CERN 94–03
26 April 1994
Proton Synchrotron
Division

ORGANISATION EUROPÉENNE POUR LA RECHERCHE NUCLÉAIRE
CERN EUROPEAN ORGANIZATION FOR NUCLEAR RESEARCH

WORKSHOP ON

BEAM COOLING AND RELATED TOPICS

Montreux, Switzerland
4–8 October 1993

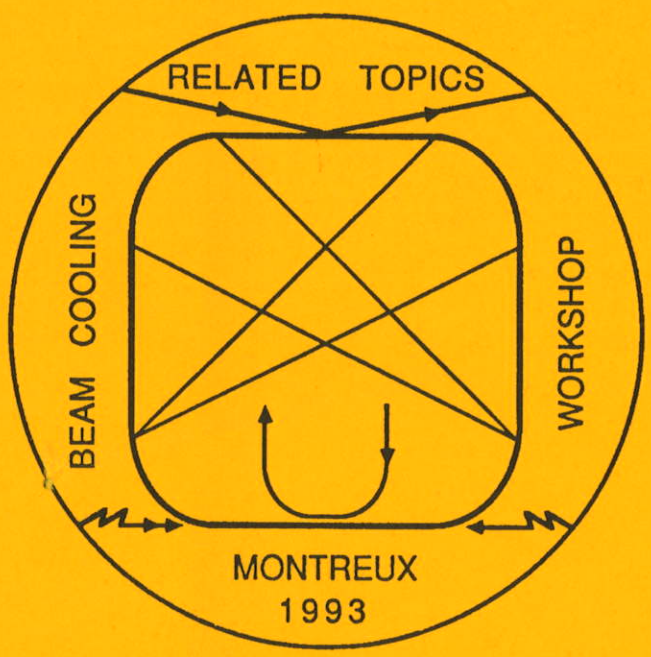

PROCEEDINGS
Editor: J. Bosser

GENEVA
1994

ISSN 0007-8328
ISBN 92-9083-060-3

CERN 94–03
26 April 1994
Proton Synchrotron
Division

ORGANISATION EUROPÉENNE POUR LA RECHERCHE NUCLÉAIRE
CERN EUROPEAN ORGANIZATION FOR NUCLEAR RESEARCH

WORKSHOP ON

BEAM COOLING AND RELATED TOPICS

Montreux, Switzerland
4–8 October 1993

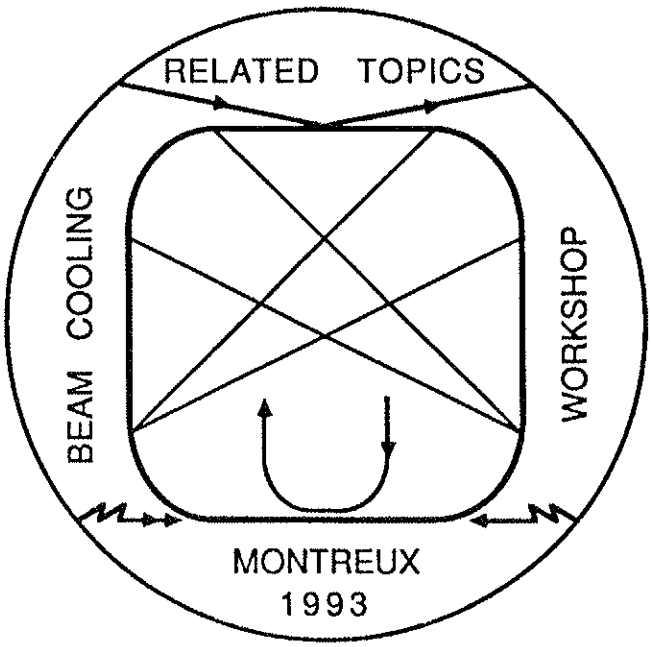

PROCEEDINGS
Editor: J. Bosser

GENEVA
1994

CERN–Service d'information scientifique–RD/922– 2500–avril 1994

ABSTRACT

The sessions of the Workshop on Beam Cooling and Related Topics, held in Montreux from 4–8 October 1993, are reported in these Proceedings. This meeting brought together international experts in the field of accelerator beam cooling. Its purpose was to discuss the status of the different cooling techniques currently in use (stochastic, electron, ionization, heavy-ion, and laser) and their actual performances, technological implications, and future prospects. Certain theoretical principles (muon cooling, cyclotron maser cooling) were discussed and are reported on in these Proceedings. Also of interest in this Workshop was the possibility of beam crystallization in accelerators using ultimate cooling. In the first part of these Proceedings, overview talks on the various cooling techniques, their implications, present performance, and future prospects are presented. More detailed reports on all the topics are then given in the form of oral presentations or poster sessions. Finally, the chairmen and/or convenors then present summary talks.

PREFACE

The Workshop on Beam Cooling and Related Topics took place from 4–8 October 1993 in Montreux, Switzerland. It was organized by the Antiproton Rings Group of the PS Division at CERN. About 80 participants from Western Europe, Russia, the USA and Japan attended this meeting which was the continuation of a series of workshops on beam cooling (Karlsruhe 1984, Wertheim 1988, Legnaro 1990 and Tokyo 1990 which were mostly devoted to electron cooling).

Following the recommendations of the International Programme Committee, emphasis was put on the wide spectrum of present and future cooling techniques for muons, protons and heavier ions.

The Workshop was divided into three main parts. During the first day, invited overview talks were given. Intended for a large audience they were presented in a tutorial form with emphasis on the present highlights and future prospects. The three following days were devoted to more specialized talks and discussions. A poster session was organized during one afternoon. On the last day the convenors gave their summary talks.

The present Proceedings contain all the papers presented at this Workshop, including the poster presentations and the session summaries written by the convenors. The wealth and the high quality of these papers underline the vigour of the field.

The Workshop received financial support from **Aubert et Duval** Steelworks (France) and from the **Société de Banque Suisse** (Switzerland). Owing to the help of the **International Science Foundation** (I.S.F., Washington D.C.) and thanks to generous financial support from the **Commission of the European Communities** (C.E.C., Brussels) we were in a position to invite a number of European students and Russian physicists. We would like to thank all these organizations for their support.

The efficient advice and help received from the members of the Organizing and Programme Committees is warmly acknowledged.

We believe that this Workshop has helped to promote cooling techniques such as electron cooling and stochastic cooling which are now being widely used in a large number of laboratories, and especially those which are under development and study such as laser cooling of ions and ionization cooling of muons.

Jacques Bosser
Chairman of the Local Organizing Committee

WORKSHOP ORGANIZATION

LOCAL ORGANIZING COMMITTEE
Chairman: J. Bosser

F. Caspers
M. Chanel
R. Ley
S. Maury
D. Möhl
G. Tranquille

PROGRAMME COMMITTEE

G. Bisoffi
T. Ellison
D. Habs
I. Hofmann
H. Ikegami
T. Katayama
P. Lefèvre
J. Marriner
I. Meshkov
D. Neuffer
O. Poulsen
D. Reistad
A. Ruggiero
A. Sessler
S. Skrinski
M. Steck
H.J. Stein
G.M. Ter-Akopian
S. van der Meer
A. Wolf

SESSION CHAIRMEN

S. Chattopadhyay
K. Hübner
T. Katayama
D. Koshkarev
V. Parkhomchuk
O. Poulsen
A. Sessler
J.P. Schiffer
D.J. Simon
A. Skrinski
A. Wolf

Workshop Secretariat

N. Gaillard
A. Molat-Berbiers

SCIENTIFIC PROGRAMME

Monday, 4 October

Morning Session	OVERVIEW TALKS (Chairman: K. Hübner)
Afternoon Session	OVERVIEW TALKS (Chairman: D.J. Simon)
Evening Session	CYCLOTRON MASER COOLING (Chairman: A.M. Sessler)

Tuesday, 5 October

Morning Session	STOCHASTIC COOLING (Chairman: T. Katayama)	TECHNIQUES & TECHNOLOGY (Chairman: V. Parkhomchuk)
	MUON COOLING (Chairman: S. Chattopadhyay)	
Afternoon Session	POSTER SESSION	
Evening Session	CYCLOTRON MASER COOLING (cont'd) (Chairman: A.M. Sessler)	

Wednesday, 6 October

Morning Session	ELECTRON COOLING (Chairmen: A. Skrinski - A. Wolf)
Afternoon Session	LASER COOLING (Chairman: O. Poulsen)
	ULTRA-COLD BEAMS, CRYSTALLIZATION (Chairman: J. P. Schiffer)

Thursday, 7 October

Morning Session	HEAVY IONS, HIGH-ENERGY COOLING (Chairman: D. Koshkarev)	
Afternoon Session	Visit to Gruyères	Work of Convenors
Evening	Banquet	

Friday, 8 October

Morning Session → 12.00	REPORTS FROM CONVENORS (Chairman: S. van der Meer)

CONTENTS

STOCHASTIC COOLING
Chairman: T. Katayama

MUON COOLING
Chairman: S. Chattopadhyay

TECHNIQUES AND TECHNOLOGY
Chairman: V. Parkhomchuk

Laser Cooling

Ultra-Cold Beams. Crystallization

Techniques and Technology

ELECTRON COOLING
Chairmen: A. Skrinski & A. Wolf

SUMMARY REPORTS FROM THE CHAIRMEN
Chairman: S. van der Meer

INTRODUCTORY REMARKS

Beam cooling is fascinating for two reasons. Firstly, it is one of the most advanced techniques for particle beam handling attracting our interest and curiosity as physicists and engineers; secondly, it has had and will have a significant impact on the advance of physics.

It had a somewhat slow start as it took quite some time before it became operationally used. This can be seen from some milestones in its development:

1966 Invention of Electron Cooling (Budker)
1968 Invention of Stochastic Cooling (van der Meer)
1974 Experimental proof of Electron Cooling (Budker et al.)
1975 Experimental proof of Stochastic Cooling and subsequent operational use in the ISR (Schnell et al.)
1977 Proposal for proton-antiproton collisions in the SPS (Rubbia et al.)
1978 Experimental proof of three-dimensional cooling in ICE
1981 Operational use of Stochastic Cooling in the CERN Antiproton Accumulator.

Subsequently, the cooling techniques were applied and refined for antiproton cooling in FNAL with a strong contribution from LBL.

In parallel, LEAR was built being the first low-energy storage ring to supply cooled hadron beams to particle physics experiments. Many other low-energy and medium-energy cooling rings in Europe, Japan and in the US have been subsequently designed and constructed mainly for nuclear and atomic physics with cooled ion beams covering the range from protons up to Uranium. Thus, the field expanded rapidly after the slowish start. The latter is partially explained by the fact that the right technology was not at hand in the early 70's.

Thanks to the cooling techniques, the experimenters now have at their disposal antiproton beams covering fifteen orders of magnitude in energy ranging from 1 meV to 1 TeV.

The lowest energy antiprotons have been used to compare the inertial masses of antiproton and proton to 4×10^{-8} and 10^{-9} seems to be within reach; furthermore, the antiprotons from these rings are also required by the experiments comparing the gravitational acceleration of antiprotons and protons. The ultimate goal at low energy might be the production of antihydrogen, which would open the possibility for a whole series of most fundamental tests.

At the high-energy side, beam cooling is indispensable to reach reasonable luminosities in the proton-antiproton colliders. This enabled the discovery of the intermediate bosons at CERN and provides the basis of the vigorous search for the top quark at FNAL.

A wealth of valuable physics is now produced by the smaller ion rings but also the performance of larger ion storage rings as RHIC might profit from advanced cooling techniques. High-luminosity ion-ion collisions in LHC cannot be envisaged without fast accumulation by ion cooling in a small buffer ring.

Laser cooling and crystalline beams may open completely new fields of application and research.

It is obvious that all these important techniques need further refinement and a better understanding. The Workshop will be the ideal place for this allowing for exchange of information and a critical review of the present status. It will generate new ideas and help the community to define the best routes to new horizons. I wish you a successful week.

K. Hübner
PS Division Leader
CERN

CERN 94–03
26 April 1994
Proton Synchrotron
Division

ORGANISATION EUROPÉENNE POUR LA RECHERCHE NUCLÉAIRE
CERN EUROPEAN ORGANIZATION FOR NUCLEAR RESEARCH

WORKSHOP ON

BEAM COOLING AND RELATED TOPICS

Montreux, Switzerland
4–8 October 1993

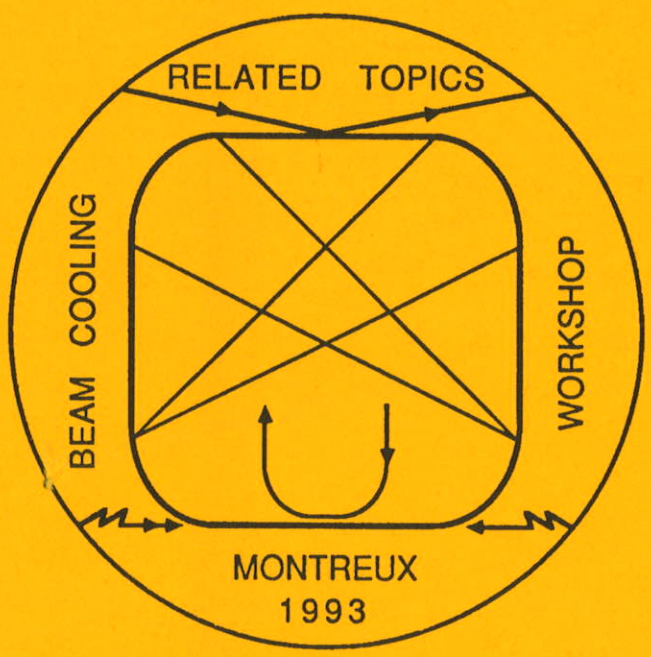

PROCEEDINGS
Editor: J. Bosser

GENEVA
1994

ISSN 0007-8328
ISBN 92-9083-060-3

CERN 94–03
26 April 1994
Proton Synchrotron
Division

ORGANISATION EUROPÉENNE POUR LA RECHERCHE NUCLÉAIRE
CERN EUROPEAN ORGANIZATION FOR NUCLEAR RESEARCH

WORKSHOP ON

BEAM COOLING AND RELATED TOPICS

Montreux, Switzerland
4–8 October 1993

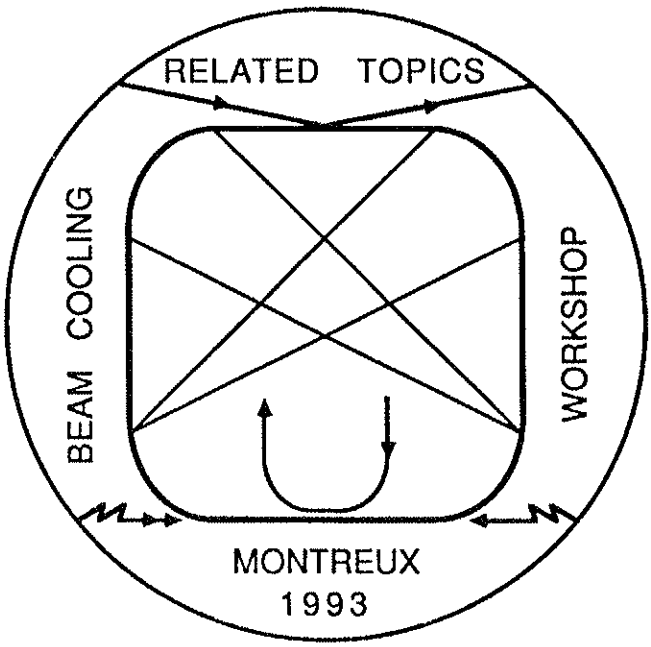

PROCEEDINGS
Editor: J. Bosser

GENEVA
1994

CERN–Service d'information scientifique–RD/922– 2500–avril 1994

ABSTRACT

The sessions of the Workshop on Beam Cooling and Related Topics, held in Montreux from 4–8 October 1993, are reported in these Proceedings. This meeting brought together international experts in the field of accelerator beam cooling. Its purpose was to discuss the status of the different cooling techniques currently in use (stochastic, electron, ionization, heavy-ion, and laser) and their actual performances, technological implications, and future prospects. Certain theoretical principles (muon cooling, cyclotron maser cooling) were discussed and are reported on in these Proceedings. Also of interest in this Workshop was the possibility of beam crystallization in accelerators using ultimate cooling. In the first part of these Proceedings, overview talks on the various cooling techniques, their implications, present performance, and future prospects are presented. More detailed reports on all the topics are then given in the form of oral presentations or poster sessions. Finally, the chairmen and/or convenors then present summary talks.

PREFACE

The Workshop on Beam Cooling and Related Topics took place from 4–8 October 1993 in Montreux, Switzerland. It was organized by the Antiproton Rings Group of the PS Division at CERN. About 80 participants from Western Europe, Russia, the USA and Japan attended this meeting which was the continuation of a series of workshops on beam cooling (Karlsruhe 1984, Wertheim 1988, Legnaro 1990 and Tokyo 1990 which were mostly devoted to electron cooling).

Following the recommendations of the International Programme Committee, emphasis was put on the wide spectrum of present and future cooling techniques for muons, protons and heavier ions.

The Workshop was divided into three main parts. During the first day, invited overview talks were given. Intended for a large audience they were presented in a tutorial form with emphasis on the present highlights and future prospects. The three following days were devoted to more specialized talks and discussions. A poster session was organized during one afternoon. On the last day the convenors gave their summary talks.

The present Proceedings contain all the papers presented at this Workshop, including the poster presentations and the session summaries written by the convenors. The wealth and the high quality of these papers underline the vigour of the field.

The Workshop received financial support from **Aubert et Duval** Steelworks (France) and from the **Société de Banque Suisse** (Switzerland). Owing to the help of the **International Science Foundation** (I.S.F., Washington D.C.) and thanks to generous financial support from the **Commission of the European Communities** (C.E.C., Brussels) we were in a position to invite a number of European students and Russian physicists. We would like to thank all these organizations for their support.

The efficient advice and help received from the members of the Organizing and Programme Committees is warmly acknowledged.

We believe that this Workshop has helped to promote cooling techniques such as electron cooling and stochastic cooling which are now being widely used in a large number of laboratories, and especially those which are under development and study such as laser cooling of ions and ionization cooling of muons.

Jacques Bosser
Chairman of the Local Organizing Committee

WORKSHOP ORGANIZATION

LOCAL ORGANIZING COMMITTEE
Chairman: J. Bosser

F. Caspers
M. Chanel
R. Ley
S. Maury
D. Möhl
G. Tranquille

PROGRAMME COMMITTEE

G. Bisoffi
T. Ellison
D. Habs
I. Hofmann
H. Ikegami
T. Katayama
P. Lefèvre
J. Marriner
I. Meshkov
D. Neuffer
O. Poulsen
D. Reistad
A. Ruggiero
A. Sessler
S. Skrinski
M. Steck
H.J. Stein
G.M. Ter-Akopian
S. van der Meer
A. Wolf

SESSION CHAIRMEN

S. Chattopadhyay
K. Hübner
T. Katayama
D. Koshkarev
V. Parkhomchuk
O. Poulsen
A. Sessler
J.P. Schiffer
D.J. Simon
A. Skrinski
A. Wolf

Workshop Secretariat

N. Gaillard
A. Molat-Berbiers

SCIENTIFIC PROGRAMME

Monday, 4 October

Morning Session	OVERVIEW TALKS (Chairman: K. Hübner)
Afternoon Session	OVERVIEW TALKS (Chairman: D.J. Simon)
Evening Session	CYCLOTRON MASER COOLING (Chairman: A.M. Sessler)

Tuesday, 5 October

Morning Session	STOCHASTIC COOLING (Chairman: T. Katayama)	TECHNIQUES & TECHNOLOGY (Chairman: V. Parkhomchuk)
	MUON COOLING (Chairman: S. Chattopadhyay)	
Afternoon Session	POSTER SESSION	
Evening Session	CYCLOTRON MASER COOLING (cont'd) (Chairman: A.M. Sessler)	

Wednesday, 6 October

Morning Session	ELECTRON COOLING (Chairmen: A. Skrinski - A. Wolf)
Afternoon Session	LASER COOLING (Chairman: O. Poulsen)
	ULTRA-COLD BEAMS, CRYSTALLIZATION (Chairman: J. P. Schiffer)

Thursday, 7 October

Morning Session	HEAVY IONS, HIGH-ENERGY COOLING (Chairman: D. Koshkarev)	
Afternoon Session	Visit to Gruyères	Work of Convenors
Evening	Banquet	

Friday, 8 October

Morning Session → 12.00	REPORTS FROM CONVENORS (Chairman: S. van der Meer)

CONTENTS

STOCHASTIC COOLING
Chairman: T. Katayama

MUON COOLING
Chairman: S. Chattopadhyay

TECHNIQUES AND TECHNOLOGY
Chairman: V. Parkhomchuk

Laser Cooling

Ultra-Cold Beams. Crystallization

Techniques and Technology

ELECTRON COOLING
Chairmen: A. Skrinski & A. Wolf

SUMMARY REPORTS FROM THE CHAIRMEN
Chairman: S. van der Meer

INTRODUCTORY REMARKS

Beam cooling is fascinating for two reasons. Firstly, it is one of the most advanced techniques for particle beam handling attracting our interest and curiosity as physicists and engineers; secondly, it has had and will have a significant impact on the advance of physics.

It had a somewhat slow start as it took quite some time before it became operationally used. This can be seen from some milestones in its development:

1966 Invention of Electron Cooling (Budker)
1968 Invention of Stochastic Cooling (van der Meer)
1974 Experimental proof of Electron Cooling (Budker et al.)
1975 Experimental proof of Stochastic Cooling and subsequent operational use in the ISR (Schnell et al.)
1977 Proposal for proton-antiproton collisions in the SPS (Rubbia et al.)
1978 Experimental proof of three-dimensional cooling in ICE
1981 Operational use of Stochastic Cooling in the CERN Antiproton Accumulator.

Subsequently, the cooling techniques were applied and refined for antiproton cooling in FNAL with a strong contribution from LBL.

In parallel, LEAR was built being the first low-energy storage ring to supply cooled hadron beams to particle physics experiments. Many other low-energy and medium-energy cooling rings in Europe, Japan and in the US have been subsequently designed and constructed mainly for nuclear and atomic physics with cooled ion beams covering the range from protons up to Uranium. Thus, the field expanded rapidly after the slowish start. The latter is partially explained by the fact that the right technology was not at hand in the early 70's.

Thanks to the cooling techniques, the experimenters now have at their disposal antiproton beams covering fifteen orders of magnitude in energy ranging from 1 meV to 1 TeV.

The lowest energy antiprotons have been used to compare the inertial masses of antiproton and proton to 4×10^{-8} and 10^{-9} seems to be within reach; furthermore, the antiprotons from these rings are also required by the experiments comparing the gravitational acceleration of antiprotons and protons. The ultimate goal at low energy might be the production of antihydrogen, which would open the possibility for a whole series of most fundamental tests.

At the high-energy side, beam cooling is indispensable to reach reasonable luminosities in the proton-antiproton colliders. This enabled the discovery of the intermediate bosons at CERN and provides the basis of the vigorous search for the top quark at FNAL.

A wealth of valuable physics is now produced by the smaller ion rings but also the performance of larger ion storage rings as RHIC might profit from advanced cooling techniques. High-luminosity ion-ion collisions in LHC cannot be envisaged without fast accumulation by ion cooling in a small buffer ring.

Laser cooling and crystalline beams may open completely new fields of application and research.

It is obvious that all these important techniques need further refinement and a better understanding. The Workshop will be the ideal place for this allowing for exchange of information and a critical review of the present status. It will generate new ideas and help the community to define the best routes to new horizons. I wish you a successful week.

K. Hübner
PS Division Leader
CERN

LIOUVILLE'S THEOREM AND PHASE-SPACE COOLING*

Robert L. Mills
Ohio State University
Columbus, OH 43210
and
Andrew M. Sessler
Lawrence Berkeley Laboratory
University of California
Berkeley, CA 94720

September 28, 1993

ABSTRACT
A discussion is presented of Liouville's theorem and its consequences for conservative dynamical systems. A formal proof of Liouville's theorem is given. The Boltzmann equation is derived, and the collisionless Boltzmann equation is shown to be rigorously true for a continuous medium. The Fokker-Planck equation is derived. Discussion is given as to when the various equations are applicable and, in particular, under what circumstances phase space cooling may occur.

1. INTRODUCTION

This workshop is devoted to cooling, so why start with a paper on Liouville's theorem [1], a theorem well-known to be "against cooling"? For very good reason, really, for it is only with a deep understanding of when one can *not* cool, that one can design—and properly analyze—cooling systems.

Back in the "old days", starting in 1955, the MURA (Midwestern Universities Research Assoc.) physicists were well aware of the limits imposed by Liouville's theorem [2]. They tried, in fact, to produce damping with tapered foils (a scheme which works in principle, but is not practical) and slaunched cavities (wrong in principle). Most of this work—for good reason—was unpublished, although publication might have prevented others from wasting many hours [3].

Besides Liouville's theorem there are other invariants, enumerated systematically by Poincare, which any dynamical system must observe [4]. In this paper we shall only consider the first Poincare invariant, i.e., Liouville's theorem. This invariant concerns over-all preservation of phase space volume and, therefore, is of relevance to the subject of cooling.

Starting in 1958 attention at MURA turned to evaluating space charge, or collective, effects; first static effects and then dynamic effects [5,6]. It seemed proper to base this analysis upon the collisionless Boltzmann equation, or Vlasov equation, but it was rather unclear, in those old days, just when that equation was a valid approximation. The present authors made a study of that matter, but never published their work [7].

It seems appropriate to re-visit the subject and now—some 35 years later—to publish the work. At the same time, it seems useful to present—in one review paper—derivations of Liouville's theorem, the Vlasov equation, and the Fokker-Planck equation. It is hoped that this will provide useful background for a proper understanding of phase space damping, i.e., cooling.

*This work was supported in part by the Director, Office of Energy Research, Office of High Energy and Nuclear Physics, of the U.S. Department of Energy under contract no. DE-AC3-76SF00098.

2. LIOUVILLE'S THEOREM

This dynamical theorem applies in a conservative Hamiltonian system such as a single particle in external magnetic and electric fields. In this case the phase density of many non-interacting systems (having slightly different initial conditions) is preserved as one follows the motion of the system.

Thus, this theorem is applicable to a beam of particles when the interaction between particles is negligible and can be ignored, which is often true—but not always true—for high energy beams.

Even within the restrictions of Liouville's theorem it is possible to arrange to interchange phase space (between, say, longitudinal and transverse degrees of freedom) or, equally interestingly, not even to exchange phase space, but to introduce correlations between the degrees of freedom, i.e., "push phase space around". A device that does just this, to distinct advantage for free-electron lasers, has recently been proposed [8].

A proof of Liouville's theorem can be found in many text books [9,10]. A simple way of looking at this theorem is to think of it as equivalent to the condition of incompressible flow in the phase space of a given system. Let the system be described by the N coordinates q_α and the N conjugate nomenta p_α, $\alpha=1,2,...,N$. The phase space is just the 2N-dimensional space with coordinates q_α and p_α, and the development in time of the state of the system is represented by the trajectory of a single point in phase space. Just as with fluid flow, there is a well-defined velocity field at each instant of time, which assigns to each point in phase space a definite velocity, with components $\dot{q}_\alpha$ and $\dot{p}_\alpha$ given as functions of the q's and p's by Hamilton's equations. For fluid flow in any number of dimensions the condition that volumes are preserved by the flow is equivalent to the vanishing of the divergence of the velocity field:

$$\nabla \cdot \mathbf{v}(x) = 0 \ . \tag{1}$$

For phase space the components of the velocity field are

$$\dot{q}_\alpha = v_\alpha(q,p,t) = \partial H/\partial p_\alpha \ , \tag{2}$$

$$\dot{p}_\alpha = F_\alpha(q,p,t) = -\partial H/\partial q_\alpha \ , \tag{3}$$

The divergence condition (1) then becomes

$$\Sigma_\alpha(\partial v_\alpha/\partial q_\alpha + \partial F_\alpha/\partial p_\alpha) = \partial^2 H/\partial p_\alpha \partial q_\alpha - \partial^2 H/\partial q_\alpha \partial p_\alpha = 0 \ , \tag{4}$$

which is automatically satisfied as a consequence of Hamilton's equations, and thus demonstrates the validity of Liouville's theorem. It is important to note that the Hamiltonian may depend explicitly on the time t.

Often a dynamical system is represented by an ensemble of possible states, with a distribution function f giving the number $n(\Delta v)$ of particles systems in a small volume ΔV of phase space:

$$n(\Delta v) = f(q,p,t)\,\Delta V \ . \tag{5}$$

If the q_i and p_i are Hamiltonian variables, then ΔV is conserved, and since the number of particles is clearly invariant, we deduce that moving with the particles (or set of systems) the density function f is constant:

$$\frac{df}{dt} = 0 \ . \tag{6}$$

It is interesting to write this out:

$$\frac{df}{dt} = \frac{\partial f}{\partial t} + \sum_{\alpha=1}^{N} \left(\frac{\partial f}{\partial q_\alpha} \frac{dq_\alpha}{dt} + \frac{\partial f}{\partial p_\alpha} \frac{dp_\alpha}{dt} \right) = 0 \quad . \tag{7}$$

From Hamilton's equations:

$$\frac{df}{dt} = \frac{\partial f}{\partial t} + \sum_{\alpha=1}^{N} \left(\frac{\partial f}{\partial q_\alpha} \frac{\partial H}{\partial p_\alpha} - \frac{\partial f}{\partial p_\alpha} \frac{\partial H}{\partial q_\alpha} \right) = 0 \quad . \tag{8}$$

From this we can see that a stationary distribution — one for which $\partial f/\partial t=0$ — must satisfy the relationship

$$\{f,H\} \equiv \Sigma_\alpha \left(\partial f/\partial q_\alpha \; \partial H/\partial p_\alpha - \partial f/\partial p_\alpha \; \partial H/\partial q_\alpha \right) = 0 \quad . \tag{9}$$

The center expression here is the Poisson bracket of f with the Hamiltonian, and the vanishing of the Poisson bracket, for a function that doesn't depend explicitly on the time, is just the condition that the expression f(q,p) be a constant of the motion and therefore, normally, a function of the standard conserved quantities. For many systems the only such constant of the motion is the energy itself, in which case f must be equal to a function of the Hamiltonian function H:

$$f = f[H(q,p)]. \tag{10}$$

This result, applied to interacting particles, for which it is not strictly true, but is a very good approximation, as we shall see in the next section, was first used in beam physics in 1958 [5]. It has been widely used since that time.

3. LIOUVILLE'S THEOREM FOR A CONTINUOUS MEDIUM WITH CONSERVATIVE INTERACTIONS

The MURA Report, which the authors wrote 35 years ago, still reads very well. This section simply consists of the old report [7], somewhat streamlined. The formal proof, of that report, is presented in Appendix A.

The study of the motion of particles in an accelerator becomes a many-body problem when the interactions between particles are taken into account. It is thus important to investigate the possibility of establishing the validity—or approximate validity—of general dynamical theorems applicable to the n-body problem. Such a powerful theorem is the one proved here to be an extremely good approximate theorem for particles in an accelerator.

Liouville's theorem asserts that in a 2fN dimensional space (f is the number of degrees of freedom of one particle), spanned by the coordinates and momenta of all particles (called γ space), the density in phase space is a constant as one moves along with any state point. It is thus a statement about the density of points, each point representing a dynamical system. The systems constitute an ensemble and of course do not interact.

The theorem proven here refers to a system of many interacting particles, and asserts that in the 2f-dimensional space spanned by the coordinates and momenta of a single system (called a μ space), the density in phase is a constant as one moves along with any phase point. It is thus a statement about the behavior of interacting particles, and thus really quite different from Liouville's theorem.

The validity of the theorem, as well as the limits of its validity, may readily be seen by the following intuitive argument:

Consider first a system of many particles, N. Suppose these particles are subject to external forces derivable from a Hamiltonian (which may even be time-dependent), but there are no interactions between the particles. Clearly density in phase in μ space is a constant of the motion as one follows the motion of a phase point. This follows then immediately from Liouville's Theorem in γ space, since with no interactions between particles μ space for N particles is simply γ space for a single particle.

Consider now a system of a great many particles N, with interactions between the particles. Imagine that the solution has been obtained so that we know the motion of all the particles as a function of time. Concentrate now on a "small" number of particles n, which initially are localized in μ space. We will define what "small" means shortly. Let all the other particles move along the trajectories appropriate to the solution of the N-body problem. If the interactions among the n particles can be neglected compared to the interactions between the N-n particles and one of the n particles, then these particles are subject to "external forces" and by the first case the density in μ space is a constant as one moves along with the sample group of n particles. This is clearly true for any sample, and hence the theorem is established.

That is, the sample size must be small enough compared to N that the influence of the n sample particles on one of their number is negligible compared with the influence of the N-n remaining particles. At the same time, n must be large enough that fluctuations within the sample can be neglected. Both of these conditions can be met if N is sufficiently large, in which case the theorem is valid to a good approximation. In the argument given below, the limit of a continuous medium is taken so that fluctuation phenomena do not exist. For applications to particle accelerators where we consider a number of particles $N \approx 10^{13}$ this approximation is very valid, corresponding to neglect of particle–particle collisions which throw a particle out of the accelerator, but *not* neglecting long range electromagnetic interactions which are responsible for space–charge limits, plasma oscillations, beam–beam interactions and possible two–stream amplification mechanisms.

Each particle of a system moves under the influence of the force fields due to all the other particles of the system, in addition to the externally imposed fields that act equally on all the particles. That particle, then, moves according to a perfectly good single-particle Hamiltonian, and you might think that Liouville's theorem would be exact for each particle. The reason this doesn't work is that the single-particle Hamiltonians are all different, and the velocity fields in μ space determined by those Hamiltonians are different also. That is, the direction that the point moves in μ space depends on which particle you are following, not on just the location in μ space, and this spoils the picture of incompressible flow that constitutes Liouville's theorem.

What makes Liouville's theorem valid to a very good approximation in μ space is that the individual single-particle Hamiltonians are so nearly similar, because the contribution of any one particle to the force fields is so small. In the continuum limit that contribution is truly negligible, and Liouville's theorem for μ space becomes exactly valid. The proof is trivially equivalent to the proof given above for an entire system; the only approximation that needs to be made is that each particle moves in the same force field and is therefore described by the same time-dependent single-particle Hamiltonian.

The density $\rho(\mathbf{r},\mathbf{p},t)$ of particles in μ space is logically equivalent to the distribution function $f(q,p,t)$ defined for an entire system by Eq. 5, and in the continuum limit it remains constant along particle trajectories in exactly the same way. In section 4 we shall see for the explicit case of relativistic particles interacting electromagnetically how this approximation yeilds the relativistic version of the Vlasov equation, or collisionless Boltzmann equation. In section 5 we shall discuss the additional collision term of the Fokker-Planck equation.

4. THE VLASOV EQUATION

For a single particle of mass m and charge e moving in an external field described by the potentials $(\mathbf{A},\varphi)$ we have the well-known Hamiltonian [11]

$$H = c\left[m^2c^2 + (\mathbf{p}-e\mathbf{A})^2\right]^{1/2} + e\varphi \quad , \tag{11}$$

with the momentum given in terms of the velocity $\mathbf{v}$ by:

$$\mathbf{p} = m\gamma\mathbf{v} + e\mathbf{A} \quad , \tag{12}$$

and

$$\gamma = \left[1 + (\mathbf{p} - e\mathbf{A})^2/m^2c^2\right]^{1/2} \quad . \tag{13}$$

The collisionless Boltzmann equation is equivalent to Eq. 6, the statement that the phase-space density, now equal to $\rho(\mathbf{r},\mathbf{v},t)$, the particle density in μ space, is constant as one follows a particle trajectory, with ρ expressed now in terms of velocity rather than momentum:

$$d\rho/dt = \partial\rho/\partial t + \Sigma v_i \partial\rho/\partial x_i + \Sigma \dot{v}_i \partial\rho/\partial v_i = 0 \ . \tag{14}$$

It is necessary only to find the acceleration $\dot{\mathbf{v}}$ in terms of the electromagnetic force $\mathbf{F}$:

$$\mathbf{F} = e(\mathbf{E} + \mathbf{v} \times \mathbf{B}) \tag{15}$$

$$= d(m\gamma\mathbf{v})/dt \tag{16}$$

$$= m\gamma(\dot{\mathbf{v}} + \gamma^2 \mathbf{v}\mathbf{v}\cdot\dot{\mathbf{v}}/c^2) \ . \tag{17}$$

Solving for $\dot{\mathbf{v}}$ yields

$$\dot{\mathbf{v}} = (1/m\gamma)(\mathbf{F} - \mathbf{v}\mathbf{v}\cdot\mathbf{F}/c^2) \ , \tag{18}$$

and substituting this result into Eq. 14 then gives the desired result:

$$\partial\rho/\partial t + \sum_i v_i \partial\rho/\partial x_i + \sum_{i,k} (1/m\gamma) F_i (\delta_{ik} - v_i v_k/c^2) \partial\rho/\partial v_k = 0. \tag{19}$$

In the non-relativistic limit

$$\frac{\partial\rho}{\partial t} + \mathbf{v}\cdot\nabla_r\rho + \frac{\mathbf{F}}{m}\nabla_v\rho = 0 \ , \tag{20}$$

the well-known Vlasov, or collisionless Boltzmann, equation.

Now the discussion of the last section allows us to extend this to many particles. In that case we must include collisions between particles which means we have on the RHS, $\left.\frac{\partial\rho}{\partial t}\right)_{\text{collisions}}$, rather than zero.

If, however, the particles *only* interact through the fields $\boldsymbol{E}$ and $\boldsymbol{B}$ then there are no collisions and we recover the Vlasov equation; but with $\boldsymbol{E}$ and $\boldsymbol{B}$ the *total* field (external field plus self-field) and ρ now the distribution function of *interacting* particles. Obviously Liouville's theorem is applicable.

5. THE FOKKER-PLANCK EQUATION

We would like to turn, now, to evaluation of the collision term $\left.\frac{\partial\rho}{\partial t}\right)_{\text{collisions}}$ on the RHS of the Boltzmann equation. Clearly, evaluation depends upon the nature of the forces between particles. For hard scattering, such as molecules in a gas undergo, Boltzmann, himself, addressed the subject.

For Coulomb forces the scattering is primarily into very small angles (i.e., hardly any change in the direction of the particle). In this case we must consider the effect of multiple scattering, thus deriving the change in ρ from many, very small, collisions. The result is the Fokker-Planck equation, which has been employed widely in physics. In accelerator physics it has been employed, amongst other things, to study intra-beam scattering, the effect of noise on the applied radio frequency, and the turbulence in intense charge bunches [12].

Let $W(\mathbf{v},\Delta\mathbf{v})$ be the probability density for a particle changing its velocity from $\mathbf{v}$ to $\mathbf{v}+\Delta\mathbf{v}$ in time Δt, and suppose for this discussion that the only changes in ρ are those due to collisions. Then

$$\rho(\mathbf{r},\mathbf{v},t+\Delta t) = \int \rho(\mathbf{r},\mathbf{v}-\Delta\mathbf{v},t) W(\mathbf{v}-\Delta\mathbf{v},\Delta\mathbf{v}) d(\Delta\mathbf{v}) \ . \tag{21}$$

Since

$$\frac{\partial \rho}{\partial t}\Big)_{\text{collisions}} \Delta t = \rho(\mathbf{r},\mathbf{v},t+\Delta t) - \rho(\mathbf{r},\mathbf{v},t) \quad , \tag{22}$$

we can Taylor expand and get

$$\begin{aligned} &\rho(\mathbf{r},\mathbf{v}-\Delta\mathbf{v},t)W(\mathbf{v}-\Delta\mathbf{v},\Delta\mathbf{v}) = \rho(\mathbf{r},\mathbf{v},t)W(\mathbf{v},\Delta\mathbf{v}) \\ &-\sum_i \frac{\partial(\rho W)}{\partial v_i}\Delta v_i + \frac{1}{2}\sum_{i,j}\frac{\partial^2(\rho W)}{\partial v_i \partial v_j}\Delta v_i \Delta v_j + \ldots \end{aligned} \tag{23}$$

By definition

$$\int W d(\Delta v) = 1 \quad . \tag{24}$$

Defining

$$\langle \Delta v \rangle_t \, \Delta t = \int W \, \Delta v \, d(\Delta v) \quad , \tag{25}$$

$$\langle \Delta v_i \Delta v_j \rangle_t \, \Delta t = \int W \, \Delta v_i \, \Delta v_j \, d(\Delta \mathbf{v}) \quad , \tag{26}$$

we have the Fokker-Planck collision term:

$$\frac{\partial \rho}{\partial t}\Big)_{\text{collisions}} = -\sum_i \frac{\partial}{\partial v_i}\left(\langle \Delta v_i \rangle_t \rho\right) + \sum_{i,j}\frac{1}{2}\frac{\partial^2}{\partial v_i \partial v_j}\left(\langle \Delta v_i \Delta v_j \rangle_t \rho\right) \quad . \tag{27}$$

The coefficients have been studied extensively in the literature.

6. DISCUSSION

Let us, first of all, review the theorems discussed in this note. Liouville's theorem applies to any Hamiltonian dynamical system, that is, a system describable by a Hamiltonian, which may be time-dependent. Thus the theorem applies, for example, to a single particle subject to a conservative external force, and also to a collection of non-interacting particles, each subject to the same external conservative force.

Does Liouville's theorem apply to highly nonlinear, stochastic motion of non-interacting particles? Clearly it does, since each particle still constitutes a Hamiltonian system governed by the same single-particle Hamiltonian. How then can we reconcile the theorem with the very non-Liouvillean motion characterized by non-zero Liapunov exponents? From a fine-grained point of view, there is no change in phase space density; Liouville's theorem is quite valid. From a coarse-grained point of view, however, the density in phase space changes significantly. The filaments of constant density become ever finer and lots of "air" mixes in, so the coarse-grained density is ever decreasing. Notice that the coarse-grained density becomes more and more relevant because, given any degree of precision with which density is observed, one only has to wait sufficiently long and the coarse-grained density will become appropriate. Notice also that the coarse-grained density can only decrease, that is, that only "heating", but not "cooling", can occur through this mechanism.

The Vlasov equation, or collisionless Boltzmann equation as usually used, is only a nonrelativistic approximation. It is applicable to a collection of particles, each subject to the same

(possibly time-dependent) external forces described by a conservative Hamiltonian, where the strong collisional interactions between particles are negligible and the particles interact with each other only through their mutual electromagnetic interactions. This interaction may be very significant; the collective behavior of plasmas, for example, which is very complicated indeed, is accurately described by the Vlasov equation.

The Fokker-Planck equation is valid when the interacting particles undergo many collisions, eah one of which only deflects the particle slightly (multiple scattering). [Is this right? The derivation doesn't seem to be limited to small momentum-transfer collisions.] It is thus a natural extension of the Vlasov equation. The Fokker-Planck equation can be used to study, for example, the effect of intra-beam scattering.

Secondly, let us now discuss under what situations one can have "cooling", that is, damping of phase space. The simplest is to have a dissipative system, as, for example, a charged particle radiatively coupled to the electromagnetic field[13]. Actually, there are quantum fluctuations in this coupling, which are usually studied by means of the Fokker-Planck equation.

A second example of a dissipative system is a beam of particles interacting with a foil[14]. This is called "ionization damping", and is very similar to radiation damping. It has been proposed for cooling a mu meson beam to make a muon collider.

A third example is provided by interaction between the "hot" beam one wishes to cool and a "cold" beam of electrons[15]. In this case, "hot" and "cold" refer to transverse temperature. Electron cooling has been employed in high-energy physics, though its most important applications have been in nuclear physics.

A rather different approach to "circumventing Liouville" is to develop a system which probes the distribution of particles in mu space and to improve that distribution by decreasing the emittance of the beam. Stochastic cooling is of this nature and, as we all know, has been very effectively used in high-energy physics[16].

Finally, let us comment on the transition from the Vlasov equation, where there is no damping of phase space, to a damping situation, such as is provided by radiation damping. Clearly, in the latter case, if we include all the modes of the electromagnetic field (photons, if we think quantum mechanically) with the particles, then the whole system is described by a Hamiltonian and Liouville's theorem applies. Thus, from this "big point of view" we only have transfer of phase volume among the various degrees of freedom and no damping of the total phase space. Nevertheless, there is damping of the particle phase space, spanned by all the particle coordinates and momenta, and "undamping" of the region spanned by electromagnetic mode coordinates and momenta.

If we have a group of particles coupled without radiative damping to one or more modes of the electromagnetic field, then the motion of the particles is described by the Vlasov equation and there is no damping in the particle phase space. In this situation of particles coupled dynamically to the electromagnetic field, one might think - erroneously - that Liouville's theorem refers only to the total phase space spanned by particle coordinates and momenta and field coordinates and momenta. Thus, especially in the case where the electromagnetic field is self-generated and growing in time (as in a free-electron laser), one might expect damping in the particle phase space and undamping in the electromagnetic field phase space, as described in the previous paragraph. The Vlasov equation shows, however, that this thinking is quite wrong. Provided the number of particles is large, as discussed in sec.3, each particle moves in the same well-determined electromagnetic field, described by a good single-particle Hamiltonian, and particle phase space is conserved. Notice that this is true whether or not the electromagnetic field is removed from the particle's surroundings (and, for example, used for some purpose); i.e., phase space is conserved whether or not the system is dissipative of energy.

What, then, is needed to achieve a violation of Liouville's theorem? There are just two ways in which the mu-space Liouville's theorem is violated at the microscopic level: through radiation damping, the dissipative self-force on the charged particles, and through the failure of the condition discussed above, that the contribution of any one particle to the electromagnetic field distribution can be neglected. The effects of radiation damping are well understood, and are not under discussion here, while the number of particles in a typical accelerator beam is so great that the latter condition is satisfied to an excellent degree. For this discussion, then, Liouville's theorem holds for mu space.

How, then, do we achieve the apparent violations of Liouville's theorem in various methods of beam cooling? As always, Liouville's theorem breaks down as soon as you work with a coarse-grained average density in phase space. The usual effect of this, due to the normal filamenting of volumes in phase space, is a reduction of phase space density, but the game we are playing is to reverse this normal effect by playing Maxwell's demon. We probe the distribution in mu space, determine which parts are occupied and which are not, and then adjust the electromagnetic fields so that the occupied parts move closer together and the unoccupied parts go elsewhere. The time-dependent fields that we introduce do not alter the fact that the same single-particle Hamiltonian governs the motion of every particle, and thus do not destroy the validity of Liouville's theorem at the microscopic level. The coarse-grained average density, though, increases in the occupied regions of phase space and decreases, necessarily, for the unoccupied regions. For occupied and unoccupied, of course, you can substitute more densely and less densely occupied.

What, then, are the limitations on how far you can play this game? The question is simply how precisely you can probe mu space, and how precisely you can dissect and manipulate it; i.e., what is the spacial resolution of the probe. In some cases a measure of this precision is the wavelength of the electromagnetic signals involved in the process; in other cases, such as in stochastic cooling, it is more the "effective wavelength", since the dipole mode sensed by the pickup has a very long wavelength, but its amplitude is measured with very great precision. If the spacial resolution is greater than the inter-particle spacing, then no further cooling is possible. Others have argued that the spacial resolution should be compared with the final beam emittance. We believe that this question is unsettled, and note that 155 years after Liouville's work there are still interesting and unresolved aspects of his remarkable theorem.

7. ACKNOWLEDGMENTS

We wish to thank Swapan Chattopadhyay, Kwang-Je Kim, Hiromi Okamoto, George Schmidt, and Simon Yu for illuminating discussions.

REFERENCES

[1] J. Liouville, Journ. de Math. 3, 349 (1838).

[2] K.R. Symon and A.M. Sessler, *Methods of radio frequency acceleration in fixed field accelerators,* Proc. of CERN Symp. on High Energy Accelerators, p. 44, CERN, Geneva (1956).

[3] Members of the MURA Group (private communication).

[4] V.I. Arnold, *Mathematical Methods of Classical Mechanics*, Springer-Verlag, New York (1978), p. 238.

[5] C.E. Nielsen and A.M. Sessler, Rev. Sci. Inst. 30, 80 (1959).

[6] C.E. Nielsen, A.M. Sessler and K.R. Symon, *Longitudinal instabilities in intense relativistic beams*, Proc. of CERN Symp. on High Energy Accelerators, p. 239, CERN, Geneva (1959); A.A. Kolomenskij and A.N. Lebedev, *Certain beam-stacking effects in fxed-feld magnet systems*, ibid p. 115.

[7] R.L. Mills and A.M. Sessler, *Liouville's theorem for a continuous medium with conservative interactions*, Midwestern Universities Research Association, MURA-433, Oct. 8, 1958 (unpublished).

[8] A.M. Sessler, D.H. Whittum and L.-H. Yu, Phys. Rev. Lett. 64, 309 (1992).

[9] H. Goldstein, *Classical Mechanics*, Addison-Wesley, Reading, MA (1980), p. 426; A.J. Lichtenberg, *Phase Space Dynamics of Particles*, Wiley, New York (1969).

[10] K. Miyamoto, *Plasma Physics for Nuclear Fusion*, The MIT Press, Cambridge, p. 102 ff (1976).

[11] J.D. Jackson, *Classical Electrodynamics*, Wiley, New York (1975), p. 574.

[12] P.J. Channell and A.M. Sessler, Nucl. Instr. and Methods 136, 473 (1976); D. Boussard, G. Dome and C. Grazini, *The influence of rf noise on the lifetime of bunched proton beams*, 11th Inter. Conf. on High-Energy Accelerators, CERN, Birkhäuser, Basel (1980), p. 620; A. Piwinski, *Intra-beam scattering*, 14th Inter. Conf. on High Energy Accelerators, SLAC, Stanford (1974), p. 405.
[13] K. Robinson, Phys. Rev. 111, 373 (1958); M. Sands, Phys. Rev. 97, 470 (1955).
[14] Members of the MURA Group (private communication); D. Neuffer, Particle Accelerators 14, 75 (1983).
[15] G.I. Budker, *Status report of works on storage rings at Novosibirsk*, Proc. Int. Symp. on Electron and Positron Storage Rings, Saclay (1966), p. II-1-1; W. Kells, *Electron cooling*, Physics of High Energy Particle Accelerators, AIP Conf. Proc. 87, AIP, New York (1982), p. 656.
[16] S. van der Meer, *Stochastic damping of betatron oscillations in the ISR*, CERN Internal Report CERN/ISR-PO/72-31 (1972); S. van der Meer, *An introduction to stochastic cooling*, Physics of Particle Accelerators, AIP Conf. Proc. 153, AIP, New York (1987), p. 1628.

APPENDIX A : Formal Proof of Liouville's Theorem for a Continuous Media

Let λ_i (i = 1, ---, 2f,) be parameters labelling the particles of the medium (2f dimensional phase space; this is the μ space); $dn = \sigma d\lambda_1 ... d\lambda_{2f}$ = number of particles in 'volume' element $d\lambda$; σ = constant 'density' with respect to λ.

Let $\pi_\alpha(\lambda)$ = momentum density = σp_x, $q_\alpha(\lambda)$ = position of particle λ.

The Hamiltonian is

$$H = \sigma \int h[q(\lambda), \pi(\lambda)] d\lambda + \sigma^2 \iint v[q(\lambda), \pi(\lambda), q(\lambda')\pi(\lambda')] d\lambda d\lambda' , \tag{A1}$$

where h and v do not depend explicitly on λ, and the equations of motion are

$$\dot{q}_\alpha(\lambda) = \frac{\delta H}{\delta \pi_\alpha(\lambda)} = \sigma \frac{\partial h[\lambda]}{\partial \pi_\alpha(\lambda)} + \sigma^2 \int \frac{\partial}{\partial \pi_\alpha(\lambda)} v[\lambda, \lambda'] d\lambda' \tag{A2}$$

$$\dot{\pi}_\alpha(\lambda) = -\frac{\delta H}{\delta q_\alpha(\lambda)} = -\sigma \frac{\partial h[\lambda]}{\partial q_\alpha[\lambda]} - \sigma^2 \int \frac{\partial}{\partial q_\alpha(\lambda)} v[\lambda, \lambda'] d\lambda' . \tag{A3}$$

Let us introduce a condensed notation:

$$\begin{aligned} \xi_s &= q_s , \ s = 1, \ldots, f \\ &= -\pi_s , \ s = f+1, \ldots, 2f . \end{aligned} \tag{A4}$$

The equations of motion may be written

$$\dot{\xi}_s(\lambda) = \sum_t \varepsilon_{st} \frac{\delta H}{\delta \xi_t(\lambda)} = \sum_t \varepsilon_{st} \left[\sigma \frac{\partial h}{\partial \xi_t} + \sigma^2 \int \frac{\partial v}{\partial \xi_t} d\lambda' \right], \tag{A5}$$

where

$$\begin{aligned} &\varepsilon_{s,f+s} = 1, \ s = 1, \ldots, f \\ &\varepsilon_{f+s,s} = -1, \ s = 1, \ldots, f \\ &\varepsilon_{st} \ = 0, \quad \text{otherwise} . \end{aligned} \tag{A6}$$

Clearly ε_{st} is antisymmetric. Now the density $\rho(q,\pi)$ in phase space is given by

$$\rho dq d\pi = \sigma d\lambda \tag{A7}$$

or

$$\rho d\xi = \sigma d\lambda \ . \tag{A8}$$

$$\begin{aligned} \frac{1}{\rho} &= \frac{1}{\sigma} \times \text{Jacobian} \\ &= \frac{1}{\sigma} \times \det \left| \frac{\partial \xi_s}{\partial \lambda_i} \right| \\ &= \frac{1}{\sigma} \Delta, \text{ say} . \end{aligned} \tag{A9}$$

The inverse matrix to $\partial\xi_s/\partial l_i$ is of course $\partial\lambda_i/\partial\xi_s$, and the adjoint to $\partial\xi_s/\partial\lambda_i$ is $\Delta \frac{\partial \lambda_i}{\partial \xi_s}$ .Thus we have for the rate of change of $\frac{1}{\rho}$ along a trajectory (λ = constant):

$$\begin{aligned} \frac{d}{dt}\left(\frac{1}{\rho}\right) &= \frac{1}{\sigma} \frac{\partial \Delta}{\partial t} \Big|_{\lambda = \text{constant}} \\ &= \frac{1}{\sigma} \sum_{i,s} \left(\Delta \frac{\partial \lambda_i}{\partial \xi_s} \right) \frac{\partial^2 \xi_s}{\partial t \partial \lambda_i} , \end{aligned} \tag{A10}$$

but

$$\begin{aligned} \frac{\partial^2 \xi_s}{\partial t \partial \lambda_i} &= \sum_t \frac{\partial}{\partial \lambda_i} \varepsilon_{st} \frac{\delta H}{\delta \xi_t(\lambda)} \\ &= \sum_t \varepsilon_{st} \frac{\partial}{\partial \lambda_1} \left[\sigma \frac{\partial h[\lambda]}{\partial \xi_t(\lambda)} + \sigma^2 \int \frac{\partial v[\lambda, \lambda']}{\partial \xi_t(\lambda)} d\lambda' \right] \\ &= \sum_{r,t} \varepsilon_{st} \frac{\partial \xi_r}{\partial \lambda_i} \left[\sigma \frac{\partial^2 h[\lambda]}{\partial \xi_t \partial \xi_r} + \sigma^2 \int \frac{\partial^2 v[\lambda, \lambda']}{\partial \xi_t(\lambda) \partial \xi_r(\lambda)} d\lambda' \right] \\ &= \sum_{r,t} \varepsilon_{st} \frac{\partial \xi_r}{\partial \lambda_i} \left[\sigma \frac{\partial^2 h[\lambda]}{\partial \xi_t \partial \xi_r} + \sigma^2 \int \frac{\partial^2 v[\lambda, \lambda']}{\partial \xi_t(\lambda) \partial \xi_r(\lambda)} d\lambda' \right] \\ &= \sum_{r,t} \varepsilon_{st} \frac{\partial \xi_r}{\partial \lambda_i} M_{tr} \quad \text{and } M_{tr} \text{ is symmetric,} \end{aligned} \tag{A11}$$

so

$$\begin{aligned}\frac{d}{dt}\left(\frac{1}{\rho}\right) &= \frac{1}{\sigma}\Delta \cdot \sum_{i,s,t,r} \frac{\partial \lambda_i}{\partial \xi_s} \varepsilon_{st} \frac{\partial \xi_r}{\partial \lambda_i} M_{tr} \\ &= \frac{\Delta}{\sigma} \sum_{s,t,r} \delta_{r,s} \varepsilon_{st} M_{tr} \\ &= \frac{\Delta}{\sigma} \sum_{s,t} \varepsilon_{st} M_{ts} \\ &= 0\end{aligned} \tag{A12}$$

since ε is antisymmetric and M is symmetric. So the density in μ space does indeed remain constant along any trajectory.

THEORY, TECHNOLOGY, AND TECHNIQUE OF STOCHASTIC COOLING

John Marriner
Fermilab* , P.O. Box 500, Batavia, IL 60510

ABSTRACT
The theory and technological implementation of stochastic cooling is described. Theoretical and technological limitations are discussed. Data from existing stochastic cooling systems are shown to illustrate some useful techniques.

1. THEORY

1.1 Introduction

The theory of stochastic cooling has been discussed by a number of authors [1,2,3,4,5,6,7]. I will try to describe the theory and to make the results seem plausible, but I will not give a detailed derivation of the results.

A prototypical transverse stochastic cooling is shown in Fig. 1. The system senses the particle position at the pickup by measuring the difference in induced current between the two pickup electrodes. The electronic signal is amplified and applied to the kicker electrode when the particle passes between the electrodes. Transverse electric and magnetic fields in the kicker deflect the particle. The angular deflection at the kicker will decrease the amplitude of the betatron oscillations provided that it has the correct sign.

1.2 Schottky Signals

An understanding of Schottky signals is central to the understanding of stochastic cooling. A particle passing a point in the ring with revolution frequency makes a current

$$\begin{aligned} i(t) &= e\sum_{n=-\infty}^{\infty}\delta\left(t+\tau-\frac{n}{f_0}\right) \\ &= ef_0\left[1+2\sum_{n=1}^{\infty}\cos n\omega_0(t+\tau)\right]. \end{aligned} \tag{1}$$

The current consists of an infinite series of lines at multiples of the revolution frequency. If we consider a beam of particles with random values of τ then the total current will be nearly zero because of the random phase factor in Eq. (1). The rms current is not zero and is known as the Schottky current. In a beam the revolution frequencies are similar but not identical for all particles. Thus, the Schottky currents organize themselves into bands around the average revolution frequency. The total power per Schottky band for a beam of N particles is

$$P_t = 2Ne^2 f_0^2. \tag{2}$$

The betatron motion of particle in the beam at the observation point is given by

$$x(t) = A\cos(\omega_0 Qt + \phi). \tag{3}$$

The dipole moment of the beam is the current times the displacement and can be written in terms of sine waves as

$$d(t) = ef_0 A\left[\sum_{n+Q>0}\cos(n+Q)\omega_0(t+\tau)+\sum_{n-Q>0}\cos(n-Q)\omega_0(t+\tau)\right]. \tag{4}$$

There are 2 Schottky sidebands per harmonic of the revolution frequency. Each band has a total power

* Operated by the Universities Research Assoc. under contract no. DE-AC02-76CHO3000 with the US Dept. of Energy

$$P_t = \frac{1}{2} N e^2 A^2 f_0^2. \tag{5}$$

Schottky signals are often observed with a pair of strip-line pickups. The beam current is observed when the top and bottom pickups are added. The dipole moment is obtained when the two pickups are subtracted. An example of the observation of the dipole signal is shown in Fig. 2.

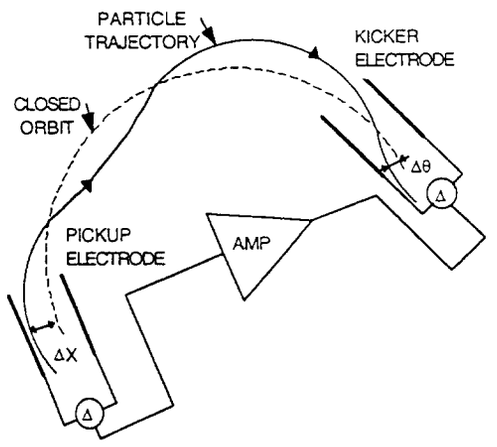

Fig. 1. Schematic of a typical stochastic cooling system. The particle position is sensed at the pickup and a corresponding deflection is applied at the kicker.

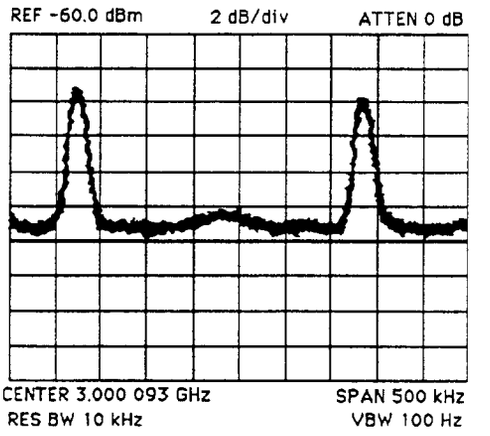

Fig. 2. The Schottky signal from the two betatron sidebands in the FNAL Debuncher ring is shown. The pickup is most sensitive to the dipole moment but has some direct sensitivity to the current which produces a small enhancement at harmonics of the revolution frequency as seen near the center of the trace.

1.2 Action of the Feedback

We consider the action of the feedback system in Fig. 1 on a coasting beam. A more schematic representation is shown in Fig. 3. The dipole moment will be the sum of the dipole moment $d_i(\omega)$ in the absence of the feedback system and a dipole moment $d_f(\omega)$ induced by the excitation applied to the kicker. If this excitation is not too large, then the dipole moment will depend linearly on the deflection.

$$d_f(\omega) = F(\omega)\theta(\omega). \tag{6}$$

We further assume that the angular deflection depends linearly on the dipole moment of the beam:

$$\theta(\omega) = G(\omega)\left[d_i(\omega) + d_f(\omega)\right]. \tag{7}$$

Using the circuit shown in Fig. 3, one can infer that

$$\begin{aligned} \theta(\omega) &= \frac{G(\omega)d_i(\omega)}{1 - F(\omega)G(\omega)} \\ &= H(\omega)d_i(\omega). \end{aligned} \tag{8}$$

Fig. 3 and this formalism are intended to demonstrate that stochastic cooling is formally identical to purely electronic feedback circuits. Thus, one can apply the techniques used in dealing with these more commonplace feedback circuits directly to stochastic cooling systems. Network analyzers can be effectively employed to measure the denominator in Eq. (8). The denominator, in fact, is of considerably more importance than the numerator. Not only does it determine system stability according to the criterion of Nyquist [8], it also provides a measure of the cooling rate relative to the maximum rate that can be obtained.

In order to understand the relationship between the denominator of Eq. (8) and the cooling effect, consider Fig. 4. A segment of a beam is shown in coordinate space. Suppose that a random clumping of particles gives the beam a net dipole moment near the center of the beam. The action of the stochastic cooling

system serves to reduce the dipole moment by displacing the centroid of the beam by making the "kink" shown in Fig. 4. This effect of the cooling system is known as "signal suppression." When signal suppression is present, the motion of the beam centroid produces a signal which is opposite in sign to the Schottky signal. If the cooling system is turned off, the Schottky signal will return to its former level.

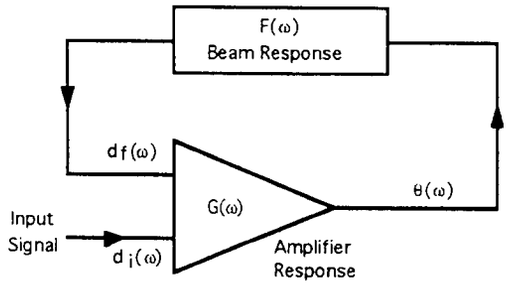

Fig. 3. Equivalent circuit of the beam feedback. The input signal d_i is modified by the addition of the feedback d_f.

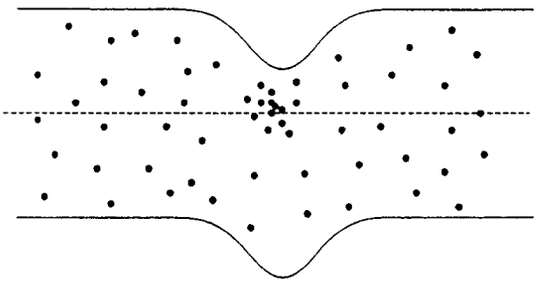

Fig. 4. A cartoon of the behavior of a fluctuation in the dipole moment of the beam under the influence of a stochastic cooling system.

The kink in the beam reduces the amplitudes of the particles that constitute the clump of beam. These particles have slightly different revolution frequencies, so the clump will dissipate as time elapses. After the clump dissipates these particles will continue to have their reduced amplitudes – even if the cooling system is turned off. Note that some particles have their amplitudes increased in this process. However, the net effect is beam cooling since more particles are in the clump of beam than outside it. The length of time that it takes for fluctuations to disappear is defined to be M times the revolution period, where M is known as the mixing factor. Large values of M reduce the maximum cooling rate. The power of the cooling system to resolve two nearby fluctuations is approximately $1/W$, where W is the cooling system bandwidth.

1.3 Betatron Cooling

In order to quantitatively connect the signal suppression phenomenon and the cooling rate, consider the equations of motion. The emittance is a constant of motion in the absence of the cooling system. Under the action of the cooling system the change in amplitude of the i^{th} particle is:

$$\begin{aligned}\Delta\left(A_i^2\right) &= \frac{\beta}{2}\left[\left(\theta_i + \Delta\theta\right)^2 - \theta_i^2\right] \\ &= \beta\theta_i\Delta\theta + \frac{\beta}{2}\Delta\theta^2,\end{aligned} \tag{9}$$

where β is the beta function at the kicker, θ_i. is the angle of the ith particle at the kicker, and $\Delta\theta$ is the angular deflection at the kicker. The deflection at the kicker depends linearly on the signals the various particles created at the pickup. Therefore one can write the deflection as a sum over particles

$$\Delta\theta = \sum_{j=1}^{N}\Delta\theta_j, \tag{10}$$

where part of the deflection due to the motion of the ith particle. We can use Eqs. (9) and (10) to compute the change in emittance as follows:

$$\Delta\varepsilon = \frac{1}{N}\sum_{i=1}^{N}\Delta\left(A_i^2\right) = \frac{\beta}{2N}\sum_{i=1}^{N}\left(2\theta_i\Delta\theta_i + N\Delta\theta_i^2\right). \tag{11}$$

In writing Eq. (11) it has been assumed that the particle motions are random, so that the $i\neq j$ terms do not *on the average* contribute to $\Delta\varepsilon$ and the double sum collapses to a single sum.

An evaluation of $\Delta\theta$ and a more detailed account of some other significant points are given in reference 7. The result is that the cooling rate is given by

$$\frac{1}{\varepsilon}\frac{d\varepsilon}{dt} = \frac{1}{4\pi N}\sum_{i=1}^{N}\omega_{0ii}\sum_{n=-\infty}^{\infty}\Big\{-2\,\mathrm{Re}\Big[jH\big((n+Q)\omega_{0i}\big)e^{j\mu_k}e^{-j(n+Q)\omega_{0i}t_{ik}}\Big]$$
$$+\Big[M\big((n+Q)\omega_{0i}\big)+U\big((n+Q)\omega_{0i}\big)\Big]\Big|H\big((n+Q)\omega_{0i}\big)\Big|^2\Big\}, \qquad (12)$$

where Q is the betatron tune, μ_k is the phase advance between pickup and kicker, ω_{0i} is the angular revolution frequency, and t_{ki} is the transit time delay between pickup and kicker. The first term on the right hand side of Eq. (12) is the cooling term. The cooling rate is maximized when $\mu_k = \pi/2$ and $H(\omega)$ is real and except for a phase factor $\exp(j\omega_{0i}t_{ik})$. The phase factor corresponds to a delay equal to the particle pickup to kicker delay.

The mixing factor M is the ratio of the Schottky power density of particles with the same revolution frequency as the i^{th} particle to the average Schottky power. Since no particles have *exactly* the same revolution frequency as the i^{th} particle, the calculation of M must be understood as a limit. If the cooling is applied for a time T, the number of particles that have a revolution frequency that is indistinguishable from the i^{th} particle is proportional to $1/T$. The growth in amplitude squared from the remaining particles, however, is proportional to T^2. Thus the net effect of the particles is a growth in amplitude squared that is linear with time.

The factor $U(\omega)$ is the ratio of thermal noise power to the average schottky power. It enters into the equations in exactly the same way as the schottky power. The only difference between the Schottky noise and thermal noise is that the system designer has some control over the value of the thermal noise. In fact, in low density beams the major design challenge may be to achieve an acceptable signal to noise ratio.

Since the cooling term in Eq. (12) is proportional to $H(\omega)$ and the heating term is proportional to $|H(\omega)|^2$, there is a value of H that achieves the highest cooling rate. This value is known as the optimum gain. Gain values which exceed the optimum gain will result in a reduced cooling rate.

Equation (12) is the exact expression for cooling in the frequency domain. The cooling of particles with different frequencies will vary because of the differences in the phase factors in the cooling term and the mixing factor M. The cooling system is usually phased for the center of the beam distribution – where M usually has a peak. The heating term decreases as the frequency departs from the center, but the phase error of the cooling term increases so the cooling rate doesn't vary too much. It is convential to estimate the cooling rate by using the cooling value at the peak value of M If H is at the optimum gain, the formula for the cooling rate becomes:

$$\frac{1}{\varepsilon}\frac{d\varepsilon}{dt} = \frac{W}{N\big(\overline{M}+\overline{U}\big)}. \qquad (13)$$

where $W = f_{max} - f_{min}$ is the cooling system bandwidth and $\overline{M}$ and $\overline{U}$ are the peak values of M and U.

1.4 Momentum Cooling

Momentum cooling is similar to betatron cooling except that a technique is required to develop a signal that is proportional to the momentum of the particle. The simplest technique is to place a difference pickup in a region of non-zero dispersion. A pickup that measures the dipole moment of the particles in a region of dispersion will produce a Schottky voltage proportional to the momentum fluctuations in the beam. This voltage can be made to accelerate or decelerate the beam in a kicker and therefore cool the momentum spread. This cooling method is sometimes called the Palmer method. A second technique is to use a notch filter. The filter response changes sign depending on whether the particle revolution frequency is above or below the desired frequency. This method of cooling [9] is sometimes called the Thorndahl method.

The two methods have disadvantages and advantages. The pickup placed in the region of dispersion will have poor signal to noise ratio (nominally 0) at the center of the pickup. The notch filter method avoids the low signal to noise ratio by filtering the noise as well as the signal, and the signal to noise ratio follows the particle density throughout the notch. The filter method can only be used if the revolution frequency versus momentum relationship is unique (non-overlapping Schottky bands). The filter introduces undesirable phase characteristics that reduce the cooling rate. Thus, the filter method is used in situations where the signal to noise ratio is critical; otherwise the pickup in dispersion is used.

Momentum cooling is conventionally described by a Fokker-Planck equation. The beam is described by a distribution $N(E,t)$, which is the number of particles greater than energy E at time t. The density Ψ is given by

$$\Psi(E,t) = \frac{\partial N(E,t)}{\partial E}, \tag{14}$$

and the flux is given by

$$\Phi(E,t) = \frac{\partial N(E,t)}{\partial t}. \tag{15}$$

The flux is related to the beam distribution by the Fokker-Planck equation

$$\Phi = F\Psi + \left(D_0 + D_1 + D_2\Psi\right)\frac{\partial \Psi}{\partial E}. \tag{16}$$

The term proportional to $F = F(E)$ is the cooling term. $F(E)$ is proportional to the cooling system gain G. The term D_1 is a heating term that is proportional to thermal noise in the system. The term proportional to D_2 is the Schottky heating term. The Schottky heating is proportional to $\Psi(E,t)$ the number of particles at that energy (or equivalently that revolution frequency). Both D_1 and D_2 are proportional to G^2. The term D_0 is used to describe external heating mechanisms such as intrabeam scattering that are independent of cooling system gain.

One can describe momentum cooling in terms of moments similar to the equation describing momentum cooling. However, moments tend to be less useful because of the non-linear nature of Eq. (16): as the cooling proceeds the density increases and the Schottky heating term increases. Similarly, one can write a Fokker-Planck equation to describe betatron cooling. However, most betatron cooling applications are fairly well described by gaussian distributions where the variation in the rms beam size completely describes the beam evolution. Momentum cooling, however, has been applied to antiproton momentum stacking, working with non-gaussian distributions. Eq. (16) can be solved analytically for a number of situations where $\Phi(E,t) = \Phi_0 =$constant. A solution for antiproton stacking is discussed by van der Meer [10].

1.5 Good and Bad Mixing

Perhaps the most fundamental limitation in achieving effective cooling comes from limitations in the mixing. The fastest cooling is achieved if the Schottky signal is completely randomized between successive passes through the pickup. The randomization is complete in the limit that $M = 1$. However, the Schottky signal should not change between pickup and kicker (M should be large). The randomization between successive passes through the pickup is sometimes called the "good mixing" and the randomization between pickup and kicker is sometimes called the "bad mixing". A reasonable rule of thumb is that M=3 for an optimized betatron cooling system.

Antiproton sources CERN AA and FNAL Accumulator were engineered to have a specific value of mixing but using special magnetic lattice design techniques. The lattice parameter $\eta = 1/\gamma_t^2 - 1/\gamma^2$ specifies the spread in revolution periods. At a particular frequency in the cooling band the time spread in revolution frequencies leads to phase errors. As the frequency is increased, the phase error increases. Thus, attempts to upgrade the antiproton source cooling systems are constrained by the limitation imposed by the "bad mixing." At other accelerators it is a matter of luck if the lattice parameter η is appropriate for effective cooling at some frequency.

Possible solutions to the mixing problem are special lattices that have no mixing between pickup and kicker and yet have large mixing between kicker and pickup. Such a lattice was considered at least briefly as a possible design for the CERN Antiproton Collector, but I do not know of any accelerator built on this principle. Another possibility is to design a special pickup placed in a region of dispersion to cancel the transit time differences of the particles in the beam. The basic idea is that both the transit time difference and the position at the pickup are proportional to the momentum offset. If the signal at the pickup can be made to have a time-delay that is proportional to the horizontal position of the particle, it may be possible to have the time delay difference in the pickup exactly compensate the pickup to kicker transit time difference.

2. TECHNOLOGY

2.1 Bandwidth considerations

Stochastic cooling systems have been built with bandwidths ranging from 100 MHz to 4 GHz. The highest frequency systems operate in the 4-8 GHz band. Systems typically are chosen to operate in a band where the upper frequency is twice the lower frequency (known as an octave bandwidth). It becomes extremely difficult for a variety of technological reasons to maintain uniform gain amplitude and phase over bands that exceed one octave.

From a technological point of view it appears possible to extend present stochastic cooling technology to frequencies in the 10's of GHz. Aside from the good mixing/bad mixing problem mentioned above some of the technical difficulties in extending the frequency range of stochastic cooling systems are discussed below.

2.2 Pickups and Kickers

Pickups are devices that convert the mechanical beam energy into electrical energy. Kickers perform work on the beam with the applied electrical energy. The same structure can act as either a pickup or a kicker. The reciprocity theorem states that any device that converts the mechanical energy of the beam into electrical energy can be used to convert electrical energy into mechanical energy with the same coupling. A more precise statement of this theorem and other theoretical and practical pickup considerations can be found in the article by Lambertson [11]. The major practical differences between pickup and kicker design is that pickups may be cooled to cryogenic temperatures to reduce the thermal noise level while kickers may be required to dissipate significant rf power.

2.3 Stripline Pickup Response Model

Although other types of pickups are possible [12,13], the most common pickup is the strip-line type indicated in Figs. 5 and 6. These figures are also intended to suggest an electrical model of the beam current and stripline. The beam current is given by:

$$i(z,t) = i_b e^{j(kz-\omega t)} \tag{17}$$

where $v = \omega / k$ is the beam velocity. A current equal in magnitude but opposite in sign (the image current) flows on the walls of the beam chamber. A fraction f of the image current flows onto the strip line at one end and off at the other end. The pickup response can be modeled as a transmission line with the beam acting as a current source at the two ends. The solution of these equations shows that the output voltage is given by

$$V_p = f Z_p i_b \sin k\ell \tag{18}$$

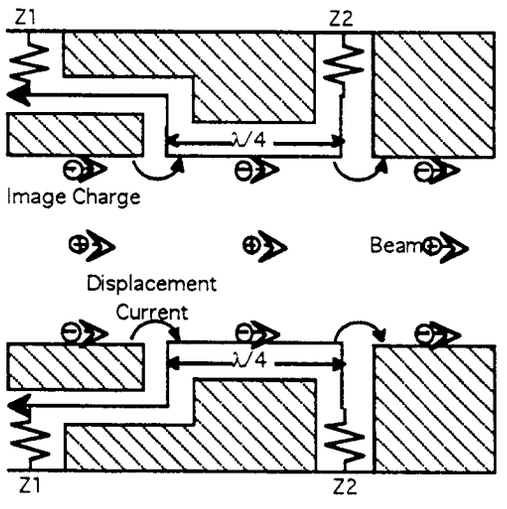

Fig. 5. Schematic representation of a quarter-wave strip-line electrode interacting with a high energy charged particle (side view).

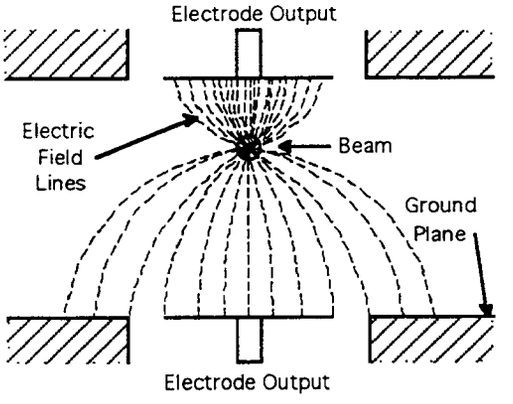

Fig. 6. The electric field lines from a single particle in the vicinity of a pickup electrode. More field lines terminate on the upper plate because the particle is closer to it than to the lower plate (cross-section).

The peak in the response occurs at $k\ell = \pi/2$. Thus the length is chosen to be a 1/4 wavelength long at the band center frequency. The fraction f of image current that is sensed by the pickup may be estimated by assuming that the pickup is infinitely long in z and solving the following wave equation for the scalar potential:

$$\left(\frac{1}{c}\right)^2 \frac{\partial^2 \Phi}{\partial t^2} - \nabla^2 \Phi = \rho(x,y) e^{j(kz-\omega t)} \tag{19}$$

where $\rho(x,y)$ is the beam density. Writing the potential as:

$$\Phi = \Theta(x,y) e^{j(kz-\omega t)}, \tag{20}$$

the equation for the potential becomes

$$\nabla_t^2 \Theta - \left[k^2 - \left(\frac{\omega}{c}\right)^2\right]\Theta = \rho(x,y) \tag{21}$$

For some simple geometries Eq. (21) can be solved analytically. If b is the transverse dimension of the beam chamber and $kb << 1$. the term in the [] is small and can be neglected. Under these conditions Eq. (21) reduces to the 2-dimensional Poisson's equation, and it can be solved by any of a large arsenal of techniques. The image currents are obtained by integrating the normal component of the electric field over the surface of the pickup.

2.4 Design Considerations

Schottky signal beam currents are often small compared to the noise current from thermal fluctuations. Arrays of 100 or more pickups are commonly used to obtain an adequate signal to noise ratio. The output power of two pickups is conveniently combined by connecting them to transmission lines of the same characteristic impedance as the pickup. The two transmission lines can be joined together and they will transmit all their power to a transmission line of half the impedance (assuming that the transmission lines are of the proper length so that the signals arrive in phase where the lines are joined). The transmission line with half the characteristic impedance can be transformed to a higher impedance with a series of stepped 1/4 wavelength transmission lines (or a single tapered line) and the combination process can be cascaded several times. This technique is easily implemented for bandwidths of an octave or less using stripline or microstrip circuit board techniques. In fact, the need for extensive combiner boards has recently led to the construction of the pickups themselves by using standard printed circuit board techniques [14,15]. These techniques have substantially reduced the cost of building pickup and kicker arrays.

Since the signal level tends to be low, it is important to maximize the signal seen by each individual pickup. Since the beam is an excellent current source, the signal is maximized by using a high impedance pickup. Typical pickup impedances are in the range 50-100 Ω. In principle, one can obtain larger impedances by leaving the electrode dimensions fixed and increasing the wall dimensions indefinitely. However, the impedance only increases logarithmically for large wall dimensions. Furthermore, unless the frequency is very low, the electrode would not act much like a transmission line since its height would greatly exceed its length.

The electrode sensitivity is also maximized by using wide electrodes to intercept a large fraction of the image currents (see Fig. 6). If the beam chamber is small or the energy is high, the electric field will be transverse and the currents at a given z will all be in phase. However, the energy from different parts of the electrode may be collected with slightly different transit times. The resulting phase errors are likely to be a limiting factor in the performance of large electrodes in the GHz region.

2.5 Wave Guide Modes

Another problem in the design of pickups is suggested by Eq. (21). The general solution of this equation is any solution of the inhomogeneous equation plus the general solution of the homogeneous equation. The solution of the homogeneous equation is the well-known infinite set of wave guide modes. The solution becomes mathematically unique if one applies boundary conditions at the two ends of cylinder. Physically, these wave guide modes arise from discontinuities in the beam chamber. The discontinuities are excited by the beam current and then radiate energy into the wave guide modes.

The presence of wave guide modes causes two problems. The wave guide modes propagate with velocities that depend on frequency and are different from the beam velocity. Thus, it tends to be difficult to use them for cooling over a significant bandwidth because of the large and unpredictable phase errors that are present with these modes. Even more annoying is the fact that these modes may show resonant behavior – especially if the pickup chamber is not well matched in cross-section to the rest of the beam chamber. In this case, there may be a peak in the amplitude of the gain function $G(\omega)$ and a corresponding rapid change in phase of 180° or more. This situation inevitably leads to system instability at gains lower than the optimum cooling gain.

There are two defenses against undesired microwave modes. The first comes naturally when many pickups are combined. The pickups are phased for the beam velocity. The microwave modes are rejected because their propagation velocities are different (typically slower). The second defense is to place microwave absorbers in the pickup. Possible absorbers include bulk and film resistors, lossy dielectrics, and lossy magnetic materials.

2.6 Limitations to Pickup Sensitivity at High Frequencies

The most fundamental limitation on building pickups that are sensitive to Schottky signals at very high frequency is the reduction in wall current intensity at high frequency. To illustrate the point, consider Eq. (21) for a beam in a circular pipe of radius b. The charge density $\rho(x, y)$ is assumed to be uniform for radii less than a It is straight-forward to show that the radial electric field at the beam chamber wall is:

$$E_\rho(b) = \frac{\rho_0 a I_1(k'a)}{\varepsilon_0 k' b I_0(k'b)} e^{j(kz-\omega t)} \tag{22}$$

where ρ_0 is the uniform charge density, I_0 and I_1 are modified Bessel's functions, $k' = k/\gamma$, $\gamma = \sqrt{1-(v/c)^2}$, and ε_0=8.85x10^{-12} F/m. Equation (22) reduces to a $1/\rho$ dependence for $k' \to 0$. However, the electric field falls exponentially with asymptotically large k'. This asymptotic condition is avoided by either $b \to 0$ or $\gamma \to \infty$. Thus the cutoff frequency is an important limitation for high frequencies, large apertures, and low energies. For example, $I_0(k'b) = 1.2$ at k=0.6 cm^{-1}, b=5 cm, and γ=3.7, which are approximately the parameters that correspond to the stochastic cooling systems at the CERN Antiproton Collector Ring.

2.7 Amplifier and Resistor Noise Minimization

In many cooling systems the signal to noise ratio is a significant concern. Maximizing the number and sensitivity of the pickups is crucial to obtain an adequate signal. Other techniques are available to reduce the thermal noise. The thermal noise comes from two sources which are comparable in magnitude: the back termination in the pickup and the preamplifier itself. The thermal noise voltage $V_n = 2\sqrt{k_B T R}$ from the resistance R at temperature T is easy to characterize. Normally R is chosen to be the characteristic impedance of the system (50 Ω). If one makes R smaller, then the system is mismatched and the noise power will be a function of frequency. The noise power in the frequency band of interest may be reduced by this technique. A more universally applicable technique is to lower the resistor temperature. Resistors are cooled to cryogenic temperatures extensively at both the CERN and FNAL antiproton sources. The physics of low noise amplifiers is considerably more complicated – and certainly beyond my understanding. Fortunately, there is a large industry working on making low noise microwave amplifiers, so the problem of being clever is reduced to the more tractable problem of being adequately funded.

2.8 Filters and Equalizers

Filters are used extensively in stochastic cooling systems. One type of filter is intended to have a shape that repeats (more or less) each Schottky band. These filters are used, for example, to suppress noise or shift the phase of the cooling signal. A simple filter that is used extensively at the FNAL antiproton source is shown in Fig. 7. The output transfer function is the sum of a prompt and a delayed signal: $T(\omega) = (1 - e^{j\omega\tau})/2$, where τ is the difference in length between the short and long legs.. This type of filter has transmission zeroes when $\omega\tau = 2\pi$ and is sometimes referred to as a "notch filter." Other types of notch filters are possible: the stack tail filters at the AA utilize shunt transmission lines. However, all these filters require one or more elements that delay the signal by a multiple of τ, where $1/\tau = 4f_0$, and f_0 is the average revolution frequency. In order for the filter to work properly the delay elements must be accurately described by a pure delay, i.e., the attenuation and the group delay must be independent of frequency. Thus, the problem of building a periodic filter is essentially that of building an ideal transmission line.

A number of transmission line techniques can be used. The simplest technique uses coaxial cable as the delay element. The diameter of the cable must be large to avoid large attenuation. The skin and dielectric losses are inversely proportional to the radius. The skin loss increases with the square root of the frequency. The dielectric loss is more complicated but tends to increase with frequency also. However, the size of the coaxial cable is limited because of the need to avoid the lowest wave guide mode (TM_{01}). While it is possible to calculate the cutoff frequency for the mode, the effect of non-propagating modes can be significant depending on the construction of the cable. Thus, the maximum usable frequency of a cable is best determined by measurements. The combination of increasing skin losses and being forced to smaller diameter cable can be very dramatic. For example, foam dielectric 7/8 inch heliax cable can be used up to a frequency of 5 GHz where it has a power transmission of 7% over a distance of 100 m, but a similar 3/8 inch cable has a power transmission of 0.001% at 11 GHz [16].

Fortunately other techniques are available. One technique used at the FNAL antiproton source involves the use of super-conducting delay lines to avoid the skin losses [17]. Another technique involves amplitude modulation of a laser coupled to an optical fiber followed by demodulation using a photo diode at the far end of the fiber [18,19]. Very long (10's of μsec) delays are possible with this technique. Bulk acoustic wave (BAW) devices have been more recently used to replace the super-conducting delay lines at FNAL to achieve lower operational costs [20]. Both the BAW and the optical modulation techniques suffer from large inefficiencies in converting energy from one form to another.

Equalizers are filters that have nearly constant gain over a single Schottky band. They are used, for example, to attenuate low frequencies to compensate for the high frequency attenuation that occurs in cables and other devices. Equalizers are extensively used commercially, and they may be conveniently constructed of strip-line or microstrip. A number of computer aided design programs can be used to accurately predict performance and to take most of the guess work out of equalizer design. Typically a stochastic cooling system will be built and the gain measured with an open-loop gain measurement (see below). Then an equalization filter will be constructed to flatten the gain and phase [21].

3. TECHNIQUES

3.1. Open-loop gain measurements

One of the most important diagnostic measurements made on a stochastic cooling system is a measurement of the open-loop gain. A typical experimental setup for this type of measurement is shown in Fig. 8. The cooling system is opened at some point and a sine-wave excitation is applied to the portion of the system leading to the kicker. The signal is transmitted via the beam, detected by the pickup, and brought back to the point of excitation. The propagation delay along the signal path ($T_1+T_4+T_3$) is equal to the difference in cooling system delay and beam transit time ($T_2-T_1-T_3$) plus one revolution period. Since the revolution period contributes a 360° phase shift, the open-loop gain measurement measures directly and precisely the transit time difference between the electronic signal and the beam motion.

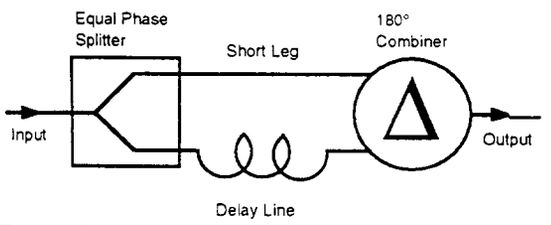

Fig. 7. Schematic of a simple filter of the type used in the FNAL antiproton source.

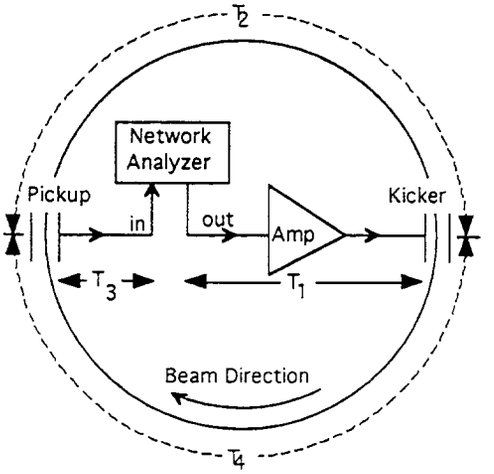

Fig. 8. Schematic of a typical setup for a cooling system open-loop gain measurement.

The open-loop gain measures the quantity $F(\omega)G(\omega)$ in Eq. (8). An open-loop gain measurement is shown in Fig. 9. The structure of the curves is dominated by the beam response since $G(\omega)$ is nearly constant

over the narrow frequency range in this measurement. There are four peaks in the amplitude corresponding to the four betatron sidebands inside the frequency interval that was measured. Each peak is accompanied by a rapid 180° change in phase. The phase at the peaks of the amplitude response is 180° when $G(\omega)$ phased for cooling. The data in Fig. 9 indicate a phase at the peaks of the betatron sidebands of around 90°, so the phase of this system is not properly adjusted to achieve cooling.

In order to get more information about $G(\omega)$, it is useful to measure many Schottky bands. Normally, this measurement is accomplished by measuring a few points per Schottky band and measuring 100 or so Schottky bands throughout the frequency range of the cooling system. Such a measurement is shown in Fig. 10. The phases and amplitudes of the upper and lower sidebands are shown separately. It can be seen that the phases of these bands are slightly different. This difference occurs because the phase advance between pickup and kicker is not exactly an odd multiple of 90°. The amplitude curves give a good estimate of the phase and relative amplitude of $G(\omega)$. Data like those in Fig. 10 are useful in designing equalizers that can be used to optimize the cooling rate.

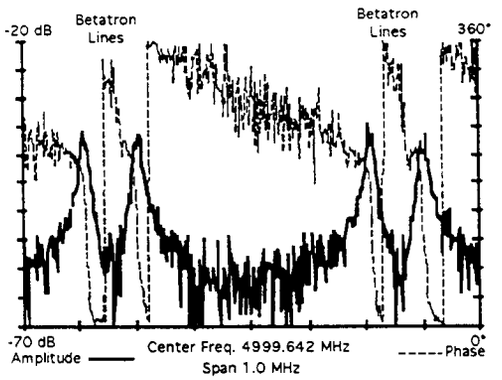

Fig. 9. Open-loop gain of a 4 to 8 GHz betatron cooling system at the FNAL Accumulator ring. The revolution frequency is 629 kHz. The four peaks correspond to the four betatron peaks that lie in the 1-MHz interval. The phase changes rapidly by 180° in the vicinity of the amplitude peaks.

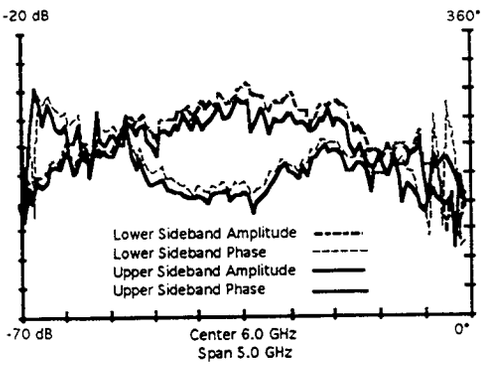

Fig. 10 Open-loop measurement of the same system shown in Fig 9. One point is measured on every 40th betatron line. The average phase is about 180°, as required for cooling.

3.2 Schottky signal suppression

Since the cooling system works using the Schottky signal it is useful, if not essential, that one be able to monitor the Schottky signal at some point in the stochastic cooling system. With these observations one can measure the signal to noise ratio and the mixing factor.

The phenomena of Schottky signal suppression (discussed above) is an especially useful diagnostic. A signal suppression amplitude of 6 dB indicates that the system is operating at the optimum gain. The measurement is made by observing the difference between the open-loop and closed-loop Schottky signal. A measurement showing about 6 dB of signal suppression is shown in Fig. 11. The closed-loop response in Fig. 11 is lower than the open-loop noise floor. This phenomenon occurs because the beam response acts to cancel a portion of the electronic noise. Signal suppression measurements are particularly useful to check the operation of cooling systems where the cooling rate is very slow and difficult to measure directly.

3.3. Cooling rate

There are a large number of ways of directly measuring the cooling rate. One commonly used method is to observe the rate of change of the Schottky signal. In addition to providing the cooling signal, Schottky signals can be used to measure the momentum spread, tune, transverse beam size, and chromaticity of the beam[22]. An example of the measurement of the horizontal betatron amplitude cooling rate is shown in Fig. 13. The horizontal beam emittance is changed by approximately two orders of magnitude while the beam current and vertical beam emittance are nearly constant. One can avoid the signal suppression effect by observing a Schottky band that is outside the bandwidth of the cooling system.

It is also possible to measure the transverse size of the beam using a variety of other techniques including using flying wires or extracting the beam and measuring the beam shape with segmented ion or secondary emission chambers. Measurements of the profile of the circulating beam were made in the FNAL Debuncher ring by imaging the residual gas that is ionized by the beam. The profiles thus obtained are shown in Fig. 13.

One can determine the optimum system delay for the FNAL Debuncher transverse cooling systems to a few psec by minimizing the width of the beam profile on a secondary emission chamber.

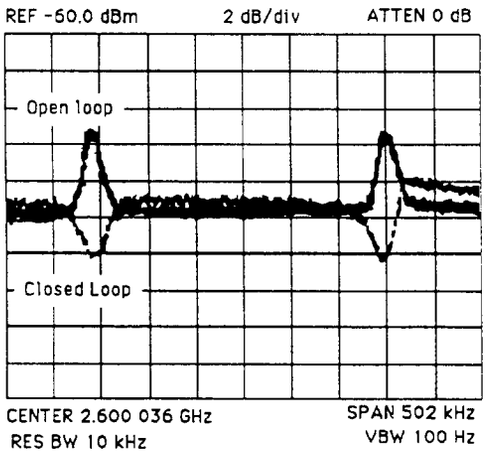

Fig. 11. Spectrum analyzer traces showing the difference between the open-loop and closed-loop signals coming from the pickup.

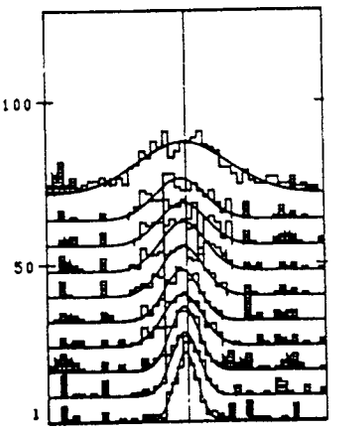

Fig. 12. Beam profiles in the FNAL Debuncher ring. The profiles were obtained at 0.22-sec intervals. The earliest time is at the top of the plot; the latest, at the bottom.

3.4. Instabilities

The presence of the denominator in the cooling equations suggest the possibility that $1-F(\omega)G(\omega)$ might vanish, and the system could become unstable. A stability diagram of a betatron cooling system operating near the optimum gain with a pickup to kicker phase advance of 70° is shown in Fig. 14. The system is unstable if the stability curve encircles the value of +1 (on the real axis). The two loops on the plot correspond to the two Schottky sidebands. At the frequencies that correspond to the peaks of the betatron sidebands the function is approximately -1. Between the sidebands the gain is less than 0.2. Raising the gain of the system a factor of 10 beyond the optimum gain will cause an instability. Of course, any one Schottky band can cause an instability. Variations in gain and phase from one Schottky band to another can erode the margin between the optimum gain and the unstable gain.

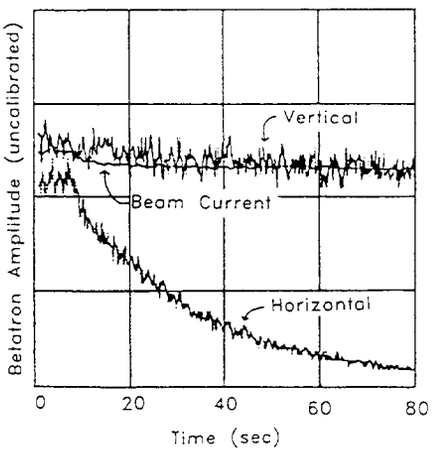

Fig. 13 A spectrum analyzer is tuned to receive the power from a single Schottky band.

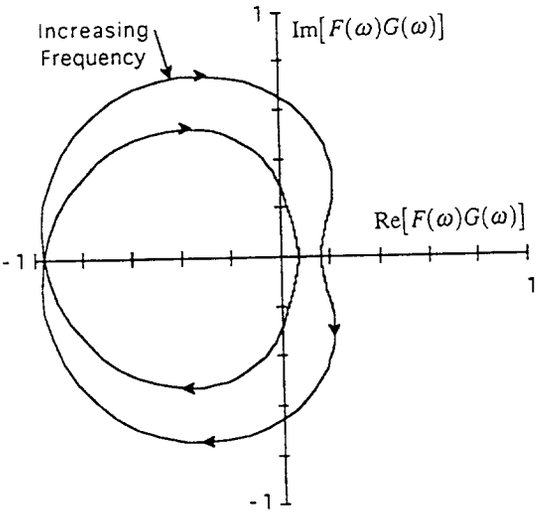

Fig. 14. A stability plot of a betatron cooling system. The plot is drawn for a betatron cooling system at the FNAL accumulator for the frequency range $(n-0.5)f_0$ to $(n+0.5)f_0$ .with n=5000 and f_0=629 kHz.

CONCLUSION

The theory, technology, and techniques of stochastic cooling have been reviewed. Where possible I have tried to indicate the limitations of our current techniques and technology.

REFERENCES

[1] D. Mohl,, G. Petrucci, L. Thorndahl, and S. van der Meer, Phys. Rep. **58**, 73 (1980).

[2] J. Bisognano and C. Leeman, **AIP Conf. Proc. 87**, Physics of Particle Accelerators, Fermilab Summer School 1981, Ed. R.A. Carrigan, et al., American Institue of Physics, New York, 1982, p 583.

[3] S. Chattopadhyay, IEEE Trans. Nucl. Sci. **30**, 2649 (1983).

[4] J.J. Bisognano, **AIP Conf. Proc. 127**, Physics of Particle Accelerators, BNL/SUNY Summer School 1983, Ed. M. Month et al., American Institue of Physics, New York, 1985, p 443.

[5] N.S. Dikanskii and D.V. Pestrikov, Sov. Phys. Tech. Phys. **29**, 271 (1984).

[6] D. Mohl, Proceedings, Advanced Accelerator Physics, Oxford, 1985, Vol 2, p.453.

[7] Marriner JP, McGinnis D, **AIP Conf. Proc. 249**, Physics of Particle Accelerators, Eds. M Month and M Dienes, American Institute of Physics, New York, 1992, p 693.

[8] H. Nyquist, Bell S. Tech. J., **11**, 126 (1932).

[9] G. Carron G and L. Thorndahl, CERN Internal Report, CERN-ISR-RF/78-12 (1978)

[10] S. van der Meer , CERN Internal Report, CERN/PS/AA/78-22 (1978).

[11] Lambertson, G., **AIP Conf. Proc. 153**, Physics of Particle Accelerators, SLAC Summer School 1985, Fermilab Summer School 1984, Vol. II, Ed. M. Month and M. Dienes, American Institue of Physics, New York, 1987, p. 1414.

[12] L. Faltin, Nucl. Instr. Meth., **A241** , 416 (1985).

[13] G. Di Massa, Nuovo Cim., **100A**, 249 (1988).

[14] F. Caspers, IEEE Trans. on Nucl. Sci., **34**, 1866 (1987).

[15] J. Petter et al., Proceedings of the IEEE Particle Accelerator Conf. (Chicago), Vol. 1, 636 (1989).

[16] Andrew Corporation, Catalog 35, Orland Park, IL, USA.

[17] R.J. Pasquinelli, Proceedings of the 12th International Conference on High-Energy Accelerators (Fermilab), p 584 (1983).

[18] J.D. Simpson and R. Konecny, IEEE Trans. Nucl. Sci. xxx, 2129 (1985).

[19] R. Pasquinelli, Proceedings of the 1989 IEEE Particle accelerator Converence (Chicago), Vol 1, p 694.

[20] R. Pasquinelli, Conf. Rec. of the 1991 IEEE Particle Accelerator Conf. (San Francisco), Vol. 3, p. 1395 (1991).

[21] D. McGinnis, Conf. Rec. of the 1991 IEEE Particle Accelerator Conf. (San Francisco) Vol 3, p. 1392.

[22] S. van der Meer S, CERN Internal Report, CERN/PS/88-60 (AR), (1988).

ELECTRON COOLING: STATUS AND PERSPECTIVES

I.N.Meshkov

Centre of Applied Physics and Technology
of Budker Institute of Nuclear Physics
Moscovskaya Str., 398055, Lipetsk, Russia

ABSTRACT

The electron cooling method became now conventional instrument of accelerator technique. Storage rings with electron cooling – the so-called coolers, permit generate very dense and high intensive beams of charged heavy particles – protons, antiprotons, ions. 9 such coolers – one for antiprotons and 8 for ions are operating effectively now in laboratories for high energy and nuclear physics. The review of the present understanding and of related problems is given in this report.

1. INTRODUCTION

The electron cooling method went through a long way of development, from the first Budker's idea [1], based on the model of two component electron – ion plasma, to very rich physics of a magnetized electron beam with "the flattened distribution" of electron velocities. It is a method of introduction of an effective "friction" in a particle beam that makes it possible to reduce the beam phase space volume (emittance) and, correspondingly, to compress the beam size and to decrease its particle momentum (energy) spread. As a result, an intensive, dense and "cold" particle beam can be generated. To produce such a friction, an "absorber" has to be brought into the beam.

In principle, one can use the mechanism of ionization losses in any material transparent for fast particles. Unfortunately, nature does not present us with such a gift, and ionization ("muon") cooling does not work for barions because of a short life time of the beam, limited by particle losses in strong interaction with absorber nucleons.

Budker's idea had two remarkable points:

1. to use "free" electrons, i.e. electron beam as an absorber;

2. to equalize average velocities of heavy particles and electrons, what gives the maximal value of the cross section of electromagnetic interaction.

Later these points were supplemented with a fortunate proposal to use homogeneous (solenoidal) magnetic field to form and transport the cooling electron beam [2], what gives additional advantages in cooling efficiency. It was discovered and understood later – in experimental studies of electron cooling [3].

The electron cooling method was successfully tested and developed in experimental studies done in the 1970-th at Budker Institute of Nuclear Physics [3-5], CERN [6] and Fermilab [7]. It is used now in 9 coolers (see [8]).

The development of the method is progressing in several directions that have a common goal of improving electron cooling efficiency and expanding the parameter area where the method can be applied. They are:

– generation of electron beams with the maximally achievable intensity and the lowest electron temperature possible: the guns with adiabatic optics, adiabatic acceleration, photocathode guns;

- elaboration of electron cooling systems with the neutralized space charge of an electron beam;

- extension of electron energy to the level in tens MeV;

- development of high effective recuperators of electron beam energy.

Today one can point out three main directions of the method application:

- storing, forming and keeping circulating antiproton beams in high energy physics, during the interaction with an internal target or slow extraction;

- the same for ions in nuclear atomic physics;

- storing and preliminary forming of heavy particle beams for following acceleration in a cascade of machines up to TeV-th energies (SSC and LHC projects).

The method can be used also for positron cooling, which permits to generate intensive flow of antihydrogen atoms[9]. The physics of cold intense beam of heavy particles – "beam crystallization"[10,11] – is also very interesting subject of the research. Numerical examples are given through at the report for some parameters, typical for middle energy coolers.

Unfortunately, the limited size of the report does not admit of any full review of the problem at all. Thereupon, one had to choose the mostly interesting, in author's opinion, points in the present status of electron cooling – some for a brief discussion, others – only to formulate. One can recommend a few review reports: [8,10-17].

2. THE PHYSICS OF ELECTRON COOLING

2.1. The uniform Maxwellian plasma relaxation

Two component plasma with a density n_e, consisting of heavy particles (mass M, the charge Ze) and electrons (m, e) , each with uniform Maxwellian distribution and different initial temperatures T_p, T_e. Its relaxation process obeys Landau equation [18], which gives the instantaneous value of relaxation (cooling) time, or decrement

$$\tau_{plasma} = \frac{3Mm}{8\sqrt{2\pi}qL_c} \cdot \left(\frac{T_p}{M} + \frac{T_e}{m}\right)^{3/2} = \frac{3Mm}{8\sqrt{2\pi}qL_c} \times \begin{cases} \Delta_p^3, & \Delta_p \gg \Delta_e \ , \\ \Delta_e^3, & \Delta_p \ll \Delta_e \ . \end{cases} \tag{1}$$

$$q = n_e Z^2 e^4, \ T_p = M\Delta_p^2, \ T_e = m\Delta_e^2 \ ,$$

and the equilibrium condition:

$$T_p = T_e, \ \Delta_p = \sqrt{m/M} \cdot \Delta_e \ , \tag{2}$$

L_c is Coulomb logarithm. The decrement does depend on particle velocity for high magnitude of the last one. This relaxation process is "a competition" of friction force and diffusion, which appear, when a heavy particle penetrates an electron cloud.

2.2. The flattened distribution

The peculiarity of an electron beam is (see Sec. 3) a sharply nonuniform velocity distribution, called "flattened" [3,10,17]:

$$f_{Flat}(\bar{v}) \ d^3v = \frac{m^{3/2}}{(2\pi)^{3/2}T_\perp\sqrt{T_\parallel}} \cdot exp\left\{-\frac{mv_\perp^2}{2T_\perp} - \frac{mv_\parallel^2}{2T_\parallel}\right\} \cdot 2\pi v_\perp \ dv_\perp dv_\parallel \ , \tag{3}$$

$$v_\perp^2 = v_x^2 + v_z^2, \ m < v_\perp^2 > \equiv m\Delta_\perp^2 = T_\perp \gg T_\parallel \ .$$

The flattened distribution has three different regions of particle velocities V:

$$\begin{array}{lll} \text{high} & (\text{"H"}) & V > \Delta_\perp \ . \\ \text{low} & (\text{"L"}) & \Delta_\| < V < \Delta_\perp \ . \\ \text{superlow} & (\text{"S"}) & V < \Delta_\| \ . \end{array} \tag{4}$$

The friction force and the diffusion power for the particle in the electron beam with the flattened distribution and in the absence of any focusing magnetic field somewhat differs from these for free electrons (see [14,17,19]).

2.3. The magnetized electron beam

In a longitudinal magnetic field B electron trajectories are spirals with a radius (the transversal Larmor radius) and a "step"

$$\rho_\perp = mv_\perp c/eB, \ \lambda_\| = 2\pi m v_\| c/eB \ll \rho_\perp \ , \tag{5}$$

and the peculiarity of the distribution plays a crucial role. The magnetization defines also electron beam temperature formation, decreases the beam angular spread and limits its space charge influence (see Sec. 3).

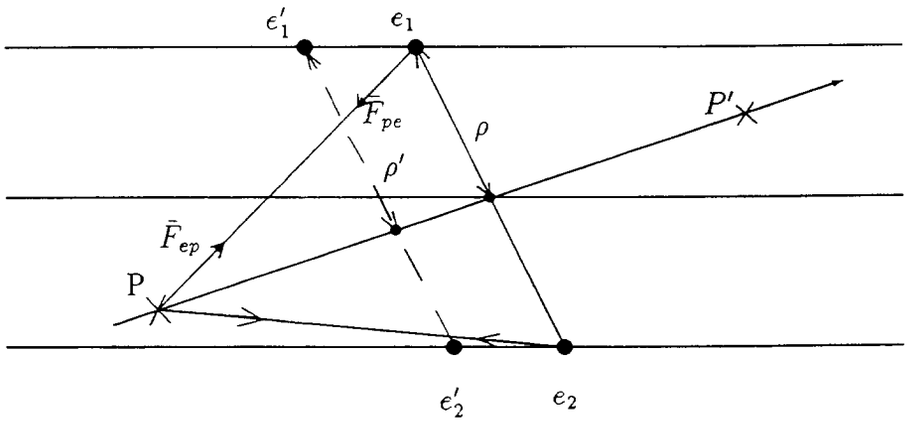

Fig.1. The schematics of collision of the particle with a magnetized electron: PP' – the particle trajectory, $e_1e_1'(\Delta\rho > 0)$ and $e_2e_2'(\Delta\rho < 0)$ – electron trajectories.

In the case of infinitely strong magnetization ($\rho_\perp \to 0$) the electron-particle interaction looks like the attraction ($Z > 0$) of an amber bead strung on a knitting needle, by a moving charged object (Fig. 1). When "the bead" can not move absolutely, the particle scattering is elastic, without any energy loss and, consequently, no friction force appears in this case. A free displacement of "the bead" along "the needle" leads to some energy transfer from the particle to the bead, so a friction force appears. In terms of a force action and a momentum transfer it means that the impact parameter alters during the collision – it increases or decreases depending on the mutual disposition of the electron and the particle (see Fig.1). Therefore, the attraction force also alters during collision, and it is weaker or stronger after the electron displacement. The total result for the whole

electron ensemble is that the particle experiences the action of a decelerating (friction!) force. The calculations give (see [14,20,19]:

$$\mathbf{F}_\perp = -\frac{2\pi q L_c}{mV^3}\cdot\frac{V_\perp^2 - 2V_{||}^2}{V^2}\cdot\mathbf{V}_\perp\ , \tag{6}$$

$$\mathbf{F}_{||} = -\frac{2\pi q L_c}{mV^3}\cdot\frac{3V_\perp^2}{V^2}\cdot\mathbf{V}_{||}\ ,\quad L_c = ln\frac{\rho_{max}}{\rho_{min}}\ ,$$

$\mathbf{V}$ - the vector of the particle velocity.

One should point out important differences between the force (6) and that one for free electrons: $\mathbf{F}_{||} \to 0$ when $V_\perp \to 0$ and $\mathbf{F}_\perp$ changes its sign and becomes positive, when $V_\perp < 2V_{||}$, that is cooling turns in heating.

The Coulomb logarithm L_c deserves a special discussion. So far as the electron transverse motion is "frozen", the response of the electron cloud to electric field of the particle occurs only through a longitudinal displacement of electrons, therefore Debay shielding radius is equal to

$$R_D = \frac{U_M}{\omega_{pe}} = \begin{cases} V/\omega_{pe} \sim 0.05cm, & V > \Delta_{||}, \\ \Delta_{||}/\omega_{pe} \sim 5\cdot 10^{-4}cm, & V < \Delta_{||}, \end{cases} \tag{7}$$

$$U_M = <|\ \mathbf{V} - \mathbf{\Delta}_{||}\ |>\ ,$$

ω_{pe} - electron plasma frequency. On the other hand, Debay shielding needs some amount of electrons, therefore, it can not be less than

$$R_D > R_e \equiv (k/n_e)^{1/3},\ k \gg Z\ . \tag{8}$$

This condition can be violated for the superlow particle velocity and Debay radius should be taken equal to R_e . It is, certainly, a very rough estimation, and a more accurate analysis of collective effects at superlow velocities is an open question yet.

Thus, the maximal impact parameter for a magnetized electron beam is the subject of a complicated choice:

$$\rho_{max} = min\begin{cases} a & \sim 1.5cm, \\ max\{R_D, R_e\} & \sim 0.05 - 0.1cm, \\ U_M\cdot\tau & \sim 0.5 - 6\cdot 10^{-2}cm. \end{cases} \tag{9}$$

Here a is beam radius, τ - time of flight of the particle trough the cooling system.

A finite magnetic field brings into existence three regions of impact parameter magnitudes (Fig.2), which are defined by the beam parameters - electron Larmor radius (5) and longitudinal velocity spread $\Delta_{||}$ and the particle velocity.

Small impact parameters - the particle interacts with an electron without any influence of magnetic field, if the collision time is less than the period of Larmor (cyclotron) revolution of an electron - "the fast collisions" ("F"):

$$\tau_{col} \sim \rho/U_M \le \omega_B^{-1} \equiv mc/eB\ . \tag{10}$$

It defines the scale of small impact parameters:

$$\rho_{min} \le \rho \le \rho_F,$$

$$\rho_{min} = \frac{Ze^2}{mU^2} = \frac{Ze^2}{m} \cdot \begin{cases} V^{-2}, & V > \Delta_{||}, \\ \Delta_{\perp}^{-2}, & V < \Delta_{||}, \end{cases} \tag{11}$$

$$U = <| \mathbf{V} - \mathbf{\Delta}_{\perp} |>, \quad \rho_F = U_M/\omega_B.$$

The friction force and diffusion are described here with formulae for flattened distribution [14] with $\rho_{max} = \rho_F$.

Intermediate impact parameters $\rho_F \leq \rho \leq < \rho_{\perp} >$. In such collisions the particle and the electron travel together during a few periods of a cyclotron revolution while the electron rotates "around" the particle, colliding with it N times:

$$1 \leq N \leq \frac{\tau_{col}}{2\pi} \cdot \omega_B \leq \frac{\Delta_{\perp}}{U_M} \sim \begin{cases} \Delta_{\perp}/V, & V > \Delta_{||}, \\ \Delta_{\perp}/\Delta_{||}, & V < \Delta_{||}. \end{cases} \tag{12}$$

The friction force and diffusion in these "adiabatic collisions" ("A") are amplified N times in comparison with a free electron beam [10,14,19].

At **large impact parameters** $\rho_{\perp} \leq \rho \leq \rho_{max}$ (see (5), (9)) the electron looks like a small "Larmor circle" and the collision has the same character as for strongly magnetized electrons (6).

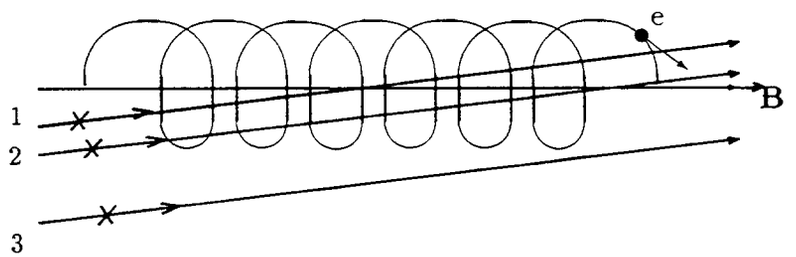

Fig.2. Three kinds of particle-electron collisions: fast (1), adiabatic (2) and magnetized (3).

It can be distinctly seen from the discussion above, that the choice of the impact parameter magnitude depends primarily on particle velocity (for the given parameters of an electron beam). Hence the three regions of particle velocities (4) exist as before. At a **high velocity** the friction force has only two parts - the fast one and the magnetized one: no adiabatic collisions exist here, because $N < 1$, if $V > \Delta_{\perp}$.

Low and superlow velocities of the particle admit the existence of all three regions of impact parameters, and the friction force contains here three parts - fast, adiabatic and magnetized ones. However, the magnetized collisions **at superlow velocity** demand some additional analysis, because $\Delta_{||}$ can not be neglected as before. The simplified estimation of a momentum, transferred to the particle in a collision with an electron, gives [19]

$$\mathbf{F} \sim -\mathbf{V} \cdot \frac{2\pi q}{\Delta_{||}^3} \cdot L_{MS}, \; L_{MS} = ln \frac{\rho_{max}}{< \rho_{\perp} >}, \tag{13}$$

which only slightly differs from the result of the exact calculation [14].

Thus, the friction force in the magnetized electron beam is

$$\mathbf{F}_\perp = -\frac{2\pi q}{m}\cdot\mathbf{V}_\perp\cdot\begin{cases}\frac{1}{V^3}\left(2L_{FH}+\frac{V_\perp^2-2V_\parallel^2}{V^2}\cdot L_{MH}\right), & "H";\\ \frac{L_{FL}}{\Delta_\perp^3}+\frac{L_{AL}}{\Delta_\perp^2 V}+\frac{V_\perp^2-2V_\parallel^2}{V^2}\cdot\frac{L_{ML}}{V^3}, & "L";\\ \frac{L_{FS}}{\Delta_\perp^3}+\frac{L_{AS}}{\Delta_\perp^2\Delta_\parallel}+\frac{L_{MS}}{\Delta_\parallel^3}, & "S";\end{cases} \tag{14}$$

$$\mathbf{F}_\parallel = -\frac{2\pi q}{m}\cdot\mathbf{V}_\parallel\cdot\begin{cases}\frac{1}{V^3}\left(2L_{FH}+3L_{MH}\cdot\frac{V_\perp^2}{V^2}\right), & "H";\\ \frac{2L_{FL}}{\Delta_\perp^2 V_\parallel}+\frac{2L_{AL}}{\Delta_\perp V V_\parallel}+\frac{V_\perp^2}{V^2}\cdot\frac{3L_{ML}}{V^3}, & "L";\\ \sqrt{\frac{2}{\pi}}\frac{L_{FS}}{\Delta_\perp^2\Delta_\parallel}+\frac{2L_{AS}}{\Delta_\perp V V_\parallel}+\frac{3L_{MS}}{\Delta_\parallel^3}, & "S".\end{cases}$$

The Coulomb logarithms are gathered below by groups for each velocity region:

High particle velocity

$$L_{MH} = ln[(\rho_{max})_H / <\rho_\perp>] \sim ln[(V\omega_B)/\omega_{pe}\Delta_\perp] \sim 3;$$
$$L_{FH} = ln[\rho_{FH}/(\rho_{min})_H] \sim ln[mV^3/\omega_B Ze^2] \sim 10 - lnZ.$$

Low particle velocity

$$L_{ML} = ln[(\rho_{max})_L / <\rho_\perp>] = ln\frac{min\left\{V/\omega_{pe}, (k\!\!\!/_e)^{+1/3}\right\}}{<\rho_\perp>} \sim 3 \div 1;$$

$$L_{AL} = ln[<\rho_\perp>/\rho_{FL}] = ln[\Delta_\perp/(\Delta_\perp \to \Delta_\parallel)] \sim 0 \to 4;$$

$$L_{FL} = ln[\rho_{FL}/(\rho_{min})_L] = ln[mV^3/Ze^2\omega_B] \sim 5 - lnZ$$

Superlow particle velocity

$$L_{MS} = ln[(\rho_{max})_S / <\rho_\perp>] = ln[(k\!\!\!/_e)^{1/3} / <\rho_\perp>] \sim 2;$$

$$L_{AS} = ln[<\rho_\perp>/\rho_{FS}] = ln[\Delta_\perp/\Delta_\parallel] \sim 4;$$
$$L_{FS} = ln[\rho_{FS}/(\rho_{min})_S] = ln[m\Delta_\parallel\Delta_\perp^2/Ze^2\omega_B] \sim 5 - lnZ.$$

This Coulomb logarithm "Zoo" shows that the friction force is nonlinear very significantly, because the logarithms themselves alter during the cooling process.

The Formulae (14) lead to one important conclusion: the friction force for a magnetized electron beam differs essentially from that for a nonmagnetized one: when a particle velocity diminishes under the cooling action, the force grows up as V^2, and this growth does not stop at $V \sim \Delta_\perp$, as for a nonmagnetized beam, but continues in the region of

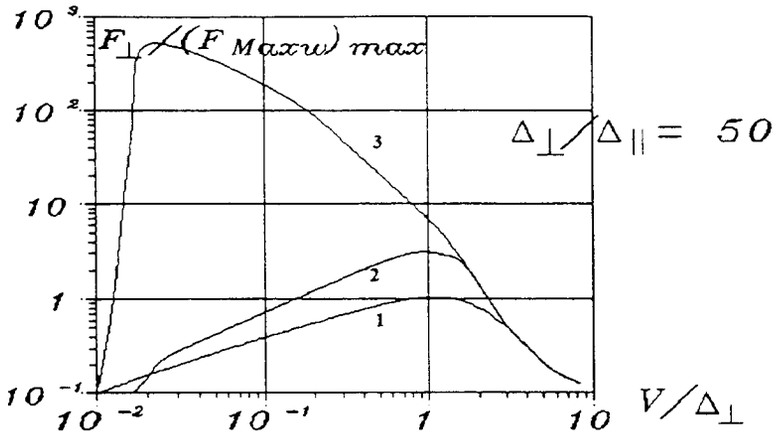

Fig.3. The dependence of the transversal friction force on particle velocity: 1 - the uniform Maxwellian plasma, 2 - the flatened distribution at $B = 0$, 3 - the magnetized electron beam.

a low velocity due to "adiabatic" and "magnetized" terms (Fig.3). The force reaches its maximum near $V \sim \Delta_{||}$ and then drops linearly with V at $V < \Delta_{||}$.

One can formulate at last the criterion of magnetization of an electron beam:

$$< \rho_\perp > < (\rho_{max})_S \sim 3n_e^{-1/3} , \tag{15}$$

or

$$B > \frac{m\Delta_\perp c}{3en_e^{-1/3}}.$$

The diffusion is important only in the region of a superlow velocity, because it defines the equilibrium state namely here. The estimations similar to (13), give for its power

$$Q \equiv \frac{M}{2} \cdot \frac{d < V^2 >}{dt} \sim \frac{4\pi q}{M\Delta_{||}} \cdot L_{MS} . \tag{16}$$

It differs insignificantly with results of exact calculations [14]. The equalizing of the power of the friction force (13) and diffusion (16) gives equilibrium state in a magnetized electron beam:

$$\sqrt{\mathbf{V}^2_{equi}} \approx \sqrt{\frac{m}{M}} \cdot \Delta_{||} . \tag{17}$$

The law of particle velocity behavior one can find with (14), neglecting with angular dependence of the friction force and the term with L_{AL}:

$$\sqrt{\mathbf{V}^2_\perp(t)} = \begin{cases} V^o_\perp (1 - t/\tau_\perp)^{1/3}, & "H"; \\ \left[\left((V^o_\perp)^3 + \alpha\Delta^3_\perp\right) e^{-t/\tau_\perp} - \alpha\Delta^3_\perp\right]^{1/3}, & "L"; \\ \left[(\mathbf{V}^2_\perp)_{equi} + \left((V^o_\perp)^2 - (\mathbf{V}^2_\perp)_{equi}\right) \cdot e^{-t/\tau_\perp}\right]^{1/2}, & "S"; \end{cases} \tag{18}$$

$$\alpha = L_{ML}/L_{FL};$$

where characteristic times $\tau_\perp$ are

$$\tau_\perp \approx \frac{mM}{2\pi q} \times \begin{cases} \left(V_\perp^o\right)^3 /3\left(2L_{FH} + L_{MH}\right), & "H"; \\ \Delta_\perp^3/3L_{FL}, & "L"; \\ \Delta_{||}^3/L_{MS}, & "S". \end{cases} \tag{19}$$

These $\tau_\perp$ can be treated as cooling time only in "H" and "S" cases. For "L" region it is some characteristic parameter, and time duration necessary to cool the particle from $V_\perp^o$ to $\Delta_{||}$ is equal to

$$\left(\tau_{cool}\right)_L = \left(\tau_\perp\right)_L \cdot ln\frac{\left(V_\perp^o\right)^3 + \alpha\Delta_\perp^3}{\Delta_{||}^3 + \alpha\Delta_\perp^3} \sim \frac{mM}{6\pi q L_{ML}} \cdot \left(V_\perp^o\right)^3, \quad "L" \ . \tag{20}$$

This result demonstrates the effect of "The fast electron cooling", when τ_{cool} depends on particle velocity even at $V < \Delta_\perp$.

For a longitudinal component the law of $V_{||}(t)$ is the same as (18) for the "H" and "S" regions, but with different characteristic time (see (23)). For the "L" region the law is very intricate:

$$t(V_{||}) = \tau_0 \left\{ \frac{V_{||}^o - V_{||}}{\Delta_\perp} - \kappa \cdot Arctg\left(\frac{V_{||}^o - V_{||}}{1 + V_{||}^o V_{||}/(\kappa\Delta_\perp)^2} \cdot \frac{1}{\kappa\Delta_\perp} \right) \right\} , \tag{21}$$

$$\tau_0 = mM\Delta_\perp^3/4\pi q L_{FL}, \quad \kappa = \sqrt{3L_{ML}/2L_{FL}} \sim 1.$$

For typical parameters $\kappa \sim 1$, therefore the cooling time for a particle with a low initial velocity is about

$$\left(\tau_{||}\right)_L \sim \frac{\tau_0}{3\kappa^2} \left(\frac{V_{||}^o}{\Delta_\perp} \right)^3 . \tag{22}$$

Then

$$\tau_{||} \approx \frac{mM}{2\pi q} \times \begin{cases} \left(V_{||}^o\right)^3 /3\left(2L_{FH} + 2L_{MH}\right), & "H"; \\ \left(V_{||}^o\right)^3 /9L_{ML}, & "L"; \\ \Delta_{||}^3/L_{MS}, & "S". \end{cases} \tag{23}$$

The comparison of (20) and (23) shows, that for low velocities the longitudinal cooling time is about 3 times shorter than the transversal one.

The question of practical interest is the cooling time for a particle with high initial velocity. As could be seen from (19), (23), it slightly differs from the case of a non-magnetized electron beam (1). Besides, what is much more significant: the influence of magnetization on cooling time in the region of low velocities is also very modest. It's not very surprising, because, notwithstanding a very fast increase of friction force (and instant increment!) with V decreasing, the full cooling time is defined mostly by large magnitudes of the initial particle velocity $V \sim \Delta_\perp$.

Nevertheless, instant value of friction force plays crucial role when equilibrium state is concerned. It is very important, particularly, in consideration of particle beam interaction with internal target.

3. THE FINE EFFECTS IN ELECTRON COOLING

3.1. The additional friction force for a negatively charged particle

In a collision with the low impact parameters a negatively charged particle reflects magnetized electrons, while a positively charged one attracts them. The addition to the friction force for a negatively charged ion is equal to [19]

$$\Delta F_{||} = -n_e V \cdot 2mV \cdot \pi \rho_{min}^2 \approx -\frac{2\pi q}{m} \times \begin{cases} 1/V^2\,, & V > \Delta_{||}; \\ V^2/\Delta_{||}^4\,, & V < \Delta_{||}; \end{cases} \tag{24}$$

and the maximal friction force is nearly 2 times more powerful for negatively charged particle (see [19], Fig.7).

3.2. The additional diffusion for a positively charged particle[19]

The junction of electron and particle beams in a cooling device is a very fast process in the particle rest frame: an electron displaces in the junction section for one period of Larmor revolution in the direction transversal to the particle trajectory by the distance, which is much larger of $< \rho_\perp >$. Hence, the particle and the electron meet together "instantly". Then, the positively charged particle attracts the electron, which travels close enough to the particle, oscillating along the magnetic field and slowly rotating around the particle trajectory due to the drift in a transversal electric field of the particle and a longitudinal magnetic field of the cooler. The particle-electron interaction gives the additional diffusion power [19]:

$$Q \approx \frac{e^2}{M\tau_0} \cdot \left(\frac{Bq\tau^2}{c}\right)^{2/3} . \tag{25}$$

τ_0 – period of particle revolution in the storage ring, τ – time of flight through cooling section. As result,

$$\sqrt{(\mathbf{V}^2)_{equi}} \approx \sqrt{\frac{m}{M}} \cdot (1+\delta)\,, \delta = \frac{1}{\sqrt{2\pi\tau_0 \Delta_{||} L_{MS}}} \cdot \left(\frac{r_e c^2 \tau^4 \omega_B^2}{Z^2}\right)^{1/6} \sim 0.2 \cdot Z^{-1/3} . \tag{26}$$

3.3. The Coulomb logarithm and multi-charged ions

It became "a tradition" in electron cooling numerical estimations to put the Coulomb logarithm in any formula of order 10-15. However, a more attentive analysis shows that one should be careful with such estimations. The influence of the Coulomb logarithm is the only possible way of explanation of the results, obtained recently in experiments at TSR [21,22]. It was found, that longitudinal friction force and its decrement decrease with ion charge Z. These results do not contradict the dependence of the Coulomb logarithm L_{FL} on ion charge in formulae (14). Our analysis shows, that TSR experiment results stricly follow the law (Fig.4)

$$\lambda_{||} = \lambda_1 - \lambda_2 \cdot lnZ, \quad \lambda_{||} = \left(\tau^{-1}\right) \cdot A / Z^2. \tag{27}$$

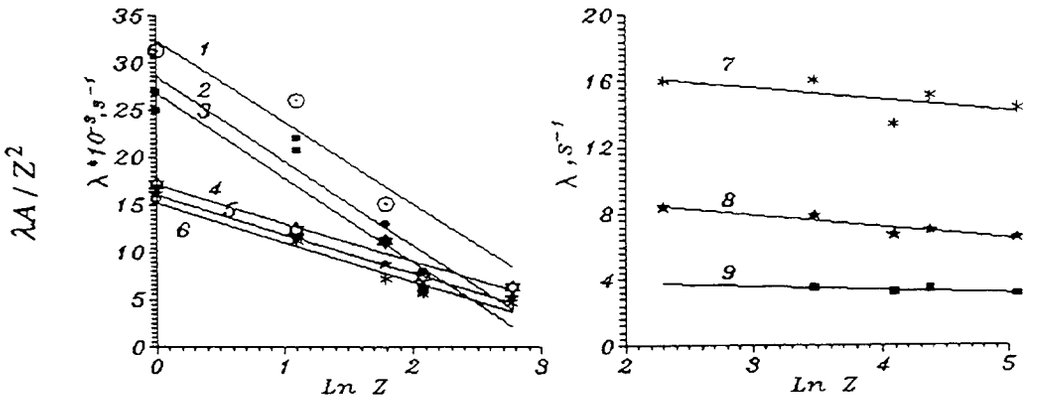

Fig.4. The dependence of longitudinal decrement of ion transverse velocity for different Z, obtained from the analysis of TSR-experiment [21].

4. THE COOLING ELECTRON BEAM

4.1. The electrostatic acceleration and the flattened distribution

The distribution (3) has a kinematical origin in a low intensity beam. Because distribution function is the solution of the collisionless Vlasov equation with full energy as the function argument, one can write (in Laboratory frame after acceleration):

$$f(v_{||}) = A \cdot e^{-\varepsilon_c/T_c}, \quad \varepsilon_c \approx p_0 \cdot (p - p_0)/\gamma m \ , \tag{28}$$

$$p_0 = < p > = \beta\gamma mc \ ,$$

p, p_0 – electron momenta in Lab. frame, ε_c – electron kinetic energy at the cathode, T_c – cathode temperature. The transformation of (28) from the Lab. frame to the electron one and normalization by unit leads to

$$f(v_{||}) = \frac{\beta\gamma mc}{T_c} \cdot e^{-\beta\gamma mcv_{||}/T_c} \tag{29}$$

$$T_{||} = m \int_{-\infty}^{\infty} v_{||}^2 \cdot f(v_{||}) \cdot dv_{||} = 2T_c^2/\beta^2\gamma^2 mc^2 \ \rightarrow \ T_c^2/\varepsilon_0 \ , \ \ \varepsilon_0 \ll mc^2 \ . \tag{30}$$

This distribution function is not an equilibrium one. Electron gas comes to thermoequilibrium after some relaxation time, that is very short (see Sec. 4.3).

Electron transverse momentum does not change during the acceleration, if optical aberrations of the gun can be neglected. Hence

$$T_\perp \sim T_c \ . \tag{31}$$

N^o	1	2	3	4	5	6	N^o	7	8	9
$V_\perp$, $10^5 cm/s$	6	7	8	6	7	8	$V_{||}$, $10^7 cm/s$	2.4	3.4	4.8
$n_e \cdot 10^8 cm^{-3}$	0.72			3.42			–	–	–	–

4.2. The electron density fluctuations and longitudinal temperature

The result (29),(30) is correct for an electron beam of very low density, when the Coulomb interaction between electrons is negligible. The beams used in electron cooling are fairly dense and this interaction plays an important role. Because of a random character of distances between electrons, the local electric field in a beam is not equal to zero and such a field accelerates or decelerates electrons, i.e. transfers to them additional kinetic energy (temperature)[10,19]:

$$\Delta T \sim e^2/l_e \sim 10^{-4} eV \ , \quad l_e = n_e^{-1/3} \sim 1.5 \cdot 10^{-3} cm \ - \tag{32}$$

the average distance between electrons in the beam (all parameters are taken in the particle rest frame). The result of a strict analysis differs by the numerical coefficient of order of unit.

4.3. Electron relaxation. "Fast" and "slow" acceleration

The relaxation of the distribution function (29) occurs due to electron-electron collisions and, in principle, is the same process of the Coulomb interaction, as the electron cooling. If the electron beam is magnetized, one can use for the estimation of the relaxation time formulae (23), the case "S", if to put $m = M$. Then for the longitudinal relaxation one has [24,19]

$$(\tau_{||})_{e-e} \sim \frac{\Delta_{||}^3}{2\pi n_e r_e^2 c^4 L_{MS}} \sim 2 \cdot 10^{-9} sec \ . \tag{33}$$

This relaxation works very fast and the electron beam comes from the gun into the cooling section (a distance of about 0.5 m) very well "maxwellized". The relaxation does not influence in a conventional electron gun because of a high acceleration rate. Therefore electrons do not redistribute their additional energy (32) and come to the gun exit, where after relaxation time electron energy becomes equal to

$$T_{||} \sim \frac{T_c^2}{\varepsilon_0} + e^2 n_e^{1/3} \approx e^2 n_e^{1/3} \ . \tag{34}$$

One can write the criterion of slow acceleration, when relaxation "intermixes" electrons and maxwellizes electron velocity distribution in the gun:

$$\frac{1}{T_{||}} \cdot \frac{dT_{||}}{dt} < min \left\{ (\tau_{||})_{e-e}^{-1}, \omega_{pe} \right\} \ . \tag{35}$$

In this case the instant value of the electron longitudinal temperature follows the law (30), and

$$\frac{1}{T_{||}} \cdot \frac{dT_{||}}{dt} = \frac{1}{\varepsilon} \cdot \frac{d\varepsilon}{dt} = \frac{v}{\varepsilon} \cdot eE \ , \tag{36}$$

where E is accelerating electric field in the gun. Then, the criterion has the form

$$E < 2.1 \sqrt{j \cdot \sqrt{m\varepsilon_0/e^2}} \ . \tag{37}$$

The electric field of the Pierce's gun is about 3 times higher, the Pierce gun is too "fast" and forms the electron beam with a temperature, which follows the law (34), with the flattened distribution, generally speaking.

Numerical estimations show, that the effect of density fluctuations defines the longitudinal temperature of the electron beam. A special design of the gun is required to reach a lower temperature limit (30). Such a gun consists of two parts: a Pierce gun with "fast" acceleration and section of slow ("adiabatic") acceleration. One can show, that for given $T_{\|}$ the maximal beam current generated with such a gun does not exceed

$$I(T_{\|}) \approx \frac{mc^3}{e} \cdot \left(\frac{\pi a^2}{r_e^2}\right)^{9/8} \cdot \left(\frac{T_{\|}\varepsilon_0}{m^2c^4}\right)^{3/8}, \quad \frac{T_c^2}{\varepsilon_0} \leq T_{\|} \leq e^2 n_e^{1/3}, \tag{38}$$

and the current corresponding $T_{min} = T_c^2/\varepsilon_0$ does not depend on energy ε_0 :

$$I(T_{min}) = \frac{mc^3}{e} \cdot \left(\frac{a}{r_e}\right)^{3/4} \cdot \left(\frac{T_c}{mc^2}\right)^{9/4} \approx 40mA \times a_{cm}^{3/4} \ \ at \ \ T_c = 0.1 \ eV \ . \tag{39}$$

To generate the beam with T_{min} the gun at $\varepsilon_0 = 30keV$ has to have about 5 mm "the Pierce gap" and 0.7 m long slow section. First experimental achievements [23] look promising.

The conservation of flattened distribution during beam transportation is limited with electron-electron collisions, which lead to the so called transversal - longitudinal relaxation. It equalizes the longitudinal temperature to the transversal one. A longitudinal magnetic field suppresses essentially the transversal - longitudinal relaxation, if [24] $\rho_{\perp} \leq l_e$.

4.4. The magnetized intense electron beam in a drift chamber

The space charge of an intense electron beam, travelling in a longitudinal magnetic field, creates two effects: electron drift in the plane, transversal to the beam axis and electron energy variation across the beam. Both are essential for electron cooling process. Therefore the neutralization of the space charge is a problem of great practical interest [25].

REFERENCES

[1] G.I.Budker. Atomnaya Energiya, No 22, p.346-348.(1967)

[2] V.I.Kudelainen, I.N.Meshkov, R.A.Salimov. Preprint INP 72-70, Novosibirsk (1970); translated in CERN 77-08, Geneva (1977)

[3] N.S.Dikansky, V.I.Kononov, V.I.Kudelainen, I.N.Meshkov, V.I.Parkhomchuk, D.V.Pestrikov, A.N.Skrinsky and B.N.Sukhina. Proc. of 6-th USSR Meeting on Charged Part. Accel., Dubna, 1978

[4] G.I.Budker, N.S.Dikansky, V.I.Kudelainen, I.N.Meshkov, V.I.Parkhomchuk, A.N.Skrinsky and B.N.Sukhina. Proc. of 4-th USSR Meeting on Charged Part. Accel., Moscow, 1974, vol 2, p 309 (1975). IEEE Trans. Nucl.Sci. VS-22 pp. 2093-7 (1976)

[5] G.I.Budker, N.S.Dikansky, V.I.Kudelainen, I.N.Meshkov, V.I.Parkhomchuk, A.N.Skrinsky and B.N.Sukhina. Particle Accelerators No 7, pp.197-211, (1976)

[6] M.Bell, J.Chaney, H.Herr, F.Krienen, P.Moller-Petersen and G.Petrucci. Nucl. Instr. & Meth. No 190, pp. 237-255. (1981)

[7] T.Ellison, W.Kells, V.Kerner, F.Mills, R.Petas, T.Ruthbun and D.Young. IEEE Trans. Nucl. Sci. NS-30 pp. 2370-92 (1983)

[8] J.Bosser. CAS-1991, CERN 92-01, Geneva pp.147-203 (1992)

[9] A.S.Artamonov, Ya.S.Derbenev and E.L.Saldin. Part. Accel.,v.23, pp.79-92 (1988); I.N.Meshkov. The talk at CERN 40-th PS/AR seminar 22.03.1993

[10] V.V.Parkhomchuk and A.N.Skrinsky. In "Reports on progress in physics", Vol. 54, N 7 , July 1991, p. 919

[11] I.Hoffman. Overview talk on this Workshop

[12] G.I.Budker, A.N.Skrinsky. Sov. Uspekhi phisich. nauk, v. 124, p.561 (1978)

[13] N.S.Dikansky, I.N.Meshkov, A.N.Skrinsky. Nature, v.276 (1978)

[14] Ya.S.Derbenev and A.N.Skrinsky. Physics Reviews, ser. Soviet Physical Reviews , 1981, vol. 3, p.165

[15] A.H.Sorensen and E.Bonderup. Nucl.Instr. & Meth. v.215, pp.27-54 (1983)

[16] H.Poth. CERN EP/90-04, Geneva (1990)

[17] Ya.S.Derbenev and I.N.Meshkov. CERN 77-08, Geneva, (1977)

[18] L.D.Landau, Zh. Eksp. Teor. Fiz. 7, 203 (1937)

[19] N.S.Dikansky, V.I.Kudelainen, V.A.Lebedev, I.N.Meshkov, V.I.Parkhomchuk, A.A.Seryj, A.N.Skrinsky and B.N.Sukhina. Preprint INP 88-61, Novosibirsk (1988)

[20] V.V.Parkhomchuk. In Proc.of The Workshop on electron cooling and related applications, KfK, Karlsruhe, pp.71-85 (1984)

[21] A.Wolf. Wechselwirkung zwischen hochgelanden Ionen und freien electronen. Univ.Heidelberg (1992)

[22] A.Wolf, C.Ellert, M.Grieser, D.Habs, B.Hochadel, R.Repnow and D.Schwalm. The Proc. of this Workshop

[23] A.V.Aleksandrov, R.Galaberese, N.S.Dikansky, V.Guidi, N.Ch.Kot, V.I.Kudelainen, V.A.Lebedev, P.V.Logachov and L.Tecchio. Europhys.Lett v.18 (2), pp.151-156 (1992)

[24] V.I.Kudelainen, V.A.Lebedev, I.N.Meshkov, V.V.Parkhomchuk and B.N.Sukhina. JETP v.83, N6, p.2056-2064

[25] A.V.Burov, V.I.Kudelainen, V.A.Lebedev, V.V.Parkhomchuk, A.A.Seryj and V.D.Shiltzev. Preprint INP 89-116 (1989)

LASER COOLING OF STORED ION BEAMS

R. Grimm, M. Grieser, A. Gruber, D. Habs, H.-J. Miesner, D. Schwalm, B. Wanner

Max-Planck-Institut für Kernphysik and Physikalisches Institut der Universität,
D-69029 Heidelberg, Germany

ABSTRACT

An introduction is given into the basic concepts of laser cooling with special regard to stored ion beams. As an example recent experimental results obtained with 7.3 MeV $^9Be^+$ ions at the Heidelberg Test Storage Ring are discussed.

1. INTRODUCTION

The resonant interaction with laser light offers unique possibilities for the phase-space cooling of ensembles of atoms and ions [1]. Since the first proposals for laser cooling in '75 [2] and the first successful experiments on trapped ions in '78 [3] and on neutral atoms in the early '80s [4] enormous progress has been made in the development of various cooling methods [1]. Now, by standard laser cooling techniques very slow and cold atomic beams are produced from thermal beams, and atoms can even be captured directly from a room-temperature gas into laser traps, where they can easily be cooled down to temperatures in the range of several 10 μK. For ions in traps laser cooling has served as a unique tool for a variety of fascinating experiments like, e.g., ultrahigh-resolution laser spectroscopy and the recent observations of phase transitions of ion ensembles to ordered structures [5-7].

A very young field for laser cooling is the phase-space compression of high-velocity ion beams in storage rings, where longitudinal cooling times and limit temperatures can be reached which are several orders of magnitude lower as compared to electron cooling. In the regime of the extremely low temperatures attainable with laser cooling, the kinetic energy in the rest frame of the ion beam can be considerably smaller than the potential energy between the ions due to their Coulomb repulsion and ordering effects may result in a liquid or solid behavior of the ion beam or even in crystallization [8]. Such an ultracold Coulomb plasma will exhibit a considerably different behavior with quite interesting properties as compared to a hot ion beam or to neutralized plasmas [9]. Moreover, ultracold fast ion beams may be used to improve precision measurements such as, e.g., the test of special relativity presently in progress at the TSR [10] or Ramsey-type experiments [11].

The first successful laser-cooling experiments on stored ion beams were performed in '89 at the Test Storage Ring (TSR) in Heidelberg on a 13.3 MeV $^7Li^+$ beam [12] and in '90 at the ASTRID ring in Aarhus on a 100 keV $^7Li^+$ beam [17]. More recent results obtained on $^7Li^+$ beams at ASTRID are reported in [14], and [15] gives a detailed description of laser cooling at the TSR with experimental results on a 7.3 MeV $^9Be^+$ beam. The most recent results on the cooling of $^{24}Mg^+$ at ASTRID and $^9Be^+$ at the TSR can be found in other contributions to these proceedings [16-18].

2. BASICS OF LASER COOLING

The mechanical forces exerted by laser light on resonantly excited atoms or ions can be understood by the photon momentum transfer connected with the elementary processes

absorption, spontaneous emission and stimulated emission. If an ion with initial momentum $\vec{p}_0$ absorbs a laser photon of momentum $\hbar\vec{k}$ its new momentum will be $\vec{p}_0 + \hbar\vec{k}$. If the excited ion then emits a photon of momentum $\hbar\vec{k}'$ the corresponding recoil will result in an ionic momentum $\vec{p}_0 + \hbar\vec{k} - \hbar\vec{k}'$ (see Fig.1). Let us now assume that a single laser beam, which we idealize as a plane traveling wave with wave vector $\vec{k}$ and frequency $\omega = 2\pi\nu = kc$, interacts with an optical transition of the ions with frequency $\omega_0 = 2\pi\nu_0$. As a very important condition, we furthermore assume that the driven *transition is closed* so that the excited state is only allowed to decay back into the same ground state and no optical pumping to other levels can occur. The interaction will then result in a principally unlimited number of cycles of photon absorption and emission. In an average over many cycles of absorption and *spontaneous*[1] reemission the momentum change per cycle is just the absorbed momentum $\hbar\vec{k}$ because the recoil momentum in spontaneous emission averages to zero ($\langle\hbar\vec{k}'\rangle = 0$). The rate at which these cycles take place is given by the product of the excitation probability p_e and the spontaneous decay rate Γ (inverse lifetime) of the upper state. Therefore the average force resulting from the repeated scattering of photons is

$$\vec{F}_{sp} = \hbar\vec{k} \times \Gamma \times p_e. \tag{1}$$

This force is often called *spontaneous force*, *scattering force*, or *radiation-pressure force.* The excitation probability p_e displays the well-known Lorentzian lineshape

$$p_e = \frac{S/2}{(2\Delta/\Gamma)^2 + 1 + S} \tag{2}$$

as a function of the frequency detuning

$$\Delta = (1 - v_{||}/c)\,\gamma\,\omega - \omega_0 \tag{3}$$

seen by the moving ion; $v_{||} = \vec{v} \cdot \vec{k}/k$ is the longitudinal ion velocity, S is the optical saturation parameter defined as the ratio between laser intensity I and saturation intensity I_{sat} of the transition, and $\gamma = 1/\sqrt{1 - v^2/c^2}$ is the relativistic factor. As the crucial point for laser cooling, the *Doppler effect* in Eq.(2) makes the laser force extremely sensitive to the ion velocity (see Fig.1).

For simplicity in the following, we now assume that the ion beam propagates collinearly with the laser beam ($v_{||} = v$) and we treat the ion motion in a nonrelativistic way. The relativistic factor γ is only considered as far as the laser frequencies are concerned.

The spontaneous force of a single laser beam copropagating or counterpropagating with the ion beam can accelerate or decelerate the ions in a narrow velocity interval fulfilling the Doppler condition within the optical linewidth, but the force is *no cooling force on its own.* For cooling a stable point must exist, i.e. at a certain velocity v^* the total force must vanish ($F(v^*) = 0$) and must display a negative slope ($\partial F/\partial v|_{v=v^*} < 0$). In this case, the motion of ions in the vicinity of the stable point is damped toward v^*. Let us now discuss two schemes of interest for stored ion beams which provide a real cooling force with such a stable point.

(i) The first scheme uses *two laser beams* and was applied in the experiments reported in Refs. [12, 17]. As illustrated in Fig.2(a), the first laser beam copropagates with the ion beam and accelerates ions of velocity v_1 and the second one is counterpropagating and decelerates ions of velocity $v_2 > v_1$ with the resonant velocities v_1 and v_2 being determined by the laser frequencies ω_1 and ω_2 via the Doppler condition Eq.(3) with $\Delta = 0$. If $v_2 - v_1$ corresponds to a few optical linewidths, the combined action of the two laser fields creates a dispersion-like total

[1] In a single traveling laser wave cycles of absorption and *stimulated* emission do not lead to a net force since an identical photon is placed back into the laser beam as absorbed before so that the emission recoil exactly cancels the absorbed momentum.

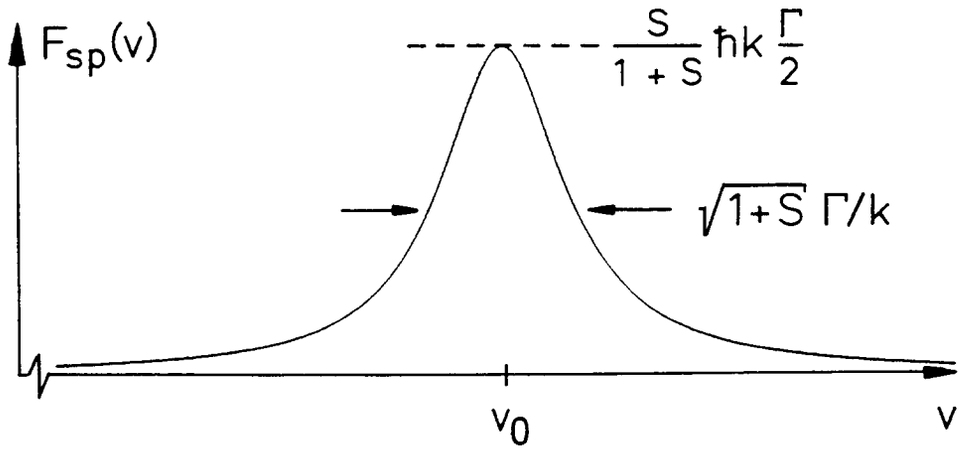

Figure 1: The spontaneous laser force $F_{sp}(v)$ as a function of longitudinal ion velocity, reflecting the Lorentzian-shaped optical excitation probability. The resonant velocity v_0 is determined by the laser frequency via the Doppler condition (Eq.(3) with $\Delta = 0$).

force[2], which is similar to the electron cooling force and has a stable cooling point in its center (see Fig.2(a)). Usually the initial ion velocity distribution is much wider than this narrow laser force. Therefore the cooling in this scheme is usually started with a large $v_2 - v_1$, including all ions between v_1 and v_2. Then $v_2 - v_1$ is steadily reduced by scanning one or both laser frequencies in order to compress the ion ensemble into a narrow velocity interval. After this a continuous and efficient cooling of all collected ions can be achieved with a small value of $v_2 - v_1$.

(ii) The second cooling scheme employs a *single laser beam* counter- or copropagating with the ion beam in combination with a counteracting nonresonant *auxiliary force* (see Fig.2(b)). In a storage ring such an auxiliary force can quite easily be realized with an induction accelerator [20] and also with the electron cooler [21]. The cooling process takes place in the following way: First the auxiliary force accelerates or decelerates the whole ion distribution toward resonance with the laser beams. The motion of the ions coming close to resonance is damped toward the stable point. In this way all ions are successively collected at the cooling point. This scheme has the obvious advantage that only a single fixed-frequency laser beam is required for cooling, since the nonresonant auxiliary force can push all ions toward the stable point. A drawback ot this scheme, however, is the existence of an unstable region, where the auxiliary force accelerates the ions away from the narrow, resonant laser force (see also Miesner et al. in these proceedings).

The final longitudinal temperature $T_{||}$ reached in the laser cooling process can be understood as an equilibrium of cooling and heating. With D denoting the total longitudinal heating rate (in K/s) and Λ being the laser cooling rate (in s^{-1}) the longitudinal equilibrium temperature (in K) is simply given by the fundamental relation

$$T_{||} = \frac{D}{\Lambda}, \tag{4}$$

which was already derived by Einstein for the Brownian motion.

The laser cooling rate Λ is directly related to the friction coefficient $-\partial F/\partial v|_{v=v^*}$ at the stable point by

$$\Lambda = -\frac{2}{m}\left.\frac{\partial F}{\partial v}\right|_{v=v^*}, \tag{5}$$

[2]For low laser intensities the total force can be understood simply as a sum of the two individual contributions. This is still a reasonable approximation for optical saturation parameters of $S \approx 1$. For high intensities, however, the situation can be very complicated because of a stimulated redistribution of photons among the two light fields [19].

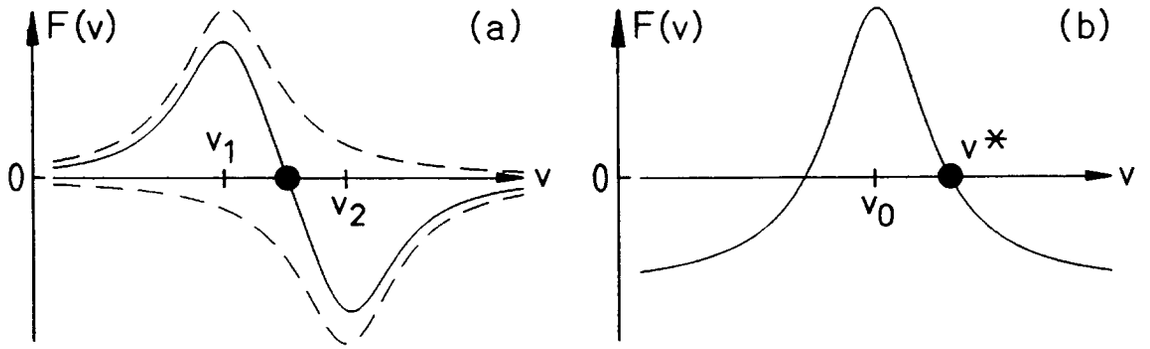

Figure 2: Illustration of the cooling forces obtained in the two discussed schemes. (a) In a pair of counterpropagating laser beams a dispersion-like cooling force (solid curve) can be created for an appropriate choice of the laser frequencies. The dashed curves show the individual contributions to the total force by each of the two lasers. (b) A single laser beam can lead to a cooling force in the presence of a counteracting auxiliary force. The big dot in each scheme marks the stable cooling point.

where m denotes the ion mass.

The heating caused by the laser itself as a consequence of fluctuations in the absorption processes and the randomness of the spontaneous emission recoils is well approximated (see [15]) by the corresponding rate[3]

$$D_{laser} = \frac{7}{10}\frac{\hbar^2 k^2 \Gamma}{k_B m} \times p_e \,, \tag{6}$$

where k_B is Boltzmann's constant and p_e is the excitation probability of Eq.(2).

The limit temperature T_{Dopp} of laser cooling by means of the spontaneous force, which is often referred to as Doppler limit[4], is

$$T_{Dopp} = \frac{7}{20}\frac{\hbar\Gamma}{k_B} \,. \tag{7}$$

This temperature is reached in the absence of other heating processes for low optical saturation ($S \ll 1$) and for $k(v_2 - v_1) = \Gamma$ in the first cooling scheme or $k|v^* - v_0| = \Gamma/2$ in the second scheme discussed above.

In storage rings, both the laser cooling rate Λ and the laser-induced heating rate D_{laser} are reduced by the fact that laser beam and ion beam are merged only within a fraction η_L (typically 10%) of the ring circumference. If, on one hand, the velocity change of the ions in a single passage through the laser field is small compared with the velocity Γ/k corresponding to the natural linewidth of the optical transition and if, on the other hand, the time for a such a single passage is long enough ($\gg \Gamma^{-1}$) for reaching stationary optical excitation conditions, then the above formulae are also valid for the ring-averaged quantities

$$\langle F_{sp} \rangle = \eta_L F_{sp} \tag{8}$$

$$\langle \Lambda \rangle = \eta_L \Lambda \tag{9}$$

$$\langle D_{laser} \rangle = \eta_L D_{laser} \,. \tag{10}$$

[3]Eq.(6) is valid for arbitrary intensities in the second cooling scheme discussed above, but as a consequence of stimulated heating processes [19] only for low intensities in the first scheme.

[4]In literature the definition $T_{Dopp} = \hbar\Gamma/(2k_B)$ is widely used for reasons discussed in [15]. Our definition gives the true cooling limit, being a factor of 7/10 lower.

Stored ion beams are heated by intrabeam scattering (IBS) processes (heating rate D_{IBS}), which are often much stronger than the laser heating. Therefore the equilibrium temperature is given by

$$T_{||} = \frac{D_{IBS} + \langle D_{laser} \rangle}{\langle \Lambda \rangle} \tag{11}$$

This means that one can in general not expect to reach the Doppler limit when laser cooling a stored ion beam, except for very dilute beams. When cooling a relatively dense beam, the laser heating can usually be completely neglected compared to the IBS heating.

3. CANDIDATES FOR LASER COOLING

The number of ion species, for which an efficient laser cooling is possible, is limited by the stringent requirement of a closed strong optical transition accessible to present-day continuous-wave laser sources. Suitable electric dipole (E1) transitions from the ground state are found in light ions of low charge states as Be^+ and Mg^+. In addition, the metastable triplet-state fractions of beams of heliumlike ions such as Li^+ and Be^{2+} are good candidates for laser cooling via strong E1 transitions. The main properties of the ion species that have been successfully laser-cooled at the TSR and at ASTRID are listed in the following table:

	$^{6,7}Li^+$	$^{9}Be^+$	$^{24}Mg^+$
lower state	$2s\,^3S_1(F=2,\frac{5}{2})$	$2s\,^2S_{1/2}$	$3s\,^2S_{1/2}$
upper state	$2p\,^3P_2(F'=3,\frac{7}{2})$	$2p\,^2P_{3/2}$	$3p\,^2P_{3/2}$
lifetime lower state	~ 50 s	ground state	ground state
lifetime upper state	43 ns	8.2 ns	3.5 ns
natural linewidth (fwhm)	3.7 MHz	19.4 MHz	45.5 MHz
wavelength (rest frame)	548 nm	313 nm	280 nm
saturation intensity (*)	2.9 mW/cm^2	83 mW/cm^2	270 mW/cm^2
maximum force (+)	8.8 meV/m	81 meV/m	210 meV/m
maximum cooling rate (+)	5.7×10^4 s^{-1}	1.4×10^5 s^{-1}	6.4×10^4 s^{-1}
cooling limit T_{Dopp}	62 μK	330 μK	770 μK

(*) calculated under the assumption of a pure two-level system

(+) ring-averaged values assuming $\eta_L = 0.1$

In heavy, highly charged ions, laser cooling via magnetic dipole (M1) transitions may also be feasible. In highly charged boronlike or carbonlike ions (e.g., S^{11+}, Cl^{12+}, Ar^{13+}, K^{14+} or K^{13+}, Ca^{14+}, Sc^{15+}, Ti^{16+}), M1 transitions in the fine structure of the ground state are accessible to cw lasers at optical wavelengths. Furthermore, M1 transitions between hyperfine levels of very heavy, highly charged ions such as Bi^{82+} may be considered. Possible ways to overcome the low cooling rates provided by the spontaneous light force for long lifetimes of these M1 transitions are offered by new laser forces utilizing the stimulated emission of photons [22, 23]. Further perspectives for laser cooling might exist in high-energy storage rings [24], where the highly relativistic Doppler effect could shift x-ray transitions in the electron shell of partially stripped ions or even nuclear transitions of bare ions into the optical spectral region.

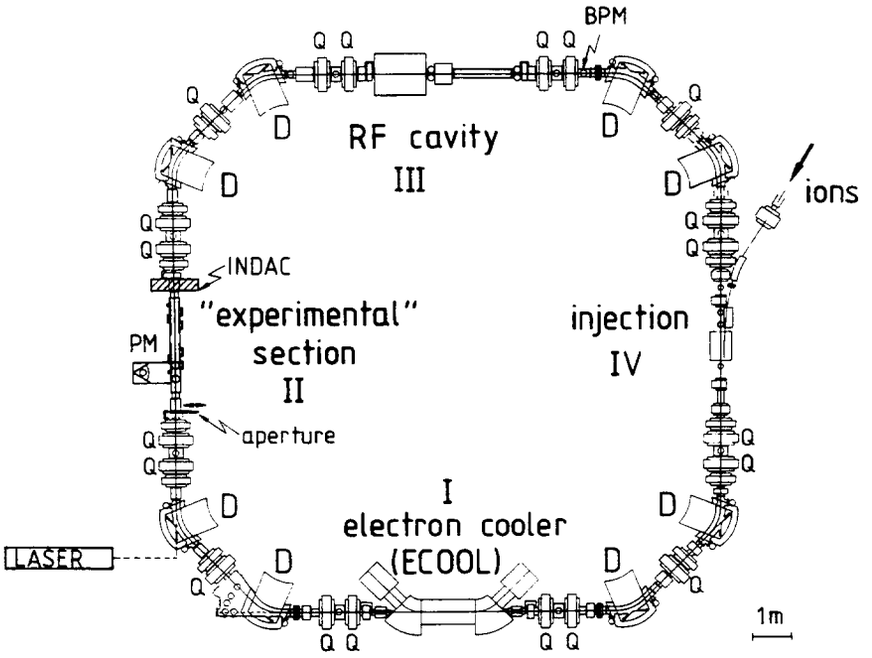

Figure 3: Schematic view of the Test Storage Ring (TSR) at the Max-Planck-Institut für Kernphysik in Heidelberg (D, dipole bending magnets; Q, quadrupole singlets; BPM, beam profile monitor; PM, photomultiplier). The circumference of the TSR is 55.4 m.

4. LASER COOLING OF $^9Be^+$ AT THE TSR

As an example for the laser cooling of stored ion beams, we now discuss some basic aspects of the experiments performed at the TSR on 7.3 MeV $^9Be^+$ ions. Here we focus on new measurements of the laser cooling force and on the lowest longitudinal beam temperature we have observed. Other important new developments at the TSR, concerning intrabeam scattering losses in the cooling process and the first observation of an indirect transverse cooling of a longitudinally cooled ion beam, are described by Miesner et al. in these proceedings.

The ions are accelerated by a tandem accelerator facility and typically 3×10^7 ions are injected into the ring. In Fig.3 the main components of the TSR are shown. In the first section following the injection the electron cooler (ECOOL) is located. By electron cooling right after the injection we reduce the transverse temperature of the ion beam from an initial temperature of $T_\perp \approx 10^6$ K down to $T_\perp \approx 5000$ K. Correspondingly the ion beam diameter, which can be measured by the TSR beam profile monitor, decreases from 2 cm (after injection) to approximately 1 mm (after electron cooling). The typical time for electron cooling is 7 s, about half the typical storage lifetime. Usually the ECOOL is switched off before the laser cooling begins.

The laser-cooling experiments on $^9Be^+$ are carried out in the TSR experimental section with the use of a laser beam that is copropagating with the ion beam. The maximum overlap of ≈ 5 m ($\eta_L \approx 0.09$) is roughly determined by the length of the field-free region between the quadrupole magnets. The lasers used in $^9Be^+$ experiments are fixed-frequency, high-power argon-ion lasers at a wavelength of 300.3 nm, where they give a typical power of 100 mW in a single longitudinal mode. The velocity is chosen to 4.16% of the speed of light, so that the ions see the resonant wavelength of 313 nm in their rest frame. The ground state of the ions shows a hyperfine splitting of 1.30 GHz in the laboratory frame. Therefore it is of crucial importance to avoid the effect of optical pumping. As the most efficient way to do this [15] we use two-argon ion lasers, the beams of which are combined to provide a two-frequency laser-field with a

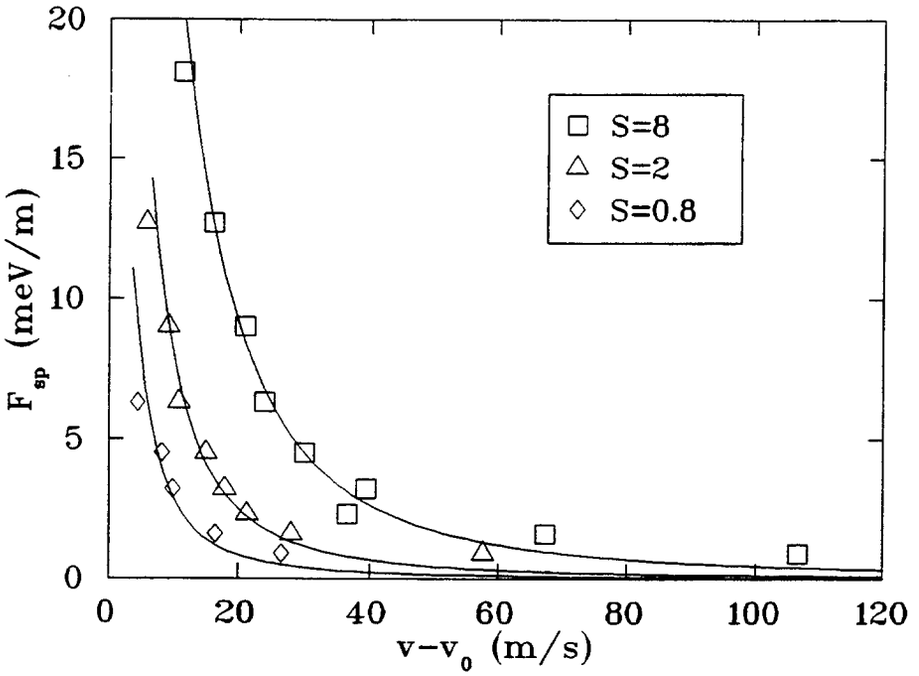

Figure 4: The ring-averaged laser force measured as a function of the ion velocity v relative to the resonant velocity v_0 for three different laser intensities. The solid lines are corresponding theoretical curves assuming an overlap length of 4 m ($\eta_L = 0.075$).

frequency separation of 1.30 GHz. As a very important point for obtaining the optimum cooling effect, the two argon-ion lasers are frequency-stabilized to better than 1 MHz. The long-term stability is ensured by locking the first laser to a commercially available, frequency-stable HeNe-laser via a double-resonant cavity. The second argon-ion laser is locked at the correct frequency difference of 1.30 GHz to the first one by making use of the beat signal, which is detected by a fast photodiode.

The cooling is performed in the second scheme discussed in Sec.2 (see Fig.2(b)), and the necessary auxiliary force is provided by an induction accelerator (INDAC) [20] in a well defined way.

For diagnostics the fluorescence light emitted by the ions perpendicular to the beam at the rest frame wavelength 313 nm is detected by a photomultiplier tube. By a high-quality interference filter this light can efficiently be discriminated against direct stray light from the laser beams. As an important tool for diagnostics, a drift tube of about 65 cm length is used, which can be biased by a variable voltage in order to locally change the velocity of the ions in the detection region. A simple scan of the bias voltage corresponds to a frequency scan seen by the ions in the tube and thus allows to scan the ion velocity distribution; for the 7.3 MeV $^9Be^+$beam a voltage of 100 V corresponds to a velocity change of 86 m/s [15].

Systematic measurements of the laser cooling force are performed in the following way: For various values of the INDAC force, diagnostic scans are made by ramping the bias voltage of the drift tube and observing the fluorescence light intensity. The voltage where the fluorescence maximum occurs corresponds to the velocity difference between the stable cooling point v* and the resonant velocity v_0 (see Fig.2(b)). This allows to measure the relative position $v^* - v_0$ of the stable point as a function of the auxiliary force F_{aux}. Since at the stable point the auxiliary force exactly cancels the laser force, this measurement directly yields $F_{sp}(v^* - v_0)$. Corresponding experimental results obtained for three different laser intensities are shown in Fig.4. These curves are in good agreement with the expected Lorentzian lineshapes if a length of 4 m is assumed for

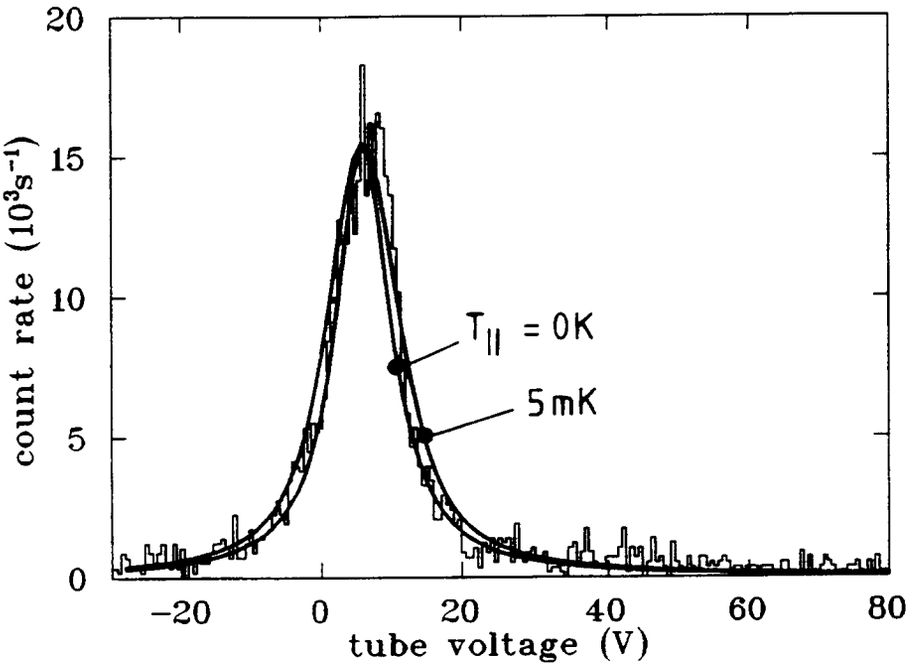

Figure 5: A diagnostics scan showing the fluorescence intensity as a function of the bias voltage of the drift tube for the high cooling rate $\langle\Lambda\rangle = 3 \times 10^4\,\mathrm{s}^{-1}$. The two theoretical curves are fitted to the data under the assumption of $T_{||} = 0\,\mathrm{K}$ and 5 mK and correspond to a lower and upper limit for the longitudinal beam temperature.

the overlap of the ion beam with the laser beam. Furthermore, these measurements allow us to derive the laser cooling rate $\langle\Lambda\rangle$ for a given intensity and INDAC force according to Eq.(5).

Let us now consider a diagnostics scan which we have recorded close to the highest cooling rate we can achieve ($\langle\Lambda\rangle = 3 \times 10^{-3}\,s^{-1}$ for $S = 0.8$ and $F_{aux} = -6.3\,\mathrm{meV/m}$). In Fig.5 the intensity of the fluorescence light emitted by the $\sim 1.5 \times 10^6$ laser-cooled ions as a function of the relative velocity $v - v_0$ shows a resonance, which is only slightly wider than one would expect for the homogeneous, saturation-broadened optical linewidth alone, i.e. for an arbitrary narrow velocity distribution with zero temperature. In this situation, where the narrow Gaussian velocity distribution is convoluted with the wider Lorentzian excitation profile, temperature measurements as we have reported in previous work [15] for much lower cooling rates are very difficult. From the measurement displayed in Fig.5 we can only derive an upper limit, which is $T_{||} < 5\,\mathrm{mK}$.

The longitudinal heating rate D_{IBS} resulting from intrabeam scattering can be measured independently of the cooling process. This is made by switching off the laser cooling and observing the following increase of the longitudinal velocity spread by laser diagnostics. Under the same conditions as for Fig.5 we measured $D_{IBS} = 100\,\mathrm{K/s}$. The equilibrium condition Eq.(4) together with the cooling rate $\langle\Lambda\rangle = 3 \times 10^4\,\mathrm{s}^{-1}$ predicts a longitudinal temperature of 3 mK, which agrees with the upper limit $T_{||} < 5\,\mathrm{mK}$ from our experiment.

5. CONCLUSION AND OUTLOOK

Since the first successful experiments performed only a few years ago, great progress has been made in the laser cooling of stored ion beams: With respect to the *longitudinal* degree of freedom, we are now close to the cooling limit given by the maximum laser cooling rate and the heating caused by intrabeam scattering. For the conditions reached in our experiments on $^9Be^+$ ions, the thermal energy of an ion is at least a factor of 20 lower than the nearest-neighbor Coulomb

energy. This means that we are already in a parameter range where ordering effects may lead to a longitudinal behavior of the ion beam that is more like a liquid or a solid rather than like a gas. In our present experiments, however, the hot transverse degrees of freedom do not allow the formation of any three-dimensional crystalline structure.

Further progress in the laser cooling of stored ion beams is promised by various possible improvements. A substantial further reduction of the longitudinal beam temperature can be expected with more elaborate laser cooling mechanisms [1], which can lead to temperatures far below the Doppler-limit. With respect to the transverse beam temperature first experimental results at the TSR and at ASTRID [18, 16] have already shown that the heat exchange between the longitudinal and the transverse degrees of freedom that is connected with intrabeam scattering can lead to a significant transverse cooling in a longitudinally laser-cooled ion beam. Corresponding computer simulations based on an intrabeam scattering code [25] agree with these observations and indicate the feasibility of order-of-magnitude reductions of the transverse temperature. Our experiments in the near future will explore this promising possibility for the cooling of ion beams to extremly low temperatures in all degrees of freedom.

We gratefully acknowledge support by the Bundesministerium für Forschung und Technologie under contract No. 06HD525I.

References

[1] *Laser Manipulation of Atoms and Ions*, proceedings of the Varenna summer school 1991, edt. by E. Arimondo, W.D. Phillips, and F. Strumia (North Holland, Amsterdam, 1992), and refs. therein.

[2] T.W. Hänsch and A.L. Schawlow, Opt. Commun. **13**, 68 (1975); D.J. Wineland and H. Dehmelt, Bull. Am. Phys. Soc. **20**, 637 (1975).

[3] D.J. Wineland, R.E. Drullinger, and F.L. Walls, Phys. Rev. Lett. **40**, 1639 (1978); W. Neuhauser, M. Hohenstatt, P. Toschek, and H. Dehmelt, Phys. Rev. Lett. **41**, 233 (1978).

[4] S.V. Andreev, V.I. Balykin, V.S. Letokhov, and V.G. Minogin, JETP Lett. **34**, 442 (1981); W.D. Phillips and H. Metcalf, Phys. Rev. Lett. **48**, 596 (1982).

[5] F. Diedrich et al., Phys. Rev. Lett. **59**, 2931 (1987); D.J. Wineland et al., Phys. Rev. Lett. **59**, 2935 (1987).

[6] S.L. Gilbert, J.J. Bollinger, and D.J. Wineland, Phys. Rev. Lett. **60**, 2022 (1988).

[7] I. Waki, S. Kassner, G. Birkl, and H. Walther, Phys. Rev. Lett. **68**, 2007 (1992).

[8] Proceedings of the Workshop on Crystalline Ion Beams, Wertheim, Germany, edt. by R.W. Hasse, I. Hofmann, and D. Liesen, Gesellschaft für Schwerionenforschung, report No. GSI-89-10, 1989.

[9] S. Ichimaru, Rev. Mod. Phys. **54**, 1017 (1982).

[10] R. Klein et al., Z. Phys. A **342**, 455 (1992).

[11] P. Forck, MPI für Kernphysik, report No. MPIH-V20-1991, 1991; M. Kristensen et al., Phys. Rev. A **46**, 4100 (1992).

[12] S. Schröder et al., Phys. Rev. Lett. **64**, 2901 (1990).

[13] J. Hangst et al., Phys. Rev. Lett. **67**, 1238 (1991).

[14] J. Hangst et al. in [1]; M. Kristensen et al. in Atomic Physics 13, edt. by H. Walther, T.W. Hänsch, and B. Neizert (AIP, New York, 1993).

[15] W. Petrich et al., Phys. Rev. A **48**, 2127 (1993).

[16] J.S. Nielsen et al., these proceedings.

[17] J.S. Hangst et al., these proceedings.

[18] H.-J. Miesner et al., these proceedings.

[19] V.G. Minogin and V.S. Letokhov, *Laser Light Pressure on Atoms* (Gordon and Breach, New York, 1987).

[20] C. Ellert et al., Nucl. Instr. and Meth. A **314**, 399 (1992).

[21] A. Wolf et al., in *Electron Cooling and New Cooling Techniques*, edited by R. Calabrese and L. Tecchio (World Scientific, Singapore, 1991).

[22] A. Aspect et al., Phys. Rev. Lett. **57**, 1688 (1986); R. Grimm et al., Phys. Rev. Lett. **65**, 1415 (1990); J. Söding et al., Europhys. Lett. **20**, 101 (1992).

[23] B. Wanner et al., these proceedings.

[24] D. Habs et al., in *Electron Cooling and New Cooling Techniques*, edited by R. Calabrese and L. Tecchio (World Scientific, Singapore, 1991).

[25] B. Hochadel et al., these proceedings.

MUON COOLING AND APPLICATIONS

David V. Neuffer
CEBAF, 12000 Jefferson Avenue, Newport News, VA 23606, USA

Abstract

The challenges in obtaining high-intensity muon bunches are described and discussed. In a reference scenario, a high-intensity pulsed proton accelerator produces large numbers of secondary π's in a nuclear target, which produce muons by decay. (Other sources are also considered.) The muons are collected and cooled (by "ionization cooling") to form high-intensity bunches. The principles of the application of ionization cooling to obtain high-phase space density muon beams are described, and its limitations (μ-decay, multiple scattering, fluctuations) are discussed. Constraints on cooling scenarios are discussed, and methods of bunch combination and compression are described. Possible applications include muon-collider scenarios such as a 100-GeV Higgs-discovery machine and future multi-TeV high-luminosity lepton colliders. Significant challenges remain in obtaining the intensities and cooling needed for high-luminosity scenarios.

Introduction

Leptonic (e^+-e^-) colliders have had the valuable property of producing simple, single-particle interactions with little background, and this property is essential in the exploration of new particle states. However, extension of e^+-e^- colliders to ultrahigh energies is constrained in energy, luminosity, and resolution by radiative effects, and these limitations imply a need for a "new paradigm" in accelerators, as was discussed at the Port Jefferson workshop (1992).[1] These limiting radiative effects scale inversely as the fourth power of the lepton mass. Therefore, extension to much higher energies is possible by colliding heavier leptons, such as muons. Muons also have a much greater direct coupling into the mass-generating "Higgs-sector", the next frontier in particle physics.

The challenges associated with developing a μ^+-μ^- collider were discussed at the Port Jefferson workshop and in subsequent mini-workshops at Napa and Los Alamos.[2,3,4] A "Higgs-factory" collider[5] (μ^+-μ^- at energy E $\approx$ 100GeV, luminosity L $\approx 10^{30}$ cm^{-2}-s^{-1}) and an ultrahigh-energy lepton collider (E > 1 TeV, L > 10^{33}) were identified as important goals. Sample parameter sets with these goals are displayed in Table 1, and a μ^+-μ^- facility is outlined in Figure 1. These collider goals would require μ-beam bunches with much greater intensities and phase-space densities than previously attempted. Substantial achievements in μ^+-μ^- production, collection, and bunch combination and compression with beam cooling will be required to meet these goals.

In the present paper we explore aspects of this collider challenge, with an emphasis on the beam cooling problem. We first describe μ-production, noting that a large μ-acceptance will probably imply a large initial phase space, and estimate its size. We describe the possibilities in phase-space compression obtainable by "muon cooling", and emphasize in particular the technique called "ionization cooling".[6,7,8] The physics of ionization cooling and its limitations are discussed. Other beam-cooling options are also discussed (i. e., stochastic cooling, stopped μ's). Incorporation of beam cooling into collider scenarios with μ-production, and bunch combination and compression methods is discussed, and topics requiring further development toward achievement of collider parameters are indicated. (Improved μ-production and cooling techniques may, of course, have other applications than the μ^+-μ^- collider, such as μ-p colliders, and improved μ-beams for deep-inelastic scattering, g-2, μSR, and neutrino experiments, and possibly even advance progress toward μ-catalyzed fusion.)

Muon Production

Several options for μ^+-μ^- production have been proposed in the workshops. Following $\bar{p}$-source experience, we consider as a base-line reference a high-energy hadronic (HEH) source as described in refs. (8, 9), and displayed in Fig. 2. A high-energy (10—100 GeV), high-intensity, hadron beam is transported onto a high-density target. The hadronic interactions produce large numbers of GeV-scale π's and the π's are confined in a transport channel where they decay to produce μ's.

The π-production parameters can be estimated using measured and calculated p-X interaction spectra.[10,11]

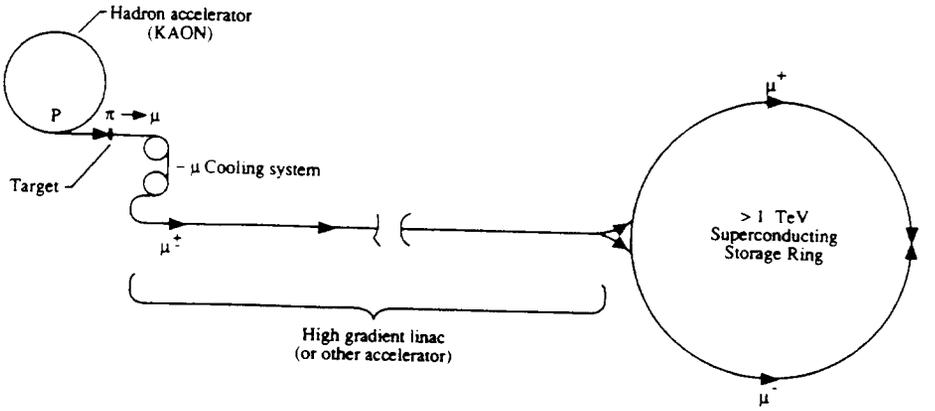

Figure 1. Overview of a μ^+—μ^- collider, showing a hadronic accelerator, which produces π's on a target, followed by a π-decay channel ($\pi \rightarrow \mu\ \nu$) and μ-cooling system, followed by a μ-accelerating linac (or recirculating linac or rapid-cycling synchrotron), feeding into a high-energy storage ring for μ^+—μ^- collisions.

Table 1: Parameter lists for High-Energy and Higgs-Factory μ^+-μ^- Colliders

Parameter	Symbol	High-Energy	Higgs Factory
Energy per beam	E_μ	2 TeV	100 GeV
Luminosity	$L=f_0 n_\tau n_b N_\mu^2/4\pi\sigma^2$	5×10^{33} cm^{-1}s^{-1}	4×10^{29} cm^{-1}s^{-1}
HEH-Source Parameters			
Proton energy	E_p	40 GeV	40 GeV
Protons/pulse	N_p	2×10^{14}	10^{14}
Pulse rate	f_0	30 Hz	10 Hz
μ production efficiency	μ/p	2×10^{-3}	10^{-3}
Collider Parameters			
Number of μ^+/μ^- per bunch	$N_{\mu\pm}$	2×10^{11}	2.5×10^{10}
Number of bunches	n_B	2	4
Storage turns	n_τ	1200	1000
μ-beam emittance	ε_t	0.5×10^{-8} m-rad	10^{-7} m-rad
Interaction focus	β_0	0.1 cm	0.5 cm
Beam size at interaction	$\sigma = (\varepsilon_t\beta_0)^{1/2}$	2.2 μm	22 μm

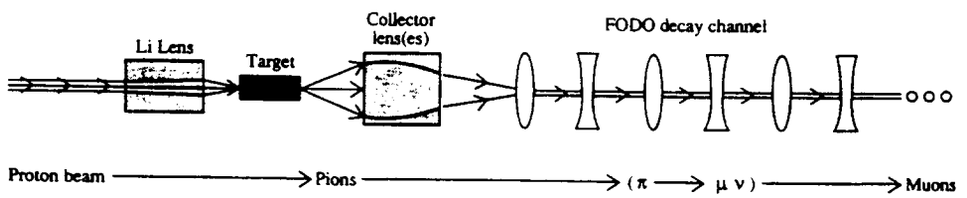

Figure 2. Schematic view of μ-production from π-decay, with π's produced from hadrons. A high-energy hadronic beam is focussed onto a target; a collector lens(es) collects the resulting π's into a strong-focussing "FODO" channel, where π-decay produces μ's for collider use.

The single-interaction spectra show a slow rise in π-production with primary p energy E_p ($\sigma \propto \ln(E_p)$ for $E_p >$ 100GeV), and a broad optimum for π collection at $E_\pi \approx 0.1E_p$. The transverse momentum is limited to the pion-mass scale; $P_t < \sim 0.3$ GeV/c. In the decay channel, π-decay ($\pi \rightarrow \mu + \nu$) produces μ's within a uniform energy distribution (between 0.57 and 1.0 E_π) and a maximum transverse momentum of 0.03 GeV/c. Calculated estimates indicate that an HEH source, with momentum acceptances < 10% and transverse acceptances reasonably matched to π-production and decay, can produce > 1×10^{-3} μ/p for the collider, even after including many inefficiency factors (target efficiency, acceptances, decay losses, etc.).[9, 8] Some improvements are possible, but obtaining much more than $\sim 10^{-2}$ μ/p seems difficult.

The HEH source produces medium energy μ's (1–10 GeV) within a broad energy spread given by the production and decay channel acceptances (~±5%). The transverse emittance ε_t is set by the beam size and P_t acceptance from the production target, as well as the phase-space dilution in π-decay. The dominant term is likely to be the projected production emittance, which is given by:

$$\varepsilon_{N,rms} \approx \frac{l_T}{2}\left[\frac{P_t}{P}\right]^2 \beta\gamma \quad , \tag{1}$$

where $\varepsilon_{N,rms}$ is the normalized rms emittance, l_T is the target length, P_t/P is the acceptance angle, and $\beta\gamma = p/m_\pi c$, the usual kinetic factor. At typical parameters (l_T=5 cm, a single-interaction length W target, P = 3 GeV/c, P_t=0.3 GeV/c), $\varepsilon_{N,rms} \approx 5 \times 10^{-3}$ m-rad and, in general, $\varepsilon_{N,rms} \approx 10^{-2} - 10^{-3}$ m-rad may be expected from an HEH source.

Particle production can be magnified from the above single-interaction case by sending the beam instead into an extended target, where multiple interactions of primary and secondaries would occur, forming a "hadronic cascade",[8] from which the optics would extract relatively-low energy π's and μ's. Total production could be increased, but the initial phase-space area of the beam would also be magnified, and more cooling would be needed. (Similar multiplication could also occur in an extended electroproduction source.) In all cases, μ-production at collider intensities will require extremely large beam powers on the production targets (> ~10 MW in the baseline HEH scenario of table 1). Multitarget arrays and beam sweeping can reduce target loads. Silvestrov has proposed the use of liquid metal jet technology in targets and lenses to handle the required power levels.[12]

Other possible source scenarios were proposed at the workshops. Lower-energy sources, using a "π-factory" (~GeV/nucleon p or d beams) to produce non-relativistic (or stopped) μ's are possible. A π-factory source can produce large numbers of μ's with low energy and momentum spread, which may require little or no further cooling. The difficulty is in extracting sufficient μ's in small-phase-space bunches suitable for a μ^+-μ^- collider. Further study is needed. Another possible μ-source can be obtained by colliding multi-GeV e^- beams into a hadronic target, producing muons from μ^+-μ^- pair creation. Barletta and Sessler[13] have developed a collider based on electroproduction of muons from a 50 GeV electron beam, identifying innovations needed to upgrade the scenario to desired performance. These (and other) possibilities have not been explored to the level that an optimal and satisfactory approach is identified; further development and invention is desired.

Muon Cooling – Ionization Cooling

In almost all proposed production schemes, the muons are produced within a much larger phase-space volume than that desired for high-luminosity collisions (see table 1); this volume must be reduced by beam-cooling and compression. Much of the needed compression is obtained from adiabatic damping; acceleration from GeV-scale μ collection to TeV-scale collisions reduces phase-space by ~10^9 (10^3 per dimension). Additional phase-space reduction may be obtained by "ionization cooling" of muons ("μ-cooling"), in which beam transverse and longitudinal energy losses in passing through a material medium are followed by coherent reacceleration, resulting in beam phase-space cooling.[6, 7, 8] This is conceptually similar to radiation damping, in which energy losses in synchrotron radiation followed by rf acceleration results in beam-cooling. (Ionization cooling is not practical for protons and electrons because of nuclear scattering (p's) and bremstrahlung (e's) effects, which do not limit μ's, and other methods of obtaining high-density p- and e-beams exist.)

The basic mechanism of transverse μ-cooling is shown graphically in figure 3. Muons passing through a material medium lose energy (and momentum) through ionization interactions. The losses are parallel to the particle motion, and therefore include transverse and longitudinal momentum losses. The beam positions and divergences

(x, x') are unchanged by the coherent energy loss; therefore the unnormalized emittance is unchanged. (The normalized emittance is reduced by the reduction in beam momentum.) Reacceleration of the beam (in rf cavities) restores only longitudinal momentum. The combined process of ionization energy loss plus rf reacceleration reduces transverse momentum and hence reduces transverse emittance. The emittance change in a cycle with an energy loss of $\Delta E = dE_\mu/dz\ \Delta z$ and regain can be written as:

$$\varepsilon_\perp \rightarrow \frac{E_\mu - \Delta E}{E_\mu}\varepsilon_{\perp 0} = \left(1 - \frac{dE_\mu}{dz}\frac{\Delta z}{E_\mu}\right)\varepsilon_{\perp 0} \qquad (2)$$

where $\varepsilon_\perp$ is the (unnormalized) transverse emittance, dE_μ/dz is the absorber energy loss per transport length z.

However, the random process of multiple scattering in the material medium increases the emittance; the increase in transverse emittance is $\Delta\varepsilon_\perp \approx \beta^*\langle\theta_{rms}^2\rangle/2$, where β^* is the betatron function in the absorber and θ_{rms} is the mean accumulated multiple scattering angle in the absorber. The cooling and heating effects can be combined in a differential-equation for transverse cooling:

$$\frac{d\varepsilon_\perp}{dz} = -\frac{(dE_\mu/dz)}{E_\mu}\varepsilon_\perp + \frac{\beta^* d\langle\theta_{rms}^2\rangle}{2\ dz} \qquad (3)$$

(The differential-equation form of eq. (3) assumes the cooling system is formed from small alternating absorber and reaccelerator sections; similar difference equations would be correct if individual sections are long. Also relativistic kinematics is assumed.)

Note that $dE_\mu/dz = f_A\ dE_\mu/ds$, where f_A is the fraction of the transport length occupied by the absorber, which has an energy absorption coefficient dE_μ/ds, given by the Bethe-Bloch formula:[14]

$$\frac{dE_\mu}{ds} = \frac{4\pi N_0 e^4}{m_e c^2 \beta^2}\frac{Z}{A}\left[\ln\left(\frac{2m_e c^2\beta^2\gamma^2}{I}\right) - \beta^2\right] \qquad (4)$$

where N_0 is Avogadro's number, Z and A the atomic number and weight of the material medium, and I is the mean ionization energy ($I \approx 10Z$ eV). (β, γ) are the muon kinetic parameters. The energy loss function for muons, dE_μ/ds, is rapidly decreasing with energy for $E_\mu < 0.3$ GeV, where the beam is non-relativistic, but is slightly increasing for $E_\mu > 0.3$ GeV. The multiple scattering can be estimated from:

$$\frac{d\langle\theta_{rms}^2\rangle}{dz} \cong \frac{f_A}{L_R}\left(\frac{0.014}{E_\mu}\right)^2 \qquad (5)$$

where L_R is the material radiation length and E_μ is in GeV.[15] Table 2 lists some candidate absorber properties.

If the parameters remain constant, equations 3 and 5 may be combined to find a minimum cooled (unnormalized) emittance of

$$\varepsilon_\perp \rightarrow \frac{(0.014)^2}{2E_\mu}\frac{\beta^*}{L_R(dE_\mu/ds)} \qquad (6)$$

(All energies are in GeV.) or, when normalized:

$$\varepsilon_N = \varepsilon_\perp\beta\gamma \Rightarrow \frac{(0.014)^2}{2m_\mu c^2}\frac{\beta^*}{L_R\,(dE_\mu/ds)} \qquad (7)$$

Some properties of the cooling process can be deduced from equations 2—7. The cooling term of Eq. 4 results in exponentially decreasing emittances with a scale length of $L_{cool} = E_\mu/(dE_\mu/dz)$, which implies than an e-folding in cooling requires absorption and reacceleration by $\Delta E_{total} = E_\mu$, as in radiation cooling. To cool before decay

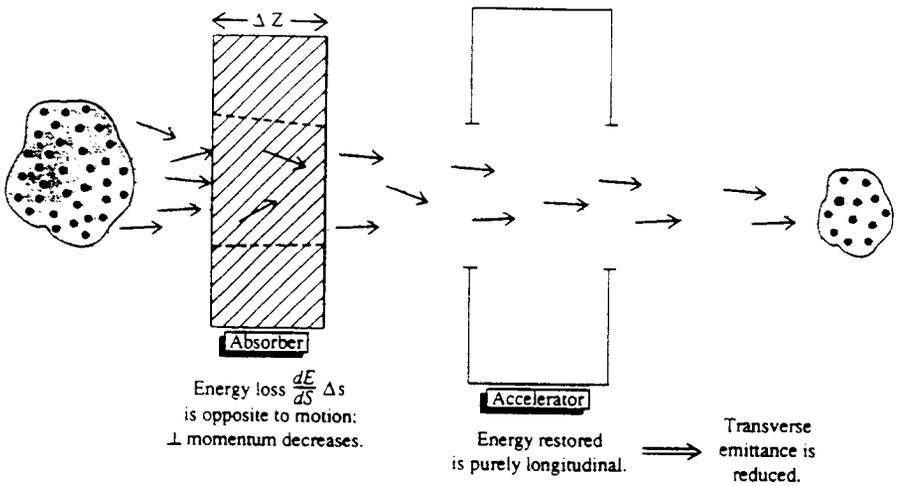

Figure 3. Schematic view of transverse "ionization cooling." Energy loss in an absorber occurs parallel to the motion; therefore transverse momentum is lost with the longitudinal energy loss. Energy gain is longitudinal only; the net result is a decrease in transverse phase-space area.

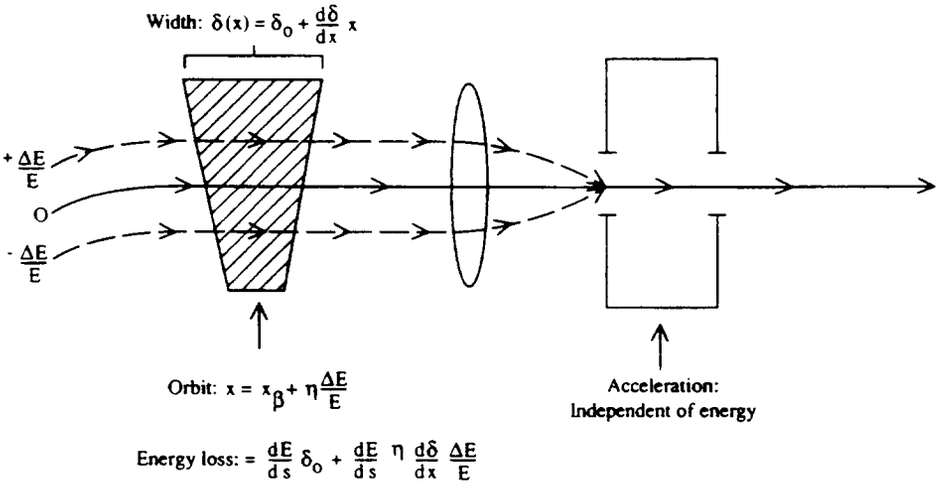

Figure 4. Enhancement of energy cooling by using a wedge absorber placed in a non-zero dispersion region. The thickness of the absorber depends on transverse position ($\delta(x) = \delta_o + (d\delta/dx)\ x$), and the position at the absorber depends on the energy ($x = \eta\ (\Delta E/E) + x_\beta$), producing an enhanced energy dependence of energy loss, decreasing energy spread. Energy recovery in the accelerator is independent of energy. (Transverse cooling decreases with enhanced energy cooling.)

Table 2: Properties of Some Absorber Materials

Material	A	Z	Density gm/cm^2	dE/ds(min) MeV/cm	L_r (rad. length) cm	L_r dE/dz(min) MeV
Li	7	3	0.53	0.70	155	110
Be	9	4	1.85	2.61	35.3	92
C	12	6	2.27	3.57	18.8	67
Al	27	13	2.7	3.8	8.9	34.
Cu	63.5	29	9.0	12.0	1.43	17.2
W	184	74	19.3	21.1	0.35	7.4

it is necessary to have $L_{cool} << L_{decay}$, where $L_{decay} = 660\beta\gamma$ m. $\approx 6250\ E_\mu$(GeV) m. To minimize the heating term, it is desirable to obtain small β^* (strong focusing) at the absorber and to use materials with large $L_R dE_\mu/ds$. $L_R dE_\mu/ds$ is largest for light elements (0.1 GeV for Li, Be but ~0.01 GeV for W, Pb), indicating a desirability of light absorbers. (However, heavier absorbers have larger dE/ds, and therefore shorter cooling lengths.) With current technology (see below), focussing systems obtaining $\beta^* < 1$cm are possible. With $\beta^* \approx 1$ cm, and $L_R dE_\mu/ds \approx 0.1$ GeV, a normalized emittance of $\varepsilon_N \approx 10^{-2}\beta^* \approx 10^{-4}$ m-rad is obtained as a reasonable goal for transverse cooling.

Longitudinal (Energy) Cooling

Longitudinal (energy-spread) cooling is also possible, if the energy loss increases with increasing energy. In passing through an absorber, the energy spread ΔE_μ is reduced by the coherent energy loss following the equation:

$$\Delta E_\mu \rightarrow \Delta E_{\mu,0} - \frac{\partial(dE_\mu/dz)}{\partial E_\mu}\Delta z\ \Delta E_{\mu,0} \tag{8}$$

The derivative $\partial(dE_\mu/dz)/\partial E_\mu$ is steeply negative (heating) for nonrelativistic muons ($E_\mu < 0.3$ GeV), but is weakly positive (cooling) for larger energies, with a maximum of ~0.2 m^{-1} at 0.6 GeV. This cooling term can be compared with the similar emittance cooling term by considering their ratio $R_{E/x} = \partial(dE_\mu/dz)/\partial E_\mu\ /\ (dE_\mu/dz)/E_\mu$. This ratio $R_{E/x}$ is roughly constant for $E_\mu > 0.6$ GeV, with a material-dependent value of ~0.15 (0.125 for Li, 0.175 for U). This indicates the energy cooling is naturally weaker than the emittance cooling. This natural cooling is probably insufficient to obtain the large energy-cooling factors needed in some scenarios.

However, this natural dependence can be enhanced by placing a wedge-shaped absorber at a "non-zero dispersion" region where position is energy-dependent ($x = \eta\ \Delta E/E + x_\beta$), and the absorber is arranged so that higher-energy beam passes through thicker absorber sections (see Fig. 4). The enhanced cooling derivative is:

$$\left(\frac{\partial\frac{dE_\mu}{dz}}{\partial E_\mu}\right)_{total} = f_A\left(\frac{\partial\frac{dE_\mu}{ds}}{\partial E_\mu}\right)_0 + f_A\frac{dE_\mu}{ds}\frac{d\delta}{dx}\frac{\eta}{E_\mu\delta_o} \equiv \frac{\frac{dE_\mu}{dz}}{E_{cool,E}} \tag{9}$$

where η is the dispersion at the absorber, δ_0 and $d\delta/dx = \delta'$ are the thickness and tilt of the absorber. A cooling parameter $E_{cool,E}$ has been introduced for comparison of enhanced cooling rates with emittance cooling rates; it is the total energy of absorption and reacceleration needed to obtain 1/e cooling.

The statistical fluctuations in the number and energy of muon-atom interactions will heat the beam and limit the longitudinal cooling. The energy loss $\Delta E = dE/dz\ \Delta z$ occurs in a number of collisions $N_{coll} = \Delta E/\ \delta E_I$, where δE_I is the mean energy exchange ($\delta E_I \approx f_I I \sim f_I\ 10Z$ eV, where f_I is a multiplifying factor depending on energy absorption statistics.) The energy spread is expected to increase as $\sqrt{N_{coll}}\ \delta E_I$, following :

$$\frac{d\langle(\Delta E)^2\rangle}{dz} \approx \frac{dN_{coll}}{dz}\delta E_I^{\,2} \approx \frac{dE_\mu}{dz}\,\delta E_I \tag{10}$$

Combining cooling and heating effects, an equation for energy cooling is:

$$\frac{d\langle(\Delta E)^2\rangle}{dz} \approx -2\left(\frac{\partial(dE_\mu/dz)}{\partial E_\mu}\right)_{total}\langle(\Delta E)^2\rangle + \frac{dE_\mu}{dz}\,\delta E_I \tag{11}$$

where the derivative with energy combines natural energy dependence with dispersion-enhanced dependence.

Note that using a wedge absorber to increase energy cooling will reduce transverse cooling, through phase-space mixing.[7] In passing through an absorber the total particle position $x_t (x_t = \eta\ \Delta E/E + x_\beta)$ remains constant. Changing ΔE changes x_β, following:

$$\Delta E \rightarrow \Delta E(0) - \frac{dE}{ds}(\delta_0 + \delta' x_t)$$
$$x_\beta \rightarrow x_\beta(0) + \frac{\eta}{E}\frac{dE}{ds}[\delta_0 + \delta'(\eta\frac{\Delta E}{E} + x_\beta)] \quad (12)$$

The thickness variation with position changes the rms beam size ($\Delta\langle x_\beta^2\rangle \approx 2\delta'\eta/E\ dE/ds\langle x_\beta^2\rangle$), which, after averaging over betatron phases, changes the emittance cooling term, following:

$$\Delta\frac{d\varepsilon_x}{dz} = \frac{\eta\delta' dE_\mu}{E\delta_0 dz}\varepsilon_x \quad (13)$$

This heating term is exactly the opposite of the energy cooling enhancement term. The sum of the cooling rates however is an invariant (as in radiation cooling) :

$$\frac{1}{E_{cool,x}} + \frac{1}{E_{cool,y}} + \frac{1}{E_{cool,\Delta E}} = \text{Constant} \approx \frac{2.15}{E_\mu} \quad (14)$$

With some cooling enhancement, and including the heating terms (eq. 11), it appears possible to cool 1 GeV μ-beams to $\Delta E/E \leq 10^{-3}$. Synchrotron oscillations and/or rf compression can then rotate the reduced energy spread to obtain reduced bunch lengths needed in some scenarios.

Cooling Constraints and Scenarios

Implementation of ionization cooling requires high-acceptance beam transport containing both material-absorber and acceleration sections. This can be implemented in storage-ring, linac and/or recirculating-linac configurations. The critical constraint is that cooling must be completed within a fraction of the muon lifetime ($2.2 \times 10^{-6}\gamma$ s), which is a path length of $L_\mu = 660\beta\gamma$ m or $300\bar{B}$ (T) turns in a storage ring, where $\bar{B}$ is the mean bending field. Also, since cooling by e^{-1} requires E_μ energy loss and recovery, and many e-foldings are needed for effective cooling, we require that the energy loss and recovery rate in the transport be much greater than $(E_\mu/L_\mu) = 0.15$ MeV/m, independent of energy. This independence implies that there is no sharp optimum in choice of cooling energy, except the beam must be relativistic for energy cooling ($E_\mu > 0.3$ GeV), and that higher cooling energies require longer cooling distances. We can choose $E_\mu = 1$ GeV as a reference case.

Obtaining $\Delta E/\Delta l >> 0.15$ MeV/m is easy to obtain within absorbers and acceleration cavities. The dominant space constraints come from other transport requirements, such as space for bending magnets and beam focussing. Transverse cooling requires strong focusing of the beam to small β^* at the absorber, which implies a need for strong and possibly long focusing elements. The depth of focus condition implies that each absorber section must also be shorter than $\sim\beta^*$, unless the absorber is an active, strong-focussing element, and this may imply a transport with relatively long matching sections between short absorbers. We discuss three possible approaches to the focusing lattice problem:

1 - Magnetic quadrupole focusing: Conventional or superconducting quadrupoles can be arranged to obtain low-β^* at absorbers, using optics similar to those used for collider low-β^* interaction points. Figure 5A shows an example absorber-transport cell, which has a five-quad OFDFDFO layout. In an example which is suitable for μ-cooling, this layout can be used to obtain β^* as small as 1cm in a cell with 1m half-length. (Other example cell parameters include: $\beta_{max} \approx 75$m (at $\beta^* = 1$cm) , quad strength $B'/B\rho = 15$ m^{-2} or 50 T/m for 1 GeV/c μ's.) However the cell magnifies the μ-transport scale from the absorber length (~cm) to the cell length (~m), reducing the effective energy loss rate from 2.6 MeV/cm to 2.6 MeV/m (for Be). This is acceptable, but much further dilution (in stronger-focusing) would probably not be acceptable.

2 - Metal-lens absorbers: The depth of focus constraint on the absorber lengths can be avoided by using an actively focusing absorber such as a high-current conductor, similar to the Li lenses used in $\bar{p}$-sources,[16] and these conductors are naturally strong-focusing devices. (see figure 5B) A conductor focuses radially (both x and y) and

can maintain the beam at small β^* indefinitely, provided the focusing is greater than the beam divergence, or:

$$\frac{B'}{B\rho} = \frac{\mu_0 I}{2\pi a_0} \geq \frac{1}{\beta^{*2}} \tag{15}$$

where I, a_0 are the absorber current and radius, $\mu_0 = 4\pi \times 10^{-7}$ (MKS), $B\rho$ is the magnetic rigidity (3.3 T-m for 1 GeV/c), and B' is the field gradient. For example, $\beta^* = 2$cm can be maintained at 1 GeV/c with B' =8000T/m (16T at a_0= 2mm), parameters similar to those of existing Li lenses. A Be lens (higher conductivity and melting point) and/or a liquid-metal lens could achieve even smaller β^*. Conducting lens-absorbers will probably be part of any practical cooling scheme, because of the natural match to the concurrent requirements of energy absorption and strong focusing.

3 - Plasma lens focusing: Because of multiple scattering, metal-lenses must be placed only at small β^*, and that limits performance. Very-strong high-current radial focusing can also be obtained with plasma lenses, and their relatively-low density limits multiple scattering effects. The focusing strength K in a plasma lens is given by:

$$K = \frac{B'}{B\rho} = \frac{2\pi r_\mu}{\gamma} n_p \tag{16}$$

where r_μ is the classical muon radius, and n_p is the plasma (or beam) density for an underdense (or overdense) plasma lens. At projected densities of $n_p \approx 10^{22\text{-}23}$ m^{-3}, $K \approx 10^{5\text{-}6} m^{-2}$ (at γ = 10), which is orders of magnitude stronger than metal-lens or magnetic focusing. Barletta[17] has suggested incorporating plasma lenses between absorbers in a cooling channel (see Fig. 5C). Smaller β^* (< 1 mm) within shorter distances should be possible.

Further research on these focusing methods and detailed scenario development is needed before optimum solutions incorporating these and/or other methods can be obtained.

Other μ-Cooling Methods

Ionization cooling of relativistic muons may not be the only or best method of μ-cooling. Other possibilties were discussed at the workshops, and these include:

1. Stopped μ-beams: A low-energy source can produce large numbers of stopped π's, which decay producing 30 MeV/c μ's (4MeV), which can lose more energy in the absorber, forming a slow-μ beam (keV), which may be extractable for acceleration. Nagamine[18] has suggested using a "surface-muon" source, in which muons are stopped and trapped near the surface (in muonium (μ^+)or muonic atoms ($d\mu^-$)), from which they can be emitted (thermally or laser-ionized) for acceleration. The major inefficiency is in obtaining stopping close enough to the surface to permit emission. The resulting beam is very cold, but current techniques obtain only < 10^{-7} μ/p.

2. Stochastic μ-cooling has been discussed by Ruggiero.[19] The limitation is that the cooling rate must be less than $W/N_{\mu c}$ where W is the bandwidth and $N_{\mu c}$ is the number of muons in the cooling system, and this cooling rate must be much greater than the decay rate. With W ≈ 10 GHz with present technology, $N_{\mu c}$ must be relatively small. The muons could be split up into many small bunchlets (with $N_{\mu c} \approx 10^3$–10^4) for cooling. However, either the bunchlets must then be combined or a many-bunchlet (highly-cooled) μ-collider scenario must be used. Cooling power requirements also appear formidable.

Bunch Combination and Compression Techniques

The scenarios of Table 1 envision colliding a few μ-collider bunches, but these bunches were produced from HEH proton bunches extracted from a rapid cycling synchrotron (RCS), which would hold ~100—200 bunches/turn. A major problem in longitudinal space is in combining the RCS bunches to the few μ-collider bunches. Phase-space manipulations with cooling will be needed. Bunch combination procedures could include:

1. Proton-bunch Overlap: Before extraction from the RCS, the proton bunches can be compressed with a lower harmonic (or sideband) rf system to provide spatially overlapping bunches (with different momenta) onto the π-production target. Since target spot sizes need not be very small and π-production is not very energy-dependent, a broad primary energy spread can be accepted at the target, with no degradation of π-production. Combination by

a factor of ~10 should be obtainable. (A separate extraction-energy proton compressor ring for the rf bunch manipulations may be desired.)

2. Non-Liouvillian "Decay-stacking"[20]: Bunch-combination without phase-space dilution can occur during π-decay, by "decay-stacking" into a μ-storage ring, as shown in figure 6. In this process a train of π-bunches from a hadronic target is injected into a decay channel, which is also a zero-dispersion straight-section of a μ-storage ring. The π-bunch spacing is matched to the storage ring period (or a low harmonic) and successive π-bunch arrivals are timed to overlap an accumulating μ-bunch. π decays that produce μ's within the ring momentum acceptance add to the μ-bunch. At reasonable parameters, μ's from 10—30 π-bunches can be accumulated in a single bunch, without large μ-decay losses. (The storage ring can also be used for cooling the accumulated μ's.)

3. Beam Cooling with Bunch Combination: Transverse or energy cooling of μ-bunches can compress beams to a degree where bunches can be stacked together, using conventional Liouvillian bunch-combination optics. The stacked bunch can then be further cooled to a phase-space volume $\leq$ the previous cooled single-bunch size. The process can continue through several stacking and cooling steps.

Some combination of these three (plus other to-be-developed) methods can be used to reduce the number of μ bunches to a few enhanced-intensity bunches. (The first two procedures are complementary: proton bunch stacking combines nearby bunches while decay stacking more naturally combines widely spaced bunches.) Ionization cooling can then be used for further compression, in bunch-length or energy-spread, for collider use.

Concluding Comments

We have outlined some useful concepts toward obtaining cooled muon beams at high-intensities. Substantially more design, invention, optimization and development work is needed to obtain a practical collider scenario. More experimental development is also needed on μ-production and cooling. The observation of $>10^7$ parasitic stored μ's in the $\bar{p}$-debuncher[21] can be extended to an optimization experiment. A wedge-absorber experiment to reduce μ momentum spread could be attempted as a first step toward cooling. A low-energy e^--cooling demonstration is a possibility. Improvement and development of these concepts will continue during the present Beam Cooling Workshop.

I thank D. Cline, A. Ruggiero, J. D. Bjorken, S. Glashow, H. A. Thiessen, P. Channell, R. Palmer and R. Noble (and any others I forgot) for important conversations contributing to the ideas expressed in this paper. This work was suppported by US DOE contract #DE-AC05-84ER40150.

References

1. M. Tigner, in Advanced Accelerator Concepts, Port Jefferson, NY 1992, AIP Conf. Proc. 279, 1 (1993).
2. P. Chen and K. T. MacDonald, in AIP Conf. Proc. 279, 853 (1993).
3. Proceedings of the Mini-Workshop on μ^+-μ^- Colliders: Particle Physics and Design, Napa CA, to be published in Nucl Inst. and Meth. A (1993).
4. Proceedings of the Muon Collider Workshop, February 22, 1993, Los Alamos National Laboratory Report LA-UR-93-866 (1993).
5. D. Cline, unpublished communication (1992).
6. initial speculations on ionization cooling have been variously attributed to G. O'Neill and/or G. Budker .
7. D. Neuffer, Particle Accelerators, 14, 75 (1983), D. Neuffer, Proc. 12th Int. Conf. on High Energy Accelerators, F. T. Cole and R. Donaldson, eds., 481 (1983), D. Neuffer, in Advanced Accelerator Concepts, AIP Conf. Proc. 156, 201 (1987).
8. E. A. Perevedentsev and A. N. Skrinsky, Proc. 12th Int. Conf. on High Energy Accelerators, F. T. Cole and R. Donaldson, eds., 485 (1983).
9. R. Noble, in Advanced. Accelerator Concepts, Port Jefferson, NY 1992, AIP Conf. Proc. 279, 949 (1993).
10. C. L. Wang, Phys Rev D9, 2609 (1973) and Phys. Rev. D10, 3876 (1974).
11. H. Grote, R. Hagedorn, and J. Ranft, Particle Spectra (CERN, Geneva, 1970).
12. G. Silvestrov, Proceedings of the Muon Collider Workshop, February 22, 1993, Los Alamos National Laboratory Report LA-UR-93-866 (1993).
13. W. Barletta and A. Sessler, in Proceedings of the Mini-Workshop on μ^+-μ^- Colliders: Particle Physics and Design, Napa CA, to be published in Nucl Inst. and Meth.(1993).
14. U. Fano, Ann. Rev. Nucl. Sci. 13, 1 (1963).

15. V. L Highland, Nucl. Inst. and Meth. 129, 497 (1975) and Nucl Inst. and Meth. 161, 171(1979).
16. B. Bayanov, J. Petrov, G. Silvestrov, J. MacLachlan, and G. Nicholls, Nucl. Inst. and Meth. 190, 9 (1981).
17. W. Barletta, private communication (1993); see also Barletta et al. "Plasma Lens Experiments at the Final Focus Test Beam" to appear in Proc. of the 1993 Particle Accelerator Conference (1993).
18. K. Nagamine, private communication(1987), and K. Nagamine and K. Ishida, Perspectives of Meson Science, Chapter 11 (1992).
19. A. G. Ruggiero, in Advanced. Accelerator Concepts, Port Jefferson, NY 1992, AIP Conf. Proc. 279, 958 (1993).
20. D. Neuffer, IEEE Trans. NS-28, 2034 (1981).
21. A. Bross, M. Gormley, Y. Ho, C. Kim, W. Lee, E. Mannel, M. Murtagh, S. O'Day, H. Park, Nucl. Inst. and Meth. in Physics Research A 332, 27-31 (1993).

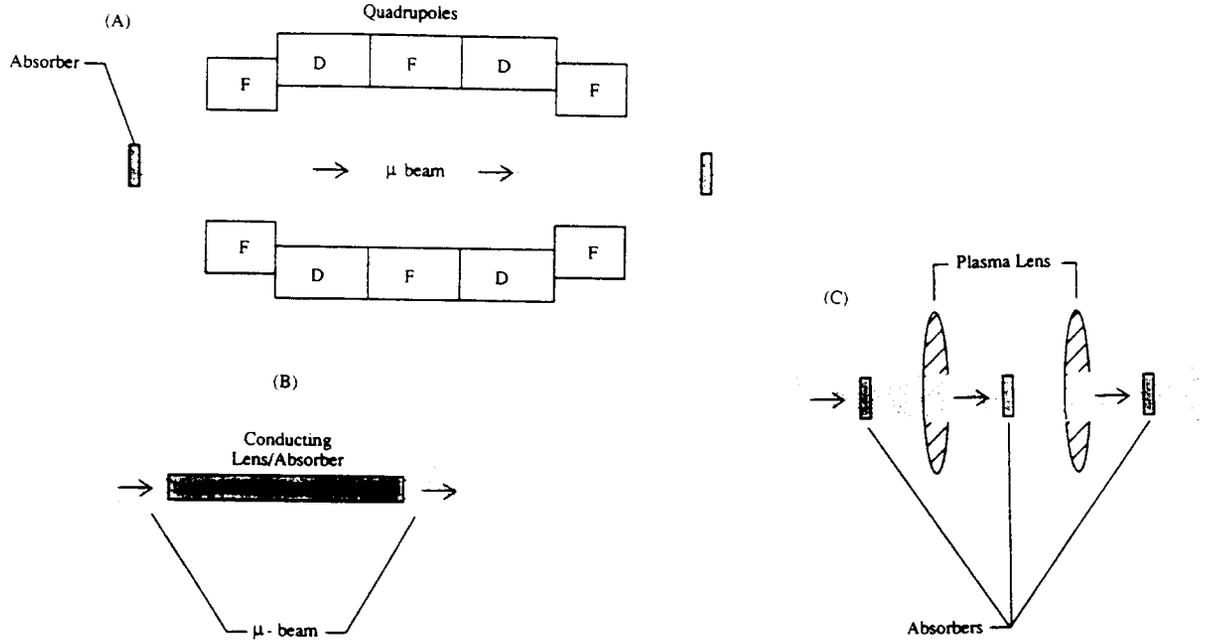

Figure 5 A) A transport cell for ionization cooling, with five quadrupoles/cell (FDFDF) focusing the beam to small β^* (small beam size) at the absorbers; the cooling system would contain many cells. B) Use of a metal lens/absorber to contain the beam at small β^* for extended distances. C) Two transport cells with radially focusing plasma lenses to obtain small β^* at absorbers in a compact structure.

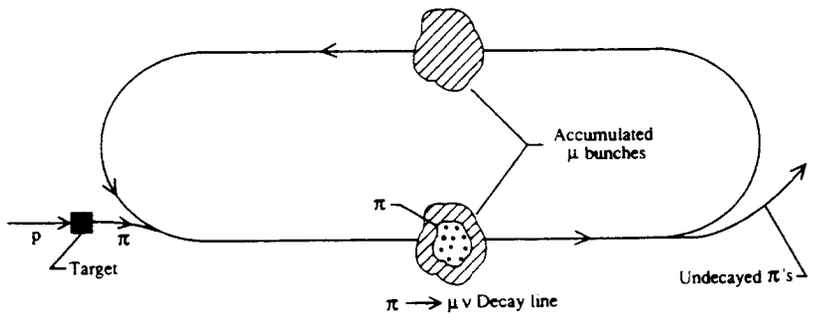

Figure 6. Schematic view of "decay-stacking" into a storage ring. A train of p-bunches produces π-bunches, which are injected into a storage ring for multi-turn stacking. The initial spacing is matched to a ring harmonic (h=2 in the figure), so that following π-bunches overlap accumulated μ's from previous bunches. π-decays in the straight section which produce μ's within the ring acceptance add to the accumulation. (Note that the short but finite π lifetime is nearly optimally matched to make this scheme practical.)

MEDIUM AND HIGH ENERGY ELECTRON COOLING

Tim Ellison
IUCF - 2401 Milo Sampson Ln., Bloomington IN 47405

ABSTRACT

Electron cooling in the medium and high energy regimes may be an overlooked technology. Medium energy electron cooling system provide economically-justifiable improvements in the performance of many existing and proposed rings; high energy electron cooling could be of benefit to high energy heavy ions colliders, such as RHIC. This paper reviews the projected performance of electron coolers in the medium and high energy regimes. The status of the development of the technology needed for medium energy electron cooling is briefly discussed. A number of possible applications of medium energy electron cooling systems for use in existing and proposed rings are summarized, and a design of a system for RHIC is used to illustrate electron cooling in the high energy regime.

1. INTRODUCTION

I begin with my classification scheme for low, medium or intermediate, and high energy electron cooling systems. All systems built to date would be classified as *low energy* systems. These systems are characterized by the use of a conventional Cockcroft-Walton (C−W) power supply to bias the cathode with respect to the cooling region, and by a continuous longitudinal (solenoidal) magnetic field to confine (focus) the electron beam. With the exception of increased electron beam energies, the movement to non-resonant-focussing electron guns, and the possible future use of adiabatic electron beam expansion to obtain lower electron beam temperatures, this technology is almost indistinguishable from the original Novosibirsk design[1] -- a great tribute to its designers.

Compact commercial C−W voltage generators are limited to about 0.6 − 1 MV, about a factor of 2 − 3 times higher than the IUCF, CELSIUS, and GSI electron systems; this is the principal technical limitation in the low energy regime. In the *medium energy* regime Pelletron electrostatic accelerators, having an operating range of about 2 − 20 MV, would replace the C−W generators. In this regime the continuous longitudinal magnetic field is no longer necessary for focussing, though such a scheme cannot be entirely ruled out. The beam focussing requirements in the medium energy regime are discussed in more detail in section 3.2.

In the *high energy* regime, the single-pass recirculating electron technology, which would provide $> 99\%$ beam energy recovery and $> 99.99\%$ current recovery in the medium energy regime, no longer works; instead the electrons must be stored in a ring (the power requirement alone -- a few amperes times hundreds of MeV -- rules out the possibility of a linac). One might ask whether the medium energy regime even exists -- could not one go immediately from the low energy technology directly to storage ring technology? The answer is no: as will be discussed in later sections, the performance of a Pelletron-based medium energy cooler would be far superior to that of a storage ring due to the electron storage ring space charge tune shift and radiation damping time limitations.

In section 2 an expression for the cooling time is presented; later in sections 3 and 4 the relativistic scaling of this expression is explored for the medium and high energy regimes making assumptions concerning the technical limitations which would apply. In section 3 the status of the technological development necessary for the medium energy regime is summarized. This regime is illustrated with a number of applications for existing and proposed rings. Section 4 discusses electron cooling in the high energy regime; the possibility of using electron cooling in RHIC to counteract intrabeam scattering (IBS) in heavy fully-ionized ion beams is explored.

2. COOLING RATES

For all regimes I will use the following relation to estimate the transverse emittance damping time, $\tau \equiv \epsilon_I / (d\epsilon_I / dt)$:

$$\tau = \frac{A}{Z^2} \frac{\beta\gamma^2}{4\eta\Lambda} \frac{M}{m} \left(\frac{r_b}{r_e}\right)^2 \left(\frac{kT}{mc^2}\right)^{3/2} \frac{e}{I_e} \left[\left(\beta\gamma \frac{\epsilon_I}{\beta_I} \frac{mc^2}{kT} + \beta \frac{\Delta p}{p} \sqrt{\frac{mc^2}{kT}} \right)^{3/2} + \sqrt{\frac{8}{\pi}} \right] \qquad (1)$$

where A and Ze are the ion atomic number and charge, respectively; β and γ are the usual relativistic parameters and β_I is the beta function, or the ratio of the ion beam size to its divergence, in the cooling region; η is length of the cooling region, L_c, divided by the ion storage ring circumference, C; Λ is the coulomb logarithm ≈ 10; M and m are the proton and electron mass, respectively, and c is the speed of light; r_e is the classical electron radius and r_b is the electron beam radius; T is the electron beam temperature and k is the Boltzmann constant; I_e is the electron current; ϵ_I will *always* be the *rms normalized* beam transverse emittance, and the subscripts I and e will refer to the ion and electron beams, respectively; finally, $\Delta p/p$ is the ion beam relative rms momentum spread. This analytical relation provides a reasonably good fit to a numerical calculation[2] of the cooling time using the simple nonmagnetized model for cooling. The model assumes a flattened electron velocity distribution, and accounts for both synchrotron and betatron oscillations[a]; τ is strictly an exponential damping time only in the regime where the addend $(8/\pi)^{1/2}$ dominates the last factor in Eq. (1).

The relativistic scaling is, well, relative! Two different sets of assumptions can lead to very different scaling relations, for example, $\tau \propto \beta\gamma^2$ or $\tau \propto \beta^4\gamma^6$. Both relations assume that I_e and η remain constant with energy. The first relationship results from the additional assumption of constant temperature beams (i.e., a constant *normalized* emittance and transverse beam size); the second assumes a constant *non-normalized* emittance and constant beta functions. Below we investigate these scaling laws for both the medium and high energy regimes. We shall also see that the relativistic scaling is *not* continuous when crossing from one regime to another, and that even within a single regime the scaling law is a function of the beam energy and intensity.

3. The Medium Energy Regime

3.1 Relativistic Scaling in the Medium Energy Regime

We assume that the electron gun design is independent of the beam energy[b] and that the electron beam can be adiabatically accelerated. Consequently, I_e, r_c (the cathode radius), and kT_c (the cathode temperature) are independent of the beam energy. We also assume that η remains constant. In the regime $\theta_I \ll \theta_e$ (i.e. $\beta\gamma\epsilon_I/\beta_I \ll kT/mc^2$), where θ_I and θ_e are the ion and electron beam angular divergences, we find $\tau \propto \beta\gamma^2$ assuming that we keep r_b constant; one factor of γ results from time dilation, and a factor of $\beta\gamma$ results from the reduction in the rest frame electron density for constant current. In this regime the cooling time depends strongly on the electron beam temperature ($\propto T^{3/2} = T_c^{3/2} r_c^3 / r_b^3$) and can always be decreased by increasing the electron beam radius (adiabatic expansion):

$$\tau \propto \beta\gamma^2 T_c^{3/2} \frac{r_c^3}{r_b}, \qquad (\theta_I < \theta_e) . \qquad (2)$$

In the regime where $\theta_I \gg \theta_e$, however, the cooling time also depends strongly upon the manner in which the ion beam emittance and the cooling region beta functions are scaled. In this regime we assume that the

---

[a]Note that when considering the betatron and synchrotron motion the *transverse* cooling time increases as the cube of rest frame transverse velocity, but only as the three halves power of the rest frame longitudinal velocity.

[b]One actually finds that, due to focussing constraints, the electron beam current needs to be reduced $\propto (\beta\gamma)^2$ for electron energies less than about 2 MeV in a variable energy machine.

electron beam size scales in proportion to the ion beam size, $r_b^2 \propto \beta_I \epsilon_I / \beta\gamma$. This set of assumptions yields:

$$\tau \propto \beta^{3/2}\gamma^{5/2} \frac{\epsilon_I^{5/2}}{\beta_I^{1/2}}, \quad (\theta_I > \theta_e) . \tag{3}$$

Thus for constant ϵ_I and β_I, $\tau \propto \beta^{3/2}\gamma^{5/2}$; such would be the case for cooling in a variable-energy machine assuming that the ion beam were adiabatically accelerated. Alternately if we increase $\beta_I \propto \beta\gamma$, thus keeping the ion beam size and consequently temperature constant, we would again have $\tau \propto \beta\gamma^2$; such might be the case if comparing the performance of a cooling system in different rings within a chain of accelerators where the beam is adiabatically accelerated, since it is reasonable to assume that $\beta_I \propto L_c \propto \eta$ ($C \propto \beta\gamma$).

If instead we kept the non-normalized beam emittance constant, we would have $\tau \propto \beta^4\gamma^6/\beta_I$; such might be the case if investigating the cooling of a variable energy antiproton beam emerging from a target and injected into a ring with a fixed lattice and aperture, though it is difficult to imagine a large range of $\beta\gamma$ in this situation.

3.2 Focussing Requirements in the Medium Energy Regime

The simplest electron focussing channel in the cooling region is a series of very weak solenoids[3] with focal length f_{sol} spaced by the distance L_{sol}. From here on we assume the radius of the uniform electron distribution is $\sqrt{2}$ times the rms radius of the normal ion distribution, and $\epsilon_e \leq \epsilon_I$ before cooling. The magnetic confinement system maintains the space charge (rather than emittance) dominated beam divergence to a value less than the incoherent divergence due to the beam temperature. This condition then determines both f_{sol} and L_{sol}:

$$f_{sol} > \frac{\beta_I}{\sqrt{2}} > L_{sol} = \frac{2\bar{\lambda}^2}{f_{sol}} = \sqrt{2}\,(\beta\gamma)^2 \frac{\epsilon_I}{r_e} \frac{ec}{I_e} \tag{4}$$

where λ-bar is the electron beam plasma wavelength divided by 2π (i.e., $\beta c/\omega_p$, where ω_p is the plasma frequency). Note that L_{sol} is independent of β_I.

If the electron beam radius (or divergence) is not properly matched to this focussing channel, it will oscillate around the equilibrium size at the plasma frequency. The effective temperature due to this mismatch is then merely $m(\Delta r_b w_p{}^*)^2/4$; typically $\lambda > L_c$, and Δr_b can be $\approx 0.1 r_b$ before the effective temperature becomes significant. Consequently, 3 or 4 profile monitors can be used to resolve the "sine" and "cosine" like amplitudes to provide feedback for correcting any mismatch.

Neglecting obvious limits to size of β_I, such as magnet apertures, β_I is limited by the precision of the beam position monitors used for the relative alignment of the electron and ion beams. Assuming the position electrodes are located inside the solenoids and have an rms resolution δ, the angular misalignment can be limited to $2\delta/L_{sol}$ thus limiting β_I as:

$$\beta_I < \beta^3\gamma^3 \left(\frac{ec}{I_e r_e}\right)^2 \frac{\epsilon_I^3}{\delta^2} . \tag{5}$$

A three dimensional particle tracking study has shown that the electron beam, with a uniform spatial distribution and Gaussian angular distribution, develops small tails and a slight amount of hollowness in this transport system; the emittance growth, however, is negligible. Since a solenoid is a second order focussing element, the focal length for ions is $(AM/Zm)^2$ times greater than for the electrons. The ion beam tune shift and betatron plane coupling is consequently negligible. The ion beam space charge can, however, adversely affect the less rigid electron beam and provisions must be made to prevent space charge neutralization of the electron beam. Since the electrons on the outer radius of the electron beam are given an angular kick which is the same as the beam angular spread due to the cathode temperature, the solenoid aberrations are unimportant. Quadrupole triplets could be used in place of solenoids[4]; these ion optical elements, however, require more insertion space and have a larger effect upon the ion beam.

Low energy electron cooling systems use a continuous solenoidal field to confine the electron beam. The electrostatic repulsion causes the electron beam radius to expand fractionally by an amount Δr_b, given by:

$$\Delta r_b = r_c \frac{\Omega^*}{\omega_c^*} = 2\pi r_b \frac{n_e^* r_e c^2}{\omega_c^{*2}} \tag{6}$$

where r_c is the cathode radius, Ω the beam angular rotation frequency due to the $(\mathbf{E} \times \mathbf{B})/B^2$ drift where $\mathbf{E}$ is the radial electric field due to the electron space charge and $\mathbf{B}$ is the solenoidal field strength; ω_c is the cyclotron frequency, n_e the electron density, and the superscript * refers to the value in the moving frame. The energy gained by particles due to this expansion, $E\Delta r_b$, is transformed into beam rotation such that the resulting Lorentz focussing force exactly cancels the defocussing space charge force. This effective transverse temperature, increasing with the square of the distance from the beam axis, scales $\propto 1/\gamma$ for a constant electron beam current density. It has been suggested[5] that this same technique could be used in the medium energy regime. It does not seem feasible to inject the beam into this solenoidal confinement field after being accelerated in a field free region since the acquired beam temperature would be $\approx (\omega_c r_b /c)mc^2/8$, a value equal to the cathode temperature for a 4 mm radius beam only if the confinement field is less than 5 Gauss! This puts one in the regime where $\omega_c \approx \omega_p$; the focussing would not be strong enough, and such a beam may be quite susceptible to instabilities. Consequently it would be necessary to have the solenoidal confinement field surround the entire cooling system, including the inside of the Pelletron accelerator. Although very weak fields are needed to confine the electron beam at high energies ($\approx 0.1\ \mathrm{T}/\gamma$), fields of about 0.1 T may still be necessary in the gun and collector regions, since in the medium energy regime small beams are required and adiabatic expansion is probably not an option. Although such a Pelletron may be constructed[6], such a system would be inelegant, consume a large amount of power, and be difficult to service. There is the additional problem of adiabatic transport which I have not considered.

3.3. Status of Technology

The Luis Elias and Gerry Ramian, U. of California--Santa Barbara (UCSB), first proposed and demonstrated Pelletron-based *pulsed* electron recirculation in the early 1980's using a 3 MV Pelletron at the National Electrostatics Corporation (NEC). In 1984, a 6 MV version began operation as a FEL driver in Santa Barbara[7]. The UCSB system reports extremely good reliability, operating for over 1 year without opening the Pelletron for servicing[8]. A U. of Wisconsin, FNAL and NEC collaboration proposed using this technology

Table I. Pelletron-based electron recirculation systems.

System	Energy (MeV)	Current (A)	DC Pulsed	Collection Efficiency (%)	Year
UCSB	2.5	1.25	Pulsed	99.4	1983
	3	1.25	Pulsed	97	1985
	6	1-3	Pulsed	99.7	1993
NEC	2	0.12	DC	99.99	1989
CREOL	0.9	0.20	DC/Pulsed	99.9	(1994)
	1.7	0.20	DC/Pulsed	99.9	
IUCF/NEC Test System	2	1-2	DC	> 99.995	(1994)

for electron cooling[9], and using the prototype UCSB system at NEC, measured the emittance of a 2.5 and 3 MeV electron beam to be, within errors, equal to the emittance at the cathode. The UCSB group reports similar adiabatic acceleration[7][10]. The U. of Wisconsin collaboration later demonstrated *DC* recirculation of a 0.12 A electron beam[11]. As can be seen in the next section, such a beam is suitable for cooling medium energy heavy ion beams, such as in the proposed KEK PS-Collider or low energy beams in RHIC. Elias, now at CREOL, is building a 1.7 MV machine which will operate with DC beams, and produce kW's of laser power with 10−30% wall power efficiency[12][13]. More recently, an IUCF collaboration has been retro-fitting the NEC Pelletron to demonstrate DC recirculation of multi-ampere electron beams[14]; this project is on hold due to a lack of funding.

3.4 Examples of Medium Energy Electron Cooling Systems

Table I summarizes 5 possible applications of intermediate energy electron cooling. In most cases these systems are not optimized, but rather designed to fit into existing lattices.

The system for CoSy[15], a ring being commissioned at KFA-Jülich, would fit into 1 of the 4 straight sections currently reserved for stochastic cooling. The electron system would cool beams approximately 10 times faster to much smaller equilibrium emittances than could the stochastic system. It is necessary to reduce

Table II. Proposed intermediate energy electron cooling systems.

Parameter	Symbol	CoSy	KEK-PS	Petra II	MEB-1	MEB-2	Units
Ring Properties							
Circumference	C	0.1835	0.283	2.3	3.96	3.96	km
Cooling region length	L_c	4	3.5	50	25	40	m
Fraction (L_c/C)	η	2.2×10^{-2}	1.2×10^{-2}	2.2×10^{-2}	6.3×10^{-3}	1×10^{-2}	
Cool region beta funct.	β_I	8	10	40	50_x; 20_y	100	m
Ion Beam Properties							
Ion species	H^+	H^+	$^{197}Au^{79+}$	H^+	H^+		
Momentum/nucleon	p	3.2	5; 8	8.4	13		GeV/c
Norm rms emittance	ϵ_I	2.5	2	4	0.70		π μm
Rms mom. sprd.	$\Delta p/p$	1×10^{-3}	4×10^{-4}	5×10^{-4}	2×10^{-4}		
Peak ion current	$I_{I,\,peak}$		$Z \times 1.6$	1,000	800		mA
Lasslet tune shift	ΔQ_{SC}		$8; 3 \times 10^{-4}$	0.03	0.07		
Beam-beam tune shift	$\Delta Q_{b\text{-}b}$		1×10^{-5}		8.6×10^{-4}		
Electron Cooling System Parameters							
Electron current	I_e	2	2	2	2	2	A
Electron kinetic energy	U	1.3	2.2; 3.8	4.1	6	6	MeV
Cathode radius	r_c	3.2	3.2	3.2	3.2	3.2	mm
Electron beam radius	r_b	3.2	3.2	4.2	3.2	4.5	mm
Electron temperature	T_e	0.12	0.12	0.07	0.12	0.06	eV/k
Solenoid focal length	f_{sol}	5	none	28.4	19	91	m
Solenoid spacing	L_{sol}	1	none	2.5	6	2	m
Emittance damp. time	τ						s
initial		6	0.4; 1.2	35	100	30	
for cold beams		0.5	0.05; 0.13	5	35	20	
Approximate cost		1	2	4	6.5	6.5	M$

$I_e \sim (\beta\gamma)^2$ as the proton beam momentum is reduced from its rigidity limit of 3.3 GeV/c due to fixed L_{sol}; τ, however, remains almost constant.

Cooling would be extremely fast in the proposed KEK-PS[16] heavy ion collider due to the A/Z^2 scaling of the cooling time and relatively low beam energy. This system would counteract intrabeam scattering consequently increasing the luminosity by a factor of $\approx$ 10.

The emittance of proton beams in HERA is limited by space charge effects in the first synchrotron, DESY III. In the following ring, PETRA II, $\Delta Q_{SC} \approx 0.03$; consequently the emittance could be reduced by $\approx \times 10$ in about 1/3 the ring ramp time, 108 s.

Cooling in the SSC MEB has been investigated in great detail[17]. MEB-I is a design which leaves the ring lattice entirely unmodified; MEB-II re-arranges the ordering of a few elements in the long straight insertion to increase β_I and L_C.

A medium energy system should also be considered for cooling heavy ion beams in RHIC with energy less than $\approx$ 40 MeV/n. The cooling time would be similar to those projected for the PS-Collider, γ(0.01 to 0.1 s). Such a system could counteract emittance growth due to IBS and could potentially provide order of magnitude increases in the machine luminosity. Such a system would also nicely complement the high energy electron cooling system discussed in the following section.

4. THE HIGH ENERGY REGIME

High energy electron cooling was proposed as early as 1978[18][19][20]. Ruggiero [17] presented a scenario for cooling high energy protons at FNAL and CERN which is very similar to what I present below for cooling heavy ions at RHIC. I first discuss the relativistic scaling in the high energy regime, then consider cooling heavy ions at RHIC.

4.1 Relativistic Scaling in the High Energy Regime

I will use a different set of assumptions for scaling τ in the high energy regime, beginning with a first order optimization by assuming that the electron and proton beams have the same emittance and size (i.e., $r_b^2 = \beta_I \epsilon_I / \beta\gamma$, and $kT = \beta\gamma mc^2 \epsilon_I / \beta_I$). The electron beam current is no longer constant, as in the low and medium energy regimes, but is instead limited by its space charge tune shift, ΔQ_{SC}, given by:

$$\Delta Q_{SC} = \frac{1}{4\pi(\beta\gamma)^2} \frac{r_e}{\epsilon_e} \frac{I_e C_e}{ec} \tag{7}$$

where C_e is the electron ring circumference. Assuming a fairly compact electron ring, such that $C_e \approx 3L_c = 3\eta C$, and substituting Eq. (7) into Eq. (1), we obtain the following expression for the cooling time:

$$\tau \approx 0.15 \frac{A}{Z^2} \frac{1}{\Delta Q_{SC} \Lambda} \left(\frac{\gamma}{\beta}\right)^{1/2} \frac{M}{m} \left(\frac{\epsilon_I^3}{\beta_I r_e^2}\right)^{1/2} \frac{C}{c} \tag{8}$$

Since at high energies we expect $C \propto \beta\gamma$, and $\beta_I \propto (\beta\gamma)^{1/2}$ or $\gamma\beta$, we thus have $\tau \propto \beta^{1/4}\gamma^{5/4}\epsilon_I^{3/2}$ or $\tau \propto \gamma\epsilon_I^{3/2}$, an almost linear dependence with energy. Note that there is no longer any η dependence since ΔQ_{SC} is fixed: any increase in L_c must be offset by a decrease in I_e. Using some reasonable values for large rings ($C \approx 20\beta\gamma$ m, and $\beta_I \propto 0.5\,(\beta\gamma)^{1/2}$ m) we can rewrite Eq. (8) as:

$$\tau \approx \frac{A}{Z^2 \Delta Q_{SC}} \left[\beta\gamma^5 \left(\frac{\epsilon_I}{1\,\pi\mu\text{m}}\right)^6\right]^{1/4} \text{s}. \tag{9}$$

The ΔQ_{SC} limitation in the high energy regime makes clear the need for the Pelletron solution in the medium energy regime. One can easily envision a 2 A electron beam with a 1 $\pi\mu$m emittance[c] in either the low or medium energy regime. If we set η to 0.1, and again assume $C \approx 20\beta\gamma$ m, ΔQ_{SC} for this beam would be $\approx 60/\beta\gamma$! Consequently we can see that the high energy scenario *cannot* compete with the medium energy scenario for any energy within the range of the Pelletron. In the *low* and *medium energy* regimes the electron beam current density is limited by the current density at the cathode; in the *high energy* regime, the electron current density is limited by the space charge tune shift in the electron ring. One consequently sees that relativistic scaling relations, in general, can be used only within a the range of a single technical regime. The electron beams in low and medium energy electron cooling are *space charge dominated beams* -- the transverse phase space diagrams for these beams are typically "lines", not the familiar ellipses; the focussing is necessary to correct the space charge defocussing force, not the negligible emittance defocussing force. Such beams cannot be stored in rings which are typically limited to $\Delta Q_{SC} < 0.1$.

4.2 Example of High Energy Electron Cooling -- the RHIC Scenario

For a high energy application we investigate cooling fully-stripped 100 GeV/n $^{197}Au^{79+}$ beams in RHIC. Although the nominal 1σ rms normalized emittance, ϵ_I, is 1.6 $\pi\mu$m, the AGS is capable of providing smaller emittance beams. This larger value was apparently chosen during the RHIC design[21] to minimize the emittance growth due to intrabeam scattering (IBS). Using Eq. (9) with $\gamma = 100$, $A = 197$, $Z = 79$,

---

[c]The rms normalized emittance of an electron beam is $(r_c^2 kT_c/4mc^2)^{1/2}$ πm, though I hesitate characterizing the emittance of an electron beam with a uniform spacial and normal angular distribution (or the emittance of an aberrated beam) in this manner.

Table III. RHIC electron cooling system parameters; those shown in parenthesis are variable.

PARAMETER	SYMBOL	VALUE	UNITS
Electron Ring Parameters			
Cooling Length	L_c	40	m
Electron ring circumference	C_e	$133 = fC$	m
Fraction of RHIC used for cooling	$\eta = L_c/C$	0.01	
C_e/C	f	2/57	
Electron beam tune shift	ΔQ_{SC}	0.05	
Electron beam emittance	ϵ_e	(1.6)	$\pi\mu$m
Beta functions in cooling region	β_e	162	m
Electron beam temperature	T	(1.3)	eV/k
Electron beam rms radius	r_b	(1×10^{-3})	m
Electron beam current	I_e	(1.26)	A
Synchrotron radiation power	P_s	190	W
Synchrotron radiation damping time	τ_{SR}	0.3	s
RHIC Parameters			
Circumference	C	3800	m
Beta functions in cooling region	β_I	100	m
Ion Beam Parameters			
Atomic number	A	197	
Atomic charge	Z	79	
Ion current	I_I	57	mA
Emittance	ϵ_I	(1)	$\pi\mu$m
Momentum spread	$\Delta p/p$	(1×10^{-3})	

$\Delta Q_{SC} = 0.05$, and $\epsilon_I = 1$ $\pi\mu$m, we get a first order estimate for the cooling time of only 200 s -- an extremely short period of time in light of the projected storage time of 36,000 s!

4.3 Electron Damping Limitation

Such a cooling system sounds too good to be true, and indeed, there is a complication. We have not considered the heating of the electron beam by the proton beam, a concern which is not relevant for single-pass electron recirculators in the low or medium energy regimes, nor for cooling low intensity ion beams in the high energy regime. If energy is to be conserved, there is a straightforward relationship between the ion and electron beam intensities, masses, emittances, and damping times, i.e.:

$$\tau_{SR} \leq \frac{m}{AM}\frac{ZI_e}{I_I}\left(\frac{C_e}{C} \equiv f\right)\left(\frac{\epsilon_e\beta_I}{\epsilon_I\beta_e} = \frac{\epsilon_e^2}{\epsilon_I^2}\right)\tau \qquad (10)$$

where τ_{SR} is the synchrotron radiation damping time, approximately twice the time needed for a particle to radiate away all its energy:

$$\tau_{SR} \approx \frac{3}{2\pi\gamma^3}\frac{R_{bend}}{r_e}\frac{C_e}{c} \qquad (11)$$

where R_{bend} is the bending magnet radius of curvature.

If the condition given by Eq. (10) does not hold true for the conditions assumed, then another approach must be used to calculate the cooling rates. Such is the case in this RHIC example: a τ_{SR} of 0.01 s is necessary to cool a 0.057 A, $^{197}Au^{79}$ beam with a similar emittance 1 A electron beam for $C_e/C = 0.01$ and $\beta_I = \beta_e$,

whereas even a relatively small R_{bend} of 0.25 m (B = 0.68 T) yields a τ_{SR} of 5 s. We now consider a ring in which a third of its circumference consists of 1 T wigglers, and another third the cooling section; this would yield τ_{SR} = 0.3 s; since RHIC will operate with 57 bunches, we set $f = C_e/C = 2/57$. Note that the total synchrotron radiation power is only 150 W/A.

In this regime, the electron beam emittance is determined by ion beam heating, and the electron beam space charge tune shift limit determines the electron beam current and hence the ion beam cooling rate. We begin with a simpler relation for the ion beam emittance damping time:

$$\tau = \frac{3}{2}\sqrt{\frac{\pi}{2}}\,\frac{A}{Z^2}\,\frac{\beta^{3/2}\gamma^{5/2}}{\eta\Lambda}\,\frac{M}{m}\,\frac{\epsilon_e^{\,3}}{\sqrt{\epsilon_I\beta_I}\,r_e^2}\,\frac{e}{I_e}\,. \tag{12}$$

This relation is valid in the regime where $\epsilon_e > \epsilon_I$ for a spherical, rather than flattened, electron velocity distribution (thus only the last addend in Eq. (1), which we have increase by a factor[22] of $3\pi/4$, has been kept). We have further assumed that the ion and electron beams have the same radius (though independent emittances), and have increased the value of r_b by $\sqrt{2}$ to account for the Gaussian, rather than uniform, electron spatial distribution. Using Eqs. (10) and (12), we can solve for ϵ_e:

$$\epsilon_e = \left(\frac{2}{3}\sqrt{\frac{2}{\pi}}\,\frac{\eta}{f}\,\frac{Z\Lambda}{\beta^{3/2}\gamma^{5/2}}\,\frac{I_p\tau_{SR}}{e}\,\sqrt{\epsilon_I^{\,5}\beta_I}\,r_e^2\right)^{1/5}\,. \tag{13}$$

The value for ϵ_e obtained using Eq. (13) can then be used in the relation for the electron beam tune shift, ΔQ_{SC} [Eq. . (7)], to determine I_e; Eqs. (10) or (12) can then be used to solve for τ :

$$\tau = \frac{1}{4\pi}\left(\frac{9\pi}{8}\,\frac{r_e}{\beta_I}\right)^{1/5}\left(\frac{f}{\eta\Lambda}\right)^{2/5}\left(\frac{I_p\tau_{SR}}{e}\right)^{3/5}\,\frac{A}{\Delta Q_{SC}\gamma(Z\beta)^{7/5}}\,\frac{M}{m}\,\frac{C}{c}\,. \tag{14}$$

Using the values from Table III for the parameters in Eq. (14), we find the RHIC cooling time to be

$$\tau_{RHIC} = 1{,}100\ \text{s}\cdot\left(\frac{I_p}{0.057\ \text{A}}\,\frac{\tau_{SR}}{0.5\ \text{s}}\right)^{3/5}\,. \tag{15}$$

The parameters for this system are summarized in Table III. The value of parameters which vary are shown in parenthesis; their nominal values for ϵ_I = 1 $\pi\mu$m are listed. The 1,100 s cooling time could conceivably be reduced by about another factor of 2 by using super-ferric wiggler magnets. (The focal length of the wiggler magnets, assuming they bend by 90°, is twice their bend radius; thus the beam is quite small; the wiggler strength could be varied to synchronize the electron and RHIC revolution frequencies).

The synchrotron radiation damping limit is another reason why the storage ring technology cannot compete with the Pelletron technology in the medium energy regime. One should be wary of using Eqs. (14) or (15) to scale to higher energies: assuming $C \propto \gamma$ and noting $\tau_{SR} \propto 1/\gamma$, one might expect $\tau \propto 1/\gamma^{3/5}$; however, at higher energies, with faster synchrotron radiation damping, the electron beam emittance will no longer be determined by ion beam heating and our assumption that $\epsilon_e > \epsilon_I$ is no longer valid. At very high energies, the equilibrium electron beam emittance would be determined by quantum fluctuations and would scale as $(C_e/R_o)(\gamma/Q_x)^3$ where Q_x is the horizontal tune in the electron ring.

4.4 Radiative Recombination

Another concern is the ion radiative recombination lifetime, τ_{RR}, given by[23]:

$$\tau_{RR} = \frac{\gamma^2}{\eta r}, \quad r \approx \frac{2\pi^2}{\alpha}\,r_e^2\,n_e c\,\sqrt{\frac{\pi E_0^2}{2kTmc^2}}\cdot\left(1.12 + 0.5\ln\frac{E_o}{kT}\right) \tag{16}$$

where α is the fine structure constant, $E_o = Z^2 \times 13.6$ eV, and where we have assumed a spherical electron

velocity distribution. Using the values from Table III, we obtain $\tau_{RR} \approx 42$ ks, somewhat larger than the anticipated beam storage time. This does not appear to be a serious problem: the cooling system could be used intermittently; this could also provide a method for slow beam extraction for external target experiments. Alternatively this problem could be completely eliminated by cooling with positrons.

4.5 Discussion of High Energy Electron Cooling in RHIC

The basic theory of electron cooling has been thoroughly tested, and is not in doubt; the technology needed to build such a high energy electron cooler for RHIC has also been demonstrated. Such a system, which would cost approximately 20 M$ (100 k$/m) would have many obvious benefits:

--The luminosity of RHIC is a direct measurement of the potential physics research which can be accomplished. An electron cooling system could potentially increase the luminosity of beam in RHIC by over an order of magnitude by reducing the beam emittance. An electron cooling system thus appears to be economically viable in light of the capital (600 M$) and operating costs of RHIC.

--The reduced beam momentum spread would lead to a shorter diamond region, and reduce the storage rf power requirements by over an order of magnitude.

--The reduced beam size would increase the available machine aperture, ease the closed orbit error tolerances, improve the ease of operation, and possibly decrease the commissioning time.

--Most importantly, this system would be a great insurance policy: any shortcomings in the machine or the injector complex which would lead to a large beam emittance or energy spread could be compensated by cooling.

Such a system should be seriously considered.

5. SUMMARY AND CONCLUSIONS

Medium and high energy electron cooling may be overlooked technologies which should be re-examined. In the late 1970's it was investigated as a tool for accumulating antiprotons; however, due to the large cooling times associated with these large emittance beams, it was not a suitable tool. Nor was it a suitable tool for cooling the large emittance ion beams in accelerators. In recent years, as colliding beam experiments have pushed the requirements for low emittance beams, electron freezing may be a more appropriate tool. Today the beam emittance in many proton machines is limited by the space charge tune shift at low energies. However, since the tune shift varies as $C/(\beta\gamma)^2$ for a constant normalized emittance, the beam qualities can be improved through the use of medium energy electron cooling part way through the chain of accelerators. This could reduce the required apperture for all the following machines. The luminosity of heavy ion colliders is limited by IBS, which can be effectively counteracted by both medium and high energy electron cooling.

ACKNOWLEDGEMENTS

Many thanks to Lee Teng (Argonne APS) for reading an earlier version of this manuscript and answering my questions about electron storage rings; to Mike Ellison and Sergei Nagaitsev (IUCF) for many enjoyable and productive discussions, and for all their ideas. I would also like to thank John Cameron (IUCF director), who first sparked my interest in medium and high energy cooling with a conversation in late 1989 concerning the possibility of electron cooling beam in LISS (the Light Ion Spin Synchrotron) -- an envisioned 16 GeV version of the IUCF Cooler. This work was supported by the Texas National Research Laboratory Commission under grants RGFY 9158 and RGFY 9258 and by the National Science Foundation under grant NSF PHY 90-15957.

REFERENCES

[1] G.I. Budker, N.S. Dikansky, V.I. Kudelainen, I.N. Meshkov, V.V. Parkhomchuk, D. Pestrikov, A.N. Skrinsky, B.N. Sukhina, "Experimental studies of electron cooling", Part. Acc. **7** (1976) 295−235.

[2]. *MEB E-Cool Design Report 1992*, The MEBEC Group (IUCF publication, 1992).

[3] Tim Ellison and Sergei Nagaitsev, "Electron beam optic and electron /proton beam alignment in the Medium Energy Booster electron cooling region", (IUCF technote IU/AP/MEBEC009a, February 1992).

[4] D. Reistad, "Electron beam optics for proposed 6 MeV electron cooler at MEB", internal IUCF technote (IU/AP/MEBEC/003, March 1991).

[5] V. Lebedev (Budker Institute of Physics/SSC) private E-Mail communication (31 August 1992).

[6] Jim Ferry (National Electrostatics Corporation), private (FAX) communication 17 September 1993.

[7] Luis R. Elias and Gerald Ramian, "Recirculating electrostatic accelerators", IEEE Trans. Nucl. Sci. **NS-32** No. 5 (October 1985) 1732.

[8] Jerry Ramian (UCSB) private communication 26 January 1990.

[9] D.B. Cline, D.J. Larson, W. Kells, F.E. Mills, J. Adney, J. Ferry, and M. Sundquist, "Intermediate energy electron cooling for antiproton sources using a Pelletron accelerator", IEEE Trans. Nucl. Sci. **NS-30** (1983) 2370.

[10] Gerry Ramian, UCSB, Quantum Laboratory, private (telephone) communication (30 September 1993)

[11] D.J. Larson, R.R. Adney, D.R. Anderson, F.E. Mills, M.L. Sundquist, "Operation of a prototype intermediate-energy electron cooler", NIM **A311** (1992) 30-33.

[12] Luis R. Elias, Isidoro Kimel, Delbert Larson, Dan Anderson, Mufit Tecimer and Zhong Zhefu, "A compact cw free electron laser", NIM **A304** (1991) 219-223.

[13] Luis Elias, CREOL, U. of Central Florida, private (telephone) communication (30 September 1993).

[14] S. Nagaitsev, D. Anderson, M. Ball, D. Caussyn, T. Ellison, B. Hamilton, P. Schwandt, J. Adney, J. Ferry, M. Sundquist, D. Reistad, M. Sedlaček, "The development of the technology for electron cooling in the 2−20 GeV/nucleon energy range", these proceedings.

[15] R. Maier, U. Pfister and J. Range for the COSY-Team, "The COSY-Jülich project April 1991 status", in *Proc. 1991 IEEE Part. Acc. Conf.* (IEEE cat. no. 91CH3038-7, IEEE Piscataway NJ)2808-2900.

[16] J. Chiba et al., "The PS Collider design report 2 (in English)", KEK Report 90-13 (September 1990).

[17] The MEBEC group, *MEBEC E-Cool Design Report 1992*, (IUCF publication, October 1992).

[18] C. Rubbia, "Relativistic electron cooling for high luminosity proton-antiproton colliding beams at very high energies", *Proceedings of the Workshop on Producing High Luminosity High Energy Proton-Antiproton Collisions* (27-31 March 1978, Berkeley CA, LBL-7574, UC-34c, CONF-780345).

[19] Mel Month, "Electron cooling of high energy beams", ibid.

[20] A.G. Ruggiero, "High energy electron cooling", ibid.

[21] *Conceptual Design of the Relativistic Heavy Ion Collider RHIC* (BNL publication BNL 52195, May 1989).

[22] Allan H. Sørensen and Ejvind Bonderup, "Electron cooling", N.I.M. **215** (1983) 27−54.

[23] R. Neumann, H. Poth, A. Winnacker, and A. Wolf, "Laser-enhanced electron-ion capture and antihydrogen formation", Z. Phys. A **313** (1983) 253 - 262.

PHYSICS OF COOLED BEAMS

I. Hofmann and G. Kalisch

GSI Darmstadt, Postfach 110552, D-64220 Darmstadt, Germany

Abstract

Various aspects of diagnostics and its interpretation for coasting and bunched beams cooled by electrons are presented. Schottky spectra and their modification by impedances are central subjects in this discussion. We show that the noise generated by numerical simulation is closely related to the noise due to the graininess of a real beam, which helps interpreting coasting and in particular bunched beam spectra. Noise spectral analysis is used for determining the phase space density and the vicinity to instability. For bunched beams at higher currents some not yet understood instability phenomena are described by means of streakcamera images.

1. INTRODUCTION

For low phase space density beams the momentum spread can be obtained directly from the frequency span of the Schottky spectrum. This is not possible for cooled high phase space density beams, where the observed spectrum can be modified by collective effects and also by the friction force as was made evident in the first electron cooling experiments [1, 2]. It is thus necessary to use theoretical tools in order to obtain the desired information from measurements. In this context a close comparison between experiment and computer simulation is necessary. We confine the studies presented here to phenomena in the longitudinal phase space, where space charge effects can be significant. In transverse direction there is a limitation set by the maximum tune shift, which is determined by nonlinear resonances. Experimental observations are made at the GSI electron cooling storage ring ESR [3].

2. INTERPRETATION OF SCHOTTKY SPECTRA

2.1 Experimentally Obtained Spectra

The origin of the Schottky spectrum is the noise from the statistical distribution of particles. This gives rise to current fluctuations, which induce a voltage on a pick-up. Schottky spectra for a Ne^{10+} beam at 250 MeV/u are shown in Fig. 1, where we compare the spectrum with electron cooler current nearly zero and increased in steps up to 0.5 A [4]. The Schottky power is proportional to the square of the current fluctuations, which is proportional to the momentum distribution function only in the low phase space density case [5], where particles are completely uncorrelated in phase around the machine. With cooling there are collective effects (waves), which correlate particle phases. This leads to peaks at the frequencies of the collective motion.

2.2 Analytical Support and Interpretation

For high phase space densities the beam responds collectively on the field excited by the statistical fluctuations of the uncorrelated particles ("source field"). This results in a total electric field, which is obtained as usual by dividing the source electric field by the dielectric

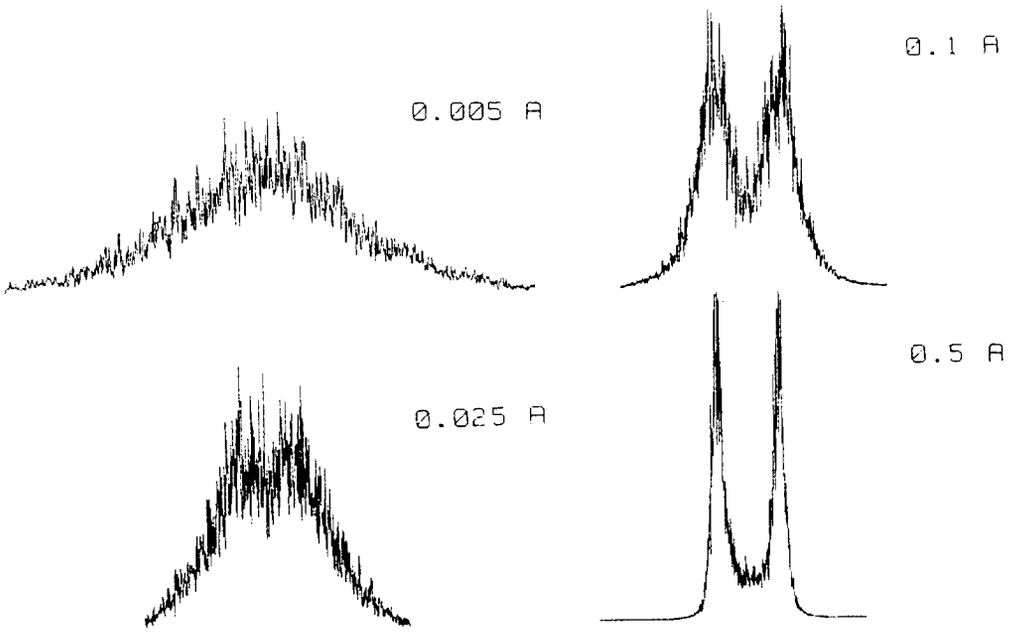

Fig. 1: *Schottky spectra for increasing cooler current to maximum of 0.5 A.*

function ϵ (see also Ref. [6]). Using Vlasov's equation (see Ref. [1, 2, 7, 8]) one thus obtains the modified expression for the Schottky power spectrum for harmonic n according to

$$P(\Omega, p) = \frac{q^2 e^2}{\pi} \frac{N}{n} \frac{\Psi_0(\Omega/n)}{|\epsilon|^2} \tag{1}$$

with the plasma dielectric function given by

$$\epsilon(\Omega, n) = 1 - iZ_{||} \frac{\eta q I}{\beta^2 \gamma A m c^2 / e} D(\Omega, n) \tag{2}$$

$Z_{||}$ is the coupling impedance, $\eta = 1/\gamma^2 - 1/\gamma_t^2$ (transition energy $\gamma_t >> 1$), and D a dispersion integral involving the distribution function of frequencies:

$$D = \int \frac{\partial \Psi_0 / \partial \omega}{\Omega - n\omega} d\omega = PV \int \frac{\partial \Psi_0 / \partial \omega}{\Omega - n\omega} d\omega + i \frac{\pi}{n} \partial \Psi_0 / \partial \omega \tag{3}$$

For the low-intensity limit $\epsilon \approx 1$, Equ. 1 yields directly the distribution function. For high phase space density ϵ can be close to zero for frequencies, which correspond to longitudinal "plasma waves". They are excited by the noise and can propagate in beam direction or opposite to it (fast and slow waves). This is responsible for the sharp peaks in the spectrum at these frequencies. The peaks would be infinite, if Landau damping were absent. At the band center the power is suppressed strongly, which is due to the shielding of the noise by the collective motion. This phenomenon is analogous to the well-known Debye shielding of a test particle in a plasma.

If the coupling impedance were known at sufficient accuracy, the distribution function could be determined in an iterative way: assuming a first guess for Ψ_0 one can calculate ϵ. Inserting this approximate ϵ into Equ. 1 and using the measured P one obtains a new Ψ_0, with which one can repeat the iteration. With unknown impedance the method still works if a second independent measurement exists, which is the beam transfer function method (see below), hence both impedance and distribution function can be determined consistently (see Ref. [8, 6]).

With only Schottky spectra and an uncertainty in the impedance - noting that the space charge impedance depends logarithmically on the beam size - it is thus not straightforward to obtain the correct $\Delta p/p$. A comparison with analytically derived spectra by calculating ϵ can be useful to determine $\Delta p/p$ in an approximate way [9, 6].

2.3 Simulation Noise

The above outlined interpretation of collectively distorted noise spectra on the basis of analytical calculations of a dielectric function can be strongly supported by calculating "real noise" by means of computer simulation. As we shall see below this is of particular interest for bunched beams. In simulation working with discrete particles one has natural fluctuations in the line density, which are analogous to the fluctuations in real beams. In Fig. 2 we show such an instantaneous line density for a coasting beam simulated by the "particle-in-cell" program SCOP-RZ. "Particle-in-cell" refers to the technique of calculating the self-interaction of the beam by creating each time-step a density function on a grid in r,z and solving Poisson's equation for an infinitely conducting pipe. This procedure takes care of what is usually described by the space charge impedance. In Fig. 2 we also show a projection of the beam into the x,z plane (different scales in x and z!). By Fourier analyzing the line density we can also include the measured machine impedances and thus obtain a full description of the electromagnetic interaction of the beam.

The simulation Schottky noise is obtained by recording the line density over a large number of revolutions and carrying out a Fourier transformation. Smooth spectra (high "confidence level") can be obtained only by carrying out an averaging over a number (typically several ten) of independent spectra, which is the same procedure as in the experiment.

In Fig. 3 we show spectra for large (uncooled) and 10 times smaller (cooled) momentum spread with no external machine impedance (i.e. only space charge active), and with a resistive component. The uncooled case corresponds to $\Delta p/p = 10^{-3}$ for a 20 mA Ne^{10+} beam at 250 MeV/u. The momentum distribution is Gaussian in all cases and remains unchanged during the simulation. The different noise spectra are related to longitudinal correlations between particles due to the collective interaction. The latter is absent for large momentum spread due to Landau damping.

Simulation noise is particularly valuable to study directly the effect of extra contributions to the coupling impedance, which can be turned on and off separately, while the momentum distribution is well-known as input. This is also shown in Fig. 3 for an additional real part of the coupling impedance $Z_{||}/n$ of 50 Ω, which could be due to a low impedance rf cavity. The left peak corresponding to the slow wave is strongly enhanced, whereas the right peak is reduced. A further enhancement of the resistive impedance (at constant $\Delta p/p$) would lead to a growing left peak.

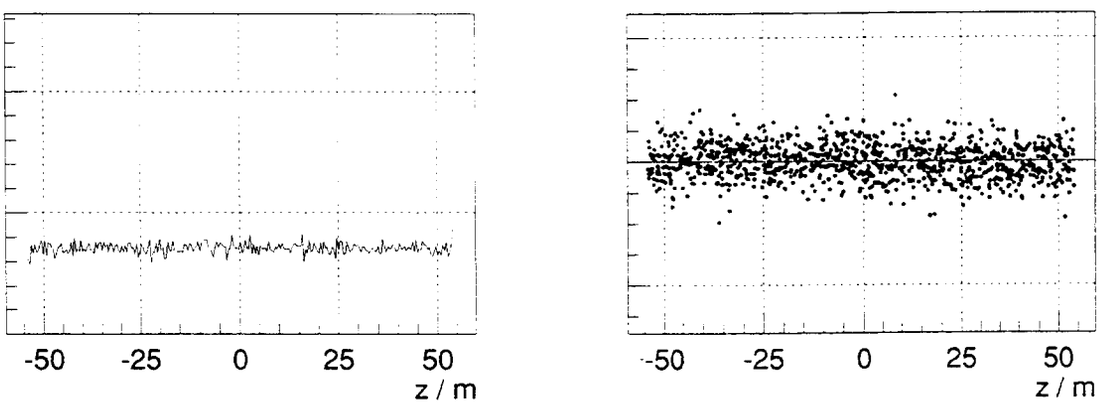

Fig. 2: *Fluctuations of line density (left) and scatter plot (right) of coasting beam simulation.*

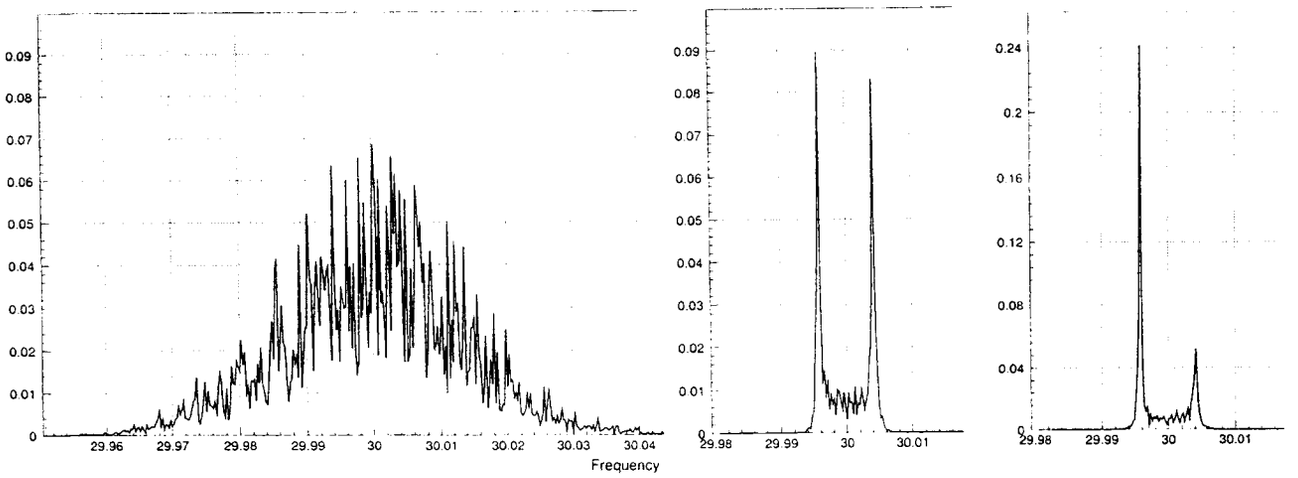

Fig. 3: *Simulation Schottky noise for large (left), 10 times smaller (center) and additional resistive impedance (right; different vertical scale).*

3. STABILITY AND INSTABILITY

3.1 Transition to Instability

The limit of instability in Fig. 3 would be characterized by an infinitely large left peak of the Schottky noise. This happens at a sufficiently large resistive part of the coupling impedance depending on the inductive part. For a more detailed discussion of stability one introduces the beam transfer function (BTF), which is the inverse response function [11]:

$$\frac{1}{r_{||}} = \frac{1}{r_{||,0}} + Z_{||} \tag{4}$$

with (using Equ. 3)

$$r_{||,0} = -i\frac{eZ\eta I}{\beta^2\gamma A m_p c^2} D \tag{5}$$

A measured BTF diagram for an electron cooled beam is shown in Fig. 4 [10]. According to Eq. 4 the effect of the impedance is a shift of the origin, which must lie in the interior of the curve to ensure stability. Due to the equilibrium with the cooling mechanism (Coulomb scattering) the momentum distribution is very close to a Gaussian. The tails of the Gaussian lead to a largely extended stable area in the direction of inductive impedance (space charge). This is beneficial for energies far below the transition energy. There the space charge impedance (inductive) is large, which has the effect of shifting the coherent frequencies into the tails of the distribution function.

We note that the worst case in the sense of stability is a parabolic distribution, for which the boundary of stability is described by a small circle in the BTF diagram. The small size of this area is due to the absence of Landau damping in the tails. This circle is described by the "Keil-Schnell criterion":

$$I_{th} = \beta^2\gamma\frac{Am_pc^2}{Ze}|\eta|(\frac{\Delta p}{p})^2_{fwhm}/|\frac{Z_{||}}{n}| \tag{6}$$

According to Fig. 4 the allowed impedance (or in an equivalent sense beam current, following Equ. 6) is much larger for a Gaussian distribution as long as it is mainly in the inductive direction.

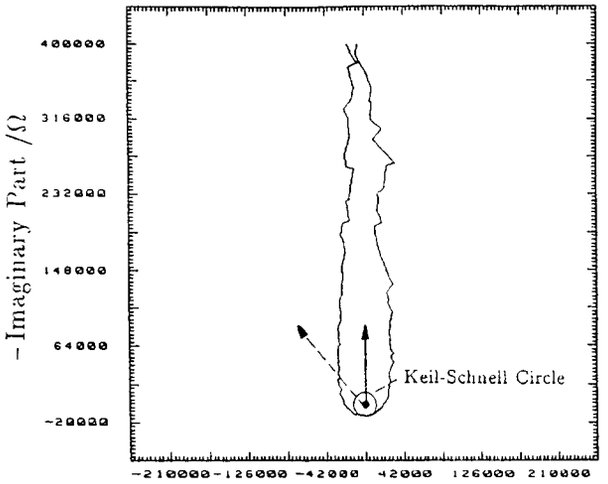

Fig. 4: *Measured stability diagram (BTF measurement) for cooled beam, with Keil-Schnell circle indicated; arrow corresponding to cooled case of Fig. 3 (center), dashed arrow to unstable case of Fig. 5.*

For the simulation example of Fig. 3, I/I_{th} has been as large as 7 (arrow in Fig. 4) without loss of stability. Measurements in various cooler rings have shown that I/I_{th} can indeed exceed 5 due to such Gaussian-like momentum distributions [13, 14, 12].

Obviously an additional resistive component of 1 kΩ (i.e. comparable with the space charge impedance) in the simulation example of Fig. 3 would shift the origin far beyond the boundary of stability. To show the onset of instability we have simulated such a case in Fig. 5. Such a resistive impedance could stem, for instance, from a ferrite loaded rf cavity tuned at resonance with the beam.

It is noted that the coasting beam develops a self-bunching effect, which leads to a trapping of particles in the longitudinal self-field. The instability saturates at a broadened momentum distribution, which is almost a factor 3 broader than the initial distribution. Due to the quadratic dependence of the threshold current on the momentum spread (Equ. 6) it is clear that this broadening leads to a final distribution, where $I/I_{th} \approx 1$. We thus confirm that $I/I_{th} >> 1$ is only possible for small resistive compared with inductive impedance.

A different behaviour of the longitudinal microwave instability for a resistive impedance much smaller than the space charge impedance, but with I/I_{th} as large as 50 was studied by simulation in connection with heavy ion fusion storage rings [15]. In this case the instability was found to develop extended "stabilizing tails", which would suppress further growth and leave the small initial momentum spread for most of the beam unchanged.

3.2 Role of Intrabeam Scattering

The question can be raised what the maximum I/I_{th} is in a given cooler ring. Why are we not approaching the limit of stability, which would be accompanied by a large growth of the "slow wave" peak in the Schottky spectra as indicated by the simulation experiment of Fig. 3? It must be assumed that intrabeam scattering (IBS) plays a crucial role in this context. A possible consequence of IBS could be that the beam is longitudinally colder only if it is made transversely hotter.

In the lack of systematic measurements such a statement can be supported by calculations of IBS equilibria, which we have carried out for the ESR lattice. In Fig. 6 we plot $\Delta p/p$) as a function of the horizontal emittance under the asumption of a constant longitudinal cooling rate. The curve shows theoretical equilibria starting from an experimentally observed equilibrium at $\Delta p/p = 4.1 \cdot 10^{-5}$ and $\epsilon_h = 0.08 \cdot 10^{-6}$ m-rad for Au^{79+} at 250 MeV/u and $N = 2.7 \cdot 10^6$. It is recognized that considerably smaller momentum spreads can be expected if the transverse

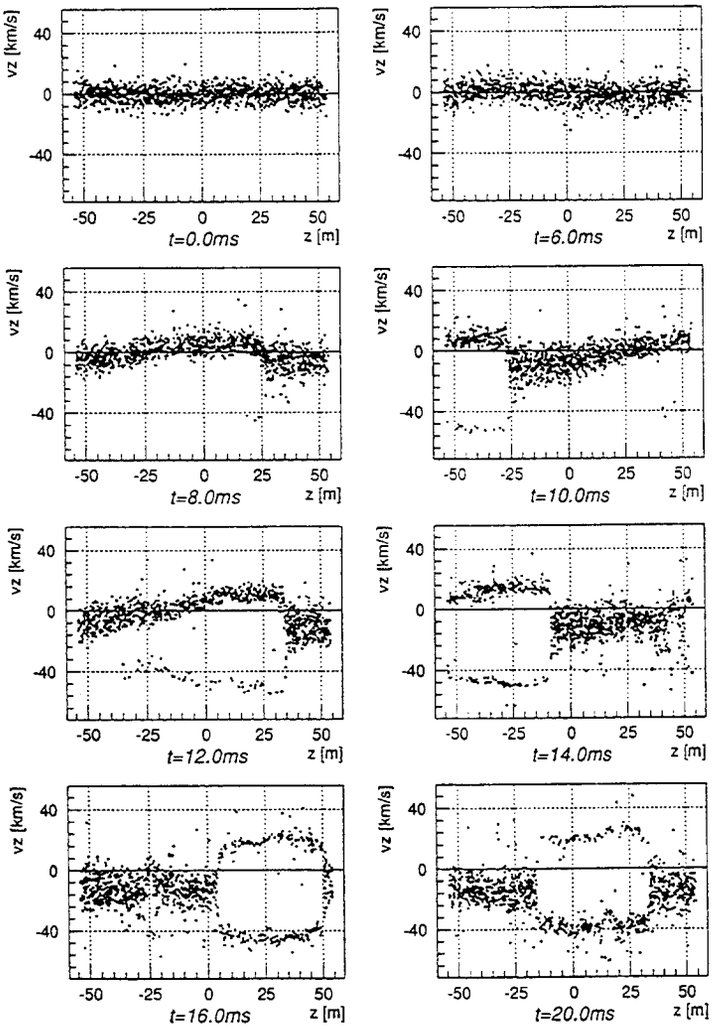

Fig. 5: *Simulation of longitudinal microwave instability for C^{6+} at 250 MeV/u, $\Delta p/p = 3{\cdot}10^{-5}$, I=30 mA and 1kΩ resistive impedance at fundamental harmonic.*

emittances are blown up. This can be achieved by an extra transverse heating source (rf noise) or by spoiling the transverse cooling optimization. We can understand this result by noting that the transfer of heat from the transverse to the longitudinal degree of freedom happens at a rate, which is the slower the larger the velocity mismatch is between both degrees of freedom.

3.3 Influence of Cooling Force

It is necessary to examine whether the observed Schottky noise is only a consequence of the ion beam properties and the impedance, or whether it is also influenced by the cooling friction force. This is conceivable if one notices that the stability behaviour depends on the Landau damping provided by the tails of the momentum distribution. Electron cooling is also a damping mechanism with a rate given by the cooling rate ν_{cool}. The friction force can be ignored, if the ratio of cooling rate to phase mixing rate (given by the spread of angular frequency) is small. This criterion can be approximately written as (for a more detailed model and further references see Ref. [8])

$$\frac{\nu_{cool}}{n\delta\omega} << 1 \tag{7}$$

It is noted that the influence of the friction force is largest for small n. By comparing spectra for small and large n it should be possible to identify such an influence, if the cooling rate is large enough; no experimental evidence seems to exist yet for such an observation.

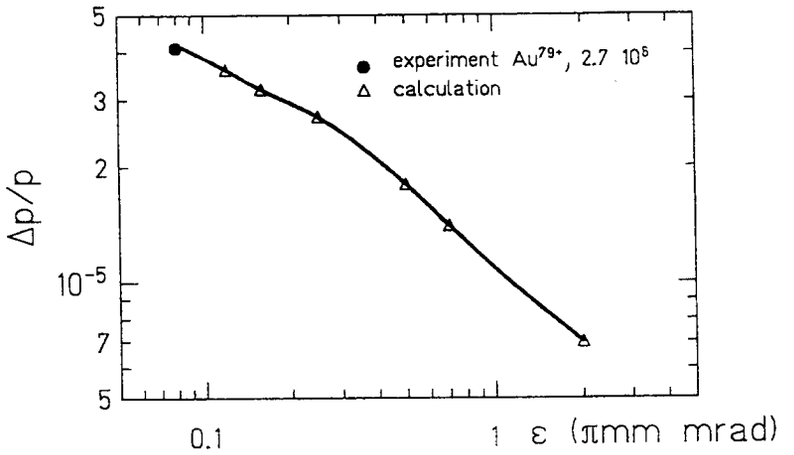

Fig. 6: *Calculated IBS equilibria in the vicinity of experimental data.*

4. BUNCHED BEAMS

4.1 Effect of Space Charge

We are interested in an appropriate measure for the phase space density of cooled bunches. The analogue of noise suppression in the center of the Schottky band for coasting beams is the reduction of the applied rf potential well due to space charge ("potential well flattening"), which results in an effective potential reduced by a factor α:

$$V_{eff} = V_{rf}/\alpha \tag{8}$$

We can compare this expression with Equ. 1 for a coasting beam locally equivalent to the bunched beam center. This comparison suggests that α is equivalent to the dielectric function ϵ, which describes the Schottky current ($\propto$ (power)$^{1/2}$) suppression in the band center. Provided that in both cases space charge is the dominant contribution to the impedance one thus has - ignoring a geometry factor of order unity depending on the bunch shape - :

$$\alpha \approx 1 + I/I_{th,b.c.} \approx \epsilon_{b.c.} \tag{9}$$

with the understanding that $I_{th,b.c.}$, $\epsilon_{b.c.}$ are for coasting beams equivalent to the bunched beam center. α is thus an an appropriate measure for the longitudinal phase space density. $\alpha >> 1$ would indicate strongly space charge dominated bunches, which have been observed for cooled proton bunches [16].

The potential well flattening leads to a bunch lengthening effect and a reduction in synchrotron frequency ω_0. In harmonic approximation one immediately has the following relation:

$$\frac{\omega_{eff}}{\omega_0} = \alpha^{-1/2} \tag{10}$$

From an experimental point of view an accurate measurement of α is desirable. We suggest that the most reliable way is to directly measure ω_{eff} and ω_0.

4.2 Frequency Spectra

As an example we have measured in the ESR bunched beam spectra of a Ne^{10+} beam of 250 MeV/u and 3x10^8 particles at an rf voltage of 100 V (Fig. 7).

Such measurements have been successful only for sufficiently stable operation of the electron cooler and relatively low intensity. The spectrum contains as a central line a multiple of the revolution frequency and a large number of sidebands. Some of the sidebands are at multiples of 50 Hz; we assume they are due to the power supply of the cooler or rf. To obtain a more

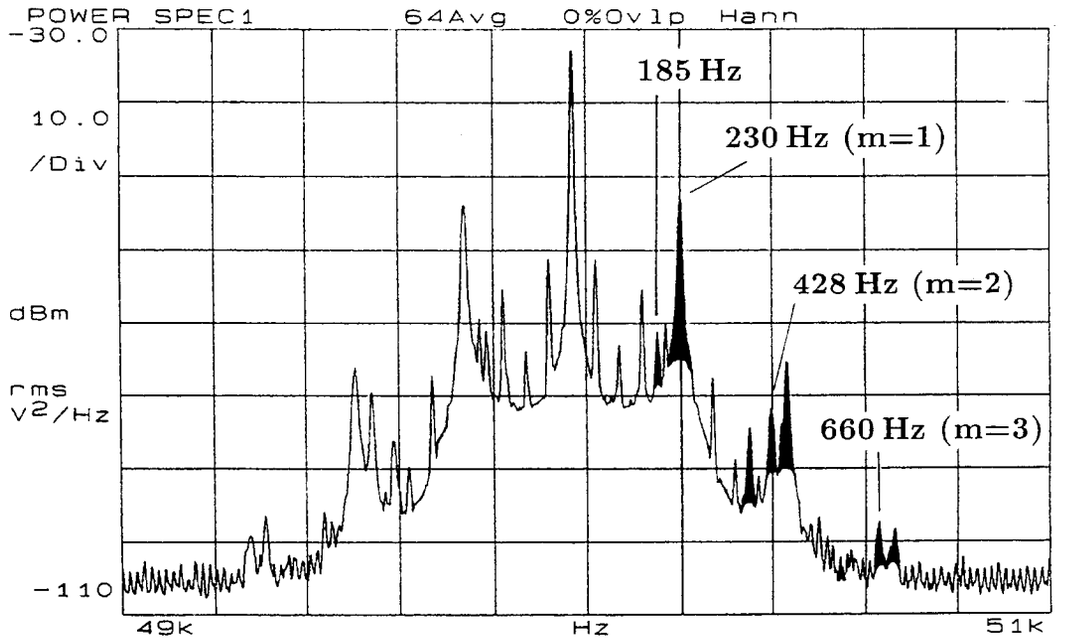

Fig. 7: *Split Schottky lines for bunched beam with moderate space charge (relevant satellites filled black).*

solid ground for a physical interpretation we have calculated the simulation noise for a bunched beam, which allows a direct comparison with the experimental observation and helps interpreting them. Simulation results are shown in Fig. 8 for zero space charge and finite space charge of comparable strength as in the above experiment. The band width has been increased to reduce computer time. For zero space charge one obtains simply the multiples of the synchrotron frequency.

For finite space charge each sideband is split into several lines for coherent and incoherent (low-level signals) frequencies. The coherent frequencies refer to dipole (bunch center, m=1), quadrupole (bunch length, m=2) and sextupole (shape unsymmetry, m=3) oscillations. The height of these lines reflects the amplitude of excitation of a particular mode. The notion of multipole oscillations in this context is applied to the shape of the distribution in longitudinal phase space. The dipole oscillation is unaffected by space charge since the bunch center oscillates carrying along its own space charge. The relevant frequency is thus the zero space charge synchrotron frequency ω_0 (230 Hz in Fig. 7). We note that for each observed line there are also higher harmonics, which are just multiples. This explains the increasing number of lines at higher sidebands. The incoherent frequency peaks of single particles are much less pronounced

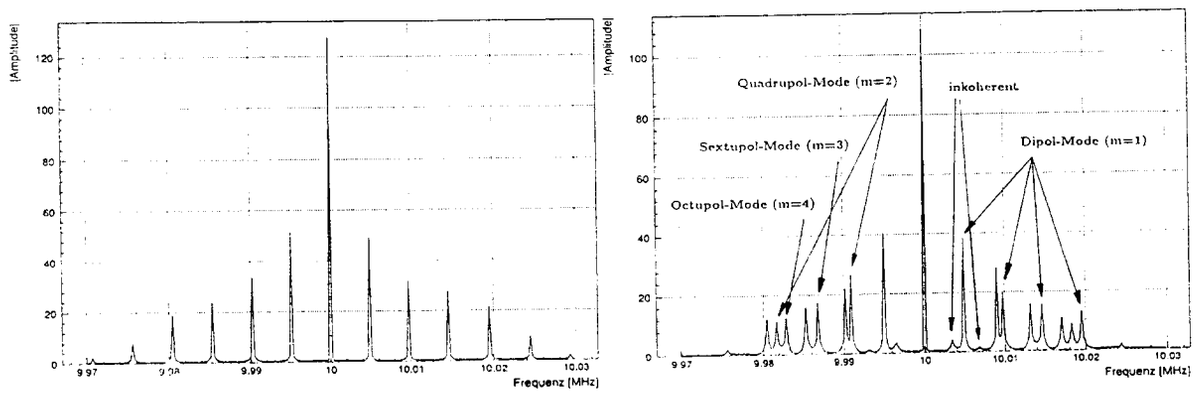

Fig. 8: *Simulation noise for bunched beam without (left) and with moderate space charge (right).*

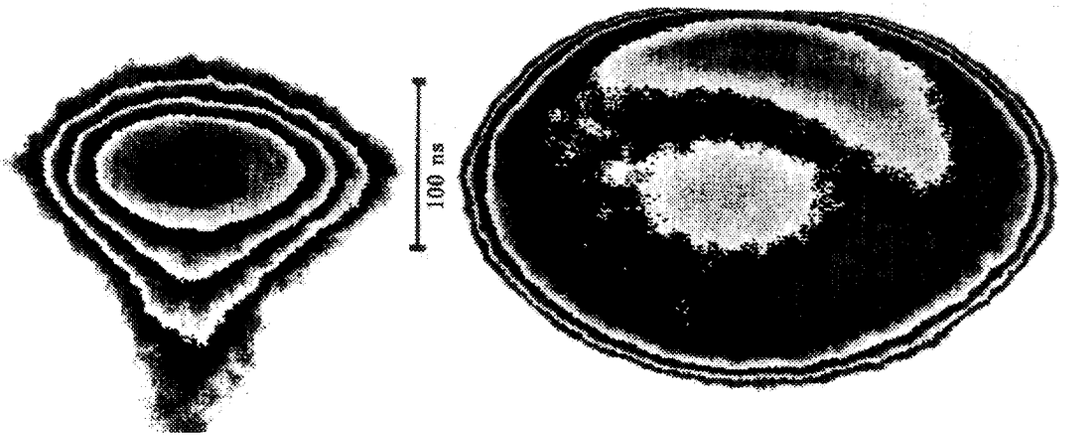

Fig. 9: *Streakcamera pictures of 0.6 mA (left) and 1.9 mA (right, unstable) bunches of Ne^{10+} at 250 MeV/u, with time running downwards.*

due to the random summation of signals from individual particles. This incoherent synchrotron frequency ω_{eff} (185 Hz in Fig. 7) is thus a direct measure of the effective potential.

From these frequencies we calculate with Equ. 10, $\alpha = 1.55$, which indicates that 35% of the applied rf voltage is compensated by space charge. We assume that intrabeam scattering heating of the momentum distribution is the main reason why the observed α was not any larger.

4.3 Bunches at Higher Intensities

Experiments in the ESR with bunches at larger intensities have so far not lead to sufficiently stationary conditions to measure Schottky spectra. For total currents exceeding typically 1 mA (i.e. 10% of the maximum stable stored coasting beam currents for Ne, C beams) it was found that bunches were not in a stable equilibrium with the electron cooling. Periodically (in intervals of the order of a second) a phase of cooling to short bunch length was followed by a disintegration of the bunch profile. In Fig. 9 we show streakcamera pictures of a low intensity stable bunch and a snapshot during the unstable phase at three times higher intensity, both at an rf voltage of 1 kV. Each picture is for a single bunch extracted from the ring and hitting a plastic scintillator (NE102) with ns time resolution. The camera records the light through a horizontal slit centered on the spot. At subsequent times the light is deflected (vertically downwards in Fig. 9) which yields a longitudinal - horizontal cut through the bunch in real space. The overall time resolution is 1-2 ns.

The horizontal size of the image gives the instantaneous horizontal beam size ($\propto \epsilon_h^{1/2}$) as a function of position along the bunch. Shown are equi-intensity contours of the scintillator light, which are converted alternatively into black and white. In the low-intensity picture the unsymmetry of the image is due to a scintillator afterglow. For the three times higher intensity it is seen that the bunch has suffered an unstable behaviour both in longitudinal and in horizontal direction. In this case peak intensity is in the center and in the half-moon shaped area at the head of the bunch. This instability phenomena might be connected with a de-tuning between cooler energy and rf frequency, which requires careful study in the future.

Acknowledgment: The authors are indebted to B. Franzke and the ESR-group for their support in the measurements.

References

[1] V. Parkhomchuk and D. Pestrikov, "Thermal noise in an intense beam in a storage ring",

Sov. Phys. Tech. Phys. 25(7), p.818 (1980)

[2] E.N. Demente'ev et al., Sov. Phys. Tech. Phys. 25(8), 1001 (1980)

[3] B. Franzke, Proc. Part. Acc. Conf., San Francisco, May 6-9, 1991, p. 2880 (1991)

[4] M. Steck, private communication

[5] J. Borer et al., Proc. IXth Conf. on High Energy Accelerators, Stanford, 1974, p.53

[6] I. Hofmann, K. Beckert, S. Baumann-Cocher and U. Schaaf, Proc. European Part. Accel. Conf., Nice, June 12-14, 1990, p.229

[7] S. Chattopadhyay, "Some fundamental aspects of fluctuations and coherence in charged particle beams in storage rings", CERN 84-11 (1984)

[8] S. Cocher and I. Hofmann, Part. Accel. **34**, 189 (1990)

[9] H. Poth, Report CERN-EP/90-04 (1990)

[10] U. Schaaf, Dissertation, Frankfurt University (1991)

[11] J. Borer et al. IEEE Trans. Nucl. Sci. **NS-26**, 3405 (1979)

[12] I. Hofmann, Proc. Part. Acc. Conf., San Francisco, May 6-9, 1991, p. 2492 (1991)

[13] P. Baumann et al., Nucl. Instr. and Meth. **A 268**, 531 (1988)

[14] J. Bosser et al., Proc. Part. Acc. Conf., San Francisco, May 6-9, 1991, p. 2509 (1991)

[15] I. Hofmann, Laser and Particle Beams, **3**, 1 (1985)

[16] T.J. Ellison et al., Phys. Rev. Lett. **70**, 790 (1993)

COHERENT MICROWAVE COOLING (CMC) OF ELECTRON AND ION BEAMS

Hidetsugu Ikegami

Research Center for Nuclear Physics, Osaka University
Mihogaoka 10-1, Ibaraki, Osaka 567, Japan
and
Department of Radiation Sciences, Uppsala University
Box 535, S-751 21 Uppsala, Sweden

ABSTRACT

A new principle "coherent microwave cooling" (CMC) of charged particle beams is described. Particles are forced, by a magnetic field over some length of their trajectory, to move in a helical path and interact with an rf field. The validity of the principle has been examined experimentally. The experimental results provided some inspiring indications of the "cooling" in the transverse energy-time phase space of the electrons. Electrons initially in the range $8 - 12$ keV, were all found to accumulate at one discrete energy, 23 keV. Phase bunching, a feature of the cyclotron maser, was observed indirectly in the gyration of the accumulated electrons of 23 keV energy. The agreement between the prediction and the experimental results implies that in principle any kind of charged particle beam can be cooled in a single pass through the CMC sections regardless of its energy.

1 INTRODUCTION

The invention of beam cooling has opened up new ways of reducing drastically the phase space of circulating particles [1-6]. In *electron cooling* the ion beam is merged with a parallel beam of mono-energetic electrons in a cooling section. The *thermal* energies of the ions seen in the rest frame of the electrons, are transferred to the electron beam as a low temperature reservoir through *heat conduction*. However for the case of ion beams of higher energy, the cooling times are much longer because of the γ^2 dependence of the relativistic time dilation effect in the interacting two body system where $\gamma = (1-\beta^2)^{-1/2}$ is the relativistic energy factor [1].

In *stochastic cooling*, some pick-up systems are installed in a particle storage ring to measure the average positions of circulating particles. Corresponding kicker systems are placed downstream from the pick-up systems to correct any beam excursion at the pick-up systems [3]. In this cooling scheme, especially shaped space and time characteristics of the electric pulses are essential in the kicker systems to yield non-linear effects such as the cooling of particle beam.

This cooling scheme is, in the physical sense, analogous to the action of sheepdog against flocks and thus it is easy to understand that the cooling time is lengthening in proportion to the number of particles in the pulses.

The *radiation cooling* due to the synchrotron radiation is at present the best mastered scheme for the cooling of the longitudinal phase space of electrons and of protons of extremely high energies but at the sacrifice of heating in their transverse phase space [2]. Other cooling schemes such as *laser cooling* [5] and cooling by inelastic scattering [6] are applicable to only partially ionized ions.

Now, it would be of particular importance to note that most cooling schemes of transverse phase space so far developed are based on the mechanism of *spontaneous* transfer of the *thermal* movement of a particle beam to a low temperature reservoir through heat conduction or radiation but none has been developed based on the stimulated cooling mechanism. From this viewpoint, the most crucial low temperature reservoir would be the coherent microwave field. The newly presented principle *coherent microwave cooling* (CMC) dramatically enhances the *thermal* transfer mechanism by the stimulated coherent emission or absorption of photons and removes drawbacks of present cooling schemes such as the slow cooling speed and the limitations on the energy and the intensity of particle beams to be cooled [7]. Of particular interest is that CMC is in principle applicable to any kind of charged particles with arbitrary energy resulting in an *rapid cooling* in the transverse energy-time phase space. CMC may be understood as a *forced radiation cooling* which is a typical non-Liouvillean phenomenon [7]. This talk outlines the basic concept of CMC [7,8] and presents the first experimental results which provide some indications of CMC supporting the prediction of *cooling* in the transverse phase space of electrons [8,9].

2 MECHANISM OF CYCLOTRON MASER – OSCILLATOR APPROACH

The mechanism of CMC has been discussed so far [7,8] on the basis of the quantum mechanical oscillator approach. In this talk, I would like to present the CMC principle again in the simple quantum mechanical approach for the simplicity of the discussions. However, it would be of significance to understand the mechanism also as a classical physics phenomena in the scheme of dynamics of gyrating particles. For this purpose, a simple approach has been developed based on classical particle dynamics (Appendix). Of special interest is that both approaches lead to identical results!

The CMC can be applied to particles circulating in a storage ring as shown in Fig. 1. In the CMC sections a stimulating rf field is sent antiparallel or parallel to a particle beam in the presence of a solenoidal magnetic field B_0. A fraction of the longitudinal energy of particles with rest mass m_0 and charge e is changed into transverse energy by introducing the particles in the CMC sections at an angle of inclination to the longitudinal axis of the solenoidal magnetic field B_0 yielding a gyration of the particles with the cyclotron frequency $\omega_c^* \equiv eB_0/m_0$. Quantities with an asterisk refer to the particle system with no longitudinal velocity and MKSA units are used throughout this talk. In the presence of an rf field of angular frequency ω_{rf}^*, electric field amplitude E_{rf}^* and energy flow density defined by the absolute value of the Poynting vector $I^*(\omega_{rf}^*)$ of which electric field vectors are perpendicular to the axis of the solenoid, the gyrating particles are governed by the Lorentz force $F_m^* = ec\beta_\perp B_0$ generated by the magnetic field B_0 and an electric force $F_e^* = eE_{rf}^* \cos(\omega_{rf}^* t^*)$ in the particle rest frame where their longitudinal momentum is zero on average. Here, c and $c\beta_\perp$ denote the speed of light and the gyration speed, respectively.

The particles gyrating in the solenodial magnetic field may be described as harmonic oscillators with Landau level spacings, $\hbar\omega_c^*$ in the particle rest frame. In the presence of the rf field,

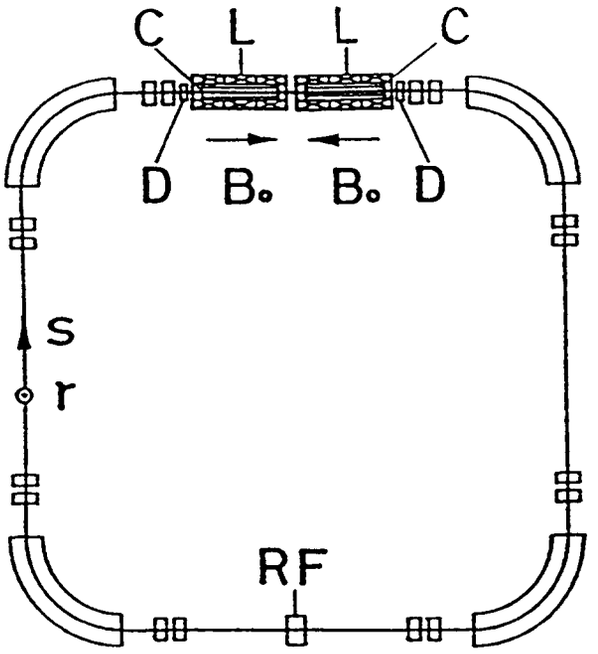

Figure 1: A basic configuartion of a facility for coherent microwave cooling. C: rf cavity for stimulating emission or absorption of photons; D: small deflection magnet; L: solenoidal magnet; RF: accelerating rf system. Elements without abbreviation are lattice magnets and r and s are the transverse and longitudinal coordinates, respectively.

the gyrating particles, described by harmonic dipole oscillators, undergo radiative transitions leading to a change of their transverse energy $\gamma_\perp m_0 c^2$ with time,

$$\frac{\mathrm{d}\gamma_\perp^*}{\mathrm{d}t^*} = \frac{1}{2}\left(\frac{eE_{\mathrm{rf}}^*}{m_0 c}\right)^2 \tau^* F(x_0) = \frac{4\pi r_{\mathrm{p}}}{m_0 c} I^*(\omega_{\mathrm{rf}}^*)\tau^* F(x_0) \ , \tag{1}$$

where

$$F(x_0) \equiv (1 + x_0^2)^{-1} \ , \tag{2}$$

$$x_0 \equiv 2\tau^*(\omega_{\mathrm{c}}^* - \omega_{\mathrm{rf}}^*) \ . \tag{3}$$

Here, $\gamma_\perp = (1 - \beta_\perp)^{-1/2}$ and $r_{\mathrm{p}} (= e^2/4\pi\varepsilon_0 m_0 c^2)$ denote the relativistic energy factor and the classical radius of particles, respectively, and τ^* is the damping time of the oscillator – hereafter called *phase debunching time*. The subscription $\perp$ and $\parallel$ denote the transverse and longitudinal directions, respectively. It is seen that Eq. (1) is a well-known formula of a damping dipole oscillator, which can also be derived classically [10]. The function $F(x_0)$ defined by Eq. (2) is the harmonic oscillator response function of Lorenzian shape, which corresponds to the normalized energy gain of gyrating particles.

As a matter of fact, the gyro-frequency of the particles is $\omega_{\mathrm{c}}^*/\gamma_\perp^*$ instead of ω_{c}^* due to the relativistic mass effect on the gyration. The gyrating particles should thus be described as unharmonic oscillators with non-equal Landau level spacings $\hbar\omega_{\mathrm{c}}^*/\gamma_\perp^*$, resulting in a shift of resonance frequency. Thus the variable x_0 in Eq. (2) has to be replaced by x,

$$x \equiv 2\tau^* \left[(\omega_{\mathrm{c}}^*/\gamma_\perp^*) - \omega_{\mathrm{rf}}^*\right] \ . \tag{4}$$

However, this replacement of variable is not enough to describe the unharmonic oscillators. The response function $F(x)$ associated with an unharmonic oscillator generally consists of the dipole term $(1+x^2)^{-1}$ and an additional quadrupole term which is proportional to $(x-x_0)$ and the derivative of the dipole term having the form $(x-x_0)\mathrm{d}(1+x^2)^{-1}/\mathrm{d}x$ [8]. We have thus,

$$F(x) = \frac{1}{1+x^2} + \frac{2ax}{(1+x^2)^2} \ , \tag{5}$$

$$a \equiv x_0 - x = 2\omega_c^*\tau^*(1-\gamma_\perp^{*-1}) = 2\omega_c\tau(1-\gamma_\perp^{-1}) \ . \tag{6}$$

It should be noted that an opposite sign of a in Eq. (5) would result in $F(x) \rightarrow F(x_0)$ losing unharmonicity. The first term of $F(x)$ in Eq. (5) describes incoherent absorptive transitions of dipole oscillator with a relativistically shifted resonance frequency $\omega_c^*/\gamma_\perp^*$ while the second a-dependent term is concerned with the transitions of quadrupole oscillator of the same resonance frequency. The correction of the gyro-frequency is essentially due to the relativistic mass effect on the gyration, which causes the replacement of m_0 in Eq. (1) by $\gamma_\perp m_0$ and hence we have,

$$\frac{\mathrm{d}\gamma_\perp}{\mathrm{d}t^*} = \frac{1}{2}\left(\frac{eE_{\mathrm{rf}}^*}{\gamma_\perp m_0 c}\right)^2 \tau^* F(x) = \frac{4\pi r_{\mathrm{p}}}{\gamma_\perp^2 m_0 c} I^*(\omega_{\mathrm{rf}}^*)\tau^* F(x) \ . \tag{7}$$

The transition rates, Eqs. (5-7), are identical with those derived in the Appendix on the basis of classical dynamical approach, in which a damped dipole oscillator term corresponds to the gyration speed $c\beta_\perp$ dependent frictional term whereas an unharmonic quadrupole oscillator term corresponds to the gyro-frequency $\omega_c^*/\gamma_\perp$ dependent frictional term. As seen in Eq. (5), the unharmonic oscillation due to the relativistic effect on the gyro-frequency causes a drastic rate in the change of energy proportional to $(\tau^*)^3$ because both a and x are proportional to τ^*. On the contrary, the rate of damped dipole oscillation varies only linearly with the phase debunching time τ^*, which has no coherency of gyration due to the lack of phase bunching effect as explained in the classical dynamical approach (Appendix).

As seen in Fig. 2, the unharmonic quadrupole transition rate is remarkably enhanced with increase of a – hereafter called *coherency factor*. In fact, this mechanism is explained as an effect of the stimulated radiation caused by the coherent gyration, i.e. the bunched particle gyration with respect to the rf field as described below. The unharmonic oscillation may be understood as a *super damped oscillation* which is a consequence of a large flow of energy from the system of gyrating particles and the rf field to the outside, and *vice versa*. This phenomenon has been known as the *cyclotron maser* mechanism and utilized extensively in *cyclotron maser* amplifiers and/or oscillators to extract radiation of high power from gyrating electrons [11].

To understand the phase bunching mechanism, consider the case where particles of the same transverse energy $\gamma_\perp^*$ are initially randomly distributed in phase and are gyrating at the same frequency as the rf field. Some of the particles will gain energy and hence increase their mass. The phase of these particles will slip behind the rf wave since their gyro-frequency decreases. The particles which are initially in the opposite phase and lose energy will similarly advance in phase. After a certain number of gyrations depending on the initial conditions, most particles gyrate at similar phases. After some time, the phase debunching time τ^*, the bunching action is interrupted for example when particles enter the space without rf field. This consideration can be generalized to the case where the particles have initially different transverse energies. More detailed explanations on the phase bunching mechanism are developed in the classical dynamical approach presented in the Appendix.

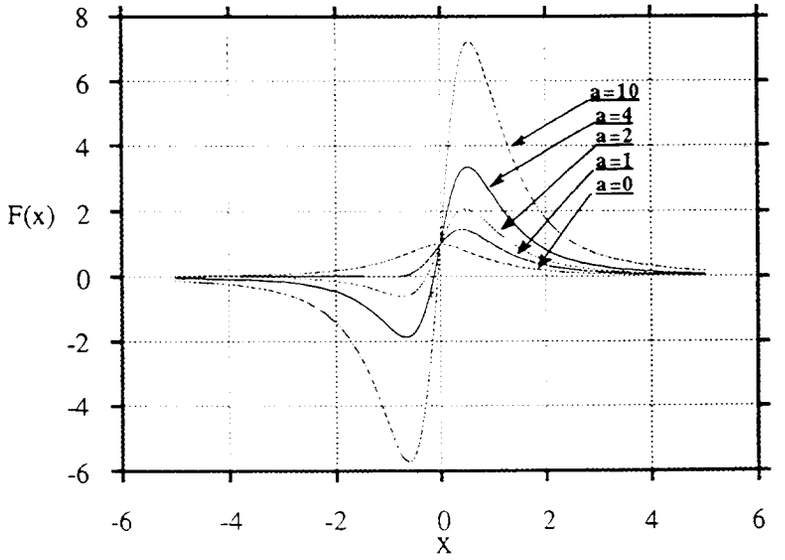

Figure 2: The response function $F(x)$ gives the normalized energy gain of a gyrating charged particle. As seen in the response function $F(x)$ for $a \gg 1$, the particles with the high energy, i.e. $x < 0$ or $\gamma_\perp > \omega_c^*/\omega_{rf}^*$, emit coherently radiation while the particles with the low energy, i.e. $x > 0$ or $\gamma_\perp < \omega_c^*/\omega_{rf}^*$ absorb coherently radiation through the stimulation of the rf field resulting in the CMC.

3 CMC IN THE TRANSVERSE ENERGY-TIME PHASE SPACE

Since the derivation so far is based on quantum mechanics, the behaviour of the phases of the particles can not be treated explicitly. Classically, the trapping of a DC beam can, however, be discussed by means of the synchrotron phase space. When the phase angles $\phi(t^*)$ of the gyrating particles are distributed uniformly with respect to the rf field and when the mismatching frequency $\Omega^* \equiv (\omega_c^*/\gamma_\perp) - \omega_{rf}^*$ is smaller than the region of stability of synchrotron phase space, a significant portion of the particles will be trapped. For this case, the range of phase angles will be reduced by an amount which depends on the so called maser instability [12].

We have shown that stimulated coherent transitions are caused by the effect of the relativistic mass increase on the gyro-frequency leading to a bunching of the phases of the gyrating particles. Whenever the *coherency condition*,

$$a \gg 1 \,, \tag{8}$$

is satisfied, the unharmonic oscillator term in Eq. (5) becomes predominant. The unharmonic oscillator term predicts the coherent absorptions for $x > 0$, i.e. $(\omega_c^*/\gamma_\perp^*) > \omega_{rf}^*$, which is interpreted as that the coherently gyrating particles absorb the rf power to increase their mass so as to yield the resonance $\omega_c^*/\gamma_\perp^* = \omega_{rf}^*$. While the coherent emissions are favored to yield the

resonance in the case $x < 0$. This feature is seen in the $F(x)$ curves with $a \gg 1$ in Fig. 2. This finding indicates the possibility of CMC, since the particles with the higher transverse energy i.e. $\gamma_\perp^* > \omega_c^*/\omega_{rf}^*$ undergo coherent emissions while the particles with the lower energy i.e. $\gamma_\perp^* < \omega_c^*/\omega_{rf}^*$ undergo coherent absorptions under the stimulation of the rf field.

Though the principle of CMC is based on the cyclotron maser mechanism, the kernel of the CMC problem is that how control the dynamics of gyrating particles but not to extract extensively radiations from the particles on the contrary to the cyclotron maser developments devoted so far. On the basis of this viewpoint, the following basic conditions are introduced for CMC.

1) At the CMC section, the solenoidal magnetic field is so uniform that its fractional non-uniformity is negligibly small compared to $2\omega_c\tau$ over the field space.

2) The rf cavity is uniformly long so that the unharmonicity of the rf field due to the edge effect can be neglected.

3) The power of stimulating rf field fed to the cavity is much stronger than that radiated or absorbed by the gyrating particles and thus its disturbance or heating can be completely disregarded.

Under these conditions, the CMC mechanism in the transverse energy can be investigated through a simple analytical treatment based on the transition rate formulae Eqs. (5) and (7).

In an experimental situation, the phase debunching time τ^* is not necessarily constant and determined generally by the gyration state of particles which is influenced by the intrabeam scattering, the irregularities of electromagnetic fields and so on. However, in the case of single pass cooling, the phase debunching time τ^* is basically the flight time t^* in the rf field. Eqs. (4) and (6) are, as a consequence, replaced by the following equations:

$$a \equiv 2\omega_c^* t^* (1 - \gamma_\perp^{-1}) \,, \tag{9}$$

$$x \equiv 2t^* \left[(\omega_c^*/\gamma_\perp) - \omega_{rf}^* \right] \,. \tag{10}$$

The basic discussions of CMC are developed here mostly along the treatments in the previous CMC papers [7,8] which provide a very simple estimate of CMC speed. The rate formula, can be approximated as

$$\frac{d\gamma_\perp}{dt^*} = \frac{4\pi r_p I^*(\omega_{rf}^*) t^*}{\gamma_\perp^2 m_0 c} 2ax \,, \tag{11}$$

under the *coherency condition*, $a \gg 1$, and further the initial transverse energy distribution limited between the emission and the absorption maxima i.e. $-3^{-1/2} < x < 3^{-1/2}$ neglecting the second and higher order terms of x. The cooling time $\tau_\perp$ for the transverse energy is now defined in the laboratory frame by the logarithmic decrement as,

$$\tau_\perp \equiv \frac{t}{\ln \left[(\Delta\gamma_\perp)_0 / \Delta\gamma_\perp \right]} \,, \tag{12}$$

where $(\Delta\gamma_\perp) m_0 c^2$ and $(\Delta\gamma_\perp)_0 m_0 c^2$ are the half width of transverse energy spread at the half maximum and its initial value, respectively. The value of $\tau_\perp$ is obtained by specifying the tuning conditions which are required for CMC. In the region, $-3^{-1/2} < x < 3^{-1/2}$, the mean value of the distribution shall be such that the gyro-frequency of particles of mean transverse energy $\gamma_\perp \cdot m_0 c^2$ is in coincidence with the rf frequency and the energy spread such that the corresponding x-values of the particles are kept in the range between the peak values of $F(x)$ in Eq. (5). We have thus $\omega_c^*/\bar{\gamma}_\perp = \omega_{rf}^*$, i.e.

$$\omega_c/\bar{\gamma}_\perp = (1 - \beta_\parallel \beta_{rf}) \omega_{rf} \,, \tag{13}$$

recalling $\omega_c^* = \omega_c\gamma_\parallel$ and $\omega_{rf}^* = \omega_{rf}(1-\beta_\parallel\beta_{rf})\gamma_\parallel$. Here, $c\beta_{rf}$ denotes the propagation velocity of the rf field along the particle travelling axis. Also we have

$$\Delta\gamma_\perp/\bar{\gamma}_\perp \sim \bar{\gamma}_\perp/2\omega_c t \ . \tag{14}$$

Eq. (14) provides an estimate of coolable energy range. Around the resonance $x = 0$, x may be approximated as

$$x \sim -(2\omega_c t/\bar{\gamma}_\perp)(\Delta\gamma_\perp/\bar{\gamma}_\perp) \ . \tag{15}$$

Using Eqs. (11), (14) and (15), the transition rate formula is now rewritten in the laboratory frame as,

$$\frac{\mathrm{d}}{\mathrm{d}t}(\Delta\gamma_\perp) = -\frac{4\pi r_p I(\omega_{rf})}{ceB_0}\left(\frac{2\omega_c t}{\bar{\gamma}_\perp}\right)^3 \frac{(1-\beta_\parallel\beta_{rf})(\bar{\gamma}_\perp - 1)}{\bar{\gamma}_\perp^2}\Delta\gamma_\perp \ . \tag{16}$$

and we obtain,

$$\Delta\gamma_\perp = (\Delta\gamma_\perp)_0 \exp\left[-\frac{\pi r_p I(\omega_{rf})}{ceB_0}\left(\frac{2\omega_c}{\bar{\gamma}_\perp}\right)^3 \frac{(1-\beta_\parallel\beta_{rf})(\bar{\gamma}_\perp - 1)}{\bar{\gamma}_\perp^2} t^4\right] \ . \tag{17}$$

The cooling time $\tau_\perp$ defined in Eq. (12) becomes,

$$\tau_\perp \sim \frac{ceB_0}{\pi r_p I(\omega_{rf})}\left(\frac{\bar{\gamma}_\perp}{2\omega_c t}\right)^3 \frac{\bar{\gamma}_\perp^2}{(1-\beta_\parallel\beta_{rf})(\bar{\gamma}_\perp - 1)} \ . \tag{18}$$

It may be of particular importance to note that *the cooling time $\tau_\perp$ is not affected by the relativistic time dilation, that is, independent of the longitudinal velocity of particles, except for the Doppler shift factor $(1-\beta_\parallel\beta_{rf})$. However, this factor will shorten the cooling time when the backward travelling rf wave is used*, which may be the natural choice in high energy particle accelerators and storage rings since the frequency in the laboratory frame becomes lower and high power levels may more easily be achieved.

4 CMC IN THE LONGITUDINAL ENERGY

As seen in Fig. 1, a fraction of the longitudinal energy is changed to the transverse energy by introducing the particles in the CMC section at a small angle θ to the longitudinal axis of the section (s-axis in Fig. 1). Further, particle orbits of equimomentum are adjusted to be nearly parallel. Then the particles gyrate keeping a mean value of $\gamma_\perp^*$, where

$$\gamma_\perp^* = \gamma_\perp = \gamma - \gamma_\parallel + 1 \sim 1 + (1/2\gamma_\parallel)\left[(\theta\beta_\parallel\gamma)^2 + (p_\perp/m_0c)^2\right] \ , \tag{19}$$

with $\gamma^2 = 1+\beta^2\gamma^2$, $\gamma_\parallel^2 = 1+\beta_\parallel^2\gamma^2$. Here $p_\perp$ denotes the intrinsic transverse momentum of the particles, that is, the transverse momentum outside the CMC section. The mean width of $\gamma_\perp$ is given by

$$\Delta\bar{\gamma}_\perp = \left[D' + (\theta/2)(1+\gamma_\parallel^{-2})\right]\theta\Delta\gamma_\parallel + (1/2\gamma_\parallel)(p_\perp/m_0c)^2 \ , \tag{20}$$

recalling that $\Delta\theta = D'\Delta(\beta_\parallel\gamma)/\beta_\parallel\gamma$ and $\beta_\parallel\gamma\Delta(\beta_\parallel\gamma) = \gamma_\parallel\Delta\gamma_\parallel$. Here D' is the derivative of momentum dispersion of the ring or accelerator lattice at the entrance of the section. The positive sign of D' is defined along the deflection of ange θ. The peak value and the width of the transverse energy distribution can therefore be controlled practically by tuning the lattice elements.

In the practical cases $\gamma_\perp \gg \Delta\gamma_\perp$, the substantial part of $\gamma_\perp$ is transformed from $\gamma_\parallel$ implying that the first term of $\Delta\gamma_\parallel$ in $\Delta\gamma_\perp$ is much larger than the second term of $p_\perp$ in

Eq. (20). The change in the transverse energy, $d\gamma_\perp/dt$, therefore reflects to the change in the longitudinal energy, $d\gamma_\parallel/dt$, resulting in the cooling or heating in the longitudinal energy. Besides this an additional change in the longitudinal energy is resulted from the momentum conservation between the particle and the rf field along the longitudinal axis of the rf cavity,

$$\frac{d(\beta_\parallel\gamma)}{d\gamma} = \beta_{rf} \ . \tag{21}$$

The momentum conservation, Eq. (21) leads to

$$\frac{d\gamma_\parallel}{dt} = \frac{\beta_\parallel\beta_{rf}}{(\gamma_\parallel/\gamma) - \beta_\parallel\beta_{rf}} \frac{d\gamma_\perp}{dt} \ , \tag{22}$$

recalling again $\beta_\parallel\gamma\Delta(\beta_\parallel\gamma) = \gamma_\parallel\Delta\gamma_\parallel$ and $\Delta\gamma = \Delta\gamma_\parallel + \Delta\gamma_\perp$. Summing the change in Eq. (22) and $d\gamma_\perp/dt$ as a function of $\gamma_\parallel$ in Eq. (19), we obtain

$$\frac{d\gamma_\parallel}{dt} = \frac{(\gamma_\parallel/\gamma)}{(\gamma_\parallel/\gamma) - \beta_\parallel\beta_{rf}} \frac{d\gamma_\perp}{dt} \ . \tag{23}$$

If we replace the above $d\gamma_\perp/dt$ by the right-hand side of Eq. (11) in the laboratory frame and use Eq. (20) taking out the $\Delta\gamma_\parallel$ independent term, we have the associated cooling time for the longitudinal phase space,

$$\tau_\parallel = \frac{(\gamma_\parallel/\gamma) - \beta_\parallel\beta_{rf}}{\left[D' + (\theta/2)(1+\gamma_\parallel^{-2})\right]\theta\gamma_\parallel/\gamma} \tau_\perp \ . \tag{24}$$

It is seen in Eq. (24) that the cooling in the transverse energy results in also the cooling in the longitudinal energy i.e. $\tau_\parallel > 0$ whenever

$$|D'| < |\theta/2|(1+\gamma_\parallel^{-2}) \quad \text{or} \quad D'\theta > 0 \ . \tag{25}$$

5 PHASE LOCKING OF GYRATION

As seen in the previous sections, CMC depends critically on the phase debunching time τ which affects the CMC speed and determines together with ω_c and $\gamma_\perp$, the *coherency condition* $a \gg 1$. High energy particles pass through a single CMC section of length L_0 in a short time $\tau = L_0/\beta_\parallel c$ which limits the number of gyrations and hence the coherent emission or absorption as compared to that of cyclotron maser devices such as a gyrotron in which electrons usually gyrate some 10 times. As an example, 2 GeV electrons traverse a CMC section of $L_0 = 6.0\,\mathrm{m}$ and $B_0 = 3\,\mathrm{T}$ in a time $\tau = 20\,\mathrm{ns}$ with a gyro-frequency $\omega_c/2\pi = 1.3 \times 10^8$ and the value of $2\omega_c\tau = 5$. This gives $a < 2$ for $\gamma_\perp < 1.4$ and hence the *coherency condition* $a \gg 1$ is not fulfilled. For ion beams, the situation is evidently worse and $a = 0$.

However, since a circulating particle passes the CMC section many times, the effective length over which CMC may act is much greater than L_0. Furthermore subdivided multiple CMC sections, in which gyration angles of the particles are very small, would be greatly useful in the practical cases in order to make the electrode gap of rf cavities very narrow. It is therefore essential to keep the bunched phases of gyrations unchanged in order to have an additive coherent emission or absorption of radiations during multiple traversals of the particles through the multiple CMC sections. The phase of the gyration can be controlled within a certain range, if the stimulating rf field is synchronized with the phase of the accelerating rf field which determines the synchrotron phase stability of the circulating particles. The condition of *phase*

locking of gyration will therefore be introduced and this concept is especially essential to the cooling of ion and high energy electron beams.

The condition of *phase locking* is derived by considering the change of the angle ϕ_0 of the gyration during one particle revolution in the synchrotron or ring:

$$\phi_0 = \frac{1}{\beta_\parallel \gamma_\parallel c} \oint \omega^*(r,s)\mathrm{d}s = \frac{\omega_c^*}{\beta_\parallel \gamma_\parallel \gamma_\perp c B_0} \oint B_s(r,s)\mathrm{d}s \ . \tag{26}$$

Here, $\omega^*(r,s)$ is the angular frequency of the gyration due to the longitudinal component of the magnetic field $B_s(r,s)$. The integrals are the closed line integral along the reference particle orbit. If $\phi_0 = 2n\pi$ $(n = 0,1,2,\ldots)$ is independent of orbits, the particle would recirculate in the ring without any change of gyration phase. The relativistic phase bunching due to $\gamma_\perp$ could therefore act in a repetitive fashion and yield the coherent emission or absorption of radiations in the CMC sections thereby affecting remarkably the transverse kinetic energy.

If the phase angle shifts by an amount $\Delta\phi_0$ per turn, the number of phase bunched recirculations is limited within $\pi/\Delta\phi_0$ resulting in an effective length for CMC of about $\pi L_0/\Delta\phi_0$. This determines the phase debunching time $\tau = \pi L_0/\beta_\parallel c\Delta\phi_0$ and hence $\gamma_\perp/2\omega_c\tau$ as

$$\begin{aligned} \frac{\gamma_\perp}{2\omega_c\tau} &\sim \frac{\beta_\parallel\gamma_\parallel\gamma_\perp}{2B_0L_0}\Delta\left[\frac{1}{\beta_\parallel\gamma_\parallel\gamma_\perp}\oint B_s(r,s)\mathrm{d}s\right] \\ &= \frac{1}{2B_0L_0}\left\{\beta_\parallel\gamma_\parallel\gamma_\perp\oint B_s(r,s)\mathrm{d}s\,\Delta\left[\frac{1}{\beta_\parallel\gamma_\parallel\gamma_\perp}\right] + \oint \Delta B_s(r,s)\mathrm{d}s\right\} \ . \end{aligned} \tag{27}$$

The first of the two terms in the large parentheses can be made to vanish independently of $\gamma_\parallel$ and $\gamma_\perp$ under the condition of *phase locking*:

$$\oint B_s(r,s)\mathrm{d}s = 0 \ . \tag{28}$$

This can be achieved by introducing CMC sections consisting of a pair of solenoidal magnets with antisymmetric configuration and corresponding rf cavities as shown in Fig. 1. The second term in Eq. (27) takes into account variations in the fields and consists of those of solenoidal magnets

$$\int \Delta B_s(r,s)\mathrm{d}s = -\frac{1}{4}\frac{\mathrm{d}}{\mathrm{d}s}B_s(0,s)r^2 + \ldots \ , \tag{29}$$

and of lattice magnets,

$$\int \Delta B_s(r,s)\mathrm{d}s = B_r(0,s)r + \frac{1}{6}\frac{\mathrm{d}^2}{\mathrm{d}s^2}B_r(0,s)r^3 + \ldots \ . \tag{30}$$

However, these field integrals vanish for any symmetric equilibrium orbit. Hence any beam dynamical effects cannot cause the accumulation of these field integrals for a ring of symmetric lattice. This means that a ring of symmetric lattice does not break the phase bunching mechanism under the condition of *phase locking*.

Phase debunching may occur due to transverse impulses received by the particles in the fringing fields of solenoidal and lattice magnets. However, the impulses received at the entry and the exit of a magnet are oppositely directed and hence the perturbation is of second order. Moreover, the duration of one pass is small compared with the time period of the stimulating rf field $2\pi/\omega_{rf}$ and this fact will reduce the perturbation further.

The particles may exchange longitudinal and transverse energies during their passage through a rippled magnetic field of averaged value B_{av} defined by the relation $eB_{av}/m_0 =$

$2\pi\beta_{\parallel}\gamma_{\parallel}c/L_p$, L_p being the periodicity of the field [13]. This nonadiabatic process has a resonance feature like a depolarizing resonance in the acceleration of spin-polarized particles and hence, if necessary, a correction can be applied to the accelerator working point.

There are many other phase debunching mechanisms such as beam dynamical effects caused by interactions between the beam particles and lattice elements including vacuum chambers of ring, intrabeam scattering, frequency band widths of the stimulating and synchrotron accelerating rf fields, phase mismatching between multiple CMC rf cavities and so on. Some of them may be useful to adjust the value of coolable energy range, $\Delta\gamma_{\perp}/\gamma_{\perp}$ given in Eq. (14). Detailed investigations on these matters are left for further studies and developments.

6 EXPERIMENTAL TEST OF CMC

The most crucial problems to be tested experimentally are: does CMC work under the *CMC conditions* on the resonance, Eq. (13), can particles be cooled in the energy range according to Eq. (14) and can the extraordinarily rapid cooling be realized as predicted by Eq. (18). These problems have, in fact, so far never been investigated. On the other hand the maser mechanism has been utilized to extract radiation of high power from gyrating electrons. Since CMC is, in principle, applicable to any kind of charged particles with arbitrary energy, experimental tests using low energy electrons will provide indications of CMC, from which one may deduce features of CMC applied to high energy electron and ion beams.

In Fig. 3 is shown the experimental arrangement employed to test CMC. An electron beam of about 1 μA and 10 keV is accelerated by a thermionic electron gun with an active domain of about 0.5 mm in diameter. The gun is located outside a solenoidal magnetic field. The electrons pass through dual sets of electrostatic horizontal and vertical deflectors towards an orifice of 40 mm in diameter in a 15 mm thick iron end plate attached to the cylindrical iron yoke at the entrance of the solenoidal coil 500 mm long and 200 mm in inner diameter. The dual deflector system is arranged so as to adjust the position and direction of the electron beam at the fringing region of the magnetic field. This serves to transform adiabatically any desired fraction of the total kinetic energy into transverse kinetic energy with respect to the solenoid axis. Computer calculations of magnetic field distribution and electron trajectories also verified that this way of generating a helical motion worked with full efficiency up to the maximum beam energy but at the sacrifice in the very broad longitudinal energy, i.e. energy associated with the longitudinal momentum. After passing through the orifice, the gyrating electrons drift along the magnetic field and pass through an rf cavity with rectangular cross section located at the center of the solenoidal coil. Though three series of experiments are carried out through at different cavity modes, here described are typical results obtained using a cavity which is 100 mm wide, 50 mm high and 200 mm long and resonant at 2.09 GHz in the TE_{102} mode with the quality factor $Q = 8000$. The rf power fed to the cavity, adjustable between 0.1 μW and 400 mW, is monitored by means of a spectrum analyzer connected to the cavity. Over the cavity space the magnetic field is axially homogeneous within $\pm 10^{-4}$. The gyrating electrons are collected at a conductive ZnS screen of 25.3 mm in diameter, which is placed just behind an rf gird ring attached to the end window of the rf cavity. The ZnS screen can be electrostatically biased to measure the longitudinal drift energy of the electrons. Following the cavity, a video camera equipped with a read out system is set to measure the intensity of the ring shaped trace on the ZnS screen. Evidence as to the effectiveness with which the fringing region of the magnetic field and the dual deflector system function is also provided by comparing the value of accelerating voltage and the transverse kinetic energies of electrons obtained from the Larmor radius of the rings. The entire apparatus consisting of steel, copper and aluminum is evacuated by a turbo-molecular pump to about 6×10^{-5} Pa without any treatment such as baking out for desorption of gasses.

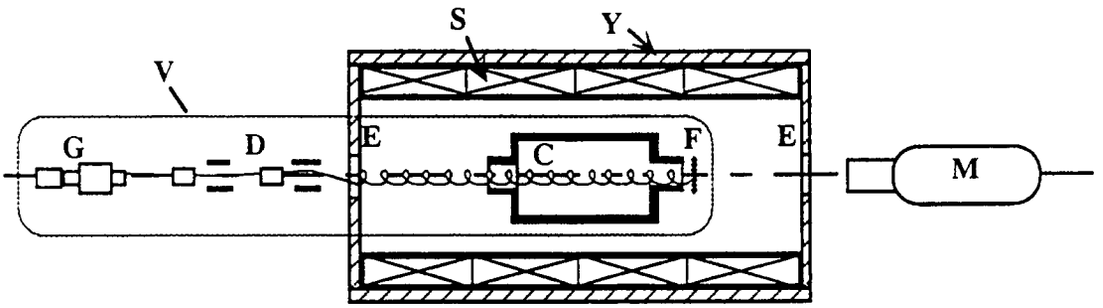

Figure 3: Experimental arrangement. G: electron gun; D: dual deflector system; E: end plate of magnet; C: rf cavity; F: conducting ZnS screen; Y: magnet yoke; S: solenoidal coil; V: vacuum enclosure; M: monitoring system.

Electrons pass through the rf cavity of axial length $L_0 = 0.20\,\mathrm{m}$ only once, which mostly determines the maximum permissible phase debunching time $L_0/c\beta_\parallel$ and hence a as,

$$a < (2\omega_c L_0/c\beta_\parallel)(1-\gamma_\perp^{-1})\ . \tag{31}$$

The phase debunching time was estimated for the collision of electrons with the residual gas and also for effects of the non-uniformities of the rf field and solenoidal magnetic field. It was found to be longer as much as two orders of magnitudes than the transit time of electrons in the cavity and thus neglected in Eq. (31). In the cavity, the rf field of the TE_{102} mode consists of two travelling waves of $\beta_{rf} = \pm 0.72$ propagating along the axis. The interaction of electrons with the rf field will thus be characterized by two different values of ω_{rf}^* and hence x due to the Doppler effect. The resulting two response functions $F(x)$ will have to be taken into account for analyzing the present experimental data based on electrons with extremely low longitudinal drift energy less than 100 eV. This consideration is, of course, unnecessary in the practical cases of high energy particles, since they interact with only one of the forward- or backward-travelling waves. In the present experiment using a short rf cavity, it is essential to reduce the drift energy of the electrons to realize a sufficient *phase debunching time* and hence a sufficiently large value of *coherency factor a* for fully developing the CMC effect. Further, the low drift energy exludes strictly the possibility of the transfer of the longitudinal energy to the transverse energy.

To find the resonance, the magnetic field was swept around the value $B_0 = 0.075\,\mathrm{T}$ which corresponds to the non-relativistic cyclotron resonance, $\omega_{rf} = \omega_c$. A very strong rf power loss was found at $\omega_{rf} = \omega_c$ regardless electron sources such as the electron gun and the ionization vacuum gauge. Most likely the rf power loss is caused by stray electrons emitted from the walls of the apparatus generating an avalanche driven by the rf field, so called *multifactoring effect.* Any CMC effect close to the resonance at $\omega_{rf} = \omega_c$ is therefore difficult to observe. The difficulty of resolving the CMC effect due to the absorption of stray electrons is related to the particular condition of present small scale experiment with low energy electron beam and a small drift velocity resulting in two overlapping response functions mentioned above. For instance, the response function $F(x)$ for 10 keV electrons is partially located in the region where the rf power is absorbed by the stray electrons resulting in an insufficient rf power for the CMC effect to take place in the coherent emission mode, $x < 0$. Throughout the present experiments, only the

CMC condition of coherent absorption mode,

$$\frac{\omega_c}{(\gamma_\perp)_{\max}} = (1 - \beta_\parallel \beta_{rf})\,\omega_{rf} \ , \tag{32}$$

was therefore carefully investigated, $(\gamma_\perp)_{\max}$ denoting the maximum value of $\gamma_\perp$. In fact, it was found that the coherent absorption mode was much more clearly observed than the coherent emission mode due to less interference with the stray electron resonances.

7 OBSERVATION OF CMC – COMPRESSION OF ENERGY SPREAD

In spite of the problems outlined in the previous section, we have obtained some first inspiring indications of *cooling* of the transverse energy-time phase space.

In the experiments, the transverse kinetic energy ranged from below 10 keV to beyond 20 keV while the longitudinal drift energy was set at 50 – 300 eV. It is thus possible to deduce the transverse kinetic energy distribution precisely by measuring the broadening of the Larmor radii of gyrating electrons depicted on the ZnS screen assuming that the centers of gyration are remained fixed. The latter point was verified experimentally as explained below.

As a demonstration of CMC, the Larmor radii arising from *heating* and *absorptive cooling* of electrons are compared in Fig. 4 at a fixed rf power of 100 mV for the cases of initial transverse kinetic energies of 8, 10 and 12 keV. The cyclotron frequency $\omega_c/2\pi = 2.16\,\mathrm{GHz}(B_0 = 0.772\,\mathrm{T})$ was fixed so that electrons of $(\gamma_\perp)_{\max} = 1.04$ were resonant with the rf frequency $\omega_{rf}/2\pi = 2.09\,\mathrm{GHz}$. The longitudinal drift energy was adjusted to be in the range 50 – 300 eV independently of the initial transverse kinetic energy values. Because of this large spread of longitudinal drift energy, the electrons were expected to consist of groups, such as those of $a \sim 1$ and $a \gg 1$ depending on their drift velocity $\beta_\parallel c$ (see Eq. (31)). The main feature of the pictures with *rf on* in Fig. 4, in which circular patterns are found, is the formation of discrete circles enclosing the broad band of circles.

For the electrons of $a \sim 1$, only incoherent transitions are expected from discussions in Section 2 (see also Appendix), which are verified by the inner broad band of circles as seen in the pictures of *rf on* in Fig. 4. The broad band is generated by the rf field and expands with the increase of initial transverse kinetic energy. The mean radius is almost same as the initial Larmor radius with *rf off*. It is thus a crucial problem whether the formation of the broad band of circles is an effect of the possible oscillation of the centers of gyration or a result from axially symmetric broadening of the Larmor radius due to *heating*. In order to settle the problem, an experiment was performed. A copper baffle was inserted perpendicular to the transverse plane outside the cavity exit aperture. The baffle served to cut out a part of the gyrating electrons. The electrons were shifted by means of the deflector system, laterally towards the copper baffle. If the broad circles were formed by electrons gyrating about different centers, the successive cutting of the outer periphery would have resulted in visible effects also at the inner periphery. By cutting away so much of the broad circle that the remaining width was less than the width of the circle observed without the rf field applied, it was confirmed that the oscillations of centers caused by the rf field were negligible. The rf field thus accelerated or decelerated the electrons transversely without any marked change of the center of curvature. The feature should be associated with the broad band of circles, where the phases of gyration are homogeneously distributed with respect to the rf field.

The sharp outer circle in Fig. 4 corresponds to a transverse kinetic energy of 23 keV and its radius is independent of the initial transverse kinetic energy. This energy coincides with the transverse energy at the resonance, $x = 0$, for a longitudinal drift energy around 50 eV. If the

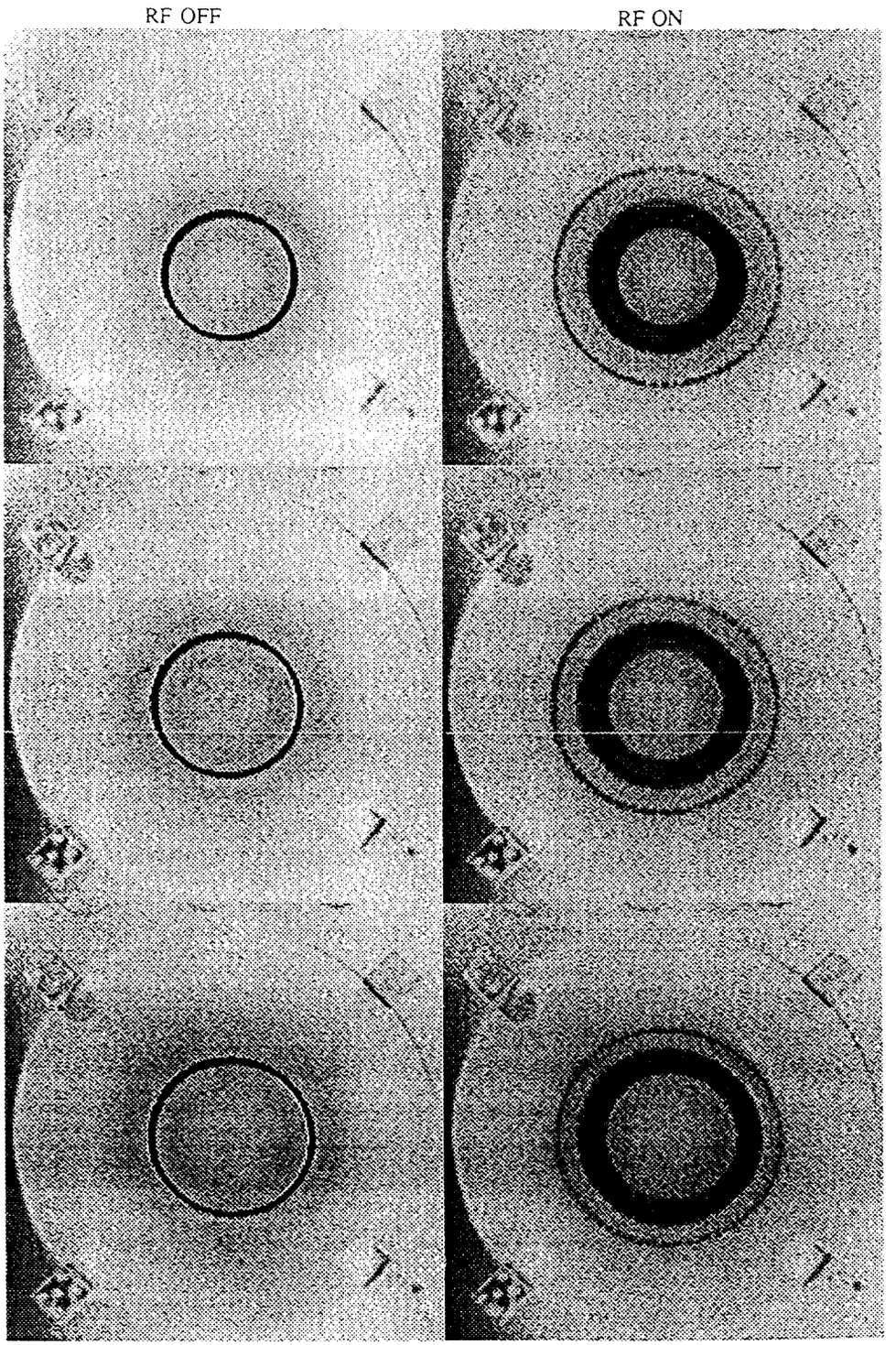

Figure 4: Comparison of the Larmor radii arising from *heating* and *absorptive cooling* of electrons. The patterns depicted on the ZnS screen for *rf on* and *rf off* at $\omega_c/2\pi = 2.16\,\mathrm{GHz}$ and $\omega_{rf}/2\pi = 2.09\,\mathrm{GHz}$ for the initial transverse kinetic energies: (a) 8 keV, (b) 10 keV, (c) 12 keV. The sharp outer circles correspond to the electron energy of 23 keV, which were observed without accompanied by the broad band of inner circles when the longitudinal drift energy spread was reduced.

pictures for the three cases in Fig. 4 are superimposed, under the assumption that electrons were strictly governed by the rf field only, it can be visualized how three initial sets of electrons, 8, 10 and 12 keV will reach a final energy 23 keV. Hence, an energy spread of 4 keV has been eliminated as far as these electrons concerned. The above assumption is reasonable for electrons undergoing coherent emission or absorption of radiation since any spontaneous or incoherent effects such as intrabeam scattering effect can be neglected. From the reduction of the energy spread, $\Delta\gamma_\perp/(\Delta\gamma_\perp)_0 < 0.1$, the cooling time $\tau_\perp$ was estimated to be $\tau_\perp < L_0/\beta_\parallel c \ln 10 \approx 20$ns using the transit time of electrons in the cavity $L_0/\beta_\parallel c = 50$ ns. The value is consistent with the value $\tau_\perp = 10$ ns predicted from Eq. (18) using the values $B_0 = 0.077$ T, $I(\omega_{rf}) = 2 \times 10^4$ Wm^{-2}, $\gamma_\perp = 1.04$, $\beta_\parallel = 0.014$ and $\beta_{rf} = -0.72$. The value of $I(\omega_{rf})$ was obtained from the volume 10^{-3}m^3 and $Q = 8000$ of the cavity at a power of 100 mW.

The simultaneous appearance of broad inner band of circles and sharp outer circle is due to the extremely large fractional spread of longitudinal drift energy. In fact, the broad circle and the sharp circle were separately observed in the other experiments by reducing the spread of longitudinal energy. This indicates that the *cooling* and *heating* of electrons are controllable. It is however very curious that the electrons with a broad band of longitudinal energies split clearly into two groups, one of *heating* and one of *cooling*.

Once electrons with $a > 1$ gain their transverse kinetic energy through the coherent absorption of rf energy, the *coherency factor* a increases drastically with time together with the gain of the transverse kinetic energy. The increase of a is further intensified by the decrease of drift velocity $\beta_\parallel c$ due to the recoil effect in the coherent absorption of backward travelling rf wave energy. The amount of the recoil energy, $\Delta T_\parallel = \beta_\parallel \beta_{rf} \Delta T_\perp$ is of the same order as the longitudinal energy $T_\parallel$. For instance, $\Delta T_\parallel = 70$ eV for a gain of transverse energy $\Delta T_\perp = 5$ keV. For these electrons the effective value of the *coherency factor* was estimated to be $a > 15$. Then the electrons reach the resonance point $x = 0$ *instantly*. On the contrary, for electrons with higher drift energy, $T_\parallel > 100$ eV and hence $a = 1$, their transverse kinetic energy is almost unchanged due to their incoherent interaction with the rf field losing a chance of coherent absorption of stimulating rf energy.

8 OBSERVATION OF CMC – COMPRESSION OF PHASE ANGLE SPREAD

The CMC principle so far discussed has been based on the mechanism of bunching of phases of gyrating particles with respect to the applied rf field caused by the relativistic effects. However, in the experiments, the indication of phase bunching was obtained only indirectly through the drastic energy gain associated with the outer circles in Fig. 4. In fact, there was no way of explaining the energy gain and the sharpness of the outer circles other than assuming that the electrons are in resonance at a defined phase with the rf field. However, the arc or spot pattern was not observed on the ZnS screen. This was again caused by the very broad spectrum of longitudinal energies. Further, this rounding off effect on the patterns was enhanced by the recoil effect due to the radiation absorbed coherently by the electrons as described in the previous section.

The indication of phase bunching in CMC was provided by another experiment in which the sharp outer circle was not necessarily concentric with the broad band of inner circles. When the initial center of gyration was shifted away from the central axis of rf cavity, the center of the sharp circle shifted towards the central axis of cavity, where the strength of rf field was maximum, while the broad band of inner circle was always concentric with the initially shifted center of gyration. This effect can not be explained unless the electrons forming the sharp circle are assumed to have a certain degree of phase correlation with respect to the rf field,

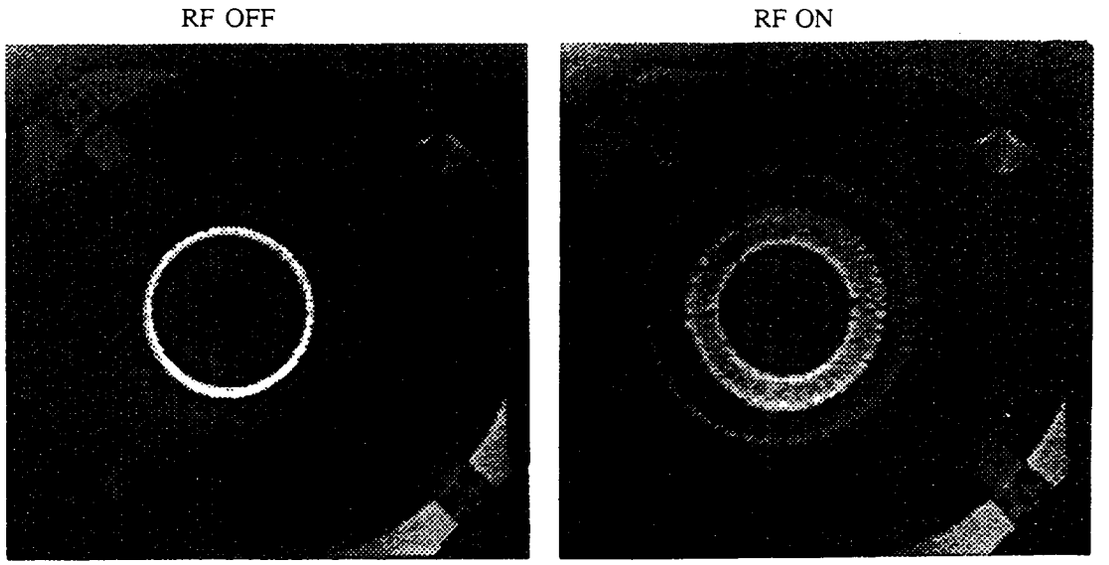

Figure 5: Indication of phase bunching for the cooled electrons of sharp circle. When the initial center of circle is shifted away from the central axis of the rf cavity, the sharp outer circle with *rf on* picture shifts back towards the central axis where the strength of the rf field is maximum. The broad band of inner circle is symmetric with the initial center of *rf off* circle. The shift tends to be larger for the further away from the central axis of the rf cavity. The electron beam is prepared with a high transverse to longitudinal kinetic energy ratio. The total energy 9 keV, cathode current 0.5 μA, rf field of 2.091 GHz and 200 mW, cyclotron frequency 2.165 GHz. (The pictures are displayed without inversion.)

since electrons with phase matched gyration of absorption mode are always pulled towards the maximum field area. In Fig. 5, the magnetic field is directed out of the paper and the electrons gyrate in the counter clockwise direction. The axis of the solenoid as well as the central axis of the cavity crosses the ZnS screen slightly to the left of the top of the *rf off* circle. The electric field vector of the rf field is in the vertical direction. When the rf field is on, the broad band of circles is always concentric with the initial *rf off* circle. The sharp circle is however laterally shifted as seen in Fig. 5. The shift tends to be larger for the further away from the central axis of cavity.

9 SUMMARY

A new principle for the cooling of charged particle beams has been presented. The formalism for this *coherent microwave cooling* (CMC) was derived in a quantum mechanical oscillator approach and in a classical dynamical approach (Appendix). Both approaches lead to the same results. It was shown that both the energy cooling and the phase bunching of particles are caused by the relativistic effects on the particle gyro-frequency resulting in the compression in the energy-time phase space of gyrating particles.

The new principle has been tested experimentally. The experimental results provided some inspiring indications of the *cooling* of the transverse energy-time phase space of electrons. Dramatically rapid cooling, < 20 ns as predicted, was observed for the transverse energy. Electrons initially in the range $8 - 12$ keV, were all found to accumulate at one discrete energy, 23 keV. A phase bunching effect was observed indirectly in the gyration of the accumulated electrons of 23 keV energy.

The agreement between the prediction and the experimental results implies that in principle any kind of charged particle beams can be cooled in a single pass through the CMC sections regardless of their energy.

10 ACKNOWLEDGEMENT

I would like to acknowledge to Professor Sven Kullander of Uppsala University for his stimulating discussions and continuous encouragements throughout the CMC research. My greatest thanks are also directed to Dr. Fredrik Kullander for his excellent activities shown in the CMC experiments. Without their mighty promotion, this work might not be completed. I am also indebted to the kind help of members of Osaka University and Uppsala University, especially, Drs. A. Ando, Y. Mizuno, E. Brändas, V. Pavlenko, B. Karlsson and Professor A. Johansson for their collaboration at some stages of the projects. Also appreciated are grants from the Monbusho (Ministry of Education, Japan) International Scientific Research Program and the Royal Swedish Academy of Sciences through their Nobel Committee for Physics.

APPENDIX

MECHANISM OF CYCLOTRON MASER – PARTICLE DYNAMICAL APPROACH

We start from the equation of motion and rewrite it in the instantaneous transverse energy transition rate for a particle as,

$$\frac{\mathrm{d}\gamma_\perp}{\mathrm{d}t^*} = \frac{e\beta_\perp E^*_{\mathrm{rf}}}{m_0 c}\cos\phi(t^*)\ , \qquad \text{with} \quad \begin{cases} \phi(t^*) \equiv \Omega^* t^* + \phi_0\ , \\ \Omega^* \equiv (\omega^*_{\mathrm{c}}/\gamma_\perp) - \omega^*_{\mathrm{rf}}\ , \end{cases} \tag{33}$$

$\phi(t^*)$, ϕ_0 and Ω^* being the phase, the initial phase and the mismatching frequency of particle gyration, respectively, with respect to the rf field.

If the energy of the system of gyrating particles and the rf field were conserved, the speed $\beta_\perp c$ and the frequency $\omega^*_{\mathrm{c}}/\gamma_\perp$ are constant on average. Eq. (33) gives only the fluctuation in the transition rate occurring during the course of a single period of gyration and thus the state of gyration is stable. That is to say, nothing happens in the energy-time phase space of gyrating particles yielding a typical Liouvillean system. However, according to the electromagnetic theory, gyrating charged particles generally emit radiation associated with their acceleration or deceleration resulting in the loss of energy of the system. Such radiation loss introduces kind of frictional forces, such as the speed dependent – and the gyro-frequency dependent – forces yielding a non-Liouvillean system of unharmonic gyration. These frictional forces cause the radiation loss of the system in proportion to $\mathrm{d}\beta_\perp$ and $\mathrm{d}(\omega^*_{\mathrm{c}}/\gamma_\perp)$ as,

$$\mathrm{d}\left(\frac{\mathrm{d}\gamma_\perp}{\mathrm{d}t^*}\right) = \mathrm{d}\left(\frac{\mathrm{d}\gamma_\perp}{\mathrm{d}t^*}\right)_1 + \mathrm{d}\left(\frac{\mathrm{d}\gamma_\perp}{\mathrm{d}t^*}\right)_2\ , \tag{34}$$

with

$$\mathrm{d}\left(\frac{\mathrm{d}\gamma_\perp}{\mathrm{d}t^*}\right)_1 \equiv \frac{\partial}{\partial\beta_\perp}\left(\frac{\mathrm{d}\gamma_\perp}{\mathrm{d}t^*}\right)\mathrm{d}\beta_\perp \ , \tag{35}$$

$$\mathrm{d}\left(\frac{\mathrm{d}\gamma_\perp}{\mathrm{d}t^*}\right)_2 \equiv \frac{\partial}{\partial(\omega_c^*/\gamma_\perp)}\left(\frac{\mathrm{d}\gamma_\perp}{\mathrm{d}t^*}\right)\mathrm{d}\left(\frac{\omega_c^*}{\gamma_\perp}\right) \ , \tag{36}$$

where both $\mathrm{d}\beta_\perp$ and $\mathrm{d}(\omega_c^*/\gamma_\perp)$ are functions of t^* through Eq. (33) and hence,

$$\mathrm{d}\beta_\perp = \frac{\partial\beta_\perp}{\partial\gamma_\perp}\mathrm{d}\gamma_\perp = \frac{1}{\beta_\perp\gamma_\perp^3}\frac{\mathrm{d}\gamma_\perp}{\mathrm{d}t^*}\mathrm{d}t^* = \frac{eE_{\mathrm{rf}}^*}{m_0c}\frac{1}{\gamma_\perp^3}\cos(\Omega^*t^*+\phi_0)\mathrm{d}t^* \ , \tag{37}$$

$$\mathrm{d}\left(\frac{\omega_c^*}{\gamma_\perp}\right) = \frac{\partial}{\partial\gamma_\perp}\left(\frac{\omega_c^*}{\gamma_\perp}\right)\mathrm{d}\gamma_\perp = -\frac{\omega_c^*}{\gamma_\perp^2}\frac{\mathrm{d}\gamma_\perp}{\mathrm{d}t^*}\mathrm{d}t^* = -\frac{eE_{\mathrm{rf}}^*}{m_0c}\frac{\beta_\perp\omega_c^*}{\gamma_\perp^2}\cos(\Omega^*t^*+\phi_0)\mathrm{d}t^* \ . \tag{38}$$

Here, the factor $\mathrm{d}\gamma_\perp/\mathrm{d}t^*$ in Eqs. (37) and (38) has been replaced by the right-hand side of Eq. (33). Substituting Eqs. (37) and (38) into Eqs. (35) and (36), respectively, we obtain

$$\mathrm{d}\left(\frac{\mathrm{d}\gamma_\perp}{\mathrm{d}t^*}\right)_1 = \frac{1}{2}\left(\frac{eE_{\mathrm{rf}}^*}{\gamma_\perp m_0c}\right)^2\gamma_\perp^{-1}\cos(2\Omega^*t^*)\mathrm{d}t^* \ , \tag{39}$$

$$\mathrm{d}\left(\frac{\mathrm{d}\gamma_\perp}{\mathrm{d}t^*}\right)_2 = \frac{1}{2}\left(\frac{eE_{\mathrm{rf}}^*}{\gamma_\perp m_0c}\right)^2(1+\gamma_\perp^{-1})\omega_c^*t^*(1-\gamma_\perp^{-1})\sin(2\Omega^*t^*)\mathrm{d}t^* \ . \tag{40}$$

The energy loss in Eqs. (39) and (40) is the sum of energy of radiation induced by the rf field. The induced radiation has the same phase with the rf field which means $\phi(t^*) = 0$ at the resonance $\Omega^* = 0$. The initial phase ϕ_0 has therefore been dropped in Eqs. (39) and (40). Due to the presence of the frictional forces, the gyration of particles is not stable but damps with the mean life τ^*, – so called *phase debunching time*. For the particles of damped gyration, the transition rate due to the radiation loss can be obtained by means of Laplace transformation.

$$\frac{\mathrm{d}\gamma_\perp}{\mathrm{d}t^*} = \int_{t^*=0}^{\infty}\mathrm{e}^{-t^*/\tau^*}\mathrm{d}\left(\frac{\mathrm{d}\gamma_\perp}{\mathrm{d}t^*}\right) = \left(\frac{\mathrm{d}\gamma_\perp}{\mathrm{d}t^*}\right)_1 + \left(\frac{\mathrm{d}\gamma_\perp}{\mathrm{d}t^*}\right)_2 \ , \tag{41}$$

with

$$\left(\frac{\mathrm{d}\gamma_\perp}{\mathrm{d}t^*}\right)_1 = \frac{1}{2}\left(\frac{eE_{\mathrm{rf}}^*}{\gamma_\perp m_0c}\right)^2\gamma_\perp^{-1}\frac{\tau^*}{1+x^2} \approx \frac{1}{2}\left(\frac{eE_{\mathrm{rf}}^*}{\gamma_\perp m_0c}\right)^2\frac{\tau^*}{1+x^2} \ , \tag{42}$$

$$\left(\frac{\mathrm{d}\gamma_\perp}{\mathrm{d}t^*}\right)_2 = \frac{1}{2}\left(\frac{eE_{\mathrm{rf}}^*}{\gamma_\perp m_0c}\right)^2(1+\gamma_\perp^{-1})\frac{\tau^*ax}{(1+x^2)^2} \approx \frac{1}{2}\left(\frac{eE_{\mathrm{rf}}^*}{\gamma_\perp m_0c}\right)^2\frac{2\tau^*ax}{(1+x^2)^2} \ , \tag{43}$$

where

$$a \equiv 2\omega_c^*\tau^*(1-\gamma_\perp^{-1}) \ , \tag{44}$$

$$x \equiv 2\Omega^*\tau^* = 2\tau^*\left[(\omega_c^*/\gamma_\perp) - \omega_{\mathrm{rf}}^*\right] \ . \tag{45}$$

The rate formula, Eq. (41), is now represented as,

$$\frac{\mathrm{d}\gamma_\perp}{\mathrm{d}t^*} = \frac{1}{2}\left(\frac{eE_{\mathrm{rf}}^*}{\gamma_\perp m_0c}\right)^2\tau^*F(x) = \frac{4\pi r_{\mathrm{p}}}{\gamma_\perp^2 m_0c}I^*(\omega_{\mathrm{rf}}^*)\tau^*F(x) \ , \tag{46}$$

with

$$F(x) \equiv \frac{1}{1+x^2} + \frac{2ax}{(1+x^2)^2} \ . \tag{47}$$

The physical implication behind the derivation of Eqs. (41-47) is now found to be the extraction of the non-Liouvillean components caused by the stimulated radiation through elimination of the Liouvillean components, i.e. the fluctuation part from Eq. (33).

Comparing Eqs. (7) and (46), it is seen that both the particle dynamical approach and the oscillator approach lead to the same result. Though both approaches have so far been contrasted in the last three decade discussions on the cyclotron maser, nevertheless they are essentially identical and further they need not actually any assumptions such as the very weakly relativistic. However, the physics implicated behind the two different approaches is of special importance to note. As seen in the particle dynamical approach, the transition rate of unharmonic quadrupole oscillator term, Eq. (43), is derived as the first order effect as well as that of damped dipole oscillator term, Eq. (42). Therefore, the quadrupole oscillator term is, of course, not a second order effect, which has so far been misinterpreted after Schneider's theory based on the very weakly relativistic approximation [11].

The second order effects due to the second order derivatives of $\beta_\perp$ and $\omega_c^*/\gamma_\perp$ are small compared with the first order effects as much as the factor $(\omega_c^*/\gamma_\perp - \omega_{rf}^*)/\omega_c^*$ being negligibly small at the resonance. Another ones yield from the coupled two first order derivatives of $\beta_\perp$ and$\omega_c^*/\gamma_\perp$ which are, however, smaller than the first order effects by the factor of $(eE_{rf}^*\tau^*/2\gamma_\perp m_0 c)$ and thus practically again negligible.

MECHANISM OF PHASE BUNCHING OF GYRATION – PARTICLE DYNAMICAL APPROACH

We are ready to elucidate the mechanism of the phase bunching of particle gyration caused by relativistic effects. Due to the relativistic effects, the phase $\phi(t^*)$ is not a linear function of t^*. Recalling Eqs. (38) and (33), we obtain the derivative of $\cos\phi(t^*)$ as,

$$\mathrm{d}\left[\cos\phi(t^*)\right] = -\sin\phi(t^*)\frac{\partial\phi(t^*)}{\partial\gamma_\perp}\frac{\mathrm{d}\gamma_\perp}{\mathrm{d}t^*}\mathrm{d}t^* = \frac{e\beta_\perp E_{rf}^*\omega_c^* t^*}{2\gamma_\perp^2 m_0 c}\sin(2\Omega^* t^* + 2\phi_0)\mathrm{d}t^* \ . \tag{48}$$

When particles with the random distribution of initial phase ϕ_0 are subjected to the rf field during the phase debunching time τ^*, the average value of $\overline{\cos\phi(\tau^*)}$ is found through Laplace transformation. Recalling the discussion on the phase of induced radiation regarding Eqs. (39) and (40), we have

$$\overline{\cos\phi(\tau^*)} = \int_{t^*=0}^{\infty} \mathrm{e}^{-t^*/\tau^*}\mathrm{d}\left[\cos\phi(t^*)\right] = \left(\frac{eE_{rf}^*\beta_\perp c\tau^*}{\gamma_\perp m_0 c^2}\right)\left(\frac{\omega_c^*\tau^*}{\gamma_\perp}\right)\frac{2\Omega^*\tau^*}{[1+(2\Omega^*\tau^*)^2]^2} \ . \tag{49}$$

In the right-hand side of Eq. (49), the numerator in the first parenthesis denotes the energy transferred through the rf field to a particle during the phase debunching time τ^* and the second parenthesis is the gyration angle of the particle. Along the discussion in Section 3, τ^* is replaced by t^* for the case of single pass cooling and hence Eq. (49) may be replaced by

$$\overline{\cos\phi(t^*)} \approx \left(\frac{eE_{rf}^* a t^*}{\beta_\perp\gamma_\perp m_0 c}\right)\frac{2\Omega^* t^*}{[1+(2\Omega^* t^*)^2]^2} \ . \tag{50}$$

In Fig. 6 are shown phase diagrams, $|\overline{\cos\phi(t^*)}|$ vs $2|\Omega^*|t^*$. Here, $\Omega^* > 0$ and $\Omega^* < 0$ correspond to the cases of absorption and emission, respectively. The curve a) corresponds to the case $(eE_{rf}^* a t^*/\beta_\perp\gamma_\perp m_0 c) \gg 1$ at $2|\Omega^*|t^* = 3^{-1/2}$. Along the curve, a series of arrows indicates how the averaged value of $\overline{\cos\phi(t^*)}$ changes with $\Omega^* t^*$. At $t^* = 0$, the phases of

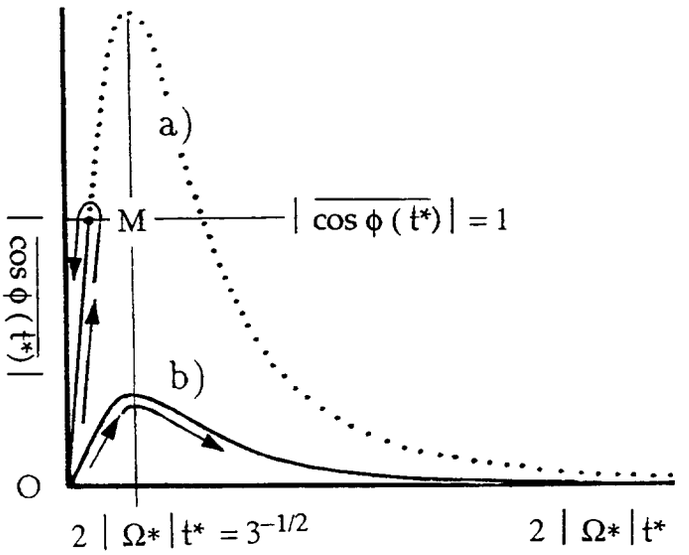

Figure 6: Phase diagram: $|\overline{\cos\phi(t^*)}|$ vs $2|\Omega^*|t^*$. Here the absorption and emission correspond to $\Omega^* > 0$ ($\overline{\cos\phi} > 0$) and $\Omega^* < 0$ ($\overline{\cos\phi} < 0$), respectively. The curve a) corresponds to the case $(eE^*_{rf}at^*/\beta_\perp\gamma_\perp m_0c) \gg 1$ at $2|\Omega^*|t^* = 3^{-1/2}$. At $t^* = 0$, the phases of particle gyration distribute at random and hence $\overline{\cos\phi(t^*)} = 0$. However, the phase bunching caused by the relativistic effect grows up with time t^* towards the phase matching point M where $|\overline{\cos\phi(t^*)}| \sim 1$. Then the mismatching frequency $|\Omega^*|$ falls off towards the resonance point O where $\Omega^* = (\omega^*_c/\gamma_\perp) - \omega^*_{rf} = 0$. At this M$\rightarrow$O process, the bunched phase shifts such that $|\overline{\cos\phi(t^*)}| \rightarrow 0$. If the value of $(eE^*_{rf}at^*/\beta_\perp\gamma_\perp m_0c)$ is not sufficiently large, the phase bunching cannot be fully developed missing both the matching point M and the resonance $\Omega^* = 0$ as seen in the curve b). In this case, $\overline{\cos\phi(t^*)}$ vanishes finally resulting in the random phase gyration

particle gyration distribute at random and hence $\overline{\cos\phi(t^*)} = 0$. However, the phase bunching caused by the relativistic effects grows up with flight time t^* towards the phase matching point M where $|\overline{\cos\phi(t^*)}| \sim 1$. At the matching point, the cooling action is maximum resulting in the drastic change of Ω^* towards the resonance point O where $\Omega^* = 0$. In the process M$\rightarrow$O, the bunched phase shifts such that $|\overline{\cos\phi(t^*)}| = 1 \rightarrow 0$.

In Fig. 6, the curve b) is another phase diagram where the value of $(eE^*_{rf}at^*/\beta_\perp\gamma_\perp m_0c)$ is not sufficiently large at $2|\Omega^*|t^* = 3^{-1/2}$ so that the phase bunching can not be fully developed missing both the matching point M and the resonance $\Omega^* = 0$. In this case, the value of $\overline{\cos\phi(t^*)}$ vanishes finally going back to the random phase gyration.

TABLE OF RADIATION OF GYRATING CHARGED PARTICLES

Gyration / Radiation	Incoherent gyration (Random phase)	Coherent gyration (Bunched phase)
Spontaneous radiation ($E_{rf} = 0$)	Cyclotron Radiation Incoherent emission $P \propto n$ $G = 1$ 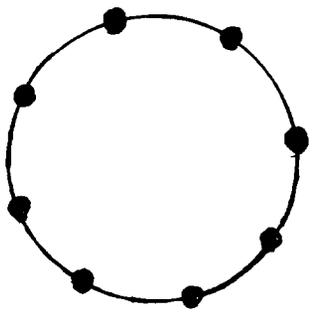	Bunched Cyclotron Radiation Coherent emission $P \propto n^2$ $G = n$ 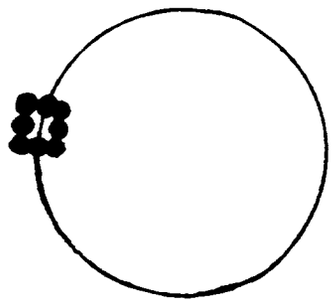
Stimulated radiation ($E_{rf} \neq 0$)	Damped Harmonic Oscillator Emission or absorption in phase with rf field $P \propto nE_{rf}^2$ $G = N_{photon}$ 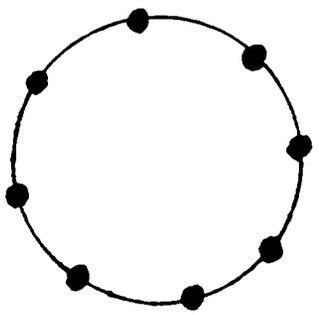	Super-damped Oscillator Emission or absorption in phase with rf field $P \propto anE_{rf}^2$ $G = aN_{photon}$ 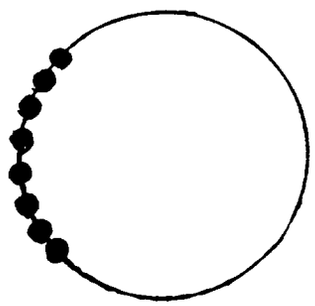

Table 1: Radiation of gyrating charged particles. E_{rf}: Electric field amplitude of stimulating rf field, P: Power of radiation, G: Enhancement of radiation rate, n: Number of gyrating charged particles, N_{photon}: Number density of photons of stimulating rf field, $a \equiv 2\omega_c\tau(1 - \gamma_\perp^{-1})$: Coherency factor ($a > 10$ for CMC).

REFERENCES

[1] G.I. Budker *et al.*, *Part. Acc.* **7** (1976) 197;
G.I. Budker and A.N. Skrinsky, *Usp. Fiz. Nauk.* **124** (1978) 561. [*Sov. Phys. Usp.* **21** (1978) 277];
H. Poth, *Phys. Rep.* **196** (1990) 135.

[2] A.N. Skrinsky and V.V. Parkhomchuk, *Fiz. Elem. Chastits At. Yadra* **12** (1981) 557. [*Sov. J. Part. Nucl.* **12** (1981) 223], and references cited therein.

[3] D, Möhl, G. Petrucci, L. Thorndahl and S. van der Meer, *Phys. Rep.* **58** (1980) 73.

[4] M. Sands, *Proc. Int. School "Enrico Fermi", 46th Course, Varenna, Italy*, ed. B. Touschek, Academic Press, New York, 1969.

[5] E. Bonderup, *CERN 90-04*, ed. S. Turner, (*Proc. CERN, Third Advanced Accelerator Physics Course, Uppsala, Sweden, 18-29 september 1989.*)

[6] K.Kilian, *Proc. Workshop on Electron Cooling and New Cooling Techniques*, (p. 239), eds. R. Calabrese and L. Tecchio, World Scientific Press, Singapore, 1991.

[7] H. Ikegami, *Phys. Rev. Lett.* **64** (1990) 1737; **64** (1990) 2593.

[8] H. Ikegami, *Phys. Scripta.* **48** (1993) 32;
(*Proc. Second International Conference on Particle Production near Threshold*, (Opening Talk), ed. C. Ekström).

[9] F. Kullander, *Cyclotron Maser Cooling*, PhD Thesis, Osaka University, 1993.

[10] L. Page, *Introduction to Theoretical Physics*, (3rd ed., p. 573), D. Van Nostrand, Toronto, 1952.

[11] R.Q. Twiss, *Aust. J. Phys.* **11** (1958) 564;
J. Schneider, *Phys. Rev. Lett.* **2** (1959) 504;
A.V. Gaponov, *Izv. VUSOV. Radiofiz.* **2** (1959) 450; **2** (1959) 837;

[12] P. Sprangle and A.T. Drobot, *IEEE Trans. Microwave* **MTT 25** (1977) 528.

[13] E.W. Laing and A.E. Robson, *Plasma. Phys.* **3** (1961) 146.

Particle Simulation of Cyclotron Maser Cooling Experiment

D. R. Whaley, M. Q. Tran, T. M. Tran

Centre de Recherches en Physique des Plasmas,
Association Euratom-Confédération Suisse,
Ecole Polytechnique Fédérale de Lausanne, 21 Av. des Bains,
CH-1007 Lausanne, Switzerland

Abstract

Cyclotron Maser Cooling has been proposed as a process by which the width of the energy distribution of a beam of particles can be significantly reduced[1]. A numerical simulation of the experiment demonstrating this process has been performed using classical equations to propagate the electron beam across the resonant cavity described in [1]. Results show that for conditions described, the beam/wave interaction results in a spreading of the beam in energy. Only for either a modulated or correctly phased beam does a decrease in energy spread occur.

Simulation

The experimental setup is shown in Fig. 1. An axis-circling electron beam with $E_{//} \sim 50eV$ and $8keV < E_{\perp} < 12keV$ is injected into a rectangular resonant cavity operating in the TE_{102} mode and fed with $\sim 100mW$ of rf power at $f_{res} \sim 2.12GHz$. Beam and cavity characteristics are shown in the figure. The beam is reported to emerge from the cavity with a significant decrease in the perpendicular energy spread accompanied by an overall increase in the perpendicular energy, i.e. $E_{\perp} = 22keV$ and $\Delta E_{\perp} \sim 0keV$.

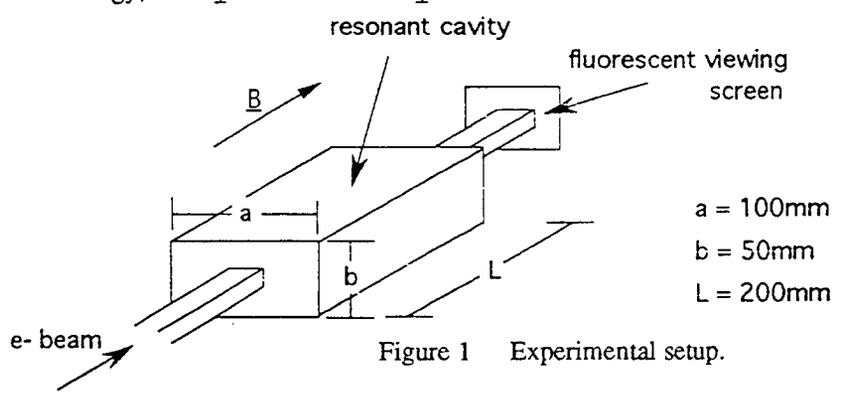

Figure 1 Experimental setup.

The above experiment has been simulated numerically by injecting a beam of particles whose energy is either fixed at a constant value or distributed as defined in the above figure. The simulation is run for an rf field defined in two ways: a) forward traveling wave - as defined in [1] b) standing wave - a more realistic structure for a cavity field. The wave fields are defined for the TE_{102} mode as:

$$E_y = E_0 \sin k_x x \; e^{-i\omega t} \times \begin{cases} e^{i k_z z} & \text{traveling wave} \\ \sin k_z z & \text{standing wave} \end{cases} \tag{1a}$$

$$H_x = E_0 \frac{k_z}{\mu\omega} \sin k_x x \; e^{-i\omega t} \times \begin{cases} -e^{i k_z z} & \text{traveling wave} \\ i \cos k_z z & \text{standing wave} \end{cases} \tag{1b}$$

$$H_z = E_0 \frac{i k_x}{\mu\omega} \cos k_x x \; e^{-i\omega t} \times \begin{cases} -e^{i k_z z} & \text{traveling wave} \\ -\sin k_z z & \text{standing wave} \end{cases} \tag{1c}$$

$$E_x = E_z = H_y = 0, \tag{1d}$$

and $k_x = \pi/a$, $k_z = 2\pi/L$. The above constant E_0 is determined from an energy balance in the cavity using $Q = \omega W_{st}/P_{rf}$ where ω = *excitation frequency* and

$$W_{st} = \text{stored energy} = \int_V \frac{1}{2}\varepsilon_0 E^2\, dV + \int_V \frac{1}{2}\mu_0 H^2\, dV$$
$$= \varepsilon_0 E_0^2\, abL \left(1 + \frac{k_x^2 + k_z^2}{\mu_0 \varepsilon_0 \omega^2}\right) \times \begin{matrix} 1/8 & \textit{traveling wave} \\ 1/16 & \textit{standing wave} \end{matrix} \qquad (2)$$

Using Eqs. 1-2, E_0 is determined to be $E_0 = 3.7\times10^3 V/m$ for the traveling wave case and $E_0 = 7.4\times10^3 V/m$ for the standing wave case. At the input to the cavity the particles appear in the position and momentum planes as shown in Figs. 2. The phase of the injected beam relative to the rf field is random as inferred from the experiment. The classical equations of motion are used to propagate the beam through the rf field of the cavity - $\boldsymbol{F} = d\boldsymbol{p}/dt = q_e(\boldsymbol{E} + \boldsymbol{v}\times\boldsymbol{B})$, $\boldsymbol{p} = \gamma m \boldsymbol{v}$. The particle simulation is stopped when the last of the particles reaches the far end at $z = L$. It should be noted that effects of beam space charge are not included in the model. However, the experiment operates at such small currents ($I_{beam} = 1\mu A$) that any space charge effects may be considered negligible ($\omega_p^2/\omega_c^2 << 1$ [2]).

A run for a typical set of parameters is shown in Fig. 3. In this case all particles are injected with equal energy, $E_\perp = 10keV$ $E_{//} = 50eV$. The relativistic gyro frequency is set slightly below the wave frequency, $B = .0768T$ ($\Delta = (2/\beta_\perp^2)(1-qB/\gamma m\omega) = 0.36$). The figure shows the time evolution of the particles as they traverse the cavity. One can see that the initial phase quickly determines the path that the particles follow. The paths become straight lines when the particles reach the end of the cavity where they are viewed on the florescent screen. During the passage through the cavity, the particles acquire a spread in longitudinal velocity due to the Lorentz force resulting in different transit times for particles of different initial phase. The run shown in Fig. 3(a) is typical of all runs performed for both the traveling and standing wave case. The mean energy of the distribution can either increase or decrease depending on the detuning between the wave frequency and the particles relativistic gyro frequency. There is though always a significant increase in the energy spread. For the case shown in Fig. 3(a), the spread becomes more than 20% of the final energy.

Figure 3 (b) and (c) shows the particles of Fig. 3(a) in the x-y and p_x-p_y plane at the end of the simulation. It is clear that, though the mean energy of the beam has increased, the *spread* in energy results in wide "rings" in the position and momentum planes of the beam. For this choice of parameters, "cooling" in the p_x-p_y momentum plane has not occurred.

Simulations similar to those of Figs. 3 are performed for the entire range of magnetic field, or detuning, values of interest. The mean energy change and energy spread is plotted in Figs. 4 as a function of magnetic field for both the forward traveling and standing wave fields. As is seen in both cases, the mean beam energy can be increased or decreased, given the correct magnetic field. However, the final energy spread is *always* greater than *10%* for zero initial energy spread, and increases to as high as *40%*, for any beam energy change of more than a few percent. The possibility therefore of injecting a random-phase beam with an initial energy spread and reducing this spread by the method described here seems unlikely.

Contrary to the experiment described in [1], if one could fix the phase of the injected beam with respect to the wave, the reduction in the energy spread of the beam may be possible. An example is shown in Figs. 5 where a distribution of particles with energies $E_{//} \sim 50eV$ and $8keV < E_\perp < 12keV$ is injected into the cavity of Fig. 1. As seen by the time trajectories of the particles in Fig. 5(c), a reduction in the width of the energy distribution occurs as all particles, regardless of their initial energy state, reach the cavity end at a near constant energy. This though is only possible if the initial phase of all particles in the distribution is fixed at the same value. Figures 5(a) and (b) shows the required initial state of the particles to achieve this effect. At the cavity exit, the energy distribution is seen to be narrower, though the particles have now spread out over the entire 2π radians of phase.

Conclusions

A particle simulation of the cyclotron maser cooling effect has shown that the electron beam/wave interaction can result in either a decrease or increase in the mean energy of the injected beam. The energy spread induced however as a result of the interaction, is seen to be unacceptably large, varying between *10%* and *40%*, depending on the detuning between the electron gyro frequency and the wave frequency. These results are in contradiction to those presented in [1] and cannot

explain the observed "cooling" of the electron beam in the p_x-p_y momentum plane shown in the experiment. Contrarily, if the phase of the injected beam can be controlled, the simulation shows that a reduction in the energy spread of the injected electron beam can be attained. This requires a constant particle input phase and though the interaction results in a reduction of the energy spread it also results in a spreading of the beam to all phase values.

References

1. H. Ikegami, this conference, and references contained therein.
2. R. G. Kleva, T. M. Antonsen Jr., and B. Levush. "The effect of the time-dependent self-consistent electrostatic field on gyrotron operation", *Phys. Fluids* **31**, 375-386. 1988.

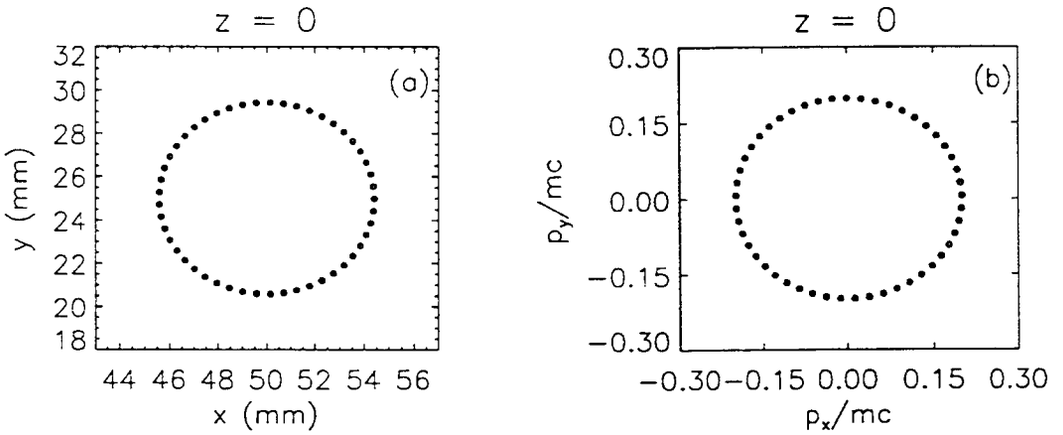

Figure 2. Initial phase space distribution of injected beam. Beam parameters are $E_{//} = 50eV$ and $E_{\perp} \sim 10keV$ (a) x-y plane (b) p_x-p_y plane.

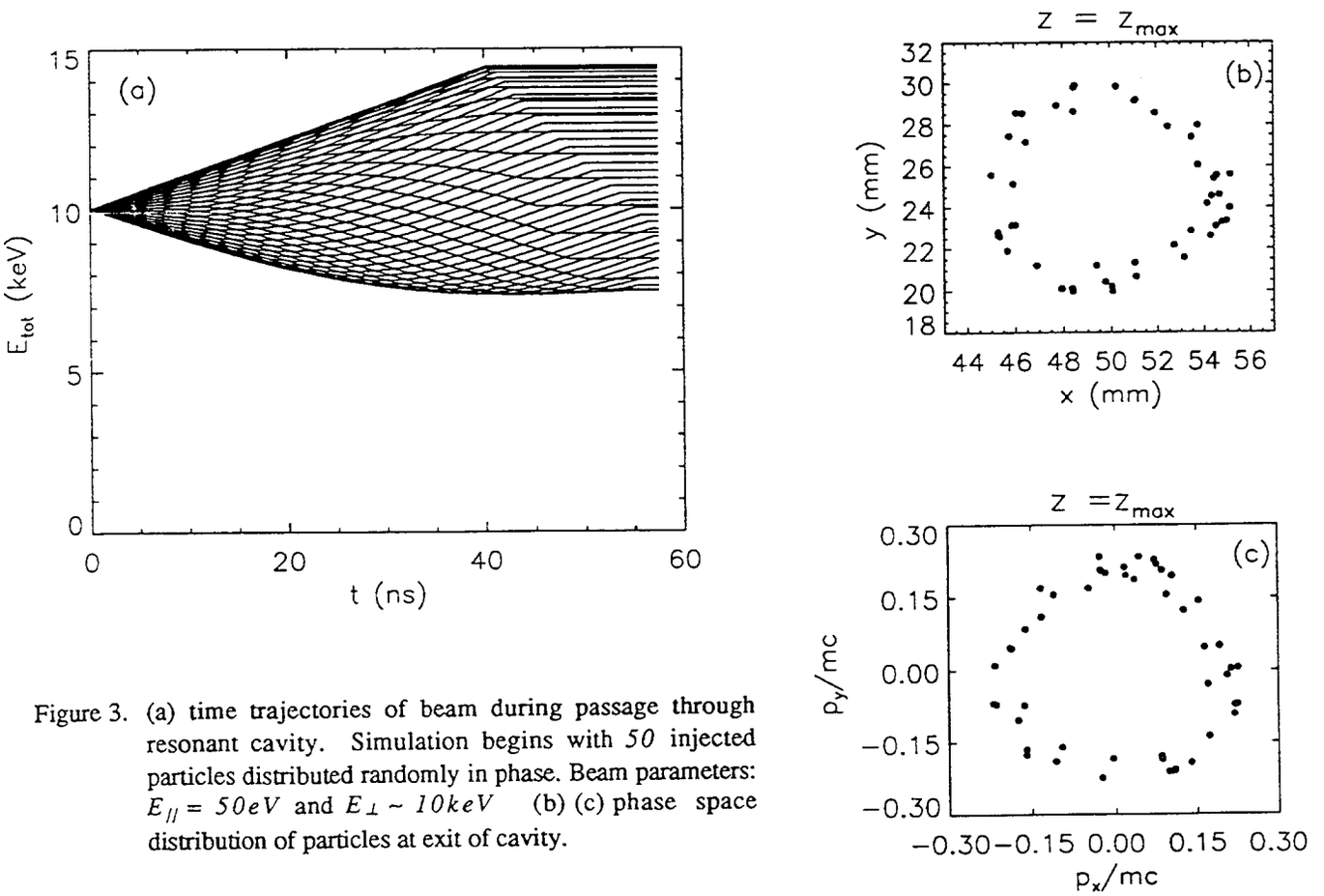

Figure 3. (a) time trajectories of beam during passage through resonant cavity. Simulation begins with 50 injected particles distributed randomly in phase. Beam parameters: $E_{//} = 50eV$ and $E_{\perp} \sim 10keV$ (b) (c) phase space distribution of particles at exit of cavity.

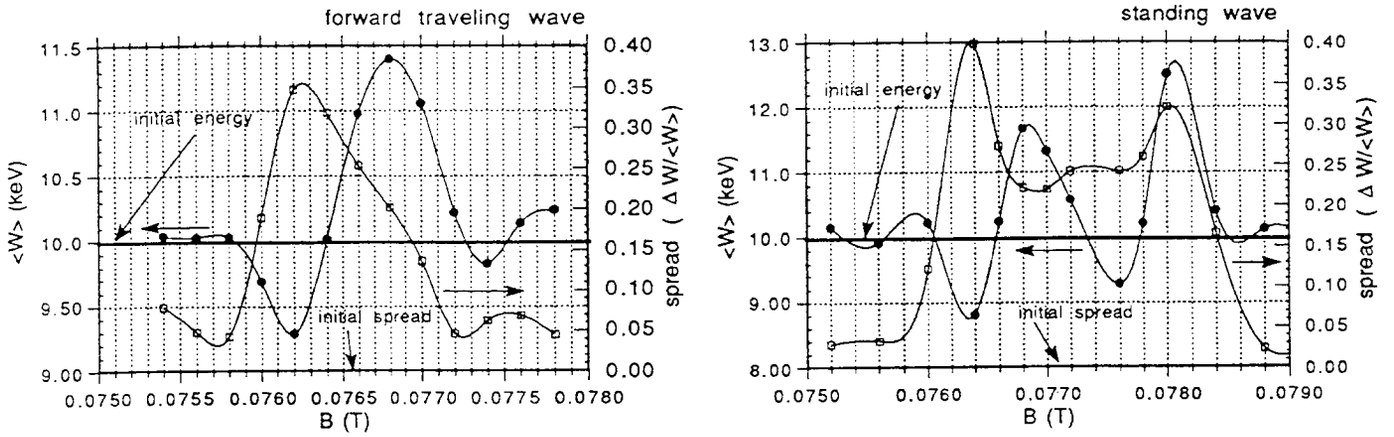

Figure 4. Mean energy of distribution and energy spread of beam at exit of resonant cavity vs. magnetic field for (a) forward traveling rf wave field (b) standing rf wave field.

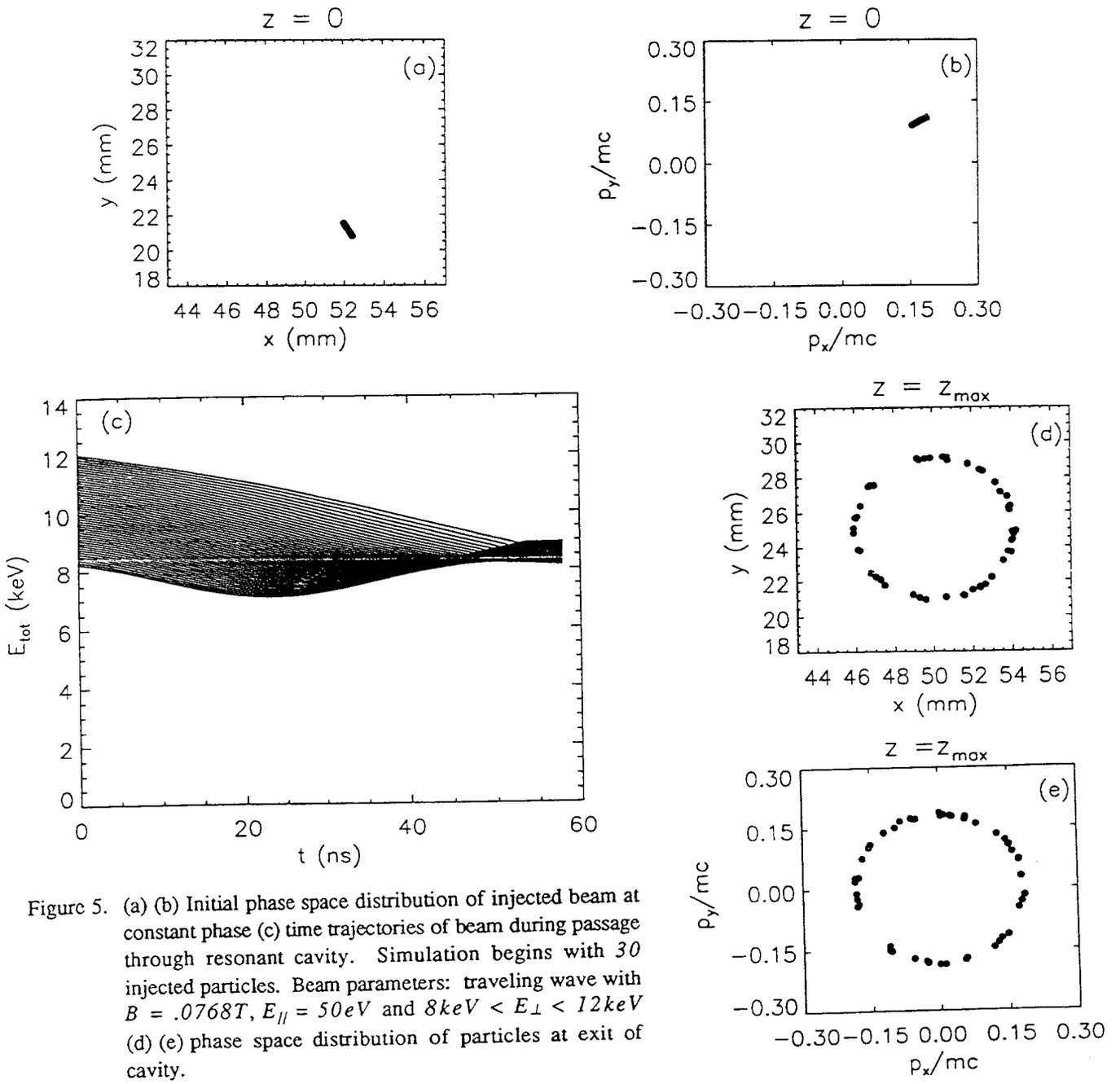

Figure 5. (a) (b) Initial phase space distribution of injected beam at constant phase (c) time trajectories of beam during passage through resonant cavity. Simulation begins with *30* injected particles. Beam parameters: traveling wave with $B = .0768T$, $E_{//} = 50eV$ and $8keV < E_{\perp} < 12keV$ (d) (e) phase space distribution of particles at exit of cavity.

ORGANIZATION OF PARTICLE BEAMS – A POSSIBLE NEW COOLING CONCEPT

Erkki J. Brändas
Department of Quantum Chemistry, Uppsala University
Box 518, S-751 20 Uppsala, Sweden

ABSTRACT

A preliminary report on the theoretical possibility of cooling electrons (and ions) by means of coherent microwaves also called cyclotron maser cooling (CMC) is presented. It is concluded that the derivation of the so-called CMC gainfunction, using standard results known in classical and quantum theory of spontaneous and stimulated emission, will not yield the necessary increase of phase space density and thus can not explain any proposed cooling effects. However, using modern quantum statistical methods involving coherent, non-linear collective effects, a possible cooling principle is indicated. The principle is discussed in connection with Ikegami's recent CMC experiments and a brief reference to laser cooling is also given.

1. INTRODUCTION.

The advent of intense pulsed relativistic electron beams has renewed interest in the cyclotron maser instability. At the same time the invention of electron cooling has suggested new ways of improving the properties of circulating particle beams. The combination of the two ideas, namely to force radiation cooling due to enhanced emission of cyclotron radiation may lead to new maser cooling principles which, if applicable to circulating particles in a storage ring, should lead to dramatically refined and organized beam qualities.

A historic account should start with the classical linear mechanism for a possible electron cyclotron maser, first proposed by Twiss [1] in 1958, followed, one year later, by Schneider's [2] quantum mechanical (linear) formulation based on the relativistic Landau oscillator. The general nonlinear theory, including the importance of relativistic effects associated with gyrating electrons about an external magnetic field, was finally reviewed and thoroughly treated by Sprangle and Drobot [3] in their classic paper on the electron cyclotron maser instability.

The observed maser action, see Ref.[4] for the earliest definite confirmation of the electron maser mechanism, is mainly due to relativistic corrections, which remove the degeneracy in the level spacings for free electrons in a magnetic field. If higher magnetic moments are in sufficient population excess, the system can support enhanced stimulated emission of electric dipole radiation at the electron cyclotron frequency.

The pioneering work of Schneider [2] indicated that a net stimulated emission should be possible in certain regimes provided the linear mechanism for the maser instability is valid. Starting from Schneider's result, Ikegami [5] suggested the principle of "cyclotron maser cooling" (CMC) by assuming that the loss of transverse energy through cyclotron radiation should equal the radiated net transfer of power in the quantum mechanical linear theory.

Nonlinear effects, in the Ikegami experiments [5] should be controlled within a certain range of the cyclotron gyration phase, if the stimulating rf field is synchronized with the phase of the accelerating

rf field. Phase locking of cyclotron gyration is thus essential to the "cooling" of the beam [5], and the phase locking condition can be achieved by introducing compensating solenoidal magnets, see Ref.[5] for details. Recent CMC experiments [6] seem to demonstrate rapid cooling times for the transverse as well as the longitudinal phase spaces of the electron beam and thus would imply that forced radiation cooling due to enhanced emission of cyclotron radiation should be possible.

A similar idea, due to Hirshfield and Park [7], i.e. to reduce the energy spread of the electron beam during passage through a gyrotron and thereby allowing entropy to flow from the hot electron beam to the surroundings, was strongly criticized by Larson [8]. His arguments run as follows:
"All known mechanisms for particle beam cooling clearly obey the second law of thermodynamics by transferring entropy away from the beam that is to be cooled. Electron cooling transfers entropy from a hot beam to a cold electron beam, and the spent electron beam is discarded. Stochastic cooling transfers entropy from a hot beam into the electronics of the cooling system. Synchrotron-radiation emittance damping in storage rings transfers entropy from beam particles to radiated photons".
Larson further argued that since no known mechanism exists which would lead to the corresponding entropy exchanges between the electrons in the beam and the photons in the electromagnetic cavity, any cooling effects would indeed lead to a violation of the second law.

He also observed that the gainfunction proposed in [7] was essentially derived by averaging over initial gyration phases and hence any initial preparation of the beam, i.e. to have the beam energies correlated with phase - a possibility for reducing the energy spread - was not at issue here.

In Uppsala we have had, during the last two months, an interdisciplinary science group working to analyse and evaluate the CMC principle of Ikegami, namely that it should be possible to "cool" electrons via coherent microwaves or from the use of appropriate knowledge in the arena of the electron cyclotron maser instability. We have penetrated the various requirements that a satisfactory CMC theory should require. E.g. in these proceedings B. Karlsson [9] solves numerically the exact dynamical equations of motion for an electron in a constant magnetic field perturbed by an oscillating electric rf field (as specified in the experimental setup). He then demonstrates that a classical gainfunction $F(x)$, where x is essentially the mismatch of frequences between gyromotion and rf field, after averaging over the initial phase, can be derived which furthermore has the "desired" characterization, i.e. $F(x)$ splits into the "usual" domains of positive and negative absorption. Since the system is Hamiltonian there can be no cooling associated with this particular CMC concept.

The first conclusion thus becomes, based on [8,9], that *a derived gainfunction with positive and negative domains of absorption does not guarantee cooling.* Next, is it possible to explain the CMC experiments by alternative theories which do not imply an increase of the phase space density. Third, if this question is not answered beyond doubt, what would be the main features of such a new theory that actually would provide organization or cooling.

Since Ikegami [6] does not invoke any average over initial gyration phases, albeit works in a classical setting with specifically included friction terms, it is not immediately clear to what extent the present critique, see [8,9] apply. On the other hand it can be simply proven that the above mentioned friction terms vanish exactly under random (initial) phases. As standard results of classical and quantum theory of spontaneous and stimulated transitions do not lead to any cooling effects, it is therefore necessary to develop a "new" theory which are based on coherent properties and collective nonlinear behaviour of the particle beam. In other words we are in search for a "Maxwell Demon" which can provide negentropy to the individual particles (or samples of particles).

It also becomes obvious that we need a theory which explicitly accounts for general predominant nonlinear collective effects as well as incorporates specific saturation mechanisms, i.e. depletion of free energy and phase trapping of gyrating electrons, in order to fully understand the general "cooling" effect, if it exists. Hence, we will here indicate a possibility based on the modern theory of micro-dynamical

correlations in dissipative systems far from equilibrium [10]. For a general account of subdynamics and dissipativity in complex non-linear systems, see Nicolis and Prigogine [11]. We will also have additional motivations for this endeavour by a quick look in the direction of laser cooling mechanisms.

2. CORRELATED TRANSITIONS OF FERMIONS.

Since electrons are fermions obeying the Pauli principle, it is obvious that a quantum formulation of the present situation somehow should incorporate Fermi statistics. At the same time the beam contains electrons at relativistic energies. It is hence of great interest to find out if these electrons would be sufficiently correlated for a stimulated emission of cyclotron radiation to take place so that organization rather than increased entropy would result. Before we quote some recent results along these lines we remark that any cooling effects must be directly coupled to the phase space dynamics through the Liouville equation

$$i\frac{\partial \rho}{\partial t} = \hat{L}\rho \tag{1}$$

As usual $\hat{L}$ is the commutator with the Hamiltonian ($\hbar$ should be inserted unless we deal directly with energies in terms of frequencies) in the quantum case and $i\hat{L}$ is the Poisson bracket in the classical domain. We will return to this in the next section.

In order to develop the micro-dynamical picture we must first give the following brief background with reference to correlated fermions. We will also, when possible, have the CMC setup [5,6] in mind, i.e. consider gyrating electrons in a constant magnetic field perturbed by a suitable time dependent electromagnetic field, but first we will review some general results from the interactions and the correlations in a manybody fermionic system. It is a well-known fact that these correlations manifest themselves in the appearance of occupation numbers fulfilling [12] (due to the Pauli principle) $0 \leq \lambda^{(1)} \leq 1$. For weekly correlated particles these occupation numbers are close to one, but in strongly correlated situations, e.g. in high-T_c superconductivity, (HTSC), or in the fractional quantum Hall, (FQHE), effect these occupancies may deviate significantly from unity.

Next, the fermionic statistics may under optimal conditions lead to the so-called extreme case of maximum coherence (Coleman [13]) which further could develop into off-diagonal long-range order (ODLRO) (Yang [14]). We emphasize that these correlations can extend over macroscopic dimensions in condensed matter applications, cf. HTSC and FQHE mentioned above. In the domain of accelerator physics, however, such extensions have not been predicted previously, but it should be further investigated whether such effects could appear for instance during bunching in the CMC experiments. In general, quantum effects are entering accelerator physics e.g. through laser cooling and the new fascinating area of crystalline beams. It is therefore important to keep in mind that correlations (not to be confused with the concept of interactions) might play a more active role than before in storage ring physics due to the statistical (fermionic or bosonic) origin of the participating particles with commensurate consequences for possible organizations of beam quality. A more clear cut example would of course be to apply this in the context of laser cooling, but we will leave this for later. In the correlated (extreme) case the occupation number is given by

$$\lambda^{(1)} = \frac{N}{2r} \tag{2}$$

where N is the number of fermions and $2r$ is the number of available spinorbitals. Equivalently r is the rank of the fermion (geminal) pair subspace. It is now a simple task to set up a "correlation matrix" which describes quantum mechanically the excitation of an electron from one (Landau) level to another as correlated with or stimulated by other electronic excitations [10]. The off-diagonal element is simply given by the product of the probability of the correlated electron being in the appropriate spinorbital, i.e. $\frac{N}{2r}$ with the probability of the other spinorbital being empty, i.e. $\frac{N}{2r} \cdot \frac{(2r-N)}{2(r-1)}$.

The detailed statistical analysis have been carried out in [10] so we do not repeat it here. It is perhaps strange to discuss fermions here, while at the same time having Landau oscillators and Landau levels in mind as given by the CMC experimental set up [6], since they refer to bosonic entities. First we realize that we are indeed considering the fermion pair subspace and the associated second order reduced density matrix, and fermion pairs behave as (quasi) bosons. Analogously the two dimensional projection of gyrating electrons, which leads to the (highly degenerate) Landau oscillator formulation, again subscribe to boson statistics. In both cases there is a "hidden" fermionic origin of the problem, which cannot be completely forgotten. The analogy, which will be carried out in more detail in the next section, implies, cf. HTSC and FQHE above, that the structure, see discussion below, exhibited by correlated electrons is transferred to the (relativistic) Landau oscillator picture.

Returning to the "correlation matrix" above it is a simple matter to diagonalize it. This leads to a large eigenvalue λ_{L} and a small one λ_{S} given by

$$\lambda_{\mathrm{S}} = \frac{N(N-2)}{4r(r-1)}; \quad \lambda_{\mathrm{L}} = \frac{N}{2} - (r-1)\lambda_{\mathrm{S}}. \tag{3}$$

For the identification with Coleman's extreme case or with Yang's concept of ODLRO, see [10]. Note that in the oscillator picture, referred to above, the large eigenvalue λ_{L} will be directly related to the stimulated part of the transition leading to amplification through ODLRO and cooling. Whether this mechanism is a possibility in CMC is now to be analysed, but first we will briefly look at the fermionic correlation problem.

For our purpose we will start with a localised basis of electron pair functions of rank r given by $\mathbf{h} = |h_1, h_2, \ldots, h_r\rangle$. It may here be chosen as a real localized set of spin paired reference determinants but in general it is important to realize that a dynamic formulation necessitates transformations to complex Gamow like representation, see Ref.[10] and further below. To arrive at the above mentioned structure, see e.g. [10], we introduce a delocalised coherence basis $\mathbf{g}$ and a complex correlation basis called $\mathbf{f}$ via

$$|\mathbf{h}\rangle\mathbf{B} = |\mathrm{g}\rangle = |g_1, g_2, \ldots, g_r\rangle \tag{4a}$$

and

$$|\mathbf{h}\rangle\mathbf{B}^{-1} = |\mathbf{f}\rangle = |f_1, f_2, \ldots, f_r\rangle \tag{4b}$$

with $\mathbf{B}$ given by

$$\sqrt{(r)} \cdot \mathbf{B} = \begin{pmatrix} 1 & \omega & \omega^2 & \ldots & \omega^{r-1} \\ 1 & \omega^3 & \omega^6 & \ldots & \omega^{3(r-1)} \\ \ldots & \ldots & \ldots & \ldots & \ldots \\ 1 & \omega^{2r-1} & \omega^{2(2r-1)} & \ldots & \omega^{(r-1)(2r-1)} \end{pmatrix} \tag{4c}$$

and $\omega = \exp(i\frac{\pi}{r})$.

The (relevant part of) the reduced second order density matrix for the correlated electron problem reads [10,13]

$$\Gamma^{(2)} = \Gamma^{(2)}_{\mathrm{L}} + \Gamma^{(2)}_{\mathrm{S}} = \lambda_{\mathrm{L}}|g_1\rangle\langle g_1| + \lambda_{\mathrm{S}} \sum_{k=1}^{r}\sum_{l=1}^{r} |h_k\rangle(\delta_{kl} - \frac{1}{r})\langle h_l| \tag{5}$$

with $Tr\{\Gamma^{(2)}\} = \frac{N}{2}$ i.e. the correlation matrix is normalized to the number of fermionic pairs. In passing we mention that we have neglected an uninteresting "unpaired" contribution to the full $\Gamma^{(2)}$ in the trace relation above, but here this technicality will not be pursued [10]. It is interesting to note that, for a given value of r, i.e. $2r$ much greater than N, it follows from Eqs.(2-5) that λ_{L} first "grows" linearly with N until the quadratic term, see Eq.(3), starts contributing. The parabola "ends" for $2r = N$, where coherence and delocalization (in the sense given above) no longer persists [10]. We have put the words

"grows" and "ends" within quotation marks to issue a warning that changes in N and/or r are not to be interpreted as in linear theories, i.e. to see what happens with the system when certain parameters vary. Here the formulation is *manifestly nonlinear* and therefore N and/or r are not at "our disposal" since they simply reflect that all parts of the system are intrinsically coupled as a dissipative structure.

We have earlier showed how Eq.(5) via complex dilations [15-17] and thermalization, see e.g. [10,18], assumes a Jordan block structure which for Γ_S takes the simple form, i.e.

$$\Gamma_S = \lambda_S \sum_{k=1}^{r-1} |f_k\rangle\langle f_{k+1}| = \lambda_S J \tag{6}$$

with the important property

$$J^r = 0, \quad J^{r-1} \neq 0. \tag{7}$$

As mentioned above we may take our reference space real and let all dynamic complexities be invoked through effective reduced Hamiltonians (and/or Liouvillians) and associated partitioning techniques. We must remember, however, that in this formulation the Liouvillian is no longer self-adjoint and hence there is the possibility of a spontaneous breaking of time reversibility. We will also see what consequences the present extension has for the Liouville phase space density or rather the associated space of reduced density matrices.

3. LIOUVILLE FORMULATION OF SPONTANEOUS AND STIMULATED TRANSITIONS.

Since our aim is to couple a suitably defined gainfunction directly to a relevant Liouville formulation, we will transfer the structure of the correlation matrix displayed in section 2 to a super-operator framework in terms of correlated relativistic Landau oscillators. The crucial assumption is thus that the coherent-dissipative properties of the electrons in a bunch, let us say, manifest itself so that organization or cooling appears through a new term of the Liouvillian to be described below.

We will denote the density matrix corresponding to a transition (system absorbs) between the Landau levels $i+1$ and i by $||h_{k(i)} \gg = |\{i+1\}(k)\rangle\langle i(k)|$, where k denotes a particular transition involving Landau levels i and $i+1$ characterized by the angular frequency $\omega_{i+1,i} \approx \omega_L$ given by the eigenvalue (of the "zero order" Liouvillian) $\hbar\omega_{i+1,i} = E_{i+1} - E_i$.

In the same way as before we obtain a super-operator transformation between the transition matrices $||\mathbf{h} \gg$, $||\mathbf{f} \gg$ and $||\mathbf{g} \gg$ via the $r \times r$ transformation matrices $\mathbf{B}^{-1}$ and $\mathbf{B}$, respectively. In the basis $||\mathbf{f} \gg$ the transitions are correlated and in $||\mathbf{g} \gg$ coherent according to the properties of respective transformations. For example, $||g_1 \gg$ describes simultaneous coherent transitions by the frequence $\omega_{i+1,i}$, while $||f_1 \gg$ represents transitions that are phase correlated through the factors $\exp(\frac{i\pi}{r}(k-1))$, $k = 1, 2, \ldots r$. Note also that $\ll \mathbf{g}||$ and $\ll \mathbf{f}||$ describe coherent and correlated emissions with the eigenvalues $\hbar\omega_{i,i+1} = E_i - E_{i+1}$ of the corresponding (zero order) Liouvillian.

Absorption and emission are therefore intrinsically connected through the bra-ket correlated transformations based on $||\mathbf{h} \gg \mathbf{B}$ and $||\mathbf{h} \gg \mathbf{B}^{-1}$.

Note also that the usual transformation property for timereversal, i.e. $t \rightarrow -t$; $\hat{L} \rightarrow -\hat{L}$, will not work here, since we will have an intrinsic coupling with the environment through the new terms, see below, obtained from the dissipative dynamics.

In the present formulation the scalar product hence becomes

$$\ll h_{k(i)}||h_{l(j)} \gg = Tr\{h^{\dagger}_{k(i)} h_{l(j)}\} \tag{8}$$

One should observe here that in general one must use the generalized scalar product for $||\mathbf{h} \gg$ complex

$$\ll h^*_{k(i)}||h_{l(j)} \gg = Tr\{h^*_{k(i)}{}^\dagger h_{l(j)}\} \tag{8'}$$

Since our reference basis is chosen real we may not dwell on this complication here. Suffice it to say that meaningful scalar products should in general be taken between components of the two conjugate Hilbert spaces and all vectors in the bra position should have a complex conjugate sign to show that we take a component from the dual space, see [18] for details. Note that we are here treating non-selfadjoint Liouvillians with real reference spaces, and that unitary transformations in this context therefore will lead to nonsymmetric Jordan blocks [18].

We will now proceed to construct the relevant Liouvillian $\hat{L}$ commensurate with the above mentioned Jordan block structure. Note that we will obtain a time independent effective Liouvillian even if the original Liouvillian may contain time dependent parts. We will return to this question below. In analogy with the previous section we write (note that Γ here means the resonance width related to the characteristic (collision or phase debunching) lifetime of the state via $\frac{\hbar}{\Gamma} = \tau$ not to be confused with the density matrix which have indices S or L)

$$\hat{L} = (z_{\mathrm{L}} - i\Gamma)\hat{I} + \hbar\omega_{\mathrm{S}}\hat{J} \tag{9}$$

In Eq.(9) the identity stands for $\hat{I} = \sum_{k=1}^{r} ||g_k \gg\ll g_k|| = \sum_{k=1}^{r} ||f_k \gg\ll f_k||$, $\hat{J} = \sum_{k=1}^{r-1} ||f_k \gg\ll f_{k+1}||$, $z_{\mathrm{L}} = \hbar\omega_{\mathrm{L}}$ with ω_{L} being the characteristic angular frequency associated with specific transition in question, and finally ω_{S} to be determined. Although this construction appears quite *ad hoc* - our intention is clearly not to derive the details of the full Liouvillian - but rather to see how the second term in (9) arises from first principles and further to demonstrate the subsequent consequences with respect to its Liouvillian properties.

From Eq.(9) we now deduce the relation (from inspection with Eq.(5)), that the large component (in the identity operator) scales with the Jordan block component as

$$\omega_{\mathrm{S}} = \omega_{\mathrm{L}} \cdot \frac{\lambda_{\mathrm{S}}}{\lambda_{\mathrm{L}}} \tag{10}$$

which means that the quotient between ω_{S} and ω_{L} can be expressed in terms of N, the number of particles in the system (or bunch) and r, the dimension of the pairspace, see Eq.(3). Our density matrix is now properly specified.

In the discussion of the exact underlying Liouvillian for this construction we must realize that the Liouvillian is time dependent through the perturbing electromagnetic rf field. Of course we can derive appropriate equations from partitioning technique with the attempt to continue analytically the nonlinear equations via well-defined regularization techniques. This complication can be delt with, see next section. Here we will therefore only briefly express the abstract resolvent equations for a general Liouvillian referring to a particular timescale, where explicit time dependencies on a shorter scale have been averaged out.

The full nonlinearity of the problem can now in principle be explicitly specified giving the precise condition for the characteristic angular frequency as well as the one determining $\Gamma = \frac{\hbar}{\tau}$. This follows from the unique analytic continuation of the Liouville problem

$$\{\hat{P}\hat{\mathcal{L}}\hat{P} + \hat{\Psi}(z) - z\hat{\mathcal{I}}\}||f_l \gg = 0; \quad l = 1, 2, \ldots r. \tag{11a}$$

in which $\hat{P} = \sum_{k=1}^{r} ||g_k \gg\ll g_k|| = \sum_{k=1}^{r} ||f_k \gg\ll f_k||$ with $\hat{P} + \hat{Q} = \hat{\mathcal{I}}$ and

$$\hat{\Psi}(z) = -\hat{P}\hat{\mathcal{L}}\hat{Q}(\hat{Q}\hat{\mathcal{L}}\hat{Q} - z\hat{\mathcal{I}})^{-1}\hat{Q}\hat{\mathcal{L}}\hat{P} \tag{11b}$$

In the equations above the Liouvillian $\hat{\mathcal{L}}$ describes (in principle) the complete physical mechanisms, including relativistic effects, involved in e.g. the maser instability, see e.g [3] for details. Further $\hat{\mathcal{I}}$ is the complete unit operator and Eqs. (11a) and (11b) give the condition for ω_{L} and Γ including all the non-linearities of the problem. The construction in (9) obtains from (11) by the choice $\hat{P} = \hat{I}$ and $\hat{L} = \hat{P}\hat{\mathcal{L}}\hat{P} + \hat{\Psi}(z_{\mathrm{L}} - i\Gamma)$. See also [19,20] for more details.

Before we continue to demonstrate how the associated dynamics of the present model evolves, we will go back to the particular situation experienced in CMC. It is clear that the desired "Maxwell Demon" should work as follows. At first we note the enormous degeneracies of the Landau oscillator problem, which, however, are coupled to decreasing level spacings as energy increases. Secondly, this implies that stimulated absorption and emission must be correlated so that excited oscillators in some specified energy levels should be phase correlated with the corresponding oscillators, already situated at higher energies, with appropriate de-excitation properties for stimulated emission to occur. Obviously this collective effect (intuitively) could lead to decrease of energy spread and thus cooling. The intriguing possibility that appears here is the following. The "classical" Maxwellian probability for an appropriately defined excitation reads

$$p = \exp -(h\nu/k_{\mathrm{B}}T)$$

where $h\nu$ is the frequency multiplied by Planck's constant, k_{B} is Boltzmann's constant and T is the relevant temperature. We have put "classical" within quotation marks, since the famous Einstein relation between spontaneous and stimulated emission involving the intensity $I(\nu)$ and the famous A and B coefficients, i.e.

$$\frac{AI(\nu)}{B} = \frac{1}{\exp(h\nu/k_{\mathrm{B}}T) - 1} = \delta \tag{12a}$$

is equivalent to the (quantum) Planck radiation law. The interesting analogy with the previous derivations follows by considering the correlation matrix, cf. discussions in connection with Eq.(2), with diagonal elements p and off-diagonal elements $p(1-p)$, where the latter corresponds to the phase correlated coupling between a particular oscillator being excited and another one being de-excited.

It is a remarkable coincidence that this simple correlation matrix has the same algebraic structure as the one appearing in condensed matter, albeit for a weakly correlated situation. Thus we obtain

$$\lambda_{\mathrm{L}} = sp - (s-1)p^2, \ \lambda_{\mathrm{S}} = p^2 \tag{12b}$$

where in the weakly correlated regime $s \approx r \approx N/2$. Relation Eq.(10) then obtains

$$\omega_{\mathrm{S}}/\omega_{\mathrm{L}} = \delta/s \approx 2 \cdot \delta/N \tag{12c}$$

Eq.(12c) will be the main result of this contribution, since it will be shown that it leads to the desired gainfunction at the same time coupling it, through the present dissipative subdynamics model, to an organization (or cooling) property of the CMC problem.

4. SELF-ORGANISATION AND DYNAMIC CORRELATION PATTERNS.

We will now see how the Liouvillian, obtained in the previous section directly connects a suitable gainfunction with cooling through the mechanism of spontaneous and stimulated transitions. We will start with the general relation between the propagator and resolvent ($t > 0$ and C^+ contour in the upper half plane and $\hbar = 1$, see [20] for details)

$$e^{-i\hat{L}t} = \frac{i}{2\pi}\int_{C+}(z - \hat{L})^{-1}e^{-izt}dz \tag{13}$$

Eq.(13) is convenient when working directly with angular frequencies and inverse lifetimes. For the remainder of this section we will, however, insert $\hbar$ again in order to a connect with the Liouvillian

of the previous section, e.g. Eq. (9). Regarding the aforementioned problem of timescales, it is easy to see that one can replace the lefthand side of (13) with a general expression corresponding to a more complicated correlation function. It follows immediately that the righthand side through the general relationship between correlation functions and the spectrum exhibits an analogous resolvent like structure as displayed in (13). Through appropriate dispersion relations a relevant timeindependent operator can be constructed so that (13) and in principle (11), can be expressed without contradictions.

Thus leaving this technicality aside as solved in principle, the resolvent straightforwardly becomes

$$(z-\hat{L})^{-1} = \frac{1}{z-(\hbar\omega_{\mathrm{L}}-i\Gamma)}\hat{I} + \frac{\hbar\omega_{\mathrm{S}}}{(z-(\hbar\omega_{\mathrm{L}}-i\Gamma))^2}\hat{J} + ..\frac{(\hbar\omega_{\mathrm{S}})^{r-1}}{(z-(\hbar\omega_{\mathrm{L}}-i\Gamma))^r}\hat{J}^{r-1} \tag{14}$$

and the propagator

$$\exp(-\frac{i\hat{L}t}{\hbar}) = \exp(-i\omega_{\mathrm{L}}t)\exp(-\frac{\Gamma t}{\hbar})\cdot\ \exp(-i\omega_{\mathrm{S}}\hat{J}t)\hat{I} \tag{15}$$

with

$$\exp(-i\omega_{\mathrm{S}}\hat{J}t) = (1 - i\omega_{\mathrm{S}}t\hat{J} \ldots + \frac{(-i\omega_{\mathrm{S}}t)^{r-1}}{(r-1)!}\hat{J}^{r-1})$$

The formula can be obtained either from simple matrix algebra or from the general resolvent propagator expression above [21].

Let us briefly look at correlated transitions described by $||f_1 \gg$ correlated with the transitions $||f_k \gg$ characterized by the operator $\hat{J}^{k-1}$ with $k = 2,3,\ldots r$. Note that the characteristic (collision) lifetime τ is still given by $\frac{\hbar}{\Gamma}$. The time rule for, let us say, transitions involving $||f_1 \gg$ and $||f_k \gg$ are given by (note that the present resonance model is only realistic or relevant "in between" small and large times, i.e. does not describe the evolution for very short or very large times compared to multiples of $\frac{\hbar}{\Gamma}$)

$$N(t) = |\ll f_1||\exp(-\frac{i\hat{L}t}{\hbar})||f_k \gg| \propto t^{k-1}\exp(-\frac{\Gamma t}{\hbar}) \tag{16a}$$

which yields

$$dN \propto t^{k-2}(k-1-\frac{\Gamma t}{\hbar})\exp(-\frac{\Gamma t}{\hbar})\cdot dt. \tag{16b}$$

Eqs.(16) show that $dN > 0$ for $t < (k-1)\cdot\frac{\hbar}{\Gamma}$, $k = 2,3,\ldots r$. Thus the occurrence of Jordan blocks in the Liouville picture lead to increase of $N(t)$ for the times specified above, i.e an increase of number of particles in the correlated state given by $||f_1 \gg$ by correlated transitions from all other states $||f_k \gg$, $k = 2,\ldots,r$. In general there may be a certain balance between increase and decrease in coherence, correlation and dissipation. Since there is an overall decay out of $\hat{I}$ given by

$$N(t) = |\ll f_1||\exp(-\frac{i\hat{L}t}{\hbar})||f_1 \gg| \propto \exp(-\frac{\Gamma t}{\hbar}) \tag{17a}$$

yielding the standard exponential decay rule

$$dN \propto (-\frac{\Gamma}{\hbar})\exp(-\frac{\Gamma t}{\hbar})\cdot dt. \tag{17b}$$

the summing up of all contributions or transitions to (or from) the correlated state $||f_1 \gg$ may lead to dissipative structures which during certain timespans of order $r\tau$ have increasing order etc., and in this sense we may speak of self-organisation on a microscopic level "created" by the Jordan block term in $\hat{L}$. In the following section we will attempt to find a possible relation with CMC or cooling principles in general.

5. CONNECTION WITH THE GAINFUNCTION.

Based on Schneider's work, Ikegami expanded the expression for the radiated net transfer of power in the quantum mechanical linear theory [5]. Later he attempted a derivation based on classical expressions involving specifically obtained friction terms, see discussion in the introduction.

He obtained, for particles gyrating in a magnetic field undergoing radiative transitions leading to a change of the transverse energy, the rate formula

$$\frac{d\gamma_\perp^*}{dt^*} \propto \tau \frac{2ax}{(1+x^2)^2}$$

where $a = \omega_L^* \tau^* (\gamma_\perp^* - 1)$; $x = \tau^*(\omega_L^* - \omega)$, $\omega_L^* = \frac{\omega_c^*}{\gamma_\perp^*}$ is the relativistic cyclotron frequency, $\tau^* = \frac{1}{\nu^*}$ with ν^* being the phase bunching frequency and finally $\gamma_\perp^*$ is the relativistic energy factor. The "constant" above involves the energy flow density (Poynting vector), the classical radius of the particles divided by $m_0 c$, with m_0 being the restmass and c the speed of light.

We may also compare the Schneider expression where $a = Q\frac{W}{m_0 c^2}$, $Q = \omega_0 \tau$ and $x = (\omega_{i+1,i} - \omega)\tau$, with τ being the characteristic time, W the kinetic energy of the electron and ω_0 the cyclotron frequency.

From Eq.(11) we obtain the nonlinear equations determining $\hbar\omega_L - i\Gamma$. The analytic continuation - necessary to obtain the complex solutions corresponding to the full subdynamics - rests on the dispersion relation, see [20] for details

$$\Psi(\hbar\omega + i0) = \mathcal{P}(\hat{P}\hat{\mathcal{L}}\hat{Q}(\hbar\omega - \hat{Q}\hat{\mathcal{L}}\hat{Q})^{-1}\hat{Q}\hat{\mathcal{L}}\hat{P}) - i\pi\delta(\hat{P}\hat{\mathcal{L}}\hat{Q}(\hbar\omega - \hat{Q}\hat{\mathcal{L}}\hat{Q})\hat{Q}\hat{\mathcal{L}}\hat{P})$$

with $\mathcal{P}(\Psi)$ and $\delta(\Psi)$ denoting the principal part and the delta function contribution of Ψ respectively.

Using the Obcemea-Brändas construction [20], the $\delta(\Psi)$ contribution can be retrieved from the corresponding Hamiltonian dynamics via a dispersion relation for $\overline{H}(E+i0) = H + HG(E+i0)H$, where $G(E+i0)$ is a suitably defined reduced resolvent and $H = H_0 + V$ with V a suitable optical potential [22]. For a sufficiently monochromatic beam of wavepackets φ with kinetic energies given by H_0, one can identify $\overline{H}(E+i0)$ with the t-matrix, i.e. $\overline{H}(E+i0) = H_0 + V + VG(E+i0)V = H_0 + t(E+i0)$ with G being the full resolvent $G = (E+i0-H)^{-1}$, $t = 1/2\pi(\hat{S} - \hat{\mathcal{I}})$ and $\hat{S}$ being the scattering matrix.

Eigenvalues of $\overline{H}(E)$ are then given by $E_i(E) - i\epsilon(E)$ with

$$E_i(E) = \langle\varphi_i|H_0 + V + \mathcal{P}(V(E-H)^{-1}V)|\varphi_i\rangle$$

and

$$\epsilon_i(E) = \pi\langle\varphi_i|V\delta(E-H)V)|\varphi_i\rangle.$$

Further the construction [20] amounts to finding an analytic continuation based on $\hat{\mathcal{L}}$ with eigenvalues

$$E_i(E) - E_j(E) - i(\epsilon_i(E) + \epsilon_j(E)).$$

We hence note that $\epsilon_i(E) = \pi\{-\Im t_{\varphi_i\varphi_i}\} \propto \sum_\gamma \sigma_{i\to\gamma}$, where $\sigma_{i\to\gamma}$is the cross section for the transition $i \to \gamma$ and the sum is the total cross section.

We therefore conclude that the absorption curve for the electron beam in the experimental setup [5] should follow a Lorentzian curve as described above in this section. However, the fundamental nonlinearities of this problem require additional work in the degeneracy space $\hat{I}$. Under "normal" conditions, i.e. with no Jordan blocks present, the dispersion relation for $(z-\hat{L})^{-1}$ should give the projector associated with $\hat{P}$, see Eq.(11), and hence trivially only heating of the particle beam is possible. In the present case, however, we need to study the the resolvent $(z-\hat{L})^{-1}$, including the Jordan block term, in order to find

the appropriate evolution commensurate with the degenerate root manifold spanned by $||\mathrm{f} \gg$. Thus we obtain from Eq.(14)

$$(z-\hat{L})^{-1} = \frac{\tau}{\hbar}\{\frac{1}{(y+i)}\hat{I} + \frac{\omega_S \tau}{(y+i)^2}\hat{J} + \ldots \tag{18}$$

with $y = \tau(z/\hbar - \omega_L)$. Intuitively we might conclude that we only have to put $y = -x$, with x defined in connection with the previous identification with Schneider's gaincurve [2]. Even if the contributions to the rate, see below, will look similar in nature, there will be some important differences. First of all it is important to realize that ω_L, obtained from Eq.(11), *is not equivalent to* Ikegami's ω_L^*, or the gyrofrequency. Our ω_L is the energy parameter divided by $\hbar$ and thus contains relativistic corrections, with the leading terms obtained from the relativistic Schrödinger (or Klein-Gordon) equation, small collective effects, and possibly contains a weak interaction with the longitudinal degrees of freedom. Furthermore, there are higher order terms in the resolvent expansion Eqs.(14,15) which might completely blur out the simple and clear cut information produced by a "well-behaved" gainfunction. It is nevertheless an interesting coincidence that that such a gainlike function indeed can be obtained here. To see that consistent gains can be obtained, which has the desired domain of negative absorption, we briefly return to our scattering theoretic review above.

Since the cross section (or associated spectral density) refers to taking the imaginary parts of the factors in front of $\hat{I}, \quad \hat{J}, \ldots, \hat{J}^r$ we can directly find the contributions, i.e from the first term

$$\frac{d\gamma_\perp^*}{dt^*} \propto\ll f_1||\Im\{-(z-\hat{L})^{-1}\}||f_1 \gg = \frac{\tau}{\hbar}\frac{1}{(y^2+1)} \tag{19}$$

and from the second term (and similarly for higher orders)

$$\frac{d\gamma_\perp^*}{dt^*} \propto\ll f_1||\Im\{-(z-\hat{L})^{-1}\}||f_2 \gg = \frac{\tau}{\hbar}\{(\frac{2\omega_S\tau \cdot y}{(y^2+1)^2})\} \tag{20}$$

We note that for $\omega_L > z/\hbar$, or $y < 0$, we obtain the desired negative absorption. Even if comparison with Schneider's and Ikegami's expressions obviously has lost its significance, it might be tempting to estimate the value of $a = \omega_S\tau$, determined from Eq.(10), i.e.

$$a = \omega_S\tau = \omega_L\tau \cdot 2\delta/N$$

as related to Schneider's relativistic factor $\omega_0\tau \cdot W/m_0c^2$ (W is the kinetic energy of the electrons) or Ikegami's parametrization.

The gainfunction has, as we have repeatedly pointed out, lost its fundamental "cooling" property, namely

- (i) it does not guarantee organization or increase of phase space density
- (ii) it may be blurred out in connection with cooling effects.

Nevertheless, the absolute size of $a = \omega_S\tau$ may in the present context still be of fundamental importance for any cooling effects to appear. This conclusion is only indirectly drawn from Eq.(20), since $|a|^2$ appears in the proportonality factor of Eq.(16), see also (15).

In summary, we find that our correlated picture contains collective effects including relativistic ones through the non-linear conditions (11). Note also that the presently derived gainfunction, (or rather the parameter a), in contrast to earlier derivations, simultaneously yields cooling as well as contains explicitly terms which refer to relativistic *and* collective corrections through the relativistic energy $\hbar\omega_L$, the factor δ for stimulated emission and N for the number of particles in the bunch. Even if the characteristic time τ is much smaller than the transit time (of electrons through the cavity), and further that $\omega_L\tau$ might be smaller than Ikegamis"s $\omega_L^*\tau^*$, it is still plausible that δ, which may attain values as high as 10^{14} at

radio frequencies in connection with maser devices, also in the present connection might yield a crucial contribution. Since multiples of τ also appear in the expression (16b), it needs to be investigated whether the replacement $\tau \rightarrow r \cdot \tau$, or replacing τ with the transit time, whichever is smallest, may significantly improve the situation when δ/N is small.

Of course, all these comparisons would be quite meaningless, save a complicated derivation of a gainfunction from quantum statistics including in principle nonlinear collective behaviour, if they did not refer to experimental conditions and associated non-Liouvillian self-organizational properties. However, as we have stressed earlier, the present derivation immediately yields a general principle of organization due to relations (16a) and (16b). Hence if nonlinear collective effects are prominent in CMC, cooling is possible.

Irrespective of the possible application of self-organizational principles in the microwave regime it should nevertheless be important to analyse more clearcut situations, e.g. in connection with laser cooling. For instance using the non-Liouvillian term proportional to

$$\hat{J} = ||f_1 \gg\ll f_r|| \tag{21}$$

with $f_r = f_1^*$ corresponding to the two given CW-laser pulses with frequencies $\omega_1 - \omega_0 - kv_1$ and $\omega_2 - \omega_0 + kv_2$. Here as usual v_1, v_2 are the relevant longitudinal velocities and $k = \omega/c$, c=velocity of light. If the characteristic width, including correction for saturation etc. is denoted by Γ we can immediately derive a resonance condition from the analogy with Eq.(18). It follows that

$$k(v_1 - v_2) = (2/\sqrt{3})\tau,\ \tau = \Gamma/\hbar$$

From the analysis given here, this resonance condition is commensurate with cooling.

Acknowledgements.

I thank the Swedish Natural Science Research Council and the Swedish Research Council for Engineering Sciences for financial support. I am also indebted to our interdisciplinary CMC group for helpful comments and discussions in connection with the classical background for this potentially important problem. In particular I am thankful to Prof. H. Ikegami for his neverfailing enthusiasm to communicate and provoke new ideas and Prof. S. Kullander for stimulating this enterprise in the broadest possible sense.

REFERENCES.

[1] R. Q. Twiss, Aust. J. Phys. **11**, 564 (1958).
[2] J. Schneider, Phys. Rev. Lett. **2**, 504 (1959).
[3] P. Sprangle and A. T. Drobot, IEEE Trans. Microwave Theory Tech. **25**, 528 (1977).
[4] J. L. Hirshfeld and J. M. Wachtel, Phys. Rev. Lett. **12**, 533 (1964).
[5] H. Ikegami, Phys. Rev. Lett. **64**, 1737 (1990); *ibid.* 2593 (1990).
[6] H. Ikegami, these proceedings.
[7] J. L. Hirschfield and G. S. Park, Phys. Rev. Letters, **66**, 2312 (1991).
[8] D. J. Larson, Phys. Rev. Letters, **68**, 133 (1992).

[9] B. Karlsson, these proceedings.
[10] E. Brändas and C. A. Chatzidimitriou-Dreismann, Int. J. Quant. Chem. **40** 649 (1991).
[11] G. Nicolis and I. Prigogine, *Exploring Complexity.* W.H. Freeman and Company, New York (1989).
[12] P. O. Löwdin, Phys. Rev. **97**, 1474 (1955).
[13] A. J. Coleman, Rev. Mod. Phys. **35**, 668 (1963); J. Math. Phys **6**, 1425 (1965); see also *Density Matrices and Density Functionals, Proceedings of the A. John Coleman Symposium,* (Eds. R. Erdahl and V. H. Smith, Jr.), (D. Riedel Publishing Company, Dordrecht 1987).
[14] C. N. Yang, Rev. Mod. Phys. **34**, 694 (1962).
[15] E. Balslev and J. M. Combes, Commun. Math. Phys. **22**, 280 (1971).
[16] C. van Winter, J. Math. Anal. **47**, 633 (1974).
[17] B. Simon, Ann. Math. **97**, 247 (1973).
[18] C. E. Reid and E. J. Brändas in *Resonances - The Unifying Route towards the Formulation of Dynamical Processes*, Eds. E. Brändas and N. Elander), Lecture Notes in Physics, Vol. **325**, pp. 475-483, (Springer, Berlin 1989).
[19] I. Prigogine, C. George, F. Henin, and L. Rosenfeld, Chem. Scripta **4**, (1973).
[20] CH. Obcemea and E. Brändas, Ann. Phys. **151**, 383 (1983).
[21] E. Brändas in *Quantum Science Methods and Structure A Tribute to Per-Olov Löwdin*, Eds. J-L. Calais, O. Goscinski, J. Linderberg and Y. Öhrn, Plenum New York, p.381 (1976); see also E. Brändas and P. Froelich, Int. J. Quant. Chem. **S 17**, 113 (1983).
[22] D. A. Micha and E. Brändas, J. Chem. Phys. **55**, 4792 (1971).

THE CMC CONCEPT AND TEST EXPERIMENT

Bengt R. Karlsson
Department of Radiation Sciences, Uppsala University,
Box 535, S-751 21 Uppsala, Sweden

ABSTRACT

It is argued that the CMC (Cyclotron Maser Cooling, or Coherent Microwave Cooling) concept can be captured in a simple model that by construction conserves the density in phase space. In particular, it is shown that the results of the CMC test experiment are well reproduced in this model.

1. INTRODUCTION

The cyclotron motion gyro frequency ω_c/γ for a relativistic particle in a constant magnetic field depends on energy through the relativistic factor γ. If a beam of such particles is exposed to an electromagnetic field with a frequency ω close to the gyro frequency, the energy flow between the beam and the field will be resonance enhanced. Furthermore, and due to the energy dependence of the gyro frequency, in the resonance region there will be a net flow of energy *into* the beam if $\omega_c/\gamma > \omega$, and *out of* the beam if $\omega_c/\gamma < \omega$. In both cases it therefore appears as if the energy of the beam would approach the value for which $\omega_c/\gamma = \omega$, and as if an energy spread of the beam would be diminished accordingly. Since the energy flow is resonance enhanced, this "cooling" of the beam would also be anticipated as efficient.

The above scheeme for particle beam cooling has recently been proposed twice, by Ikegami [1] and by Hirshfield and Park [2]. In the latter case, agreement has been reached [3, 4] that the "cooling" referred to is not phase space cooling: for a system of (mutually non-interacting) particles moving under the influence of an external electromagnetic field, the phase space density is constant (Liouvilles theorem).

It was also pointed out by Larson [3] that the outlined argument for "cooling" is misleading. The energy flow referred to is the net flow, applicable to a set of particles uniformly distributed in initial gyro phase. The energy transferred to individual particles depends strongly on the initial gyro phase, and may show large deviations from the average value. The true outcome is therefore a beam with an increased rather than a decreased energy spread. This point will be further illustrated below, see Figs. 1 and 2.

The concept proposed by Ikegami [1] is termed CMC (for Cyclotron Maser Cooling, or more recently for Coherent Microwave Cooling), and has been further developed in Refs. [5, 6]. It has also been the subject of an experimental investigation [7, 5, 6] which here will be referred to as the CMC test experiment. In spite of early claims of phase space cooling, and reference to frictional forces due to radiation, the basic concept is as outlined above, i e involving the (resonance region) motion of non-interacting particles under the influence of external electromagnetic forces. Therefore, neither in this case can the "cooling" referred to be identified as phase space cooling.

In order to corroborate this conclusion, the CMC test experiment will be taken as the canonical implementation of the CMC concept, and will be discussed in some detail. The main goal will be to sharpen the contours of the CMC concept. In the process it will also be shown how the experimental results follow from a simple model that by construction precludes phase space cooling.

2. THE CMC TEST EXPERIMENT

In the CMC test experiment, a low current electron beam (0.5 μA) gyrates in a constant magnetic field $\vec{B} = B_0\hat{z}$ with a radius of gyration of about 5 mm. The longitudinal energy (10-300 eV) associated with the motion along $\vec{B}$ is much smaller than the transverse energy (6-20 keV). This beam is allowed to drift through an RF cavity, with $0 < x < a$, $0 < y < b$ and $0 < z < d$, in which a TE_{101} or TE_{102} mode is externally excited at a large amplitude (5-20 kV/m). Thanks to the low longitudinal energy, the

beam completes of the order of 50-100 turns inside the cavity, and conditions for strong resonance effects have thereby been created. The electron beam is observed through its impact pattern on a luminescent screen behind the cavity. Away from resonance, the beam is seen as a thin ring, the radius of which is the gyration radius (the point corresponding to a monoenergetic beam is spread out in angle because of the spread in longitudinal energy). In the resonance region, this ring is broadened as a result of the enhanced energy transfer between the field and the electrons. Under judiciously chosen conditions, an additional outer ring may be observed, at a gyration radius that is found to be almost independent of the initial energy. This phenomenon has been at the focus of interest in the CMC test experiment, and is interpreted as CMC "cooling": (a subset of) particles with a large initial spread in gyration radius display a tendency to leave the cavity at a much smaller spread.

Unfortunately, the observed intensity distribution on the luminescent screen is an unknown function of the intensity of impacting electrons. It is therefore not known how the intensity in the outer ring is related to the total intensity or to the total current.

In order to model the CMC test experiment, the beam will be treated as a sequence of independent electrons exposed to a constant magnetic field $B_0\hat{z}$ and to an externally excited cavity mode TE_{10p}. This combination of fields can be generated from the vector potential $\vec{A} = A_y\hat{y}$, where

$$A_y = B_0 x - E_0\frac{c}{\omega}\sin(\frac{\pi x}{a})\sin(\frac{p\pi z}{d})\sin(\omega t - \phi_i) \tag{1}$$

In principle, these external fields are not the only fields in the cavity. The gyrating electrons also radiate, but it is easy to verify that under the conditions of the experiment, this contribution is much smaller than the externally generated field. The dominance of the external field is intentional, as is stressed in [6], and leaves no doubt that the CMC concept involves the motion of charges in external fields rather than in, for instance, the fields radiated by the beam itself. [1]

It may be noted that this distinction between motion in the external field and motion caused by radiation losses is not upheld elsewhere in the formulation of the CMC concept. In particular, in the attemps to derive a rate formula for CMC cooling [6], the starting point is the motion generated by the external fields. At a later stage in the derivation, however, part of the induced energy changes is reinterpreted as originating from frictional forces associated with radiation loss. This, however, is a misidentification, and if disregarded, the basic CMC concept remains as outlined above.

In summary, it has been argued that the CMC test experiment can be modelled using the vector potential of Eq.(1), and the dynamical equations that follow from the relativistic Hamiltonian

$$H = \sqrt{m^2c^4 + \left(\vec{P} - \frac{e}{c}\vec{A}\right)^2 c^2} \tag{2}$$

For this model, Liouvilles theorem precludes phase space cooling. If indeed the results of the CMC experiment can be reproduced, it will be claimed that the CMC concept has been captured and that the "cooling" referred to is not phase space cooling.

3. NUMERICAL RESULTS

The electron motion in the cavity is often quite complicated, even to the extent that some electrons may turn around and never reach the far end of the cavity. The cavity fields are large considering the energy and distance scales involved, and the resonance conditions are affected by Doppler effects and the nonlinearity of the relativistic dynamics. Accurate numerical solutions of the equations of motion therefore seem appropriate, and have been generated for parameters and initial conditions pertinent to the CMC experiment. The parameters that will be used here are specified in the Appendix, and correspond to experimental results presented in [7] and in [5, 6].

In order to simulate an incoming direct current beam, several solutions differing only in initial gyro phase have been generated. Figures 1, 3 and 4 have been obtained using 1800 initial phases, while Fig. 3 was obtained upon averaging over 180 initial phases for each value of ω_c. Figure 1 shows the relative energy gain $\gamma_f/\gamma_i - 1$ for an electron that has passed through the cavity, as a function of the initial phase ϕ_i. In those cases where the electron never reaches the far end of the cavity, the gain is displayed as zero. Obviously, the average energy gain is much smaller than the spread in energy gain, as was

[1] This fact makes the CMC concept clearly distinct from the otherwise related cyclotron resonance maser.

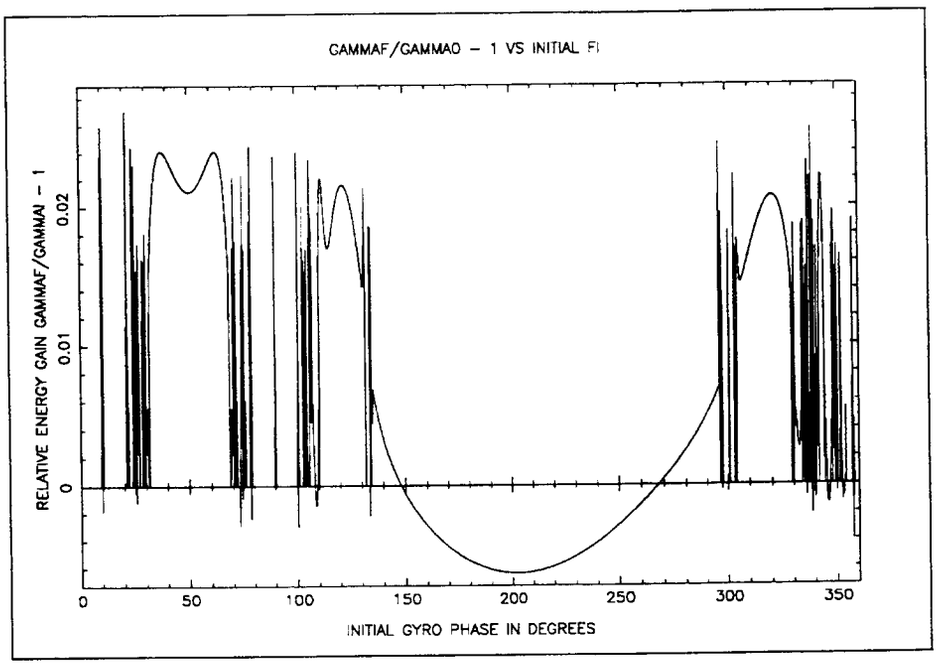

Figure 1: Relative energy gain as function of initial gyro phase

discussed in the Introduction. Figure 2 shows the average energy gain as a function of $\omega_c = eB_0/mc$, other parameters as in the Appendix (note the difference in scale between Fig. 1 and Fig. 2). Particles that never arrive (within 200 ns) at the far end of the cavity have not been included in the evaluation of the average gain. This omission (and not insufficient numerical accuracy) gives rize to the irregular shape seen in Fig.2. The working point corresponding to the parameter set specified in the Appendix is clearly in the resonance absorption region, where the net gain function for the electron is the largest.

The gain curve of Fig. 2 differs from the approximate, small amplitude gain curves presented for instance in [8]. The main reasons for the discrepancy is that Fig. 2 shows a large field amplitude gain curve, and that the TE_{102} mode electric field changes polarity halfways down the cavity. The results shown in Figs. 2 and 3 could not easily have been obtained using analytical methods, and provide an after the fact justification for the numerical approach persued here.

It may be noted in passing that the attempted derivation of a gain formula in [6] is affected by the "frictional force" misidentification referred to in the previous section. If averaged over initial phases, Eqs.(39) and (40) of reference [6] in fact vanish identically, and the final expression must therefore be considered as obtained in an ad hoc manner.

It should be emphasized that the gain curve in Fig. 2 has been obtained in a Hamiltonian model corresponding to a constant phase space density. Such a gain curve is therefore neither a signature for frictional forces, or for non-Liouvillian motion, nor well suited as starting point for beam cooling considerations.

For the generation of an impact pattern to be compared with the CMC test experiment results, it must be recalled that the experimental pattern has been obtained under conditions that have not been entirely under control. In particular, the distribution of initial longitudinal energies is largely unknown (in an interval, say, of 10-300 eV), and different assumptions regarding this distribution may lead to quite different results (the resonance condition depends via the Dopplershift on the precise value of this energy). An experimental problem of perhaps even greater relevance is related to chargeup of the recording luminescent screen. With the small longitudinal energies involved, there is a considerable risk that through this effect a significant part of the electrons actually fail to reach the screen. In order to counteract this phenomenon, the backing of the screen is held at a bais voltage, but it is not known to what extent this voltage balances the repulsive barrier created by the chargeup.

When generating impact patterns from the model considered here, the initial longitudinal energy has been chosen as 25 eV which positions the solution well in the strongly resonant regime. The resulting

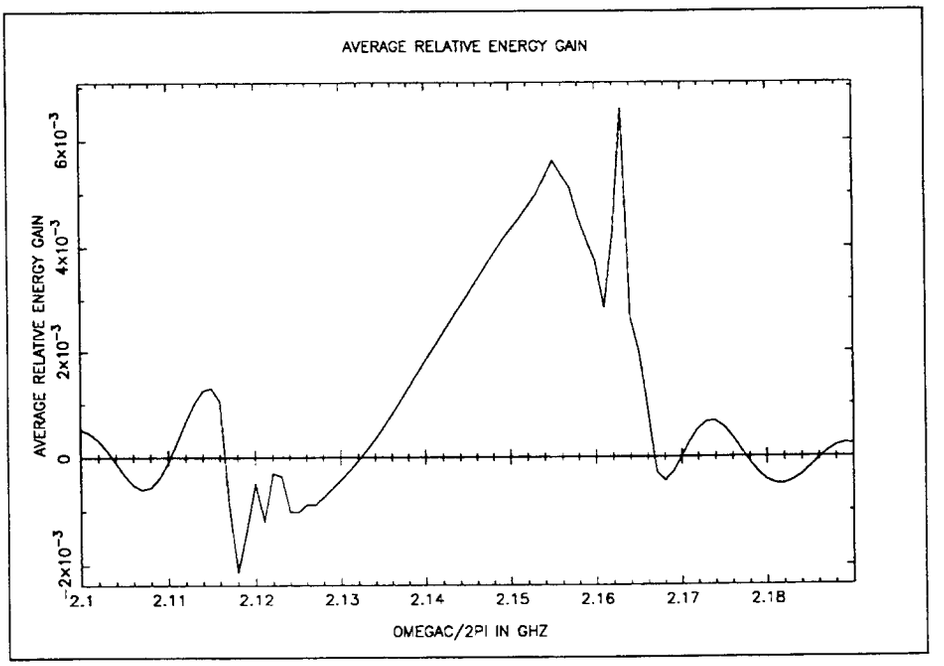

Figure 2: Average (net) relative energy gain as function of $\omega_c/2\pi$

impact pattern in Fig. 3 is based on 1800 initial electrons, uniformy distributed in initial gyro phase (most of these electrons actually arrive at the end of the cavity, as is evident from Fig. 1). In order to show how the pattern can be made more distinct through bias voltage finetuning, Fig. 4 shows the pattern obtained imposing a recording threshold at 25 eV, i.e. upon recording only those electrons that have gained longitudinal energy in the cavity. The sharpness of the outer ring in Fig.4 as compared to the ring in Fig.3 is therefore a feature of a selection proceedure rather than of a "cooling" mechanism. These impact patterns should be compared with Fig. 5.7B3 of reference [7] and Fig.4 of reference [6]. Considering the uncertainties in the experimental conditions, the agreement must be considered as good. It is particularly satisfactory that the (parameter sensitive) outer ring not only is reproduced, but also comes out at the experimentally observed value.

Impact patterns similar to those in Figs. 3 and 4 have been produced for several other values of the initial transverse energy (other parameters as in the Appendix). The radius of the outer ring is

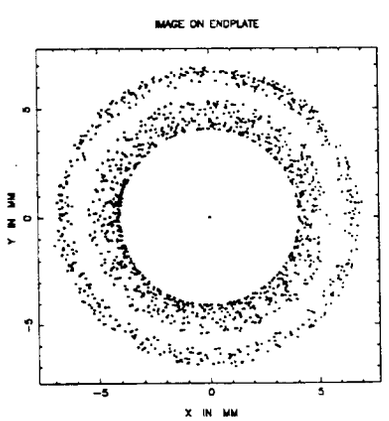

Figure 3: Electron intensity pattern, no bias

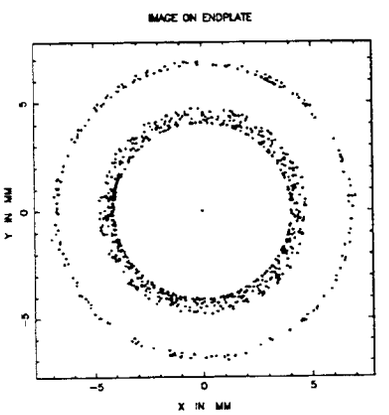

Figure 4: Electron intensity pattern, bias = 25 eV

found to grow only very slowly with this energy, and a by eye determination from Fig. 4 and for instance the corresponding pattern at 17 keV yields the same value for the radius. It has also been verified that electrons with other longitudinal energies produce impact points inside, or on, the outer ring in Fig. 4. The experimental observation that the radius of the outer ring is essentially independent of the initial transverse energy is therefore also reproduced.

3. CONCLUSIONS

It has been shown that the "cooling" observed in the CMC test experiment can be reproduced in a simple model that by construction is phase space density conserving. These results reinforce the general arguments given in the Introduction, and the conclusion of the present investigation is therefore that the CMC concept is not a phase space cooling scheeme.

4. ACKNOWLEDGEMENTS

The present study grew out of several discussions with D Reistad of the The Svedberg Laboratory, Uppsala, in the fall of 1992. Supplementary information concerning the CMC experiments was given by H Ikegami and F Kullander, and was very helpful. Finally, several discussions on all aspects of CMC and related concepts with the members of the CMC workshop in Uppsala in the late summer of 1993 are gratefully acknowledged.

APPENDIX

The CMC test experiments were carried out for a number of parameter combinations, with similar results [7]. For comparison with the results quoted in [5, 6], the parameter set B3 of [7] will be considered here. For this case $a = 103$ mm, $b = 50$ mm, $d = 200$ mm, $\omega/2\pi = 2.0911$ GHz, $\omega_c/2\pi = 2.1627$ GHz, $E_0 = 7.5$ kV/m and the initial total (or transverse) energy = 12 keV. Since the initial longitudinal energy was not well under control, a representative value = 0.025 keV has been used. The value of the electric field amplitude E_0 has been obtained from the quoted input power P through the expression for the stored energy in the cavity,

$$P\frac{Q}{\omega} = \frac{\epsilon_0}{8} abd\ E_0^2 \tag{3}$$

where $Q \approx 8000$ is the quality factor of the cavity (note that the input power quoted in [5] is in error). The resulting value for E_0 is probably not very precise.

REFERENCES

[1] H. Ikegami, Phys. Rev. Lett. **64**, 1737 (1990); *ibid* 2593 (1990).

[2] J. L. Hirshfield and G.S.Park, Phys. Rev. Lett. **66**, 2312 (1991).

[3] D. J. Larson, Phys. Rev. Lett. **68**, 133 (1992).

[4] J. L. Hirshfield and G.S.Park, Phys. Rev. Lett. **68**, 134 (1992).

[5] H. Ikegami, in *Proc. 2nd Int. Conf. on Particle Production Near Threshold*, Uppsala, Aug 1992 (ed. C Ekström); Physica Scripta **48**, 32 (1993).

[6] H. Ikegami, these proceedings.

[7] F. Kullander, *Cyclotron Maser Cooling*, Thesis, Osaka University, Nov 1992.

[8] T.W.Hsu and P.N.Robson, Electronics Letters **1**, 84 (1965).

DISCUSSION ON IKEGAMI'S PAPER

S. van der Meer
CERN, Geneva, Switzerland

ABSTRACT
I would like to describe Liouville's theorem in a way slightly different from what Sessler did on Monday, October 4. It comes to the same in the end, but I think this description clarifies thinking about what cooling is and, therefore, also applies to Cyclotron Maser Cooling.

1. INTRODUCTION

Normally, one considers particles that are pushed around by electromagnetic fields. In my description, I also look at how empty phase space (6-dimensional) is pushed around. This seems crazy, but I can define precisely what I mean. In fact, in this description every point in phase space moves as a particle would do if it would be at that point. Thus, I can describe how empty phase space is distorted by fields. Of course, these are external fields, and Liouville's theorem applies.

2. DESCRIPTION

We now add particles. I shall apply Liouville's theorem to pieces of phase space whose volume approaches zero. (I think this is what Liouville intended.) If the volume of a phase-space element goes to zero, the chance that it contains a particle also becomes zero. Thus, we are talking about empty pieces of phase space, and now all fields are external ones. Therefore, on this microscopic scale, Liouville's theorem can never be violated. Whether we have space charge, radiation, or cooling, this remains valid.

How then can cooling work? It must necessarily be through deformation of phase space, such that particles move to the centre of the distribution and (to satisfy Liouville) the empty phase space between the particles moves outwards. Clearly, the fields that do this must have a very particular shape, strongly correlated with particle position. In fact, at least two conditions must be satisfied:

1) The field that cools a particular particle must be correlated with the particle's phase-space position. In short, the field must know where each particle is.
2) The field that pushes a particular particle towards the centre should preferably push the empty phase space around it outwards. It should therefore treat each particle separately.

With stochastic cooling, these two conditions are clearly corresponding to the function of the pick-up and kicker. Both must be wide-band in order to see individual particles as much as possible.

For electron cooling, we have a similar situation. Each proton is mainly influenced by the field of a particular electron with which it collides. Both conditions are more or less satisfied. It is not difficult to convince oneself that the two conditions are also satisfied for radiation cooling, ionisation cooling and laser cooling. This is not an accident; Liouville's theorem makes it necessary.

Of course, the two conditions are rarely completely satisfied. With stochastic cooling, the pick-ups and kickers usually see many particles at the same time (typically 10^3 to 10^6). This is why stochastic cooling is so slow. If we wanted to cool in a single turn, we would have to treat the particles one by one.

3. CONCLUSION

Cyclotron Maser Cooling is claimed to be very fast; cooling times of a few turns are said to be possible. However, the coherent radiation used has no knowledge of individual particles. It satisfies neither condition 1) nor condition 2). This is the reason why Cyclotron Maser Cooling will not work.

BUNCHED BEAM STOCHASTIC COOLING IN THE FERMILAB TEVATRON COLLIDER

G. Jackson
Fermi National Accelerator Laboratory, MS 341, P.O. Box 500, Batavia IL, 60510, USA

ABSTRACT
In order to double the integrated luminosity of the Tevatron collider in the next running period, a 4-8 GHz bunched beam betatron stochastic cooling system has been designed. The horizontal and vertical emittances of the protons and antiprotons will be each cooled to counteract the effects of power supply noise, beam-beam interaction, and intrabeam scattering. A vertical proton test system has been installed in the Tevatron and tested. In addition to measurement results, details of the hardware, measurements, and cooling calculations are reviewed.

1. INTRODUCTION

The purpose of the Tevatron bunched beam stochastic cooling project is to improve the luminosity lifetime of the Tevatron [1,2,3]. Horizontal and vertical emittance growth [4,5] induced by power supply noise and ripple is the dominant cause of short luminosity lifetime, which can vary anywhere between 8 and 30 hours. During the present Tevatron upgrade and maintenance period the horizontal and vertical proton and antiproton 4-8 GHz stochastic cooling systems are being installed. The design of these systems is based on the lessons learned from two earlier proton vertical prototype systems [6,7,8,9]. In this paper these lessons are discussed.

2. TEVATRON AND COOLING

When the Tevatron is configured as a collider it is expected to store 6 proton and 6 counter-rotating antiproton bunches for tens of hours each fill. These bunches are generated using the RF manipulation called coalescing [10,11] and therefore tend to have rather long bunch lengths. During stores the transverse and longitudinal emittances slowly grow due to the decoherence of excited of coherent oscillations.

Table 1: List of typical Tevatron Collider parameters of relevance to bunched beam stochastic cooling.

Parameter	Value	Units
Beam Energy	900	GeV
Circumference	2π	km
Transverse Tune	20.6	
Gamma-T	18.75	
Synchrotron Frequency	39	Hz
RF Voltage	1	MV/turn
Fractional rms Momentum Width	.00014	
Bunch Length	50	cm
Invariant Bunch Area	4	eV-sec
Bunch Area Growth Rate	0.07	eV-sec/hr
Invariant Transverse Emittance	20	π mmmr (95%)
Emittance Growth Rate	0.3	π mmmr/hr
Proton/Antiproton Bunch Intensity	120/40	10^9
Bunch Intensity Lifetime	100	hrs

The beam energy during high energy physic stores has traditionally been limited to 900 GeV per beam. During Tevatron Collider commissioning in December 1993 the new cold compressors will increase the maximum energy to 1 TeV. With the addition of the second low-β region for the new D0 detector, the transverse tune is 20.6, up from the value of 19.4 during fixed target operations and the 1988-89 Collider run. The transverse emittance growth rates, once as high as 5 π mmmr/hr, have been reduced to the value of 0.3 by modifying power supplies. The cause of the observed 60 psec coherent longitudinal dipole oscillations which decohere into bunch area growth has not yet been identified. Coherent longitudinal quadrupole oscillations have also been observed.

Table 2: List of typical Tevatron Collider parameters of relevance to high energy physics stores.

Parameter	Value	Units
Store Length	24	hrs
Injection Time	2	hrs
Beta-star	25-50	cm
Luminosity	8	10^{30}
Luminosity Lifetime	15-30	hrs
Number of Interaction Regions	2	
Total Proton Beam-Beam Tune Shift	0.010	
HEP Interactions per Crossing	2	

Store lengths are chosen to maximize integrated luminosity. The actual number depends on the antiproton stacking rate, the stack intensity, the charge efficiency of antiproton transfers from the antiproton Accumulator ring to the Tevatron, the luminosity lifetime, and the value of the initial luminosity. The time from dumping the residual Collider beam at the end of a store to the start of the store on the next cycle has been as short as 45 minutes and as long as 4-5 hours. The value of β^*, though designed to be 50 cm during the last Collider run, was actually closer to 35 cm due to errors in the low-β quadrupole strengths. During the next run it will be reduced to 25 cm. The total beam-beam tune shift of the antiprotons was once as high as 0.025, but is presently reduced by the addition of helical orbits in the arcs using electrostatic separators. The average number of HEP interactions per crossing is presently at 2 and climbing. Either the detectors will have to separate more and more events each crossing or it will be necessary to inject more bunches and reduce the charge per bunch as luminosity continues to increase.

The most important parameter which must be established before designing a stochastic cooling system is the required cooling time. The criterion is the Tevatron Collider is a system which preserves the initial luminosity without excessively rapid increases beam density. Because the linear beam-beam tune shift parameter is already of the order of 0.01 (and is limited to 0.02) and there are already 2 high energy physics interactions per crossing, a transverse emittance can not decrease by more than a factor of 2 without the beam intensities also dropping substantially. Based on operational models, a cooling time of 20 hours was initially chosen. Since the proton intensity is now higher than original designed and the antiproton bunch intensity is lower than designed, the expected cooling rates during the next Collider run for protons and antiprotons are 50 and 18 hours. The average mixing factor is expected to be 4.3.

3. MEASUREMENTS OF BEAM PROPERTIES

The dominant difficulty in making bunched beam stochastic cooling in the Tevatron a reality is the unanticipated large dynamic range of the signals measured by the pickup electrodes. In this section the observations of the longitudinal and transverse beam spectra are reviewed.

When the beam signals from the proton vertical pickup electrodes were first measured, it was immediately noted that the power in the revolution harmonics was far greater than that in the transverse or longitudinal Schottky bands. Figure 1 is an example of such a spectral measurement. Note that the typical dynamic range needed to propagate an undistorted Schottky signal through the cooling electronics was 50 dB. Because dynamic ranges of this magnitude are extremely difficult to maintain, a considerable amount of effort was dedicated toward understanding the origin of these lines. Another reason for reducing the amount of coherent power is the limit of 200 watts of peak power the traveling wave tubes can send to the kicker plates. Since the system power is dominated by these lines, the maximum gain of the system is limited.

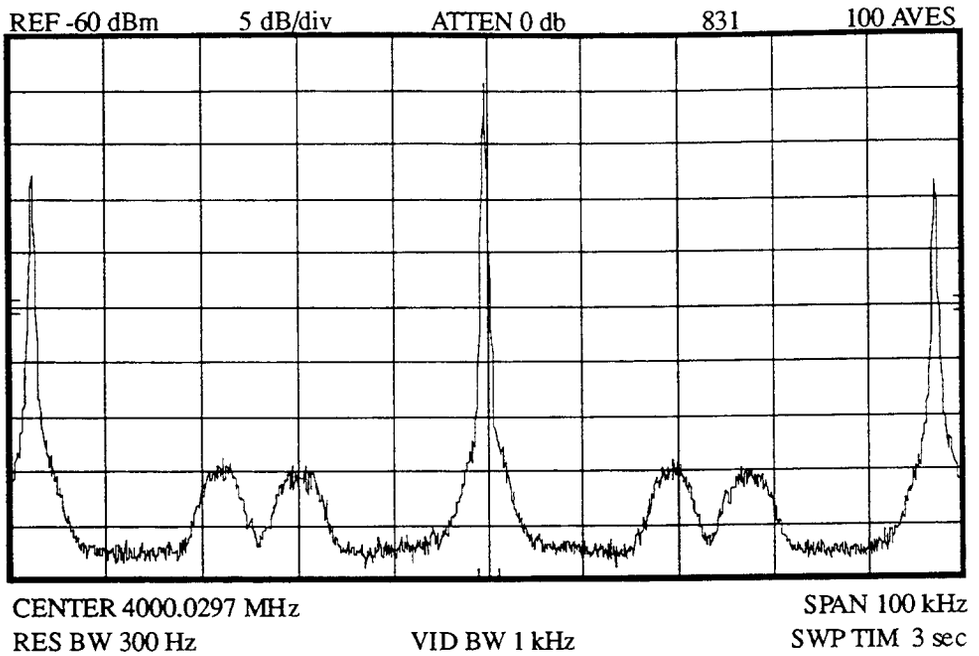

Figure 1: Example of a typical open loop proton vertical power spectrum measured with a spectrum analyzer.

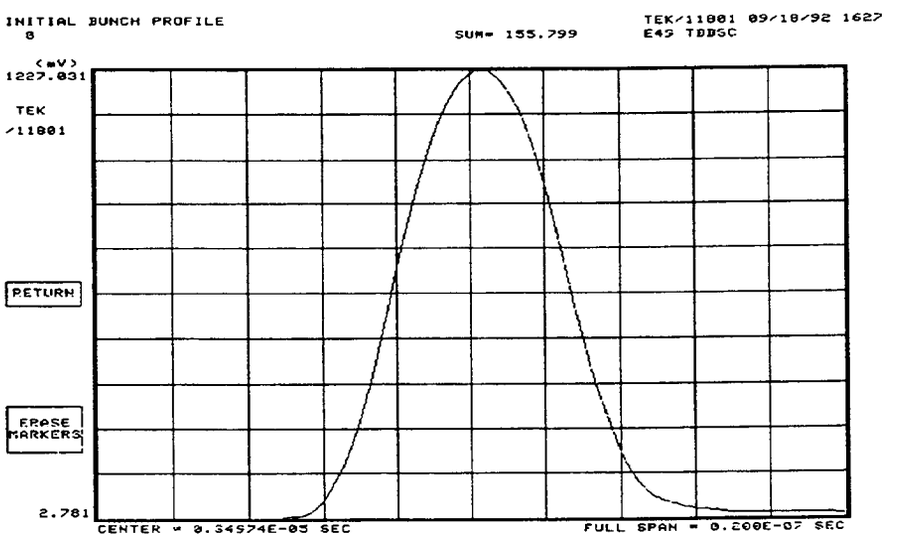

Figure 2: Longitudinal current profile of a typical proton bunch as measured by a resistive wall monitor. The horizontal scale is 2 nsec/div.

Figure 2 contains a measurement of the proton longitudinal profile as measured with a 20 GHz analog bandwidth sampling scope recording the signals from a 6 GHz bandwidth, uniform spectral response resistive wall monitor [12]. Since the bunch appears to have a Gaussian or perhaps Lorentzian temporal shape, the envelope of the spectral beam current should be described by the Fourier transform of this shape, which should have an extremely small amplitude at frequencies above 4 GHz. The actual power in the lines at harmonics of the RF frequency (f_{rf} =53.104708, h=1113) are shown in figure 3. Note that the

decrease in revolution harmonic power with increasing frequency is much to slow too be explained by the macroscopic longitudinal shape of the beam.

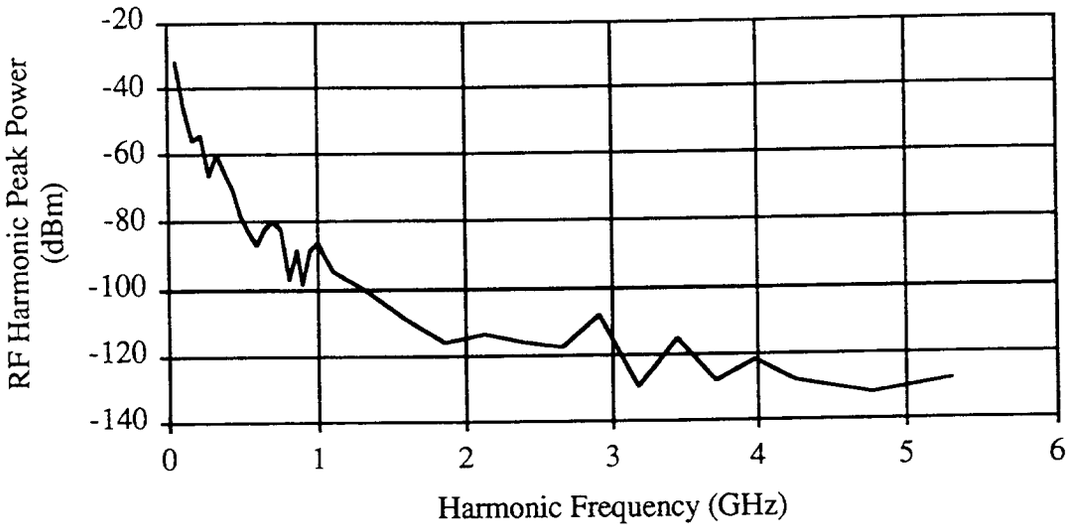

Figure 3: Measurement of the revolution harmonic power at harmonics of the RF frequency.

4. Dynamic Range Mitigation

In the past a number of techniques have been used to try and reduce the power at harmonics of the revolution frequency. In fact, most of the effort on the Tevatron bunched beam stochastic cooling system has been dominated by attempts to reduce the required dynamic range in the system by reducing this power.

The first technique to minimize the revolution harmonic power was based on high resolution stepping motors, which were used to center the proton bunches between the vertical pickup electrodes. Second, a radically new hybrid design was invented to improve the vector balance between the inputs over all frequencies in the system bandwidth. In order to be completely effective, the signals from the opposing pickup arrays must reach the hybrid a exactly the same time, down to a precision of 1 psec. This requires a longitudinal array placement tolerance of 1 mil, which cannot be guaranteed with such movable structures. Therefore, an inchworm [13] motor with a step size of 1 micron is used to move one array longitudinally with respect to the other.

Third, a repetitive notch filter which utilizes a photon storage ring (instead of a single turn delay) is undergoing commissioning. This design was developed in order to eliminate unwanted phase slope and provide uniform gain in the bandpass region of each revolution harmonic interval. This improvement comes from the fact that instead of using both closed orbit (wanted) and betatron oscillation (unwanted) information from the previous turn, the storage ring exponentially averages away the betatron oscillation modulation, and hence the phase and gain changes. Preliminary tests indicate that 30 dB of revolution harmonic power reduction is possible with this filter.

Finally, a circuit has been tested in which the sum signal is partially superimposed on the difference signal to actively null the DC and AC portions of the closed orbit contribution in the difference signal. Beam tests have already shown reductions in the revolution harmonic power of 15-20 dB. Both the repetitive notch filter and this sum/difference nullification circuit will be installed into the proton vertical test system in December 1993.

5. Observation of Signal Suppression

Tests so far have not exhibited any measurable change in the observed proton vertical emittance growth rate or luminosity lifetime. On the other hand, on one of the last days available during the last Collider run signal suppression was successfully observed. By installing a filter aimed at removing the portion of the bandwidth around 4 GHz which exhibits the largest peak revolution harmonic powers, the

system gain could be raised sufficiently to approach its optimum value. Figure 4 contains the resultant vertical betatron Schotty signals during this test.

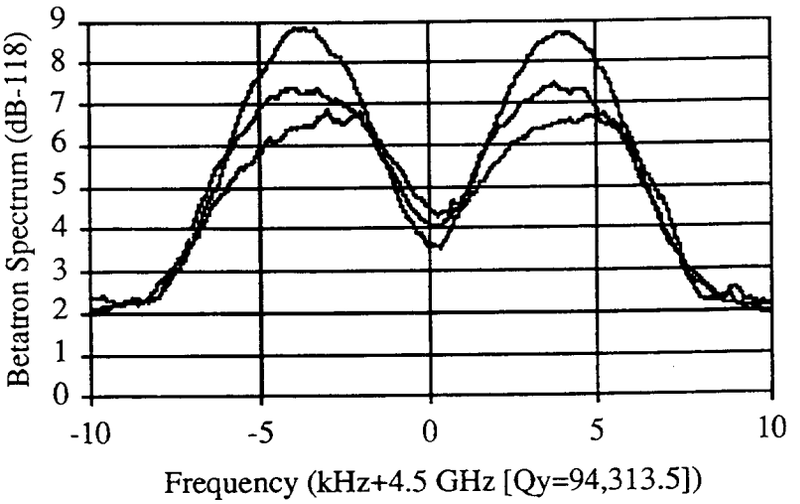

Figure 4: Observation of signal suppression in the proton vertical test system. The lowest curve was measured with the system at the correct phase and maximum unsaturated gain. The highest curve was taken under the same conditions with the exception that the system phase was changed by 180°. The middle curve is the proton vertical signal when the system is open loop.

6. REFERENCES

[1] G. Jackson, et. al., "Luminosity Lifetime in the Tevatron", Proc. of the European Part. Acc. Conf., Rome (1988), pg. 556.

[2] G. Jackson, "Winter 1988 Luminosity Lifetime Studies Analysis Results", Interanl Fermilab Memo EXP-154 (1988).

[3] D. Herrup, D. Finley, and G. Jackson, "Luminosity Lifetime in the Tevatron Collider", Proc. IEEE Part. Acc. Conf., Chicago (1989), pg. 1824.

[4] G. Jackson and S. Mane, "Studies and Calculations of Transverse Emittance Growth in Proton Storage Rings", Nucl. Instr. and Methods in Phys. Research A276, 8 (1989).

[5] G. Jackson, "Observations of Emittance Growth at Fermilab", Proc. 5th Adv. ICFA Beam Dyn. Workshop, Corpus Christi (1991).

[6] G. Jackson, "Bunched Beam Schottky Signal Measurements for the Tevatron Stochastic Cooling System", Proc. Adv. Instr. Workshop, KEK (1991).

[7] G. Jackson, "Bunched Beam Stochastic Cooling", Proc. IEEE Part. Acc. Conf., San Francisco (1991).

[8] G. Jackson, et. al., "A Test of Bunched Beam Stochastic Cooling in the Fermilab Tevatron Collider", Proc. IEEE Part. Acc. Conf., San Francisco (1991).

[9] G. Jackson, et. al, "Bunched Beam Stochastic Cooling in the Fermilab Tevatron Collider", Proc. IEEE Part. Acc. Conf., Washington DC (1993).

[10] I. Kourbanis, G. Jackson, X. Lu, Proc. IEEE Part. Acc. Conf., Washington D.C. (1993).

[11] P. Martin, K. Meisner, and D. Wildman, Proc. IEEE Part. Acc. Conf., Chicago (1989) 1827.

[12] C.D. Moore, et. al., Proc. IEEE Part. Acc. Conf.,Chicago (1989) 1513.

[13] P. Hurh, G.Jackson, "The Mechanical Design of a Bunched Beam Stochastic Cooling Tank for the FNAL Tevatron", Proc. IEEE Part. Acc. Conf., Washington D.C. (1993).

STOCHASTIC COOLING AND INTRA-BEAM SCATTERING IN RHIC*

Jie Wei
Brookhaven National Laboratory, Upton, New York 11973, USA

ABSTRACT

During the storage of the heavy ion beam in the Relativistic Heavy Ion Collider (RHIC), the luminosity deterioration due to beam growth and particle loss caused by intra-beam scattering (IBS) is of primary concern. In this paper, we study compensation methods using bunched beam stochastic cooling. With longitudinal and transverse stochastic cooling of 4–8 GHz bandwidth, the longitudinal beam loss resulted from the inadequacy of the rf voltage can be eliminated, and the transverse normalized beam emittance can be confined to about 30π mm·mrad. With such an emittance, the β^* at the crossing point can be lowered under 1 meter without exceeding the transverse aperture limit at the focusing triplets. The achievable luminosity can thus be significantly improved.

1. INTRODUCTION

Hadron beams of species from proton to Au^{79+} will be injected, accelerated, and then stored for 10 hours in the Relativistic Heavy Ion Collider (RHIC), currently under construction at the Brookhaven National Laboratory. For the highly charged ions like Au^{79+}, the luminosity deterioration due to beam growth and particle loss caused by Coulomb intra-beam scattering (IBS)[1] is of primary concern. During the 10-hour storage, beam loss of about 40% is expected due to the IBS beam growth and the inadequacy of the rf voltage. Furthermore, the transverse beam emittance grows from 10π mm·mrad to about 40π mm·mrad. When β^* at the collision point is squeezed down to 1 meter to increase luminosity, transverse beam loss may also occur. Stochastic cooling potentially provides an effective and economic method to reduce the beam size, eliminate beam loss, and thus improve luminosity.

In this paper, we summarize our study on the effects of IBS and the compensation method of bunched-beam stochastic cooling. Expressions for IBS beam growth rates and for transverse cooling rates are presented in sections 2 and 3, respectively. Section 4 discusses the Fokker-Planck approach to evaluate the longitudinal beam loss and beam evolution under IBS and longitudinal stochastic cooling. Conclusions and discussion are given in section 5.

2. INTRA-BEAM SCATTERING BEAM GROWTH

Because of the dispersion that correlates the horizontal closed orbit to the momentum, the scaling behaviour of the IBS growth rates are drastically different at energies low and high compared with the transition energy.[2] At high energies, the rates are approximately independent of the energy. Asymptotically, the horizontal and longitudinal beam amplitudes are linearly related by the average dispersion. At low energies, the beam evolves such that the velocity distribution in the rest frame becomes isotropic in all the directions.

The IBS theories[1] typically assume that the particle distribution remains Gaussian in the six-dimensional (6-D) phase space. Provided that the lattice of the accelerator mainly consists of regular cells, the rates of growth in the rms beam amplitude that are typically expressed in complex integral form, can be simplify into simple analytical form.[2] In particular, the beams in RHIC are stored at energies (γ) much higher than the transition energy (γ_T). Due to injection conditions and transverse coupling, the horizontal and vertical emittances are about the same. In terms of the normalized transverse emittance $\epsilon_{x,y} = \beta\gamma\sigma_{x,y}^2/\beta_{x,y}$ and longitudinal bunch area $S = \pi m_0 c^2 \gamma \sigma_s \sigma_p / \beta^3 cA$, the growth rate of the rms

* Work performed under the auspice of the U.S. Department of Energy.

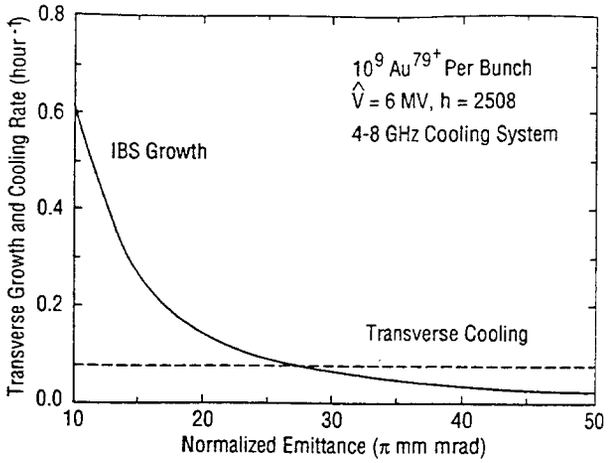

Figure 1: Transverse IBS growth rate and cooling rate as functions of the emittance.

betatron amplitude σ_x and fractional momentum deviation σ_p can be written

$$\begin{bmatrix} \frac{1}{\sigma_p}\frac{d\sigma_p}{dt} \\ \frac{1}{\sigma_x}\frac{d\sigma_x}{dt} \end{bmatrix} = \frac{Z^4 N}{A^2}\frac{\pi r_0^2 m_0 c^2 L_c}{16\beta^4\gamma_T\epsilon_x\epsilon_y S}\begin{bmatrix} n_b(1-d^2)/d \\ d/n_c \end{bmatrix} \tag{1}$$

where N is the number of particles per bunch, γ is the Lorentz factor, A is the atomic number, the Coulomb logarithm L_c is about equal to 20, $r_0 = e^2/m_0c^2$, n_b is equal to 1 if the beam is azimuthally bunched, and is equal to 2 if it is not, and n_c is equal to 1 if the horizontal and vertical motions are not coupled, and is equal to 2 if they are fully coupled. The quantity $d = D_p\sigma_p/(\sigma_x^2 + D_p^2\sigma_p^2)^{1/2} < 1$ is the effective ratio between the longitudinal and horizontal total amplitude, where D_p is the average dispersion in the cell.

The growth rates are shown to be linearly proportional to the beam intensity, and are strongly dependent ($\sim Z^4/A^2$) on the charge state Z of the particle. Except for the factor d, the rates are inversely proportional to the 6-D phase-space area. The dependence on the beam energy is usually weak. After the initial stage of storage, the asymptotic configuration $n_b n_c \sigma_x^2 \approx D_p^2\sigma_p^2$ will be approximately reached.

In the case of storage of 10^9 Au^{79+} ions per bunch in RHIC, the beam of initial area 0.3 eV·s/u fills up the entire rf bucket of area 1.28 eV·s/u in less than 30 minutes. Thereafter, beam loss occurs in longitudinal dimension. Without cooling, the transverse emittances grow in 10 hours from 10π mm·mr to about 40π mm·mr. Assuming full transverse coupling, the solid line in Fig. 1 shows the transverse IBS growth rate at different emittances.

3. TRANSVERSE STOCHASTIC COOLING

With a stochastic cooling system of properly chosen bandwidth, the IBS growth in transverse beam emittances can be compensated. The equilibrium state can be reached when the cooling rate is equal to the IBS growth rate.

With the highly charged ions, the system thermal noise is often negligible. The transverse cooling rate can thus be obtained using the Fokker-Planck approach[3, 4]

$$\begin{aligned} \frac{1}{\sigma_{x,y}}\frac{d\sigma_{x,y}}{dt} &= -\frac{f_0^2\sin(\nu_x\theta^{PK})}{2}\sum_{m=-\infty}^{\infty}\sum_{l=-\infty}^{\infty} G(m^{\pm}\omega_0 - l\Omega_i)e^{il\Omega_i\theta^{PK}/\omega_0}J_l^2(m\omega_0\tau_i) \\ &+ \frac{\pi f_0^4}{4}\sum_{l=-\infty}^{\infty}\sum_{k=-\infty}^{\infty}\frac{\rho(J')}{|l|\left|\frac{d\Omega_s(J')}{dJ'}\right|}\Bigg|_{\Omega_s(J')=k\Omega_s(J)/l}\{|G_D(-)|^2 + |G_D(+)|^2 + 2Re\,[G_D(-)G_D(+)]\}, \end{aligned} \tag{2}$$

where

$$G_D(\pm) = \sum_{m=1}^{\infty} G(m^{\pm}\omega_0 \pm l\Omega_j)J_{\mp l}(m\omega_0\tau_j)J_{\mp k}(m\omega_0\tau_i), \tag{3}$$

θ^{PK} is the distance in azimuthal angle between the pick ups and the kickers, $\omega_0 = 2\pi f_0$ is the revolution frequency, Ω_s is the synchrotron-oscillation frequency, J_l is the Bessel function of lth order, $\rho(J)$ is the

density in J, and $2\pi J$ is the longitudinal phase-space area enclosed by the particle trajectory. The quantity $\left|\frac{d\Omega_s}{dJ}\right|$ appeared in Eq. 2 is a monotonically increasing function of J,

$$\frac{d\Omega_s}{dJ} = -\frac{\pi^2 C_W}{8}\frac{1}{k^2\mathrm{K}^3(k)}\left[\frac{\mathrm{E}(k)}{1-k^2} - \mathrm{K}(k)\right] \sim -\frac{C_W}{4}, \text{ with } J = \frac{4}{\pi}\sqrt{\frac{C_\phi}{C_W}}\left[(k^2-1)\mathrm{K}(k) + \mathrm{E}(k)\right] \sim \sqrt{\frac{C_\phi}{C_W}}k^2, \tag{4}$$

where $C_W = h^2\omega_0^2\eta/2E\beta^2$, $C_\phi = Ze\hat{V}/\pi h$, $\hat{V}$ is the peak voltage, h is the harmonic number of the rf system, η is the slip factor, and K and E are complete elliptical integrals of first and second kind. Here in Eq. 4, the sign $\sim$ denotes the value in the small-amplitude limit. The summation on the revolution bands in Eq. 2 is performed over the system bandwidth, while the summation on the synchrotron side-bands is actually performed from $l = 1$ to $m\omega_0\tau$, with $\tau = \arccos\left(1-2k^2\right)/h\omega_0 \sim 2k/h\omega_0$ the oscillation amplitude in time. The factor $e^{il\Omega_s\theta^{PK}/\omega_0}$ represents the phase slip that non-synchronous particles experience during their passage from the pick-up to the kickers. In order to minimize this undesirable "mixing", the distance between the pick-up and the kickers should be chosen such that $\theta^{PK}n\hat{\tau}\Omega_0 \ll 1$, where $\hat{\tau}$ is the half bunch length in time, Ω_0 is the zero-amplitude synchrotron frequency, and n is the average harmonic number of the cooling system. The optimum cooling rate can be obtained from Eq. 2 by using numerically methods. With a bandwidth of 4–8 GHz, the dash line in Fig. 1 shows the optimum cooling rate that can be achieved when the rf bucket is nearly full (Fig. 2b). The transverse emittance at equilibrium is about 30π mm·mr.

For the convenience of order-of-magnitude estimate, the optimum cooling rate is[5] estimated

$$\frac{1}{\sigma_{x,y}}\frac{d\sigma_{x,y}}{dt}\bigg| = \frac{\langle l\rangle^2}{8\pi\langle\rho(J)\rangle}\left|\frac{d\Omega_s}{dJ}\right| = \frac{nf_0}{\pi^{3/2}hN\langle M\rangle}\frac{\langle J\rangle^{3/2}}{J_{max}^{3/2}} \tag{5}$$

where $2\pi J_{max} = 8\sqrt{C_\phi/C_W}$ is the bucket area, $\langle\ \rangle$ denotes the average over all the particles, and $\langle M\rangle = \omega_0/\langle l\rangle\Omega_0$ is the mixing factor. Cooling becomes very difficult when the bunch area $2\pi\langle J\rangle$ is small compared with the bucket area.

4. BEAM LIFETIME IMPROVEMENT WITH LONGITUDINAL COOLING

Because of the severe boundary limitation and the particle loss in longitudinal direction, the beam evolution can not be adequately described by the growth rates. The transport equation is thus derived to describe the time evolution of the longitudinal density distribution in the presence of IBS and stochastic cooling.

A transport equation in terms of action-angle variables can be obtained by averaging the 6-D Fokker-Planck equation over all transverse variables x, x', y, and y'. Because the time for IBS and stochastic cooling to produce appreciable effect is typically much longer than the synchrotron-oscillation period, which is again much longer than the correlation time of the collision process, this equation can be further reduced by averaging over the angle variable for one synchrotron-oscillation period

$$\frac{\partial\rho}{\partial t} = -\frac{\partial}{\partial J}(F\rho) + \frac{1}{2}\frac{\partial}{\partial J}\left(D\frac{\partial\rho}{\partial J}\right), \quad \text{with} \quad \begin{cases} J = 0: & -F\rho + \dfrac{D}{2}\dfrac{\partial\rho}{\partial J} = 0\ , \\ J = J_{max}: & \rho = 0\ . \end{cases} \tag{6}$$

For intra-beam scattering, the so called coefficient of dynamic friction F and diffusion D are obtained by assuming an 4-D transverse Gaussians distribution and[4] integrating over all the transverse components of the test particle

$$F(J) = \int\frac{2dz}{\pi R}\int_0^{\frac{1}{4}} dQ\ \frac{\partial W}{\partial J}\bigg|_\phi^{-1}(Q,J)\int_{J_{min}}^{J}\frac{\partial W}{\partial J}\bigg|_\phi(Q',J')\left[A_F(\lambda_1)+A_F(\lambda_2)\right]\rho(J')dJ' \tag{7}$$

and

$$D(J) = \int\frac{2dz}{\pi R}\int_0^{\frac{1}{4}} dQ\left[\frac{\partial W}{\partial J}\bigg|_\phi^{-1}(Q,J)\right]^2\int_{J_{min}}^{J}\frac{\partial W}{\partial J}\bigg|_\phi(Q',J')\left[A_D(\lambda_1)+A_D(\lambda_2)\right]\rho(J')dJ' \tag{8}$$

where $2\pi R$ is the circumference,

$$A_F(\lambda) = -\frac{2Z^4r_0^2L_cE}{A^2\beta^2\gamma^4}\frac{I_F(\lambda)}{\sigma_x\sigma_y},\quad A_D(\lambda) = \frac{Z^4r_0^2L_cE^2}{A^2\gamma^3h\omega_0}\frac{I_D(\lambda)}{\sigma_x\sigma_y},\quad \lambda_{1,2} = \frac{h\omega_0 a}{\gamma\beta^2E}(W\mp W'),\ a = \frac{1}{2}\sqrt{\frac{6\beta\gamma\beta_{x,y}}{\epsilon_{x,y}}}, \tag{9}$$

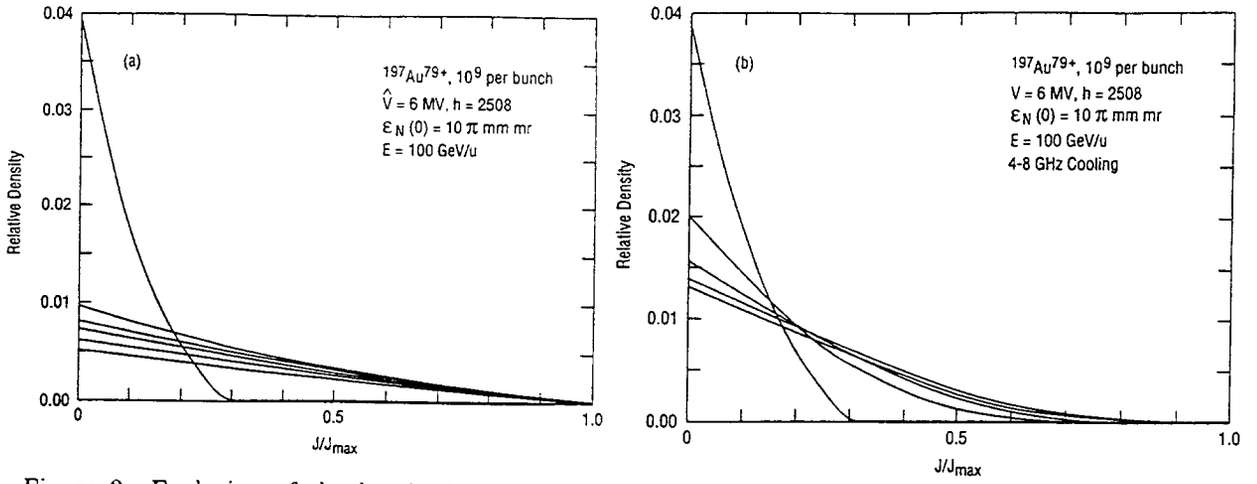

Figure 2: Evolusion of the longitudinal distribution function a) under IBS; b) under IBS when both longitudinal and transverse coolings are applied.

$$\left.\frac{\partial W}{\partial J}\right|_{\phi}^{-1} = 8k\ \mathrm{K}(k)\cos 2\pi Q\ \left[1 - 4\xi\sin^2 2\pi Q + O(\xi^2)\right],\quad \xi = \exp\left[-\pi \mathrm{K}'(k)/\mathrm{K}(k)\right],\quad \mathrm{K}'(k) = \mathrm{K}(\sqrt{1-k^2}). \tag{10}$$

The first integrals in Eqs. 7 and 8 represents the average over the machine lattice; the second integral represents the average over synchrotron-oscillation period; while the third integral describes particles of different action J' involved in the collision. The integration over J' is performed such that $k(J')\sin 2\pi Q' \approx \sin\left[\phi(Q,J)/2\right]$, extending from J_{min} to the bunch edge $\hat{J}$, with $k(J_{min}) \approx \left[\sin\phi(Q,J)/2\right]$. For a round beam with $\beta_x D_p' + \alpha_x D_p \sim 0$, we have

$$I_F(\lambda) = 2a^2\mathrm{sgn}(\lambda)\chi\left\{1 - \sqrt{\pi}|\lambda|e^{\lambda^2}\left[1 - \Phi(\lambda)\right]\right\},\ I_D(\lambda) = a\chi\left\{\sqrt{\pi}(1+2\lambda^2)e^{\lambda^2}\left[1-\Phi(\lambda)\right] - 2|\lambda|\right\}, \tag{11}$$

where $\chi = e^{-(D_p\gamma\lambda/2\sigma_x)^2}$, Φ is the error function, and $\mathrm{sgn}(\lambda)$ is 1 if $\lambda \geq 0$, and is -1 if otherwise.

For longitudinal stochastic cooling, the corresponding coefficient of coherent correction F and Schottky diffusion D can be obtained[3, 4]

$$F(J) = \frac{Z^2e^2\omega_0}{\pi}\sum_{m=1}^{\infty}\sum_{l=1}^{\infty}\frac{l}{m}J_l^2\left[m\omega_0\tau(J)\right]Re\left[G_F(m,+l) - G_F(m,-l)\right] \tag{12}$$

with

$$G_F(m,\pm l) = G\left[mf_0 \pm l\Omega_s(J)\right]\ e^{\pm il\Omega_s(J)\theta^{PK}/\omega_0}, \tag{13}$$

and

$$D(J) = \frac{NZ^4e^4f_0^2}{\pi}\sum_{l=1}^{\infty}\sum_{k=1}^{\infty}\left.\frac{k^2\rho(J')}{l\left|\frac{d\Omega_s(J')}{dJ'}\right|}\right|_{\Omega_s(J')=k\Omega_s(J)/l}\left\{|G_D(k,l)|^2 + |G_D(-k,-l)|^2 - 2Re\left[G_D(k,l)G_D(-k,-l)\right]\right\} \tag{14}$$

where the double summation on l and k represents synchrotron sideband overlapping, and

$$G_D(k,l) = \sum_{m=1}^{\infty}\frac{1}{m}G\left[m\omega_0 + l\Omega_s(J')\right]J_k\left[m\omega_0\tau(J)\right]J_l\left[m\omega_0\tau(J')\right]. \tag{15}$$

With F and D obtained for various mechanisms, Eq. 6 can be solved numerically with any given initial distribution $\rho(J)$ at $t = 0$. Note that at the vicinity of the separatrix, the synchrotron-oscillation period approaches infinity. Consequently, the assumptions that Eq. 6 is based upon is no longer valid (The quantity ξ in Eq. 10 is large compared to 1.). In our numerical calculation, we have conservatively assumed that the particle is lost if its action J exceeds 95% of the bucket value J_{max}. Our study also shows that the results are not sensitive to the closeness of the chosen boundary to the separatrix. This is partly due to the low particle density near the boundary.

Fig. 2a shows the time evolution of $\rho(J)$ during the 10-hour period with 2.5-hour time interval in the absence of cooling. The voltage of the 196 MHz rf system is kept at the maximum value 6 MV. The

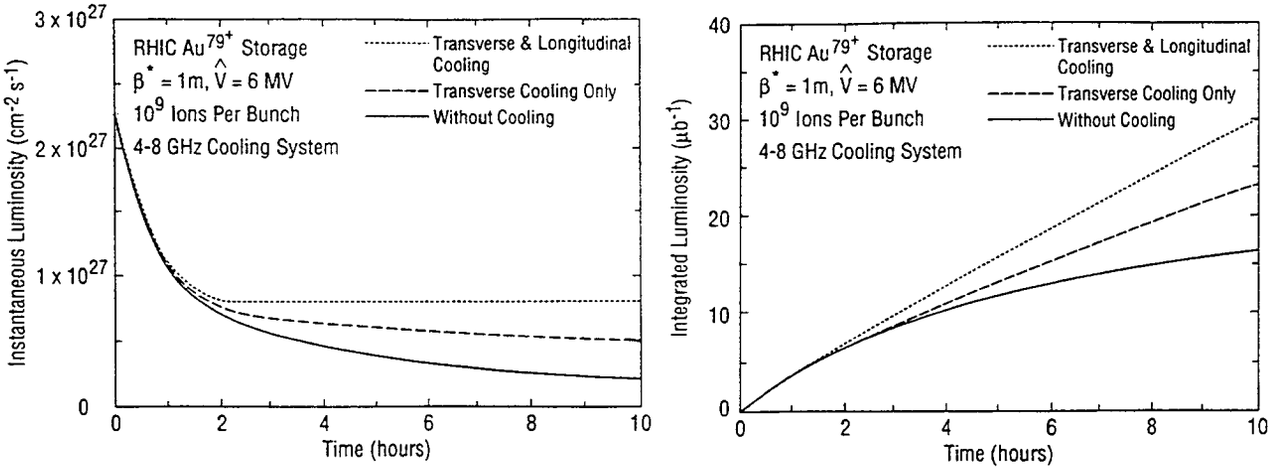

Figure 3: Improvements on a) instantaneous and b) integrated luminosity in RHIC when stochastic cooling is applied.

total beam loss is about 40%. The asymptotic distribution in longitudinal phase space is found to be Gaussian-like, insensitive to the initial conditions.

With both longitudinal and transverse stochastic cooling of 4-8 GHz bandwidth, Fig. 2b shows that the bunch approximately reaches the equilibrium state in several hours. Longitudinal beam loss is essentially eliminated, while the transverse emittance is kept to about 30π mm·mr. With a reasonable number (about 128) of kickers, the peak power needed is of the order of kW. Since the mixing factor is large compared to 1, full-turn delay between pick-ups and the kickers is plausible for this bandwidth.

Figs. 3a and b show the improvement in the instantaneous and integrated luminosity when stochastic coolings in different planes are applied. With both transverse and longitudinal cooling, the instantaneous luminosity can be significantly increased for the later period of the storage. The integrated luminosity is increased by about a factor of 2 over the entire 10-hour period.

5. CONCLUSIONS AND DISCUSSION

Bunched-beam stochastic cooling in both longitudinal and transverse planes provides an effective method to compensate for the beam growth, particle loss, and luminosity deterioration caused by IBS. With longitudinal and transverse cooling of bandwidth 4–8 GHz, the longitudinal beam loss resulted from the inadequacy of the rf voltage can be eliminated, and the transverse normalized beam emittance can be confined to about 30π mm·mrad. With such an emittance, the β^* at the crossing point can be lowered under 1 meter without exceeding the transverse aperture limit at the focusing triplets. The integrated luminosity can be increased by a factor of 2 during the 10-hour storage period.

To accommodate for the future upgrade of the beam intensity in RHIC, a wider cooling bandwidth of 8–16 MHz is desirable. To optimize the performance, the delay between the pick ups and kickers may be chosen to be 1/6 of the machine circumference. More detailed technical aspects, however, are still to be explored.

ACKNOWLEDGEMENTS The author would like to thank A.G. Ruggiero, M. Harrison, and S. Peggs for many stimulating discussions, and also D. Boussard, S. Chattopadhyay, G. Jackson, J. Marriner, G. Parzen, and A.M. Sessler for helpful discussions.

REFERENCES

[1] For example A.Piwinski, Proc. CERN Accelerator School, Gifsur-Yvette, Paris, 1984, p405; Noordwijkerhout, Netherlands, 1991, p.226; J. Bjorken and S.Mtingwa, Particle Accelerators **13**, 115 (1983); M.Martini, CERN PS/84-9 (AA) (1984); and G.Parzen, Nucl. Instr. Meth. **A256**, 231 (1987); Proc. 1988 EPAC, Rome, p.821.

[2] J.Wei, Proc. 1993 Particle Accelerator Conference, Washington DC, to be published.

[3] S. Chattopadhyay, LBL report LBL-14826 (1982).

[4] J. Wei and A.G. Ruggiero, BNL Informal Report BNL-45269, AD/RHIC-81 (1993); J. Wei and A.G. Ruggiero, Proc. 1991 Particle Accelerator Conference, San Francisco, p.1869 (1991).

[5] J. Wei, Proc. 1991 Particle Accelerator Conference, San Francisco, 1866-1868 (1991); J. Wei, Proc. XVth Inter. Confe. on High Energy Accelerators, Hamburg, Germany, p.1028 (1992).

STOCHASTIC PRECOOLING OF FRAGMENT BEAMS AT GSI IN DARMSTADT: CONCEPTS AND STATUS

F. Nolden, W. Bourgeois, H. Eickhoff, B. Franzke, P. Raabe, A. Scior, A. Schwinn, G. Trageser
GSI Darmstadt, Germany

Abstract

Stochastic Precooling at the ESR storage ring of GSI in Darmstadt will be used to cool 'hot' secondary beams on the injection orbit, before rf stacking and further electron cooling on the stack orbit [1]. The secondary beams arise from nuclear reactions at the GSI fragment separator. A maximum momentum spread of $\delta p/p_0 < \pm 0.35\%$, as well as transverse emittances of $< 20\pi$ mm mrad are to be cooled. The beam energy will be about 500 MeV/u and the number of particles per shot will be $< 10^8$. The system will be used for heavy ions up to uranium. It will operate on all three phase planes.

1. BASIC DESIGN FEATURES

The Palmer method is used for longitudinal cooling. Because of the excellent signal–to–noise ratio of heavy ion beams, notch filtering is unnecessary. There are two pick–up and two kicker stations. The presence of the stacked beam leads to the constraint of placing all electrodes in regions of sufficient dispersion. The optical parameters of the pick–up and kicker stations are given in table 1. We use the signal line P1–K1 for both vertical and longitudinal cooling. The line P2–K2 serves for horizontal cooling. As the P2 signal contains a large contribution of unwanted longitudinal Schottky noise, the P1 and P2 signals are adequately superposed at K2 in order to get a clean betatron signal.

The system works in the frequency band 0.9–1.7 GHz where Schottky bands overlap during the first few seconds of cooling. This is due to the large value $\eta \approx 0.25$ of the frequency dispersion. The time of flight between pick–up and kicker for particles at the high and low momentum ends $\delta p/p_s = \pm 0.35\%$ differs by an amount of up to ± 223 ps. In the chosen frequency band, this would lead to intolerable phase errors. Therefore the signal from the left and right plates of the pick–ups can be delayed by $T_D = \pm 200$ ps in order to restore synchronism. The delays can be varied in steps of 50 ps during each cooling cycle.

The pick–up and kicker modules consist of eight quadruplets of superelectrodes placed around the injected beam. The electrodes are conventional quarter wave plates in 50 Ω geometry. They are mounted on microstrip lines which also serve for the signal combination inside superelectrodes. For the signal transmission to the vacuum feedthroughs, vacuum coaxial lines are used. Near the electrodes, resistive dampers are installed to suppress higher waveguide modes. All modules are completely designed, the first unit (P2) has been built.

The cut–off frequency of the large ESR vacuum chamber is at about 750 MHz. Electromagnetic feedback from the kickers to the pick–ups is suppressed by means of resistive dampers installed in the chambers of ring quadrupoles.

Twelve horizontal and eight vertical steerers are available in order to center the beam at the pick–ups and kickers. With the ordinary electron–cooled beams, precision measurements of the

location	D	β_x	β_z	μ_x	μ_z
P1	3.99 m	1.6 m	17.3 m	0^0	0^0
P2	5.76 m	39.5 m	4.3 m	65^0	66^0
K1	3.99 m	1.6 m	17.3 m	414^0	432^0
K2	5.76 m	39.5 m	4.3 m	479^0	498^0

Table 1. Ion optical parameters at pick-up and kicker locations

sensitivity as a function of position are planned, in order to allow for quantitative comparisons with theory.
Electronic and rf components are ready. A total rf power of 2 kW is available. The power amplifiers are of the CERN band I type [2].

2. ELEMENTS OF THEORY

2.1. Microscopic Description

The clearest way to describe the dynamics of the cooling process is to use Hamiltonian time dependent perturbation theory. The non-perturbed Hamiltonian is expressed by the action and angle variables for a coasting beam [3]. The vector potential seen by the beam at the kickers is treated as a perturbation. The complete Hamiltonian reads

$$\begin{aligned} H(\psi_x, J_x, \psi_y, J_y, \theta, -J_s; s) &= -\frac{J_s}{R} + \frac{J_x}{\beta_x(s)} + \frac{J_y}{\beta_y(s)} \\ &- \frac{Qe}{p_s} A_s\left(x(\psi_x, J_x, J_s), y(\psi_y, J_y), s, t(\psi_x, J_x, \theta, J_s)\right). \end{aligned} \quad (1)$$

Betatron motion is characterized by the action variables $J_{x,y}$ and the angle variables $\psi_{x,y}$. Longitudinal motion is described by the action variable $J_s = Rp/p_s$ where R is the effective radius of the design orbit and p_s denotes the corresponding momentum. θ can be interpreted as an azimuthal angle. A_s is the longitudinal component of the vector potential at the kickers. The transformation equations for the coordinates x, y, and t are

$$x = D(s)\frac{\delta p}{p_s}(J_s) + x_+(s)\exp(i\psi_x) + x_-(s)\exp(-i\psi_x), \quad (2)$$

$$y = y_+(s)\exp(i\psi_y) + y_-(s)\exp(-i\psi_y), \quad (3)$$

$$t = \frac{1}{v(J_s)}\left[\theta R + \delta C(J_s)\right] + t_+(s)\exp(i\psi_x) + t_-(s)\exp(-i\psi_x). \quad (4)$$

The familiar betatron amplitudes are described by the coefficients

$$x_\pm(s) = \frac{\pm 1}{2i}\sqrt{2J_x\beta_x(s)}. \quad (5)$$

An analogous relation holds for the y components. The equation for the particle arrival time t at s contains the well-known momentum dependent term $\delta C = \delta p/p_s \int D/\rho\, ds$ as well as a less familiar expression which is caused by oscillations of the arrival time due to betatron motion:

$$t_\pm(s) = -\frac{\sqrt{2J_x}}{2v(J_s)}\left[\frac{D(s)}{\sqrt{\beta_x(s)}}\left(1 \pm \frac{\beta_x'(s)}{2i}\right) \pm iD'(s)\sqrt{\beta_x(s)}\right]. \quad (6)$$

This expression is only non-zero at locations with finite dispersion. It has a considerable impact on Hamilton's equation of motion for the horizontal action variable which reads

$$\frac{dJ_x}{ds} = -\frac{\partial H}{\partial \psi_x} = \frac{Qe}{p_s}\left(\frac{\partial A_s}{\partial x}\frac{\partial x}{\partial \psi_x} + \frac{\partial A_s}{\partial t}\frac{\partial t}{\partial \psi_x}\right). \tag{7}$$

The first term in the brackets is equivalent to the Panofsky-Wenzel theorem [4],[5].
The second term describes the change of horizontal emittance by longitudinal kicks at locations of finite dispersion [6]. In the Hamiltonian formalism, this effect is mediated by the oscillatory behaviour of the arrival times due to betatron motion.
Writing (7) as an integral equation with the unperturbed solution in the integrand yields the first order solution of (7):

$$J_x(s) \approx J_x - \frac{Qe}{p_s}\int_{s_0}^{s} ds' \left(\frac{\partial A_s}{\partial x}\frac{\partial x}{\partial \psi_x} + \frac{\partial A_s}{\partial t}\frac{\partial t}{\partial \psi_x}\right)\Bigg|_{\text{unperturbed solution}}. \tag{8}$$

The integral over vector potentials is replaced by discrete sums over kicks during subsequent revolutions. A single interaction at one kicker can be represented as the *convolution* of the voltage V_k at the input port of the kicker k with a sensitivity function S_k:

$$\int ds\, A_s(x, s, t(s)) = S_k(x, t(s_k)) * V_k(t(s_k)). \tag{9}$$

The calculation of S at a given geometry is a considerable task [7].
As the coordinate x at the nth revolution at the kicker k depends on the betatron phase angle, it is necessary to expand the sensitivity function [8]:

$$S_k(x(n,k),t) = \sum_{l=-\infty}^{\infty} S_k^l(J_s, J_x, t)\exp(il\psi_x(n,k)). \tag{10}$$

For small betatron amplitudes, the coefficients S_k^l are approximately

$$S_k^l(J_s, J_x, t) \approx \frac{(2J_x\beta_x(s_k))^{l/2}}{(2i)^l l!}\left.\frac{\partial^l S_k(x,t)}{\partial x^l}\right|_{x\,=\,D\delta p/p_s}. \tag{11}$$

In ordinary geometries, the dominating terms are those with $l = 0$.
Because of (7) we introduce functions $K_{x;k}$ describing the coupling of the applied rf field to horizontal betatron phase space at the kicker k,

$$K_{x;k}^l(J_s, J_x, t) = \sum_{\pm}\left[\pm i x_{\pm}\frac{\partial S_k^{l\mp1}(J_s, J_x, t)}{\partial x} \pm i t_{\pm}\frac{\partial S_k^{l\mp1}(J_s, J_x, t)}{\partial t}\right], \tag{12}$$

the sum being over positive and negative signs. The $K_{x;k}^{\pm1}$ terms are the dominant ones. Similarly, there is a coupling function to longitudinal phase space:

$$K_{s;k}^l(J_s, J_x, t) = -\frac{R}{v}\frac{\partial S_k^l(J_s, J_x, t)}{\partial t}. \tag{13}$$

Using these coefficients it is possible to derive simple, general expressions describing the cooling process.

2.2. Cooling drift

After 'sampling' over many revolutions it turns out that the change of the action variables is due to kicks only at the harmonics m and betatron sidebands l of the particle revolution frequency:

$$\omega_{m,l} = (m - lQ_x)\,\omega \tag{14}$$

With the usual assumptions about reciprocity ([8], [4]), the pick–up response can be described by the coupling of the electric field with the beam current. We therefore introduce the pick–up sensitivity $E_p = -\partial S_p/\partial t$. Now the drift of the horizontal action can be written

$$F_x = \left\langle \frac{\Delta J_x}{T} \right\rangle = \frac{(Qe\omega)^2 Z}{8\pi^2 p_s} \sum_{p,k} \sum_{m,l} \tilde{E}^l_p(J_s, J_x, \omega_{m,l}) G_{p,k}(\omega_{m,l}) \tilde{K}^l_{x;k}(J_s, J_x, \omega_{m,l}) \exp(i\phi). \quad (15)$$

The first sum extends over all pick–ups and kickers, the second sum over all integers m and l. Z is the pick–up impedance, and the tilde ˜ denotes the Fourier transform. $G_{p,k}$ is the voltage amplification between pick–up and kicker, without consideration of electrical delays. If we assume the electrical length of the amplification chain to be adjusted to the time of flight of the particle with momentum p_s plus some variable delay $T_D^{p,k}$, the phase ϕ in (15) becomes

$$\phi = l\,(\mu_k - \mu_p) + \omega_{m,l} \left(-t_{p,k} \eta_{p,k} \frac{\delta p}{p_s} \mp T_D^{p,k} \right). \quad (16)$$

Here, $\mu_k - \mu_p$ is the betatron phase advance between pick–up and kicker, $t_{p,k}$ is the time of flight of the design particle, and η is the local time of flight dispersion between p and k.
The advantage of the formalism presented above is due to the fact that for getting the average change of the longitudinal action J_s, one simply has to change the $\tilde{K}_{x;k}$ terms in (15) into $\tilde{K}_{s;k}$ terms, everything else remaining unchanged.

2.3. Schottky power and diffusion

The Schottky power densities and the voltage correlation at two pick-ups are delta correlated [9], i.e. $< \tilde{V}_p(\Omega)\tilde{V}_{p'}(\Omega') >= 2\pi C_{p,p'}(\Omega)\delta(\Omega + \Omega')$, with

$$C_{p,p'}(\Omega) = \frac{(QeZ)^2 \omega_s R}{8\pi|\eta|} \sum_{\text{bands}} \frac{\int dJ_x \Psi(J_s, J_x) \tilde{E}^l_p(J_s, J_x, \Omega) \left(\tilde{E}^l_{p'}(J_s, J_x, \Omega) \right)^*}{|m - lQ_x|} \exp(i\phi), \quad (17)$$

where $\Psi = \partial^2 N/\partial J_s\, \partial J_x$ is the particle distribution function, normalized to the number of particles. J_s is chosen such that the Schottky frequency $\omega_{m,l}$ is equal to Ω. In the case of Schottky overlap, there is more than one choice of m and l. ϕ is a phase similar to (16). Using the appropriate gain factors, the expression $C_{k,k'}$ for the power at the kickers is easily calculated. The components of the diffusion tensor are proportional to $C_{k,k'}$ and the appropriate coupling functions K. For example, the off–diagonal term is

$$D_{xs} = \left\langle \frac{\Delta J_x\, \Delta J_s}{T} \right\rangle = \left(\frac{Qe\omega}{2\pi p_s} \right)^2 \sum_{m,l} \sum_{k,k'} \tilde{K}^l_{x;k}(J_s, J_x, \omega_{m,l}) C_{k,k'}(\omega_{m,l}) \left(\tilde{K}^l_{s;k'}(J_s, J_x, \omega_{m,l}) \right)^*. \quad (18)$$

The other diffusion matrix elements are gained simply by exchanging K_x and K_s coupling functions.

2.4. Scaling Laws for Heavy Ions

In the following we shall assume that the thermal noise can be neglected in comparison with the Schottky noise. This is always true for heavy ion beams with intensities that are appreciated as useful by the experimental physicists. Furthermore we suppose to be power–limited, i.e. cooling is above the diffusion limit or the Ψ function is far from equilibrium. Then it makes sense to look at the scaling of the drift and diffusion coefficients under constant power conditions, which means that $G \propto \sqrt{P}/Q$. Then the drift coefficients (and the initial cooling rates) scale according to $F_i \propto Q/A$ and the diffusion due to Schottky noise scales according to $D_{ij} \propto Q^2/A^2$. Hence the cooling rates and equilibrium beam temperatures are roughly independent of the heavy ion species provided they are fully stripped.

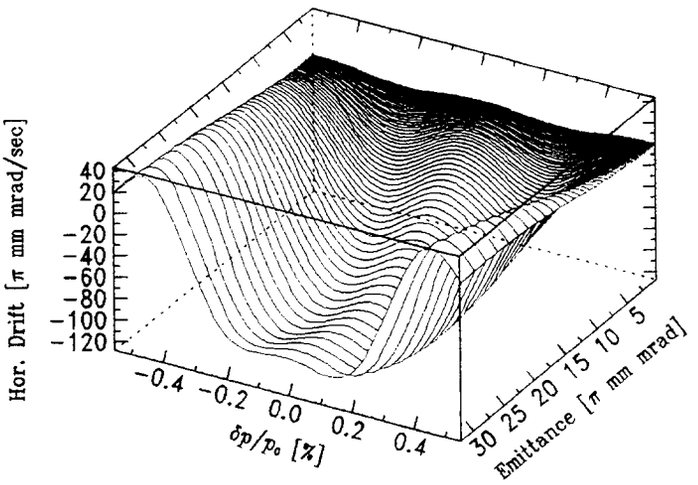

Figure 1. Horizontal drift in model calculation

3. PRELIMINARY MODEL CALCULATION

The model is calculated for a $^{238}U^{92+}$ beam with 10^7 particles. The initial distribution extends up to the limits at which the system is intended to cool, decreasing smoothly and ending closely beyond these limits. The mean power at the K1 and K2 kickers is set to about 100 W. The power due to thermal noise is of the order of a few (1–2) per cent of the total power. At the horizontal kicker K2, the power due to both betatron sidebands is about 40 W compared to 40 W from the longitudinal bands. If the signal from P1 was not used at K2 for compensating for the large longitudinal component of the P2 signal, G_{22} would have to be lowered by 7 dB, leading to a reduction of the horizontal cooling rate by about a factor of 2.2. This indicates that a proper bias between the G_{12} and G_{22} amplifications may be crucial for getting optimum cooling rates. The component of the horizontal diffusion D_{xx} which is due to horizontal kicks is larger than the one due to longitudinal kicks by about a factor of ten. Correlations between both lead to negligible corrections.
The enhancement of the cooling rate due to the variable delays T_D is verified by the calculations. As an example, fig. 1 shows the horizontal drift F_x as a function of $\delta p/p_s$ and 'emittance' $2J_x$. The valleys along the off-momentum lines at about $\pm 0.2\%$ are due to delays of ± 150 ps in the P2–K2 line. Cooling times are in the order of seconds.
Detailed numerical solutions of the 2D Fokker-Planck equation are in preparation.

References

[1] F. Nolden et al., Proc. Europ. Part. Acc. Conf., Rome 1988 (World Scientific), 579-581

[2] G. Carron, F. Caspers, L. Thorndahl, CERN Report 85-01

[3] R. Ruth, in Physics of High Energy Accelerators, AIP Conf. Proc. **153** (1985)

[4] G. Lambertson, in Physics of High Energy Accelerators, AIP Conf. Proc. **153** (1985)

[5] W. Panofsky, W. Wenzel, Rev. Sci. Inst. **27**, 967 (1956)

[6] D. Möhl, in CERN Report 84-15, 97-153

[7] P. Raabe, PhD thesis, TH Darmstadt (1992)

[8] J. Bisognano, C. Leemann, in Physics of High Energy Accelerators, AIP Conf. Proc. **87** (1982)

[9] S. Chattopadhyay, CERN 84-11

STOCHASTIC COOLING IN MUON COLLIDERS

William A. Barletta and Andrew M. Sessler
Lawrence Berkeley Laboratory, Berkeley CA 94720

ABSTRACT
Analysis of muon production techniques for high energy colliders indicates the need for rapid and effective beam cooling in order that one achieve luminosities > 10^{30} $cm^{-2}s^{-1}$ as required for high energy physics experiments. This paper considers stochastic cooling to increase the phase space density of the muons in the collider. Even at muon energies greater than 100 GeV, the number of muons per bunch must be limited to ~10^3 for the cooling rate to be less than the muon lifetime. With such a small number of muons per bunch, the final beam emittance implied by the luminosity requirement is well below the thermodynamic limit for beam electronics at practical temperatures. Rapid bunch stacking after the cooling process can raise the number of muons per bunch to a level consistent with both the luminosity goals and with practical temperatures for the stochastic cooling electronics. A major advantage of our stochastic cooling/stacking scheme over scenarios that employ only ionization cooling is that the power on the production target can be reduced below 1 MW.

1. INTRODUCTION

In a previous paper we have analyzed the design of a muon collider with a center-of-mass energy of 200 to 400 GeV with a time-averaged luminosity > 10^{30} $cm^{-2}s^{-1}$ [1]. In that scheme, the muons are generated as secondary beams from an electron beam striking a production target. The muons which emerge from the target are gathered and accelerated rapidly to an intermediate energy and cooled, at which point they can be accelerated to the final, high energy and injected into a storage ring collider with superconducting magnets. The chief advantage of producing the muons with an electron beam from a high energy, linear accelerator is that the muons are naturally formed in short bunches (< 1 cm) for subsequent acceleration to the desired high energy in a linear accelerator. As the muons retain their short bunch length in the collider, a low β interaction region can be employed.

The analysis of ref. 1, based on the use of ionization cooling [2] of the muon bunches, concluded that even with optimistic assumptions, it is difficult to envision a 200 GeV $\mu^+\mu^-$ collider functioning with a luminosity > 10^{27} $cm^{-2}s^{-1}$. In the scenario of Ref. 1 achieving a luminosity ≈10^{30} $cm^{-2}s^{-1}$ would require major advances in several of the constituent technologies: superconducting dipoles and quadrupoles, multi-kiloampere electron beam sources, and multi-megawatt muon production targets.

In this paper we consider the extent to which the inclusion of a stage of stochastic cooling after the ionization cooler can improve the prospects of designing muon colliders with luminosity exceeding 10^{30} $cm^{-2}s^{-1}$.

2. COLLIDER CONSIDERATIONS

The number of muons per bunch, $N_\mu{}^*$, that circulate in the collider will be determined by the production efficiency, A_μ, by the charge, N_e in the electron bunch that strikes the production target, and by the path length through the cooling lattice. The electron bunches will be produced in a macropulse of duration, τ_e, that is chosen to match the circulation period. If the average dipole field in the collider is B_{ave}, and if the muon energy is E_μ, the circulation period will be

$$\tau_e = 2\,\mu s \left(\frac{3\ T}{B_{ave}}\right)\left(\frac{E_\mu}{100\ GeV}\right). \qquad (1)$$

For N_b bunches per macropulse, the collision frequency will be

$$f_{coll} = \frac{N_b}{\tau_e}. \qquad (2)$$

The electron linac is pulsed at a rate, τ_μ^{-1}, where τ_μ is the muon lifetime as seen in the laboratory. As the duty factor of the linac is τ_e/τ_μ, the average power of the electron beam on the muon production target is

$$P_{beam} = \frac{N_b N_e}{\tau_e}\frac{\tau_e}{\tau_\mu} E_e = \frac{N_b N_e}{\tau_\mu} E_e. \quad (3)$$

The peak luminosity of the collider containing muons with a geometrical emittance, ε, can be written as

$$L = \frac{N_\mu^{*2} f_{coll}}{4\pi \varepsilon \beta^*} , \quad (4)$$

where $\gamma = E_\mu/\mu$ and β^* is the value of the beta function at the collision point. Following the analysis of ref. 1, we obtain the average luminosity of a collider of repetition rate, R,

$$\langle L \rangle = \frac{A_\mu^2 N_e^2 N_b \gamma C_\mu}{4\pi r_{sh} \phi_{accept} \beta^* \tau_e} \left(\frac{\gamma}{\gamma_{prod}}\right) \exp\left(-\frac{2 L_{cool}}{c \tau_\mu \gamma_c}\right)\left[1 - \exp\left(\frac{2}{\tau_\mu \gamma R}\right)\right]\left(\frac{\tau_\mu \gamma R}{2}\right). \quad (5)$$

In eq. (5) r_{sh} is the shower radius, ϕ_{accept} is the acceptance angle of the muons, and C_μ accounts for the possibility of cooling the muons; in the absence of transverse cooling, $C_\mu = 1$ and $L_{cool} = 0$.

3. STOCHASTIC COOLING SCENARIOS

The average luminosity of a muon collider will be far more sensitive to the decay lifetime of the muons than to the depopulation of the beams due to colisions. Therefore, for maximum luminosity, the beam emittance should be made as low as possible. In dealing with unstable particles such as muons, the technique of ionization cooling has the advantage that the rate of cooling the beam to the limiting emittance is independent of the number of particles. The limiting emittance of the beam is set by multiple scattering in the cooling cells. Our previous analysis suggests that it will be difficult to increase C_μ to > 1000 via ionization cooling.

Rather than relying solely on ionization cooling, one might also consider using stochastic cooling in a linear array [3] or in a storage ring to reduce the emittance of the muon beams. The difficulties of this approach derive from the limited number of particles that can be effectively cooled stochasticly. In a single pass by the pickup and kicker electrodes of the ring the emittance of the beam can be reduced by an amount

$$\frac{\Delta \varepsilon}{\varepsilon} = \frac{g}{N_{bunch}} . \quad (6)$$

With optimized amplifiers g = 1.

In eq. (6) N_{bunch} is the number of particles that are within the resolution bandwidth of the electronics. For our purposes, a bandwidth of 3 GHz is a reasonable assumption that would match the use of an S-band rf-system in the ring. For a ring with revolution frequency, f_S, containing P pairs of pickups and kickers, the maximum rate at which the emittance can be damped is

$$\alpha_s = \frac{f_S P}{N_{bunch}} . \quad (7)$$

If the beam of initial, geometrical emittance, ε_o, is cooled over a period of ζ muon lifetimes, then the final emittance of the bunch will be

$$\varepsilon_f = \varepsilon_o \exp[-\alpha_s \zeta \gamma \tau_\mu] . \quad (8)$$

Consider that in the absence of cooling the luminosity of the collider is L_{nc}; then for the collider to operate with a required luminosity, L_{req}, the cooling rate and cooling time should satisfy

$$\zeta \gamma \tau_\mu (2 - \alpha_s) = \ln \left[\frac{L_{nc}}{L_{req}} \right] . \quad (9)$$

For rapid damping $\alpha >> 1$; hence, for stochastic cooling of a 100 GeV muon beam

$$\zeta \frac{f_s P}{N_{bunch}} \approx 455 \ln \left[\frac{L_{req}}{L_{nc}} \right] . \quad (10)$$

Using eq. (6), we can rewrite eq. (10) as

$$\zeta \frac{f_s P}{N_{bunch}} \approx 455 \ln \left[\frac{4\pi \beta^* \varepsilon_o L_{req}}{N_{bunch}^2 f_{coll}} \right] . \quad (11)$$

Solving of eq. (11) for a system to reach any desired luminosity is complicated by the implicit dependence of ε_o on N_{bunch}. The indentification of a starting point for numerical investigations is simplified by the slow variation of the right-hand-side of the equation. For 100 GeV muons in a stochastic cooling ring with an average dipole field of 6 T and with 5 feedback pickups and kickers per ring, $f_s P \approx 3 \times 10^6$. Further numerical experimentation with eq. (11) suggests that if stochastic cooling is to be useful, the number of particles per bunch must be limited to the order of 10^3. It follows that the number of bunches in the collider ring must be as large as possible and that the original emittance must be as low as possible. Applying the considerations described above to the case of electro-production of muons, we find that a very high luminosity muon collider with stochastic cooling might have the characteristics described in Table 1.

Table 1. Characteristics of a 100 GeV × 100 GeV muon collider using electro-production, ionization cooling and stochastic cooling. The quantities with daggers require technological inventions or are of dubious validity.

Production			**Stochastic Cooler**	
E_e (GeV)	30		E_{cool} (GeV)	100
P_{beam} (MW)	1		Number of rings	1
N_e (particles)	3.3×10^8		No.of feedbacks	8
$N_{bunches}$	3000		$\langle B_d \rangle$ (T) in arcs	$6^\dagger$
E_{accept}(GeV)	4.5		V_{ring} (GeV/turn)	< 0.05
$(\Delta p/p)_\mu$ (%)	± 2		C_{ring} (m)	260
N_μ(nC)	3.6×10^4		Muon lifetimes	1.55
ε_n (π m-rad)	4.3×10^{-5}		$\varepsilon_{n,eq}$ (π m-rad)	1.8×10^{-16} †
Ionization Cooler			$C_{\mu\text{-tot}}$	2.3×10^{11}
E_{cool} (GeV)	60			
Number of rings	1		**Collider**	
F_{cool}	0.6		Repetition rate (Hz)	200
$\langle B_d \rangle$ (T) in arcs	4.5		N^*_μ (particles)	530
V_{ring} (GeV/turn)	0.3		N_{bunch}	3000
C_{ring} (m)	1110		B_{ave}(T)	4
$(B_q$ (T), a_q (cm))	$(7^\dagger, 1)$		$C_{collider}$ (m)	520
β_{cool} (cm)	0.1		f_{coll} (GHz)	2
$\varepsilon_{n,eq}$ (π m-rad)	4.1×10^{-7}		β^* (cm)	0.4
$N_{\mu\text{-out}}$ (particles)	2500		$(\Delta E/E)_{collider}$ (%)	< 0.1
C_μ	103		$\langle L \rangle$ ($cm^{-2}s^{-1}$)	1.2×10^{30}

The algebra suggests that the muon emittance can be reduced by eleven orders of magnitude to the incredible value of 1.8×10^{-16} π m-rad. Why is this "solution" absurd? First, we should check that the beam-beam tune shift is a reasonable value. The head-on tune shift is given by

$$\Delta\nu \approx \frac{r_\mu N_\mu}{4 \pi \varepsilon} \quad . \tag{12}$$

where r_μ is the classical radius of the muon. Applying eq. (12) to the case of Table 1, we find that $\Delta\nu >> 1$. Hence, the beam disruption will be so large that the beams cannot be made to collide many times.

Second, for the parameters of Table 1 the beam's transverse temperature is << 1 °K. However, the beam cannot be colder than the pick-ups, kickers, and electronics, which we can assume are all maintained at a temperature, T_f. In the best possible situation, the amplifiers do not magnify the thermal noise that is impressed on the beam. At pickups and kickers, assume the beta function is β_f. In that case minimum normalized emittance will be

$$\varepsilon_{n,min} = \beta_f \frac{2\,kT_f}{m_\mu c^2} \quad . \tag{13}$$

Let $T_f = 1$ °K and $\beta_f = 5$ cm, then $\varepsilon_{n,min} \approx 10^{-12}$ π m-rad. Using this limiting emittance in the example of Table 1, we find that the tune shift is reduced dramatically to $\Delta\nu \approx 0.001$, but the time-average luminosity is likewisw reduced to only $\approx 10^{27}$ cm^{-2} s^{-1}. This value may seem discouragingly low; however, it is not so far from what is needed. Is some invention possible?

Noting that we are allowed to increase the tune shift by roughly two orders of magnitude, we look for a way to increase the number of particles per bunch without affecting the damping rate. The obvious solution is to cool a large number of bunches in an intermediate storage ring and then to stack the bunches in the collider.

A difficulty with simply stacking directly into the collider is that the number of revolutions to accomplish the stacking would be equal to the number of bunches in the stochastic cooling ring, $N_{b,st}$. Unfortunately, in a ring with average dipole field B_{ave} the lifetime of the muons is only 300 B_{ave} turns. Too many muons would decay during the stacking process. This limitation can be overcome by the use of one or more intermediate accumulator rings. For simpilcity of design the accumulator may be assumed to have the same size and average dipole field as the cooler rings. Such an approach is illustrated in figure 1. In an arrangement with one intermediate accumulator the complete stacking can be accomplished in as few as $2\sqrt{N_{b,st}}$ turns. The technique of bunched beam cooling followed by stacking should yield $\langle L \rangle$ as high as 10^{31} cm^{-2} s^{-1} at 200 GeV.

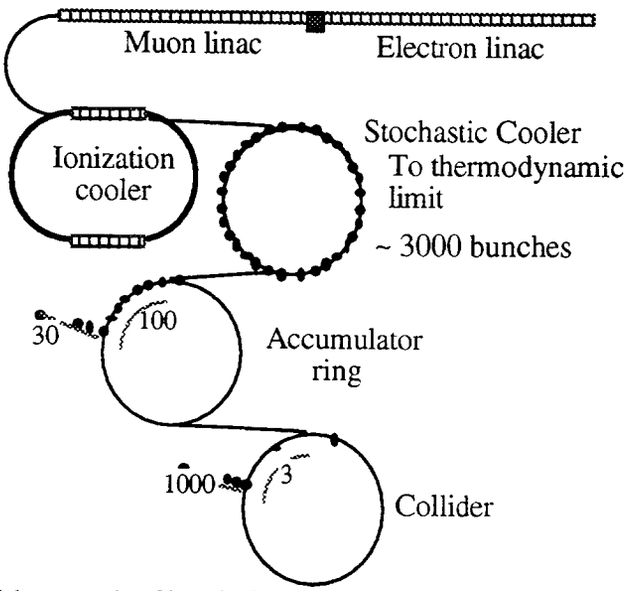

Figure 1. A schematic of the scenario of bunched beam cooling followed by stacking in a intermediate accumulator ring.

To assure a small beam size and a short bunch length we propose stacking the beams in "synchrotron space" as illustrated in Figure 2. If the 4-sigma energy spread in the cooler is Δp_{cooler}, then after cooling is complete, we must introduce an energy increment on every turn $\geq \Delta_1 = \Delta p_{cooler}$. Once the cooler is filled, we must then introduce an energy variation per turn of Δ_2, where

$$\Delta_2 \approx N_{stack}\, \Delta p_{cooler} \approx \sqrt{N_{bunch}}\, \Delta p_{cooler} \ . \tag{14}$$

Hence, the total energy spread will be

$$\Delta p_{tot} \approx N_{bunch}\, \Delta p_{cooler} \frac{E_{cooler}}{E_{collider}} \ . \tag{15}$$

If we require that the energy spread of the muon bunch in the collider, $\sigma_{E,coll}$ be 0.5%, then Δp_{cooler} should be $\approx 10^{-6}$. Such a small energy spread can be achieved only if the muons are originally selected in a rather tight momentum band ($\approx$1%) around a relatively low central energy (for example, 2 – 5 GeV). The small, final energy spread is achieved through a combination of adiabatic damping and longitudinal cooling in the ionization cooler. The consequence of this choice is a decreased conversion efficiency from electrons to muons.

The choice of stacking the bunches in synchrotron space also requires that the accumulator rings and collider be designed with a rf-system (and synchrotron frequency) carefully matched to the the phase space configuration of the stacked beams. Insufficient attention to this detail could lead to bunch lengthening and reduced luminosity.

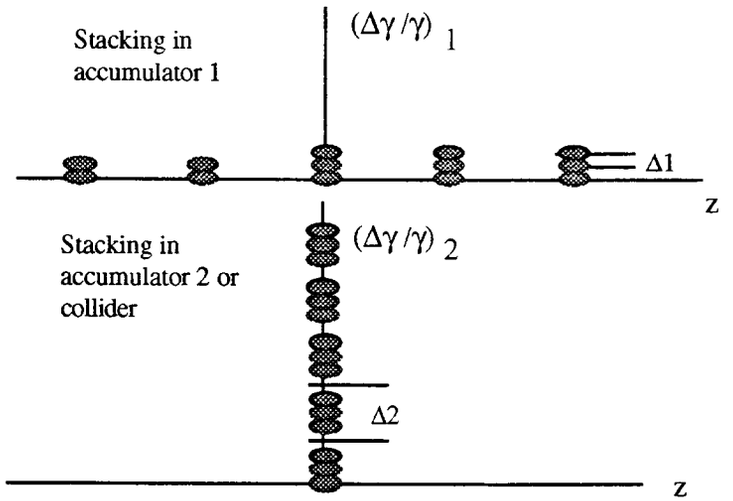

Figure 2. Schematic of stacking the muon bunches in synchrotron space

Contrary to scenarios employing ionization cooling only, the luminosity of the muon collider with stochastic cooling will be tune shift limited. In this case, the luminosity is proportional to $N_\mu \varepsilon^{-0.5}$ while the tune shift is proportional to $N_\mu \varepsilon^{-1}$. Hence, the tune shift limit can be avoided by simultaneously raising the emittance and the number of muons per bunch in the collider. Unfortunately, the number of muons per bunch in the cooler is limited to ~10^3. Hence, raising N_μ must be accomplished by increasing the number of bunches in the cooling rings.

Raising N_{bunch} in turn implies increasing the energy spread of the muon bunch in the collider. If the increase in energy spread due to two stage of stacking in synchrotron space is too large to be acceptable, the second stacking can be performed in the transverse plane with a consequent sacrifice of beam emittance and luminosity. This second approach has been adopted in the example of Table 2. Note that in our example the power on the production target is only 250 kW. The long bunch train (5000 bunches) would require the use of at least 2 rings for the first stage of stacking. In this example, the energy spread after cooling is $\approx 10^{-5}$; hence, the bunch-to-bunch energy variation that is required for the first stage of stacking can be accomplished with an rf-cavity.

One of the chief advantages of the stochastic cooling scenarios vis á vis ionization cooling is that the electron beam power on the production target is not a critical parameter. To some extent this lack of sensitivity

could be viewed as a disadvantage were one really able to design targets that could withstand 5 MW of beam power. In particular, it appears difficult to raise the luminosity by raising the power on target except by lengthening the pulse macropulse from the electron linac. One might, for example, view a 5 MW production target as an integral feature of any 5 TeV on 5 TeV e^+e^- or $\mu^+\mu^-$ collider. A cursory examination of scaling stochastic cooling schemes to such high energy suggests that it is difficult to take advantage of the faster muon production rate which a 5 MW target would provide. Specifically, the luminosity seems to increase slower than linearly with energy - much more slowly than needed to overcome the rapidly decreasing cross sections.

Table 2. The characteristics of a 100 GeV × 100 GeV muon collider using electro-production, ionization cooling and stochastic cooling. A single accumulator ring has the same circumference and average dipole field as the stochastic cooling ring. The quantities with daggers require technological innovation.

Production			**Stochastic Cooler**	
E_e (GeV)	50		E_{cool} (GeV)	100
P_{beam} (MW)	0.25		Number of rings	3
N_e (particles)	3×10^7		No.of feedbacks	12
$N_{bunches}$	5000		$\langle B_d \rangle$ (T) n arcs	6.4 †
E_{accept}(GeV)	10		V_{ring} (GeV/turn)	< 0.05
$(\Delta p/p)_\mu$ (%)	± 1		C_{ring} (m)	322
N_μ(nC)	7.3×10^3		Muon lifetimes	1.04
ε_n (π m-rad)	9.5×10^{-5}		$\varepsilon_{n,eq}$ (π m-rad)	1.05×10^{-12}
			$C_{\mu\text{-tot}}$	9×10^7
Ionization Cooler			**Accumulator**	
E_{cool} (GeV)	50		$\langle B_d \rangle$ (T) n arcs	6.4 †
Number of rings	1		C_{ring} (m)	322
Frac. of cooling cells	0.6		**Collider**	
$\langle B_d \rangle$ (T) in arcs	4.5		Repetition rate (Hz)	200
V_{ring} (GeV/turn)	0.3		N^*_μ (particles/bunch)	4.6×10^6
C_{ring} (m)	922		N_{bunch}	1
$(B_q$ (T), a_q (cm))	(5, 1.5)		$\varepsilon_{n,eq}$ (π m-rad)	7.1×10^{-11}
β_{cool} (cm)	0.1		B_{ave}(T)	6
$\varepsilon_{n,eq}$ (π m-rad)	9.5×10^{-6}		$C_{collider}$ (m)	346
$N_{\mu\text{-out}}$ (particles)	2700		f_{coll} (MHz)	1
C_μ	10		β^* (cm)	0.3
			$(\Delta E/E)_{collider}$ (%)	0.1
			$\langle L \rangle$ ($cm^{-2}\,s^{-1}$)	1.2×10^{30}

4. PROSPECTS AND CONCLUSIONS

Adding a stochastic cooling stage between the ionization cooler and the main collider ring leads to designs very different from the scenarios outlined in Ref. 1. The collider would have to contain a large number of bunches with few particles per bunch. The low initial emittance desired prior to the stochastic cooling stage must be provided by making tight cuts on both the angular spread and the momentum spread of the muons accepted from the target. As the acceleration system upstream of the production target will accept muons of a fixed geometrical emittance, one should now choose to accept lower energy muons than would be optimum in the scenarios with ionization cooling only. Accelerating the bunches to the full energy of the collider before either ionization or stochastic cooling will adiabatically damp the momentum spread of the muons that the cooling lattices must accept to values of order of

±0.1%. The stage of ionization cooling that precedes the stochastic cooler both lowers the normalized emittance further and reduces the number of particles per bunch so that the stochastic cooling can proceed more rapidly.

While our proposed approach seems to have eliminated the need for a number of the technological inventions demanded by ionization cooling, the chief difficulty is that the incredibly small normalized emittance required will put extremely severe (and perhaps unrealizable) demands on noise levels permissible in the feedback electronics and for the magnet power supplies. Additional difficulties of the approach include the need for efficient, rapid beam transfer among the several storage rings. These issues requires detailed study before one can consider the stochastic cooling option as more than a mathematical construct.

ACKNOWLEDGMENTS:

We thank Dr. Alessandro Ruggiero of Brookhaven National Laboratory for several helpful discussions concerning collider options utilizing stochastic cooling. This work was performed under the auspices of the Lawrence Berkeley Laboratory for the US Dept. of Energy Office of Energy Research under contract DE-AC03-76SF00098.

REFERENCES:

[1] Barletta, W. A. and Sessler, A. M., "Characteristics of a high energy $\mu^+\mu^-$ collider based on electro-production of muons", To be published in the Proceedings of the Workshop on High Energy Muon Colliders, Napa, California, December, 1992

[2] Neuffer, D., Particle Accelerators, **14**, (1983) 75

[3] Ruggiero, A., "Sandro's Snake", BNL report, June, 1992

STOCHASTIC COOLING REQUIREMENTS FOR A MUON COLLIDER *

Alessandro G. Ruggiero
Brookhaven National Laboratory
PO Box 5000, Upton N.Y. 11973

ABSTRACT

The most severe limitation to the muon production for a large-energy muon collider is the short time allowed for cooling the beam to dimensions small enough to provide reasonably high luminosity. The limitation is caused by the short lifetime of the particles. It appears to be desirable to accelerate the beam quickly in very short bunches. This paper describes the requirements of single-pass, fast stochastic cooling for very short bunches. Bandwidth, amplifier gain and Schottky power do not seem to be of major concern. Problems do arise with the ultimate low emittance that can be achieved, the value of which is seriously affected by the front-end thermal noise.

1. INTRODUCTION

In the quest for the Higgs bosons, a muon collider may be perceived as the experimental device more affordable and more feasible than electron-positron or very large hadron colliders [1-3]. Unfortunately, muons do not exist in nature and they have to be produced with the only technique we know these days: impinging an intense beam of protons or electrons on a target. There is also the fact that muons are intrinsically unstable particles with a very short lifetime. Accumulation, acceleration and cooling are then to be executed extremely fast.

The topic of this paper deals with the requirement of betatron stochastic cooling. The situation being described is altogether different from the usual encountered with coasting beams. Now the beam is made of short bunches with a length considerably smaller than the wavelength of the bandwidth of available electronic amplifiers. Thus a different method is to be developed based on the correction of the stochastic signal for all particles at the same time in one single-step. There is a fundamental limitation to the ultimate value of the final emittance that can be achieved, caused by the thermal noise at the front-end of the amplifier. It is found that a luminosity of about 10^{24} cm^{-2} s^{-1} can be achieved at the very most.

2. THE MUON COLLIDER

A layout of a possible scenario is shown in Fig. 1. A fast-cycling accelerator of either electrons or protons is provided as the source of the primary beam which is made to impinge on a sequence of targets for the production of muon pairs [4-8]. The secondary beam, is collected with a normalized emittance of about 100 π mm mrad. An average intensity of about 50 nA per each component of the pair production is expected. Both types of beam, μ^+ and μ^-, are accelerated in a linear rf structure, operating at 3 GHz, to the final energy which is in the range of 100 to 1000 GeV. At the end of the acceleration, each beam is transferred to a storage ring where fast stochastic cooling is done. Each beam is then taken to a stacking ring of about the same size, where several cooled beam pulses are stacked sidewise in the momentum phase space [7]. Finally, both beams are extracted from their respective stacking ring and transferred to the collider ring proper where they are made to collide.

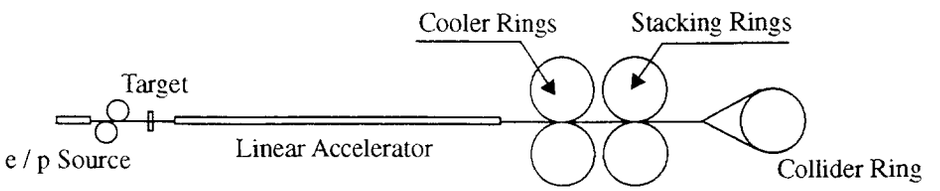

Fig. 1 - A conceptual layout of the muon collider

*Work performed under the auspices of the U.S. Department of Energy

3. THE LUMINOSITY PERFORMANCE

The average luminosity is given by the following expression

$$L = M F N_o^2 f_{bunc} \gamma / 4 \pi \varepsilon_n \beta^* = M F L_o \quad (1)$$

where $N_o \sim 100$ is the initial number of particles per bunch, $f_{bunc} \sim 3$ GHz is the beam bunching frequency during acceleration and stochastic cooling, γ is the energy relativistic factor, $\varepsilon_n \sim 25\ \pi$ mm mrad is the initial rms normalized emittance, β^* is the focussing amplitude parameter at the interaction point which is 1 cm for the single-pass mode. M is the number of beam pulses which are stacked in the momentum phase space of the stacking ring. It is to be noticed that the current $I_\mu = N_o\ e f_{bunc} \sim 50$ nA is a constant equal to the average current of each muon beam. Finally F is the form factor

$$F = F_{acc} F_{sto} F_{stac}^2 F_{col} \quad (2)$$

F_{acc} is the square of the beam survival fraction after acceleration,

$$F_{acc} = (E_{init} / E_{final})^{2E_o / cG \tau_o} \quad (3)$$

where $E_{init} \sim 1$ GeV is the beam kinetic energy at production, E_{final} is the final energy in the collider, $E_o = 106$ MeV is the rest energy, $\tau_o = 2.2\ \mu$s the lifetime of the muon at rest and G is the accelerating gradient in the linear accelerator. F_{sto} reflects the effects of reducing the betatron emittance by stochastic cooling,

$$F_{sto} = (\varepsilon_o / \varepsilon_\infty)\ exp\ (-2\ T_{sto} / \gamma_{final}\ \tau_o) \quad (4)$$

where $(\varepsilon_o / \varepsilon_\infty)$ is the ratio of the initial to the final betatron emittance and T_{sto} is the cooling period. F_{stac} is the beam survival fraction after momentum stacking of M turns during a period T_{stac},

$$F_{stac} = [1 - exp\ (-T_{stac} / \gamma_{final}\ \tau_o)] / (T_{stac} / \gamma_{final}\ \tau_o) \quad (5)$$

To avoid excessive beam losses, at most $M \sim 900$ pulses [9]. Finally, F_{col} represents the beam losses during collision and has an expression similar to the Eq. (5), except that T_{stac} is replaced by $2\ T_{col}$, that is twice the period of beam-beam collision.

4. REQUIREMENTS ON STOCHASTIC COOLING

With the values of the parameters given in the previous Sections, we have $L_o = 1.0 \times 10^{15}\ \gamma\ cm^{-2}\ s^{-1}$. To achieve a luminosity of about $1.0 \times 10^{27}\ \gamma\ cm^{-2}\ s^{-1}$, as required by the high energy physics experimental program, one needs $M F \sim 1 \times 10^{12}$. Since at most $M F_{stac}^2 \sim 1000$, even assuming $F_{acc} F_{col} \sim 1$, to meet the requirement one needs $F_{sto} \sim 1 \times 10^9$, which is a very large requirement for the betatron stochastic cooling [9]. The requirement is independent of the beam energy: a normalized emittance of $25 \times 10^{-9} \pi$ mm mrad, that is a reduction of the betatron emittance by nine orders of magnitude (!). Thus the fundamental question concerns the ultimate emittance that can be realistically achieved at the end of cooling. Fast cooling can be obtained with a low number of particles per bunch and a large electronic gain. Then a serious problem is associated with the thermal noise at the front-end of the amplifier, which will set a limitation of the final beam transverse dimension.

There are major differences between stochastic cooling for the case of bunched beams we are investigating here and the usual approach for coasting beams encountered, for instance, during production and accumulation of antiproton beams [9-11]. With good approximation, the beam bunches have no longitudinal extension. The beam current signal is therefore highly organized and coherent. The transverse beam position, on the other hand, has a very stochastic behavior. The longitudinal internal motion can be ignored and no mixing occurs between the detection of the beam signal at the pickups and the application of the deflection at the kickers. The lack of mixing causes a serious limitation on the effectiveness of stochastic cooling. Once the initial beam displacement has been corrected, there is no more signal from the beam that can be used. Thus everything is done in a single step with a relatively small reduction of the beam size. Between steps, the signal from the beam has to be regenerated, for instance by rearranging the particle mutual position with the aid of powerful magnetic lenses, like skew quadrupoles, sextupoles and nonlinear lenses. We shall assume below that this is indeed the case.

5. ANALYSIS OF THE COOLING DEVICE

Consider a very narrow bunch made of N particles all with the same electric charge. The bunch is periodically traversing a sequence of n_p position pickups made of two parallel striplines each of length ℓ and separated by a distance d. The striplines are shorted at one end and terminated at the upstream end to their characteristic impedance R_p. The bunch current can be represented as a pulse of zero duration, proportional to the average displacement $\bar{x}$. This current leaves a voltage signal which after filtering and amplification is distributed among n_k kickers of characteristic impedance R_k and having exactly the same geometrical configuration and size of the pickups.

Using the statistically relation between the average beam displacement $\bar{x}$ and the rms beam size σ, that is $\sigma^2 = N \bar{x}^2$, the total deflection angle each particle receives during the traversal of the kickers is $\theta_S = g_0 \sigma / d$ where, with E the particle total energy and βc the velocity,

$$g_0 = \frac{\ell A}{2 \beta^2 E d} \sqrt{N e^4 W^2 n_k n_p R_k R_p} \tag{6}$$

The finite temperature of the terminating resistors of the loop and of the preamplifiers creates at the input to the preamplifier a signal of power $P_T = k_B (T_A + T_R)$ W, where $k_B = 8.6171 \times 10^{-5}$ eV/°K is the Boltzmann constant, T_A the equivalent temperature of the amplifier and T_R of the resistor. We calculate also the total deflection angle due to the thermal noise

$$\theta_T = \frac{e \ell A}{\beta^2 E d} \sqrt{n_k R_k P_T} \tag{7}$$

The effectiveness of stochastic cooling is assessed by the ratio of Schottky to the thermal power

$$S = \theta_S^2 / \theta_T^2 = N e^2 W^2 n_p R_p \sigma^2 / 4 d^2 P_T \tag{8}$$

This ratio increases linearly with the bandwidth, differently from the one it was derived for coasting beams [11].

6. THE EQUATION FOR THE EVOLUTION OF THE BEAM EMITTANCE

The beam emittance can be defined as follows

$$\varepsilon = \Sigma_i (\gamma x_i^2 + 2\alpha x_i x_i' + \beta x_i'^2) / N \tag{9}$$

where α, β and γ are the lattice Twiss parameters, and x_i, x_i' are respectively the position and angle of the i-th particle. At the kickers each particle receives the same kick, that is $x_i' \rightarrow x_i' + \theta_s + \theta_T$. Since there is no correlation between particle position and thermal noise, the average change per revolution is [9]

$$\langle \Delta\varepsilon \rangle = -(2g - N g^2) \varepsilon + \beta_k \theta_T^2 \tag{10}$$

having assumed an optimum betatron phase advance between pickups and kickers, and where the dynamical gain

$$g = g_0 \sqrt{\beta_k \beta_p / N d^2} \tag{11}$$

Finally, the evolution of the beam emittance is described by the following equation

$$d\varepsilon / dt = -\lambda \varepsilon + D \tag{12}$$

where, assuming n_s identical cooling systems in the storage ring, and denoting with f_0 the revolution frequency,

$$\lambda = n_s f_0 (2g - N g^2) \tag{13}$$

is the cooling rate, and the diffusion coefficient

$$D = n_s f_0 \beta_k \theta_T^2 \tag{14}$$

7. OPTIMIZATION OF THE COOLING PERFORMANCE

An optimum cooling rate is obtained by setting $g = 1 / N$

$$\lambda_{opt} = n_s f_0 / N \tag{15}$$

which corresponds to correcting the instantaneous beam bunch displacement in one single step. At the same time we can also derive the required amplifier gain

$$A = \frac{3 \beta^2 E d^2 / e I_\mu m}{\sqrt{e^2 n_k n_p R_k R_p \beta_k \beta_p}} \tag{16}$$

and the equilibrium emittance

$$\varepsilon_\infty = D / \lambda_{opt} = N \beta_k \theta_T^2 = \frac{6 d^2 P_T / W}{m n_p \beta_p e I_\mu R_p} \tag{17}$$

Both of these expressions show the same dependence with the bunching mode number $m = 3 W / 2 f_{bunc}$ and with the average beam current $I_\mu = N e f_{bunc}$. Noticing that the thermal power P_T is proportional to W, it is seen that both A and ε_∞ do not depend explicitly on how the beam is bunched.

8. AN APPLICATION OF THE OPTIMAL SYSTEM

We take the following values: $d = 1$ cm, $\beta_p = \beta_p = 200$ m, $n_p = n_k = 1024$, $R_p = R_k = 100$ ohm. We take also m = 3, that is a bunching frequency $f_{bunc} = 3$ GHz, and a bandwidth W = 6 GHz ranging between 6 and 12 GHz. We set the temperature of the amplifier and resistor $T_A = T_R = 1$ °K which is very likely an unrealistic value. The summary of the results of our calculations are shown in Table 1 below, where we have taken the optimum gain g = 1 / N.

Table 1. Stochastic Cooling Performance

Beam Energy, GeV	100	300	1000
$2 \pi R$, m	700	2100	7000
n_s	8	24	80
$1 / \lambda$, ms	0.030	0.030	0.030
A	1×10^9	3×10^9	1×10^{10}
$\varepsilon_n = \gamma \varepsilon_\infty$, π mm mrad	32	96	320
L_o, $cm^{-2} s^{-1}$	1×10^{18}	3×10^{18}	1×10^{19}
MF	1000	300	100
L, $cm^{-2} s^{-1}$	1×10^{21}	1×10^{21}	1×10^{21}
Ng_{max}	0.0068	0.0023	0.000
f_{max}	40	120	400
L_{max}, $cm^{-2} s^{-1}$	4×10^{22}	1.2×10^{23}	4×10^{23}

The circumference of the storage ring increases with the beam energy, and the number n_s of cooling systems varies proportionally. As a consequence, the cooling rate λ is constant with energy, whereas the amplifier gain A and the equilibrium emittance ε_∞ increase linearly with energy. Even at the very low temperature of 1 °K, thermal noise dominates over the beam signal, and the equilibrium emittance is just about comparable to the initial beam emittance at the energy of 100 GeV. For larger energies, there is actually stochastic heating accompanied by an increase of the beam emittance.

Since for the optimum gain the cooling time is 0.03 ms, which is considerably shorter than the beam lifetime, it is reasonable to lower the amplifier gain. The results are shown in Fig. 2. As the gain g is lowered, both the amplifier gain and the equilibrium emittance reduce also, but on the other hand, unfortunately, the cooling time increases. If the increase is too large then the particle losses would also be too large.

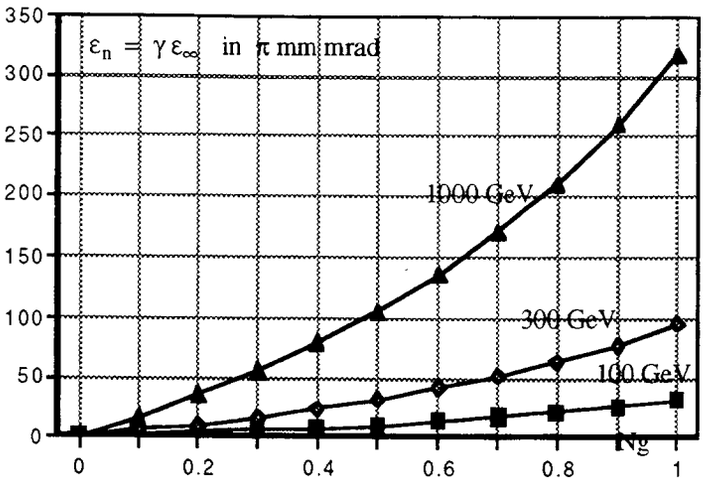

Fig. 2 - Equilibrium Emittance vs. Dynamical Gain Ng

There is an optimum [9] in correspondence of $Ng_{max} = 1 / \gamma \tau_o \lambda_{opt}$ which gives an enhancement of the luminosity by a factor $f_{max} \sim 0.04 \gamma$. The values of Ng_{max} and of f_{max} with the corresponding increased luminosity are also shown at the bottom part of Table 1. The luminosity figures are still well below the desired values.

The only other parameter that can be varied is the bunching frequency f_{bunc}. It is found [9] that as a result of the optimization with respect to the dynamical gain g, there is no optimum with the bunching mode number m.

9. CONCLUSIONS

We have determined that it is indeed feasible that the luminosity of a muon collider scales linearly with the beam energy, as it is required by physics argumentations. Unfortunately, even with the stretching of our imagination, it is seen from Table 1 that at the very most only a luminosity of 10^{20} γ cm^{-2} s^{-1} can be obtained. This is seven orders of magnitude below what it is actually required.

The limitation of thermal noise to the ultimate emittance that can be achieved is to be coupled with the requirement on the cooling rate which is to be large compared to the inverse of the beam lifetime. To achieve very fast cooling, a large amplifier gain is needed, which has also the effect to amplify to a larger level the front-end noise. Moreover large cooling rate can be obtained only with a few number of particles per bunch. Even by postulating the feasibility of momentum stacking, it is rather difficult to accumulate more than 10^5 particles per bunch.

Our estimates of the performance of stochastic cooling are based on the simple scenario of production, acceleration, cooling and collision we have proposed here. Other scenarios may be possible and we believe that an optimum configuration has still to be searched and is highly desirable. But we also believe that stochastic cooling has to be an integral part of the scheme.

REFERENCES

[1] P. Chen and K. T. McDonald, *Summary of the Physics Opportunities...*, A.I.P. Conf. Proc. **279**, 853 (1992)
[2] Proceedings of the Mini-Workshop on $\mu^+\mu^-$ colliders: Particle Physics and Design, sponsored by UCLA Center for Advanced Accelerators. Napa Valley, California, Dec. 9 - 11, 1992
[3] Proceedings of the Muon Collider Workshop, LA-UR-93-866, LAMPF Auditorium, Feb. 22, 1993
[4] A. N. Skrinsky, Proc. of the XX Intern. Confer. on High Energy Physics, A.I.P. Conf. Proc. **68**, 1056 (1980)
[5] D. Neuffer, Particle Accelerators 14, **75** (1983)
[6] R. Noble, *Particle Production and Survival in Muon Acceleration*, A.I.P. Conf. Proc. **279**, 949 (1992)
[7] W. A. Barletta and A. M. Sessler, *Characteristics of a high energy $\mu^+\mu^-$ collider based on electro-production of muons*, LBL - 33613, (January 1993)
[8] A. G. Ruggiero, *The Muon Collider*, A.I.P. Conference Proceedings **279**, 958 (1992)
[9] A. G. Ruggiero, *Stochastic Cooling Requirements for a Muon Collider*, BNL - 49553 (Sept. 1993)
[10] S. van der Meer, *An Introduction to Stochastic Cooling*, Physics of Particle Accelerators, AIP Conf Proc. **153**, Volume 2, page 1628 (1987)
[11] B. Autin, J. Marriner, A. Ruggiero, K. Takayama, IEEE Trans. on Nucl. Sci., NS-30, No. 4, p. 2593 (1983)

THE OPTICAL ANALYSIS OF THE ELECTRON BEAM TEMPERATURE

V.Golubev, I.Meshkov, V.Polyakov,
I.Seleznev, A.Smirnov, E.Syresin
Center of Applied Physics and Technology of I.N.P.
Moskovskaya St. 3980055, Lipetsk, Russia
Tel (0742)254255, Telex 101118 STAN SU, Fax (0742)256986

ABSTRACT

This method has the goal to measure the transverse temperature of electrons of an intense electron beam with energy 2 – 20 keV and current of 0.1–3 Amps. The measurement of transverse temperature are based on the measurement of transverse Larmor radius. A thin beam with a diameter of 0.06 mm is cut from the electron beam and hits a luminescent screen. The dimension of the shining spot, measured with a microscope, gives the value of the Larmor radius and consequently the transverse velocities of the electrons in the beam. The optical analysis of the electron beam temperature was performed for the new LEAR-gun and a gun, special constructed for these experiments. The difference of transverse temperature for axial and boundary electrons was found to be equal to $0.1 - 0.3eV$ for high-intensity electron beam equivalent to a perveance $1 - 5\mu A/V^{3/2}$ in a longitudinal magnetic field of 600 G. The accuracy of the method is discussed.

1. INTRODUCTION

The method of electron transverse temperature analysis is based on measurements of the transverse Larmor radius [1]. The thin electron beam cut from the base electron beam (Fig.1), comes to a luminescent screen. The dimension and coordinates of the shining spot are measured with a microscope and give the value of the Larmor radius and, consequently, the magnitudes of the transverse velocities of electrons.

The transverse velocity of the electron in the beam, generated with the gun with adiabatic optics, has radial and azimuthal components:

$$v_r = v_T \cdot cos(\varphi + \varphi_0) + v_\perp \cdot cos(\varphi) \ , \tag{1}$$

$$v_\theta = v_T \cdot sin(\varphi + \varphi_0) + v_\perp \cdot sin(\varphi) + v_d \ ,$$

where: v_T – electron thermal velocity and electron phase on the cathode, $v_\perp$ – transverse velocity, appearing due to gun optics aberrations , φ_0, φ – phase of electron Larmor rotation on the cathode and in observation point, v_d – drift velocity in the transverse electric field of the beam and the longitudinal magnetic field. The drift velocity vanishes on the cutting diaphragm, as the radial electric field of the beam transforms here in the longitudinal one.

Thus, the cut beam conserves information about v_T and $v_\perp$. The last one is the main goal of measurements.

2. THE METHOD OF MEASUREMENTS

The analysis of the transverse velocity of an electron beam was performed for two guns: new LEAR-gun [2] and CAPT gun, engineered for these experiments.

A special test bench "Analyzer" was constructed for measuring of the transverse energy of electron beam (Fig.1). This test bench consists of a vacuum chamber of 2 m in length and 30 cm in diameter, an electron gun, an analyzer of transverse velocity and a system of coils, forming a longitudinal magnetic field. The magnetic fields in the gun and the analyzer can be adjusted independently. Inhomogeneity of the magnetic field near the cathode is equal to 1–3%, in the analyzer it is equal 0.5% . The experiments were performed with a vacuum of $10^{-7} - 10^{-6}$ Torr.

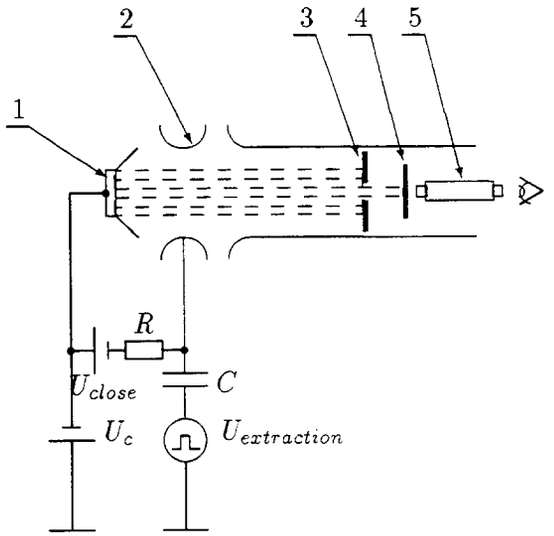

Fig.1
The schematics of the optical analyzer.
1 – the gun cathode,
2 – steering electrode,
3 – the cutting diaphragm,
4 – the luminescent screen,
5 – the microscope.

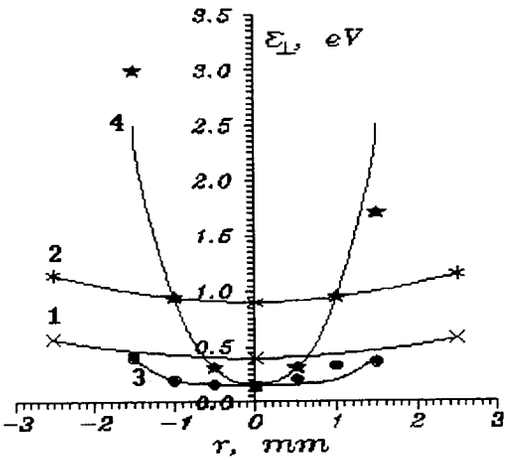

Fig.2
The dependence of the transverse energy on a radial coordinate of electron.
LEAR-gun:
1 – $I = 1\,\mathrm{A}$, $\varepsilon_0 = 5.7\,\mathrm{keV}$, $H = 600\,\mathrm{G}$;
2 – $I = 1.5\,\mathrm{A}$, $\varepsilon_0 = 5.7\,\mathrm{keV}$, $H = 600\,\mathrm{G}$;
CAPT-gun:
3 – $I = 0.3\,\mathrm{A}$, $\varepsilon_0 = 6.9\,\mathrm{keV}$, $H = 450\,\mathrm{G}$;
4 – $I = 0.5\,\mathrm{A}$, $\varepsilon_0 = 6.9\,\mathrm{keV}$, $H = 450\,\mathrm{G}$.

The optical analyzer operated in the pulsed mode, when the cathode potential is kept constant, the stearing electrode has negative "closing" potential and a periodic pulsed extracting voltage is applied to it. Pulse duration was $20-50\,\mu$sec, repetition frequency – 1–3 Hz.

The measurements of transverse velocity is based on the method of "magnetic focusing" of the cut beam. The shining spot on the luminescent screen is the exact "electron–optical" image of the cutting diaphragm, if the distance between it and the screen is equal to an integer number n of Larmor revolution periods:

$$d = 2\pi n \rho_0\,, \quad \rho_0 = v_0/\omega_H\,, \quad \omega_H = \frac{eH}{mc}\,. \tag{2}$$

When this number is half–integer, i.e.

$$d = 2\pi \rho_1 (n + 1/2)\,, \quad \rho_1 = v_1/\omega_H\,, \tag{3}$$

the spot has a maximal size, and its centre is shifted with respect to the centre of the focused optical image, observed in Regime (2). The shift value b is connected with the "optical" part of the transverse velocity $v_\perp$ and the coherent angle θ, correspondingly:

$$\theta = \frac{v_\perp}{v_1} = \frac{b}{2\rho_1}\,, \tag{4}$$

where: v_1 – electron longitudinal velocity.

The dependence of a coherent angle θ on radial coordinate was measured by scanning the beam across the diaphragm. The electron transverse energy can be found from these results with the formula

$$\varepsilon_\perp = \varepsilon_0 \theta^2(r), \tag{5}$$

where: ε_0 – kinetic energy of electrons.

The size and the form of spot for the defocusing regime (3) are defined by the Larmor radius and the coherent phase φ, which the electrons possess, when they travel from the cathode to the cutting diaphragm: $\varphi = \omega L / v_1$, where: L – distance between the cathode and the cutting diaphragm.

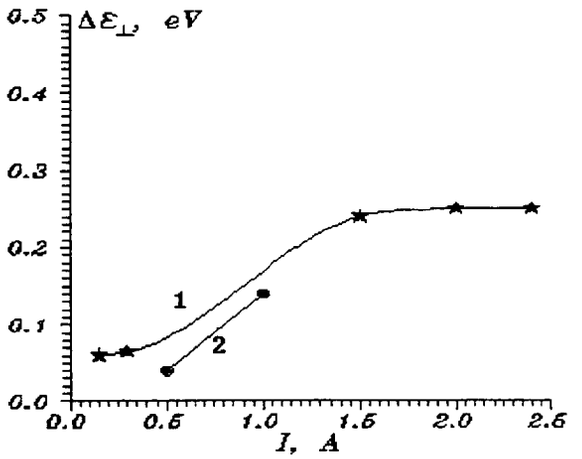

Fig.3
The dependence of difference of the transverse energy for axial and boundary electrons on beam current, forming by LEAR-gun.
$1 - \varepsilon_0 = 5.7\,\text{kV}$, $H = 600\,\text{G}$, $P = 2 - 3 \cdot 10^{-6}$ Torr;
$2 - \varepsilon_0 = 13\,\text{kV}$, $H = 600\,\text{G}$, $P = 2 - 3 \cdot 10^{-6}$ Torr.

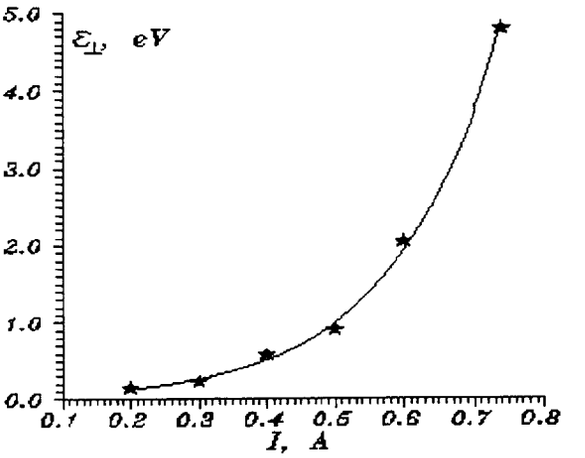

Fig.4
The dependence of the transverse energy on the beam current for CAPT-gun:
$\varepsilon_0 = 6.9\,\text{keV}$, $H = 450\,\text{G}$,
$P = 7 - 8 \cdot 10^{-7}$ Torr, $r = 1\,\text{cm}$.

The phase φ is coherent in a beam with a small current. In this case the spot has a disc form, shifted with respect to the focused spot position. The diameter of the disc is defined by thermal velocities. The incoherent angle spread $\delta\theta$ can be found from the equation

$$\delta\theta = \frac{D - a}{4\rho_1}, \tag{6}$$

where: D – size of the shining spot, a – diameter of the hole in the cutting diaphragm, $a = 0.06\,\text{mm}$.

The electron phase φ is not completely coherent for a beam with a high current, when the discharge of power supply capacitors is essential (1% of full voltage for a 1 A beam current). Such an incoherence gives a large-sized spot, which has a "banana" shape. There can exist other reasons for phase incoherence.

3. EXPERIMENTAL RESULTS

In the experiments the electron beam was scanned across the cutting diaphragm. The transverse energy was measured for axial and aperture electrons.

The results of measurements for the LEAR gun (Fig.2) show, that there exists some nonzero level of $\varepsilon_\perp$ even for axial electrons: $\varepsilon_\perp = 0.2 \div 1\,\text{eV}$. Therefore, to extract the influence of gun optics, the difference of transverse energy values

$$\Delta\varepsilon_\perp = \varepsilon_\perp(R) - \varepsilon_\perp(0)\,, \tag{7}$$

was used, where R – radius of the beam. This parameter increases with beam current (Fig.3) and has a level of $0.1 \div 0.3\,\text{eV}$ for beam perveance of $1 \div 5\,\mu A/V^{3/2}$.

The data of measurements with the optical analyzer do not contradict with the results of measurements of transverse energy with the energy analyzer [3]. The electron transverse energy, measured with help of the energy analyzer, was found to be equal $0.3 \div 1\,\text{eV}$ for the beam with perveance $1 \div 5\,\mu A/V^{3/2}$ in magnetic field $380 \div 450\,\text{G}$, while the optical analysis was realized for higher magnetic field $H = 600\,\text{G}$. It decreases transverse velocities, excited by the gun.

The results of the measurements for the CAPT gun are shown on Fig.2 and Fig.4 – 6. The dependence of $\varepsilon_\perp$ on radial coordinate (Fig.2) for different beam currents shows that it increases with radial coordinate of the electron. The transverse energy also depends very strongly on the beam current (Fig.4). The decreasing of the magnetic field and the electron energy leads to increase the transverse energy of electrons.

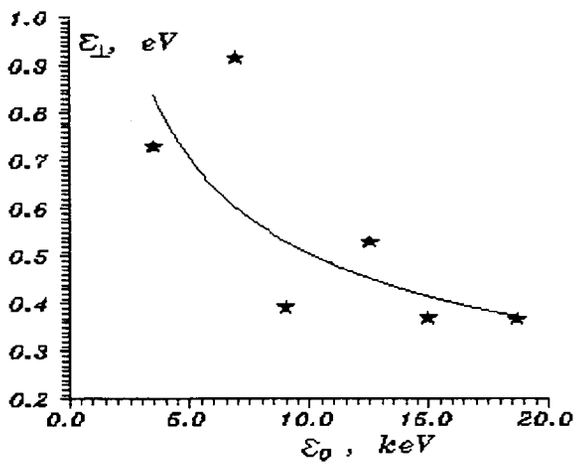

Fig.5
The dependence of the transverse energy on the electron energy:
$I = 0.5\,\text{A}$, $H = 450\,\text{G}$,
$P = 5 - 8 \cdot 10^{-7}\,\text{Torr}$, $r = 1\,\text{cm}$.

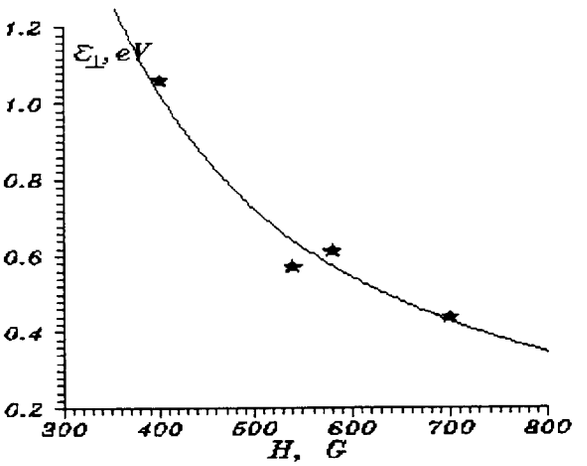

Fig.6
The dependence of the transverse energy on the magnetic field:
$\varepsilon_0 = 6.9\,\text{keV}$, $I = 0.5\,\text{A}$,
$P = 8 \cdot 10^{-7}\,\text{Torr}$, $r = 1\,\text{cm}$.

The detailed measurements of coherent transverse velocity and angular spread were produced with CAPT-gun for axial electrons. Their transverse energy spread is determined by electron thermal velocities on the cathode. Some finite value of the coherent angle $\theta \simeq 5\,\text{mrad}$ was also registered. It does not depend on the beam current for I = 0.2 ÷ 1 A and on the level of the magnetic field for $H = 300 \div 600\,\text{G}$. This coherent angle increases as $\varepsilon_0^{-1/2}$, when the electron energy decreases.

Some source of the coherent angle exists for axial electrons in the CAPT gun. It is not connected with gun optics. The increase of the coherent angle with the beam current at $H = 100 \div 200\,\text{G}$ can be connected with the distortion of gun electrodes and unparallelity of electrical and magnetic fields on the cathode. The magnetic material used in cathode elements can disturb the homogeneity of the magnetic field near cathode surface, what forms a coherent angle

$$\theta_0 \simeq \frac{2v_d}{v}\frac{R}{\rho_1}\alpha\,, \tag{8}$$

where: $v_d = 2I/\beta HR$ - electron drift velocity, α - angle between electrical and magnetic fields. Inhomogeneity of a magnetic field on the junction of the gun and the analyzer solenoids can also form some coherent angle.

The measurements of the transverse velocity of axial electrons permit to estimate the resolution of the method. It is not worse than 2 mrad both for the incoherent angle, and for the coherent one.

REFERENCES

[1] V.Ginkin, I.Meshkov, A.Skrinsky, V.Fainstein. Pribori and Tech. Exp., No.6, p.26 (1972).

[2] J.Bosser, G.Tranquille, I.Meshkov, V.Polyakov, E.Syresin, A.Smirnov, I.Seleznev, A.Zapunyako. *Project for a variable current electron gun for the LEAR electron cooler.* CERN/PS. 92-03 (1990).

[3] R.Lapik, I.Meshkov, V.Mozgunov, V.Polyakov, I.Seleznev, A.Smirnov, E.Syresin, M.Zavrazhnov, J.Bosser, G.Tranquille. *The measurement of transversal and longitudinal velocities of an electron beam.* These proceedings.

THE MEASUREMENT OF TRANSVERSAL AND LONGITUDINAL VELOCITIES OF AN ELECTRON BEAM

R.Lapik, I.Meshkov, V.Mozgunov, V.Polyakov, I.Seleznev, A.Smirnov, E.Syresin, M.Zavrazhnov
Centre of Applied Physics and Technology
of Budker Institute of Nuclear Physics
Moskovskaya st. 398055, Lipetsk, Russia
Tel. (0742)254255, Telex 101118 STAN SU, Fax (0742) 256986

J.Bosser, G.Tranquille
CERN, PS Division, CH - 1211, Geneva 23

ABSTRACT

The aim of the experiment is to measure the transverse and longitudinal velocity spreads in an electron beam. The method of measurement is based on the analysis of the energy spread in fine electron beams, cut from the main beam by small holes with diameters of 0.03–0.2 mm. The analysis is performed with a decelerating electric field of an analyzing diaphragm. The presented results give the transverse velocity spread in the electron beam, generated by the LEAR-gun, with energies up to 10 keV, and a beam current up to 3 A. The difference of transverse energy between axial and boundary electrons is less then 0.3–1 eV for the gun with perveance $1 \div 5\,\mu A/V^{3/2}$ in a longitudinal magnetic field of 350–450 G. The accuracy of the method is discussed.

1. INTRODUCTION

Forming an intensive electron beam with a low particle temperature is a well know problem in the electron cooling method [1]. The present paper is dedicated to experimental investigation of parameters of an electron beam with the current up to 3 A and energy up to 10 keV – the transverse energy and the longitudinal energy spread. The peculiarity of this experiments as compare with the analogy [2] is measurement of transverse energy in a high energy electron beam with a large perveance $\mu P = 1 \div 5\,\mu A/V^{3/2}$, when the space charge effect of an electron beam is essential. The present results are given for an electron beam generated by the new LEAR-gun [3].

2. THE PRINCIPLE OF THE METHOD

The general principle of the method is based on the analysis of the electron distribution function over longitudinal velocities in a very thin beam cut from the intense electron beam, generated by the gun immersed in a longitudinal magnetic field.

Let an electron in a cut beam have a transverse velocity

$$v_\perp = \theta v_0\,, \tag{1}$$

where

$$v_0 = \sqrt{2eU_0/m}\,, \tag{2}$$

U_0 – cathode potential. Then its longitudinal velocity is less than v_0:

$$v_\parallel^2 = v_0^2 - v_\perp^2 = (1-\theta^2)v_0^2\,, \tag{3}$$

and measurements of $v_{||}$ can give $v_{\perp}$ and θ values.

The analysis (Fig 1.) is performed with a decelerating electric field in the space between the cutting diaphragm (pos.7) and the analysing tube (pos.4), when some controlled potential difference V_{DAC} (pos.3) between cathode (pos.1) and the analysing tube is varied. By measuring the current of the collector 5 one can obtain the integral and the differential distribution functions for electrons over their energy (see Fig.2).

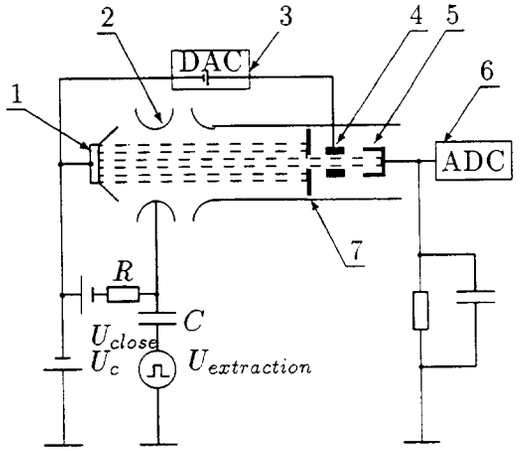

Fig.1
The scheme of the energy analyzer.
1 – gun cathode, 2 – steering electrode, 3 – DAC power supply for regulated voltage between the cathode and the analyzing diaphragm, 5 – collector, 6 – integrator and ADC, 7 – cutting diaphragm.

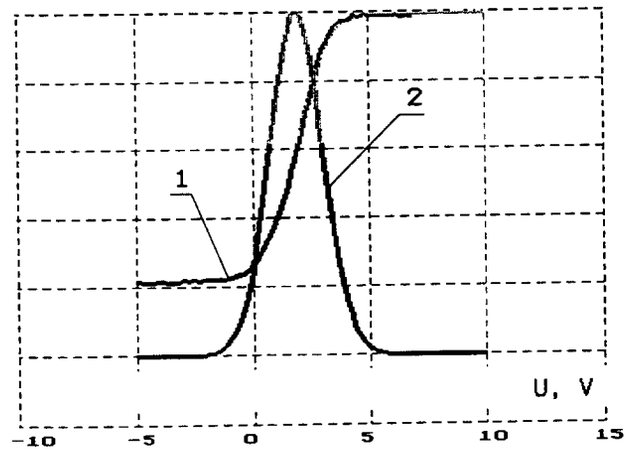

Fig.2
The integral (1) and differential (2) function of electron energy distribution, registered by the analyzer.

The excitation of transverse velocities of electrons in the gun when their total energy is constant leads to the shift of the maximum of the differential distribution function and the shift value depends on the radial position of the emitting point.

3. THE RESOLUTION OF THE METHOD

The shift of the maximum of the distribution function is determined by several effects:

1) Coherent transverse velocity of electrons connected with the imperfection of gun optics:

$$(\Delta U)_\theta = \theta^2 U_0 \,, \tag{4}$$

where U_0 – cathode potential;

2) Work function of cathode material:

$$(\Delta U)_\phi = W_\phi / e \simeq 2\,V \,; \tag{5}$$

3) Active resistance R of the emitter:

$$(\Delta U)_R = RI \,. \tag{6}$$

where: I – beam current, $R \simeq 1.4\,\mathrm{Ohm}$;

4) The potential minimum due to virtual cathode near cathode surface:

$$(\Delta U)_j = -(T_c/e) \cdot \ln \frac{j_c}{j} \approx 0.5\,V \,, \tag{7}$$

where T_c, j_c – temperature and emission current density of the cathode, j – current density of the beam generated by the gun;

5) Inclination of magnetic field lines to the analyzer axis: if electron motion is nonadiabatic near the entrance to the analysing tube, such an inclination with angle α produces

$$(\Delta U_\alpha) \approx U_0 \alpha^2 \mathbf{exp}(-\sqrt{DL}/\rho_L) \simeq U_0 \alpha^2 \mathbf{exp}\,(-2.2/(\rho_L)_{cm})) \simeq 1 \div 10\,V\,, \tag{8}$$

where ρ_L – electron Larmor radius, D – analysing tube diameter, L – distance between cutting diaphragm and analysing tube;

6) Space charge of the beam cut with diaphragm:

$$(\Delta U_I)_{Volt} \sim \frac{30 \cdot I_{Amp}}{\beta} \cdot \left(1 + 2 \cdot \ln\frac{D}{h}\right) \cdot \left(\frac{h}{a}\right)^2\,, \tag{9}$$

where I_{Amp} – current of the beam in Amps, $\beta = v/c$, v – electron velocity inside analysing tube: $v = \sqrt{2eV_{DAC}/m}$, h – diameter of the cut beam, a – cathode diameter.

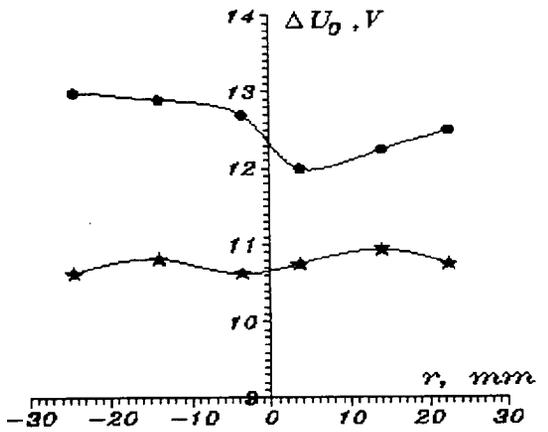

Fig.3
The dependence of ΔU on electron radial coordinate. $U_0 = 8\,\mathrm{kV}$, $H = 380\,\mathrm{G}$.

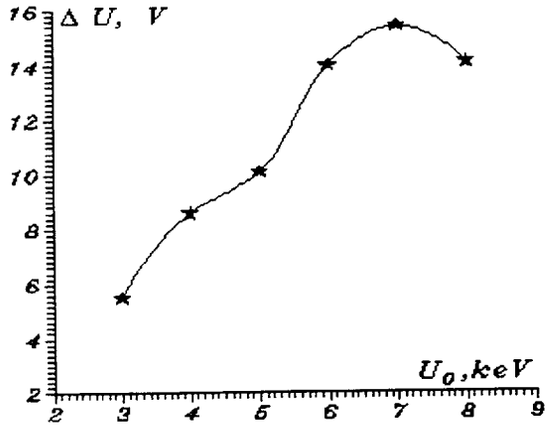

Fig.4
The dependence of ΔU on electron energy. $I = 1\,\mathrm{A}$, $H = 450\,\mathrm{G}$.

The named effects show that optical characteristic of the gun $\theta(r)$ is measured on the background of parasitic effects (2 – 6), which have a magnitude that is as large, as an optical one. To detect optical characteristic, one used the scanning of the beam across the cutting diaphragm; a dependence of $(\Delta U)_\theta$ value on the radial coordinate of the cut beam permits to obtain the necessary $\theta(r)$ characteristic – see formula (4).

The second important characteristic is the spread of electron longitudinal energy $e \cdot \delta U$. It depends on electron longitudinal temperature in the particle rest frame $T_{||}$, electron transverse energy $W_\theta \equiv e\Delta U_\theta$ and cathode temperature T_c:

$$\delta U = 2\sqrt{(T_{||}U_0 + \Delta U_\theta T_c)/e} \tag{10}$$

The results obtained in the experiments show that the achievable resolution is

$$\Delta U \approx \delta U \approx 0.2\,V\,.$$

4. THE GENERAL PARAMETERS OF THE EXPERIMENT

The experiment was performed when the gun operated in pulsed mode because of a high power of the beam. The varying voltage V_{DAC} was generated by DAC that was applied to

the cathode potential and controlled through a fiber-optics transmission line by a computer. The collector current was integrated by a capacitor, whose voltage was measured with ADC and memorized by the computer. An integral distribution function was analysed by a special program, that made an approximation of this function to the given analytical function with an RMS-method. Analytical function is equal to

$$\frac{dI}{dU_{DAC}} = \frac{I}{\delta U}\exp\left[-\left(\frac{U_{DAC}-\Delta U}{\delta U}\right)^2\right] \tag{11}$$

Such a procedure "automatically" gives the values of (ΔU)-shift and δU. The general parameters of the experiment are given in Table 1, its results – on Fig.3–6.

Table 1.
The general parameters of the experiment

Electron energy, keV	1 – 8
The beam current, mA	25 – 2500
Magnetic field, G	380 – 700
Vacuum pressure, Torr	$2 \cdot 10^{-7} - 7 \cdot 10^{-7}$
Diameter of analysing tube, μm :	
channel N 1	30
channel N 3	80 × 120 (oval)

5. ELECTRON TRANSVERSE ENERGY

The results of the beam scanning across the cutting diaphragm showed that the dependence of ΔU on the coordinate of the cut beam (Fig.3) do not look like a classical parabolic function, what could be expected from such a gun [3]. Nevertheless the difference of the ΔU magnitudes for the axial and aperture cut beams is equal to $0.3 \div 1\,\text{eV}$, which corresponds to $\theta = 6 \div 15\,\text{mrad}$ for different regimes (Table 2).

Table 2.
The results of the transverse energy measurements

Electron energy, keV	5			8		8	
The beam current, A	0.2	1.2	2	1	2.5	1	2.5
The magnetic field, G	450			450		380	
The difference of ΔU							
across the beam, eV	0.3	0.9	0.8	0.75	0.5	0.3	1.0
θ, mrad	7.7	13.4	12.6	9.7	8.0	6.1	11

The influence of the magnetic field inclination and the nonadiabatic motion near the entrance to the analysing tube, described above (Formula (8)), can explain the results shown on Fig.4 – a fast rise of ΔU with the electron energy eU_0. An essential dependence of ΔU on a magnitude of the transverse magnetic field applied in the analyser area to correct direction of the longitudinal magnetic field was discovered in the experiments.

The dependence of ΔU on the electron beam current (Fig.5) is practically linear, what corresponds to some effective resistance $R \approx 1.5 \div 1.7\,\text{Ohm}$. This magnitude includes the space

charge shift (see Formula (9)), which is about $0.2 \div 0.3$ Ohm, and the active resistance of the emitter layer of the cathode ≈ 1.4 Ohm (See Formula (6)). The curve on Fig.5 also has a shift as a whole $\Delta U \approx 2.5$ V, which can be explained as "the electron escape potential" (5).

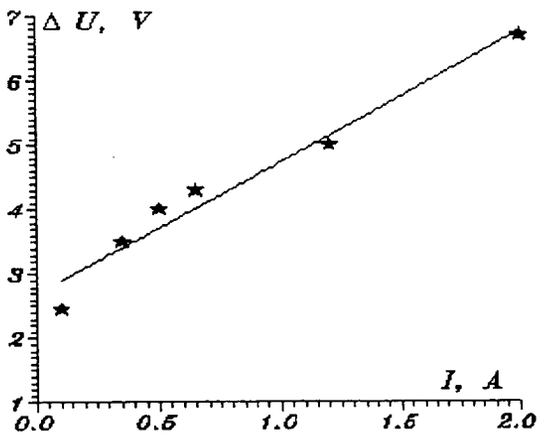

Fig.5
The dependence of ΔU on the beam current.
$U_0 = 5.2$ kV, $H = 450$ G.

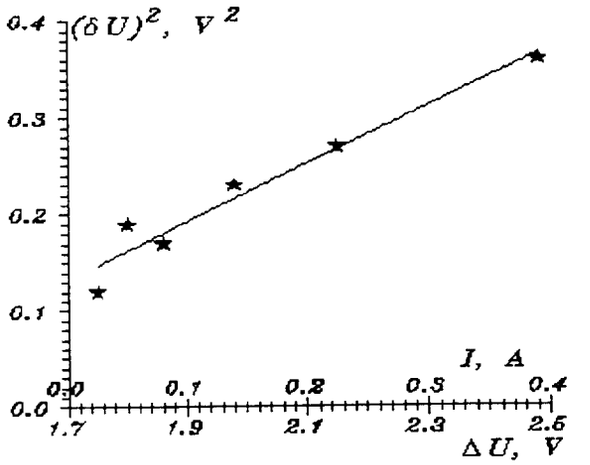

Fig.6
The dependence of the energy spread δU on the beam current and on ΔU.
$U_0 = 2$ kV, $H = 450$ G.

An increase of the cathode heating current from 30 to 35 Amps decreases ΔU by 0.5 V, what can be explained by reduction of the emitter resistance.

The important result was obtained, when heating current was switched off and measurements of integral distribution function were made with the gun beam, emitted due to thermoinertia of the heated cathode (nearly 7 min.). No difference in distribution functions was observed with and without heating current. It means that the influence of a magnetic field of the heating current is small enough.

6. THE SPREAD OF ELECTRON LONGITUDINAL ENERGY

The value of δU varies slightly with the cut beam coordinate and more strongly with the gun beam parameters. It depends on the gun beam current as square root of the current for a fixed electron energy (Fig.6), what can be explained by the transverse-longitudinal relaxation. At the same time the dependence of $(\delta U)^2$ on ΔU is linear, what can be explained by Formula (10) and by the linear dependence of ΔU on the gun current (see Fig.5).

REFERENCES

[1] G.I.Budker, A.N.Skrinsky. *Electron cooling and new perspective in the physics of elementary particles.* UFN, v.124, p.561 (1979).

[2] N.S.Dikansky, V.I.Kudelainen, V.A.Lebedev, I.N.Meshkov, V.V.Parkhomchuk et al. *Ultimate possibilities of electron cooling.* INP 88-61 (1988).

[3] J.Bosser, G.Tranquille, I.Meshkov, V.Polyakov, E.Syresin, A.Smirnov, I.Seleznev, A.Zapunyako. *Project for a variable current electron gun for the LEAR electron cooler.* CERN/PS. 92-03 (1990).

THE FIRST RESULTS OF ELECTRON COOLING AT LEAR WITH THE VARIABLE CURRENT ELECTRON GUN

J. Bosser, R. Ley and G. Tranquille
PS Division, CERN, CH 1211 Geneva 23, Switzerland

R. Lapik, I. Meshkov, V. Polijakov, I. Seleznev,
A. Smirnov, E. Syresin and A. Zapunjako
Centre of Applied Physics and Technology, CAPT, 398055 Lipetsk, Russia

ABSTRACT
A new variable current electron gun has been developed in order to improve the performance of the LEAR electron cooler. The previous gun was of the resonant type offering little operational flexibility. The new gun is of the adiabatic type with the peculiarity that it has been designed to operate in a relatively low magnetic field. It allows for the online control of the electron beam intensity whilst ensuring low transverse and longitudinal temperatures. In this paper we report on the performance of the new gun in tests made at Lipetsk and at CERN, and we present the results of first cooling tests made at LEAR on proton beams at a momentum of 310.1 MeV/c.

1. INTRODUCTION

The variable current electron gun, developed between CAPT Lipetsk and CERN, is designed to generate a high quality electron beam with intensities of up to 3 Amps for electron energies up to 30 keV. The gun and its electrical connections are shown in Fig. 1. It consists of a 5cm diameter cathode surrounded by a Pierce electrode which are bot at full potential, the 'steering electrode' which is at a positive potential with respect to the cathode, and the 'exit electrode' which is at ground potential. The cathode potential essentially determines the mean energy of the electron beam and the steering voltage the electron beam intensity. This will be discussed in more detail in section 2. Table 1 lists the main parameters of the new gun.

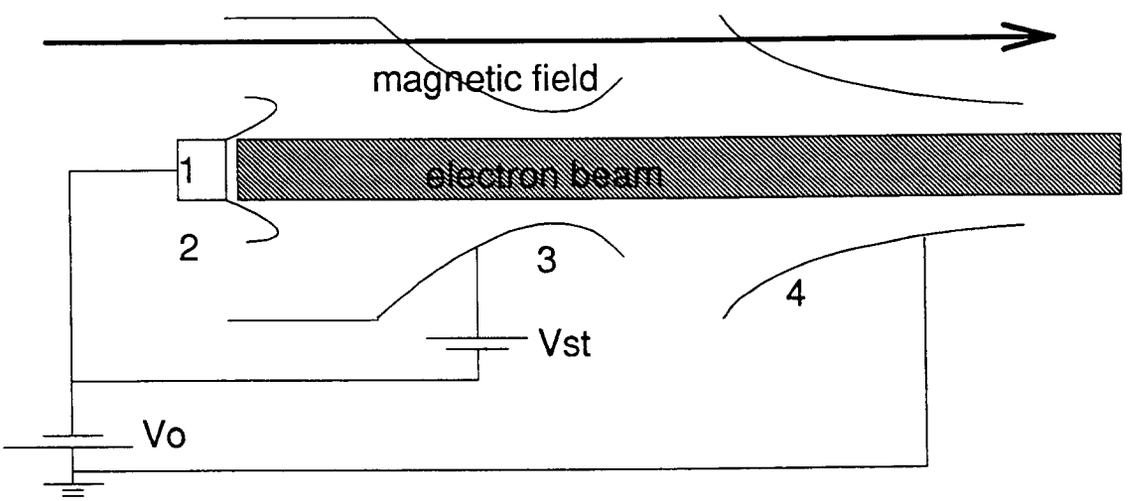

Figure 1. The electron gun. 1. cathode, 2. Pierce electrode, 3. steering electrode, 4. exit electrode

The gun was designed using the computer codes SAM [1] and EGUN [2], and by paying special attention to the shape of the steering and exit electrodes we were able to reduce the longitudinal field, in which the gun is immersed, to a relatively low value of 650 G. This is important for low energy operations at LEAR where we would be unable to compensate the coupling effect of the solenoid if the field were too strong. Computer simulations gave electron transverse energies of less than 0.4 eV, even with high intensity beams at low energy (3 Amps at 7 keV).

Table 1. Design parameters for the variable current electron gun.

Electron energy (keV)	2.3	7	20	30
Beam current (A)	0.01 to 0.53	0.07 to 2.93	0.35 to 2.83	0.65 to 2.6
Beam perveance (μP)[1]	0.125 to 5	0.125 to 5	0.125 to 1	0.125 to 0.5
Gun perveance (μP)[1]	0.58	0.58	0.58	0.58
Steering anode voltage (kV) [with respect to ground]	-1.45 to 8.1	-4.3 to 25.6	-12.5 to 11.5	-18.6 to 7.3

The gun offers a number of new facilities for the operation of the cooler :

1. the possibility to switch on and off the electron beam with the steering electrode without perturbing the circulating ion beam,
2. a very high current for electron beam energies lower than 20 keV,
3. the possibility to regulate the electron beam current during the electron cooling process.

As the electron intensity can be varied during beam cooling and with the possibility to neutralise the electron beam, a servo-system was implemented on the gun in order to maintain the mean energy of the electron beam constant. This system is described in detail in another paper presented at this workshop [3].

Because the cooler can now run with a fixed magnetic field, the compensation scheme was also modified when the gun was installed. The old tilted solenoids were replaced by a set of horizontal dipoles for the closed orbit correction and two straight solenoids powered in series with the cooler main solenoid. The whole ensemble is operated in the 'pulsed mode' as with the old system [4].

2. PARAMETER TESTS

Due to the fact that the electron intensity is determined by the steering electrode voltage, the important parameter describing the gun is the 'gun perveance' which is defined by

$$P_{gun} = I / V_{st}^{3/2},$$

where I is the beam current and V_{st} the steering electrode voltage. For a measurement of the perveance,the steering electrode voltage was fixed and V_0 varied in steps of 1 kV. For each step the beam current was measured and the gun perveance was calculated. Figure 2 shows the results for three values of V_{st}.

One sees that the gun perveance is significantly lower than the theoretical value of 0.58 μP for the regime when the steering electrode potential is positive with respect to the exit electrode i.e. with respect to ground (Fig. 3). This can be explained by the fact that when there is a positive potential difference, secondary electrons, created by collisions of the primary beam with the residual gas atoms, can be stored in this potential well and will limit the maximum beam current that the gun can deliver. This was confirmed by decreasing the cathode heating current whereby reducing the outgassing rate of the vacuum chamber around the gun which led to a slight increase of the beam current.

A value close to the design perveance could also be achieved by periodically pulsing the steering electrode voltage. If the steering voltage is forced to a negative value with respect to ground for a short period of time (<5 μs), the stored electrons are expelled from the well and the primary beam will increase in intensity. Secondary electrons will then slowly begin to fill the well and the primary beam current will decrease until the steering electrode is again pulsed. If the repetition rate for the pulser is about equal to the storage time for the secondary electrons, then the gun perveance can remain at more than 90% of the design value. The influence of this pulser on the cooling of ions has still to be tested but the effect is expected to be negligible.

The second parameter that we measured was the 'beam perveance' which is defined by

$$P_{beam} = I / V_0^{3/2},$$

[1] see section 2 'Parameter tests', for the definitions of beam and gun perveance

where V_0 is the cathode voltage. For this measurement V_0 was kept fixed and V_{st} increased until the design beam perveances shown in table 1 were obtained. Again we found that the nominal beam perveance could be reached but that the steering voltages necessary were much higher than the theoretical values (Fig. 4). The critical parameter was found to be the electron beam collector. It would seem that the collector perveance is much too low to recuperate effectively the dense electron beams that can be generated by the new gun.

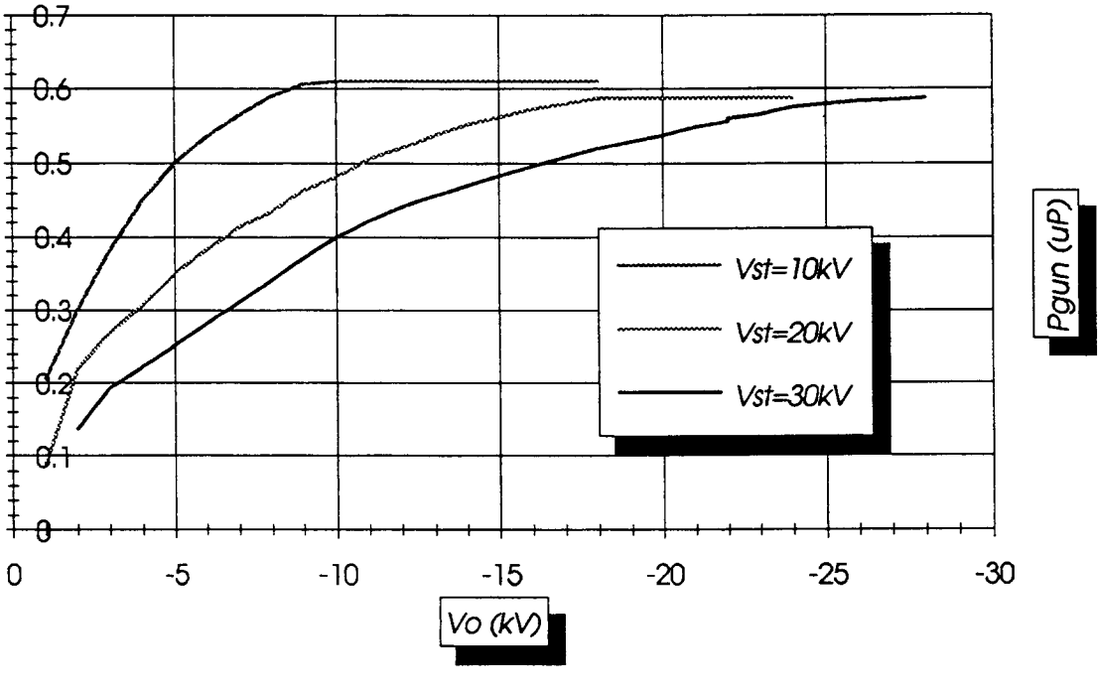

Fig 2. The variation of the gun perveance, P_{gun}, as a function of the cathode voltage V_0 for fixed values of the steering voltage V_{st}.

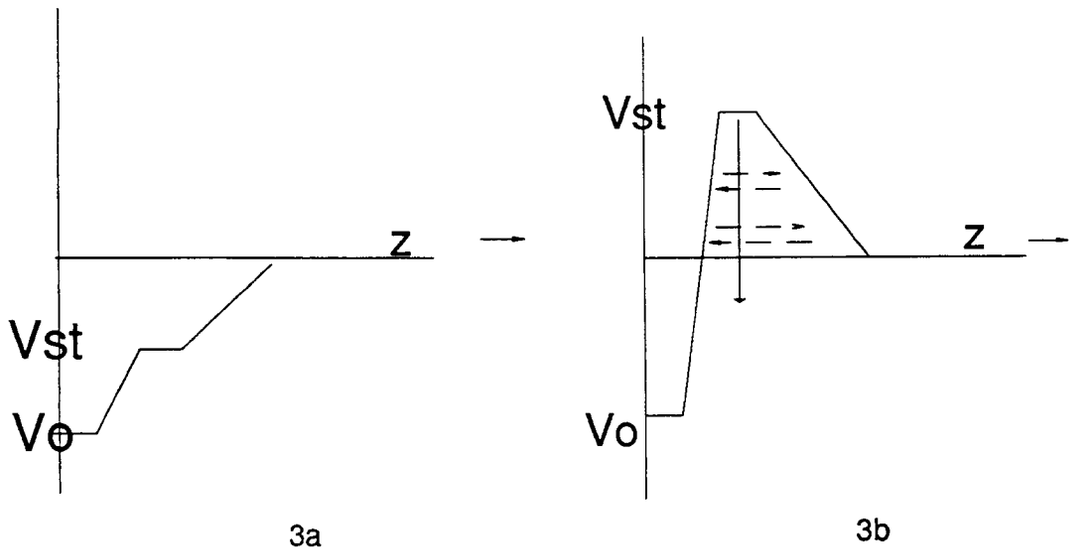

Fig. 3 The potential distribution on the beam axis. 3.a. shows the case when the electrons are smoothly accelerated to the desired energy and 3.b. shows the case when a potential well for secondary electrons is created when the steering electrode potential is positive with respect to the exit electrode. If the steering potential is made negative for a short period of time then the well no longer exists and the secondary electrons can escape.

More recently, after a fine adjustment of the collector and repeller voltages, a beam perveance of 2.8 μP was obtained at an electron energy of 10 keV. With a steering voltage of 30 kV, this corresponds to a gun perveance of 0.58 μP which is in perfect agreement with the simulations.

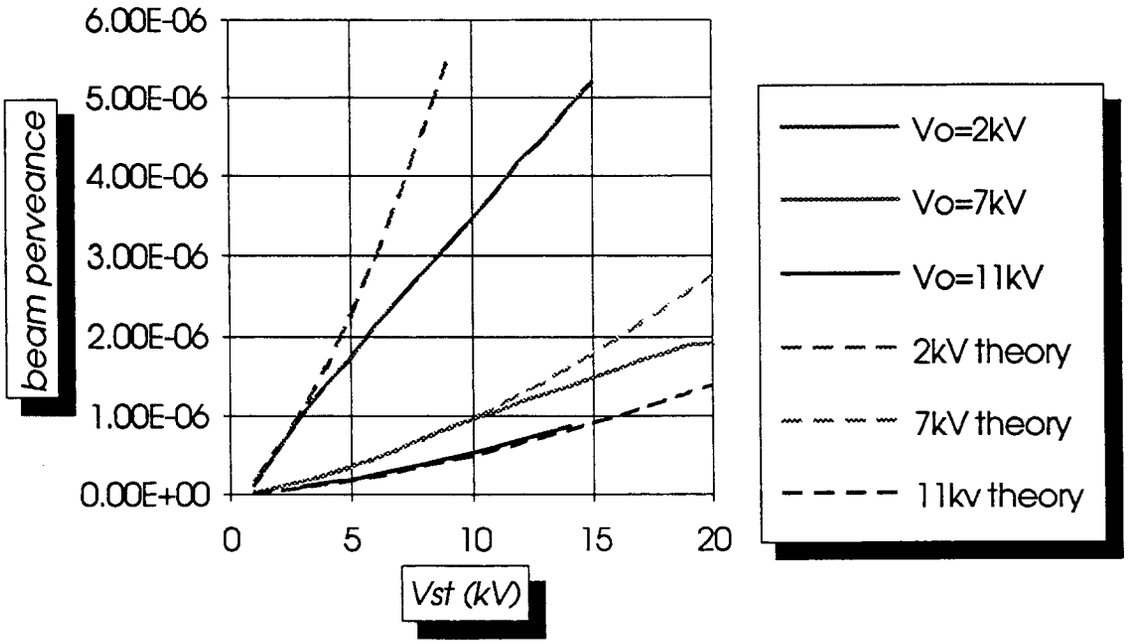

Fig 4. The dependence of the beam perveance, P_{beam}, on the steering voltage V_{st} for fixed values of the cathode voltage V_0

3. Cooling tests with 50 MeV protons

Once the parameter tests had been concluded, electron cooling tests were made at the proton injection energy of 50 MeV. A number of measurements were made in order to determine the real possibilities of electron cooling with the new gun. They comprised emittance and cooling time measurements in the transverse and longitudinal planes as a function of electron beam intensity, as well as tests on the servo-system and experiments on beam neutralisation.

3.1 Emittance measurements

During electron cooling of protons the neutral hydrogen beam, formed by the recombination with the cooling electrons, can be observed with multiwire proportional chambers or solid state detectors. This allows the shrinkage of the proton beam to be observed during cooling and one can also directly measure the equilibrium beam size. Figure 5 shows the vertical and horizontal H^0 profiles measured by a CCD camera placed at the end of the cooling section in LEAR. The video signal is displayed on a digital oscilloscope and from there it can be acquired and analysed by a program running on the LEAR μVAX cluster. The measured equilibrium emittances (2σ) were found to be $\varepsilon_v = 6.3\ \pi$ mm mrad and $\varepsilon_h = 4.3\ \pi$ mm mrad.

3.2 Cooling time measurements

The transverse and longitudinal cooling times were measured by observing the evolution of the spectral density of the beam Schottky noise around frequencies corresponding to a harmonic of the revolution frequency or a transverse sideband. This method has been used in previous cooling experiments [5] and was found to be very accurate as long as there are no beam instabilities. The measurements were made at injection, where the emittances are the largest, and the cooling time to equilibrium was estimated from the Schottky scans. Taking advantage of the fact that the electron beam intensity could be varied online, we also measured the dependency of the cooling time on this parameter. Figure 6 shows the results obtained for three settings of the electron beam current and for two different proton beam intensities. The initial values of the

transverse emittances were estimated to be about 45 π mm mrad in each plane, and the momentum spread was measured to be $4x10^{-3}$.

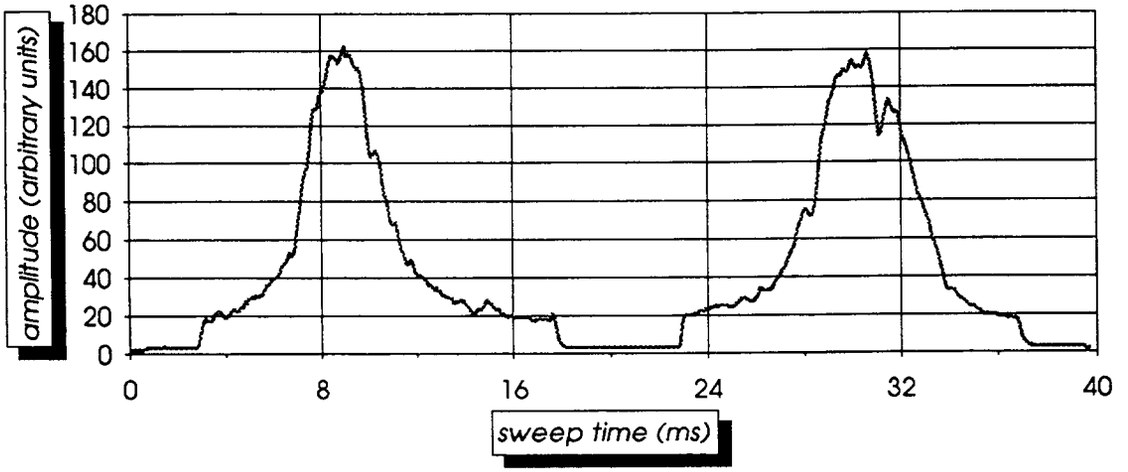

Fig 5. Vertical (left) and horizontal (right) H^0 profiles. One video signal scan takes 40 ms which is equivalent to a width of 14.3 cm. By converting the FWHM from ms to cm one obtains the equilibrium emittances.

From the results it would appear that for the transverse cooling time measurements the 1/I dependency does not satisfactorily fit the mesaured values. In the longitudinal plane however the theoretical curve agrees very well with the measurements. Moreover there seems to be a relationship between the cooling time and the number of stored protons. The difference could be due to the fact that we measured the total cooling times and not the e-fold cooling time, which is normally used. The method used for the measurement also has to be refined as the longitudinal cooling greatly influences the transverse Schottky signals. More measurements will need to be performed in order to confirm the observations already made.

3.3 Evaluation of the space charge contribution

Due to the space charge of an intense electron beam, in order for electron cooling to proceed at the correct energy the cathode must be placed at a slightly higher value than the mean kinetic energy of the electrons. The exact contribution of the beam space charge can be evaluated by varying the electron beam intensity and measuring the change in momentum of a circulating proton beam on a spectrum analyser. This momentum change is directly proportional to the mean kinetic energy of the electrons.

Figure 7 shows the variation of the space charge contribution to the electron beam energy as a function of beam intensity. The measured curve differs somewhat from the theoretical relation of $U_{sp} = 91.83I/\beta$. At high currents the contribution begins to saturate and for lower currents the behaviour follows the linear relation $U_{sp\ meas} = 78.85I/\beta$.

4. Conclusions

The variable intensity electron gun has proved to be an invaluable tool in the operation of the LEAR electron cooling device. The possibility to regulate the beam current not only opens new possibilities for cooling at ultra low energies, but has also enabled us to make a series of interesting measurements on the cooling times of protons and to investigate the influence of the electron beam space charge. The stability of stored beams should also be less of a problem as we are able to reduce the electron beam current, hence the cooling strength.

It has not yet reached the full design specifications (especially for low energy electron beams) but recent results make it clear that through careful adjustment of the cooler parameters we will soon reach the design specifications.

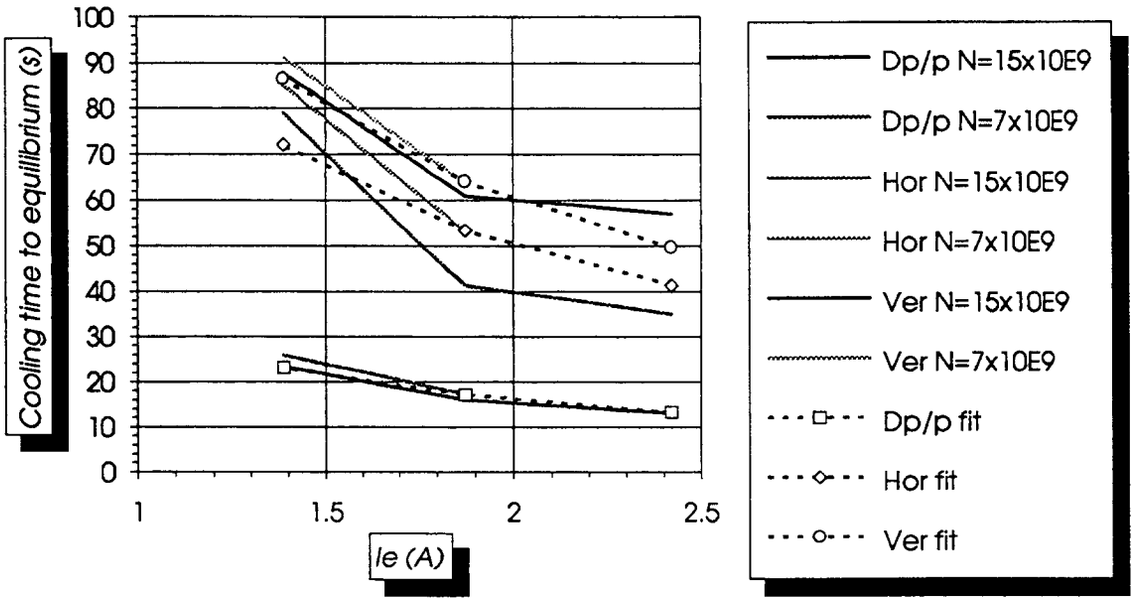

Fig 6. Cooling times to equilibrium for a proton beam at 50 MeV as a function of electron beam intensity.

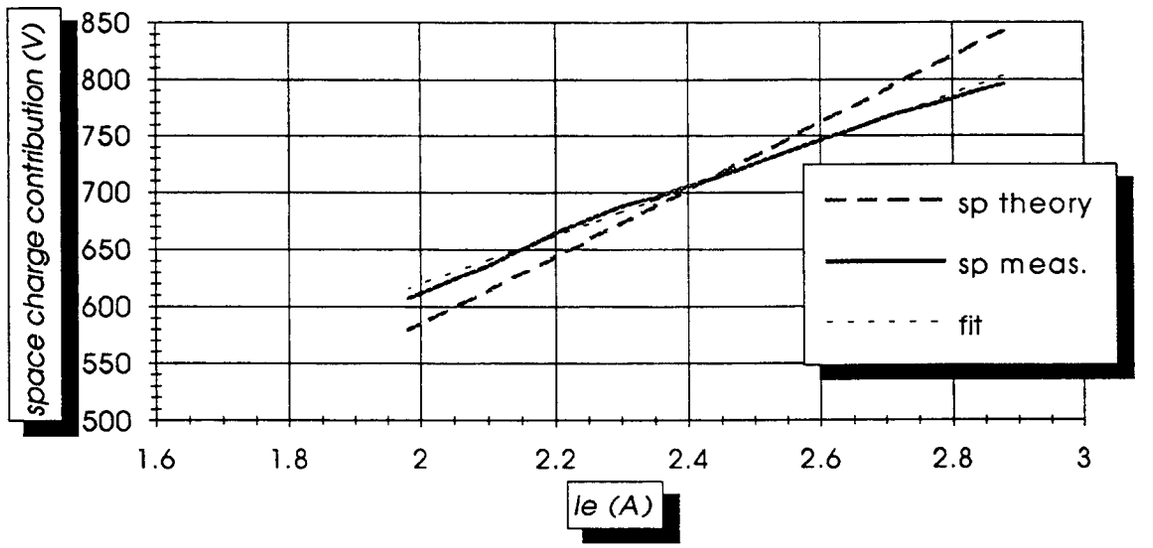

Fig 7. The space charge contribution as a function of electron beam intensity at 26.9 keV.

4. References

[1] M. Tiunov, B. Formel and V. Yakolev, "SAM Program for the calculation of electron guns on personal computers", Preprint INP 89-159 (1989).

[2] W. B. Herrmannsfeldt, "EGUN Electron trajectory program", SLAC report 226, NC 28 (1979).

[3] J. Bosser, F. Caspers, M. Chanel, R. Ley, R. Maccaferri, S. Maury, I. Meshkov, D. Möhl, G. Molinari, U. Ramos-Sanchez, E. Syresin, G. Tranquille and F. Varenne, "Neutralisation and a servo-system on the LEAR electron cooler", this workshop.

[4] J. Bosser, M. Chanel, R. Ley and G. Tranquille, "Variable energy electron cooling at LEAR", Proceedings of the 3rd European Particle Accelerator Conference EPAC92, Berlin (1992).

[5] J. Bosser, M. Chanel, R. Ley, D. Möhl, U. Oeftiger and G. Tranquille, "Electron beam cooling and beam instability studies at LEAR", Proceedings of the International Workshop on Physical Experiments and First Results on Heavy ion Storage and Cooler Rings, Smolenice (1992).

NEUTRALISATION AND SERVO-SYSTEM ON THE LEAR ELECTRON COOLER

J. Bosser, F. Caspers, M. Chanel, R. Ley, R. Maccaferri, S. Maury, D. Möhl, G. Molinari, U. Ramos Sanchez, G. Tranquille, F. Varenne
CERN, PS Division, CH - 1211 Geneva 23

I. Meshkov and E. Syresin
Centre of Applied Physics and Technology, INP, Lipetsk, Russia

ABSTRACT

The large space-charge forces introduced by a high-density electron beam induces an azimuthal drift velocity detrimental to the cooling process. To reduce this effect an electron-beam neutralisation system has been implemented. Being so, the change in the neutralisation ratio and/or of the electron beam intensity will result in a change of the cooled ion-beam energy. A servo-system has therefore been developed, which aims to maintain the ion beam at its nominal energy. The principles and the preliminary results obtained with the neutralisation and servo-system are presented.

1. INTRODUCTION

A new electron gun for the LEAR electron cooler has been designed, constructed, installed and tested at LEAR [1]. It aims to provide very intense electron beams at low energy. For example, an electron-beam intensity of 3 A was measured at a kinetic energy of 10 keV (and 0.5 A at 2.5 keV). As the cooling time is inversely proportional to the electron beam intensity this should improve the cooler performances for cooling and accumulation of ions, like the antiprotons for the present LEAR programme and the Pb^{53+} ionsat 4.2 MeV/u as required for LHC.

Such intense electron beams will induce large space-charge fields which introduce a transverse electron drift velocity detrimental to the cooling process itself.

One way to reduce the space-charge effect is to provide a neutralisation of the electron beam. This has been implemented by introducing a set of neutralisation electrodes on either side of the drift space (Fig. 1a). The electrons and the ions to be cooled are moving together in the drift tube.

Once the neutralisation is active and/or the electron-current intensity is varied, the changes in the space-charge potential will introduce a variation of the average electron velocity and, consequently, of the energy at which the ions are cooled. A "servo-system" has been installed to overcome this drawback. It aims to maintain the electron velocity and, consequently, the cooled ion beam at its nominal energy regardless of the electron-beam intensity or the neutralisation factor.

After a brief reminder of the fundamental equations, we shall present in this paper the preliminary results obtained with the neutralisation and the servo-system.

2. SOME PHYSICAL PROPERTIES OF THE ELECTRON BEAM

The electron-beam set-up is shown in Fig. 1a. In this chapter, we will neglect the influence of the steering electrodes. The electron beam of radius a passes through a steering electrode and a drift tube of radius b (Fig. 1b) to enter finally into the collector. The ion beam overlaps with the electron beam in the drift tube where cooling is effective. The overall system is surrounded by the solenoid with a longitudinal magnetic field $\vec{B} = B_0\vec{u}_s$ (see Fig. 1c for symbols).

The electron-beam intensity I is determined by the steering-electrode voltage U_s with:

$$I = p_g U_s^{3/2} \quad \text{and} \quad p_g = 5\times10^{-7}\ A\,V^{-3/2} \text{ the gun perveance}$$

The electron-beam average velocity $v = \beta c$ is determined by the following equation:

$$E_c = (\gamma - 1)mc^2 = e(U_0 + U_{sp}) \tag{1}$$

where

e, m are the electron charge and mass, respectively,
Ec is the kinetic energy,
U_{sp} is the electron-beam space-charge potential,
γ = $(1-\beta^2)^{-1/2}$, $\beta = v/c$.

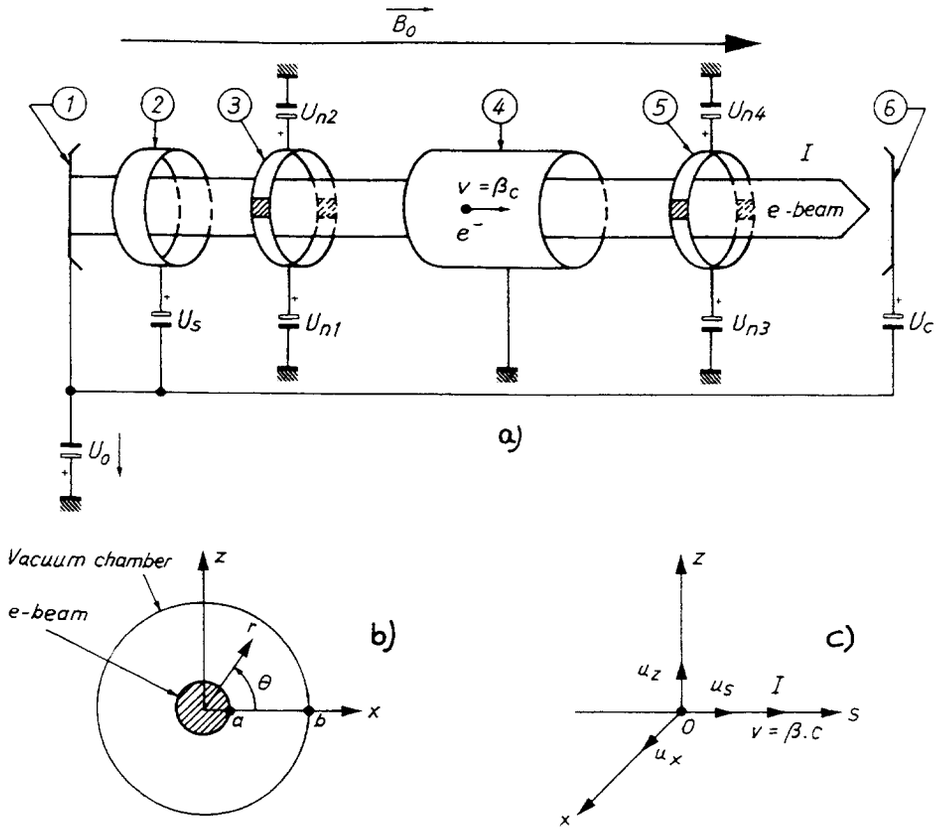

Fig. 1 - a) Principle of the electron-cooler set-up. 1: Cathode, 2: Steering electrode, 3: Cathode neutralisation electrode Elg, 4: Drift tube or drift space at ground potential, 5: Collector neutralisation electrode Elc, 6: Collector.
b) Drift-space cross section. The electron beam of radius a is at the centre.
c) Frame of reference. The electron beam is moving along the (O,s) axis.

2.1 Space-Charge Potential U_{sp}

The voltage seen by an electron at radius r, with respect to the drift tube which is at ground potential (Fig. 1b), is expressed by:

$$U_{sp} = \frac{en\left(r^2 - a^2\right)}{4\varepsilon_0} - \frac{ena^2}{2\varepsilon_0}\ln\left(\frac{b}{a}\right) \quad \text{for } r \le a$$

$$U_{sp} = -\frac{ena^2}{2\varepsilon_0}\ln\left(\frac{b}{r}\right) \quad \text{for } a \le r \le b$$

with
ε_0 = $8.854 \times 10^{-12}\ Fm^{-1}$, the permittivity of free space,
n = $(n_e - n_+)$, the density in particles/m^3,
n_e = the electron density,

$$n_e = \frac{I}{\pi a^2 \beta c e} \tag{2}$$

n_+ = the stored low-energy ion density within the electron beam when neutralisation is present.

We can define a neutralisation factor $\eta = n_+/n_e$, such that we obtain on the axis ($r = 0$):

$$U_{sp}(r=0) = -\frac{ena^2}{4\varepsilon_0}\left[1+2\ln\left(\frac{b}{a}\right)\right] = -\frac{en_e(1-\eta)a^2}{4\varepsilon_0}\left[1+2\ln\left(\frac{b}{a}\right)\right]$$

$$\cong -\frac{91.71I}{\beta}(1-\eta) \quad \text{in practical units.}$$

U_{sp} in volts, I in amperes, a = 25 mm, b = 70 mm.

We can re-write Eq. (1) as follows:

$$\left[\frac{1}{\sqrt{1-\beta^2}}-1\right]mc^2 = e\left[U_0 - \frac{91.71I}{\beta}(1-\eta)\right] \tag{3}$$

which shows that β, and consequently the cooled ion energy, will vary with I or the neutralisation factor η. Thus according to Eq. (2), for a fixed intensity I, the electron density will increase when β is decreased.

2.2 Drift Velocity

It has been shown [1] that, due to space-charge forces, an electron at radius r will acquire an azimuthal drift velocity v_d:

$$v_d = \frac{re^2 n_e(1-\eta)}{2\gamma^3 m\varepsilon_0\omega_h}; \quad \omega_h = \frac{eB_0}{\gamma m}$$

which is detrimental to the cooling efficiency. The only practical way to reduce v_d is to bring η close to unity, i.e. to neutralise the electron beam.

3. NEUTRALISATION

A way to neutralise the electron beam has been reported in Refs. [2, 3] which consists of using a set of neutralisation electrodes at each end of the drift space (Fig. 1a). The electrodes Elg are located on the gun side while Elc are on the collector side.

Each neutralisation electrode consists of two metallic half-cylinders, separated by a "conductive" glass insulator (dashed lines on parts (3) and (5) of Fig. 1a). A positive voltage up to 6 kV is applied to all the metallic cylinders.

The expression "conductive" insulator means that a high resistance is provided between the two metallic electrodes at high potential, but that a small conductivity is sufficient for discharging any electrons falling on the glass insulators.

The electron beam ionises the residual gas molecules during its passage from the cathode to the collector. The positive low-energy ions, from the molecules that have been ionised between the neutralisation electrodes, will be trapped while the "ionisation" electrons will be collected on the electrodes themselves or on the "conductive" insulator.

Computations [3] have shown that neutralisation voltages U_{ni} lower than 6 kV should be sufficient to reach full neutralisation ($\eta = 1$).

3.1 Measurements of the Neutralisation Coefficient

There are several ways to measure η depending on whether one operates with or without the cooled ion beam.

3.1.1 Measurements without cooled ion beams. Time of flight method

The accelerating voltage U_0 and the electron-beam intensity I (at U_s) are now assumed to be constant.

At a nominal dc potential U_{n1}, U_{n2}, the gun neutralisation electrodes Elg are powered to provide either longitudinal or transversal electrical field at high frequency and small amplitude superimposed on the nominal dc field (Fig. 2):

$$V_1 = V_{10}\cos(\omega t)$$

As a consequence the electron-beam density (longitudinal case) or beam position (transverse case) will be slightly modulated.

The "collector" neutralisation electrodes Elc at an effective distance L from Elg and also at their nominal dc voltages U_{n3}, U_{n4} will detect a signal:

$$V_2 = V_{20}\cos\omega\left(t - \frac{L}{v}\right); \quad v = \beta c.$$

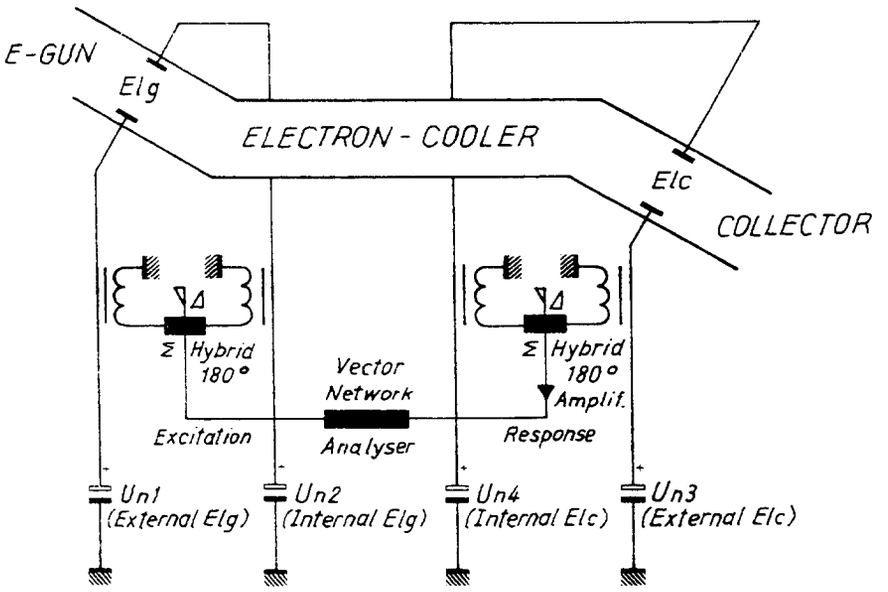

Fig. 2 - Principle of the flight method time

This method may be considered as a beam transfer function (BTF) measurement on the electron beam. Excitation frequencies between 1 MHz and 3 GHz were tested, but most measurements have been carried out between 200 MHz and 600 MHz using a vector network analyzer with a preamplifier in the receiver path. The equivalent time stability of the method is about 1 ps for an integration time of 0.1 s.

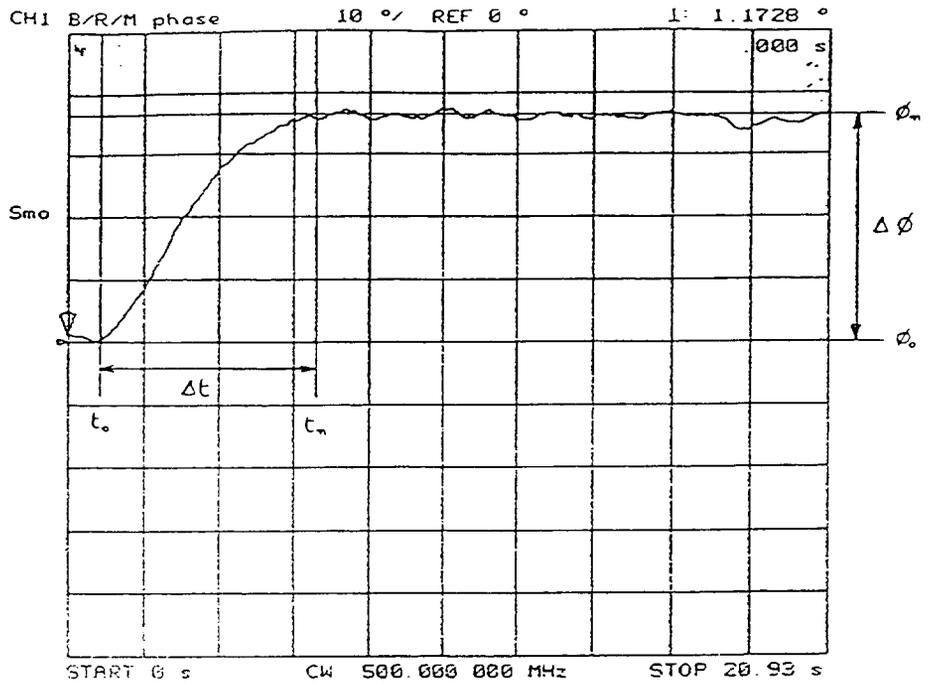

Fig. 3 - Neutralisation. Time of flight relative phase measurement. $\phi = \omega L/v$.
Vert. scale: 10°/div., Horiz. scale: 2.093 s/div., Δt: neutralisation time, ϕ_0: Phase reference, $\Delta\phi$: Phase deviation, $U_{n1} = U_{n2} = 5\,000$ V, $U_{n3} = U_{n4} = 0$ V, $I_e = 2.3$ A,
Proton nominal pc = 310.1 MeV, $U_0 = 27.852$ kV, $U_s = -668$ V, $f_{r0} = 1.197732$ MHz.

The time correlation between the two signals

$$\langle V_1 V_2 \rangle = V_{30} \cos\left(-\frac{\omega L}{v}\right) = V_{30} \cos\phi$$

has a phase ϕ which depends on $v = \beta c$, and therefore on η according to Eq. (3). This implies that L has been previously determined, e.g. by measuring the phase ϕ at different frequencies while the electrons are kept at a constant velocity.

An example of phase measurement is given in Fig. 3 and corresponds to a neutralisation factor $\eta \cong 0.5$. The time taken by the phase to reach its final value is the neutralisation time Δt (~6 s in Fig. 3).

3.1.2 Measurements with a cooled ion beam

During the electron-cooling process the cooled ions will assume the same mean velocity as the electrons. Therefore, when the neutralisation is activated and has reached its final state (by setting the appropriate fixed voltages on $U_{n1,2,3,4}$) the space-charge factor, η, will increase according to Eq. (3); the ion-beam velocity and hence its revolution frequency f_r will also increase.

The revolution frequency will be measured from a longitudinal Schottky pick-up signal displayed on a spectrum analyzer. The values of η will be determined by using the classical relation between $\Delta\beta$ and Δf_r, and the relation between $\Delta\beta$ and η. Comparing the values so measured with those obtained in Section 3.1.1 shows that the measurements are reliable (within the errors in the measurement of U_0 and I).

Once the electron beam is neutralised (even partially) another possibility is to change U_0 so as to bring the cooled ion beam to its nominal energy or revolution frequency. The change $\Delta U_0 = \Delta U_{sp}$ is directly related to the neutralisation factor η. This again gave reliable results.

3.2 Further Studies

Measurements with the neutralisation are preliminary and investigations are still underway. The reasons for not reaching the full neutralisation ($\eta = 1$) have to be studied. This may need a better understanding of the plasma behaviour through more elaborate electron-beam response measurements with the above-mentioned rf excitation and a more detailed study of the influence of the magnetic field. It is expected that for high-intensity electron beams the process of ion trapping may become unstable [3]. This must be investigated. Finally we have to check for the improvement in the transverse cooling time which is in fact the goal of neutralisation.

4. THE SERVO-SYSTEM

For a fixed value of U_0 and of I, when the neutralisation is active and the factor η is increased (see §3), β and hence the momentum of the cooled ions $cp = \gamma\beta(m_i c^2)$ and the average revolution frequency will also increase. A similar effect will occur when I is varied by modifying the steering electrode voltage U_s. It is therefore desirable to implement a system capable to maintain the cooled ions at their nominal energy (or nominal β_0 and f_{r0}) for any changes in η or I. This is the goal of the servo-system.

4.1 Principle

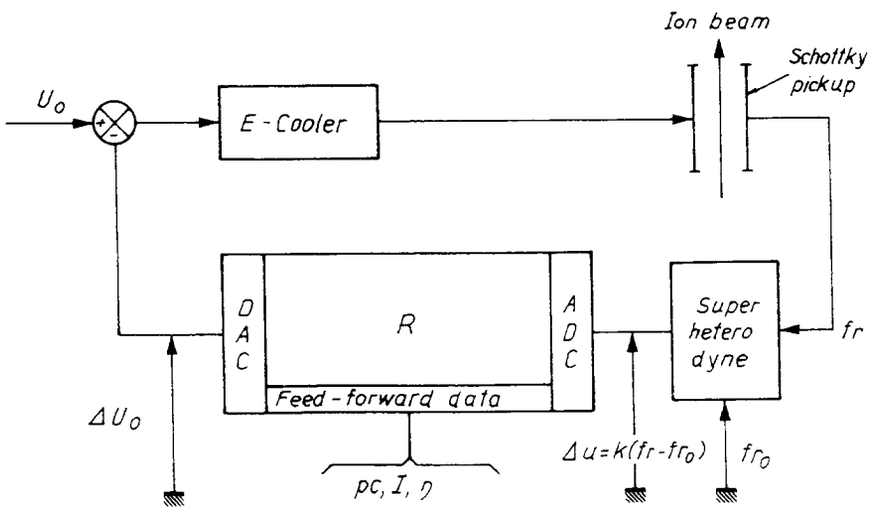

Fig. 4 - Principle of the servo-system

The principle is illustrated in Fig. 4. The actual mean revolution frequency f_r is taken from the output of a longitudinal Schottky pick-up. It is applied to a super-heterodyne receiver which is tuned to the nominal revolution frequency f_{r0}. This super-heterodyne is a commercial synthesizer-based radio receiver (25 MHz - 1 GHz) with a modified wideband (0 to ±75 kHz) FM demodulator and remote frequency setting via RS 232. The error signal at the heterodyne output $\Delta u = k(f_r - f_{r0}) = k\Delta f_r$ volts is applied to a digital system which performs the following operation (also named Proportional Integral Differential filtering, or simply P.I.D.):

$$R = \left[k_p + k_d \frac{d}{dt} + k_i \int dt \right]$$

such that the nominal gun voltage V_0 will be corrected by $\Delta U_0 = R\Delta u$.

The coefficients k_p (proportional), k_d (derivative), k_i (integral) are digitally controlled and adjusted such that after correction of U_0 by ΔU_0 the cooled ions retrieve their nominal revolution frequency (or equivalently their nominal energy).

The system has to operate for different settings of the electron cooler and at different ion energies. Therefore, to improve the servo-system response some parameters such as pc, I and η are loaded in digital form into the digital feedback loop. A microprocessor using Eq. (3) can anticipate the changes in β (or f_r) corresponding to these parameters. The microprocessor is also used to fulfill the digital filtering defined by R.

4.2 Response of the Electron Cooler Itself

The major limiting component of the servo-loop is the cooler itself since the longitudinal cooling time (or time response) on LEAR is of the order of 2 s. This implies a cut-off frequency of the order of 0.5 Hz which is much smaller than the cut-off frequency of the other components like the super-heterodyne receiver, the digital sampling period, or the U_0 power supply response time.

The open-loop response $O_l = \Delta U_0/\Delta U$ has been measured. It shows that the cooler alone behaves like a 2nd-order system which can be approximated by the following transfer function at momentum p = 310.1 MeV/c:

$$O_l(s) = \frac{G_0}{\left[1 + (s/2\pi f_1)\right]\left[1 + (s/2\pi f_2)\right]}$$

with

s the Laplace parameter,
G_0 a constant for a fixed ion energy,
f_1 = 0.32 Hz,
f_2 = 0.61 Hz.

4.3 Closed-Loop Response

The closed-loop response has been measured for k_p = 2 500 s, k_i = 35 s-1 and k_d = 8 000 s. The results are plotted in Figs. 5a and 5b together with the simulated response computed using $O_l(s)$.

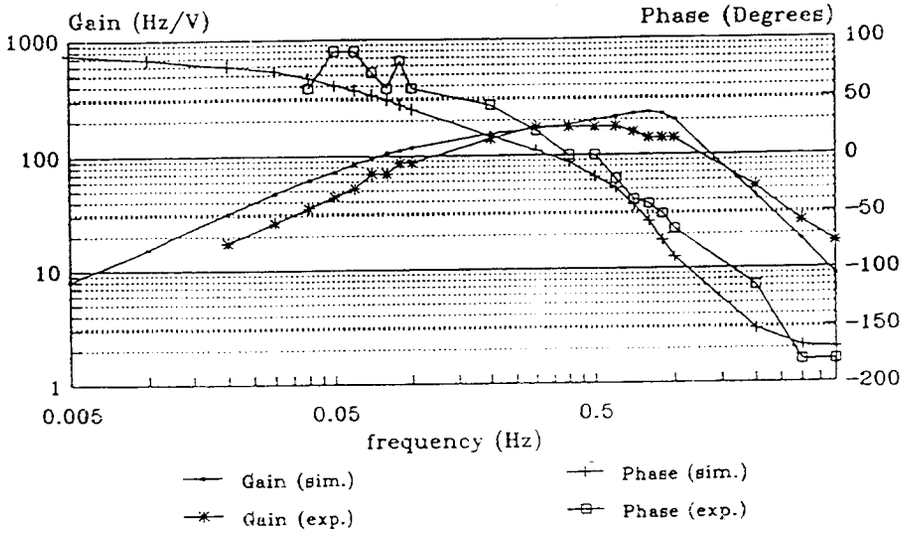

Fig. 5a - Simulated (sim.) servo-system and experimental (exp.) closed-loop transfer function. I_e = 2.3 A, Proton nominal pc = 310.1 MeV.

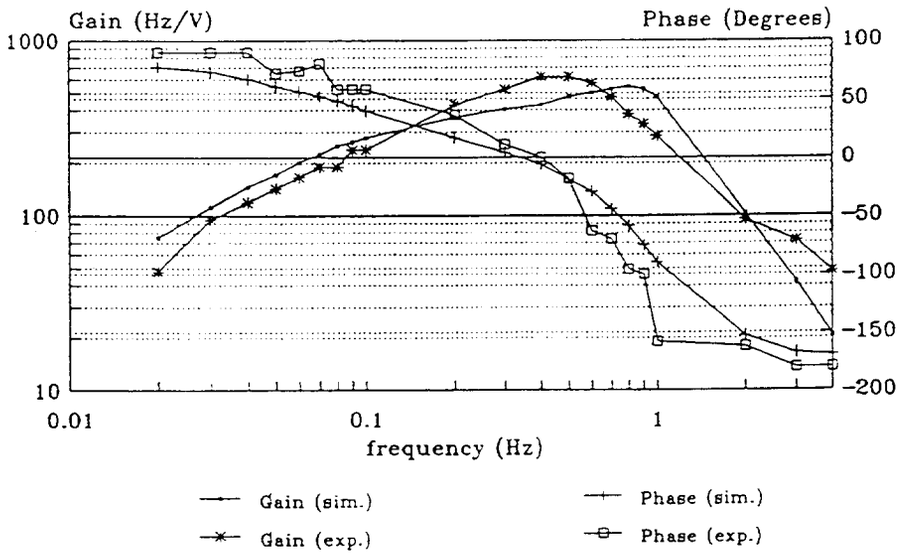

Fig. 5b - Simulated (sim.) servo-system and experimental (exp.) closed-loop transfer function. I_e = 0.64 A, Proton nominal pc = 200 MeV, U_0 = 11.9 kV, U_s = -280 V.

The response to a small voltage step on U_0 is more illustrative. The time response is shown in Fig. 6. It shows, for example (Fig. 6b), that for pc = 200 MeV to a voltage step of 21.0 V, which corresponds to a frequency shift of 728 Hz (nominal frequency f_{r0} = 0.795 MHz and so $\Delta p/p \cong 0.9 \times 10^{-3}$), the maximum excursion in frequency is 62.74 Hz and the system recovers in about 2 s. As a consequence, when ramping I (or U_s) and/or η (or U_{ni}) in 2 s or more, no change should be observed in the cooled ion-beam momentum. This has been experimentally verified.

Till now no measurements of the feedback system effects on cooling have been made.

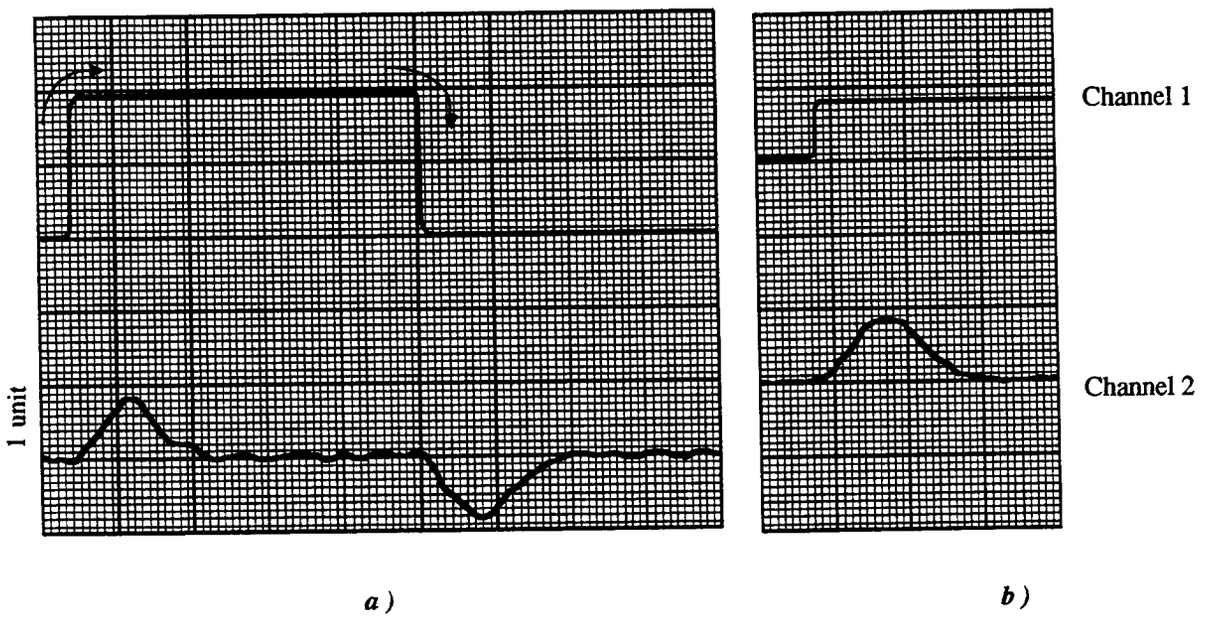

Fig. 6 - Servo-system: response to a step perturbation Δf_r versus ΔU_0.
a) Proton pc = 310.1 MeV, Horizontal scale: 1 s/unit, f_{r0} = 1.1926 MHz.,
Channel 1 - Vertical: 26.3 V/unit and so ΔU_0(max) = 52.5 V,
Channel 2 - Vertical: 235.3 Hz/unit and so Δf_r(max) = 206.0 Hz.
b) Proton pc = 200 MeV, Horizontal scale: 1 s/unit, f_{r0} = 0.795 MHz.
Channel 1 - Vertical: 26.3 V/unit and so ΔU_0(max) = 21.0 V,
Channel 2 - Vertical: 156.8 Hz/unit and so Δf_r(max) = 206.0 Hz.

5. CONCLUSIONS

The high-density electron beams foreseen to be used for the low-energy ion cooling introduce large electron transverse drift velocities which can be detrimental to the cooler performance.

A possibility to reduce this effect is to neutralise the electron beam. The neutralisation is performed by two sets of neutralisation electrodes. The electrodes, positively polarised, will trap the positive ions generated by the ionisation of the residual gas molecules by the electron beam. A neutralisation factor of about 0.5 has been reached. Studies are underway which aim at a better understanding of the neutralisation process.

The electron-beam space-charge potential is modified when introducing the neutralisation process or when the intensity is varied. As a consequence, the cooled ion energy will be modified. A servo-system has been implemented to maintain the cooled ions at their nominal energy, which is based on digital techniques, and its response time is limited by the cooler process itself. The response time is of the order of 2 s. The system has been successfully tested and will be soon used on LEAR to be operational at the ion energie levels (pc < 310 MeV/u).

REFERENCES

[1] J. Bosser, I. Meshkov, V. Poljakov, I. Seleznev, A. Smirnov, E. Syresin, G. Tranquille, and A Zapunjako, *Project for a variable current electron gun for the LEAR electron cooler*, CERN PS/92-03 (AR), 1992.
J. Bosser, R. Lapik, R. Ley, I. Meshkov, V. Poljakov, I. Seleznev, A. Smirnov, E. Syresin, G. Tranquille, and A Zapunjako, *The first results of electron cooling at LEAR with the variable current electron gun*, This Workshop.

[2] A. Burov, V.I. Kudelainen, V. Lebedev, V.V. Parkhomchuk, A.A. Sery, and V.D. Shiltev, Experimental investigation of an electron in compensated state, CERN PS/93-03 (AR), 1993 (Translation from Russian).

[3] J. Bosser, I. Meshkov, D. Möhl, E. Syresin, and G. Tranquille, *Neutralisation of the LEAR-Ecool electron-beam space charge*, PS/AR/Note 93-08, 1993.

[4] U. Ramos Sanchez, *A digital energy control system for the LEAR Electron Cooler*, PS/AR/Note 93-18 (AR), 1993.

MEASUREMENTS OF ELECTRON COOLING AND "ELECTRON HEATING" AT CELSIUS

D. Reistad, L. Hermansson, T. Bergmark, O. Johansson, A. Simonsson
The Svedberg Laboratory, Box 533, 751 21 Uppsala, Sweden

A.V. Burov
Budker Institute of Nuclear Physics, 630090 Novosibirsk, Russia

ABSTRACT
The drag rates of the CELSIUS electron cooler are similar to those of other electron coolers. On the other hand, when the stored beam is exposed to the electron beam at the injection energy at CELSIUS, a large fraction of the stored beam is rapidly lost. This is true whether the electron beam energy is tuned for cooling or whether the energy is shifted from the value, which is appropriate for cooling. One possible explanation for this phenomenon is non-linear effects due to the finite diameter of the electron beam, which is smaller than the maximum beam size.

1. INTRODUCTION

CELSIUS [1] is supplied with ions from the Gustaf Werner Cyclotron with stripping injection or multi-turn injection without stripping. These injection methods [2] make use of a vanishing orbit bump, in order to utilize the whole available horizontal acceptance of the ring. The injection energy while stripping injecting protons (starting with H_2^+ molecular ions) is 48 MeV.

An electron cooling system [3] is used to improve the momentum spread and size of beams, which travel with velocities within the velocity range of the electrons (up to 550 MeV/u). The electron cooling system will also be used to accumulate ions, which are only available with small intensity from the cyclotron.

The nominal acceptance of CELSIUS is 120 π mrad×mm in both planes, and the β-values in the electron cooler are 10 m horizontally and 7 m vertically. Thus, the nominal acceptance corresponds to a beam size of 70 mm in the horizontal plane and 58 mm in the vertical plane. The diameter of the electron beam is only 20 mm. At the design stage, it was not thought that beam-beam effects between the electron beam and the stored ion beam would be significant, because the beam-beam tune shifts are typically not more than 5×10^{-3}.

2. DRAG RATE MEASUREMENTS

The longitudinal drag rate has been measured with coasting beams of protons, deuterons, and oxygen ions with several energies. The measurement technique has been to step the output voltage from the electron cooler high voltage power supply, and to observe with a spectrum analyzer how the revolution frequency of the ions changes as a function of time after the step. Fig. 1 shows comparisons between the drag rate measured at CELSIUS with drag rates measured at other laboratories [4,5]. These measurements show, that the influence of the cooling electrons on the *cooled* ions in CELSIUS is similar to that in other electron cooling systems.

3. "ELECTRON HEATING"

When turning on the electron beam in the presence of a 48 MeV stored and bunched proton beam for the first time in 1988, the accelerator staff at Uppsala were disturbed to find that the stored beam lifetime became much shorter than before it was exposed to the electron beam. This phenomenon, which we have nick-named "electron heating," has been the subject of study for some time, however without obtaining a complete understanding.

Similar effects (although less pronounced than at CELSIUS and probably with different explanations) have been observed at NAP-M [6], Fermilab [7], Indiana [8], and TARN II [5,9]. On the other hand, they seem to be completely absent at LEAR [10], ESR and TSR [11], ASTRID [12], and CRYRING [13].

In order to separate the effects of electron heating and electron cooling, the electron heating phenomenon has often been studied with the electron beam energy offset from the value, which is appropriate for cooling (26 keV for cooling of 48 MeV protons) by one or several keV. Figure 2 shows three examples of measured intensity vs. time for a bunched proton beam with an injected intensity of about 25 mA. The three cases are: without electrons, with an electron beam of 50 mA, with energy that is tuned for cooling, and with an electron beam of the same current, which has an energy which is 1 keV too high for electron cooling to take place.

The initial lifetime of a bunched 48 MeV proton beam typically changes from 50-100 s without electrons to 0.5-1 s when it is exposed to 100 mA of electrons, and a 280 MeV bunched proton beam changed its lifetime from about 7000 s without electrons to 50 s when exposed to 500 mA of electrons.

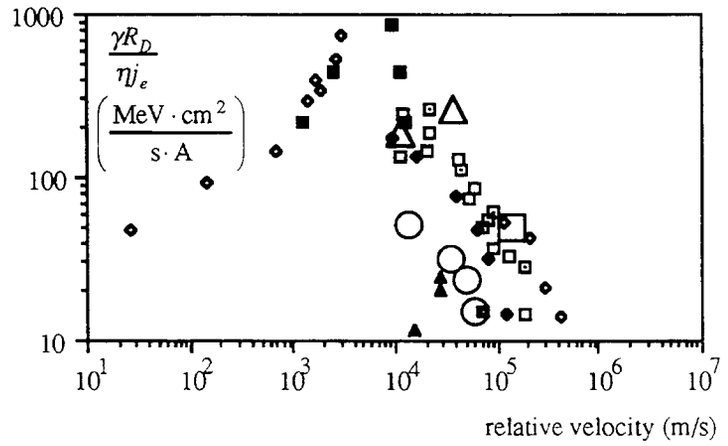

Fig. 1. Comparison between measured drag rates at LEAR (49 MeV protons, ⧈), NAP-M (65 MeV protons, ◆), FNAL (203 MeV protons, ■), IUCF (45 MeV protons, ●), Novosibirsk (850 keV protons, ■), INS (20 MeV protons, ⧈), ICE (47 MeV protons, ▲), CELSIUS (783 MeV deuterons, ◯, 296 MeV ^{16}O-ions, □, and 180 MeV protons, △).

Other observations are, that the electron heating is much worse for a bunched beam (with rf.) than for a coasting beam, and that it does not make any difference if the electron energy is detuned one or several keV or if it is increased or decreased.

The initial (just after injection) proton beam lifetime is roughly inversely proportional to the electron beam current.

A change of vacuum in the electron cooling region of nearly two orders of magnitude (from 10^{-6} Pa to a few times 10^{-8} Pa) had almost no effect on the stored beam lifetime in presence of detuned electrons.

Turning on and off the clearing electrodes, which are intended to remove low energy electrons and ions, which are trapped in the electron beam, had no effect on the stored beam lifetime in presence of detuned electrons.

When making the electron beam losses much higher than normal, by increasing the collector anode voltage or decreasing the collector voltage, then the stored beam lifetime became even shorter. For example, changing the losses of a 250 mA electron beam from 32 μA to 240 μA by increasing the collector anode voltage from 400 V to 1 kV, changed the initial 48 MeV proton beam lifetime from 0.6 s to 0.4 s.

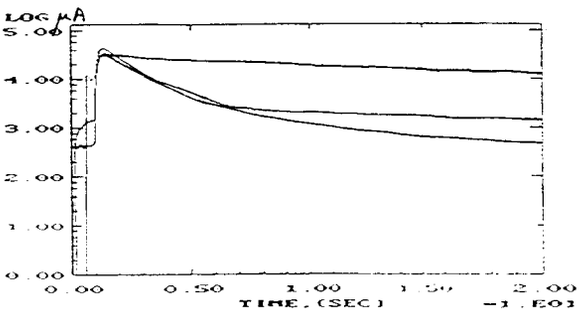

Fig. 2. Measured intensity vs. time for a bunched proton beam with an injected intensity of about 25 mA. The three cases are: without electrons (upper curve), with an electron beam of 50 mA, with energy that is tuned for cooling, and with an electron beam of the same current, which has an energy which is 1 keV too high for electron cooling to take place (lower curve).

In order to answer the question whether the electron heating effect is a coherent effect or a single particle one, the stored beam lifetime has been measured with different stored proton beam intensities. Two different methods were used to reduce the stored beam intensity from its normal value, which is about 25 mA for protons. One method was to reduce the pulse length from the cyclotron from its normal value of 8 ms. The other method was to detune the injection septum magnet in CELSIUS, in order to hit the area in horizontal phase space which is accepted by the injection process with a lower intensity.

With the first method the stored beam emittance becomes smaller at the same time as the intensity is reduced, because injection takes place only during a small part of the time during which the orbit bump is shrinking. When the proton beam intensity had been reduced with this method, the electron heating phenomenon became less pronounced than with full intensity, and completely absent if the intensity was reduced enough and the rf. was off.

With the other method on the other hand, it is thought that the emittance of the stored beam is roughly the same for different intensities. There was no significant difference in lifetime while changing the stored proton current from 25 mA to 4 mA.

This indicates, that the electron heating is not a coherent effect, but a single-particle instability, caused by the electron beam.

The instability may be due to excitation of resonances by non-linear electrical fields from the electron beam. These may be due to:

a. The electrical field increases as r inside of the electron beam, but decreases as $1/r$ outside it.

b. Non-linear electrical fields from the electron beam are seen by the ions in the toroids, where the electron beam is bent into and away from the stored beam.

c. The vacuum chamber of the electron cooler is not perfectly cylindrical. An approximately cylindrical environment for the electron beam, with 100 mm diameter, is created with 8 longitudinal wires, which are placed inside the drift tube.

d. The electron beam may be displaced from the axis of the vacuum chamber.

e. The electron beam may have an uneven effective charge density, due to inhomogeneity or asymmetry of emitter and gun, or due to an inhomogeneous distribution of secondary particles inside the electron beam.

For ions with displacement larger than the electron beam radius, the amplitude of the exciting force from the finite diameter of the electron beam itself (case a) is much larger than those from cases b and c.

This means, that we should expect the lifetime to be sensitive to changes of the electron beam radius. With a larger radius, a smaller fraction of the stored ion beam is outside the electron beam. Ions with large amplitudes should get a better lifetime. On the other hand, if the electron current density is kept constant, the ions with displacements, that are smaller than the electron beam radius will be more disturbed by the other exciting forces (b, c, d, e...) due to the higher electron current.

Measurements of such dependence have been done. The electron beam diameter in the drift tube was increased from 2 cm to 3.6, 4 and 5 cm by running the electron cooler with a smaller magnetic field in the drift tube solenoid, than in the toroids and the gun and collector solenoids. The electron current was 100 mA, 314 mA, 400 mA and 625 mA respectively in order to maintain a constant current density. The best lifetime was observed when the electron beam diameter was 4 cm and the electron current was 400 mA. In figures 3 and 4 the lifetime of 48 MeV protons in presence of detuned electron beams of 100 mA, 2 cm diameter, and 400 mA, 4 cm diameter are compared with the lifetime without electrons present.

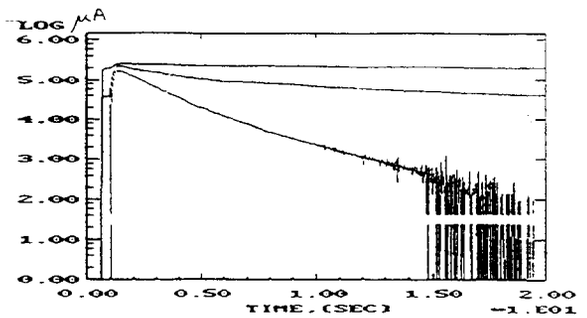

Fig. 3. Measurement of intensity (shown as ^{10}log of μA) vs. time (from zero to 20 s) for a bunched beam of 48 MeV protons (rf. voltage about 200 V), without electrons (best lifetime), with 400 mA electron beam with 4 cm diameter, and with 100 mA of electron beam with 2 cm diameter (worst lifetime).

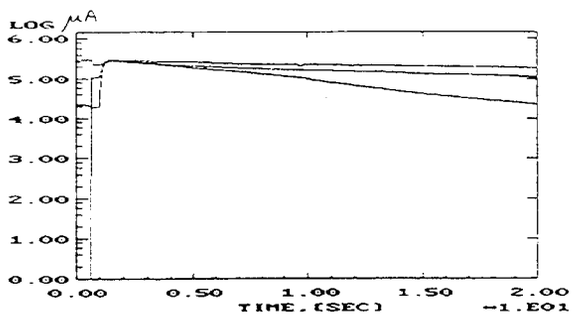

Fig. 4. As fig. 3 but for coasting beam of 48 MeV protons. The best lifetime is without electrons. The next curve is with 400 mA electron beam with 4 cm diameter. The worst lifetime is with 100 mA electron beam with 2 cm diameter.

We tested the hypothesis that the electron heating would only be due to the fact that the electron beam diameter is smaller than the ion beam size by first cooling the ion beam, then turning the electron current to zero, increasing the voltage of the high voltage power supply by 1 kV, and turning the electron current on again. The result was that beam losses do appear, with a delay after that the detuned electrons are applied, which varies with the electron current, and is a few seconds with 400 mA electron current, about 5 s with 200 mA, and 20 s with 50 mA. Thus, we have to conclude, that electron heating is present also for a beam which fits inside the electron beam, and that also other non-linear fields from the electron beam or other effects are important.

4. OTHER EXPLANATIONS

Another hypothesis to explain the electron heating phenomenon for intense stored beams has been proposed by Parkhomchuk and Pestrikov [14]. They suggest that the electron heating is also due to that the stored beam sees an additional impedance from the interaction with the electron beam. We have to conclude that several effects may play a role at the same time.

5. STUDIES OF LONGITUDINAL SCHOTTKY SPECTRA

Longitudinal Schottky noise spectra from coasting beams have been observed to see how these are influenced by the presence of a "detuned" electron beam.

The pickup which is used for these measurements is resonant at 68 MHz, which corresponds to the 60th harmonic of the revolution frequency for 48 MeV protons.

When the electron beam is present, there are dips in the measured spectra. These are absent without electrons. The density of these dips is so high, that one can usually see 3-6 of them at the same time. An example of such a measurement is shown in fig. 5. It is possible to identify resonances, which correspond to the observed peaks. These are of 6th and 7th order, see fig. 6 (Since the chromaticity is not corrected in CELSIUS, the momentum spread causes tune spread. Instead of a working point there is a "working line," as shown in fig. 6).

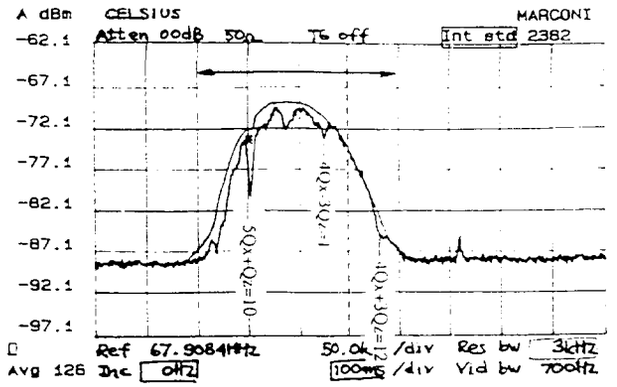

Fig. 5. Longitudinal Schottky spectra of coasting beam of 48 MeV protons with and without presence of 50 mA of "detuned" electron beam.

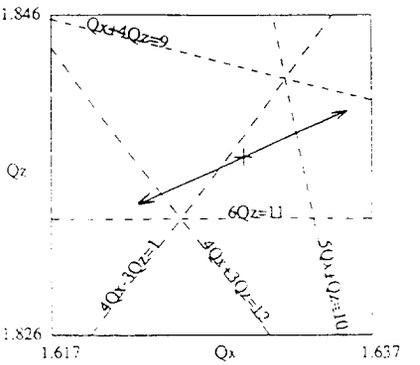

Fig. 6. Identification of resonances in tune diagram corresponding to several dips seen in the Schottky spectrum in fig. 5.

6. TRACKING CALCULATIONS

The electron heating phenomenon has been simulated in tracking calculations with SIXTRACK [15]. New subroutines have been added to represent the effects of the finite diameter electron beam, the solenoid, the electron beam in the toroid region, and our eight rods in the drift tube [16]. It was pointed out by Parkhomchuk, that it is necessary to evaluate the effect of the finite diameter electron beam by splitting the length of the interaction region into several pieces, and to calculate the kick from the displacement of the ion at each of these. Otherwise, the sharpness of the electron beam edge becomes exaggerated. We have chosen to split it in 10 pieces. With an electron beam of 0.5 A the results of the simulations seems chaotic after 10^4 - 10^5 turns of tracking of a 48 MeV proton, which starts at an amplitude just outside of the electron beam. The presence of rf. dramatically increases the chaotic behavior. The presence of a 0.1 A electron current and rf. causes a behavior which seems chaotic after about 10^6 turns. The non-linear electrical fields from the electron beam in the toroid regions, and the nonlinear electrical field from the eight rods, which surround the electron beam in CELSIUS at 100 mm diameter, seem to give rise to heating which is weaker than the electron cooling.

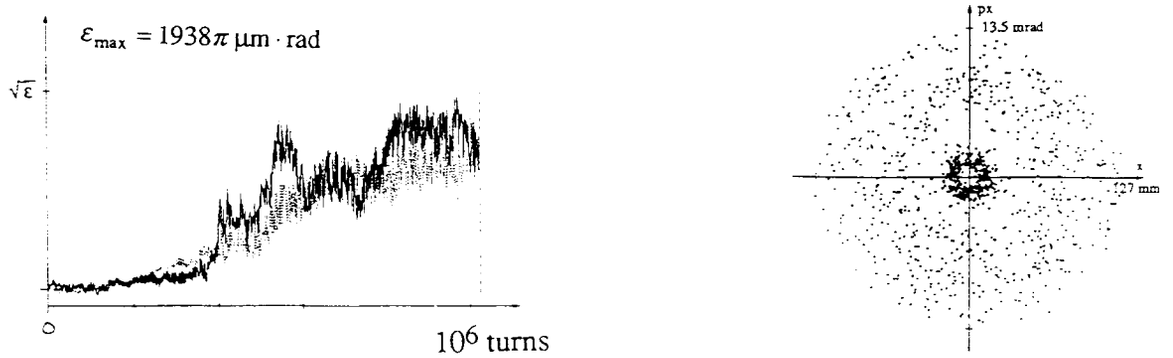

Fig. 7. Some results of tracking computation of 10^6 turns of a 48 MeV proton in presence of 0.5 A electron beam, 190 V rf., and 0.1 T solenoid field. The left figure shows how the $\sqrt{\varepsilon_x}$ (black) and $\sqrt{\varepsilon_z}$ (gray) vary as a function of turn number from 0 to 10^6, and the right figure shows the position of the proton in horizontal phase space plotted once every 10^3 turns.

As an example of the output of the tracking computations, fig. 7 shows some results of a computation of 10^6 turns of a 48 MeV proton, which starts just outside of a 0.5 A electron beam in CELSIUS. This computation is made for an rf. voltage of 190 V and a solenoid field of 0.1 T.

7. CONCLUSIONS AND PLANS

So far, we have not made any observation that contradicts our hypothesis that the electron heating is mainly due to high-order resonances, driven by the non-linear electrical fields from the electron beam. In CELSIUS, these are especially due to the fact that the diameter of the electron beam is smaller than the diameter of the injected ion beam; in fact, this seems to be the only effect, which gives rise to electron heating which is stronger than electron cooling at the injection energy.

If we gain further confidence in our hypothesis presented here, we will consider to equip our electron cooler with new solenoids for the electron gun and the collector with stronger and variable magnetic field, in order to get a variable diameter electron beam.

8. ACKNOWLEDGMENTS

Stimulating discussions and participation in experiments by Håkan Danared, Tim Ellison, Johan Jeansson, Arne Johansson, S.Y. Lee, Søren Pape Møller, Vasily Parkhomchuk, Miroslav Sedlacek, Anatoly Sharapa, Markus Steck, Tetsumi Tanabe, Gerard Tranquille, and many TSL staff members are gratefully acknowledged. Acknowledgments are also due to Frank Schmidt, who has generously provided us with SIXTRACK.

REFERENCES

[1] D. Reistad et al., *Recent Commissioning Results at CELSIUS*, Proc. 13th Int. Conf. on Cyclotrons and their Applications, Vancouver, Canada, July 6-10, 1992, 266.
[2] K. Hedblom et al., *Calculations on Multiturn and Stripping Injection in CELSIUS*, Proc. 3rd European Particle Accelerator Conference, Berlin, Germany, 24-28 March, 1992, 462.
[3] M. Sedlacek et al., *Design and Construction of the CELSIUS Electron Cooler*, these proceedings.
[4] T.J.P. Ellison, *Electron Cooling at IUCF — 0.3 MeV in 1988, 9 MeV in 1998?* Proc. Workshop on Electron Cooling and New Cooling Techniques, Legnaro, Italy, 15-17 May, 1990, 29.
[5] T. Tanabe et al., *Electron Cooling Experiments at INS*, Nucl. Instr. and Meth. in Phys. Res. **A307** (1991) 7.
[6] G.I. Budker et al., *Experimental Studies of Electron Cooling*, Particle Accelerators **7** (1976) 197.
[7] T. Ellison et al., *Fermilab 120 keV Electron Cooling System*, FNAL TM 1156.
[8] T. Ellison, private communication (1992).
[9] T. Tanabe et al., *Status of Electron Cooling at TARN II*, these proceedings.
[10] G. Tranquille, private communication (1992).
[11] M. Steck, private communication (1992).
[12] S. Pape Møller, private communication (1992).
[13] H. Danared, private communication (1992).
[14] V.V. Parkhomchuk, D.V. Pestrikov, *Coherent Instabilities at Electron Cooling*, these proceedings.
[15] F. Schmidt, *SIXTRACK version 1.1*, CERN/SL/91-52.
[16] A. Simonsson, *Simulations of Electron Heating*, TSL-Note 93-06.

A Cold Electron Beam for Cooling and Collision Experiments by Adiabatic Expansion in a Magnetic Field

D.Habs, S.Pastuszka, D.Schwalm, A.Wolf and S.Zwickler
Max-Planck-Institut für Kernphysik, Postfach 103980
and Physikalisches Institut der Universität,
D-69029 Heidelberg, Germany

ABSTRACT

All present day electron coolers have a homogeneous magnetic field of typically 0.5-1.0 kG and reach longitudinal temperatures in the region of $kT_{||} \approx 0.5meV$ while the transverse temperatures $kT_{\perp} \approx 0.1eV$ are determined by the cathode temperature. In this paper we want to outline a new design with a heated cathode, with which we expect to reach significantly lower electron beam temperatures. The basic design feature is to immerse the electron gun in the high magnetic field (of a superconducting solenoid), while the field strength in the drift region stays at its present value required for maintaining the magnetic cooling regime.

1. INTRODUCTION

An electron beam in a heavy ion storage ring is frequently used twofold: As a cooling device and as an electron target. The velocity distribution of the accelerated magnetically guided electron beam is flattened ($\Delta v_{\perp e} \gg \Delta v_{||}$), characterized by a longitudinal temperature $T_{||}$ and a larger transverse temperature $T_{\perp}$. The longitudinal temperature limits the effect of electron cooling in the magnetic cooling regime; it also limits the width of resonances in dielectronic recombination at higher relative energies. The transverse temperature is of particular importance for recombination experiments at low relative energy. The radiative recombination scales with $T_{\perp}^{-0.5}$; moreover, as the gainfactor of laser induced recombination scales with $(T_{||}T_{\perp})^{-0.5}$, the rate coefficient for laser induced recombination scales with $T_{||}^{-0.5}T_{\perp}^{-1}$. The very strong dependence of $T^{-4.5}$ of the three body collision cross section between two electrons and an ion may lead to a new local electron density distribution around the ions (Debye spheres), differing from the average electron beam density. Small transverse temperatures $T_{\perp}$ are essential to explore this new regime in electron ion interaction. For flattened situations even the temperature dependance of the three body cross section is completely unclear at present.

In this paper we explore in how far considerable smaller temperatures $T_{||}$ and $T_{\perp}$ can be achieved, when the magnetic field in the electron gun region is much larger (3-80kG) than in the drift region (0.1-1.0 kG) and an adiabatic transition is maintained between the two sides. A similar situation but with much smaller field variations has been explored already by Kudelainen et al. [1]. However, here we particularly emphasize the reduction of the transverse temperature by adiabatic expansion.

2. THE CONCEPT

Small transverse temperatures can be obtained by adiabatic expansion of the electron beam after acceleration. For a single electron the relation:

$$\frac{E_{\perp}}{B} = const.$$

can be derived from the adiabatic invariance of the magnetic moment $\mu = (\frac{-e\omega_e}{2\pi})\pi r_c^2 = -\frac{E_\perp}{B}$, where we denote the transverse energy by $E_\perp$, the cylotron frequency by ω_e and the cyclotron radius by r_c [7, 3, 4]. Since also the total energy is conserved, transverse energy is converted into longitudinal energy in a diverging magnetic field. The same principle is used in an inverse sense in a magnetic mirror, where particles are reflected via transfer of longitudinal energy into transverse energy when approaching an increasing field.

The adiabatic invariant is only preserved, if the change of the field acting on the electron during one gyration orbit is very small compared to the total field. The spiral length $\lambda_c = \frac{eB}{2\pi m v_\parallel}$ of the electrons represents the typical length scale and we can define an adiabaticity parameter:

$$\chi = |\frac{dB}{dz}|\frac{\lambda_c}{B}$$

which should be much smaller than one in the adiabatic limit.

Since the magnetic flux Φ enclosed by the helical orbit of the electron : $\Phi = \pi r_c^2|B| = -\frac{2\pi m}{e^2}\mu$ is also an adiabatic invariant and each electron adiabatically follows the flux line on which it started, one obtains for the electron density n during an adiabatic change of B :

$$\frac{n}{B} = const.$$

For intense beams with strongly coupled electrons, the Coulomb scattering between the electrons destroys the adiabatic invariant for the individual electrons, but it is interesting that for an ensemble of electrons an equivalent invariant can be derived. The transverse energy $E_{\perp i}$ divided by B but summed over all electrons is still an adiabatic invariant [6]:

$$\frac{\sum E_{\perp i}}{B} = const.$$

This invariant shows that the transverse degree of freedom is equilibrated very fast, establishing a transverse temperature $T_\perp =< E_\perp >$, while the relaxation between $T_\perp$ and $T_\parallel$, being controlled by the nonadiabaticity, takes much longer. Here, in addition to χ, the adiabaticity parameter $\kappa = \frac{r_c}{2}(n^{\frac{1}{3}} + \frac{kT_\parallel}{e^2})$ should be much smaller than one, the cyclotron radius r_c being given by: $r_c = \frac{\sqrt{2mkT_\perp}}{eB}$

We plan for adiabatic expansions of the magnetic field by a factor between 10 and 100 and expect corresponding reductions of $T_\perp$.

The very high magnetic field in the gun region also allows to reach significantly smaller longitudinal temperatures $T_\parallel$. Without relaxation processes a very low temperature $T_\parallel$[2] is obtained by electrostatic acceleration to an energy E_{kin}:

$$2 * kT_\parallel * E_{kin} = (kT_c)^2 = const.$$

where T_c is the temperature of the thermocathode. By relaxation of potential energy into kinetic energy, allowing the electrons to move along the B field lines (longitudinal-longitudinal relaxation (LLR)) a final longitudinal temperature $T_\parallel$ is obtained:

$$kT_\parallel = \frac{(kT_c)^2}{2E_{kin}} + Ce^2 n^{\frac{1}{3}}$$

where n is the electron density and C is a constant of about one for fast acceleration and significantly smaller than one for rather slow socalled adiabatic acceleration. For adiabatic acceleration the adiabaticity parameter:

$$\alpha = \frac{dT_\parallel}{dt}\frac{2\pi}{\omega_p T_\parallel}$$

with ω_p being the plasma frequency, should be much smaller than one. Experimentally adiabatic acceleration with a strongly reduced heating due to LLR has been observed [2, 5].

For the suppression of the second relaxation contributing to $T_{||}$, the transverse longitudinal relaxation(TLR), a high B field is required. This relaxation process is due to the energy exchange between the much hotter transverse degree of freedom ($T_\perp = T_c$) and the longitudinal degree of freedom with lower temperature $T_{||}$. It corresponds to the violation of the adiabatic invariant $\frac{\sum E_{\perp i}}{B}$ and is weaker than any power in the corresponding adiabaticity parameter κ. Experimentally [2] a good description of the relaxation was obtained with:

$$\frac{dT_{||}}{dz} \propto \exp(-\frac{c_1}{\kappa^{c_2}})$$

and constants $c_1 \approx 2.0, c_2 \approx 0.73$. Due to $\kappa \propto \frac{1}{B}$ this relaxation is strongly suppressed in high magnetic fields. Adiabatic acceleration enhances the importance to suppress the transverse longitudinal relaxation, because during slow acceleration a high electron density n persists for longer times and $T_{||}$ is still large, i.e. κ is large. Thus a rather high magnetic field especially in the gun region is essential to achieve minimal longitudinal temperatures $T_{||}$, as demonstrated in detailed measurements in ref.[1].

The increase of the longitudinal energy spread due to adiabatic expansion is comparable to the initial transverse energy and will yield a negligible contribution to the final longitudinal temperature in the comoving frame due to the still dominant relaxation processes. However, for typical parameters of an electron beam with adiabatic expansion it happens for electron velocities larger than about 2% velocity of light, that the transversal density change becomes nonadiabatic ($\frac{dn}{dt}\frac{\tau_p}{n} \propto \frac{dB}{dz}\frac{v_e\tau_p}{B} \geq 1$) with respect to the plasma period τ_p and a longitudinal longitudinal relaxation increases $T_{||}$ to about $e^2 n^{\frac{1}{3}}$. In order to avoid this longitudinal heating the final adiabatic acceleration has to be performed after the expansion of the electron beam in the magnetic field.

Thus our concept involving adiabatic expansion and acceleration does seem to allow a decrease of $T_{||}$ and $T_\perp$ by at least one order of magnitude.

3. THE TECHNICAL DESIGN AND NUMERICAL SIMULATIONS

The gun solenoid and the next somewhat narrower solenoid of the existing TSR electron cooler are shown in fig 1a. With the existing power supply the gun solenoid could generate a 3 kG field with a smooth transition to the next solenoid having typical fields of 0.4 -1.0 kG. In order to achieve larger magnetic expansions we studied the replacement of the gun solenoid by a super conducting magnet with a maximum field of 80 kG (fig 1b) The magnet has a length of 300 mm and a warm bore of 100 mm diameter. A field map for different equipotential lines of such a design is shown in fig 2, demonstrating the slow expansion of the field between the two solenoids with an additional coil for optimum field shaping. The electrode system of the new gun is more extended that in the present design to allow for adiabatic acceleration. The gun is separated by a valve from the rest of the existing cooler. For usual barium-oxide dispenser cathodes, operation at a current density of $1A/cm^2$ can be safely envisaged and an emission current density of $10A/cm^2$ appears possible. This will permit an electron density of $10^8 cm^{-3}$ to be obtained at a beam velocity $\leq 0.2c$ and an expansion factor ≥ 10.

When tracing the electron trajectories in the variable field region it was found, that the published computer code SLACTRA [8], infact makes a smooth interpolation of the vector potential, but produces little steps when calculating the magnetic field from the vector potential by differentiation. This unsteady B field results of course in a significant increase of the transverse electron temperature when passing the adiabatic region. By correcting to a smooth change of the B field correct temperatures were obtained. Fig.3a shows the longitudinal magnetic

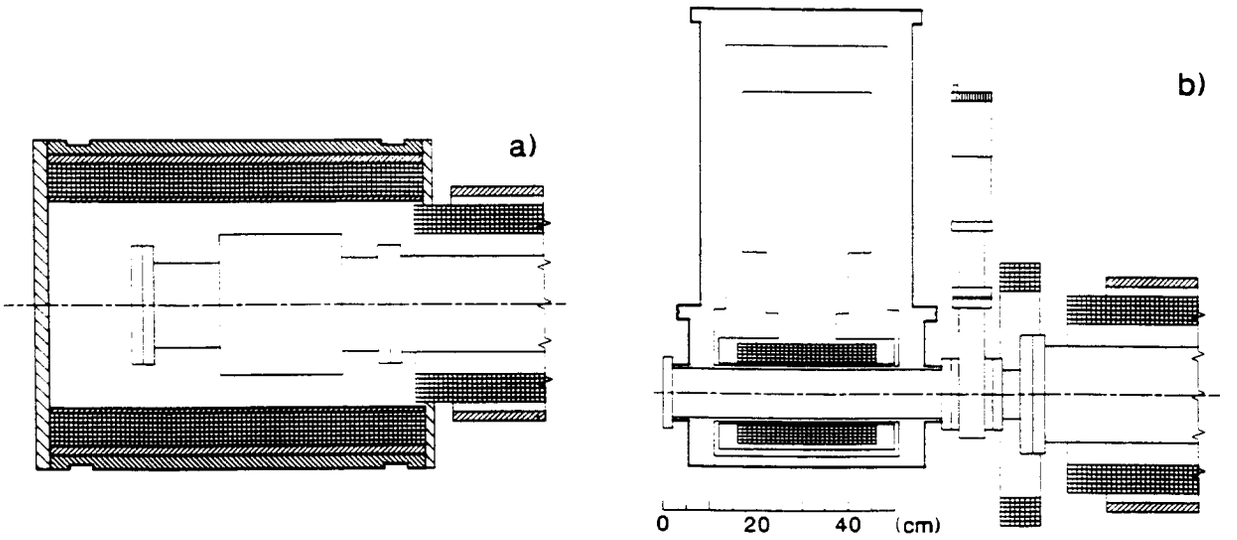

Figure 1: a) Present gun solenoid of the TSR cooler. b) New technical design with superconducting magnet and old solenoid. The electron gun is separated by a valve from the rest of the cooler.

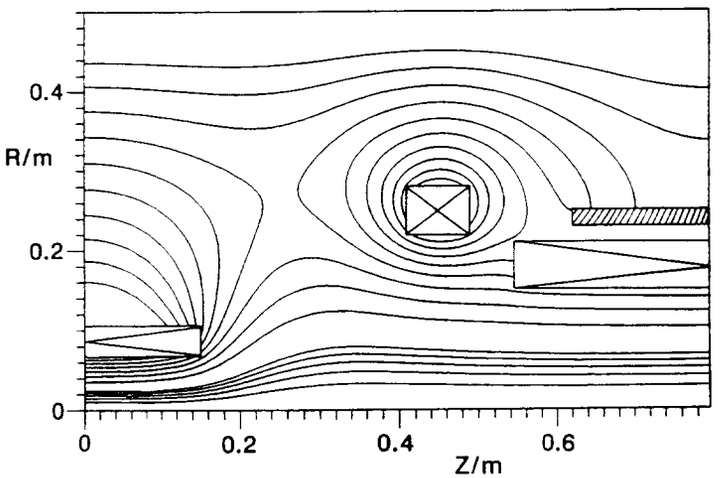

Figure 2: Magnetic field distribution for the new design with adiabatic expansion.

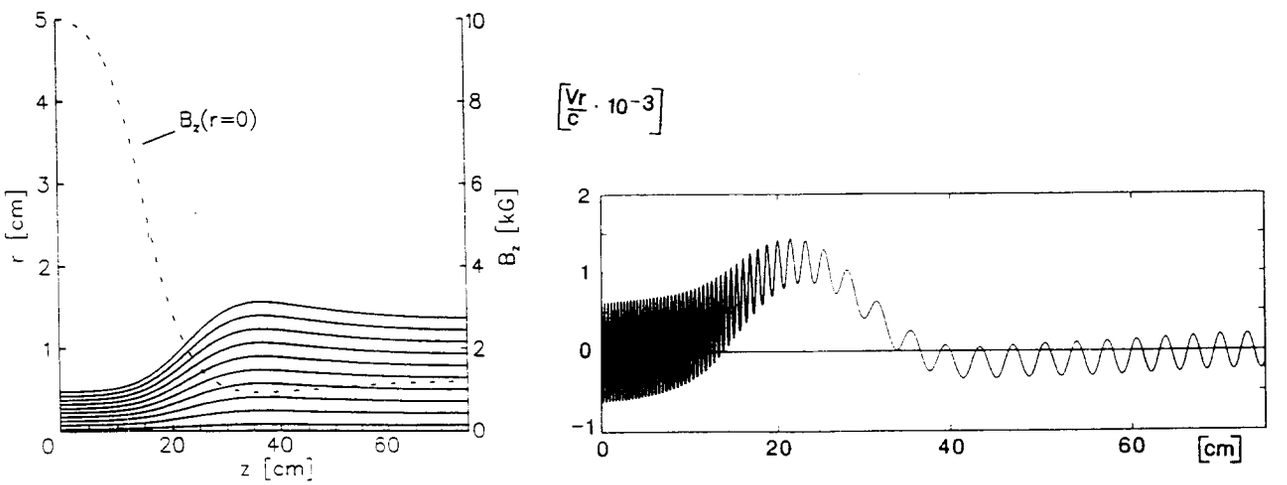

Figure 3: a) Longitudinal B field distribution on the axis and typical electron trajectories. b) Radial velocity for an electron ray starting 1mm of axis with an energy of 30 keV.

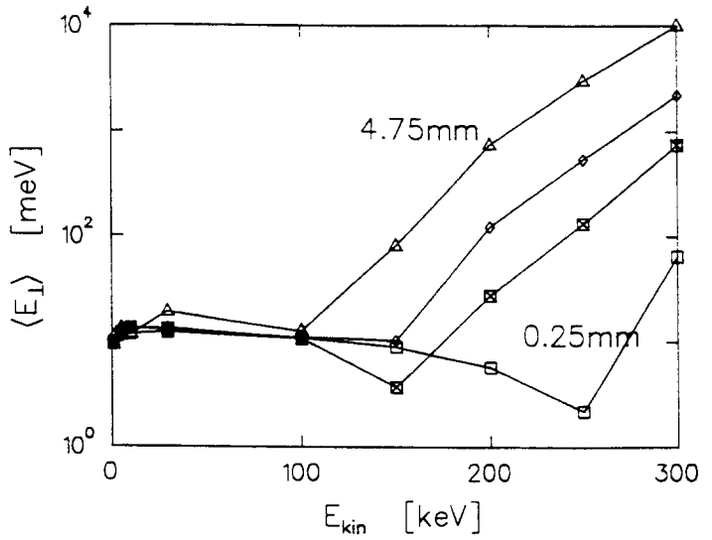

Figure 4: Transverse electron energy for electron trajectories with different initial distances from the axis as a function of the final electron energy, using the configuration of fig.2.

field distribution and typical electron trajectories. Fig.3b shows the radial velocity for one electron trajectories starting 1mm off axis. During the adiabatic decrease of the B field first an increase and then a decrease of the radial velocity is observed. The transverse energy is seen in the superimposed fast oscillation. After the adiabatic passage the oscillation amplitude is correspondingly reduced. Fig. 4 demonstrates that for typical electron energies of the TSR cooler of less than 20 keV transversal temperatures of $kT_\perp$=10 meV, i.e. a factor of 10 smaller than in standard devices, can be obtained and that nonadiabaticity effects are negligible. They start only at energies above 100 keV. Again, the nonadiabaticity can be described nicely by $\exp(-\frac{c_1}{\chi^{c_2}})$.

During the next shut down we will replace the present heated cathode by one with a smaller diameter and a compensating Pierce shield to study the adiabatic expansion with the existing solenoid system. In a second step the superconducting solenoid and a new gun design will be introduced.

References

[1] V.I.Kudelainen, V.A. Leledev, I.N. Meshkov, V.V.Parkhomchuk and B.N.Sukhina JETP56 (1982) 1191-1196

[2] P.Krause, D.Habs, S.Pastuszka, D.Schwalm, A.Wolf and S.Zwickler, to be published in Phys.Rev.E

[3] A.Picard et al. NIM B63 (1992)345

[4] P.Kruit and F.H.Read,J.Phys E:Sci Instrum 16 (1983) 313

[5] A.V.Aleksandrov et al. Europhys. Let 18 (1992) 151

[6] T.M.O'Neil and P.G.Hjorth, Phys.Fluids 28 (1985) 3241

[7] T.G. Northrop The adiabatic motion of charged Particles, ,1963, London, Interscience

[8] W.B.Herrmannsfeldt, Stanford Linear Accelerator Center Report No. SLAC-331(1988)

ENERGY ANALYSIS OF ELECTRONS EMITTED BY A SEMICONDUCTOR PHOTOCATHODE

S.Zwickler, D.Habs, P.Krause, S.Pastuszka, D.Schwalm, and A.Wolf
Max-Planck-Institut für Kernphysik, Postfach 103980
and Physikalisches Institut der Universität,
A.S.Terekhov
Institute for Semiconductor Physics,
630090 Novosibirsk, Russia

Abstract

In this paper we present measurements of the longitudinal energy spread $\Delta E_{||0}$ of electrons emitted by a $In_{0.46}Ga_{0.54}As_{.06}P_{.94}$-photocathode with current densities up to 20 mA/cm^2. Furthermore we present a method of measuring the mean transverse energy $\langle E_{\perp 0} \rangle$ making use of adiabatic invariants for the electron motion in a decreasing longitudinal magnetic field. It was successfully tested with an electron beam emitted by a thermocathode and will soon be used to measure $\langle E_{\perp 0} \rangle$ for the photoelectrons, expected to be considerably smaller than for thermal electrons.

1.INTRODUCTION

High quality electron beams needed for electron cooling devices are characterized by small temperatures $T_{||}$ and $T_{\perp}$. These can be reduced significantly by using a cold semiconductor photocathode with negative electron affinity (NEA) instead of a thermocathode employed in present devices and by accelerating these electrons adiabatically [1]. In the last few years it was demonstrated by different groups [2,3] that continuous currents of about 1mA, needed for an electron cooling device with a photocathode, where the beam diameter is 2mm [4], can be produced with a lifetime of several weeks. If the semiconductor photocathode is precleaned in a separate chamber and brought into the ultrahigh vacuum gun chamber using a fast entry lock system [2], reproducible quantum efficiencies (QE) of about 25% are reached without problems.
However, no systematic measurements concerning the initial longitudinal energy spread $\Delta E_{||0}$ and the initial mean transverse energy $\langle E_{\perp 0} \rangle$ of the electrons emitted by a semiconductor photocathode were published until now. In contrast to a heated thermocathode, where $\Delta E_{||0} = \langle E_{\perp 0} \rangle = k_B T_{cath}$, it will be shown in this paper for current densities relevant for an electron cooling device that the energy spread of electrons emitted by a NEA-photocathode is not only determined by the temperature of the cathode T_{cath} but also strongly dependent on the NEA condition.

2. LONGITUDINAL ENERGY DISTRIBUTIONS AND $\Delta E_{||0}$

The experimental setup is presented in fig.1. The photocathode (1) is a lattice-matched InGaAsP epitaxial (111)A-layer, grown on (100) GaAs by liquid phase epitaxy and p-doped with Zn to $5 \cdot 10^{18}$/cm^3. It is activated to NEA by covering it with small amounts of Cs and NF_3 in ultra high vacuum; then the vacuum level lies below the conduction band minimum in the bulk and electrons lifted from the valence to the conduction band can leave this cathode. The InGaAsP-photocathode has a better stability than a GaAs-photocathode; according to [2] this is caused by the higher band gap of E_g= 1.89eV (measured by photoluminescence) as compared to E_g= 1.42eV for GaAs. The Pierce-electrode (2) with a hole diameter of 2 mm determines the diameter

of the electron beam. The first anode (3) is situated 2mm in front of the cathode, the second anode (4) is kept on ground potential - therefore the electron energy is always given by the negative cathode voltage U_{cath}.
After leaving the cathode, the electron beam is guided in a longitudinal magnetic field of B= 1400 Gauss, produced by a pair of Helmholtz coils. This high field strength ensures that the relaxation of transverse energy into longitudinal energy is suppressed [1]. A 3-plate retarding-field energy analyzer (5), moveable in transverse direction, is located at a distance of 4 cm in front of the cathode to measure the longitudinal energy distribution $f(E_{||})$ of the electron beam. Using a 25 μm pinhole in the entrance diaphragm only a 10^{-4} fraction of the beam is analyzed. The collector current I_{coll} detected on the third plate as a function of the retarding voltage U_{ret} on the second plate gives the integrated electron distribution curve (EDC). The differential signal is obtained online via lockin-technique. Both voltages U_{cath} and U_{ret} were produced by batteries to avoid voltage ripple and are monitored continuously with differential voltmeters (accuracy 0.5meV).

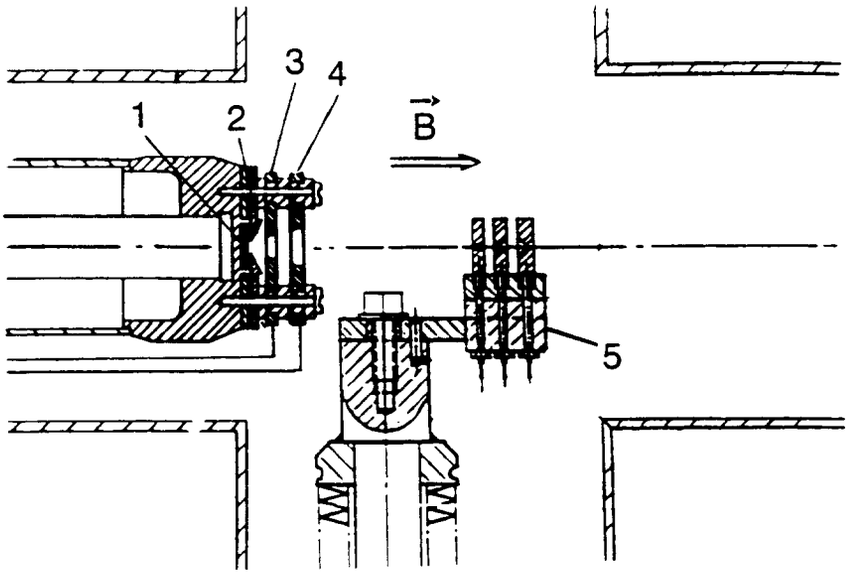

fig.1: Experimental setup with electron gun and retarding field energy analyzer (for further explanations see text).

Prior to the experiments with the NEA-photocathode, the system was tested with an electron beam produced by a conventional thermocathode. EDCs for four different currents of the thermocathode are presented in fig.2a in a semilogarithmic plot. As the gun is operated in space charge limitation, the mean energy of the electron beam decreases with increasing current: the potential produced by the space charge plasma directly in front of the cathode acts as a low energy cut-off [5]. Due to the strong magnetic field, the small current density (maximum 0.4mA/cm^2) and the low kinetic energy ($\approx$ 7eV) of the extracted electron beam, the energy distributions $f(E_{||0})$ of the emitted electrons are not substantially affected by relaxation processes [1]. Thus we have for the distribution measured by the retarding field analyzer $f(E_{||}) \approx f(E_{||0})$ and $\Delta E_{||} \approx \Delta E_{||0}$. Therefore all EDCs have the same asymmetric exponential shape. As the main part of the longitudinal energy $E_{||}$ is distributed proportional to $\exp(-E_{||}/k_B T_{cath})$, it is possible to determine $k_B T_{cath}$; the deduced value of 98 $\pm$ 2meV is in very good agreement with pyrometer measurements. The energy spread $\Delta E_{||} = \sqrt{\langle E_{||}^2 \rangle - \langle E_{||} \rangle^2}$ for each curve is $\Delta E_{||} \approx$ 102meV which also agrees with $k_B T_{cath}$.
The EDCs of photoelectrons produced by illuminating the photocathode, held at room temperature, with 30μW of a single-mode HeNe-Laser are shown in fig.2b. Again the current densities

are very small (between 3 and 30μA/cm^2) so that the EDCs reflect the longitudinal energy distributions of the electrons leaving the cathode f($E_{||}$)$\approx$ f($E_{||0}$), $\Delta E_{||} \approx \Delta E_{||0}$. For the measurement shown in fig.2b the electron gun was operated in the current limited regime (both anodes are grounded) and the different current densities are obtained after different aging times (indicated in fig.2b) of the activated photocathode. Aging is caused by pollution of the activated surface by components of the residual atmosphere which leads to an increase of the vacuum level (decrease of NEA and QE) that acts as a low energy cut-off. Due to this aging the photocathode has a so called 'dark' lifetime of about two days. Subsequent reactivations to the initial maximum NEA are possible by recesiation. The left curve in fig.2b (0min), measured after activating the cathode to highest NEA and QE, is rather broad ($\Delta E_{||} \approx$ 110meV). When NEA and QE get smaller, the EDCs become narrower (down to $\Delta E_{||} \approx$ 48meV).

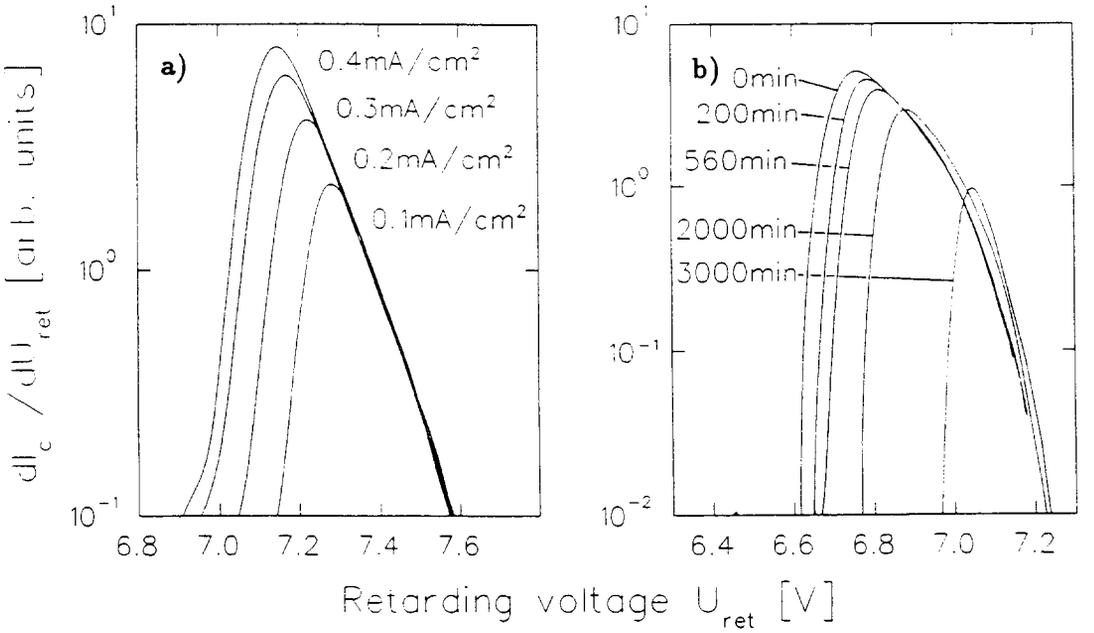

fig.2: Longitudinal EDCs measured for electrons produced a) by a thermocathode at different current densities and b) by the $In_{0.46}Ga_{0.54}As_{.06}P_{.94}$-photocathode at different aging times.

Comparison of the EDCs shown in fig.2a and fig.2b reveals a basic difference between thermo- and photocathode: the longitudinal energy spectra of the emitted photoelectrons do not have an exponential high energy slope. Hence the widths $\Delta E_{||}$ of these EDCs are not constant but they mainly depend on the potential (height of vacuum level) that the electrons have to overcome before they leave the cathode. Only in the case of very small NEA the slope of the EDC is exponential and T_{cath} as well as the photonenergy has a substantial influence on $\Delta E_{||0}$, for example $\Delta E_{||0} \approx$25meV at $T_{cath} = 150K$ and hν=2eV.

We measured the same non-exponential EDCs as shown in fig.2b when the photocathode had a constant (e.g. maximum) NEA but the gun was operated in space charge limitation. This is an important result because it shows that the electrons do not thermalize in the space charge region before they leave it.

One of the aims of these experiments was to determine $\Delta E_{||0}$ for current densities used in an electron cooling device. Therefore the photocathode was illuminated with 30mW emitted by a single mode dye-laser, U_{cath} was set to -100V and the current was extracted in space charge limitation. The measured $\Delta E_{||}$ is plotted as a function of the current density in fig.3 (dots). Due to the high kinetic energy E_{kin}, relaxation of potential energy [1] in the accelerated beam already leads to a substantial energy broadening at current densities as low as 0.2mA/cm^2. Thus the

originally asymmetric EDCs displays a Gaussian shape and the measured width $\Delta E_{||}$ is larger than $\Delta E_{||0}$ according to [1]:

$$k_B T_{||} = \frac{(\Delta E_{||})^2}{2E_{kin}} = \frac{(\Delta E_{||0})^2}{2E_{kin}} + 2\langle E^{Relax}\rangle \quad , \qquad 2\langle E^{Relax}\rangle = Ce^2 n^{\frac{1}{3}}$$

$\langle E^{Relax}\rangle$ is the mean relaxed potential energy in the rest frame, n the electron density and C a value between 0 and 1.3, depending on the number of plasmaoscillations n_{osc}, the electrons experienced on their flight to the retardation analyzer; C is a constant of about 0.7 for a nonadiabatically accelerated beam if n_{osc} is larger than one [1]. In our setup the flight time is very short and n_{osc} is smaller than one for current densities below 10mA/cm^2. To determine C, we measured $\Delta E_{||}$ as a function of n for an electron beam emitted by the thermocathode using the upper formula and $\Delta E_{||0}$ = 97meV.

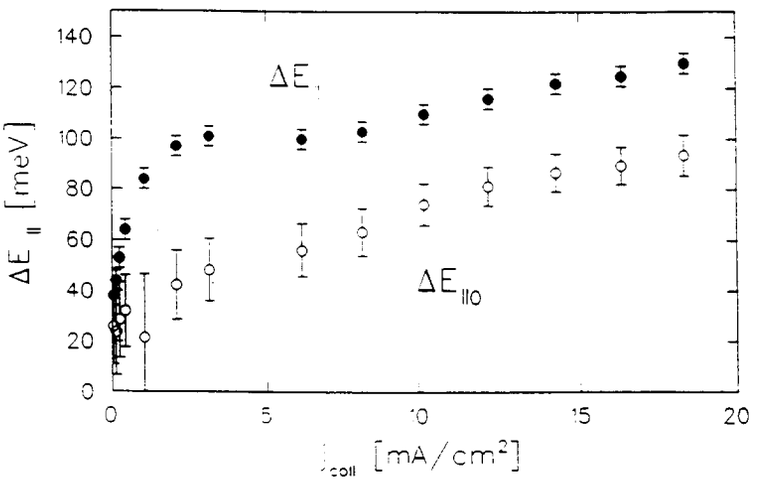

fig.3: Measured energy widths $\Delta E_{||}(\bullet)$ and deduced original widths $\Delta E_{||0}(\circ)$ for different electron current densities emitted by the InGaAsP-photocathode.

The deduced widths $\Delta E_{||0}$ for electron beams emitted by the photocathode is shown in fig.3 (circles). The situation is very similar to that shown in fig.2b; if the majority of the electrons lifted to the conduction band are not emitted because they are prevented from leaving the cathode by the vacuum level or by the space charge potential, $\Delta E_{||0}$ is rather small. By reducing this potential, the emitted current and $\Delta E_{||0}$ increases. Note that even at current densities of 20mA/cm^2 $\Delta E_{||0}$ is smaller than 100meV, i.e. $\Delta E_{||0}$ does not exceed the initial energy spread of electrons from a thermocathode.

3. MEASUREMENT OF THE MEAN TRANSVERSE ENERGY $\langle E_{\perp 0}\rangle$

In a proper accelerated electron beam, guided in a constant longitudinal magnetic field, the transverse temperature $k_B T_\perp$ is equal to the initial mean transverse energy $\langle E_{\perp 0}\rangle$ of the electrons. The great advantage of a cooled semiconductor photocathode in contrast to a heated thermocathode is a small $\langle E_{\perp 0}\rangle$; if the tangential component of the electrons momentum is conserved when they cross the interface between crystal and vacuum (like in UPS and XPS experiments), $\langle E_{\perp 0}\rangle$ is expected to be as small as 1meV due to the small effective mass of the electrons inside the semiconductor [6].

All experiments concerning $\langle E_{\perp 0}\rangle$ [6,7,8,9] measured the angular distribution of the emitted electrons but could not take into account space charge effects in the electron beam. Their results differ extremely (1meV $< \langle E_{\perp 0}\rangle <$ 120meV) and were never compared with measurements of

the well known $\langle E_{\perp 0} \rangle$ of a thermocathode. We have developed a technique for measuring $\langle E_{\perp 0} \rangle$ with an accuracy of 3meV independently of any spacecharge and relaxation effects.
For these measurements the distance between cathode and analyser (see fig.1) is increased to 26cm. Moreover, the longitudinal magnetic field $\vec{B}$, produced by three pairs of magnetic coils, decreases in a defined way (see fig.4a) from $\vec{B}_0$ (at the cathode position) to $\vec{B}_a$ (at the analyzer position). The ration $\alpha = B_a/B_0$ can be varied between 1 and 0.5 with $B_0 = 1400$G. As the electron beam expanse adiabatically [10], the mean transverse energy $\langle E_\perp \rangle$ divided by B is a constant of motion. From the energy conservation law $\langle E_{\perp 0} \rangle + \langle E_{\|0} \rangle = \langle E_\perp \rangle + \langle E_\| \rangle$ it follows that the mean longitudinal energy of the electron beam at the analyzer position $\langle E_{\|a} \rangle$ increases proportional to (1-α): $\langle E_{\|a} \rangle - \langle E_{\|0} \rangle = (1-\alpha)\langle E_{\perp 0} \rangle$. The change of the mean longitudinal energy $\langle E_{\|a} \rangle - \langle E_{\|0} \rangle$ can be measured with an error smaller than 1.5meV and thus $\langle E_{\perp 0} \rangle$ can be deduced.

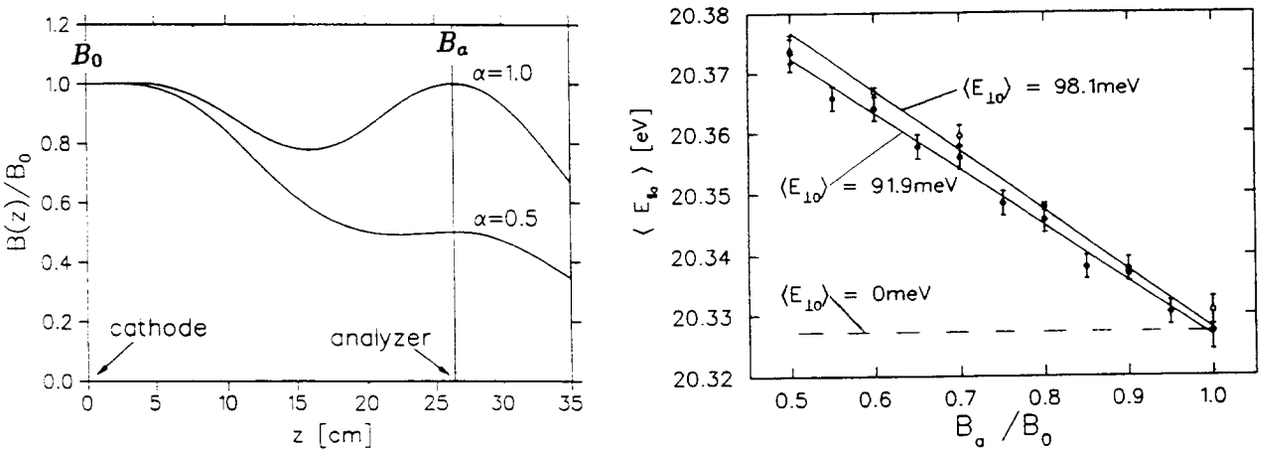

fig.4: a)Different field structures used for an adiabatic expansion of the electron beam.
In b) the measured mean energy of the electron beam $\langle E_{\|a} \rangle$ is plotted as a function of B_a/B_0 for two different T_{cath}. The broken curve would be obtained for $\langle E_{\perp 0} \rangle = 0meV$.

In fig.4b $\langle E_{\|a} \rangle$ is plotted as a function of B_a/B_0 for two different temperatures of the heated thermocathode, T_{cath}=1070K (•) and T_{cath}=1150K (○). From the slope of the fitted curves it is possible to deduce $\langle E_{\perp 0} \rangle$ with an error of 3meV, which is in very good agreement with $k_B T_{cath}$ for both curves. Corresponding measurements of $\langle E_{\perp 0} \rangle$ for InGaAsP- and also for GaAs-photocathodes are in progress.

REFERENCES

[1] P. Krause, D. Habs, D.Schwalm, S. Pastuszka, A. Wolf and S. Zwickler, to be submitted to Phys. Rev. E
[2] V. L. Alperovich, Yu. B. Bolkhovityanov, A. G. Paulish and A. S. Terekhov, subm. to NIM
[3] R. Calabrese, V. Guidi, G. Lamanna and L. Tecchio, J. Phys.3 France **2**, 473 (1992).
[4] D. Habs, J. Kramp, P. Krause, K. Matl, R. Neumann, and D. Schwalm, Physica Scripta **T22**, 269 (1988).
[5] P.T.Kirstein, G.S.Kino, W.E.Waters, Space charge flow, (Mc Graw Hill), New York, 269, (1967)
[6] R.L. Bell, Negative Electron Affinity Devices , Claredon, Oxford (1973)
[7] C.A.Sanford and N.C. Mac Donald J. Vac.Sci.Technol. **B8**(6) 1853 (1990)
[8] D.C.Rodway and M.B.Allenson, J. Phys. D: Appl. Phys. **19** 1353 (1986)
[9] D.J. Bradley et al., Jou. App. Phys. **10** (1977)
[10] T.M. O'Neil and P.G. Hjorth, Phys. Fluids **28** (1985) 3241

STUDIES OF INTRABEAM SCATTERING AT THE TSR

B. Hochadel, F. Albrecht, M. Grieser, D. Habs, D. Schwalm, A. Wolf
MPI für Kernphysik and Universität Heidelberg
G. Bisoffi
INFN, Legnaro

Abstract

We present measurements of intrabeam scattering (IBS) blow-up rates for a 63.5 MeV $^{12}C^{6+}$ and a 10 MeV p beam at the test storage ring TSR. For $^{12}C^{6+}$ also measurements of the equilibrium emittances and momentum spreads reached in electron cooling are described. The experimental findings can be well reproduced by an IBS computer code when a strong coupling between the transverse degrees of freedom is assumed. Due to the small difference of the horizontal and vertical tune in the present experiments, this coupling could be caused by the longitudinal magnetic field in the electron cooler section. Furthermore first theoretical studies of a laser cooled 7.29 MeV $^{9}Be^{+}$ beam with the IBS code are presented. The dependence of the equilibrium temperatures on the cooling rate, the particle number, and the dynamics of the beam are discussed for various longitudinal cooling rates.

1. INTRODUCTION

One of the central topics of the experimental program at the test storage ring for heavy ions TSR [1] is the development of the techniques of electron cooling [2] and laser cooling [3][4] and the study of cold, dense ion beams. The high phase-space density of stored cooled ion beams opens up many new possibilities for experiments in the field of atomic and nuclear physics.

For a proper interpretation of the cooling experiments and the planning of further developments a good quantitative knowledge of IBS is necessary, especially in the case of laser cooling: For stable working points IBS is the dominant heating mechanism for cold beams in the TSR, scattering events with the residual gas can be estimated to be negligibly small.

The motivation for the experiments described in the next two sections was to get a quantitative understanding and theoretical description of IBS at the TSR. We followed the blow-up of a 63.5 MeV $^{12}C^{6+}$ beam and a 10 MeV p beam. In the case of an electron cooled $^{12}C^{6+}$ beam also the equilibrium values of the emittances and the momentum spread in dependence of the ion current were measured. The experimental data could be reasonably well reproduced by an IBS computer code [5]. First theoretical studies for an laser cooled ion beam with this code will be presented in section 4.

2. BLOW-UP OF A $^{12}C^{6+}$ AND A PROTON BEAM

The squares in fig.1 show the results of measurements of the blow-up of the emittances and the longitudinal momentum spread of ion beams stored in the TSR. The measurements of fig.1a) refer to a 63 MeV $^{12}C^{6+}$ beam of $2 \cdot 10^7$ partices corresponding to an ion current of $11\,\mu$A; fig.1b) refers to a 10 MeV p beam of 10^9 particles corresponding to a current of $125\,\mu$A. The beams have been electron cooled to shrink the emittances and the momentum spread, then the electron cooler was switched off and the blow-up was measured as a function of time. The emittances were determined from the measurement of the horizontal and vertical beam profiles with a residual gas ionization beam profile monitor [6]. From the horizontal and vertical r.m.s. radii $\sigma_h(s_0)$ and $\sigma_v(s_0)$ measured at the position s_0 of the monitor the emittances are calculated by $\epsilon_{h,v} = \sigma^2_{h,v}(s_0)/\pi\beta_{h,v}(s_0)$, where $\beta_h(s_0)$ and $\beta_v(s_0)$ denote the local values of the horizontal and vertical lattice functions. The emittances are proportional to the ring averaged transverse temperatures T_h and T_v. The momentum spread was determined with a Schottky pick-up. In the proton case the momentum spread was only measured once at the beginning of the measurement.

For both cases shown in fig.1 a simultaneous heating of the horizontal and vertical emittance could be observed, whereas the IBS code had predicted the behaviour indicated by the dashed lines, where the vertical emittance was expected to grow slower than the horizontal one. However, the measurements can be explained assuming a strong coupling of the horizontal and vertical degree of freedom.

A coupling between the transverse degrees of freedom can occur in the presence of a longitudinal magnetic field and when the difference between the horizontal an vertical tune is very small. This is described in detail in ref.[7]. At the TSR a longitudinal magnetic field is present in the cooler section. The horizontal and vertical tunes Q_h and Q_v were measured as a function of the quadrupole strength, and for the tune difference $\Delta Q = |Q_h - Q_v|$ a minimum value of $\Delta Q_{min} \approx 0.02$ was found (see fig.2). Here the strongest coupling should occur. The measurements for $^{12}C^{6+}$ and p where performed at tune

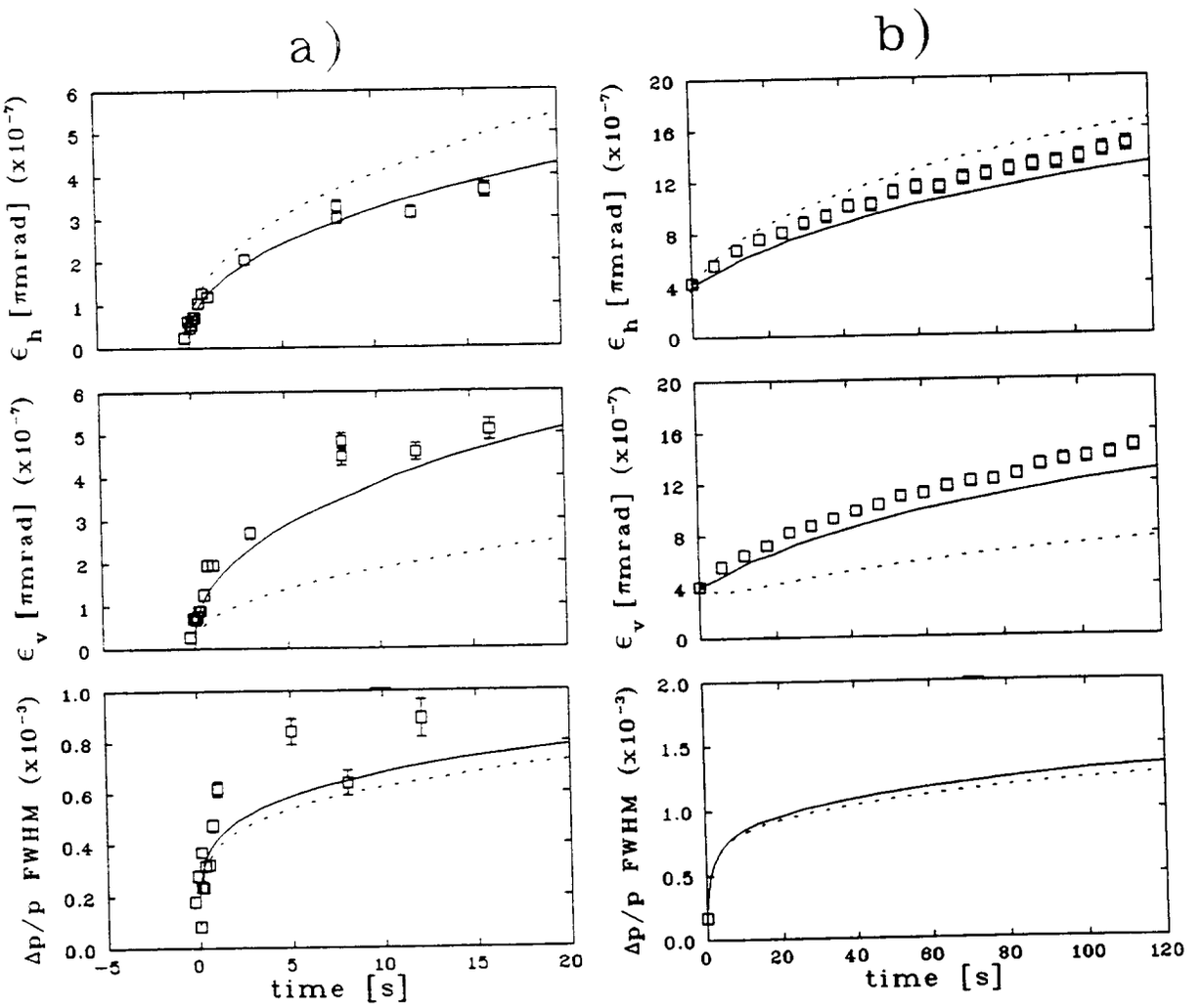

Figure 1: *Blow-up of a 63 MeV* $^{12}C^{6+}$ *beam of* 2×10^7 *particles after electron cooling (a) and of a 10 MeV p beam of* 10^9 *particles (b). Squares: measured data; full lines: result of calculations with the IBS code assuming a strong coupling of the transverse degrees of freedom; dashed lines: result of IBS calculations without coupling.*

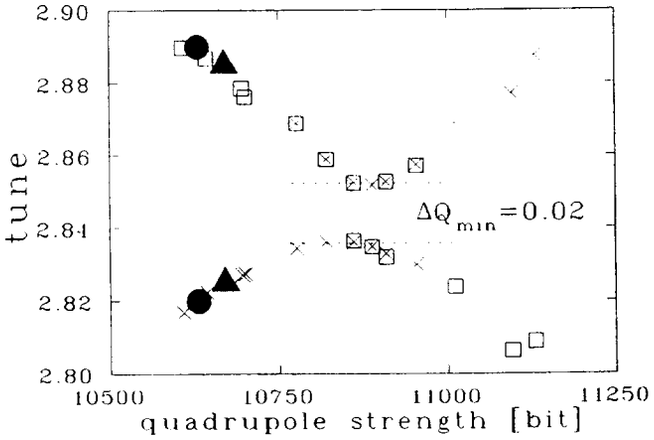

Figure 2: *Measurement of horizontal and vertical tune* Q_h *and* Q_v *as a function of the quadrupole strength (squares:* Q_h*, crosses:* Q_v*). A minimum value for the tune difference* $\Delta Q = |Q_h - Q_v|$ *of* $\Delta Q_{min} \approx 0.02$ *was found. For comparision also the values of the horizontal and vertical tunes during the described experiments are shown (bullets:* $^{12}C^{6+}$ *case,* $\Delta Q \approx 0.07$*; triangles: p case,* $\Delta Q \approx 0.06$*).*

differences of $\Delta Q = 0.07$ and $\Delta Q = 0.06$ respectively. Whether these values are small enough for a complete coupling of the transverse degrees of freedom or whether other effects are responsible will be investigated later by a more systematic study of the heating rates as a function of ΔQ.

In the IBS calculations the coupling was taken into account by finding the growth rates for both emittances from the average of the calculated horizontal and vertical IBS rates obtained from the code of ref.[5]. The result of this calculations can be seen in fig.1 as full lines, which describe the measurements reasonably good.

In fig.1 it also can be seen, that the beams don't tend to an equilibrium like in the case of a free plasma, but show an overall heating, which is caused by the coupling of the horizontal and longitudinal degree of freedom because of the dispersion in the storage ring [8]. The energy for this overall heating is taken from the kinetic energy of the beam.

Finally it should be mentioned, that additional blow-up measurements for $^{12}C^{6+}$and p were performed at various ion currents and the same reasonable aggreement of the experimental data with the IBS calculations was found. This holds also for a 7.29 MeV $^{9}Be^{+}$beam, which had been electron cooled and laser cooled before observing its blow-up rates[4].

3. EQUILIBRIUM WITH ELECTRON COOLING FOR A C^{6+} BEAM

The squares in fig.3 show the equilibrium values of the emittances and the momentum spread measured for an electron cooled 63.5 MeV $^{12}C^{6+}$ beam as a function of the ion current.

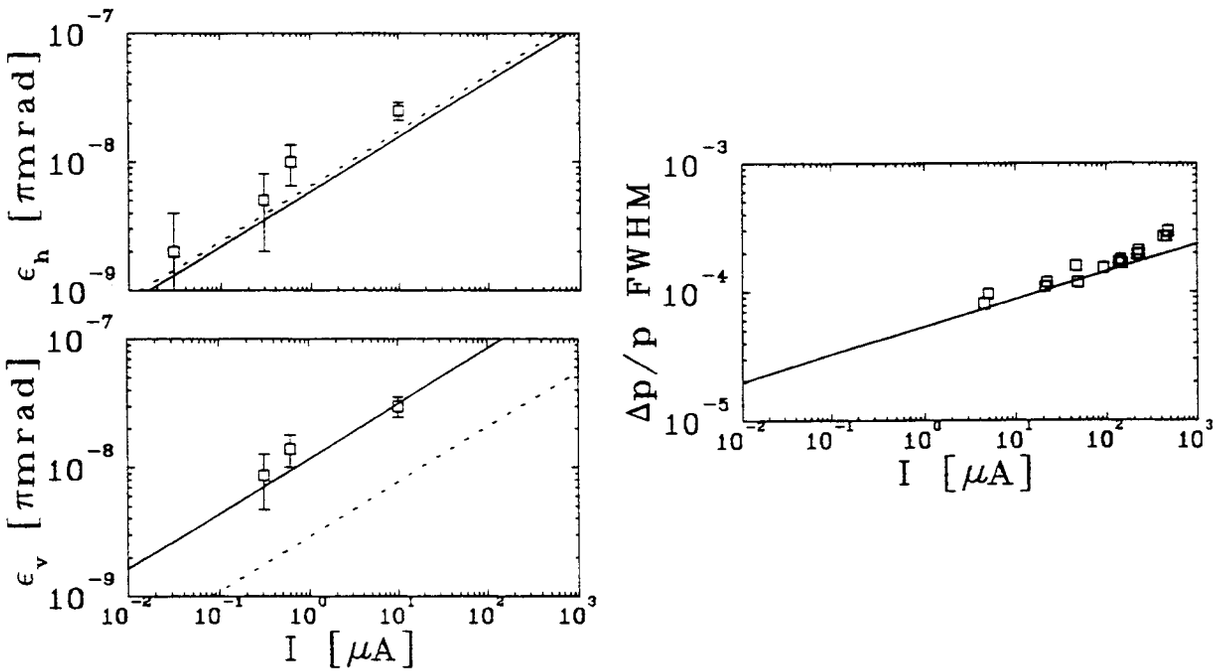

Figure 3: *Equilibrium values of the emittances and the momentum spread for an electron cooled 63.5 MeV $^{12}C^{6+}$ beam as a function of the ion current. Squares: measured data; full lines: IBS calculation assuming strong coupling of the transverse degrees of freedom; dashed lines: calculation without coupling.*

A comparision of theory and experiment was made by putting the transverse and longitudinal electron cooling rates $\lambda_\perp$ and $\lambda_\parallel$ into the IBS code. $\lambda_\perp$was determined by the relative decrease of the beam radius σ of a hot beam, which was measured with the profile monitor, and $\lambda_\perp = (d\sigma(t)/dt)/\sigma(t) = 5.5\,s^{-1}$ was found. $\lambda_\parallel$was determined from measurements of the cooling force with the induction accelerator [9] and gave $\lambda_\parallel = 250\,s^{-1}$. Like for the blow-up measurements a good aggreement with the experimental data was achieved by assuming a strong coupling between the transverse degrees of freedom, i.e. by assuming equal values of the horizontal and vertical beam temperatures. The results of these calculations are shown as full lines in fig.3. The calculations show a scaling for the emittances like $\epsilon \propto I^{0.43}$, while the momentum spread scales like $\Delta p/p \propto I^{0.21}$. For comparision the dashed lines show the results of the calculations without coupling, where the equilibrium values found for the vertical emittance are a factor of about 4 lower than the experimental values.

4. IBS STUDIES OF A LASER-COOLED $^9Be^+$ BEAM

To give proper interpretations of the laser cooling experiments at the TSR trustful quantitative theoretical studies are absolutely necessary. Of great interest are among other things the dependence of the equilibrium temperatures on the number of particles and the cooling power and naturally the dynamics of a laser cooled beam. With the IBS code first studies in this topic for a 7.29 MeV $^9Be^+$ beam, which is used in laser cooling experiments at the TSR, were made. The latest results of these measurements are presented in ref.[4]. The longitudinal laser cooling rate $\lambda_\parallel$ was put into the IBS code as the parameter describing the effect of the laser on the beam. The calculations were made with the assumption of equal ring-averaged transverse temperatures $T_h = T_v = T_\perp$ which means a strong coupling of the transverse degrees of freedom.

Fig.4 shows the behaviour of the beam temperatures $T_\perp$ and $T_\parallel$ as a function of time for three realistic values of the longitudinal laser cooling rates $\lambda_\parallel$. A typical particle number of 2×10^6 and initial temperatures of $T_\perp = 2500\,\mathrm{K}$ and $T_\parallel = 1700\,\mathrm{K}$ were assumed. Of course , a realistic initial value for $T_\perp$ of the $^9Be^+$ beam could only be roughly estimated, because the initial transverse velocity distribution of the ions that are kept in the laser cooling process is not exactly known. It can be seen that $T_\parallel$ decreases very quickly within times < 1 ms by several orders of magnitude because of the strong laser cooling force. Moreover, the coupling of the transverse and longitudinal degrees of freedom results in an indirect cooling of the transverse degrees of freedom, which results also in a decrease of $T_\perp$. From the slope of $T_\perp(t)$ it can be seen, that the coupling increases for lower values of $T_\perp$, which results in turn in an increase of $T_\parallel$. Finally an equilibrium is reached where the heating due to IBS and the cooling are equal.

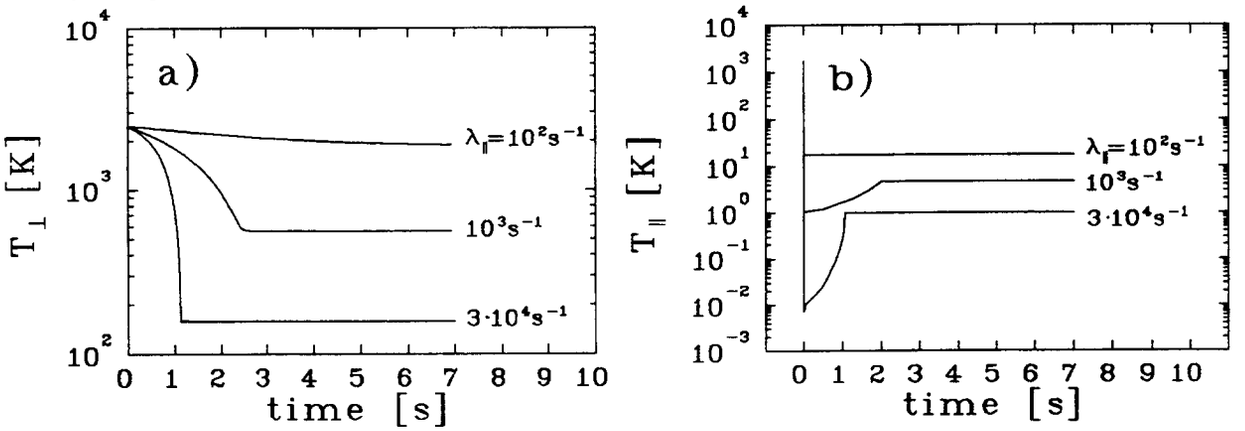

Figure 4: *a) Calculated Transverse temperature $T_\perp$ and b) longitudinal temperature $T_\parallel$ as a function of time for a laser cooled 7.29 MeV $^9Be^+$ beam of 2×10^6 particles for various longitudinal laser cooling rates $\lambda_\parallel$.*

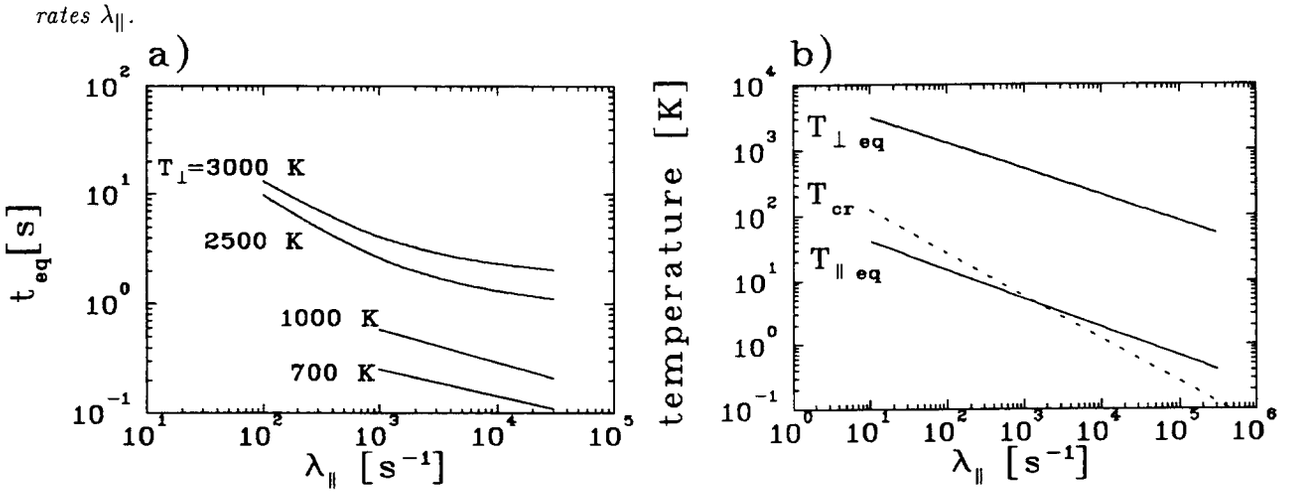

Figure 5: *a) Time t_{eq} needed to reach the equilibrium for various initial transverse temperatures $T_\perp$ and b) equilibrium temperatures $T_{\perp eq}$ and $T_{\parallel eq}$ for a laser cooled 7.29 MeV $^9Be^+$ beam of 2×10^6 particles as a function of the longitudinal cooling rate $\lambda_\parallel$. Also shown in b) is the critical temperature T_{cr}, discussed in the text.*

In fig.5a) the time t_{eq} for reaching the equilibrium is plotted for various values of the initial

transverse temperatures as a function of $\lambda_{\|}$, in fig.5b) equilibrium values of the temperatures $T_{\|eq}$ and $T_{\perp eq}$ are displayed as a function of $\lambda_{\|}$.

It can be seen in fig.5a), that lower cooling rates and higher initial values of $T_{\perp}$ lead to longer times before reaching the equilibrium. $T_{\|eq}(\lambda_{\|})$ and $T_{\perp eq}(\lambda_{\|})$ in fig.5b) show the same scaling of $T \propto \lambda_{\|}^{-0.4}$. The fact, that $T_{\perp eq}$ lies about two orders of magnitude over $T_{\|eq}$ reveals the influence of the above mentioned dispersive heating in a storage ring.

Also the dependence of the equilibrium temperatures on the particle number was studied. The result is shown in fig.6. $T_{\perp eq}(N)$ and $T_{\|eq}(N)$ scale like $T_{eq} \propto N^{0.4}$.

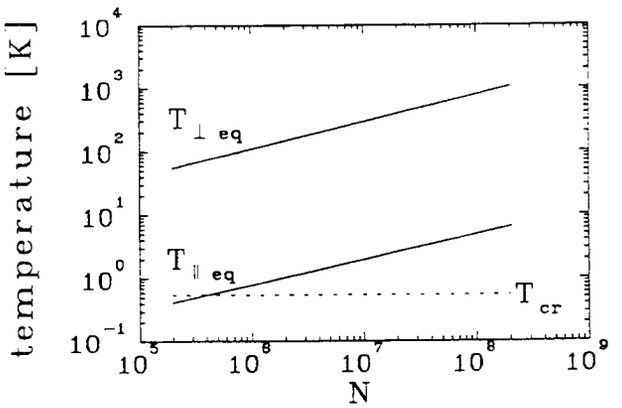

Figure 6: *Dependence of the equilibrium temperatures $T_{\|eq}$ and $T_{\perp eq}$ on the particle number N for a laser cooled $^9Be^+$ beam assuming a cooling constant of $\lambda_{\|} = 3 \cdot 10^4$. Also shown is the critical temperature T_{cr}, discussed in the text.*

In fig.5a) and fig.6 also a *critical temperature* T_{cr} is shown. It is given by $T_{cr} = \frac{m}{k_B} \Delta v_{cap}^2$, where Δv_{cap} is the velocity capture range of the laser cooling force [4]. Only for horizontal and vertical temperatures with $T_{\|} \leq T_{cr}$ and $T_{\perp} \leq T_{cr}$ the laser cooled particles are expected to be kept by the laser cooling force. In recent experiments [4], however, for a broad range of $\lambda_{\|}$rather constant values of 2×10^6 for the number of laser cooled particles could be observed, which is a contradiction to our IBS calculations, where $T_{\perp}$is always much larger than T_{cr}. Obviously effects occur that are not be taken into account in the code. One possible explanation could be the formation of a linear ordered structure, which is predicted to occur for particle numbers $N \leq 2 \times 10^6$ [10]. In this case a strong suppression of the scattering from the transverse into the longitudinal degree of freedom would be expected. Further investigations of this interesting possibility are under way.

Supported by BMFT under contract No. 06HD525I.

References

[1] D. Habs et al., NIM B43 (1989) 390.

[2] M. Steck et al., Proc. Workshop on Electron Cooling and New Cooling Techniques, Legnaro, 1990, eds. R. Calabrese and L. Tecchio (World Scientific, Singapore, 1991), p.64.

[3] W. Petrich et al., accepted for publication in Phys. Rev. A.

[4] H.-J. Miesner et al., these proceedings.

[5] R. Giannini, private communication.

[6] B. Hochadel et al., to be published.

[7] E. Wilson, CERN 85-19, p. 114.

[8] A.H. Soerensen, CERN 87-10, p. 135.

[9] C. Ellert et al., these proceedings.

[10] D. Habs in: 'Frontiers in Particle Beams', Lecture Notes in Physics **296** (1986) 310.

UPGRADING OF THE LEAR STOCHASTIC COOLING SYSTEMS

F. Caspers, M. Chanel, J.C. Perrier
CERN, PS Division, CH - 1211 Geneva 23

ABSTRACT

After presentation of the actual stochastic cooling systems with a brief historical review, recent improvements are discussed. The usable bandwidth of all systems has been increased mainly by adjustments of phase correctors and hardware modifications of the notch filters used in the longitudinal system. After identification of electromagnetic interferences at low PS-revolution harmonics in the MHz range, an efficient filter has been installed in the power supply path of the cryogenic preamplifier. In addition the power supply units are now situated as close as possible to the amplifiers in order to reduce the coupling due to the interference from the PS, which was acting via intermodulation on a large fraction of the cooling band. A new method using the time-domain function of a network analyzer to check the notch filters without disconnecting cables will be described. In conclusion the performance of all stochastic cooling systems is discussed.

1. INTRODUCTION

The stochastic cooling is an important part of the LEAR machine. It was designed mainly to reduce the beam dimensions before deceleration of the antiprotons towards 100 MeV/c. It has now been working properly for about a decade [1] and may be considered complementary to the electron cooler. The improvements made to this system, which can work for several momenta between 61 MeV/c and 2 GeV/c, are described. Some emphasis is put on the particularities of this system.

2. EVOLUTION OF LEAR STOCHASTIC COOLING SYSTEMS SINCE 1986

The LEAR stochastic cooling system consists of two chains, each working in all three planes, to cover two ranges of particle momentum in the machine. The high-momentum system (Fig. 1) can be adjusted for a momentum range from 200 MeV/c to 2 GeV/c (protons or antiprotons), corresponding to a variation of particle velocity ($\beta = v/c$) by a factor of 4.35.

The low-momentum system (Fig. 2) is adjusted for 105 MeV/c and 61 MeV/c, respectively [2].

Figures 1 and 2 illustrate the configuration used in 1993. Over the years (beginning 1986) the position of stochastic cooling pickups and kickers has been changed together with the type of coupling structure. Initially, the longitudinal cooling systems had ferrite ring pick-ups (24 rings each) and kickers. These ferrite rings were outside the vacuum (outgassing, mechanical dimensions), on a section of the ceramic vacuum chamber. With these units the usable frequency range extended from 30 MHz to 200 MHz, showing a rather poor phase response (dispersion). However, at that time only a momentum cooling (high-energy range) from $\Delta p/p = 0.6\%$ to $\Delta p/p = 0.25\%$ was required.

After the implementation of the "bunch-to-bucket" transfer from the PS into LEAR and the adiabatic debunching in LEAR, the longitudinal stochastic cooling after injection into LEAR turned out to be more important.

Because later LEAR was operated at higher momenta than injection , the increase in bandwidth for the stochastic cooling system became mandatory. Now loop couplers with variable external delays and a horizontal cooling system using the same loop couplers have been installed (BHN 30, Fig. 1). The usable bandwidth extends from 3 MHz to 1.1 GHz. In order to avoid undesired feedback between pick-ups and kickers due to imperfect shielding as well as microwave mode propagation in the beam pipe, pick-ups and kickers were placed as far apart from each other as possible.

3. DESCRIPTION OF THE COOLING SYSTEMS PRESENTLY IN USE

3.1 High-Momentum Systems

At present loop couplers for pick-ups and kickers are in use in all the LEAR stochastic cooling systems. The output of each pick-up plate is followed by a head amplifier and a well-defined delay (combiner delay) before

the signals enter a first combiner stage. To satisfy a correct phasing for all required particle momenta, these delay lines are set in steps of 5.7 cm corresponding to 190 ps. The horizontal cooling system (Fig. 1) has 12-loop pairs, also used simultaneously for the longitudinal system, and is located in the bending magnet BHN 30. The vertical system with 8-loop pairs is close to that magnet in position UCV 32 (Fig. 1). Low-noise preamplifiers with a noise figure of 1.4 dB (non-cryogenic) and a frequency range from 5 MHz to 1 GHz ensure a fairly good signal/noise ratio for the pick-up signals. Concerning the kickers, like the pick-ups, an identical coupling loop size is required since different loops could cause unacceptable phase shifts seen by the beam over the complete frequency range of the system.

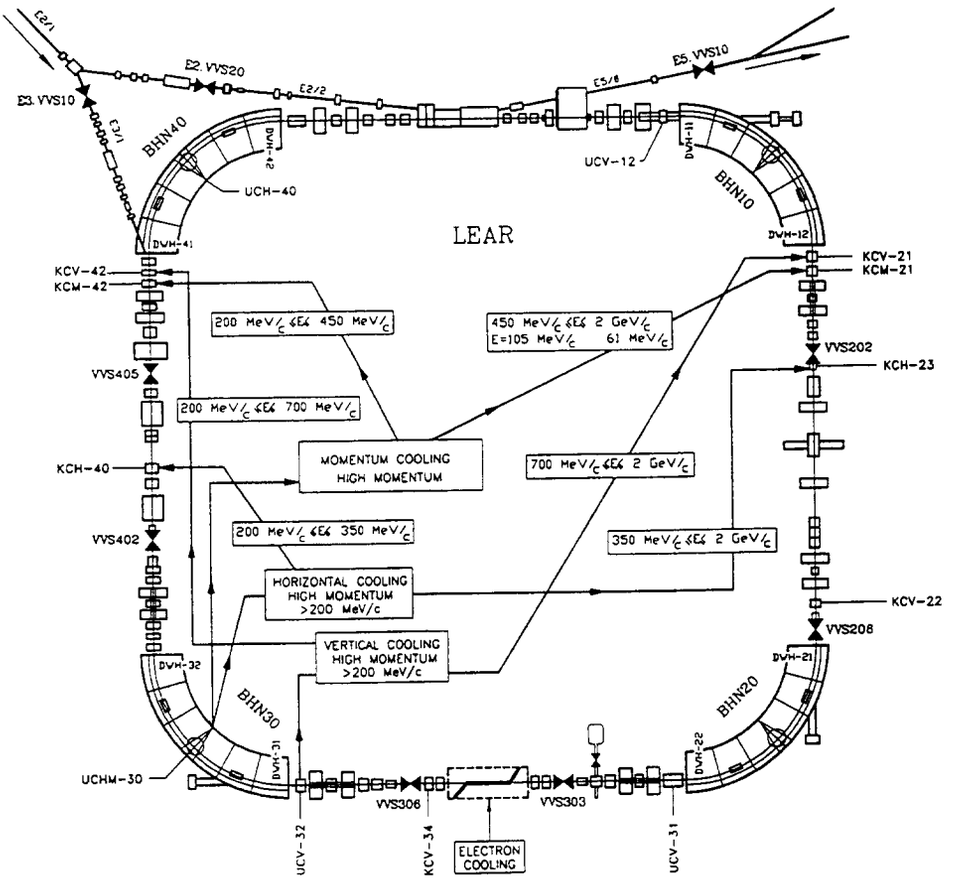

Fig. 1 - LEAR high-momentum stochastic-cooling system

The system delay is digitally set through the control system using a 16-bit data word and can be varied in steps of 41 ps from 0 to 2.7 μs. The short delay variations are implemented as printed circuits (striplines) and extend up to 336 ps. The usable bandwidth of these printed lines is limited to about 1 GHz since beyond that frequency, severe phase distortions appear due to mutual coupling of the striplines.

The maximum system gain defined as the gain sum (in dB) of all amplifiers in the chain corrected by all attenuators (cable losses, combiners, etc.) amounts to about 110 dB. Gain settings are varied by means of a PIN-diode attenuator in steps of 1 dB from 0 to -25 dB.

In some operating conditions, when cooling of particles with a large $\Delta p/p$ is required, overlapping of the Schottky bands towards higher frequencies may occur. In this case the cooling system bandwidth can be limited with an equi-ripple filter, thus allowing for a fast decay in amplitude beyond the cut-off frequency and slight phase distortion.

Until summer 1993 the power amplifier of the longitudinal high-momentum cooling system was a 10 W (CW-sine wave) unit with a passband of 5 MHz-1 GHz. Severe deviation from linear phase beyond 850 MHz led to reduced cooling speed. These phase errors cannot be compensated due to a lack of available electrical delay. A new power amplifier with 4 W output power and a linear phase up to 1.1 GHz has been built. A particular difficulty in these constructions is the requirement of very short electrical length of the unit composed of four commercial amplifier modules and line transformers, for broad-band signal splitting and combination. Practical experience with this improved version showed a considerable increase in the cooling performance, although the usable output power for noise-like signals amounts only to about 1.5 W (4 W CW). A further increase in

bandwidth is not desirable for the time being as measurements between different pick-ups and kickers have shown the onset of microwave mode propagation at about 1.3 GHz.

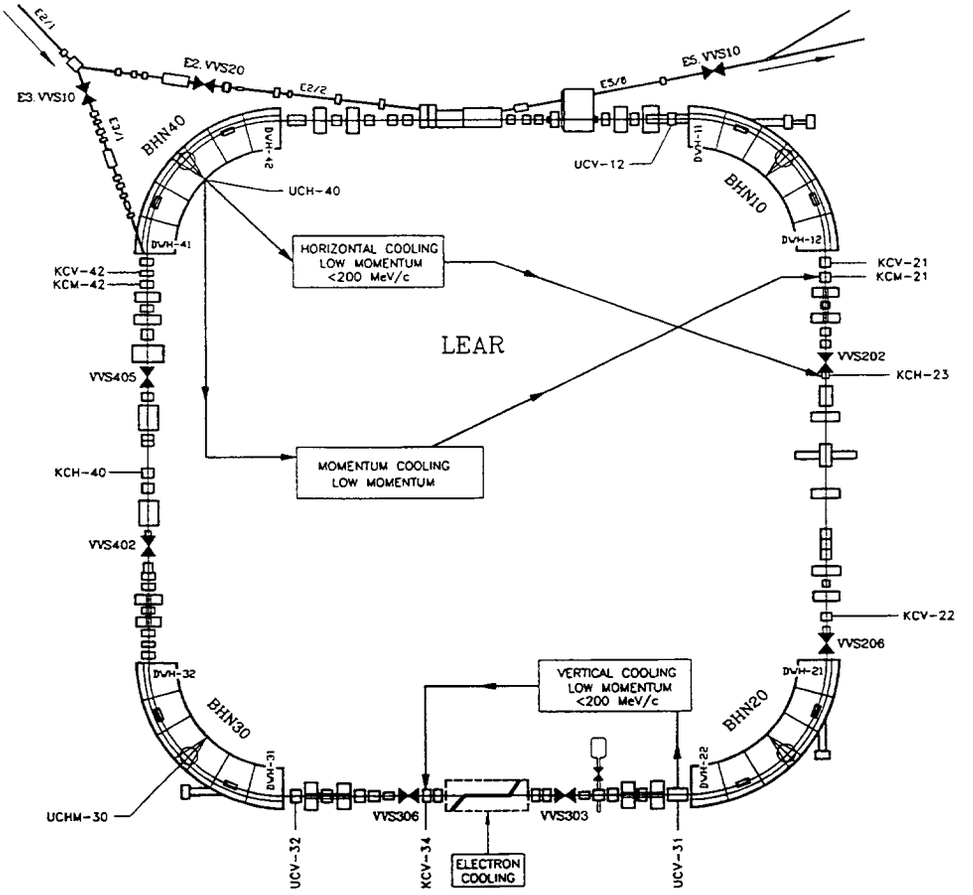

Fig. 2 LEAR low-momentum stochastic cooling systems

3.2 Notch Filters

Both active and passive (notch) filters are in use in the longitudinal cooling systems (Fig. 3). The purpose of the active filters is to increase the steepness of the notch slopes and to provide a better use of the Schottky noise power available from the power amplifier. The principal working points of these cooling systems are 105, 200, 309, 609, 1000, 1500 and 2000 MeV/c for protons and antiprotons. This implies large variations of the required delay settings for both the notch and peak filters as well as for the compensation cables (Fig. 3).

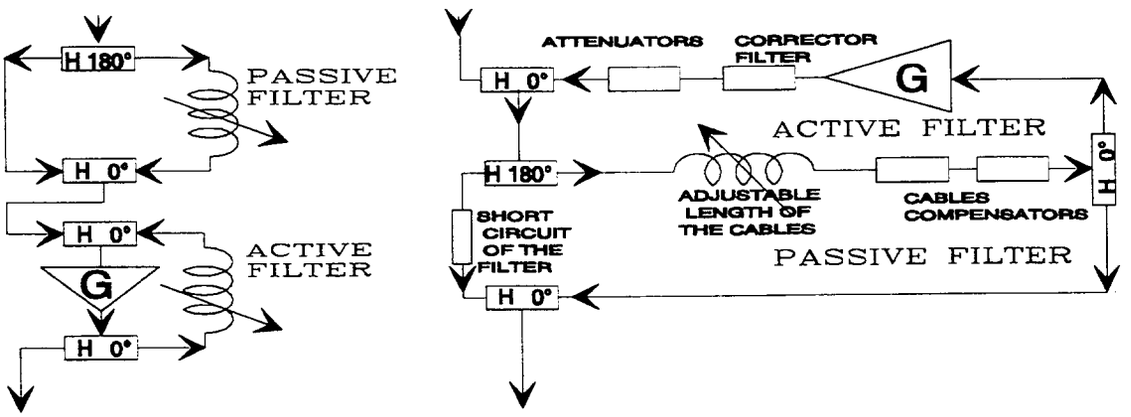

Fig. 3 - Passive and active notch filters used in LEAR. Left: old system, right: improved system. H = hybrid type power splitter/combiner.

Practical and theoretical experience has shown that for the power splitters employed in the filters, hybrid type units should be used, in preference to resistive splitters or just simple split-winding transformers (Fig. 4). As one is aiming for optimum notch depth and periodicity over the band, any asymmetry of signal and reference path will lead to a considerable distortion of notch depth and position.

The tracking of both signal paths in LEAR is within ±1 dB and ±5° of phase corresponding to about 25 dB notch depth in the worst case. If non-hybrid type elements are used for signal splitting and combination, independently of the perfect symmetry in both signal path and reference line, multiple "echos" will occur.

The configuration shown in Fig. 4 (upper part) may be considered as a heavily damped ring resonator with a round trip time corresponding to twice l_1/c. These multiple echos appear as a ripple in the frequency domain response or as a series of "echos" in the time domain. Using 0°/180° hybrid these "echos" are strongly suppressed and a nearly flat response returns. Applying a time-domain gate to a notch filter response with signal and reference paths of different lengths permits the analysis of either path response without the need to disconnect cables.

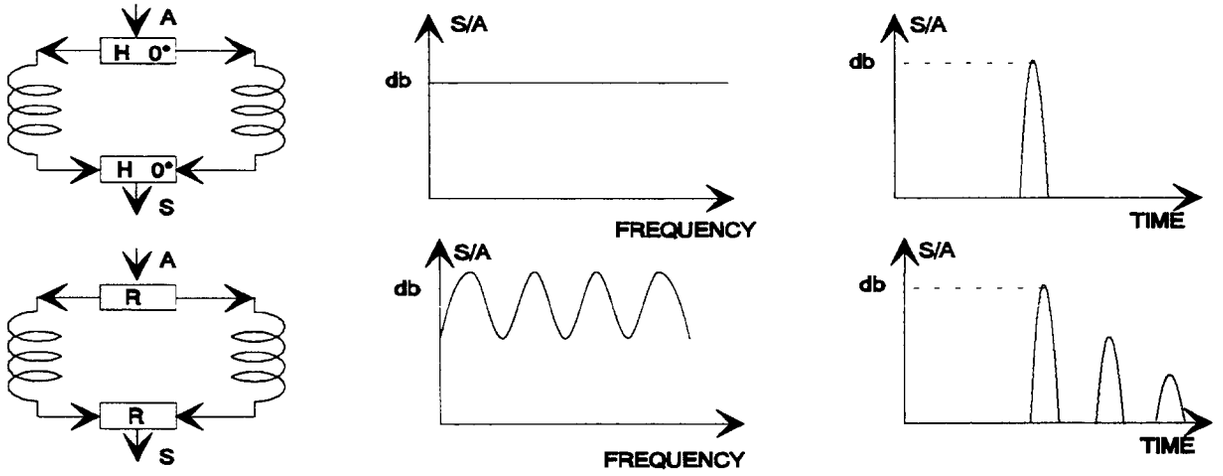

Fig. 4 - Effect of the resistive and hybrid power combiner/splitter

As already mentioned, there is a strong interest to increase the notch filter slopes' steepness, in particular for small $\Delta p/p$. Apart from using peak-filters one can set the periodicity of the notch filter to 1/2 or 1/3, which means that only every second or third notch coincides with a longitudinal Schottky band.

Even when taking into account all the improvements already mentioned, the high-energy LEAR beam fills only 1/10 of the notch width because of its very small η (η = 0.25 at 2000 MeV/c). The use of double and triple notches has significantly increased the cooling speed. It turned out to be very important in this operating condition to maintain steepness, periodicity and depth of the notches to avoid any unnecessary heating of the off-momentum particles.

3.3 Low-Momentum Systems

The low-momentum cooling systems operate at 105 MeV/c and 61 MeV/c. Pick-ups for both the longitudinal and horizontal systems are situated in the BHN 40 bending magnet, with kickers at KCM 21 and KCH 23 (Fig. 2). Similar to the high-energy pick-ups, 12 pick-up plate pairs are also in use here, connected to form a travelling wave structure with delays adapted to 105 and 61 MeV/c, respectively. To increase the signal-to-noise ratio, the termination resistors (50 Ω) are cooled to 20 K in a cryostat and the head amplifiers areoperating at 80 K physical temperature, so that a noise figure below 0.9 dB between 10 MHz and 150 MHz is obtained. There would not be much gain in total signal/noise performance by further reducing the noise figure of the head amplifier to about 0.5 dB. This is because the noise temperature of the pick-up itself (about 1 dB loss, ambient temperature) amounts already roughly to 70 K. It should be mentioned that other types of pick-up structures [3] have been tested, such as the helical and a printed meander pick-up, however with moderate sucess. Another serious problem has been noticed several years ago when interference occurred, linked to the presence of the PS beam. The PS radiates the revolution harmonics in the low MHz range because the skin depth in stainless steel is approaching the material thickness of the PS vacuum chamber. Also, the rf-bypass capacitors foreseen to short-circuit (rf-wise) the dc-isolated sections of the PS-vacuum chamber become less effective at these lower frequencies. It was found that the magnetic-field components of this leakage enter the head amplifiers through the power supply cables and lead to an intermodulation with the stochastic cooling signals. Proper shielding and filtering (cryogenic-compatible components) on this part of the amplifier chain have completely

solved the problem. New connectors and vacuum feedthroughs for the cryogenic part (50 Ω resistors, head amplifiers) are at present under construction to simplify mounting and dismantling and to improve the reliability of the contacts.

The longitudinal system uses two different types of notch filter: a conventional one, with coaxial cables and dispersion (loss) compensation is applied for 105 MeV/c; a unique digital filter consisting basically of fast AD converters followed by a digital memory and a DA converter, is applied for the 61 MeV/c range [4].

Pick-up signals from the travelling wave loop couplers with switchable delays outside vacuum (105 MeV/c) are digitized with a fast 200 Megasample 8 bit ADC. The digitized data are transferred through latches into 4 RAMs (random access memory). After storage in the RAMs for the required delay time (adjustable from 50 ns to 1280 ns) the data are read and sent to a fast DAC (500 MHz) for analogue conversion. The subtraction between delayed path and reference path takes place in a broad-band analogue hybrid (180° combiner).

The low-momentum vertical cooling has 5 pairs of coupling loops and the same types of amplifiers and terminations (cryo-pot) as the horizontal system in BHZ 40. Here also, the delays can be dialled for 61 and 105 MeV/c. Kicker signals at KCV 34 can be monitored like on the kicker KCH 23, for proper power settings and intermodulation checks.

4. PERFORMANCE

At high momenta (1 to 2 GeV/c), the stochastic cooling is used in two cases:

1. to retrieve the particles which diffused to lower momenta during the stochastic extraction process, mainly when the extraction time is very long (2 or 3 hours),
2. to get very good beam quality during operation with the Jetset experiment. A hydrogen Jet target of a density of 10^{13} atoms/cm^2 is used and a high number (3×10^{10} to 5×10^{10}) of circulating particles is needed. Then the beam characteristics must be as follows: vertical emittance $<3\pi$ mm·mrad such that the vertical beam dimension at the jet position is smaller than the jet itself (5 mm FWHM), small horizontal emittance ($\sim 3\pi$ mm·mrad) for a good vertex definition of the nuclear reaction, momentum spread <0.2% at 4π mm·mrad) for a good momentum resolution. These objectives are generally obtained despite the complexity of the operation, where at least one new momentum/day is required by the physicists.

At low momenta (105 to 609 MeV/c) the stochastic cooling has two main goals:

1. to reduce the beam dimensions before deceleration and to compensate the adiabatic emittance increase due to the deceleration. This is still applied for the injection momentum (609 MeV/c) but the electron cooling is used for momenta ≤ 309 MeV/c.
2. to counteract diffusion mechanisms such as intrabeam scattering during the slow extraction process. The need of high fluxes of particles by the experiments and the use of long spills (1 h) necessitate circulating beams of 5×10^{10} to 9×10^{10} particles. In these cases intrabeam scattering becomes important and has to be compensated by stochastic cooling. Transverse emittances of 5π mm·mrad are measured while the momentum spread is maintained below 0.3% at 4π mm·mrad.

5. CONCLUSIONS

The LEAR stochastic cooling systems have undergone several modifications and improvements over the years. Thanks to progress in technologies, better wide-band power amplifiers, the use of BAW (bulk acoustic wave) filters, and printed pick-up and kicker structures, may be considered for the future. For the time being it can be stated that globally speaking all the LEAR stochastic cooling systems work satisfactorily and are reliable. The implementation of further upgrades depends largely on the approval of new experiments and on the extension of the presently scheduled physics antiproton programme.

ACKNOWLEDGEMENTS

The authors would like to thank D. Möhl for numerous fruitful discussions, S. Maury for continuous support and A. Molat-Berbiers for typing and editing the manuscript.

REFERENCES

[1] G. Carron, J.C. Perrier and L. Thorndahl, *Status and future possibilities of the stochastic cooling system for LEAR*, Proc. of the LEAR Workshop, Tignes 1986, pp. 121-127.

[2] J.C. Perrier, *Le refroidissement stochastique de LEAR*, PS/AR Note 91-12, 1991.

[3] N. Tokuda, *Formulation of a flat-helix coupler for a pick-up of a low velocity beam*, CERN PS/LEA/Int. Note 87-05, March 1987.

[4] M. Chanel, R. Maccaferri and J.C. Perrier, *Momentum stochastic cooling with digital notches*, Proc. of the 2nd European Particle Accelerator Conference, Nice 1990, pp. 1574-1576.

THE BEAM COOLING SYSTEM OF THE ADRIA PROPOSAL

A. Dainelli,
Laboratori Nazionali di Legnaro-INFN, Legnaro, Italy

A. G. Ruggiero
Brookhaven National Laboratory, Upton (NY)

L. Tecchio
University of Torino and INFN, Torino, Italy

ABSTRACT

To define long term projects of the Laboratori Nazionali di Legnaro a proposal for a heavy ion accelerator complex has been worked out during the last three years. Such a complex, called ADRIA, is mainly foreseen for the acceleration of heavy ions to kinetic energies of about 1 GeV/u; the high energy primary beam can be used either for an experimental programme at relativistic energies or for production of Radioactive Nuclear Beams via a Projectile Fragmentation Method. The unstable nuclei are produced in a thin target and collected, after proper selection, in a Decelerator ring where they are decelerated down to 10 ÷ 20 MeV/u in order to be used in nuclear experiments around the Coulomb Barrier. To obtain the beam quality required by nuclear physics experiments a very powerful beam cooling system is mandatory and some of the general parameters are described in this contribution.

1. INTRODUCTION

In the last three years, with the collaboration of a large international community of accelerator experts, a proposal has been worked out for the construction of an accelerator complex capable to accelerate heavy ions up to the GeV/u region of specific kinetic energy with intensities in the range of 10^{12} ions/s [1,2,3].

The accelerator complex has been designed essentially for the production of Radioactive Nuclear Beams to be used in nuclear physics experiments at specific kinetic energies of about 10 ÷ 20 MeV/u. The unstable nuclei are produced by means of the Projectile Fragmentation (PF) method where the primary beam, the 1 GeV/u heavy ion beam, hits a thin target located in a dedicated area downstream the extraction channel of the Booster ring. After the production, the unstable nuclei are selected in a proper spectrometer, the Isotope Separation Line, and then injected in a Decelerator ring where they have to be stacked and cooled before the starting of the deceleration cycle. In particular the cooling requirements in the Decelerator ring are perhaps the most demanding in compairison with nowdays machines. The RNB currents delivered by the ADRIA Complex with the PF method are foreseen in the range of 10^8 ÷ 10^9 ions/s.

2. THE ADRIA PROPOSAL

In the ADRIA Complex the primary beam of heavvy ions is produced by the sequence of accelerators schematically shown in Fig. 1. The main components of the ADRIA Complex are the following:

1. a Heavvy Ion Injector (the XTU Tandem and the ALPI post-accelerator)
2. a Fast Cycling Synchrotron (the Booster ring)
3. a Slow Cycling Synchrotron (the Decelerator ring)
4. an Isotope Separation Line (connecting the two rings)
5. an Experimental Area.

The Heavvy Ion Injector is made of a Van de Graaff tandem (XTU) and a superconducting post-accelerator (ALPI). The Van de Graaff tandem can operate with a terminal voltage of 16 MV and it is able to accelerate all the ion species up to lead. The XTU tandem is fed by an ion sputter source which, working as the ADRIA injector, is pulsed at 10 Hz with a pulse width of about 300 μs and a peak current of about 200 μA according to different ion species[4].

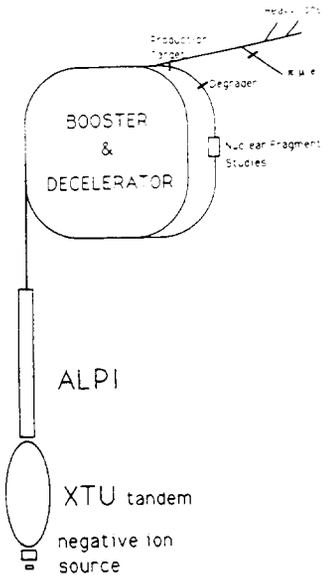

Fig. 1 : Schematics of the ADRIA Complex

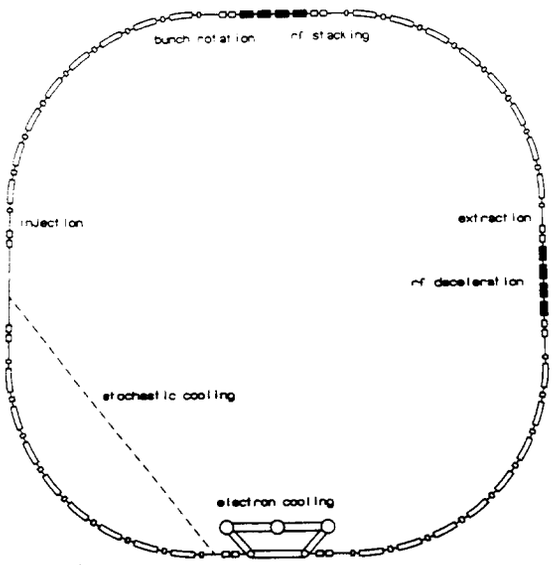

Fig. 2 Decelerator layout and arrangement

The ALPI post-accelerator [5], which is now under commissioning, is a machine made of a sequence of independently phased superconducting Quarter Wave Resonators [6] made in part of copper electroplated with lead and in part of bulk niobium [7]. The large velocity variation along the linac requires the use of different sections with specialized cavities. The low-β section at the injection of ALPI consists of 24 cavities in bulk niobium ($\beta_{opt} = 0.055$) operating at 80 MHz; the medium-β section is made of 48 copper plated cavities with $\beta_{opt} = 0.11$ working at 160 MHz which is also the working frequency of the high-β section made of 21 copper plated cavities with $\beta_{opt} = 0.15$. The average accelerating field is about 3 MV/m and the total dissipated power per cavity is around 6 W. The energy gain per cavity is about 0.5 MeV per unit charge. The time sub-structure of the beam is determined by a double-drift buncher located at the XTU entrance with a working frequency of 5 MHz [8].

The two synchrotrons (Booster and Decelerator) have the same shape and circumference, similar lattices and the same rigidity (22.25 Tm). The general parameters of the two rings are shown in Table 1. The circumference of the Booster has been chosen to correspond to the injection of 45 bunches of gold ions per turn. A "painting " procedure is applied during the multi-turn injection to fill uniformly the rf buckets. At the end of the multi-turn injection process, about $5 \cdot 10^{10}$ ions are injected. The 10 Hz repetition rate of the acceleration cycle gives the beam intensity listed in Table 2.

Table 1 : General lattice parameters of the rings

Maximum Magnetic Rigidity		22.25	Tm
Circumference		266.67	m
Bending Radius		17.62	m
Maximum Dipole Field		1.26	T
Dipole Vertical Gap		10	cm
Maximum Quadrupole Gradient		9	T/m
Quadrupole Bore Radius		7	cm
Superperiodicity		4	
Transition Energy (γ_t)		4.6	
Betatron tunes:			
Horizontal plane	ν_h	5.8	
Vertical plane	ν_v	3.8	
Natural Chromaticity :			
Horizontal plane	ξ_h	- 5.5	
Vertical plane	ξ_v	- 4.9	

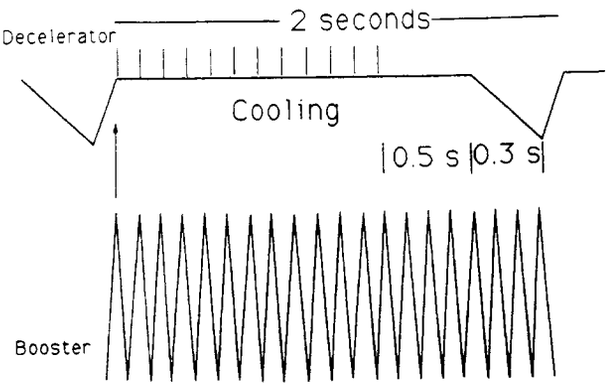

Fig. 3 : Magnetic Cycle of the ADRIA Complex

At the end of the acceleration cycle the beam can be extracted and sent toward a thin target to produce beams of exotic nuclei. The unstable nuclei produced at the target maintain almost the same longitudinal momentum per unit mass of the incident ions but they acquire a higher transverse momentum because of the fragmentation process. The exotic nuclei are then collected in the Isotope Separation Line (ISL) where they are selected first in magnetic rigidity and then in electric charge following the principle of the "momentum loss achromat" [9-10]. The transverse acceptance of the ISL has been set to 40 π mm-mrad and the momentum acceptance to 2%. The expected yeld of the ISL is of the order of 10^{-3} fragments per impinging primary ion which gives 10^{8}÷10^{9} exotic fragments per second of the desired species with assigned mass number A and atomic number Z.

The bunches of exotic fragments are then injected into the Decelerator ring where they are captured by a rf system, rotated in the longitudinal phase space [11] to reduce the momentum spread to 0.1% and displaced by an additional rf system to an off-momentum trajectory to allow stacking of twelve subsequent pulses, every 100 ms, from the Booster (Fig. 3) . During the stacking of the twelve pulses electron cooling is applied to reduce by an order of magnitude the beam momentum spread and the transverse dimension of the debunched beam. After the injection of the last pulse the electron cooling continues for additional 0.5 s together with the stochastic cooling. After the cooling process the exotic ion beam is captured by a new rf system which decelerates the ions to the specific energies required for nuclear studies around the Coulomb Barrier (10 MeV/u). The deceleration lasts 0.3 s. At the end of the cycle the beam is extracted and sent to the experimental area.

Table 2 : General Parameters of heavy ion acceleration.

	S	Cu	I	Au	U	
Atomic Number Z	16	29	53	79	92	
Mass Number A	32	63	127	197	238	u
Charge State Q	16	27	40	51	54	
Injection Kinetic Energy	16.4	10.4	6.1	4.6	3.9	MeV/u
Extraction Kinetic Energy	2.53	2.08	1.37	1.03	0.85	GeV/u
Harmonic Number	24	30	39	45	49	
Beam Intensity	2.0	1.3	0.7	0.5	0.5	10^{12} ions/s
Normalized Emittance	23	18	14	12	11	π mm-mrad
Bunch Area	0.017	0.011	0.007	0.005	0.005	eV-s/u

Table 3 : General Parameters for fragment production.

Target Thickness	1	g/cm^2
β^* @ Target	1	m
Angular Acceptance (full)	7.5	mrad
Momentum Acceptance (full)	0.7	%
No. of Booster pulses/cycle	12	
Minimum Cycle Period	2	s
Bunch Length (rms)	0.5	ns

	S	Cu	I	Au	U	
Mass Number A	32	63	127	197	238	u
Atomic Number Z	16	29	53	79	92	
No. of Fragments/s	$4.0 \cdot 10^9$	$1.6 \cdot 10^9$	$5.0 \cdot 10^8$	$1.5 \cdot 10^8$	$1.5 \cdot 10^8$	
Momentum Spread (rms)	0.09	0.11	0.2	0.28	0.38	%
Angular Spread (rms)	3.2	3.7	5.0	5.8	7.3	mrad
Harmonic Number	24	30	39	45	49	
Initial Emittance			20			π mm-mrad
Final Emittance			1			π mm-mrad
Final Momentum Spread			0.01			%

Table 4 : Parameters of the Deceleration ramp

	S	Cu	I	Au	U	
Harmonic No	24	30	39	45	49	
Bunch Area (rms)	0.0073	0.0062	0.0043	0.0034	0.0029	eV-s/u
Normalized Emittance	12.8	10.5	7.9	6.7	6.0	π mm-mrad
Top of the Cycle						
Kinetic Energy	2.53	2.08	1.37	1.03	0.85	GeV/u
β	0.963	0.951	0.914	0.880	0.852	
Magnetic Field	1.263	1.176	0.953	0.815	0.741	T
RF Frequency	25.99	32.07	40.09	44.53	46.91	MHz
Emittance	3.56	3.43	3.50	3.59	3.68	π mm-mrad
Bottom of the Cycle						
Kinetic Energy	16.45	10.43	6.13	4.59	3.87	MeV/u
β	0.186	0.148	0.114	0.099	0.091	
Magnetic Field	0.0665	0.0574	0.0485	0.0437	0.0416	T
RF Frequency	5.0	5.0	5.0	5.0	5.0	MHz
Emittance	67.6	70.1	68.7	67.0	65.4	π mm-mrad

3. COOLING REQUIREMENTS

The momentum spread of the exotic fragments after the injection in the Decelerator ring have to be continuously reduced to allow enough phase space for the subsequent pulses injected during accumulation process. Furthermore the beam momentum spread have to be sufficiently small at the end of accumulation to allow the capture in an rf bucket with a reasonable voltage.
Finally, because of the deceleration ramp, the beam momentum changes by a factor of ten and therefore the momentum spread and the betatron emittance will increase by the same factor. The most demanding requirements for cooling are imposed by the accumulation process where the momentum spread is increased of 0.2% every 100 ms due to the new pulse on the stack. Asking for an overall cooling time of 150 ms, the average momentum spread of the stack is maintained during the accumulation procedure to 0.3%. To achieve the required cooling rate, both electron cooling and stochastic cooling are required. With a second cooling period of 0.5 s, following the stacking, at the same cooling rate, the total momentum spread is finally reduced $1 \cdot 10^{-4}$.

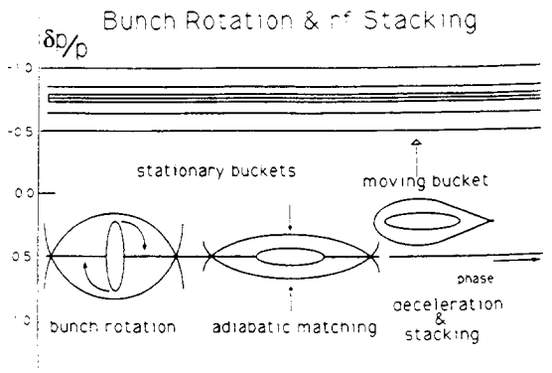

Fig. 5 : The momentum aperture of the Decelerator ring

4. THE ELECTRON COOLING SYSTEM

The design of the electron cooling system of the ADRIA proposal is based on a classical formula from which extimations of the cooling rate has been derived for different ions [12] :

$$\lambda = \frac{4\pi Q^2 2 r_e r_p L \eta (J / e)}{A \beta^4 \gamma^5 \theta^3}$$

r_e and r_p are the electron and proton classical radius; Q is the ion charge state and A the ion mass number; L is the Coulomb Logarithm, η the ratio of the electron beam length to the machine circumference, β and γ are the usual relativistic factors, J is the electron beam density ($J = I/(\pi a^2)$) and θ is the square root of the quadratic sum of the ion temperature θ_{ion} (relative velocity spread) and of the electron temperature θ_{el} ; this two temperatures are also the square root of a quadratic sum of transverse θ_{tr} and longitudinal θ_{long} components. The contribution θ_{long} is related to the momentum spread ($(1/\gamma)$ $(\delta p/p)$) while the contribution θ_{tr} is related to the ratio of the beam emittance and the beta function at the center of the interaction region (ε / β^*). In Tab. 5 the fundamental numbers for an electron cooling system capable of reducing the total momentum spread down to 0.01% in about 0.3 seconds has been reported for a 200 atomic mass number ion. The most striking parameter is the electron kinetic energy of 550 keV which is the the largest so far conceived for this kind of devices. Furthermore the high kinetic energy of the electrons and the need of fast cooling implies a continuous power of about 7 MW. To operate such demanding system it is mandatory the use of a very efficient recovery apparatus with an efficiency better than 99%; such a system has been already developed and tested at Legnaro [13].

Table 5 : Electron Cooling Parameters

Specific Kinetic Energy	1.0	GeV/u
β	0.8	
Mass number	200	
Charge State	80	
Transverse Beam emittance (rms)	3.2	π mm mrad
Momentum spread (rms)	0.047	%
β^* (h, v)	17, 6	m
Length of electron beam	8	m
Coulomb log	20	
Beam Radius	10	mm
e-beam current	12.5	A
e-beam current density	4	A/cm^2
ϑ, total	1.3	mrad
Cooling time	0.3	s
e-beam energy	0.55	keV
e-beam power	6.9	MW
Energy Recover Efficiency	99	%
Final Momentum spread (rms)	$\pm$0.0017	%

5. THE STOCHASTIC COOLING SYSTEM

As already reported above, both cooling system are designed to give a cooling time of 0.3 s. The components for stochastic cooling are shown in a schematic way in Fig. 2. The Shottky signal is detected by pick-up's made of pair of strip-lines located in a zero dispersion region; the signal is amplified and filtered through a "notch filter".
The frequency bandwidth of the electronic system which is chosen to optimize the "mixing" of the particle sample between pick-up's and kickers has been chosen around 1+2 GHz in order to obtain overlapping between neighboring bands at the upper end of the Shottky band.
The main parameters of the stochastic cooling are given in Tab. 6 ; the 1 kW total power required is mainly due to the Shottky signal after amplification; thermal power due to thermal noise at the exit of the pick-up's is low and of no consequences to the cooling performance.

Table 6: Stochastic Cooling Parameters

Total number of ions	$5 \cdot 10^7$	
Mass Number	200	u
Charge State	80	
Specific Kinetic Energy	1.0	GeV/u
β relativistic factor	0.8	
Bandwith	1+2	GHz
Method	Notch Filter	
No of Pick-up's	16	
No of kickers	32	
Skottky Power (initial)	1.0	kW
Thermal Power	negligible	
Amplifier Gain	160	dB

REFERENCES

[1] " Feasibility Study of a Hadron Facility, Conceptual Design Report", LNL-INFN (REP) 57/92, February 1992.

[2] A. Dainelli, A. Lombardi, A. Ratti, A. G. Ruggiero, Proceedings of the 1991 IEEE Particle Accelerator Conference, San Francisco (CA), May 6-9 1991, pag 2820-2822.

[3] 'The ADRIA Proposal", LNL-INFN (REP) 58/92, March 1992.

[4] P. Thieberger *et al.*, Nucl. Instr. and Meth. A-268 (1988) 513-521.

[5] G. Fortuna *et al.*, Proc. of the Third European Particle Accelerator Conf., Berlin, 24-28 March 1992, pagg. 1085-1087.

[6] I. Ben-Zvi and J. M. Brennan, Nucl. Instr. and Meth. 36 (1976) 421.

[7] A. Facco, J. S. Sokolowsky and B. Elkonin, Proc. of the Third European Particle Accelerator Conf., Berlin, 24-28 March 1992, pagg. 1266-1268.

[8] A. Facco et al., Proc. of the Third European Particle Accelerator Conf., Berlin, 24-28 March 1992, pagg. 1507-1509.

[9] G. Shatz *et al.*, Hyp. Int. 34 (1987) 555.

[10] J. P. Dufour et al., Nucl. Instr. and Meth. A-248 (1976) 267-281.

[11] J. Griffin *et al.*, IEEE tr. on Nucl. Sc., NS-30, no. 4, August 1983.

[12] T. Ogino and A. G. Ruggiero, Particle Accelerators 10 (1980) 197-205.

[13] L. Busso *et al.*, "An electron Cooling Device in the One MeV Energy Region", Proc. of the XIII International Conference on High Energy Accelerators, Novosibirsk 6-13 August 1986, Ed. A. N Skrinsky, Publ. House Nauka 1987 (344).

DERIVATION OF A FOKKER-PLANCK EQUATION FOR BUNCHED BEAMS *

Alessandro G. Ruggiero
Brookhaven National Laboratory
PO Box 5000, Upton, N.Y. 11973

ABSTRACT

This report investigates the derivation of the Fokker-Planck equation which is used to evaluate the evolution with time of an ensemble of particles under the effect of external rf forces, cooling and forces of stochastic nature. The conventional approach based on the classical work by Chandrasekhar is first outline: here the phase angle and the momentum error of the particles are used. The method is then extended to the case the distribution function is expressed in terms of the amplitude of motion. To avoid a singularity behavior, the new Fokker-Planck equation is obtained with an averaging process over the phase distribution instead of the time-averaging. The beam lifetime in the presence of the separatrix of the rf buckets is determined. Finally, the numerical estimates apply to the Relativistic Heavy Ion Collider (RHIC).

1. INTRODUCTION

The method for solving a stochastic differential equation, that is a Langevin equation [1], requires that some conditions are satisfied: the fluctuations have to take both positive and negative values, and the distribution of the errors is a Maxwell-Boltzmann distribution. An important problem is the case of a bunched beam of electrically charged particles circulating in a storage ring. The motion of the particles is determined by the presence of external rf forces, stochastic cooling and particle-particle interaction. An important issue is the determination of the beam lifetime due to the presence of an aperture limitation, like the separatrix of the rf buckets.

In the case of bunched beams, the distribution changes over periods of time considerably longer than a synchrotron oscillation period. In this case, it is desired to develop a transport equation which involves only the distribution of the amplitude of the particle motion. This creates some difficulties since with the new variable the requirements above are no longer satisfied. In previous work [2-5] a Fokker-Planck equation was derived by performing a time-averaging over synchrotron oscillation periods. Unfortunately this operation introduces a singularity; in correspondence of the separatrix, the synchrotron oscillation period diverges violating the averaging procedure itself. We propose here an approach which takes the Fokker-Planck equation in the original variables and transforms it to the one in terms of the amplitude variable. Moreover, the time average is replaced by an average over the phase distribution, avoiding the singularity.

2. CHANDRASEKHAR'S APPROACH TO LANGEVIN EQUATION

The longitudinal component of the motion of a charged particle in a storage ring is described by the rf phase angle ϕ and the angular momentum w, related to the energy error ΔE by $w = \Delta E / h\omega_0$ where ω_0 is the angular revolution frequency and h the rf harmonic number. In absence of external rf forces, stochastic cooling and intrabeam scattering, the equations of motion are

$$d\phi / dt = aw \tag{1}$$

$$dw / dt = 0 \tag{2}$$

where $a = \eta \omega_0^2 h^2 / \beta^2 E$ with E the total energy of the particle, β, γ the relativistic velocity and energy factors, γ_t the value of the transition energy and $\eta = \gamma_t^{-2} - \gamma^{-2}$. Below we shall assume $\gamma > \gamma_t$, that is the case above the transition energy, in which case both η and a are positive.

* Work performed under the auspices of the U.S. Department of Energy

When stochastic cooling and intrabeam scattering are included, the second equation is modified yielding the Langevin equation

$$d\,w / d\,t \;=\; -\lambda\, w \;+\; D\,A(t) \tag{3}$$

where λ is the cooling rate and D the diffusion parameter. A(t) is a dimensionless, time-dependent stochastic function which changes rapidly and discontinuously. The method for solving this equation is discussed in the work by Chandrasekhar [1] which we review briefly here.

Let Δt be a time sample short enough, during which the angular momentum w does not vary appreciably, and large enough to include a large number of fluctuations of the stochastic function A(t). Eq. (3) can then be formally integrated as follows

$$\Delta w \;=\; -\lambda\, w\, \Delta t \;+\; D\,B(t) \tag{4}$$

where

$$B(t) \;=\; \int_t^{t+\Delta t} A(t)\, dt \tag{5}$$

represents the net change of w which a particle may suffer during an interval of time Δt around the instant t. This parameter is subject to statistical fluctuations described by a probability distribution function given by the following Maxwell-Boltzmann equation

$$\psi(\, B[\Delta t]\,) \;=\; exp\,(\, -\, |B(\Delta t)|^2 / 4q\Delta t\,) \,/\, (4\pi\, q\, \Delta t\,)^{1/2} \tag{6}$$

where q is a parameter which defines the width of the equilibrium distribution and is related directly to the cooling rate λ and the diffusion parameter D.

The solution of the Langevin equation (3) can be described by the distribution function W(w, t) of the probability of finding the value w at the time t. With Eqs. (4) and (6) holding, it can be proven that the distribution function satisfies the following Fokker-Planck equation

$$\partial\, W / \partial\, t \;=\; \partial\,(\lambda\, w\, W) / \partial\, w \;+\; \partial^2\,(\, qW\,) / \partial\, w^2 \tag{7}$$

which in the limit $t \rightarrow \infty$ has the solution

$$W(\, w\,) \;=\; exp\,(\, -\lambda w^2 / 2q\,) \,/\, (2\pi\, q / \lambda)^{1/2} \tag{8}$$

Define the rms width δ^2 as follows

$$\delta^2 \;=\; \int_{-\infty}^{+\infty} w^2\, W(w)\, dw \tag{9}$$

The corresponding equation is obtained by multiplying both sides of the Fokker-Planck equation (7) by w^2 and integrating over the entire range of w from $-\infty$ to $+\infty$. One finds

$$d\,\delta^2 \,/\, d\,t \;=\; -\,2\,\lambda\,\delta^2 \;+\; 2\,q \tag{10}$$

which in the limit $t \rightarrow \infty$ converges to $\delta_\infty^{\,2} = q / \lambda$ in agreement with Eq. (8). Eq. (10) should be compared with the original Eq. (3). It is seen that q replaces D. It is the proper diffusion coefficient defined as the average increase of w^2 per unit of time.

It is also possible to include an external restoring force which modifies Eq.(3) as follows

$$d\,w / d\,t \;=\; -\lambda\, w \;-\; b\, sin\,\phi \;+\; D\,A(t) \tag{11}$$

where, for the case of non-accelerating, stationary rf buckets, $b = Qe\,V / 2\,\pi\,h\,A$ with Q the charge state, A the mass number of the particle and V the peak rf voltage. Introducing the distribution function $W = W(\,\phi, w, t\,)$, the Fokker-Planck equation modifies as follows

$$\partial W / \partial t + a w \partial W / \partial \phi - b \sin \phi \partial W / \partial w = \partial (\lambda w W) / \partial w + \partial^2 (qW) / \partial w^2 \quad (12)$$

which is the generalization of the Liouville's theorem according to Chandrasekhar [1]. It can be expected that the cooling rate λ and the diffusion coefficient proper q have also a dependence on the azimuthal angle ϕ, since they may depend on the actual location of a test particle within the bunch.

3. TRANSFORMATION TO ANGLE-ACTION VARIABLES

The unperturbed equations of motion in the presence of the external rf forces

$$d\phi / dt = a w \quad (13)$$

$$dw / dt = - b \sin \phi \quad (14)$$

can be derived from the Hamiltonian

$$H = a w^2 / 2 + 2 b \sin^2 \phi / 2 \quad (15)$$

Since the Hamiltonian does not depend explicitly on time, it is more convenient to operate a canonical transformation from the pair of variables (ϕ, w) to the pair (Q, J) also of canonically conjugated variables, through the generating function

$$S = S(\phi, J) = \int^{\phi} dx \sqrt{(2/a)[J - 2 b \sin^2 (x/2)]} \quad (16)$$

The variable J is identified with the Hamiltonian itself, that is J = H, and

$$Q = \partial S / \partial J = \int^{\phi} dx \{ (2a)[J - 2 b \sin^2 (x/2)] \}^{-1/2} \quad (17)$$

Q is the time required to travel around the trajectory of amplitude J. The variable J is a non-negative quantity which takes the value zero in correspondence to the center of the beam bunch and increases in value with increasing trajectory size until it reaches the value $J_s = 2b$ in correspondence of the separatrix. The motion beyond the separatrix is unstable.

4. FOKKER-PLANCK EQUATION IN THE ACTION VARIABLE

It is desirable to express the Fokker-Planck equation (12) in terms of the new transformed variables Q and J through a probability distribution function W(Q, J, t). Since J is a non-negative quantity, and its statistical fluctuations do not satisfy the Maxwell-Boltzmann distribution (6), one cannot derive the corresponding Fokker-Planck equation *ab initio* as done for the distribution W (ϕ, w, t). We propose here the following approach.

The phase oscillation period $T_o = 2\pi / (a b)^{1/2}$ in the center of the bunch is considerably larger than the sampling time Δt. Moreover, the effects due to stochastic cooling and intrabeam scattering evolve over periods of time that are both longer than T_o. Therefore it is reasonable to assume that the bunch distribution is continuously matched to the shape of the trajectories in the (ϕ ,w)-phase plane and that the distribution function depends explicitly only on J, that is W = W(J, t). This simplifies considerably the left-hand side of Eq. (12) since

$$a w \partial W / \partial \phi - b \sin \phi \partial W / \partial w = 0 \quad (18)$$

The right-hand side of Eq. (12) can also be readily transformed in terms of the variable J. The two quantities λ and q may include a dependence on ϕ. Their values have at very most a factor of 2 difference between the center of the bunch and the outer edge where particles sweep through the center twice each phase oscillation. Thus, it is a good approximation to replace λ and q with about half the peak value they take at $\phi = 0$. Finally the differential operator $\partial / \partial w$ can be easily transformed to the operator $\partial / \partial J$.

$$\partial (\lambda w W) / \partial w \sim \lambda W + \lambda \langle a w^2 \rangle (\partial W / \partial J) \quad (19)$$

$$\partial^2 (q W) / \partial w^2 \sim q a (\partial W / \partial J) + q a \langle a w^2 \rangle (\partial^2 W / \partial J^2) \quad (20)$$

In conclusion, replacing $\langle aw^2 \rangle$ with J itself,

$$\partial W / \partial t = \partial \{ J [\lambda W + \partial (qa W) / \partial J] \} / \partial J \tag{21}$$

Eq. (21) involves only coherent and stochastic variation ΔJ with Δt through the cooling rate λ and the diffusion coefficient proper q. The nature of the physical problem being investigated does not require introducing the average variation of $\langle \Delta J^2 \rangle$ over Δt.

In the limit $t \rightarrow \infty$ Eq. (21) exhibits the following equilibrium distribution

$$W(J) = exp (- J / \bar{J}_\infty) / \bar{J}_\infty \tag{22}$$

where $\bar{J}_\infty = q a / \lambda$ is the median value of the distribution at the equilibrium. We can also define the average

$$\bar{J} = \int_0^\infty J W(J, t) dJ \tag{23}$$

The equation for $\bar{J}$ is obtained by multiplying both sides of Eq. (22) by J and integrating over J

$$d\bar{J} / dt = - \lambda \bar{J} + q a \tag{24}$$

which exhibits the asymptotic value $\bar{J} = \bar{J}_\infty$ in agreement with Eqs. (22). Furthermore, reminding the relation between J and w, it is seen that Eq. (24) can be identified with Eq. (10), and that both equations yield the same equilibrium value for the width of the distribution.

5. INTEGRATION OF THE FOKKER-PLANCK EQUATION. BEAM LIFETIME.

The Fokker-Planck equation (21) is solved by assigning an initial distribution W(J) and integrating by requiring that at the separatrix $W(J = J_s) = 0$ at all times. We give below an analytical solution of Eq. (21) as the sum over fundamental modes,

$$W(J, t) = \Sigma_s C_s exp (-\beta_s t) U_s (J) \tag{25}$$

where C_s and β_s are integration constants that describe the fundamental modes and the initial distribution. The eigenmodes are described by the function $U_s (J)$ which is chosen to satisfy the boundary condition $U_s (J_s) = 0$

Inserting the series expansion Eq. (25) in the Fokker-Planck Eq. (21) gives the following equation for the eigenfunction $U_s (J)$

$$\alpha J d^2 U_s / dJ^2 + (J + \alpha) dU_s / dJ + (1 + f_s) U_s = 0 \tag{26}$$

where $\alpha = q a / \lambda$ and $f_s = \beta_s / \lambda$. Eq. (26) is Kummer's equation [6] which has as independent solutions the two Kummer's functions *M* and *U*, of which though only the first can be accepted since the second has a singularity behavior at the origin J = 0. Thus

$$U_s (J) = M(- f_s, 1, J / \alpha) exp(- J / \alpha) \tag{27}$$

The Kummer's function *M* has the s-th positive zero which in good approximation [6] is given by

$$x_s = \pi^2 (s - 1/4)^2 / (2 + 4 f_s) \tag{28}$$

The eigenmodes are determined by imposing the boundary condition $U_s (J_s) = 0$, that is

$$\beta_s = \pi^2 q a (s - 1/4)^2 / (4 J_s) - \lambda / 2 \tag{29}$$

After an initial period of time where the distribution evolves and reaches the separatrix of the rf buckets, the overall behavior is essentially determined by the lowest eigenmode corresponding to s = 1, since all the other modes will have in the meantime decayed very fast. Correspondingly the beam lifetime τ_{b0} itself can be identified with the inverse of the growth rate β_1, that is

$$\tau_{b0} = 128\, b / (9\, \pi^2\, q\, a) \tag{30}$$

This is verified by the numerical integration of the Fokker-Planck equation itself that in absence of cooling can also be written as

$$\partial W / \partial \tau = \partial W / \partial u + u\, \partial^2 W / \partial u^2 \tag{31}$$

where $u = J / J_s$, $\tau = t / T_s$ and $T_s = 2\, b / q\, a$. The result of the numerical integration [7] with the condition $W(1) = 0$ shows that the beam lifetime is about $0.7\, T_s$, in agreement with Eq. (30).

If stochastic cooling is added at the rate λ, a reasonable criterion is to adjust the cooling rate so to obtain the required beam width J_∞. In this case the beam lifetime, which we shall denote τ_{bc}, is in good approximation,

$$\tau_{bc} = \tau_{b0} / (1 - 0.36\, J_s / J_\infty) \tag{32}$$

If the cooling rate is adjusted so that $J_\infty > 0.36\, J_s$, the diffusion process will dominate resulting in a lowering and widening of the distribution and of beam particle loss at the rate given by τ_{bc}^{-1}. If on the contrary $J_\infty < 0.36\, J_s$, the cooling process will dominate, causing an increase and narrowing of the distribution at the rate $| \tau_{bc} |^{-1}$. In this case the lifetime is infinite. This case is also verified [7] by the numerical integration of the Fokker-Planck equation that can also be written as follows

$$\partial W / \partial \tau = W + (u + \alpha)\, \partial W / \partial u + \alpha\, u\, \partial^2 W / \partial u^2 \tag{33}$$

where now $\alpha = J_\infty / J_s$ and $\tau = \lambda\, t$. The optimum from the beam lifetime point of view is obtained by letting $\beta_1 = 0$, that is by setting the cooling rate so that $J_\infty = 0.32\, J_s = 0.64\, b$ which requires $\lambda = 1.56\, q\, a / b$.

6. APPLICATION TO RHIC

The performance of the Relativistic Heavy Ion Collider [8] is greatly influenced by the phenomenon of Intrabeam Scattering. This phenomenon nevertheless evolves over very long periods of time, involving several synchrotron oscillations before an appreciable effect of the beam can be noticed. Similarly, stochastic cooling of the bunched beam can be added but also with comparatively long cooling periods. In this mode of operation, the diffusion effects due to both Schottky and thermal noise can be neglected with respect to the stochastic effects of the particle-particle scattering [4]. Thus the all process can very well be described only by the cooling rate λ and the diffusion rate q due to intrabeam scattering.

The reference case is given by the case of a bunched beam of fully stripped ions of gold (A = 197, Q = 79) at the energy of 100 GeV/u. In RHIC $\gamma_t = 24.7$, $V = 4.5$ MV and $h = 2052$. From these parameters we derive $a = 15{,}650$ $(eV/u)^{-1}\, s^{-2}$, $b = 140$ eV/u and $J_s = 280$ eV/u. If the normalized betatron emittance is enlarged at the beginning of the storage to 60 π mm-mrad, and the longitudinal area of the bunch is 0.3 eV/u - s at the start, then the betatron emittance grows very little during a 10-hour long storage. At the same time the beam momentum spread increases at about a constant rate [9] which corresponds to $q = 1 \times 10^{-7}$ $(eV/u)^2$ / s. It is immediately derived that $q\, a = 0.0016$ (eV/u) / s. In absence of stochastic cooling, the beam lifetime is $\tau_{b0} = 0.7\, T_s = 34$ hour. After a storage 10-hour long 75% of the beam survives.

Stochastic cooling can be added to lengthen the beam lifetime. The cooling time required is $\tau_{cooling} = \lambda^{-1} = 0.32\, T_s = 15.6$ hrs. More generally if one requires reducing the bunch dimensions to the ratio $\alpha = J_\infty / J_s$ then the required cooling time is $\tau_{cooling} = (48.6 \text{ hrs})\, \alpha$. For instance, with $\alpha = 0.1$, we need $\tau_{cooling} = 4.9$ hrs.

REFERENCES

[1] S. Chandrasekhar, Rev. of Mod. Phy., **15**, no. 1, January 1943

[2] J. Wei, Stochastic Cooling in the RHIC. Contribution to this Workshop.

[3] J. Wei and A. G. Ruggiero, *Intrabeam Scattering and the Beam Life-Time*, BNL-45269 AD/RHIC-81 (1990)

[4] J. Wei and A. G. Ruggiero, IEEE 1991 PAC , 91CH3038-7, vol. 3, pages 1869-1871

[5] S. V. Ivanov, *Longitudinal Diffusion of a Proton Bunch under External Noise*, IHEP 92-43 (UNK), (1992)

[6] Handbook of Mathematical Functions, edited by M. Abramowitz and I. A. Stegun. National Bureau of Standards. Applied Mathematics Series 55. 9th printing, (1970)

[7] A. G. Ruggiero, *Derivation of a Fokker-Planck Equation for Bunched Beams*, BNL - 49554 (sept. 1993)

[8] Conceptual Design of the Relativistic Heavy Ion Collider RHIC, BNL 52195. (May 1989)

[9] G. Parzen, Private Communication (1993)

THEORY OF THE RELAXATION PROCESSES IN AN ELECTRON COOLING SYSTEM

V.V.Avilov
Institut für Theoretische Physik, TU-Braunschweig,
D-38106 Braunschweig, Germany

Abstract

The stopping force for the ion in a strongly magnetized plasma is calculated as a function of time. The leading contribution to the cooling force $F(t)$ (proportional to $Z^2 \ln \mid Z \mid$, where $Z = Z_i/(n_e D^3)$ is the dimensionless ion charge) is calculated in the frame of the time-dependent linearized theory for the case of small ion velocities. For very small t the stopping force is proportional to t^3 and relaxes to some finite value with the relaxation time of the order of $t_o = \mid Z \mid /\omega_{pl}$. In the case of large ion velocities the relaxation of the stopping force to its asymptotic value is determined by the parameter $\beta = Ze^2\omega_{pl}/v_0$, where Z is the ion charge in units of the electron charge e, ω_{pl} is the plasma frequency and v_0 is the ion velocity.

1 Introduction

The interest in the stopping power of ions in a magnetized plasma was stimulated by general investigations on ion cooling for the ion beams. In the framework of the linearized Vlasov-Poisson equations the problem of the potential created by an ion with charge Z moving with constant velocity v_o in a collisionless plasma was solved by Akhiezer and Sitenko [1]. On the basis of the dielectric function formalism developed in Ref.[1] the case of a magnetized plasma was investigated by Sørensen and Bonderup[2].

However, all calculations in the theory of the ion cooling are made in the case of a steady state potential in the restframe of the ion. Our purpose is to describe on the basis of linearized theory the relaxation process in an electronic plasma of the cooling system. All modern electron cooling systems have the length up to some meters and the time of interaction of a relativistic ion with a single cooling section τ_{int} is of the order of 10^{-8}s. This value is of the order of the period of the electron plasma oscillation $\tau_{pl} = 2\pi/\omega_{pl}$ in a cooler with typical electron density for modern cooling systems ($N_o \sim 10^8 \mathrm{cm}^{-3}$). It forces us to introduce a time-dependent theory of the stopping force $F(t)$ acting on the ion with a charge Z_i moving with constant velocity v_0 through a strongly magnetized plasma of an electron cooler (the Larmor radius r_L is much smaller them Debye radius r_D). We suppose that the ion is inserted at $t = 0$ into initially thermalized uniform electron plasma. We use dimensionless units: the unit of length is given by the Debye length $D = (k_B T/4\pi N_o e^2)^{1/2}$, where k_B is the Boltzmann constant, T the temperature, N_o the equilibrium density of the plasma of electrons with charge $-e$ and mass m. The potential energy is measured in units $k_B T$ and the density in N_o. The unit of velocity is the thermal velocity of the electrons $v_{th} = (2k_B T/m)^{1/2}$. In our units the ion charge Z_i is characterized by the dimensionless charge $Z = -Z_i/(N_o D^3)$. In the case of a magnetized plasma the distribution function is the function of time, space coordinates and z component of the velocity v_z parallel to the magnetic field: $f = f(\mathbf{r}, v_z, t)$.

2 The stopping force in the case of a small ion velocity.

Let us consider the ion with charge Z moving with constant velocity v_o through a collisionless magnetized plasma. In the rest frame of the ion the external charge density is

$$n_{ext}(\mathbf{r}, t) = Z\delta(\mathbf{r} - \mathbf{v}_0 t)\Theta(t) \tag{1}$$

The Fourier transform of the external ion charge is

$$n_{ext}(\mathbf{q}, \omega) = iZ/\omega \tag{2}$$

The dielectric function of a strongly magnetized plasma is

$$\epsilon(\mathbf{q},\omega) = 1 - \frac{1}{\mathbf{q}^2\sqrt{\pi}} \int_{-\infty}^{\infty} \frac{v \exp(-v^2)}{\omega/q_z + i\nu'} dv = 1 + G'(v_s)/\mathbf{q}^2, \tag{3}$$

where $v_s = v_o + \omega/q_z$, $\nu' = \nu\,\mathrm{sign}(q_z)$ and we introduce new function

$$G(\omega) = \frac{1}{2\sqrt{\pi}} \int_{-\infty}^{\infty} \frac{e^{-(\omega-\omega')^2}}{\omega' + i\nu'} d\omega' \tag{4}$$

The stopping power for the ion located in the point $\mathbf{r} = 0$ is

$$F(t) = -Z\nabla[U(\mathbf{r},t) - U_{ext}(\mathbf{r},t)]_{(\mathbf{r}\to o)} \tag{5}$$

In the frame of the dielectric formalism

$$F(t) = -\frac{Z^2}{(2\pi)^4} \int \frac{q_z \exp(-i\omega t)}{\mathbf{q}^2\omega} \left[1 - \frac{1}{\epsilon(\mathbf{q},\omega)}\right] d^3q d\omega \tag{6}$$

and with the help of the Eq. (3) we obtain the stopping power $F(t)$ for an arbitrary ion velocity v_o.

$$F(t) = -\frac{Z^2}{(2\pi)^4} \int \frac{q_z \exp(-i\omega t)}{\omega} \left[\frac{1}{q_z^2 + q_\perp^2} - \frac{1}{q_\perp^2 + q_z^2 + G'(v_s)}\right] dq_\perp^2 dq d\omega \tag{7}$$

The characteristic feature of the Coulomb potential is the divergence of power series of the perturbation theory in the vicinity of the ion, where the potential U tends to infinity. We can stop integration over $\mathbf{r}$ at some r_o where the potential energy Z/r_o is of the order of the mean kinetic energy (or 1 in our dimensionless units). It provides $r_o = Z \gg 1$ and the contribution to the stopping power of the region with $r < r_o$ is of the order of circle of this sphere with the radius r_0 or Z^2. But the contribution to the stopping power from the region $r > r_o$ contains the term of the order of $Z^2 \ln Z$ and within so called logarithmic accuracy in the case $Z \gg 1$ we can omit all terms in the stopping power that not include $\ln Z$.

In the first order in v_0 and within the logarithmic accuracy

$$F(t) = -\frac{Z^2 v_o \ln r_0}{(2\pi)^3} \int_{-\infty}^{\infty} \frac{e^{-i\omega t/r_0} G''(r_0\omega)}{\omega} d\omega \tag{8}$$

We can see that the relaxation of the stopping force to the stationary value [2] needs the characteristic time $t_o = 2Z$

$$F(t) = -\frac{Z^2 v_o \ln Z}{(2\pi)^3} 4[\mathrm{Erf}(\tau) - \tau e^{-\tau^2}], \tag{9}$$

where $\tau = t/t_o$. Fig.1 shows the stopping force as function of time.

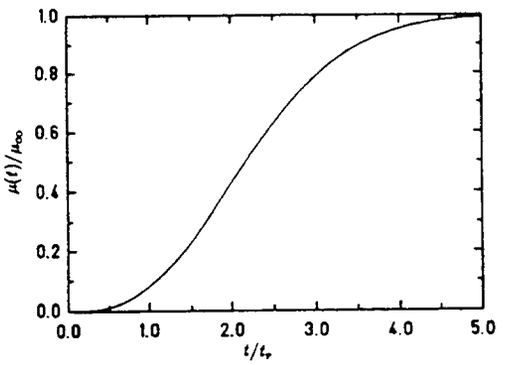

Fig.1 The cooling rate $\mu(t) = F(t)/(Mv_0)$ in units of $\mu(t = \infty)$ as a function of time in the case of small ion velocities.

3 The stopping force in the case of a large ion velocity.

If the ion velocity is larger then v_{th} the ion radiate real plasma waves. The time derivatives of the stopping force is (here we use dimensional units)

$$\dot{F}(t) = \frac{2ie^2Z^2}{(2\pi)^3} \int \frac{(k_z \exp(-i\omega t)t)d^3k d\omega}{k^2 - \omega_{pl}^2 k_z^2/(k_z+\omega)^2} \tag{10}$$

Integration over ω with the condition $F(t) = 0$ at $t < 0$ provides

$$\dot{F}(t) = \frac{e^2Z^2\omega_{pl}}{(2\pi)^2} \int 2\pi k\zeta^2 e^{ikv_o\zeta t}(e^{i\omega_{pl}\zeta t} - e^{-i\omega_{pl}\zeta t})dk d\zeta, \tag{11}$$

where $\zeta = k_z/k$.

The linearization of the kinetic equation is not valid at $r < b$, where the cut-off radius $b = Ze^2/mv_0^2$. Let us introduce some cut-off factor $g(k)$ in (10) that tends to zero at $k > b^{-1}$:

$$g(k) = e^{-kb} \tag{12}$$

It provides

$$\dot{F}(t) = \frac{2te^2Z^2\omega_{pl}^2\beta}{(\pi)(v_0/\omega_{pl})^2} \int_{-1}^{1} \frac{\zeta^3 \sin(\zeta\omega_{pl}t)d\zeta}{(\beta^2 + \zeta^2\omega_{pl}^2t^2)^2}, \tag{13}$$

where $\beta = b\omega_{pl}/v_0$. The stopping force as a function of time for some β is shown in Fig.2. For small

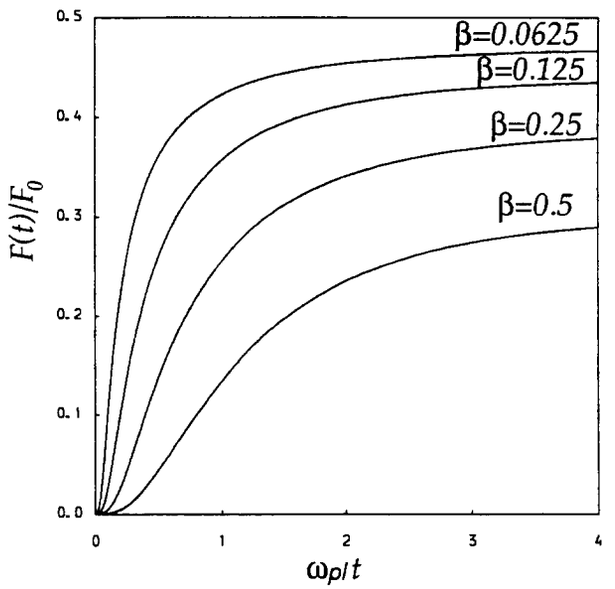

Fig.2 The stopping force (in units of $F_0 = e^2Z^2\omega_{pl}^2/v_0^2$) as a function of time for some β.

β the stopping force rapidly relaxes to its asymptotic value at large t. But if β is of the order of 1 the relaxation time is of the order of the period of plasma oscillations. In the case $\beta > 1$ we can't use the dielectric formalism, because in this case the wave length of plasma oscillations produced by the ion is smaller then b. It means that the dielectric formalism is valid in the case of very large ion velocity only:

$$v_0^3 \gg Ze^2\omega_{pl}/m \tag{14}$$

References

[1] A.I.Akhiezer and A.G.Sitenko, *ZETF*, **23**, 161 (1952); A.G.Sitenko, *Electromagnetic Fluctuations in Plasma*, Academic Press, N.Y. 1967.

[2] A.H. Sørensen, E. Bonderup, *Nucl. Instr. and Meth*, **215**, 27 (1983).

SECONDARY PARTICLES INSTABILITIES IN THE STORAGE RINGS WITH ELECTRON COOLING

A.V.Burov
Budker Institute of Nuclear Physics, 630090 Novosibirsk, Russia

ABSTRACT

The system under study consists of circulating ion beam ($i1$), cooling electron beam ($e1$), secondary ions ($i2$) and electrons ($e2$) trapped in the cooler. Interaction of this components between themselves may rouse coherent instabilities – longitudinal or transverse ones. Estimation of increments and thresholds of such instabilities is the purpose of these studies.

1. STEADY STATE PARAMETERS

Here steady state parameters of secondary particles (density n and temperature T) are investigated.

1.1 Reflected Electrons

Electrons reflected from the collector have the velocity very close to the primary electrons one. The drag force is very high, when they move in the same direction, and it is neglectfully small, when directions are opposite. This is the reason of fast blowing-up of these secondary particles. Their density $n_{e2}^{(r)}$

$$\frac{n_{e2}^{(r)}}{n} = \left(\frac{\Delta v}{v}\right)^3 \frac{r}{6\pi n_{e1} r_v^2 l L_{ee}}$$

Where $r_v = e^2/(mv^2)$, r – coefficient of reflection, Δv – initial velocity difference, n_{e1} – density of primary electrons, l – length of the cooler, $L_{ee} \simeq 10$ – Coulombian logarithm. For $\Delta v/v = 10^{-3}$, $r = 10^{-4}$, $n = 10^7 cm^{-3}$, $E = 12\,keV$, $l = 3m$ one gets $n_{e2}^{(r)}/n = 5 \cdot 10^{-3}$. (For numerical estimations prelimenary parameters of CRYSTAL project [1] will be taken.)

1.2 Ionization Electrons

Temperature: heating by primary electrons.

Collisions with primary electrons originate the temperature rising of secondary ones. For lifetime $\tau = \frac{n_{e2}}{n}\tau_c$ with $\tau_c = (n_{at}\sigma v)^{-1}$, σ – ionization cross-section it gives the temperature

$$T_{e2} = \frac{4\pi n_{e2} r_v^2 L_{ee}}{n_{at}\sigma} mv^2$$

At $n_{at} = 2 \cdot 10^7 cm^{-3}$, $\sigma = 5 \cdot 10^{-18} cm^2$, $n_{e2} = n = 10^7 \quad T_{e2} = 200\,eV$.

Density: resonance drifting.

Drift displacements Δx on turns of the cooler and in transverse electric field of special electrodes are added together to be with some phases ψ originated from helical drift in the electric field of the electron beam. The total displacements after N times is:

$$\Delta x_N = \mathrm{Re} \sum_{k=0}^{N-1} \Delta x\, e^{ik\psi} = \Delta x \frac{sin(N\psi)}{2sin(\psi/2)}$$

where $\psi = \Omega l/v_{e2}$, $\Omega = 2\pi nec/B$ – drift frequency.

For $\psi = \psi_p = 2\pi p$, p – integer, $\Delta x_N = N\Delta x$ – resonance drifting.

These resonance particles quickly leave the beam, collisions produce new ones, and so on – this is the way for secondary electrons to escape from the trap.

The life time τ estimation:

$$\frac{1}{\tau} \simeq \nu_{ee} \sum_p \frac{\Delta v_p}{w_2}$$

where $w_{e2} = \sqrt{T_{e2}/m}$ – thermal velocity, $\nu_{ee} = 4\pi n r_v^2 L_{ee} v$ — collisions frequency,

$$\Delta v_p = \frac{\Omega l}{(2\pi p)^2} \frac{\Delta x}{a}$$

is the width of resonance, a – electron beam radius.

From life time one can get the density of secondary electrons: $n_{e2}/n = \tau/\tau_c \sim 0.1 \div 10$ depending on Δx value. For centrifugal drift $\Delta x = \Delta x_c = (v_{e2}/\Omega_L)\phi_{turn}$. For electrostatic one $\Delta x = \Delta x_e = c(d/v_{e2})(E/B)$.

The temperature and density equations are connected and should be solved in pare.

1.3 Ions

Temperature: birth in potential well.
Secondary ions are born in transverse potential well, created by primary electrons. This determine their temperature $T_{i2} = U_0/2 = \pi n e^2 a^2/2$. For CRYSTAL parameters this gives $T_{i2} = 15\,eV$ which is much more than heating by primary electrons $T_{i2} = (m/M)\,T_{e2} = 0.1\,eV$.

Density: trapping in cavity-like inhomogenuity.
Ions may be trapped in cavity-like inhomogeneities of the vacuum chamber with some radius $b_2 > b$, b – radius of the vacuum chamber. Their linear density λ_{i2} is:

$$\lambda_{i2} = (\lambda_{e1} + \lambda_{e2}) \frac{\ln(b_2/b)}{0.5 + \ln(b_2/a)} \leq 0.3(\lambda_{e1} + \lambda_{e2})$$

An alternative way to secondary particles density limitation is a coherent instability.

2. LONGITUDINAL INSTABILITIES.

2.1 Dispersion Relation.

With wake potential $W(t)$ and impedance $\mathcal{Z}(k)$ determined in ordinary way, an averaged over turn electrical field $\mathcal{E}(t)$ is:

$$\mathcal{E}(t) = -\frac{e}{T_0} \int_{-\infty}^{\infty} \rho(t')W(t-t')dt' \qquad\qquad \mathcal{Z}(k) = v \int_{-\infty}^{\infty} W(t)e^{ikvt}\,dt$$

Substituting this field into Vlasov equation gives the following dispersion relation

$$\omega(k) = \pm ku \left\{ 1 - \frac{\pi i}{2} u^2 \frac{k}{|k|} f'\left(\frac{\omega}{k}\right) - i\frac{\tilde{\mathcal{Z}}}{2\mathcal{Z}} \right\}$$

where ω is the frequency of coherent oscillations, $f(u)$ — distribution function, $u = v\sqrt{\lambda r_v F}$ is the velocity of waves propagation in the beam circulating in the smooth chamber with impedance $i\mathcal{Z}(k) = ik\Pi F$, where Π is the orbit perimeter.

The second term in figured brackets describes Landau damping, the third one is responsible for coherent instability on impedance $\tilde{\mathcal{Z}}$. For Gaussian distribution $f(u) = (2\pi w^2)^{-1/2}\exp(-u^2/2w^2)$ the threshold number of circulating particles

$$N_{th} = N_{KS} \ln\left[\frac{\mathcal{Z}}{\mathrm{Re}\tilde{\mathcal{Z}}} \left(\frac{N_{KS}}{N_{th}}\right)^{3/2} \right]$$

where $N_{KS} = (\Delta p/p)^2\,\Pi/(r_v F)$ is Keil-Schnell circle threshold. At $\Delta p/p = 10^{-5}$ $N_{KS} = 3 \cdot 10^7$ for C_{12}^6, $N_{KS} = 3 \cdot 10^6$ for U_{238}^{54}.

2.2 Impedances.

Responses of primary electrons and secondary particles on the field of circulating ions may be represented in the terms of impedances. The solution of longitudinal equations of motion for these particles with fixed density perturbation of circulating ions $\rho_{i1} \sim \exp\left(ik(z - vt)\right)$ gives the following results.

2.2.1 Primary electrons.

The equations for primary electrons should be taken with zero boundary conditions at the ions entrance in the cooler. It gives the impedance

$$\frac{\mathrm{Re}\tilde{\mathcal{Z}}}{\mathcal{Z}} = \frac{l}{\Pi}\,\frac{u_{e1}}{v} \simeq 10^{-3}$$

It is the maximum value of this quantity, corresponding to $kl = v/u_{e1}$.

2.2.2 Secondary particles.

Secondary particles plasma trapped inside the electron beam has its own frequencies and may be considered as some kind of resonator. Such plasma, contained in the trap of length L has wave numbers $k_s = 2\pi s/L$ and frequencies $\omega_s = k_s u$ with Landau decrements $\gamma_s \leq k_s w$. The boundary conditions correspond to zero velocity perturbations at the edges of the trap. The equations of motion of such plasma in the external field of circulating ions give the following result:

$$\frac{\mathrm{Re}\mathcal{Z}}{\mathcal{Z}} = \frac{2}{L\Pi}\sum_s \left|\int e^{ikz}\sin(k_s z)dz\right|^2 \frac{\omega_s^2 kv\gamma_s}{(\omega_s^2 - k^2v^2)^2 + k^2v^2\gamma_s^2}$$

The interval of integrating is one of the overlapping of circulating ions and this secondary plasma. For secondary electrons one can obtain ($L > l$) :

$$\max\frac{\mathrm{Re}\mathcal{Z}}{\mathcal{Z}} = \frac{1}{(2\pi)^2}\,\frac{L}{\Pi}\,\frac{u^2}{w^2} \simeq 3\cdot 10^{-4}$$

For ions

$$L > l: \quad \max\frac{\mathrm{Re}\mathcal{Z}}{\mathcal{Z}} = \frac{1}{(2\pi)^2}\,\frac{w}{v} \simeq 6\cdot 10^{-4}$$

$$L < l: \quad \max\frac{\mathrm{Re}\mathcal{Z}}{\mathcal{Z}} = \frac{1}{2\pi}\,\frac{L}{\Pi}\,\frac{w}{v} \simeq 6\cdot 10^{-5}$$

These values are rather small, what means that $N_{th} \gg N_{KS}$ (for Gaussian distribution $N_{th} = 5N_{KS}$).

3. TRANSVERSE INSTABILITIES.

3.1 Equations of Motion.

Here only most dangerous transverse oscillations — the dipole ones will be considered. The equations of motion of four components $(e1, e2, i1, i2)$ are as follows:

$$(e1): \qquad \frac{\partial\zeta_{e1}^{\pm}}{\partial t} + v\frac{\partial\zeta_{e1}^{\pm}}{\partial z} = \pm i\sum_\alpha \Omega_\alpha(\zeta_{e1}^{\pm} - \zeta_\alpha^{\pm})$$

$$(e2): \qquad \frac{\partial\zeta_{e2}^{\pm}}{\partial t} = \pm i\sum_\alpha \Omega_\alpha(\zeta_{e2}^{\pm} - \zeta_\alpha^{\pm}) - \gamma_{e2}\zeta_{e2}^{\pm}$$

Where $\zeta^{\pm} = x \pm iy$ — transverse displacement in complex form, $\Omega_\alpha = 2\pi Z_\alpha ecn_\alpha/B$ — drift frequency in the field of particles of sort α with charge number Z_α ($\alpha = e1, e2, i1, i2$), γ_{e2} - Landau damping due to drift frequencies dispersion $\delta\Omega_\alpha$, $\gamma_{e2} \leq \sum_{\alpha\neq e2}\delta\Omega_\alpha$.

Equation for $(e2)$ needs some comments. If secondary electrons are cold $\omega l/w_{e2} \gg 1$ (ω is the coherent frequency), this equation describes displacements at every point z. The space derivative ζ_{e2} in the l.h.s. is omitted because it is neglectfully small in the comparison with the time one. In the opposite case of hot secondary electrons $\omega l/w_{e2} \ll 1$ this space derivative comes out after averaging on longitudinal oscillations of secondary electrons between edges of the trap. In this case the values in the r.h.s. should be taken also as averaged ones.

The equation for primary ions may be presented in the following form

$$(i1): \qquad x_{i1}(t) = 4\pi\sum_\alpha \xi_\alpha \sum_{k=0}^{\infty}(x_\alpha(t - kT_0) - x_{i1}(t - kT_0))\sin(2\pi\nu_x k)$$

with T_0 - period of revolution, ν_x - betatron tune, $\xi_\alpha = 0.5n_\alpha r_v l\beta_x Z_{i1}/A_{i1}$ - tune shift on charge of particles α, β_x is β-function in the cooler. Supposing $x_{i1} \propto \exp(-i\omega t)$, $\omega = \omega_0(\nu_x + p + \varepsilon)$ with p - integer and $\varepsilon \ll 1$ one gets

$$x_{i1} = -\frac{1}{\varepsilon}\sum_\alpha \xi_\alpha(x_\alpha - x_{i1})$$

The equations for y_{i1} have the same form.

And at last for secondary ions

$$(i2): \qquad \frac{\partial^2\zeta_{i2}}{\partial t^2} = -i\Omega_L\frac{\partial\zeta_{i2}}{\partial t} - \sum_\alpha \omega_\alpha^2(\zeta_{i2}-\zeta_\alpha) - 2\gamma_{i2}\frac{\partial\zeta_{i2}}{\partial t}$$

Here γ_{i2} is Landau decrement for secondary ions transverse oscillations due to the dispersion of ω_α, $\omega_\alpha^2 = 2\pi n_\alpha Z_{i2}Z_\alpha e^2/M_{i2}$ – transverse focusing on particles α, $\Omega_L = Z_{i2}eB/(M_{i2}c)$ – Larmour frequency. Equations for $(\pm)$ degrees of freedom are the same.

This system of equations is rather complicated to solve it immediately. That is why the stability problem for whole four-component system is studed below by the way of separation it on subsystems like $(e1+i1)$, $(e1+e2)$, $(e1+e2+i2)$ and so on.

3.2 Results for subsystems.

$(i1+e1)$: $\nu_x - \nu_y$ *resonance.*

When betatron tunes are equal the resonance instability takes place. In such a case dimensionless frequency of oscillations $\varepsilon = \xi\,(1 \pm i\Omega_i l/(2v))$ (When it could not be misunderstood indexes will be omitted or simplificated.) The stability condition $|\nu_x - \nu_y| > \xi\Omega_i l/v \simeq 2\cdot 10^{-4}$ (C_{12}^6, U_{238}^{54}).

$(e1+e2)$: *coherent damping.*

a. $e2$ are cold: $\omega l/w_2 > 1$. For solution $\zeta \sim \exp(-ik(\omega)z)$ one finds $k(\omega)v = -\Omega_1\Omega_2/(\omega - \Omega_1 + i\gamma)$ which corresponds to space attenuation.

b. $e2$ are hot: $\omega l/w_2 < 1$. In this case the frequency of coherent oscillations $\omega = \Omega_1 - i\gamma - i\Omega_1\Omega_2 l/(2v)$ which corresponds to additional damping. One can see that stability here depends on the sign of $\Omega_1\Omega_2$.

$(i1+e2)$: *ion-electron betatronic-drift resonance.*

This case is something like one taking place with ordinary accumulation of secondary electrons in the closed orbit of proton storage ring – see [2, 3]. When ions betatron frequency ω_b and electrons drift one $\Omega_d = \sum_{\alpha\neq e2}\Omega_\alpha$ satisfy resonance relation $\omega_b + n\omega_0 = \Omega_d$ the dimensionless frequency is $\varepsilon = i\,(\xi_{e2}\Omega_{i1}/(2\omega_0))^{1/2}$ which corresponds to instability. The stability criterion – detuning from resonance: $\Delta\nu_b > 2|\varepsilon| \simeq 0.1$

$(i1+e1+e2)$: *previous case + coherent damping* $(e1+e2)$.

$(i1+i2)$: *ion-ion resonance.*

This case looks rather similar $(i1+e2)$ one. At resonance $\omega_b + n\omega_0 = \omega_\pm$, where

$$\omega_\pm = -\left(\Omega_L/2 \pm \sqrt{\Omega_L^2/4 + \omega_\perp^2}\right)$$

are $(i2)$ transverse frequencies in the constant field of another particles with $\omega_\perp^2 = \sum_{\alpha\neq i2}\omega_\alpha^2$. In this case the dimensionless frequency of the coherent oscillations is

$$\varepsilon = i\left(\xi_{i2}\frac{\omega_{i1}^2}{\omega_0|\omega_+ - \omega_-|}\right)^{1/2}$$

The stability criterion $\Delta\nu_b > 2|\varepsilon| \simeq 10^{-2}$

$(e1+i2)$: *space amplification [4].*

This situation corresponds to the change of the sign in $(e1+e2)$, cold $(e2)$ case. Here

$$k(\omega) = \frac{\omega - \Omega_{i2}}{v} + \frac{\Omega_{i2}}{v}\,\frac{\omega_{e1}^2}{-\omega^2 + \Omega_L\omega + \omega_{e1}^2 - 2i\gamma\omega}$$

Space amplification coefficient $\mathcal{K} = \exp(ik(\omega)l)$ has its maximum value at $\omega = \omega_-$:

$$\mathcal{K}_{max} = \exp\left(\frac{\Omega_{i2}l}{v}\,\frac{\omega_{e1}^2}{\gamma|\omega_-|}\right)$$

If this coefficient is high enough even a small feedback $\eta > \mathcal{K}_{max}^{-1}$ creates an instability.

$(e1+i2+e2)$: $(e2)$ *feedback.*

For reflection electrons the feedback coefficient $\eta = n_{e2}^{(r)}/n_{e1}$. For ionization ones

$$\eta = \frac{n_{e2}}{n_{e1}}\left|\int_0^\infty dv f_{e2}(v)\exp\left(\frac{i\omega l}{v}\right)\right| \simeq \frac{n_{e2}}{n_{e1}}\exp\left(-\frac{3}{4}\left(\frac{\omega l}{w_2}\right)^{2/3}\right)$$

$(e1 + i2 + i1) : (i1)$ *feedback.*
Circulating ions create a feedback in the subsystem $(e1 + i2)$ with coefficient

$$\eta = \frac{Z_{i1} n_{i1}}{n_e} \frac{\omega_\perp^2}{|\omega_+ - \omega_-| \gamma_{i2}} \frac{\xi_{i2}}{\varepsilon} |\ln \mathcal{K}|^{-1}$$

At maximal detuning from ion-ion resonance $\varepsilon \simeq 1$. One can see that the system stability $|\eta\mathcal{K}| < 1$ strongly depends on the value of Landau decrement γ_{i2}. For rectangular transverse distribution $(e1)$ and neglectable density of $(i1)$ the dispersion of transverse frequencies of $(i2)$ is absent, hence $\gamma_{i2} = 0$. Nonzero value of Landau decrement is connected with the inhomogeneity of $(e1)$ density and with the density of $(i1)$. So, the most dangerous situation takes place when $(i1)$ density is equal to inhomogeneity of $(e1)$ one. For CRYSTAL parameters the threshold value of Landau decrement $(\omega_\perp/\gamma_{i2})_{th} \simeq 10^3$.

$(i1 + e1 + i2 + e2)$: *summing up.*

One can see from this consideration of transverse instabilities that practically all of them are resonance ones with rather small widths. Nevertheless the detuning from them at some cases might be not so easy problem: frequencies of secondary particles changes both with their own densities and with the density of circulating ions. The last one increases during the cooling, and near the crystal state it is much more than the density of primary electrons. Taking this into account one can see that for avoiding ion-ion resonance it is necessary to require $\omega_{e1} < \omega_0$; $\omega_{e1} \frac{n_{e2}}{2n_{e1}} < \omega_0$. Similarly for preventing betatron-drift instability one should demand $\Omega_{i1} < \omega_0$; $\Omega_{i2} < \omega_0$. For CRYSTAL parameters the betatron-drift resonance on primary ions density looks especially dangerous.

REFERENCES

[1] G.Bisoffi at al. LNL-INFN (REP) 59/92 , Legnaro (1992)

[2] D.G.Koshkarev, P.R.Zenkevich. Part. Acc., Vol 3, p.1 (1972)

[3] H.Grunder, G.Lamberston. Proc. of VIII IHEACC Conf., p.308, CERN (1971).

[4] A.V.Burov at al. CERN/PS 93-03 (AR) (1993).

DESIGN AND CONSTRUCTION OF THE CELSIUS ELECTRON COOLER

M. Sedlaček
Accelerator Technology, Royal Institute of Technology, Stockholm
T. Bergmark, K. Gajewski, L. Hermansson, O. Johansson, T. Johnsson, D. Reistad, R. Wedberg, L. Westerberg
The Svedberg Laboratory, Uppsala

ABSTRACT

The CELSIUS storage ring at the The Svedberg Laboratory is equipped with an electron cooling device. The cooler was taken into operation in May 1990. The paper describes the construction of the device together with some design considerations concerning the electron gun, collector, vacuum and high voltage system.

1. INTRODUCTION

CELSIUS [1] is a cooler-storage ring accelerator for protons and heavy ions from the Gustaf Werner Cyclotron. The ring is particularly suited for nuclear and particle physics with stored and cooled ion beams. The electron cooler for the ring was designed at the Unit for Accelerator Technology of the Royal Institute of Technology in Stockholm as a collaboration with the The Svedberg Laboratory in Uppsala, where the ring is situated.

A drawing of the electron cooler is shown in Fig. 1, the general data of the device in Table 1.

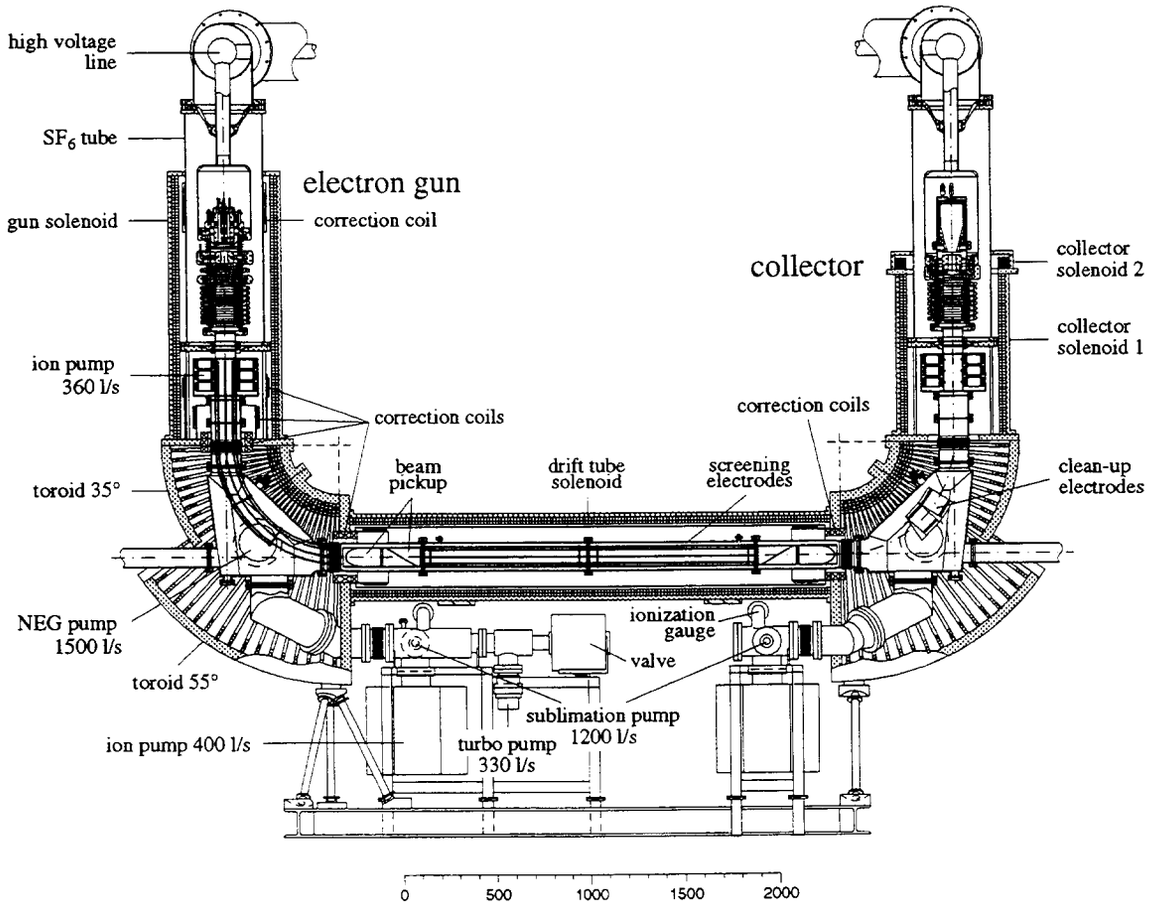

Fig. 1. CELSIUS electron cooler.

Table 1
Electron cooler data

Electron energy	5 - 300 keV
Cathode diameter	20 mm
Gun anode voltage	0 - 40 kV
Perveance	0.38 μP
Beam current	0 - 3 A
Magnetic field	0.1 - 0.18 T
Design magnetic field	0.15 T
Transverse energy	<0.2 eV @ 300 keV
Interaction space	2.5 m
Length	4.6 m
Height	4.3 m

2. MAGNETIC CIRCUIT

A homogeneous longitudinal magnetic field in the electron cooler confines the electron beam. The magnetic circuit consists of solenoids, toroids, correction, steering and dipole coils. The gun and collector solenoids have a larger diameter then the drift tube solenoid in order to accommodate the SF_6 chambers, with the high voltage insulation. The toroids consists of a 35° and a 55° section. To be able to adjust the position of the electron beam steering coils for the two perpendicular directions are included in all solenoids. Dipole coils in both toroids compensate for the drift of the electron beam.

All solenoids and toroids are connected in series to the main power supply. To compensate for differences between the necessary ampereturns in the solenoids and the toroids an additional power supply is connected to each solenoid and toroid winding. By adjusting the currents from these power supplies the same value of the longitudinal magnetic field can be obtained in the centre of each solenoid or toroid. The design value of the longitudinal field is 0.15 T.

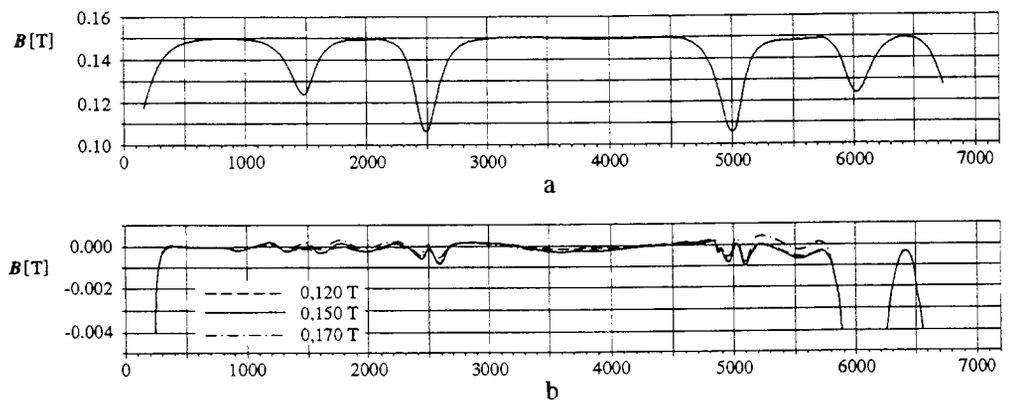

Fig. 2. Longitudinal magnetic field. **a.** Magnetic field along the axis without correction coils. **b.** Expanded corrected magnetic field at three excitations corresponding to nominal field of 0.12, 0.15 and 0.17 T.

At the transitions between the solenoids and the toroids there are missing ampereturns. The magnetic field shows a dip at these transitions, Fig. 2.a. Extensive computer simulations using the program POISSON [2] were made in order to find the number of correction coils, their shape and the number of ampereturns necessary to decrease the dips to an acceptable level.

The correction coils are necessary also for another reason. The dip in the magnetic field at the transition introduces scallop in the electron beam. Using the POISSON program a solenoidal system, where the toroids were replaced by solenoids of large diameter, was simulated. The computed field was

then used as input data in a modified version of the E-GUN program [3] and a simulation of the transit of an electron beam with different energies was made. At a beam current of 2.5 A and a beam energy of 300 keV the computed transverse energy of the outermost orbit in the drift tube was 12 eV. When all correction coils were included, the increase of the transverse energy inside the drift tube was negligible, of the order of 0.1 eV.

A special program was written to simulate the transition of the electron beam through the toroid. This program used the two-dimensional planar field obtained by POISSON computation, in the transverse direction the field was assumed constant. The space-charge of the electron beam was taken into account in a simplified way, treating the beam as concentric cylinders with variable diameter. The computations have shown two important results. The transition introduces some scallop in the electron beam, larger for higher energies. Up to about 100 keV the scallop seems to be negligible. At 300 keV the transverse energy, depending on the magnitude of the magnetic field, can reach a few electron volts. By varying the magnetic field a resonant condition can be obtained. This speaks for an electron gun construction which does not use resonant focusing to obtain a low scallop at the exit of the gun.

The longitudinal magnetic field was measured with a Hall probe connected to a Bell 600 Gaussmeter. The probe, mounted in a brass block, was pulled along the optical axis of the cooler by a synchrone motor, the output of the Gaussmeter was connected to a precision digital voltmeter and a recorder. The design value of the longitudinal magnetic field of 0.15 T was chosen for the adjustments of the correction coils. Between 0.12 and 0.17 T the differences are smaller than 0.2 mT from the gun cathode to the end of the drift tube, Fig. 2.b. All currents can be scaled proportionally to the desired magnetic field without changing the field distribution and its straightness in the drift tube solenoid.

The transverse field was measured using a small pencil beam. An electron gun with a tungsten cathode and a copper anode was placed inside the collector solenoid. The laser drilled hole in the anode was 0.05 mm in diameter. The acceleration voltage was 4.5 kV, which in a field of 0.15 T gives a Larmor radius in microns. The pencil beam is therefore forced to follow the magnetic field lines. The position of the narrow beam was monitored on a screen by a telescope, mounted on a table with digital read-out of the position. The screen was moved along the axis of the drift tube. By taking the average of a few measurements it was found that this zero method gives an accuracy of ± 0.02 mm. Fig. 3 shows the result of these measurements.

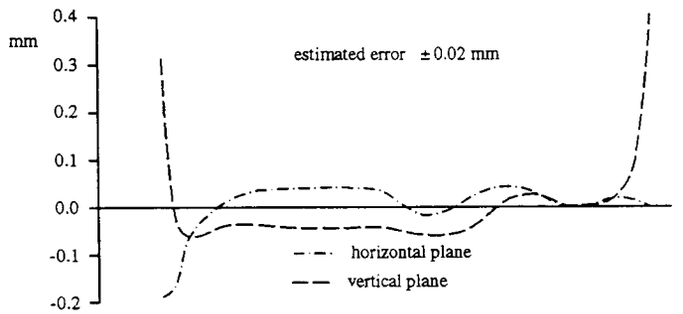

Fig. 3. Transverse magnetic field in the drift tube. Deviation from the geometric axis of the solenoid.

3. ELECTRON GUN

The design of the electron gun should result in an electron beam with a low transverse electron energy, it should be possible to vary the beam energy, the current and the magnetic field independently of each other. This speaks for an adiabatic focusing design.

A schematic drawing of the CELSIUS electron gun is shown in Fig.4. The whole gun system is placed inside a stainless steel tank filled with SF_6 in order to withstand the highest operating voltage of 300 kV. The gun uses a dispenser cathode with a diameter of 2 cm surrounded by a Pierce electrode. Two rings, the so called guard electrodes, are controlling the potential distribution in front of the cathode in order to obtain an even current density distribution across the cathode area. After passing the gun anode the electron beam is accelerated in two Large High Gradient accelerating columns made by National Electrostatic Co., a short one with 6 and a long one with 18 electrodes. A potential divider with a total resistance of 940 MΩ takes care of the potentials on all electrodes in the accelerating column. Corona rings are mounted around the electrodes. The osmium coated dispenser cathode is mounted on a holder consisting of three laser-welded Mo-Re cylinders which act as a thermal shield. The outermost cylinder

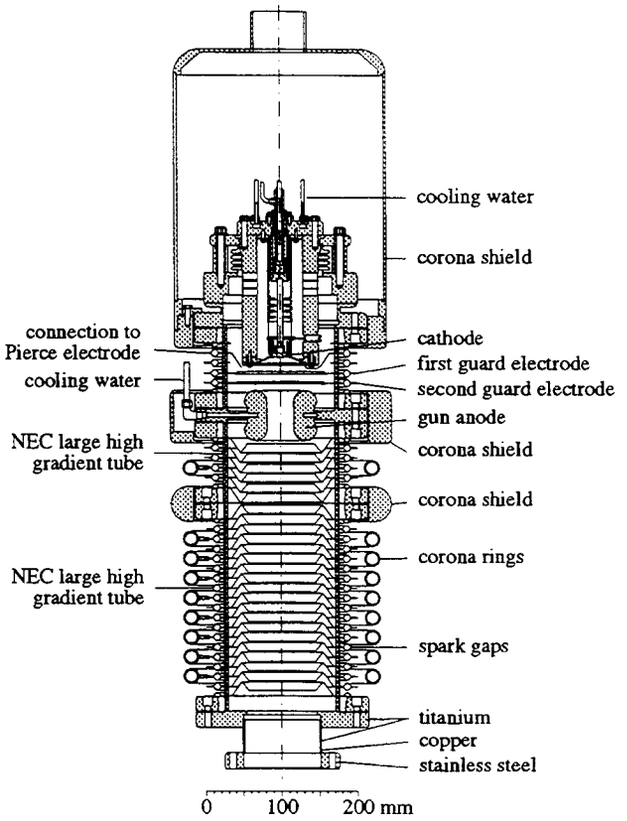

Fig. 4. Electron gun

is welded to a stainless steel cylinder with grooves to decrease the thermal conductivity losses. The cathode is heated by a pyrolytic graphite cylinder pressed against the inner cathode surface by a nimonic spring. The advantage of this kind of heating is an extremely low magnetic field at the surface of the cathode, low outgassing and a negative temperature coefficient of the material. A Mo-Re tube is the current lead. At the normal working temperature of about 1050°C the heater power is about 65 W. The power supply is power regulated. The holder of the Pierce electrode is made massive so that the outermost of the Mo-Re cylinders can be centred by three molybdenum spacers. The Pierce electrode has a standard 67.5° angle, its innermost part near the cathode is made of molybdenum, the outer part of copper. Both parts are brazed together. The electrode is mounted insulated from the holder by ceramic spacers. A ss-Cu-Ti transition connects the third Large High Gradient tube with the rest of the accelerating structure.

Inside the high voltage terminal there are three power supplies connected to the gun side of the electron cooler: the gun anode, the gun bias (guard 1) and the Pierce electrode power supply. The potential of the gun anode, the gun bias and the Pierce electrode power supply can be varied independently of the acceleration voltage on the high voltage power supply (HVPS). The voltage of the gun bias electrode can be varied between 0 and −10 kV in order to cut-off the beam current. Each power supply is connected via a series resistor and has an overvoltage spark gap in parallel. The power supplies inside the high voltage terminal are connected to the gun and to the collector side of the electron cooler by large coaxially mounted tubes insulated by SF_6.

4. COLLECTOR

A schematic drawing of the CELSIUS collector is shown in Fig. 5. Like the electron gun, the whole collector system is placed in a stainless steel tank filled with SF_6 and immersed in a magnetic field.

Table 2
Collector efficiency at 30 keV and 0.13 T

Beam current [mA]	100	200	500	1000
Gun anode voltage [kV]	3.7	5.7	10.3	16.3
Collector anode voltage [kV]	0.15	0.20	0.38	0.58
Computed minimum [kV]	0.34	0.55	1.01	1.60
HVPS current [mA]	0.049	0.049	0.063	0.124
HVPS loss current [mA]	<1 bit	0.003	0.023	0.094
Collector efficiency [per cent]	99.999	99.998	99.995	99.991
Pressure [10^{-8} Pa]	0.9	1.2	1.5	1.7

The electron beam is retarded in one Large High Gradient column, passes the collector anode and is accelerated into the collector. The column has a potential divider with equal resistors resulting in a constant field gradient. The collector is biased positive with respect to the cathode potential, like the collector anode. The potential of the collector anode is adjusted to be high enough to avoid a formation

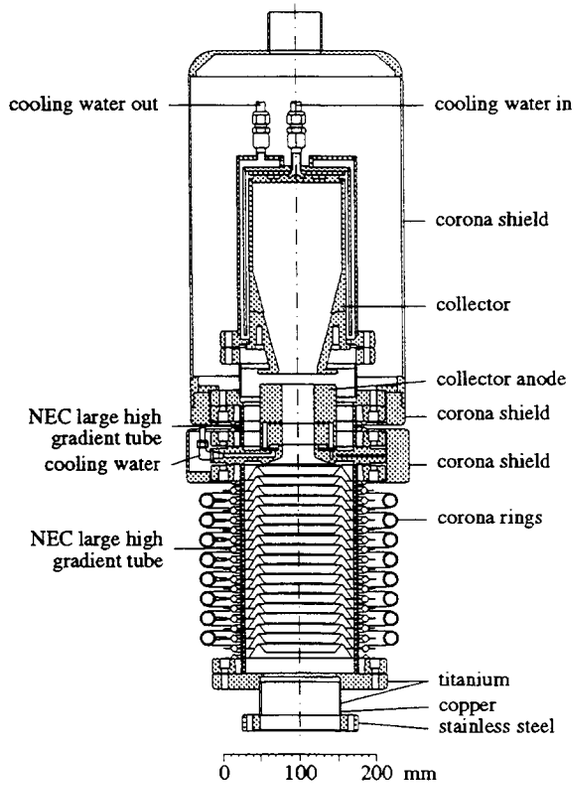

Fig. 6. Collector

of a virtual cathode and a reflection of electrons. The length of the anode ensures that a potential valley is created where positive ions, a result of the ionisation of the residual gas, are trapped [4]. The trapped ions neutralize the space-charge of the electron beam and reduce the lowest potential of the anode. The measured potential on the collector anode, Table 2, is lower than the minimum necessary to avoid the reflection of the electrons because of the space-charge depression, which confirms the formation of an ion cloud. The collector perveance is 58 μP. To optimize the collector efficiency the distribution of the magnetic field in the collector region can be changed by adjusting the current in the collector solenoid 2, Fig. 1.

Based upon the current distribution obtained from the simulation of electron orbits inside the collector, the power density and the maximum expected temperature was computed by the POISSON program. At a maximum current of 3 A the power density amounts to about 800 W/cm^2 at the centre of the collector. At a cooling water temperature of 30°C the temperature on the inside of the collector is 158°C.

5. VACUUM SYSTEM

The CELSIUS ring operates under ultra high vacuum conditions, at pressures below 10^{-7} Pa. The main pumping of the cooler is performed by a combination of ion pumps, NEG pumps and sublimation pumps, Fig. 1. A differential pumping is included on the gun and on the collector side by ion pumps, which use the gun and collector solenoid to generate the necessary magnetic field. With the valves towards the ring closed, the pressure in the cooler, as measured at the ionisation gauge mounted above the ion pump on the collector side, is $2 \cdot 10^{-9}$ Pa. With the cathode heated it increases by a factor of three. The pressure increases to about $2 \cdot 10^{-8}$ Pa with an electron current of 1 A.

All materials used in the cooler match the ultra high vacuum requirements. Stainless steel parts are made of LN316 steel, which has been fired. Other used materials are copper, titanium and ceramic. Heating jackets are wrapped around the whole vacuum system, the gun and the collector side have special baking hats. Most of the vacuum tubes have an inner diameter of 150 mm. The screening electrodes, which carry mirror charges inside the drift tube and the gun toroid chamber, are made of eight rods. This construction makes the electrodes transparent from the vacuum point of view. An estimate was made to check the possible deformation of the equipotential surfaces at the edge of the beam and found negligible.

The residual gases are ionised by the electron beam. Resulting ions and electrons drift inside the cooler along the magnetic field lines. Two clean-up electrodes are placed inside the collector toroid chamber to deflect the particles in an $\mathbf{B} \times \mathbf{E}$ field. Low conductance ceramic plates (zirconia) are connected by two stainless steel plates. The steel plates are connected to two power supplies, with variable voltage between zero an 10 kV. The electrodes are 100 mm long.

References:

[1] D.Reistad et al., *Recent Commisioning Results at CELSIUS*, Proc. 13th Int. Conf. on Cyclotrons and their Applications, Vancouver, Canada, July 6-10, 1992, 266
[2] Iselin Ch., Poisson program, CERN Program Library (1983)
[3] Herrmannsfeldt W.B., SLAC-Report #226 (1979)
[4] W.Kells et al., *The Electron Beam for the Fermilab Electron Coling Experiment*, PM918, Oct. 1979

Electron Cooling of Electron Beams

D.J. Larson
Superconducting Super Collider
2550 Beckleymeade Avenue
Dallas, Texas 75237
USA

ABSTRACT

Electron cooling of electron (and positron) sources may be important for future linear collider applications. In order to cool electrons with electrons, an intermediary positron beam must be employed, since it is impossible to merge two beams of identical particles into the cooling straight. By adjusting the beta functions of the electron and positron lattices appropriately the final emittance of the stored electron beam can be made less than the emittance of the cooling electron beam. This paper will discuss accelerator physics issues relating to an electron cooled electron beam source.

1. INTRODUCTION

Electron cooling was originally proposed by Budker in 1966[1]. The basis for his proposal came from work done by Spitzer[2] (1956) who showed that warm ions come to equilibrium with cooler electrons in a plasma. Due to the much larger mass of the ion, the final rms speed of the ions is much less than that of the electrons. Budker realized that an electron beam is simply a moving electron plasma. By superimposing an ion beam on a co-moving electron beam, warmer ions are cooled by the electron beam.

In the 1970's electron cooling was demonstrated to be an extremely good way of increasing the phase space density of proton beams. Cooling times of between one and five seconds were reported by experiments at Novosibirsk[3], CERN[4], and Fermilab[5]. Recent experiments at the Indiana University[6] and at the Low Energy Antiproton particle Ring (LEAR) at CERN[7] have made progress in extending the use of electron cooling to ion and antiproton beams, respectively. Electron cooling of positrons has also been suggested[8,9]. This paper will propose extending the use of electron cooling to electron beams.

Since electron cooling relies on a merging of beams that have identical average beam velocity, it is not possible to directly merge an electron cooling beam on a hot electron beam. An intermediate beam must be used to transfer heat from the hot electron beam to the cooling beam. The best choice for the intermediate beam is to use positrons. Positrons do not decay, and their light rest mass is the best for cooling. Figure 1 shows the proposed electron cooling scenario. A cooling electron beam is formed in an electrostatic accelerator (not shown) and merged with a positron beam in the first cooling straight. The positron beam is then transported around to a second long straight section where it is merged with the hot electron beam. The hot electron beam transfers heat to the positron beam, which in turn transfers heat to the cooling electron beam. The cooling electron beam is recirculated to the terminal of the electrostatic accelerator where it is collected. The cooling electron beam is thus continuously regenerated at the cathode, and the heat is dumped into the electron beam collector.

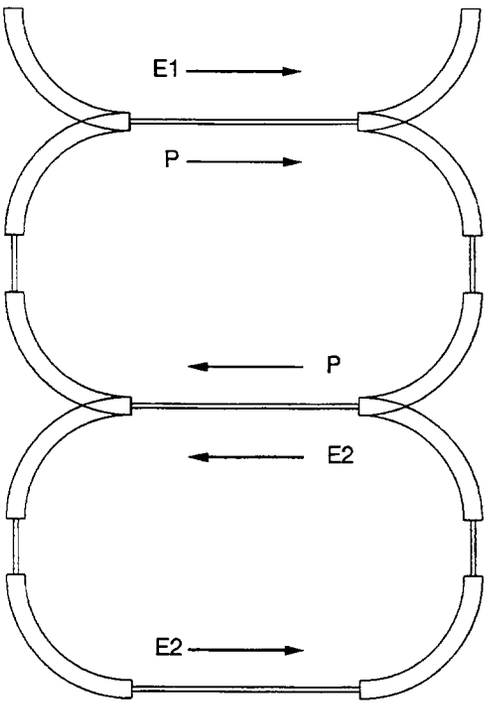

Figure 1. Schematic for electron cooling of electrons. Stored electron beam (E2) transfers heat to a stored positron beam (P) which transfers heat to the single pass cooling electron beam (E1).

2. EQUILIBRIUM OPERATION OF THE POSITRON HEAT TRANSFER RING

An earlier study of electron cooling of electrons was presented at the 1992 SPIE Conference [10]. That work was able to present a much more detailed study than the present work, due to the present page limit requirement. The earlier work derived the usual formula for the electron cooling of positrons,

$$dv_{p*}/dt = 60IL_c r_e^2 c^3/\beta\gamma^2 a^2 eCv_{p*}^2 \quad \text{(lab frame)} \ , \tag{1}$$

where v_{p*} is the positron velocity in the moving frame, t is the time, I is the electron beam current, L_c is the length of the cooling straight, r_e is the classical radius of the electron, c is the speed of light in vacuum, β is the beam velocity divided by c, $\gamma = (1-\beta^2)^{-1/2}$, a is the beam radius, e is the charge on the electron, and C is the circumference of the positron ring. The earlier study went on to compare the electron cooling rate to the intrabeam scattering rate within the electron cooled positron storage ring in order to determine where equilibrium operation of the positron storage ring would occur.

Figure 2 presents the equilibrium positron beam size within a possible positron heat transfer ring. The equilibrium vertical emittance is 0.2 π mm-mr, and the equilibrium horizontal emittance is 0.05 π mm-mr. These values compare favorably with what is desired for the next linear collider[11]. Table 1 presents parameters for the possible electron cooling system.

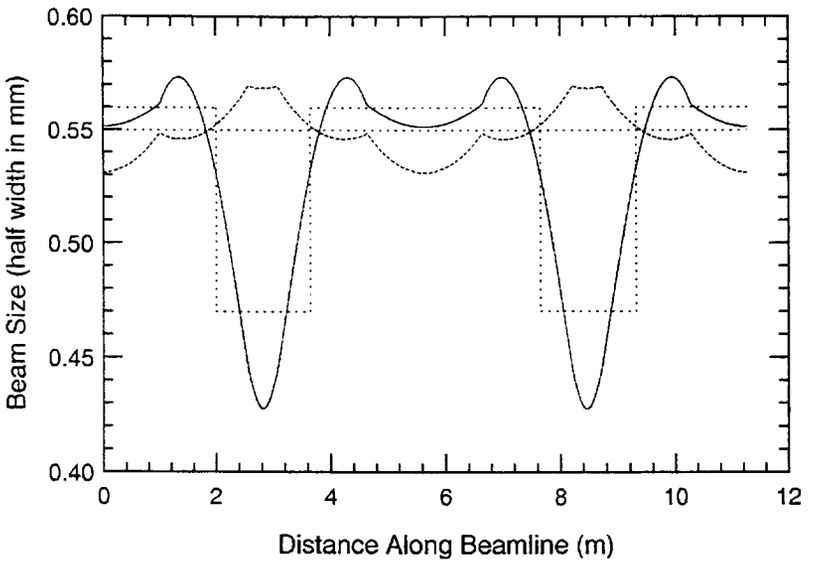

Figure 2. Equilibrium beam size in the positron heat transfer ring. Solid trace shows horizontal beam profile. Dashed trace shows horizontal beam profile. Dotted traces show beam size approximation for calculating IBS heating rates.

3. OPERATION OF THE ELECTRON COOLING RING

3.1. Determination Cooling Time

The electron cooling time can be determined by including the minus sign and rearranging Eq. (1) as

$$-v_*^2 dv_* = dt 60 I L_c r_e^2 c^3 / \beta\gamma^2 a^2 eC \qquad (2)$$

and integrating from the initial time and velocity to the final time and velocity obtains:

$$[(v_{*i} - v_{*f})^3]/3 = (t_f - t_i) 60 I L_c r_e^2 c^3 / \beta\gamma^2 a^2 eC \qquad (3)$$

Linear collider designs typically use 10^{10} particles per bunch, which here corresponds to a current of 43 mA. The hot electron beam will likely be supplied by acceleration from a thermionic gun. Thermionic guns can produce such currents with transverse emittances of 0.5 π mm-mr. This emittance is a factor of ten larger than the value of the positron horizontal emittance, and therefore the electron horizontal beam size and divergence due to emittance will each be about a factor of three greater than the equilibrium positron beam values. Therefore $(v_{*i} - v_{*f}) \approx 10^{-3}$. In this case the cooling beam is the positron beam, and I = 43 mA and a = .55 mm. But the effective cooling current will be reduced by a factor of six due to the overlap of the positron beam with the hot electron beam (Since the area of the positron beam is six times less than the area of the electron beam, 5/6ths of the electron beam will not be in contact with the positron beam on any given pass). So the effective cooling current is 7 mA. Substituting the appropriate values into Eq. (3) leads to an expected cooling time of

$$(t_f - t_i) = 1.9 \text{ ms}. \qquad (4)$$

The value of cooling time indicates that electrons could be cooled and delivered to a linear collider at a rate of 500 Hz.

Table 1. Parameters of Electron and Positron Storage Rings	
Beam Kinetic Energy (MeV)	3.0
Relativistic Factors, β, γ	0.99, 6.87
Ring Circumference (m)	11.3
Entrance and Exit Dipole Pole Face Rotations (degrees)	5
Length of Cooling Straight (m)	2
Average Value of Dispersion Function, D (m)	1.1
Transition Gamma, γ_T	1.265
Z/n Instability Limit (Ω)	20
Betatron Tunes Including Space Charge, ν_x , ν_z	1.135, 0.176
Betatron Tunes Excluding Space Charge, ν_x , ν_z	1.249, 0.452
Space Charge Tune Shift , $\Delta\nu_x$, $\Delta\nu_z$	0.114, 0.276
Electron Cooling Current (A)	0.1
Electron Cooling Beam Radius in Cooling Straight (mm)	3.2
Positron Beam Current (mA)	43
Equilibrium Positron Beam Radius in Cooling Straight (mm)	0.55
Equilibrium Normalized Positron Emittances ε_{nx}, ε_{nz} (π mm-mr)	0.05, 0.2
Equilibrium Positron Momentum Spread $\Delta p/p$	3.65×10^{-4}
Stored Electron Beam Current (mA)	43
Initial Stored Electron Beam Size in Cooling Straight (mm×mm)	1.61×1.1
Equil. Stored Electron Beam Size in Cooling Straight (mm×mm)	0.55×0.55
Initial Norm. Stored Electron Emittances ε_{nx}, ε_{nz} (π mm-mr)	0.5, 0.5
Equil. Norm. Stored Electron Emittances ε_{nx}, ε_{nz} (π mm-mr)	0.05, 0.2
Initial Stored Electron Beam Momentum Spread $\Delta p/p$	0.001
Equil. Stored Electron Beam Momentum Spread $\Delta p/p$	3.65×10^{-4}
Cooling Time (ms)	1.9

3.2. Equilibrium In The Electron Cooling Ring

If the electron cooling ring has a lattice identical to the positron transfer ring the IBS heating rate within the electron cooling ring is the same as the IBS heating rate for the positron transfer ring. But the cooling force will be much greater than the cooling force in the positron beam, since now the entire 43 mA positron beam is in contact with the electron beam. For this reason equilibrium in the electron cooling ring will be established thermally; the equilibrium emittance of the electron beam will equal that of the positron transfer beam.

The equilibrium emittances of the electron cooled electron beam will be 0.2 π mm mr vertically and 0.05 π mm mr horizontally. The momentum spread will be $\Delta p/p = 3.65\times10^{-4}$.

4. POSSIBLE INSTABILITIES

Particle beams can become unstable if they are cooled too far. If all beam particles have the same momentum, image charges generated by the particles onto the surrounding environment (such as pipes) will all be in synchronization with each other and this can lead to a field large enough to destroy the beam (the Z/n instability). Neil and Sessler[12] originally derived the criterion for onset of the Z/n instability,

$$|Z/n| = Fmc^2 \beta^2 \gamma \eta (\Delta p/p)^2 (eI)^{-1} . \qquad (5)$$

In Eq. (5) I is the stored particle beam current and η is the absolute value of the momentum compaction of the storage ring, $\eta = |(1/\gamma_t^2) - (1/\gamma^2)|$, where γ_t is the transition energy of the storage ring, here 1.265. F is a form factor of about 3. For both the electron and positron storage rings discussed here the onset of the Z/n instability will occur for

$$Z/n = 20\,\Omega \quad . \tag{6}$$

Small beam sizes lead to an increase in the relative contribution of space charge forces to the beam optics, causing a large tune spread that can cross destructive resonances, leading to beam loss. For the electron and positron lattices discussed here the horizontal tune including space charge is 1.135 and the horizontal tune excluding space charge is 1.249. The vertical tune including space charge is 0.176 and the vertical tune excluding space charge is 0.452. This region of tune space avoids the destructive integer and half integer resonances, but the vertical tune does cross the third integer resonance. It may be desirable to investigate different lattices to avoid this resonance as well.

5. CONCLUSION

This paper has presented the concept of electron cooling of electron beams. The necessary electrostatic accelerator technology for this concept has already been demonstrated[13]. The final emittance and rep rate capability of electron cooled electron sources are a fine match to future linear collider needs.

6. ACKNOWLEDGEMENTS

Due to the annual re-direction of the U.S. research program by Congress I was unable to present this work. I wish to offer my sincere gratitude to Dr. Tim Ellison of the Indiana University Cyclotron Facility who graciously offered to present this paper. This work was supported by the SSC Lab, operated by the Universities Research Association, Inc., for the U.S. Department of Energy under contract No. DE-AC35-89ER40486.

7. REFERENCES

[1] G.I. Budker, The 1966 Proc. Int. Symp. Electron and Positron Storage Rings, Saclay. Atomnaya Energiya 22: 346.

[2] L. Spitzer, "Physics of Fully Ionized Gases," (New York: Interscience, 1956) pp. 80-81.

[3] G.I. Budker, et al., Particle Accelerators, Vol. 7, 197-211 (1976).

[4] M. Bell, et al., Physics Letters, Vol. 87B, No. 3, (1979).

[5] T. Ellison, et al., IEEE Trans. Nuc. Sci., Vol. NS-30, No. 4, 2636-2638, (1983).

[6] D. L. Friesel, et al., IEEE Trans. Nuc. Sci., Vol. NS-32, No. 5, 2421-2423, 1985.

[7] A. Wolf, "Electronenkuhlung fur niederenergetische Antiprotonen," PhD thesis, KfK 4023 Kernforschungszentrum Karlsruhe, 1986.

[8] D. J. Larson, Particle Accelerators, Vol. 24, No. 2, 63-89, (1989).

[9] D. J. Larson, Physical Review Letters, Vol. 60, No. 13, pp. 1274-1277, March 1988.

[10] D. J. Larson, SPIE, Vol. 1629, pp. 446-457 (1992).

[11] Ronald D. Ruth, Proc. of the 1989 Chicago Particle Accelerator Conference, pp. 716-720 (1989).

[12] V.K. Neil and A.M. Sessler, Rev. Sci. Instrum., Vol. 36, 429 (1965).

[13] D.J. Larson, et al., NIM, A311, 30-33 (1992).

MOLECULAR DYNAMICS SIMULATION OF ELECTRON COOLING*

G. Zwicknagel, C. Toepffer and P.-G. Reinhard
Institut für Theoretische Physik II, Universität Erlangen,
D - 91058 Erlangen, Germany

ABSTRACT
We report on results of the stopping power of heavy ions in strongly coupled electron plasmas obtained by performing molecular dynamics (MD) computer simulations. A comparison with conventional theories of the stopping power shows that these fail at low ion velocities and strong coupling, where collisions between the electrons and nonlinear screening effects get important. This causes a change in the dependence of the stopping power on the ion charge Z_p at low ion velocities. From the MD simulation we find the stopping power to behave like $Z_p^{1.43}$ instead of the weak coupling behavior $Z_p^2 \ln(\text{const}/Z_p)$.

1. INTRODUCTION

The description of electron cooling of ion beams in a storage ring requires the knowledge of the stopping power on the ions due to their interaction with the cold electrons. Because of the low electron temperatures, in particular in the longitudinal component, and the possible high ion charge states, one may have to deal with strongly coupled Coulomb systems. The usual weak coupling theories for the stopping power, like binary collision approximations or linear dielectric response descriptions, are then not longer a priori applicable. To investigate the stopping power of heavy ions in strongly coupled, classical electron plasmas, with plasma parameters $\Gamma \gtrsim 1$, we perform molecular dynamics (MD) computer simulations. These simulations are an appropriate tool to study dynamical properties of strongly coupled nonequilibrium Coulomb systems and nonideal plasmas. Strong correlations and collective effects like the nonlinear dynamical screening are automatically taken into account in the MD simulations provided one succeeds in a correct treatment of both binary and higher order particle collisions.

After a description of our MD simulation technique, we discuss the stopping power obtained from weak coupling considerations and then compare this with the results we got from the MD simulations. We find that the weak coupling theories fail to predict both the velocity- and the charge-dependence of the stopping power for low ion velocities and large coupling strengths of the electron plasma. Then nonlinear dynamical screening effects and collisions between the target electrons become important for the stopping power. So far we have restricted our investigations to isotropic electron target plasmas and did not take into account the magnetic field present in the electron cooler. Such work is in progress.

2. MD SIMULATIONS OF THE STOPPING POWER

For our simulations of the stopping power [1] we consider systems consisting of heavy ions (charge $Z_p e$, mass $m_p = 0.5 \ldots 1 \cdot 10^5\, m_e$ and a non-relativistic velocity $\mathbf{v}_p$) moving through a one-component fully ionized electron plasma (density n_e, temperature T_e) with a static neutralizing background. The coupling strength between the electrons is given by the plasma parameter $\Gamma = e^2(4\pi n_e/3)^{\frac{1}{3}}/k_B T_e$, representing the ratio of mean potential to thermal energy, with strong coupling for $\Gamma \gtrsim 1$. The full dynamical description of a classical plasma only depends on this plasma parameter Γ. Here, we use different coupling strengths $\Gamma = 0.011$, 0.11, 0.34 and 1.08 corresponding to, for example, $T_e = 116 \ldots 1.16K$ and $n_e = 10^8\ cm^{-3}$. In the simulations we integrate the classical equations of motion for point particles interacting by the Coulomb force using a leap-frog algorithm and typically 500 electrons. Because of the finite number of particles and the infinite range of the Coulomb force we use periodic boundary conditions to represent an infinite system and an Ewald-sum technique to calculate the total force on a particle. There are serious problems for the stability and economy of the simulations arising from close collisions of particles with strongly curved trajectories. For this reason we have developed a special treatment for close collisions. We set a critical distance r_c and select in each time step $\triangle t$ binary and higher order clusters. A particle belongs to a cluster if its distance to any other particle in the cluster is less than r_c. The binary clusters

are propagated by taking piecewise analytical solutions of the Rutherford problem. For the less frequent higher clusters we choose a very small internal time step $\ll \Delta t$ to achieve high precision propagation. The remaining particles outside any cluster are integrated with the standard time step Δt. The influence of these surrounding particles on the motion within a cluster is taken into account by a change in momentum $\Delta \mathbf{p} = \mathbf{F}^{ext} \cdot \Delta t$ for each member of a cluster. Here $\mathbf{F}^{ext}$ is the sum of all forces from all particles outside the cluster. This technique saves a factor of about 100 in computing time and makes stable simulations of attractive plasmas with high mass ratios feasible. To study the stopping power, we performed several hundred runs for different charge states of the heavy ion $Z_p = 2 \ldots 20$, different ion velocities v_p and random initial spatial configurations of the electron plasma. Since during the simulation the ion's energy loss heats up the target, we refresh it in regular time intervals by drawing new electron velocities from a Maxwell distribution with the initial temperature. The accuracy and stability of the runs are monitored using the total energy.

3. WEAK COUPLING THEORIES AND PREDICTIONS

In the binary collision approximation [2] the stopping power of heavy ions in a dilute, weakly coupled classical plasma is calculated from the energy transfer of the ion to the electrons in isolated collisions. Integrating the Rutherford transport cross section over the impact parameters and averaging over the thermal distribution of the electron velocities yields the total energy loss as a function of the ion velocity v_p. Screening effects are accounted for by introducing a largest impact parameter b_{max}, with $b_{max}(v_p) = \lambda_D [1 + v_p^2]^{1/2}$, where λ_D is the Debye–length and v_p is scaled in $\sqrt{kT_e/m_e}$. For weak coupling with $Z_p \sqrt{3}\, \Gamma^{3/2} \ll 1$ the stopping power $-dE/ds$ then behaves in the two limiting cases of low and high ion velocities as,

$$-\frac{dE}{ds} \propto Z_p^2 v_p \ln\left(\frac{2}{Z_p \sqrt{3}\, \Gamma^{3/2}}\right) \qquad v_p \ll 1\,, \qquad -\frac{dE}{ds} \propto \frac{Z_p^2}{v_p^2} \ln\left(\frac{v_p^3}{Z_p \sqrt{3}\, \Gamma^{3/2}}\right) \qquad v_p \gg 1\,. \quad (1)$$

In the strong coupling regime, where the Coulomb logarithm becomes negative, the behaviour of the stopping power at low ion velocities changes. The binary collision approximation then predicts a cubic v_p– dependence at low velocities (Fig. 1).

A weak coupling description of the stopping power automatically including the screening effects is given in framework of the linear dielectric response formalism. In this mean-field approach the polarization potential due to the perturbation of the ion is treated selfconsistently. There one starts with a linearized Vlasov–Poisson equation for the electron distribution to derive the dielectric response function $\varepsilon(k, \omega)$ of the electron plasma. From this the stopping power of an ion is given by [3, 4]:

$$\frac{dE}{ds} = Z_p^2 \int d^3k \, \frac{\mathbf{k} \cdot \mathbf{v}_p}{v_p k^2} \, \Im\left(\frac{1}{\varepsilon(k, \mathbf{k} \cdot \mathbf{v}_p)}\right) \quad (2)$$

To avoid a logarithmic divergence at the upper limit of the k-integration in the dielectric result (2) a cutoff parameter k_{max} is necessary. It is chosen in the usual manner to exclude close Coulomb collisions with a scattering angle larger than 90^o [4].

Due to the assumption of a weak perturbation caused by the ion which is used for the linearization the genuine validity of (2) is restricted to $Z_p \Gamma^{3/2} 4\pi\sqrt{3} \ll 1$. In the weak coupling regime, however, neither the insufficient treatment of close collisions in the dielectric theory nor the treatment of screening in the binary collision approximation cause any serious problems. Both theories show almost identical results in this regime and the dielectric expression (2) yields the same limiting cases (1) as the binary collision approximation, in which no cutoff for close collisions is needed. For larger Γ and Z_p, the stopping power in the dielectric description shows a similar transition from a linear to a cubic velocity dependence at low velocities as in the binary collision approximation. However, our MD simulations show a linear veloctiy dependence at low v_p for all studied target plasma conditions.

So far both weak coupling descriptions have neglected the collisions between the target electrons, which is justified only for weak coupling, where the collision frequency ν is related to the plasma frequency ω_{p_e} by $\nu/\omega_{p_e} \propto \Gamma^{3/2}$. The dielectric response formalism, however, enables to account for collisions by adding a collision term in the underlying kinetic equation. To get a rough estimate of the effects of collisions one can employ a relaxation-time ansatz which results in the replacement $\varepsilon(k, \omega) \rightarrow \varepsilon(k, \omega + i\nu)$ in Eq.(2) [4].

The MD simulations are carried out in a finite cube. For purposes of comparison the theoretical approaches mentioned above are adapted by introducing an upper limit for b_{max} and a lower limit for the k-integration in (2) corresponding to the length of the cube.

4. SIMULATION RESULTS OF THE STOPPING POWER

The MD stopping power $-dE/ds$ is shown in Fig. 1 as a function of v_p for coupling strengths $\Gamma =$ 0.11 and 1.08 and $Z_p = 10$.

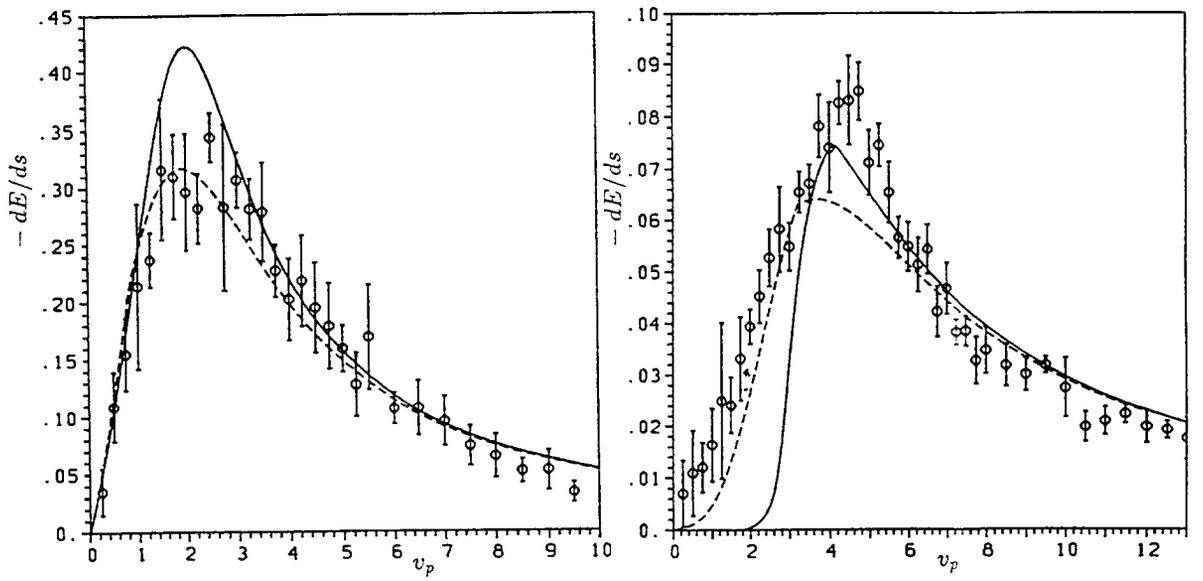

Fig. 1 - Normalized stopping power $-dE/ds\,/(Z_p^2\sqrt{3}\,\Gamma^{3/2})$ in units of k_BT_e/λ_D as a function of the ion velocity $v_p/(k_BT_e/m_e)^{1/2}$ for coupling strengths $\Gamma = 0.11$ (left plot) and $\Gamma = 1.08$ (right plot). The circles with errorbars represent the MD simulation data and the curves show the results of the dielectric description (solid) and the binary collision approximation (dashed).

The errorbars indicate the standard deviation from the mean value (circles) over an ensemble of runs differing only in the initial configuration. The solid curves represent the dielectric results from Eq.(2) (with $\nu = 0$) and the dashed curves those from the binary collision approximation. Whereas for $\Gamma =$ 0.011, which is not shown here, the three results agree quite well, there is an acceptable agreement for higher coupling strength $\Gamma \gtrsim 0.1$ only for large ion velocities. At low ion velocities we find a disagreement which grows with Γ. While the MD results show a linear increase $-dE/ds \propto v_p$ for all Γ at low ion velocities, the results of the dielectric description and the binary collision approximation exhibit the transition from a linear to a cubic behaviour mentioned above. This disagreement we think is due to an incorrect treatment of the screening in both descriptions. There the screening-length at low ion velocities is given by λ_D, which, however, becomes small compared to the mean particle distance for increasing coupling strength Γ. For intermediary v_p the dielectric description better reproduces the MD results when electron-electron collisions are included. By varying the collision frequency ν in the dielectric description to obtain the same maximal stopping power as in the MD data [1], we find collision frequencies $\nu/\omega_{p_e} =$ 0.8, 0.3 and 0.2 at coupling strengths $\Gamma = 0.11$, 0.34 and 1.08, respectively. This is in contradiction to the weak coupling gaseous behaviour $\nu/\omega_{p_e} \propto \Gamma^{3/2}$ and indicates a slowing down of the relaxation time anticipating the eventual transition to the Wigner lattice of a classical one–component plasma [5].

To investigate the Z_p-dependence of the stopping power we performed further runs for $\Gamma = 0.34$ and 1.08 and various charges Z_p. Our simulation data agree with the theoretical predictions at high ion velocity sufficiently well, showing the Z_p-dependence of (1). For low ion velocities, the linear increase of the stopping power with v_p yields an exponentially decreasing ion motion $v_p(t) = v_0\, e^{-\lambda t}$ because of

$m_p \dot{v}_p = F(v_p) = dE/ds = -m_p \lambda v_p$. In Fig. 2, the decrements λ extracted from the MD simulations are plotted as a function of Z_p.

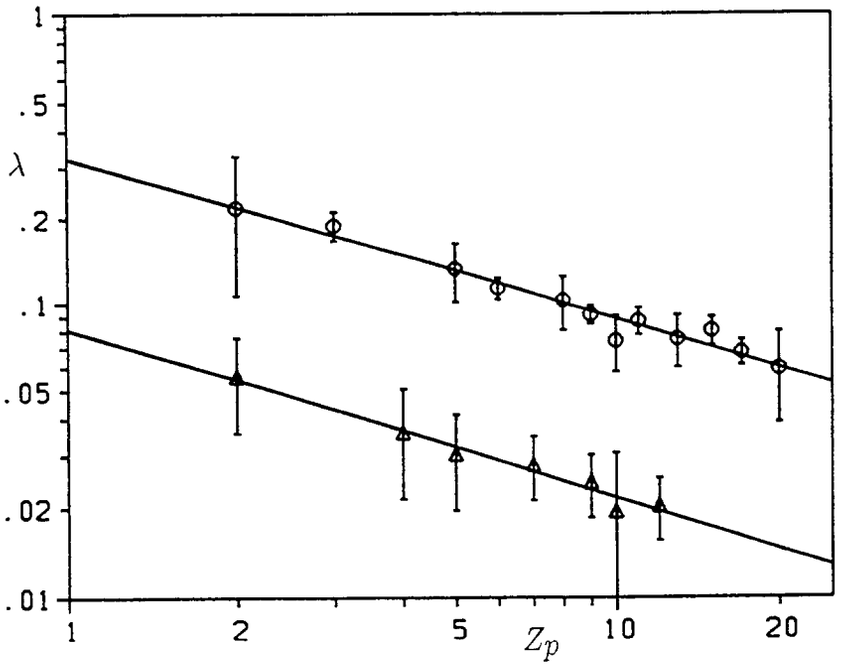

Fig. 2 - Normalized decrements $\lambda/(Z_p^2 \sqrt{3}\Gamma^{3/2}(m_p/m_e)^{-1})$ in units of ω_{p_e} as a function of the ion charge Z_p. The solid lines represent a least square fit to the MD data for $\Gamma = 0.34$ (circles) and $\Gamma = 1.08$ (triangles). In both cases the fit corresponds to a power law $\lambda \propto Z_p^{-0.57}$.

The solid lines correspond to a fit of the data by a power law $\lambda \propto Z_p^x$, with almost the same exponent $x \approx -0.57$ for $\Gamma = 0.34$ and $\Gamma = 1.08$. Thus our MD simulation show a charge dependence for strong coupling and low velocities $dE/ds \propto Z_p^{1.43}$, whereas for weak coupling one has the dependence $dE/ds \propto Z_p^2 \ln(\text{const}/Z_p)$ (1).

5. SUMMARY AND OUTLOOK

From our MD simulation results we find that the weak coupling approaches of the stopping power are not applicable for a description at strong coupling and low ion velocities. Our results confirm the importance of target particle collisions and nonlinear effects. The breakdown of linear response is clearly indicated by the Z_p-dependence of the stopping power at low ion velocities going with $Z_p^{1.43}$. Hence for the description of electron cooling care has to be taken in the extrapolation of weak coupling predictions to the strong coupling regime.

Further investigations by MD simulations of the stopping power adapted to electron cooling are in progress. We take into account an anisotropy of the electron-distribution and the presence of a magnetic field in the electron cooler.

REFERENCES

[*] Supported by the "Bundesministerium für Forschung und Technologie" (BMFT) and the "Gesellschaft für Schwerionenforschung" (GSI), Darmstadt.

[1] G. Zwicknagel, C. Toepffer, P.-G. Reinhard, Proceedings of the International Symposium on Heavy Ion Inertial Fusion, Frascati Italy, 1993, Il Nuovo Cimento A (to be published).

[2] L. de Ferrariis and N.R. Arista, Phys. Rev. A **29**, 2145 (1984).

[3] S. Ichimaru, *Basic Principles of Plasma Physics* (Benjamin, Reading, Massachusetts, 1973).

[4] Th. Peter and J. Meyer-ter-Vehn, Phys. Rev. A **43**, 1998 and 2015 (1991).

[5] G. Armbrüster and C. Toepffer, Nucl. Instrum. Methods A **333**, 282 (1993).

NEW COLLECTOR FOR THE CELSIUS ELECTRON COOLING SYSTEM

A.N. Sharapa, A.V. Shemyakin
Budker Institute of Nuclear Physics, 630090 Novosibirsk, Russia

L. Hermansson, D. Reistad
The Svedberg Laboratory, Box 533, 751 21 Uppsala, Sweden

ABSTRACT
Results of collector efficiency measurements performed on the present CELSIUS collector are given. Pecularities of such measurements in electron cooling systems are discussed. A new collector, which is expected to have a collection efficiency considerably better than the present one, has been produced and tested at the BINP test bench. The results of these measurements are presented.

1. INTRODUCTION

For the CELSIUS storage ring performance the so called "electron heating" effect is an important problem [1]. One of the possible explanations of this phenomenon may be related to secondary electrons escaping from the collector. This work was initiated in order to decrease the flow of these electrons and thus to promote understanding of the "electron heating" mechanism.

The present CELSIUS collector has a good enough efficiency to provide an electron beam energy recovery up to the current of 2 A [2]. It is important to specify the collector efficiency concept. As a rule, the ratio of the high voltage power supply current I_{hvps} to the cathode current I is considered to be a characteristic of the collector efficiency. For the case of a strong magnetic field this value is determined not only by the recuperator, but also by properties of the electron cooling device as a whole system. The current I_{hvps} may be much less than a flow δI of secondary electrons created by the primary beam on the collector surface and escaped from the recuperator. For instance, in straight systems (i.e. in devices without bending magnets), the main fraction of such electrons comes to the gun, is reflected, returns into the collector and is captured with the same efficiency as the primary beam. In this case $I_{hvps} << \delta I$. To characterize the efficiency of a recuperator itself, it is useful to introduce

$$\sigma_{col} = \frac{\delta I}{I} \qquad (1),$$

which can be called the collector secondary emission coefficient. The values of σ_{col} and $\frac{\delta I}{I}$ are the same only under definite conditions. In section 2 these conditions are discussed and results of measurements of the CELSIUS collector secondary emission coefficient are presented.

The magnitude of σ_{col} can be considerably decreased if the potential minimum in the recuperator is formed in accordance with the solution for two guns with coinciding cathodes, which was proposed in ref.[3]. A geometry of equipotentials in such a potential barrier is almost planar, therefore we will name this solution a flat electrostatic mirror. At the BINP test bench measurements were performed to compare the efficiency of the recuperators with the tube-shaped suppressor (like that used in CELSIUS) and with diaphragm-shaped one, where the flat electrostatic mirror was formed. On the base of results of these measurements a new collector for CELSIUS electron cooling system is made.

2. MEASUREMENTS OF THE CELSIUS COLLECTOR SECONDARY EMISSION COEFFICIENT.

At the CELSIUS ring a recuperator with a tube-shaped suppressor has been used. To define the coefficient of secondary emission of that, it is necessary that the whole flow of secondary electrons from the collector on its way to the gun should come to an electrode on ground potential. This is possible for a large enough displacement due to centripetal drift in the toroid bends Δ_1:

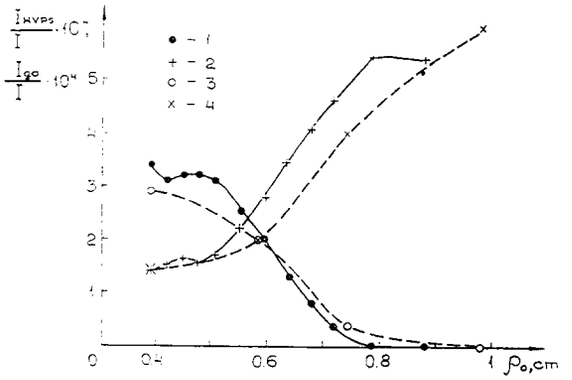

Fig.1. The current of the high voltage power supply (2,4) and the gun anode current (1,3) as functions of ρ_0. I= 1 A, U_{col} = 5 kV, U_s= 0.7 kV. 1,2- B_0= 0.15 T, U_{hvps} changes, 3,4- U_{hvps}= 30 kV, B_0 changes.

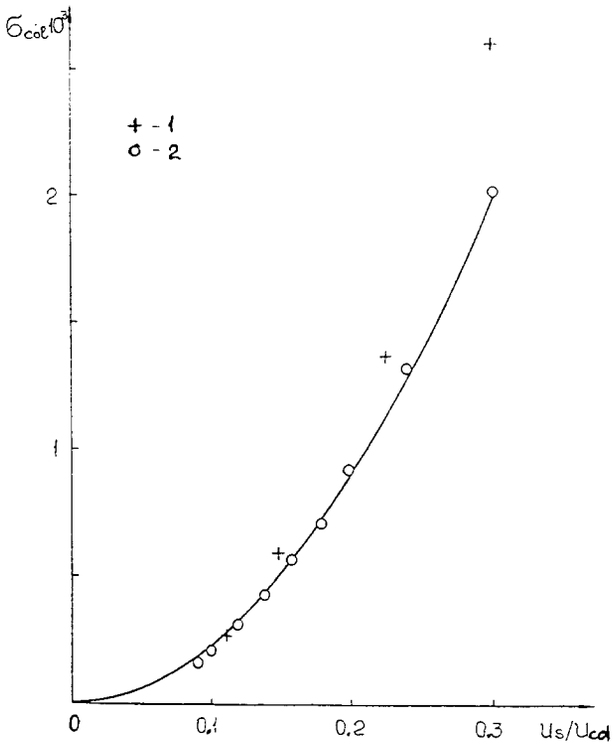

Fig.2. The collector secondary emission coefficient as function of the potential barrier depth. B_0= 0.1 T, I= 0.5 A, U_{hvps}= 30 kV. 1- U_s= 0.45 kV, U_{col} changes, 2- U_{col}= 5 kV, U_s changes.

$$\Delta_1 = 2\alpha\rho_0 > R_b + R_0,$$
$$\rho_0 = \frac{m}{eB_0}\sqrt{\frac{2W}{m}} \qquad (2),$$

where α is a turn angle of the trajectory (π for CELSIUS), $W \approx eU_{hvps}$ is the energy of these electrons, e,m are charge and mass of electron, B_0 - is magnetic field strength, R_b is the radius of the beam, R_0 is the minimal radius of electrodes on ground potential, $2\pi\rho_0$ is the gyro wave length of the electrons.

For the CELSIUS system the condition (2) can be controlled by the current I_{hvps} and the current of the gun anode power supply as a function of the value of ρ_0 (fig.1). As ρ_0 increases, the secondary beam strikes first the gun anode having the minimal diameter, and then the grounded electrode. The valuesof Δ_1, for which the gun anode current is zero, agrees with the condition (2). For $\rho_0 > 0.8$ cm $\sigma_{col} = \frac{I_{hvps}}{I}$.

Shown in figure 1 are results of two sets of measurements. For the first set the value of ρ_0 is changed by a increase in the energy of electrons, and for the other one by the magnetic field strength,. The results agree with an accuracy of 10%. It means that, firstly, the current losses are determined uniquely by the magnitude of σ_{col} and a relation between beam-electrode gaps and ρ_0. Secondly, the magnitude of σ_{col} depend weakly on the magnetic field strength.

To estimate the collector secondary emission coefficient, in the ref.[4] a simple formula is proposed:

$$\sigma_{col} = k\left(\frac{U_m}{U_{col}}\right)^2 \frac{B_c}{B_m} \qquad (3)$$

where U_m is the potential in the electrostatic barrier, U_{col} is the collector potential, B_m and B_c are the magnetic fields in the barrier and at the collector surface, respectively, the magnitude of the coefficient k depends on the collector material and vacuum conditions. The measured values of σ_{col} (fig.2) are quadratic in $\frac{U_s}{U_{col}}$ in agreement with (3). Taking U_m to be equal to a suppressor potential U_s and $\frac{B_c}{B_m}$=0.15, we obtain for CELSIUS collector conditions (a copper surface, the vacuum $5 \cdot 10^{-7}$ Pa) k= 0.15 (solid curve in figure 2).

For each value of the beam current there is a minimal possible value of the suppressor potential $(U_s)_m$ and a corresponding value of σ_{col} In experiments the magnitude of the barrier perveance [3]

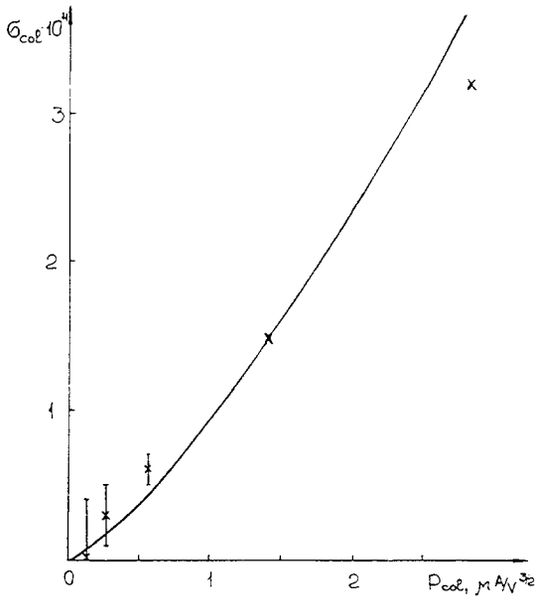

Fig.3. The minimal value of σ_{COL} as function of collector perveance. U_{hvps} 150 kV, B_0= 0.1 T, U_{col}= 5 kV, U_s is the minimum possible for each current.

$P_b = \frac{I}{(U_s)_m^{\frac{3}{2}}}$ is constant with good accuracy. Using eq. (3) iit is possible to predict a relationship between the collector secondary emission coefficient and the collector perveance:

$$\sigma_{col} \sim P_{col}^{\frac{4}{3}} = \frac{I^{\frac{4}{3}}}{U_{col}^2}(\quad (4).$$

The function σ_{col} (P_{col}) is the main characteristic of recuperator properties. For the CELSIUS recuperator it is presented in figure 3 and fits in the formula (4) (solid curve in figure 3).

Recuperators with an electrostatic barrier created by a tube-shaped suppressor are popular now (see, for example, [5], [6]). Therefore, these results of measurements of the collector secondary emission coefficient are useful also for other electron cooling systems.

3. MEASUREMENTS OF CHARACTERISTICS OF RECUPERATOR WITH FLAT ELECTROSTATIC MIRROR.

These measurements were performed with a prototype of the new collector on the INP straight test bench (fig.4).

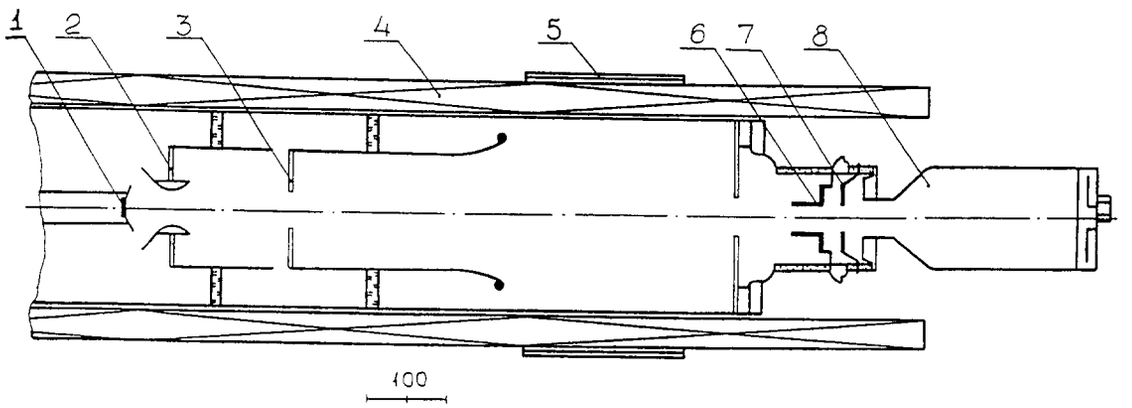

Fig.4. The BINP test bench. 1- cathode, 2,3- gun anodes, 4- solenoid, 5- correction coils, 6- collector anode, 7- diaphragm, 8- collector.

In straight systems the relative current losses are considerably lsmoller than the collector secondary emission coefficient, because the high voltage electrode current is created only by deviation of secondary electron trajectories from the primary beam ones on a value of [4]

$$\Delta = 2\rho_m = 2\frac{m}{eB_0}\sqrt{\frac{eU_m}{m}}. \qquad (5).$$

Therefore, the losses depend not only on a secondary electron flow from the recuperator, but also on distance between electrodes and the beam boundary as well as on the magnetic field strength. The goal of the measurements was a comparison of the losses for two methods of creating the potential minimum. This comparison was performed for the same geometries of the magnetic field and electrodes.

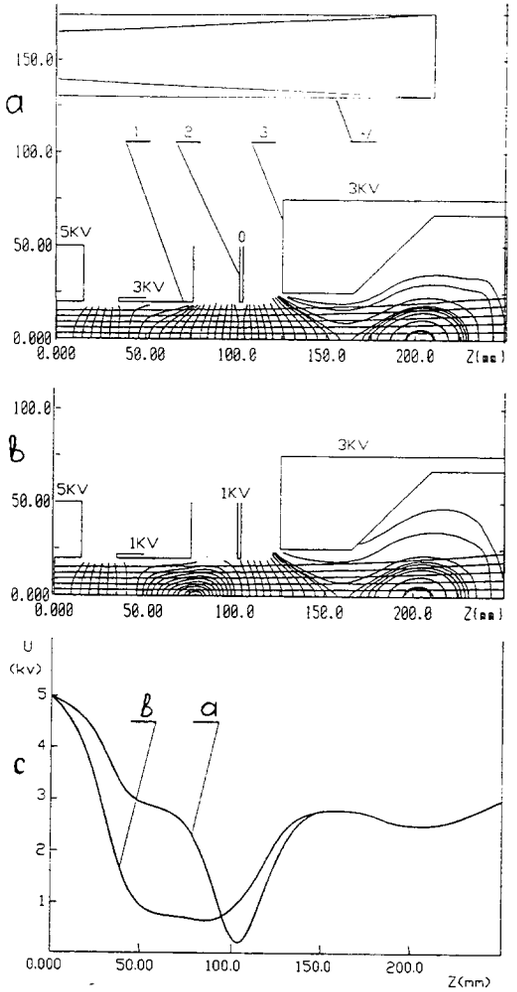

Fig.5. Results of simulation of two variants of recuperator a- tube-shaped suppressor, b- diaphragm-shaped one, c- potential distribution. 1- collector anode, 2- diaphragm, 3- collector, 4- solenoid. I=0.7 A, B_0= 50 mT.

For the first variant the suppressing potential is given to a diaphragm arranged symmetrically between the cylindrical entrance of the collector and the cylindrical collector anode. Potentials of the collector and the collector anode are equal.. The second variant models a tube-shaped suppressor used at CELSIUS: the suppressing potential is applied to the collector anode connected with the diaphragm. Results of simulations of both variant are shown in fig.5.

An electron gun with a barium oxide 30 mm cathode is used. To decrease the magnetic field on the cathode it is possible to switch off proper sections of the solenoid. The measurements were made mainly in such a regime with the 20 mm beam diameter at the recuperator entrance.

Both variants of recuperator have a good enough efficiency, and for the magnetic field strength being typical for the CELSIUS electron cooling device (about 0.1 T) the current losses are too low to be registered with good accuracy. Therefore the comparative measurements were made at the lower field level (fig.6). The losses for the diaphragm-shaped suppressor are drastically less almost in the whole range of the field strength. Note, that the level of these losses changes approximately proportionally with vacuum and is determined, apparently, by electrons created by ionization of the residual gas. A rapid growth of the losses at low magnetic fields is explained by a reflection of a peripheral fraction of the primary beam due to the development of transverse velocities of electrons in the gun at the field strength of the order of ten mT.

The minimum losses in the experiments with the diaphragm-shaped suppressor are achieved for the minimal possible potential on the diaphragm. This regime corresponds to a position of a zero equipotential near the beam boundary. Experimentally it can be observed by measuring of the current losses as a function of the transverse

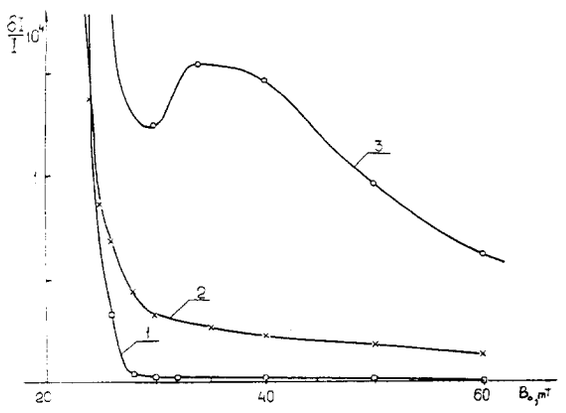

Fig.6. The current losses as a function of the magnetic field strength near the recuperator entrance. I=240 mA, U_{col}= 3 kV. 1- diaphragm- shaped suppressor, U_s= -300V, 2,3- tube-shaped suppressor, U_s= 0.75 kV (2), 1.5 kV (3).

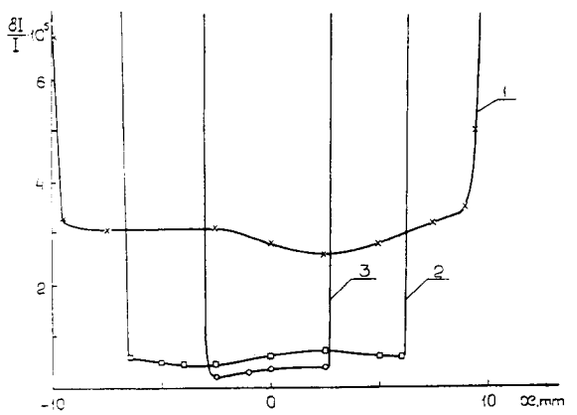

Fig.7. The current losses as function of the transverse displacement of the beam. I=240 mA, U_{col}= 3 kV, B_0= 35 mT, I= 240 mA. 1- tube-shaped suppressor, U_s= 0.75 kV, 2,3- diaphragm- shaped suppressor, U_s= -150 V (2), -300 V (3).

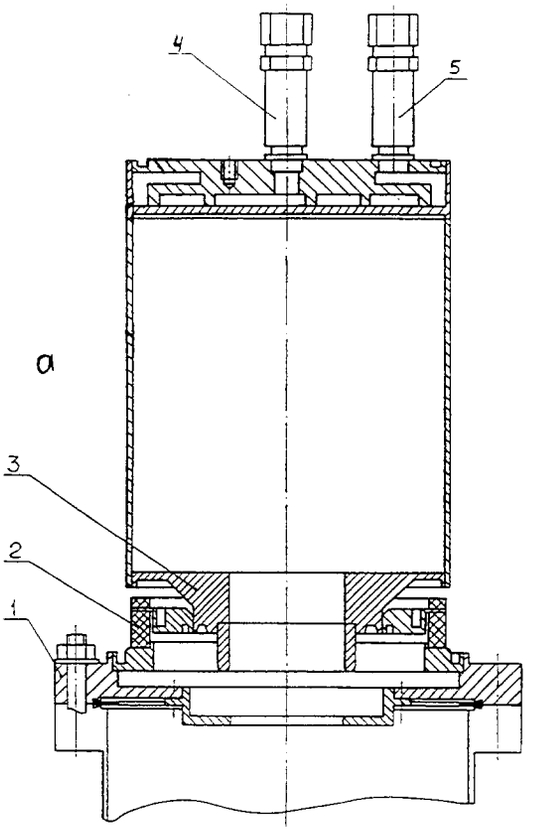

Fig.8. The new collector. 1-diaphragm, 2-isolator, 3- collector, 4, 5- input and output of water.

displacement of the beam by correction coils (fig.7). At large displacements the losses increase rapidly due to a reflection of the beam from the zero equipotential or its hitting to the collector anode. As the diaphragm potential decreases, the range of the beam positions with the low losses is reduced, which means a shift of the zero equipotential to the beam boundary.

Analogous measurements were performed also for the case of the approximately equal magnetic fields on the cathode and in the recuperator, i.e. for the beam diameter in the recuperator entrance near 30 mm. In this case the gap between the beam boundary and the collector anode is less than the one between the beam and the gun anodes, and the collector anode current is much higher than the losses. It complicates the interpretation of the results. Nevertheless, judging from the magnitude of the collector anode current, the variant with the diaphragm-shaped suppressor by optimal tuning of the diaphragm potential is essentially more effective also for 30 mm beam. Note, that for this case the collector perveance increases and for the optimal tuning is 2.4 $\frac{\mu A}{V^{\frac{3}{2}}}$.

On the base of these measurements a new recuperator for CELSIUS was made (fig.8). It consists of the collector proper, an isolator, a diaphragm, and is made to be mounted instead of the present one without an alteration of other elements of the electron cooling system. In comparison with the recuperator investigated on the test bench, the gaps between electrodes are corrected to increase the optimal collector perveance. The collector was mounted at the BINP test bench and successfully tested with a beam current of 2 A and a collector voltage of 4 kV. The results agree with those obtained previously for the prototype.

4. CONCLUSION.

The measurements made prove the advantage of the recuperator with a flat electrostatic mirror. The final result for the new collector secondary emission coefficient can be obtained only in experiments akin to those described in section 2. We hope, that with the new collector the current losses on the CELSIUS will be considerably lower.

The authors acknowledge the assistance in calculations performed by T.N. Andreeva and in the manufacturing and the assembly of the collector made by V.M. Rybkin.

References

1. D.Reistad et al., Measurements on electron cooling and "electron heating" at CELSIUS, this Workshop.
2. TSL progress report, Uppsala, 1991.
3. A.N. Sharapa, Nucl. Instr. and Meth., A329(1993), 551.
4. A.N. Sharapa and A.V. Shemyakin, Current losses in systems with the electron beam energy recovery in longitudinal magnetic field, this Workshop.
5. T.J.P. Ellison et al., Nucl. Instr. and Meth., B40/41(1983), 2636.
6. N. Angert et al., EPAC-88, Rome, 7-11 June,1988, (World Scientific, Singapore), p.1436.

OPERATION OF THE TSR CLOSE TO THE TRANSITION ENERGY

M. Grieser, F. Albrecht, D. Habs, R. v. Hahn, B. Hochadel, C.-M. Kleffner, J. Liebmann, R. Repnow, D. Schwalm
MPI für Kernphysik, Heidelberg
G. Bisoffi
INFN, Legnaro
E. Jaeschke
BESSY, Berlin

Abstract

A new operation mode of the machine close to the transition energy was investigated at the heavy ion storage ring TSR, because for sufficiently small currents and strong cooling, intrabeam scattering (IBS) is expected to be strongly suppressed. This mode is especially of interest for laser cooling experiments. At the TSR it can be obtained by increasing the dispersion function in the dipole magnets to 8.8 m and its properties were investigated in beam times with $^{12}C^{6+}$ (63 MeV, 73 MeV) and protons (21 MeV, 10 MeV). For 21 MeV protons ($\gamma = 1.02$) a γ_{tr} parameter of 1.04 could be reached. The transverse blow-up of the beam diameter after switching off the electron cooler was investigated to determine IBS heating rates and found to be about one order of magnitude higher than predicted by the calculation. The reason for these strongly increased blow-up rates is attributed to a first order resonance, since a requirement for the operation near the transition energy turns out to be $Q_x \approx \gamma_{tr} \approx 1$, where Q_x is the horizontal tune.

1 INTRODUCTION

The Test Storage Ring TSR [1] at the Max Planck Institut für Kernphysik is used for accelerator, atomic and nuclear physics experiments. The ring with 55.4 m circumference has a maximum rigidity of 1.5 Tm and receives heavy ions up to iodine from a 12 MV van de Graaff and a normal conducting RF linac combination. Electron cooling is applied to reduce the phase space of the stored beam and for accumulation [2]. The storage ring is also equipped with a laser cooling system, which can cool suitable ion species (e.g. Li^+, Be^+) down to ultra-low temperatures (so far longitudinal temperatures below 5 mK could be reached [3]). The attainable temperatures are limited by intrabeam scattering (IBS), however, for sufficiently small currents and strong cooling IBS is expected to be strongly suppressed (as already observed for protons at NAP-M in Novosibirsk [6]) if the lattice of the storage ring fulfils the isochronism condition, this means that the revolution frequencies of the particles do not depend on their momenta. A mode of operation satisfying this condition has been investigated at the TSR. The relationship between the momentum p and the revolution frequency f of the particle can be expressed by the η parameter defined as:

$$\eta = \frac{\frac{\Delta f}{f}}{\frac{\Delta p}{p}} \tag{1}$$

The desired operation mode is therefore characterized by $\eta = 0$. This parameter depends on the particle energy ($E = \gamma m_0 c^2$) and on the machine parameter γ_{tr}:

$$\eta = \frac{1}{\gamma^2} - \frac{1}{\gamma_{tr}^2} \tag{2}$$

where γ_{tr} is given by:

$$\frac{1}{\gamma_{tr}^2} = \frac{\frac{\Delta C}{C}}{\frac{\Delta p}{p}} = \frac{1}{C} \oint \frac{D(s)}{\rho(s)} ds \tag{3}$$

Here D is the dispersion function, C is the circumference and ρ the radius of curvature of the central orbit.

2 THE LATTICE OF THE TSR AT $\gamma_{tr} \approx 1$

Since in the TSR γ is about 1 also γ_{tr} must be close to 1 to achieve $\eta \approx 0$. It then follows from (3) that the average value of the dispersion function in the dipole magnets ($\rho = 1.15\ m$) should be 8.8 m. A superperiodicity of 4 was chosen in the lattice calculations in order to satisfy the isochronism requirement in every quarter of the ring; the resulting dispersion and β-functions are shown in fig. 1. Although 4 additional dipoles in the straight section of the injection break the β-function symmetry in the vertical plane, they do not alter the desired periodicity of $D(s)$.

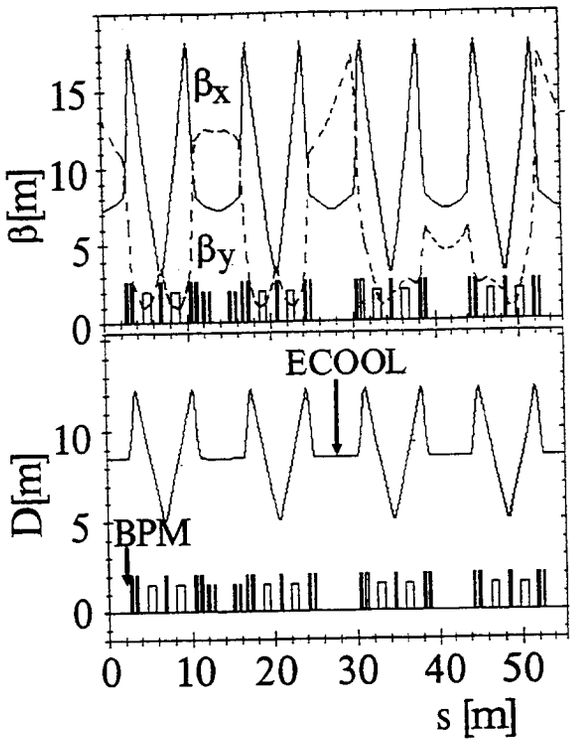

Figure 1: *Calculated β-functions and dispersion of the mode with $\gamma_{tr} \approx 1$.*

3 MEASUREMENT OF LATTICE PARAMETERS

In order to measure γ_{tr} the magnetic field of the dipoles was changed by $\frac{\Delta B}{B}$, which has the same effect on the length of the closed orbit as a change of the particle momentum by $-\frac{\Delta p}{p}$; since $\frac{\Delta C}{C} = -\frac{\Delta f}{f}$ ($\frac{\Delta f}{f}$ is the relative shift in the revolution frequency) it follows from (3):

$$\frac{1}{\gamma_{tr}^2} = \frac{\frac{\Delta f}{f}}{\frac{\Delta B}{B}} \tag{4}$$

The revolution frequency was measured via a Schottky noise analysis. Fig. 2 shows a typical Schottky spectrum of a $^{12}C^{6+}$ beam ($E = 73.3MeV$) at a γ_{tr} value of 1.06. As given by formula (1) for an η value of 0.1, the frequency spectrum is compressed by a factor of 9 compared to the standard mode with $\eta = 0.9$ for the same $\frac{\Delta p}{p}$.

Besides the transition parameter, the horizontal and vertical tunes (Q_x, Q_y) and the average value of the betatron function in each quadrupole family could be measured; a comparison between typical experimental and theoretical values, calculated with the computer program MAD [4], is given in table 1.

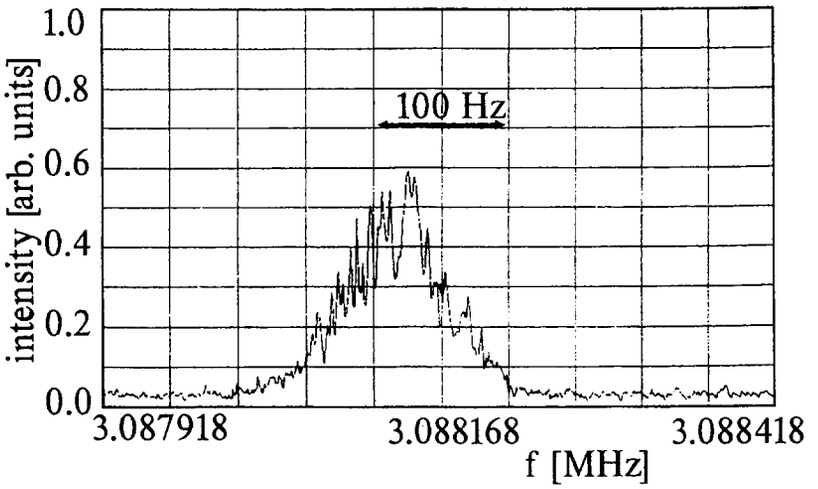

Figure 2: *Schottky spectrum for a $^{12}C^{6+}$ beam ($E = 73.3MeV$) at $\gamma_{tr} = 1.06$ corresponding to $\frac{\Delta p}{p} = 2 \cdot 10^{-4}$ measured at the fifth harmonic of the revolution frequency.*

Table 1: *Calculated and measured twiss parameters of the mode with $\gamma_{tr} \approx 1$.*

	Experiment	Theory
Q_x	1.1	1.11
Q_y	3.39	3.42
γ_{tr}	1.1	0.99
$\overline{\beta_{x,1}}, \overline{\beta_{y,1}}$[m]	3.7,12.3	8.6,13.5
$\overline{\beta_{x,2}}, \overline{\beta_{y,2}}$[m]	8.9,5.4	18.2 ,4.7
$\overline{\beta_{x,3}}, \overline{\beta_{y,3}}$[m]	2.4 ,2.3	3.0,2.5
$\overline{\beta_{x,4}}, \overline{\beta_{y,4}}$[m]	21.4,3.9	18.2,3.0
$\overline{\beta_{x,5}}, \overline{\beta_{y,5}}$[m]	10.1,7.9	8.6,8.6

4 BEAM BLOW-UP AT γ_{tr} CLOSE TO 1

By means of the beam profile monitor (its position is marked in fig. 1 with BPM) and the Schottky pickup it was possible to determine equilibrium values of horizontal and vertical emittances and momentum spread of electron cooled 63 MeV $^{12}C^{6+}$ and 21 MeV and 10 MeV proton beams. These measurements were carried out in the standard mode and in the mode where the beam energy is close to the transition energy (in the latter at various values of the transition parameter). Moreover, at different values of γ_{tr} and, for comparison in the standard mode, the heating rate of the beam after switching off the electron cooler was evaluated through the blow-up of the horizontal and vertical emittances. The experimental data of the emittance blow-up have been compared with the theoretical prediction due to intrabeam scattering calculated with a suitable IBS computer code [7]. Whereas the data are very well fitted by the theoretical calculation in the standard mode (γ_{tr}=3.1), large discrepancies between IBS theory and experiments have been observed in the cases where the γ_{tr} values were close to 1. The horizontal emittance blow-up rate was more than one order of magnitude higher than the predicted IBS value. The measured blow-up of the horizontal and vertical emittances after switching off the eletron cooling are shown in figure 3 together with the theoretical curve, which should be valid to the horizontal as well the vertical degree of freedom. The reason for these discrepancies is believed to be the heating due to the first order resonance at $Q_x = 1$ in the working diagram.

5 RELATIONSHIP BETWEEN γ_{tr} and Q_x

It is well known and easy to demonstrate that in a betatron $Q_x = \gamma_{tr}$, also for alternating gradient field mashines $Q_x \approx \gamma_{tr}$ is expected [5]. The relationship between Q_x and γ_{tr} was investigated at the TSR with different ion species and energies for several operating modes of the machine. The study was

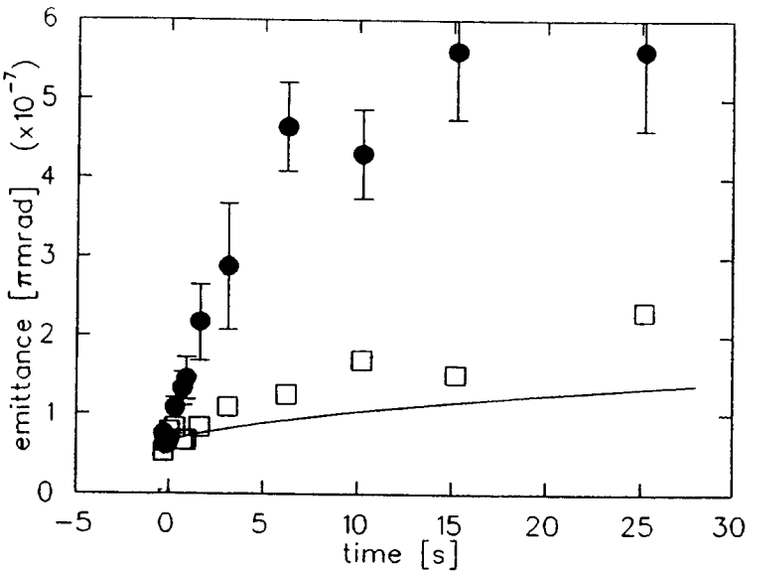

Figure 3: *Experimental horizontal (•) and vertical (□) blow-up of 21 MeV protons, measured at 7 μA.*

performed for γ_{tr} values between 1.04 and 1.7. The results are shown in fig. 4. The error of the tune and γ_{tr} measurement is about ± 0.01. The values of Q_x and γ_{tr} turn out to follow very closely a straight line given by $Q_x = \gamma_{tr}$, in contrast to the prediction of the MAD program, which always produces horizontal tune values which are at least 10 % larger than the corresponding transition parameter values. Because the range of values of the relativistic parameter γ, which can be reached in the TSR is between 1 and 1.02, this is consequently the range of γ_{tr} values one has to achiev in order to fulfill the isochronism condition. The observed relationship between $Q_x \approx \gamma_{tr}$ makes it therefore necessary to investigate the first order resonance stopband width, that is how close one can get to $Q_x = 1$ before the beam lifetime rapidly decreases. In order to disentangle the effects of the first order resonance on the beam from collective instabilities which can be expected next to $\eta = 0$, it was chosen to investigate the first order resonance $Q_x = 3$. This resonant line was approached from below with protons (E=10 MeV) by increasing the strength of a horizontal focusing quadrupole. While at $\Delta Q_x = |Q_x - 3| = 0.2$ the beam lifetime was still of the order of some hours, in good agreement with what can be expected according to the residual gas pressure in the ring ($p \approx 10^{-10} mbar$ at the time of the measurement), the lifetime was reduced to seconds below $\Delta Q_x = 0.07$ and then drastically to less than 1 ms for $\Delta Q_x \leq 0.05$. In another beamtime with $^{12}C^{6+}$(E=73.3 MeV) the same resonance line $Q_x = 3$ was approached from above. After reaching a ΔQ_x value of less then 0.08 the beam intensity rapidly decreased to zero. Also in the measurements which γ_{tr} was close to 1 (which corresponds, according to the empirical relationship shown in fig. 4, to about the same value for the tune) it was observed that the beam lifetime was limited to some seconds or less.

The tiny difference which was measured between Q_x and γ_{tr} did not permit to reach the isochronism condition $\eta = 0$ at the TSR. A chance to fulfill the isochronism condition is left to higher energy storage rings with a value of $\gamma \geq 1.1$ or find a way to enlarge the difference between γ_{tr} and Q_x. Up to 10 μA $^{12}C^{6+}$ and protons could be stored, however the beams were susceptive to longitudinal instabilities. For 21 MeV protons ($\gamma = 1.02$) a γ_{tr} parameter of 1.04 could be reached.

6 ACKNOWLEDGMENT

We would like to thank the technicians of MPI for their work which made these experiments at TSR possible.

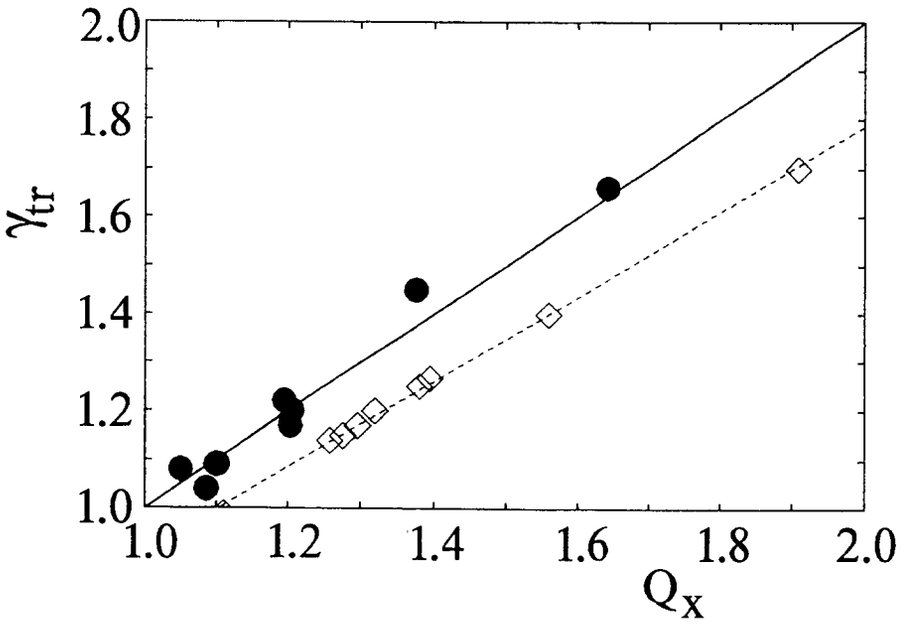

Figure 4: *Measurement of the relationship between γ_{tr} and Q_x (•), and (γ_{tr}, Q_x) values (◇) obtained by the MAD-program.*

References

[1] E. Jaeschke, D. Krämer, W. Arnold, G. Bisoffi, M. Blum, A. Friedrich, C. Geyer, M. Grieser, B. Habs, H. W. Heyng, B. Holzer, R. Ihde, M. Jung, K. Matl, R, Neumann, A. Noda, W. Ott, B. Povh, R. Repnow, F. Schmitt, M. Steck, E. Steffens, The Heidelberg Test Storage Ring for Heavy Ions TSR, 1988 European Particle Accelerator Conference, Rome, vol. 1, p. 365

[2] M. Grieser, D. Habs, R. von Hahn, C. M. Kleffner, R. Repnow, M. Stamper, E. Jaeschke and M. Steck, Advanced Stacking Methods Using Electron Colling at the TSR, 1991 IEEE Particle Accelerator Conference, San Francisco, vol. 5, p. 2817

[3] H J. Miesner, M. Grieser, R. Grimm, A. Gruber, D. Habs, W. Petrich, D. Schwalm, B. Wanner, H. Wernøe, Intrabeam Scattering in Laser Cooling Experiments at the TSR, this conference

[4] Ch. Iselin, The MAD Program, Proceedings of Computing in Accelerator Design and Operation, Berlin 1983

[5] E. D. Courant and H. S. Snyder, Theory of the Alternating-Gradient Synchrotron, Ann. Phys. 3, 1-48 (1958)

[6] N. S. Dikansky, D. V. Pestrikov , Ordering Effects in Coulomb Relaxation of a Cold, Proccedings of ECOOL 1984, Karlsruhe, p. 275

[7] R. Giannini, private Communication, 1993

COOLED $^7Li^+$ IONS IN THE TSR STORAGE RING : PRECISION EXPERIMENTS AND LASER BUNCHING

G.Huber [1], *R.Grieser, V.Jost, F.Albrecht* [2], *M.Grieser* [2], *S.Dickopf , D.Habs* [2], *I.Klaft, R.Klein, P.Knobloch, P.Merz, T. Kühl* [3], *D.Schwalm* [2]

Institut für Physik, Universität Mainz, D-55099 Mainz, Fed. Rep. Germany

[1] *CERN/PPE*

[2] *Max Planck Institut für Kernphysik Heidelberg, D-69029 Heidelberg, Fed. Rep. Germany*

[3] *Gesellschaft für Schwerionenforschung, D-64220 Darmstadt, Fed. Rep. Germany*

ABSTRACT

Laser spectroscopy of electron cooled $^7Li^+$ ions stored at 6, 4%c in the TSR storage ring have been used for an accurate test of the special theory of relativity at high velocity. Independent of assumptions on the motion of a hypothetical reference frame the best upper limits for any deviation for the time dilatation factor $\gamma = (1 - \beta^2)^{-1/2}$ have been obtained and are discussed.

The potential of such experiments depend on the unpertubed interaction between laser and ion beam. The preparation of a laser cooled and bunched ion beam can avoid beam interactions in the focussing fields of the storage ring and give moreover a direct measure of longitudinal temperatures, which up to now are only inferred from model calculations. Calculations for this bunched cooling are presented.

Laser spectroscopy in a closed three level system of fast ions can be used for a precise test of the relativistic Doppler shift formula. The moving clocks represented here by an $^7Li^+$ ion beam with well controlled parallel motion can interact with two counterpropagating laser beams. Saturation spectroscopy can be observed in the fluorescence signal of a Λ type resonance. These experiments have been performed at the TSR storage ring in Heidelberg and their results have been published in [1] [2].

For an exact collinear geometry the Doppler shifted frequencies are given

$$\nu = \nu_{1,2}(\gamma(1 + \beta cos(\theta)))^{-1} \tag{1}$$

with $cos(\theta) = \pm 1$. The parallel and antiparallel laser frequencies ν_p and ν_a and the rest frame clock frequencies of the ions ν_1 and ν_2 obey the relation $\nu_a \cdot \nu_b = \nu_1 \cdot \nu_2$ for special relativity since $\gamma^2(1 - \beta^2) = 1$. At the TSR ring ions at 6,4 % speed of light are excited with a parallel Ar^+ laser beam with $\lambda_p = 515$ nm and an antiparallel dye laser beam with $\lambda_a = 585$ nm. The Λ resonance between hyperfine levels F= $\frac{5}{2}$, F= $\frac{3}{2}$ and F'= $\frac{5}{2}$ in the $1s2p\ ^3S_1(F) \rightarrow 1s2p\ ^3P_2(F')$ line ($\lambda_{1,2} = 549$ nm at rest) is excited. All optical frequencies are measured accurately.

Any deviation given as $\gamma = \gamma_{SRT}(1 + \delta\alpha\beta^2 + \delta\alpha_2\beta^4 + \ldots)$ can be tested to second order by

$$\nu_a = \frac{\nu_1\nu_2}{\nu_p}(1 + 2\delta\alpha(\beta^2 + 2\beta\beta' cos(\Omega)) \tag{2}$$

where β' is the laboratory motion relative to a hypothetical "ether" frame comoving with the cosmic 3 K background radiation. A more complete discussion on the foundations of tests for special relativity and various classes of experimental tests can be found in [1] [3]. The frequency of the antiparallel laser beam ν_a is compared to the value $\nu_1\nu_2/\nu_p$ and from $\Delta\nu/\nu < 1.8 \cdot 10^{-8}$

a limit of $\delta\alpha < 2.1 \cdot 10^{-6}$ for any deviation from the time dilatation factor γ is obtained. The potential of the precise measurement of the Doppler effect in a stored ion beam exceeds all other test experiments and the ultimate limits are given by the accuracy of the frequency determination and by systematic perturbations related with the transverse and longitudinal velocity spread in the ion beam. This effect is of particular nuisance in the guiding and focussing magnetic fields along the merged ion and laser beams in the experimental section of the storage ring.
By the well established methods of electron cooling [5] and a combination with laser cooling [4] appropriate ion beams for precision experiments can be prepared. In the region of the quadrupole magnets and partly in the bending magnets angular misalignment occurs. As a result of the deflections in the beam transport and Zeeman effect in the magnetic fields small shifts in the optical transitions must be considered. The transient influences of angular and magnetic detuning on the (non-steady-state) resonance are partly seen in the field free section of the fluorescence detection.
These systematic errors are given as

$$\frac{\Delta\nu}{\nu} = (\gamma\beta\theta)^2 \tag{3}$$

for the misalignment of laser and ion beam by an angle θ. This shift adds to Zeeman distortion of the line and could reach $2 \cdot 10^{-9}$. In the present experiment imperfections in the laserfield and the accuracy of the restframe frequencies yield $1.8 \cdot 10^{-8}$. These limitations can be eliminated in the future. The influences from the magnetic field in the beam optical elements could be eliminated by a time dependent laser interaction with a bunched ion beam.
Whereas an electron cooled RF-bunched beam shows a large longitudinal momentum spread compared to the longitudinal temperatures found in laser and electron cooled beams, we found a mechanism for producing a bunched beam with low longitudinal temperature. This mechanism can be described in the notation given in [6]. Denoting the motion of a test particle by its momentum p_0 and its phase ϕ_0 in a circular machine, an arbitrary particle's motion is given by its momentum $p = p_0 + \Delta p$ and its phase $\phi = \phi_0 + \Delta\phi$. In our laser cooling scheme an induction accelerator [7] and a counteracting laserbeam are used. The velocity dependent laser cooling force is given by the spontaneous scattering force

$$\vec{F}_{LASER} = \hbar\vec{k}\frac{\Gamma}{2}\frac{S}{4\Delta^2/\Gamma^2 + S + 1} \tag{4}$$

with the wavevector $\vec{k}$, the detuning $\Delta = \omega_0 - \omega_{Laser}\gamma(1 + \frac{v+\Delta v}{c})$, the spontaneous scattering rate Γ and the saturation parameter S, specific for the optical transition and the laser field intensity. The induction accelerator applies to a constant acceleration for all ions by $\vec{F}_{INDAC} = const.$. Taking the total force as the sum of the laser cooling force and the force generated by the induction accelerator and using the well known relation

$$\frac{\Delta f}{f} = \eta\frac{\Delta p}{p} \tag{5}$$

which connects the revolution frequencies with the momentum spread via the machine's off momentum function η, the following equation for lasercooling can be derived for the relative phases and momenta:

$$\Delta\ddot{\Phi} - \frac{f\eta}{p} \cdot (F_{LASER(\Delta\phi,\Delta p)} + F_{INDAC}) = 0 \tag{6}$$

The phase dependence of the cooling force is shown on the right in figure (2), and is induced by a time dependent variation of the laser field's intensity. In the left of figure (2) a numerical

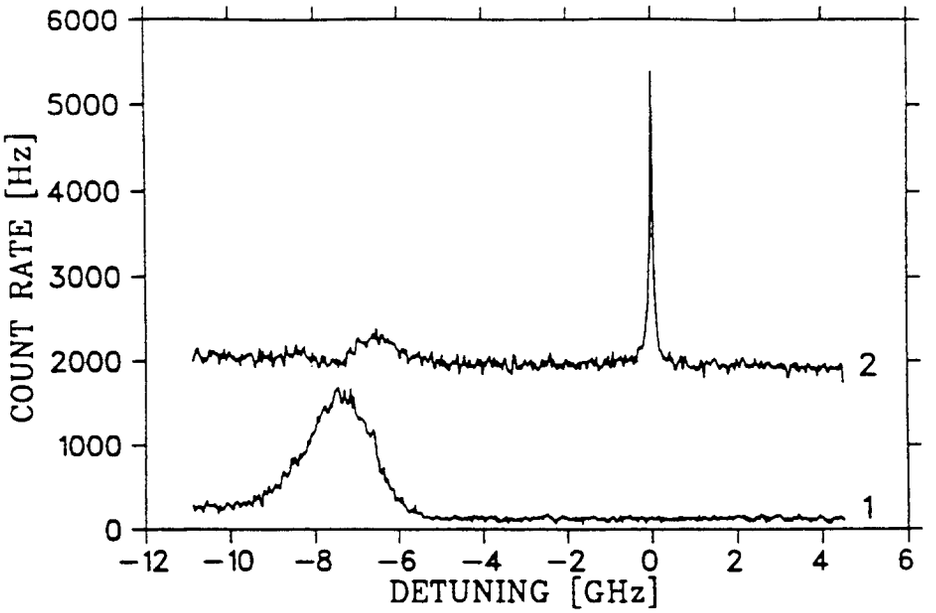

Figure 1: Fluorescence signals from the electron cooled $^7Li^+$ ion beam. In trace 1 only the dye laser's light is sent to the experiment, and the Doppler broadened fluorescence of the F= $\frac{5}{2} \rightarrow$ F' = $\frac{7}{2}$ transition is visible. The FWHM corresponds to $\frac{\Delta\nu}{\nu} = 3 \cdot 10^{-5}$. In trace 2 both lasers are sent to the ring, which increases the background, due to the stray light from the Ar^+ laser. The Ar^+ laser at resonance with the F=$\frac{5}{2} \rightarrow$ F'= $\frac{5}{2}$ transition optically pumps the ions into the F= $\frac{3}{2}$ level and the dye laser's scan shows the almost depleted F= $\frac{5}{2}$ level at the F= $\frac{5}{2} \rightarrow$ F' = $\frac{7}{2}$ transition. The resonance F= $\frac{3}{2} \rightarrow$ F' = $\frac{5}{2}$ yields a strong fluorescence from the simultaneous excitation of the Λ-system.

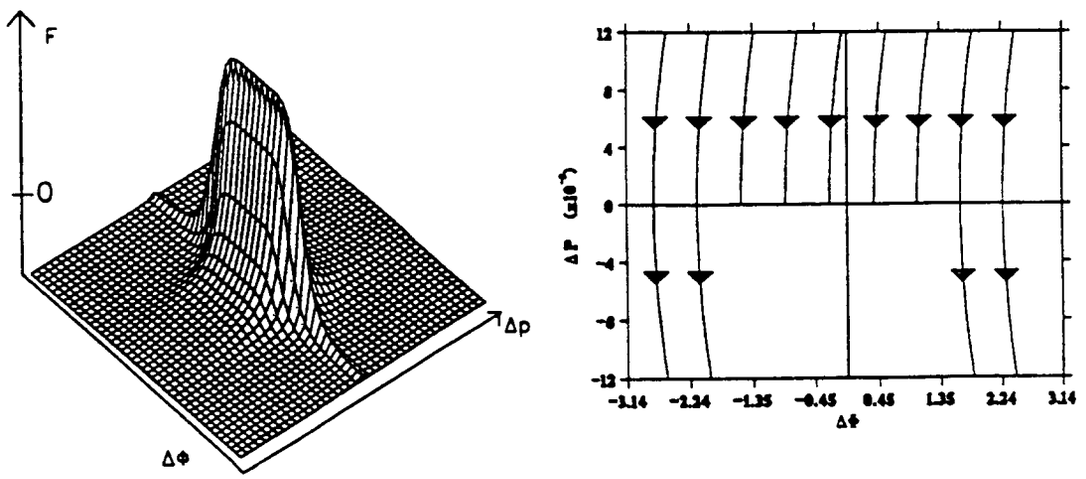

Figure 2: On the right the time dependent force acting on a stored ion beam is shown, which leads to a laser bunched ion beam. On the left solutions of equation (6) for several initial conditions are shown. The force acts as a frictional force on the particle momenta and as a spatial filter on the particle phases. Note that the scale for $\Delta\Phi$ running from $-\pi$ to $+\pi$ corresponds to exactly one revolution in the storage ring, which is the fundamental timescale for this particle preparation.

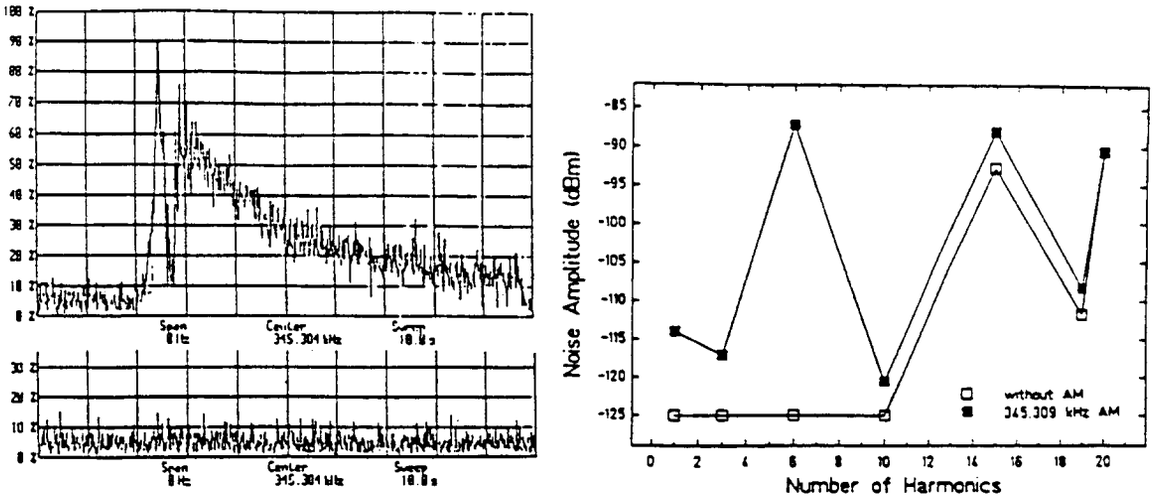

Figure 3: Schottky signals from a laser cooled and bunched $^7Li^+$ beam. The upper trace at the left shows the signal at the first harmonic as a function of time. After 2.5 s the induction accelerator brings the ions in resonance with a laser beam with its light intensity chopped at the revolution frequency of the stored ions. The signal decay is due to the beam life time in the ring. The lower trace has been recorded with a continuous laser beam and otherwise identical conditions. The figure on the right shows the Schottky noise amplitude for bunched laser cooling (full symbols) and continuous laser cooling (open symbols). The differences are visible for the lower harmonics when the bunching is produced at the revolution frequency.

solution of equation (6) is shown corresponding to the different initial conditions. The steady state condition for the cooling process is given at $F = 0$, and corresponds in this simple approach to $\Delta p = 0$ as shown on the right of figure (2).. In this model, particles having enough phase offset will not see the laser field and are thus not cooled. In this sense the force acts as a spatial filter for the stored ions, and a bunch of laser cooled particles is prepared with well defined momentum p_0. The critical parameter for this procedure is the phase stability relative to the reference particle, which results in the fact, that the laser field has to be pulsed exactly at the revolution frequency which corresponds to the steady state momentum.
The bunched beam structure is easily seen in the strong Schottky signal as shown in figure (3). With a blocked laser beam the signal relaxation allows a direct determination of the longitudinal temperature of the laser cooled ion beam.
At $\Delta p = 0$ no further spatial compression of the momentum distribution results from the force in figure (2). At very high laser intensities (S > 1000) however the phase-momentum dependence of the force gives rise to a phase shift which results in a spatial compression of the cooled beam, which develops very slowly due to the low velocity spread. This procedure is however not very useful since the cooling at very high intensities is far from optimum.

The restrictions imposed by the beam optical fields as seen in the $^7Li^+$ experiment could be avoided in a new scheme of a two photon experiment on neutral hydrogen prepared from an electron cooled particle beam in a storage ring. Proton beams can be stored and cooled up to $\beta \sim 0,2$ at the TSR ring and to $\beta \sim 0,75$ at the ESR ring at GSI/Darmstadt, and a partly neutralized beam by radiative electron capture in the 1s and 2s state of hydrogen could be extracted from the ring. The highly monochromatic low emittance atomic beam can be excited to a Rydberg state by two-photon resonance with counterpropagating parallel laser beams. By careful matching the atomic beam emittance and the laser beam in a long interaction section (L< 50 m) precise angular

alignment ($\theta < 20\mu rad$) and small signal broadening could be realized. For these conditions a state of the art frequency measurement of the 2s $\rightarrow$ nd resonance at $\lambda > 515$ nm would be limited by the line width ($\sim$ 700 kHz) and shifts in angular misalignment by $\frac{\Delta\nu}{\nu} = (\beta\gamma\theta)^2$. A frequency accuracy of $\frac{\Delta\nu}{\nu} < 5 \cdot 10^{-10}$ and a corresponding value $\delta\alpha < \cdot 10^{-9}$ should be reachable, testing the special theory of relativity over 1000 times more accurately than in the present experiment.

References

[1] R.Grieser et al. submitted to Applied Physics B

[2] R.Klein et al., Z. Phys. A 342, 455 (1992)

[3] M.Kretzschmar, Z. Phys. A 342, 463 (1992)

[4] S.Schröder et al., Phys.Rev.Lett. 64, 2901, (1990)
G.Huber et al. , Atomic Physics 12, 157,New York:AIP 1991

[5] G.I.Budker et al., Part. Accel. 7, 197 (1976)
H.Poth et al. Z. Phys. A 332, 171 (1989)
E.Jaeschke et al., Proc.European Particle Accelerator Conf. , Rome 1988. Tazzari (ed.) p, 365, Singapore: World Scientific (1989)

[6] J.Le Duff, CERN accelerator school, 125, CERN 85-19

[7] C.Ellert et al., Nucl.Instr.Meth. A 314, 399 (1992)

COMPUTER SIMULATION OF A CRYSTALLINE ION BEAM IN A STORAGE RING

A. Labrador
Laboratori Nazionali di Legnaro-INFN, Legnaro, Italy
EC Research Fellow within the "Human Capital and Mobility" Program

S. Gustafsson
Laboratori Nazionali di Legnaro-INFN, Legnaro, Italy

ABSTRACT
A storage ring dedicated to the production of crystallized ion beams is under study at the LNL Legnaro Laboratory [1]. A computer code dedicated to crystal beam simulations requiring a detailed treatment of particular features of each particle motion is under development. Here are presented the first simulations on the behavior of a two dimensional crystal beam structure: zig-zag, within a super period of the mentioned ring. Special emphasis is put on the passage of this beam through a bending magnet in order to study the importance of the shearing effect.

1. INTRODUCTION

Theoretical and numerical studies for the design of a storage ring dedicated to the production of crystal beams is under way. The use of existing simulation codes and the development of a new one constitutes a crucial part of this work. To study the detailed behavior of a crystallized beam in a storage ring a dedicated computer code is under development. A 2D-version including space charge effects is ready. The first ray tracing simulation of a crystalline beam has been done through a super period of the storage ring.

In this contribution is presented the possibility to adapt the beam not only to obtain symmetry in dimensions and divergence but also to find exactly the same internal beam structure after passing a super period. It is possible in such a way for a crystal beam to survive in a storage ring allowing a controlled shearing effect to reign within the dipoles. The state of matter inside the dipoles can be thought of as a 'LIquid Coulomb CRYstal'. This has given the name LICCRY to the code.

2. LICCRY

LICCRY is written in FORTRAN 77 and is completely developed at our laboratory. This code uses a straight forward ray-tracing method, (fourth-order Runge Kutta method due to Gills). The optical elements, drift, dipole, quadrupole,... are placed in a general Cartesian coordinate frame. Both, the geometry of the ring and the trajectories of the particles are calculated in this frame. The numerical precision (16 digits on an Alpha VAX) is sufficient to allow this choice. Options for fringing field calculations as well as edge focusing in the bending magnets are also available. Each optical element is treated in the program as a different kind of magnetic field. Fringing field are considered as a magnetic region. The problem of the passage between two zones is treated in a special routine.

The initial crystalline beam cell is generated given the length, the number of particles and the distance between them. The simulation starts with all the ions having the same longitudinal velocity, $v_l = \beta c$, without divergency and momentum dispersion.

Particles exceeding the beam cell limits enters from the opposite side of the cell, (Particle In Cell Code).

The space charge is calculated before each step of trajectory calculation. A direct Colombian particle-particle interaction is considered in a non relativistic static approach. A coasting beam is simulated by calculating the electric field contribution from all particles, placed within a cell length distance, around each examined particle in the beam cell as shown in Fig. 1. In this way the total contribution from particles further away can be neglected at first approximation. The electric field contribution from these particles must be small in the transversal direction and must be a good approximation of a DC beam in the longitudinal one. The image charge in the beam tube is also neglected. It is assumed that the focusimg forces can correct for these problems.

At each stage and before Runge Kutta calculation, the time step has been optimized to assure that the influence from the magnetic and electrical fields are correctly treated.

It is necessary, before the actual start of the calculation, to correct the given magnetic dipole fields to produce a correct reference trajectory. A reference particle is therefore sent through the beam line and the dipole fields is optimized in a way to obtain the correct angles but also the correct positions so that the reference particle pass exactly in the center of the quadrupoles and solenoids.

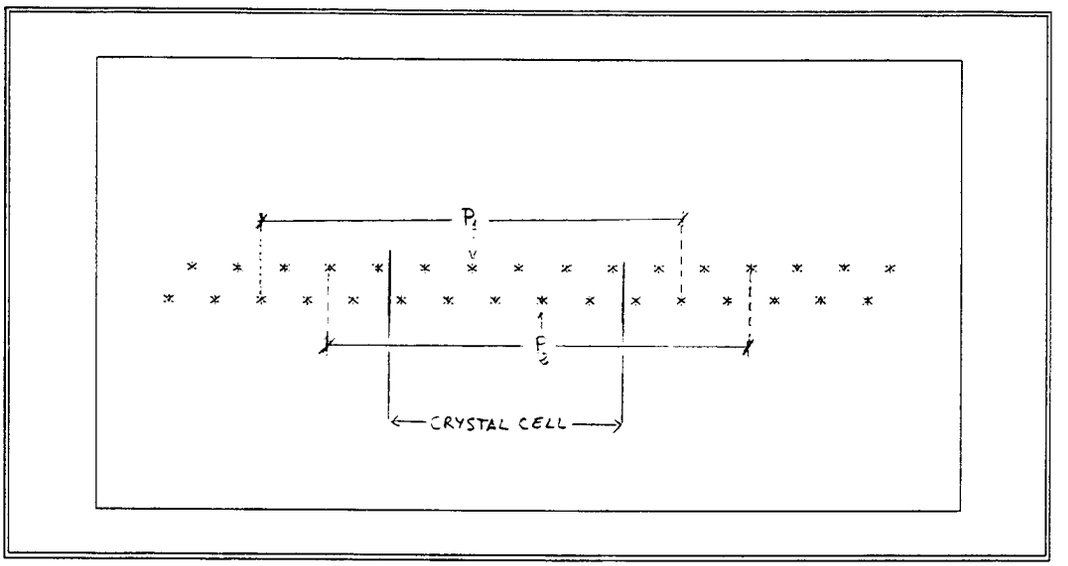

Fig. 1 - Particles considered in the space charge calculation for two particles P_1 and P_2

3. SIMULATION OF A CRYSTALLIZED BEAM IN A SUPER PERIOD

In reference [1] is presented the storage ring under study at the LNL Legnaro Laboratory, one of its super period, see Fig 2, is used for the present study.

Data files resulting from the simulation are treated with a dedicated graphical analysing program called CRANA (CRYstal ANAlysis), also developed by the authors, providing all the following graphics.

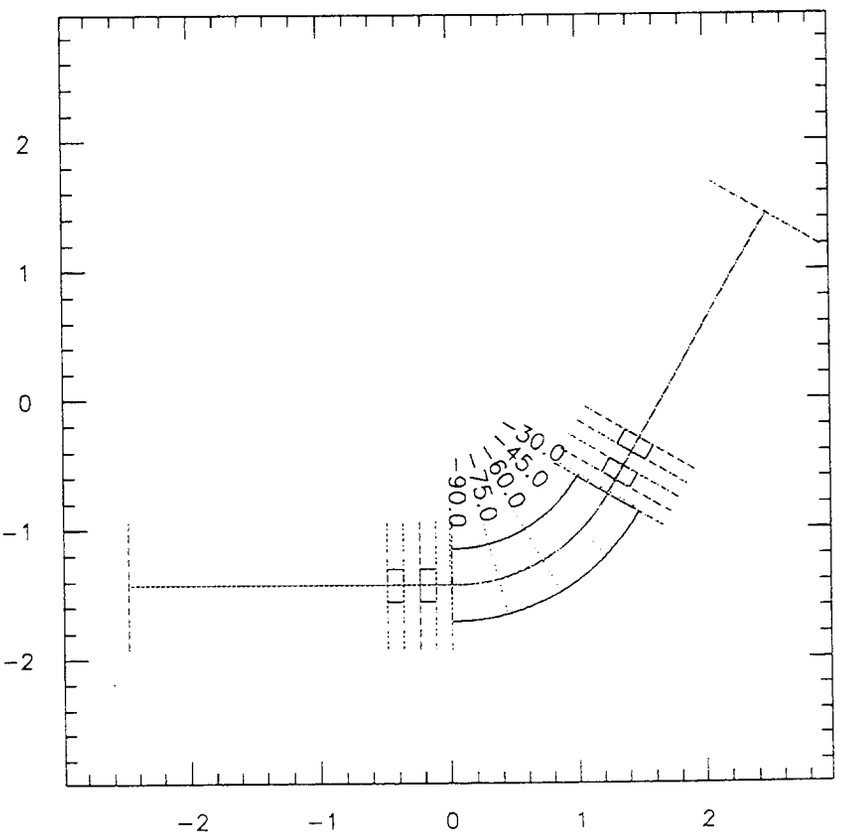

Fig. 2 - Super period of the storage ring under study at the LNL.

Simulation starts from an initial beam cell with a perfect zig-zag structure shown in Fig. 4. This structure has been chosen since it is a very simple structure and thus well adapted for demonstrative purposes. The cell makes several times the same passage through the super period allowing a fitting routine to adapt the dimensions and divergencies of the beam between the entrance and exit, Figs.3a and 3b.

A fitting routine using the optical parameters has not yet been included.

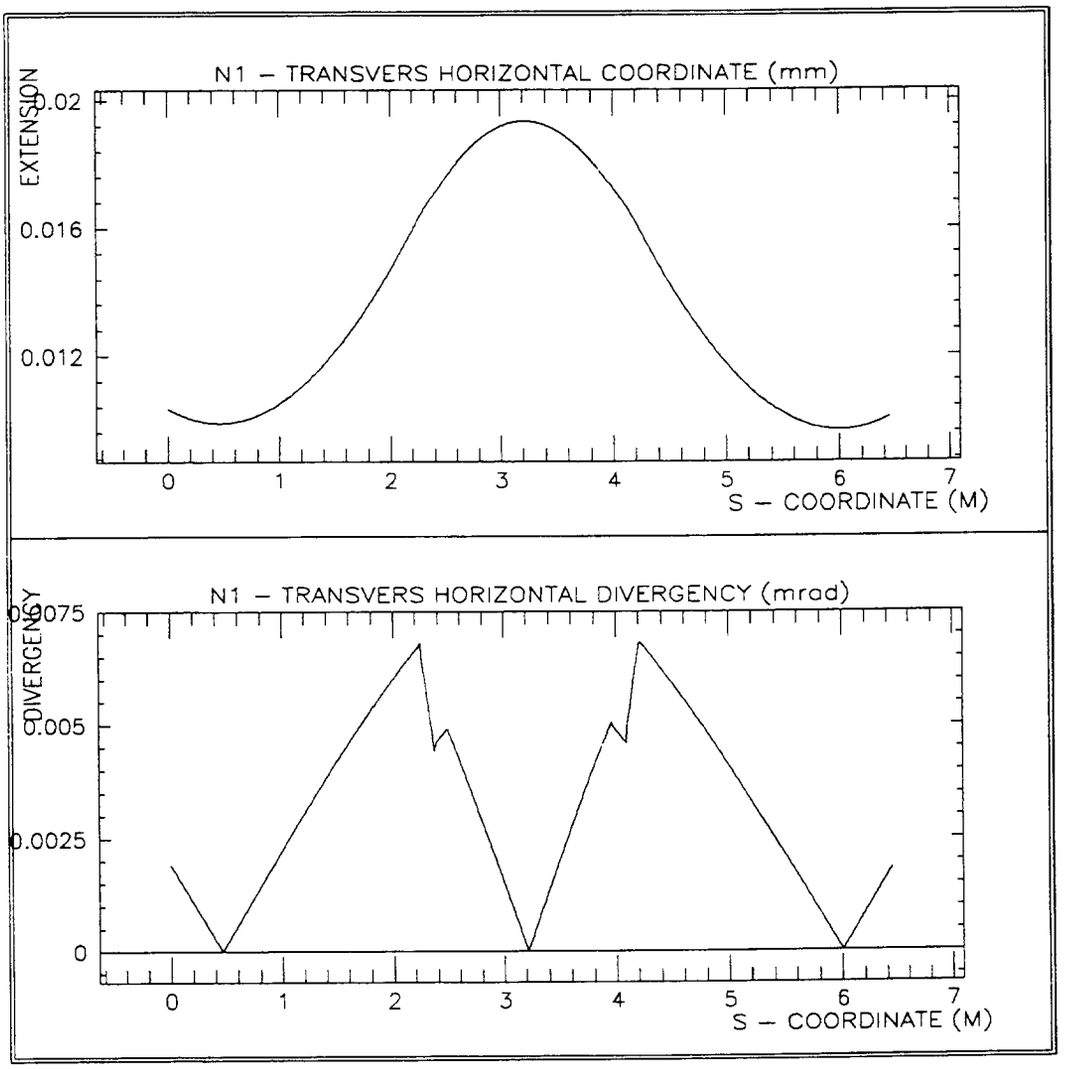

Fig. 3a - Minimum horizontal distance between a selected particle and the reference trajectory as a function of s-coordinate.

Fig. 3b - Directional angular difference between a selected particle trajectory and the reference trajectory as a function of the s-coordinate.

The matching of the internal beam structure is obtained when the relative longitudinal sliding between the two strings is equal to the distance between two neighboring particles in the same string. No fitting routine for this kind of matching has so far been developed. The matching is actually done correcting quadrupole gradients by trail and error method.

Several "snapshots" of the beam cell during the passage through the super period are presented in Fig. 4.

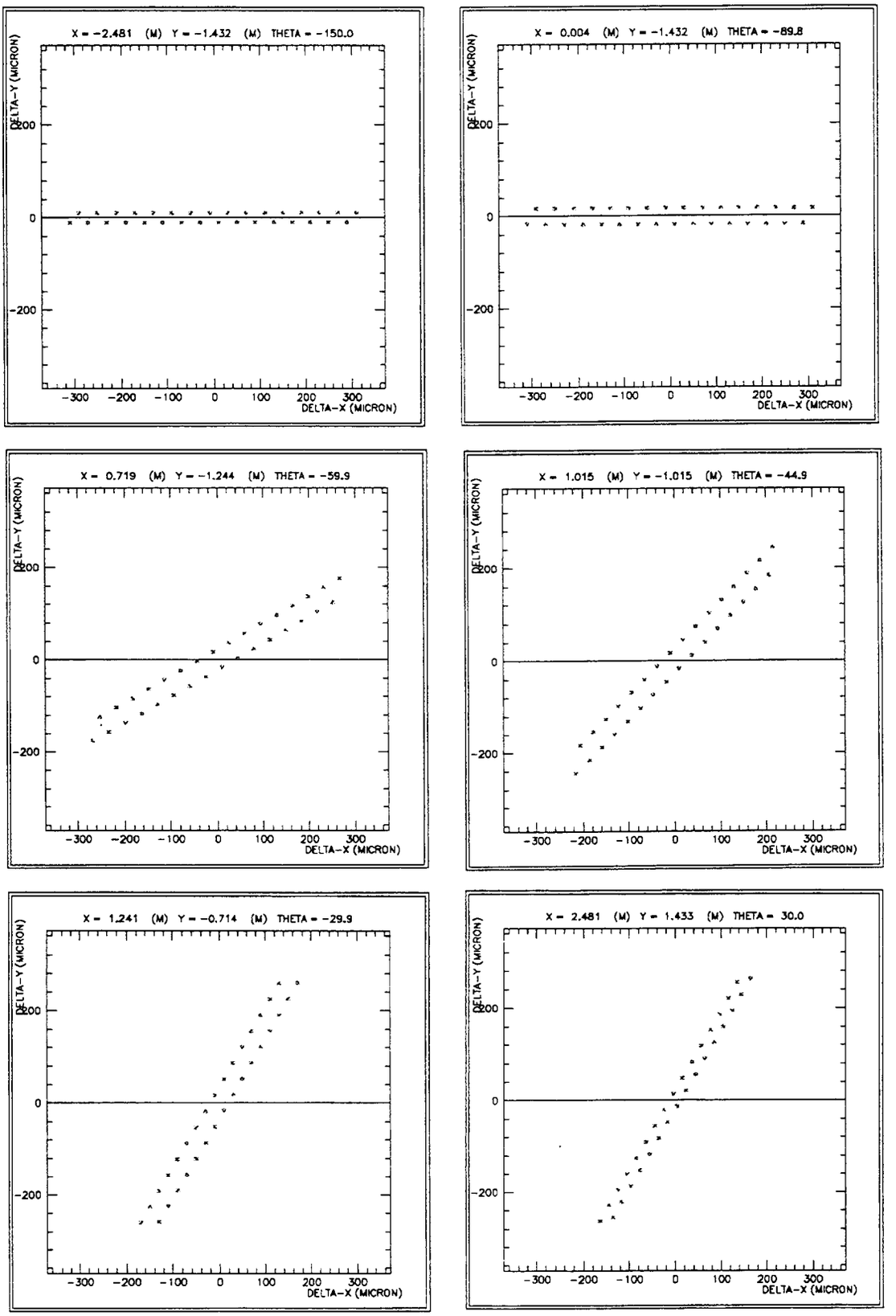

Fig. 4 - "Snapshots" of the beam cell. a) at the begining of the superperiod, b),c),d),and e) during the passage of the dipole, f) at the end of the super period. They were obtained at the angular positions indicated in Fig. 2. Note that a) and f) are identical besides a 60 degrees rotation, i.e. the initial beam structure has been reproduced

The variation of the electric field felt by one selected particle in the cell during its passage trough the super period is presented in Fig. 5. This variation is very smooth even during the passage trough the dipole. This means that the collective field contribution from the surrounding particles are much more important than the individual ones. The heating of the beam is therefore quit low for this kind of simple beam structure once the matching has been done.

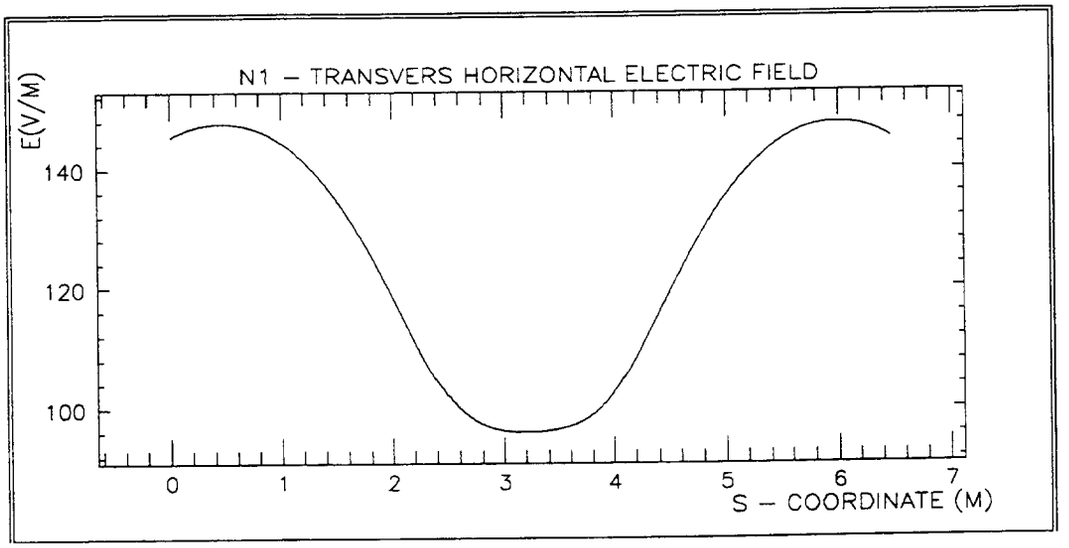

Fig. 5 - Transversal electric field on a selected particle as a function of the s coordinate.

3. CONCLUSIONS

By adapting the optical parameters to reproduce the internal beam structure is demotrated the possibility to maintain a simple crystallized 2D-beam within a storage ring. This means that it is possible to have a crystallized zig zag structure between bending magnets. Nevertheless, when passing the dipoles the structure is like a radial laminate "LIquid Coulomb CRYstal" flow.

This phenomena is very sensible to the interplay between space charge and focalizing forces. A complete 3D-study is therefore needed and will bee undertaken as soon as possible.

ACKNOWLEDGMENTS

The authors would like to thank A. Dainelli for discussions and his useful suggestions.

REFERENCES

[1] L. Tecchio et al.; A dedicated storage ring for ion beam crystallization; work presented to the Workshop on "Beam Cooling and Related Topics", October 3-8, 1993, Montreux, Switzerland.

DEMONSTRATION OF NO FEASIBILITY OF A CRYSTALLINE BEAM IN A BETATRON MAGNET*

Alessandro G. Ruggiero
Brookhaven National Laboratory
PO Box 5000, Upton, N.Y. 11973

ABSTRACT

This paper investigates the feasibility of a Crystalline Beam in a weak-focusing Betatron Magnet. The curvature effect due to the bending magnet is also investigated. The case of a circular one-dimensional string of electrically-charged particles is examined. It is found that the motion is unstable due to the dependence of the precession movement with the radial displacement. That is a form of negative-mass instability which can be avoided with an alternating-focussing structure. The calculation of the particle-particle interaction as well as of the forces due to the external magnetic field is done directly in the laboratory frame.

1. INTRODUCTION

One of the most important issue in the study of Crystalline Beams [1-3] is the determination of the best configuration of the storage ring where the formation and detection of the state should occur. Recently, Wei, Li and Sessler [4] have found that a Crystalline Beam cannot be stable in a Betatron. The method used by these Authors is based on a non-obvious transformation of general relativity to the beam rotating frame. We shall deal here with the same issue, and in particular discuss the special case of a Circular String of electrically-charged particles. The method we use applies directly to the laboratory frame and involves the correct calculation of the retarded potentials to describe the particle-particle interaction

We shall consider a circular beam of N ions all with the same electric charge Qe and mass at rest m_o. The ions are moving on the same circular trajectory of radius R, with the same constant angular frequency ω_o and are equally spaced. The particles are lying on the same plane at $z = 0$. We shall adopt a cylindrical coordinates (r, θ, z) for our study. We want to prove that the Circular String of particles is indeed an Equilibrium Configuration, compatible with a weak-focussing structure, for which we can subsequently determine the Confinement and Stability Conditions [5]. We shall also prove that such a configuration circulating in a Betatron Magnet is unstable. The instability is caused by the dependence of the precession movement of the particles with respect to each other on their radial displacement. It is the equivalent of the negative-mass instability which can be avoided by choosing a storage ring with alternating-focussing gradients, where the corresponding transition energy is above the energy of the particles. We shall work at the end an example of such a storage ring. It is also found that a large periodicity of the storage ring is required for the beam stability.

2. THE EQUATIONS OF MOTION

The equations of motion of a particle can be written in vectorial form

$$d\,\mathbf{p} / d\,t \;=\; Qe\,\mathbf{E} \;+\; Qe\,(\mathbf{v} / c)\,x\,\mathbf{B} \qquad (1)$$

where $\mathbf{p} = m_o \gamma \mathbf{v} = m \mathbf{v}$ is the ion momentum, $\mathbf{v}$ its velocity, γ the energy relativistic factor, $\mathbf{E}$ the total electric field, and $\mathbf{B}$ the total magnetic field.

The electric and magnetic fields are the sum of the particle-particle interaction, denoted in the following with the subindex "sc", and of the external fields, denoted with the subindex "ext", that is $\mathbf{E} = \mathbf{E}_{ext} + \mathbf{E}_{sc}$ and $\mathbf{B} = \mathbf{B}_{ext} + \mathbf{B}_{sc}$.

Let us define as the force acting on the particle from the interaction with all other particles

* Work performed under the auspices of the U.S. Department of Energy

$$\mathbf{F}_{sc} = Qe\,\mathbf{E}_{sc} + Qe\,(\mathbf{v}/c) \times \mathbf{B}_{sc} \tag{2}$$

We assume there are no external electric fields, that is $\mathbf{E}_{ext} = 0$. The external magnetic field $\mathbf{B}_{ext}$ corresponds to the distribution of the field in a typical Betatron Magnet. Performing an expansion and linearization around the reference circular trajectory, the field components are

$$B_r = B_0\, n\, z / R \tag{3}$$

$$B_z = -B_0 (1 - n\, x / R) \tag{4}$$

where B_0 is the guiding field on the reference orbit, n the field index which in a Betatron Magnet ranges between 0 and 1, and $x = r - R$. The azimuthal component $B_\theta = 0$.

In cylindrical coordinates, denoting with p_r, p_θ, p_z the components of the momentum $\mathbf{p}$ and with v_r, v_θ, v_z the components of the velocity $\mathbf{v}$, the three components of the vectorial Eq. (1) can be written as

$$d\,p_r/d\,t - p_\theta\, d\,\theta/d\,t = F_r + Qe\,(v_\theta/c)\,B_z \tag{5}$$

$$d\,p_\theta/d\,t + p_r\, d\,\theta/d\,t = F_\theta + Qe\,(v_z/c)\,B_r - Qe\,(v_r/c)\,B_z \tag{6}$$

$$d\,p_z/d\,t = F_z - Qe\,(v_\theta/c)\,B_r \tag{7}$$

where F_r, F_θ and F_z are the components of the vector $\mathbf{F}_{sc}$ given by Eq. (2).

3. THE EQUILIBRIUM CONFIGURATION OF THE CIRCULAR STRING

The Circular String is defined by : $x = v_r = z = v_z = 0$ and $d\,\theta/d\,t = \omega_o$, constant, at all times. It derives that γ is also a constant, $v_\theta = \omega_o R = v$ is a constant. We have also $p_r = p_z = 0$ and that the angular momentum $p_\theta = p$ is a constant of motion. It is sufficient and necessary that the following conditions are satisfied at the radius $r = R$ on the $z = 0$ plane. From Eq. (5), denoting $\beta = v/c$,

$$Qe\,B_o\,R = pc + R\,F_r/\beta \tag{8}$$

From Eq. (6), it is required that $F_\theta = 0$. Finally, from Eq. (7), we derive the condition $F_z = Qe\,\beta\,B_r$.

Equation (8) is the usual Lorentz condition where the centrifugal force is balanced by the Lorentz force. A repulsive force, due to the particle-particle interaction, appears and has to be taken into account as well. Since the beam has a perfect cylindrical arrangement, from symmetry considerations, it can be determined that F_r is constant and has the same value for all particles. For typical beam parameters this contribution is small. Using the same symmetry considerations, it is easily seen that $F_z = 0$. Thus, we need $B_r = 0$ on the $z = 0$ plane and at the radius $r = R$, which is indeed the case as shown by Eq. (3).

We have to deal finally with the condition $F_\theta = 0$. We give below a formal prove that this condition is indeed satisfied for the Circular String. We shall calculate explicitly the components of the interaction force in the following section. From symmetry considerations, if there is a non-vanishing azimuthal component of the force due to the particle-particle interaction, this component F_θ has to be the same at the same instant to all particles; that is, at the same instant all particles would suffer the same variation of the angular momentum and thus the whole system would increase or decrease its total angular momentum. This violates the principle of conservation of the angular momentum since we are dealing with a conservative isolated system where there is only an external, stationary magnetic field distribution. It derives therefore that $F_\theta = 0$ identically.

4. CALCULATION OF THE INTERACTION FORCES AT THE EQUILIBRIUM

The field distribution generated by a point-like charged particle animated of arbitrary motion is given by J. D. Jackson in *Classical Electrodynamics* [6]. We neglect the "acceleration fields", which depend linearly with $d\,\mathbf{v}/d\,t$. and that are usually very small, especially for $\beta << 1$. Let us denote with $\mathbf{E}_{ij}$ and $\mathbf{B}_{ij}$ the fields generated by the j-th particle on the i-th particle of the Circular String. Let $\mathbf{n}_{ij}$ be the unit vector directed from the j-th particle to the i-th particle, and R_{ij} the distance between the two particles. Then according to Jackson,

$$\mathbf{B}_{ij} = [\,\mathbf{n}_{ij} \times \mathbf{E}_{ij}\,]_{ret} \tag{9}$$

$$\mathbf{E}_{ij} = (Qe / \gamma^2) [(\mathbf{n}_{ij} - \boldsymbol{\beta}_j) / (1 - \boldsymbol{\beta}_j \mathbf{n}_{ij})^3 R_{ij}^2]_{ret} \quad (10)$$

where $\boldsymbol{\beta}_j = c \mathbf{v}_j$ is the velocity of the j-th particle. The square brackets with subscript "ret" mean that the quantity in the brackets is to be evaluated at the retarded time $\tau = t - R_{ij} / c$.

A more detailed and complete derivation of this result is given by R. Becker in *Theorie der Elektrizitat* [7]. Becker proves that

$$[(\mathbf{n}_{ij} - \boldsymbol{\beta}_j) R_{ij}]_{ret} = \mathbf{r}_{ij} \quad (11)$$

where $\mathbf{r}_{ij}$ is the actual distance vector between the two particles at same time t, directed from the j-th toward the i-th particle. It is also seen that

$$[(1 - \boldsymbol{\beta}_j \mathbf{n}_{ij}) R_{ij}]_{ret}^2 = \mathbf{r}_{ij}^2 - (\mathbf{r}_{ij} \times \boldsymbol{\beta}_j)^2 = s_{ij}^2 \quad (12)$$

where the quantity at the right-hand side is estimated at the same instant t. Thus

$$\mathbf{E}_{ij} = Qe \, \mathbf{r}_{ij} / \gamma^2 \, s_{ij}^3 \quad (13)$$

From symmetry considerations, the field has the same value for all particles. In particular, we can estimate the field acting on the i = 0 particle when it is located at $\theta = 0$ at the time t = 0. The vector $\mathbf{r}_{oj}$ has the following components: $[2 R \, sin^2 (\theta_j / 2), - R \, sin \, \theta_j , 0]$ where θ_j is the angular separation between the two particles. It is also seen that

$$(\mathbf{r}_{oj} \times \boldsymbol{\beta}_j)^2 = 4 \beta^2 R^2 \, sin^4 (\theta_j / 2) \quad (14)$$

and

$$s_{oj} = (2 R \, sin | \theta_j / 2 |) \sqrt{ 1 - \beta^2 \, sin^2 (\theta_j / 2) } \quad (15)$$

Since for every particle at the angular distance θ_j there is another one at $- \theta_j$, it is immediately seen that the azimuthal component of the electric field $E_\theta = 0$ whereas

$$E_r = \frac{Qe}{2 R^2 \gamma^2} \Sigma_j \frac{1}{[1 - \beta^2 \, sin^2 (\theta_j / 2)]^{3/2} \, sin (\theta_j / 2)} \quad (16)$$

where the summation is done only over those particles with $0 < \theta_j < \pi$.

It remains to estimate the components of the magnetic field $\mathbf{B}_{oj}$. According to Becker

$$[\mathbf{n}_{ij} \times \mathbf{E}_{ij}]_{ret} = \boldsymbol{\beta}_j \times \mathbf{E}_{ij} \quad (17)$$

where the quantity at the right-hand side is estimated at the instant t. Since the two vectors $\boldsymbol{\beta}_j$ and $\mathbf{E}_{ij}$ are on the same plane (z = 0), the magnetic field $\mathbf{B}_{ij}$ is directed along the z-axis and perpendicular to the z=0 plane which contains the Cylindrical String of ions. Since the velocity of any particle is directed along the azimuthal direction θ, the cross product between $\boldsymbol{\beta}_i$ and $\mathbf{B}_{ij}$ has only a radial component. In summary, from Eq. (2)

$$F_r = Qe (1 - \beta^2) E_r = \bar{F}_r \quad (18)$$

and $F_\theta = F_z = 0$. This completes the prove that the beam made of a Circular String is indeed an Equilibrium Configuration consistent with the field distribution in a Betatron Magnet.

5. DETERMINATION OF STABILITY OF THE CIRCULAR STRING

We shall apply a perturbation method where the motion of a single particle is perturbed by a small amount, whereas the motion of all other particles remains unchanged. The perturbation is described by small displacements x, Rq and z which are smaller than the unperturbed separation of two neighboring particles. Let us take as the perturbed particle the one which would be located at $\theta = 0$ at the time t = 0. Linearization of the expressions of the components of the force resulting from the particle-particle interaction gives

$$F_r = \bar{F}_r + k_r x - Qe\beta^2 E_r (dq / \omega_o dt) \quad (19)$$

$$F_\theta = - k_\theta q + Qe\beta^2 E_r (dx / v dt) \quad (20)$$

$$F_z = k_z z \quad (21)$$

where the constants k_r, k_θ and k_z have been evaluated in Ref. [8]. It is shown that for nonrelativistic beams

$$k_r \sim k_z \sim Q^2 e^2 g_o N^3 / 4\pi^3 R^3 \gamma^4 \quad (22)$$

where $g_o = 1.2$, and $k_\theta \sim 2R\gamma^2 k_z$. To first order, the energy relativistic factor γ is constant, whereas

$$p_\theta \sim p [1 + (dq / \omega_o dt) + x / R] \quad (23)$$

$$p_\theta \, d\theta / dt \sim p \omega_o [1 + 2 (dq / \omega_o dt) + x / R] \quad (24)$$

By taking into account the confinement condition Eq. (8), by inserting Eqs. (3,4) and Eqs.(19-21) into the equations of motion Eqs. (5-7), we derive the following linearized equations

$$d^2 x / dt^2 + \Omega_H^2 x = v (\omega_o x / R + dq / dt) \quad (25)$$

$$d^2 q / dt^2 + (\omega_o / R) dx / dt = - \omega_o k_\theta q / p \quad (26)$$

$$d^2 z / dt^2 + \Omega_V^2 x = 0 \quad (27)$$

where

$$\Omega_H^2 = Qe\beta B_o (1 - n) / mR - k_r / m \quad (28)$$

$$\Omega_V^2 = Qe\beta B_o n / mR - k_z / m \quad (29)$$

The equations of motion (25-27) are very general. They apply to the motion of a charged particle in a combined function magnet described by the field index n, under the action of other moving particles in a Circular String Configuration. The axial motion can be treated independently from that occurring on the z = 0 plane. Solving Eq. (27) gives a stable oscillatory solution as long as $\Omega_V^2 > 0$, that is, from Eq. (29),

$$n > R^2 k_z / \beta pc \quad (30)$$

For typical beam parameters, this condition is satisfied for positive and very large values of the field index n.

6. RADIAL-AZIMUTHAL COUPLING. NEGATIVE MASS INSTABILITY.

The first two equations of motion (25 and 26) show coupling between the azimuthal and radial components of motion. They can be solved with the conventional method of eigenvalues by assigning an angular oscillation frequency Ω_o common to the two components of motion. The following equation for Ω_o is derived [8]

$$\Omega_o^4 - M \Omega_o^2 + (\Omega_H^2 - \omega_o^2) \omega_o k_\theta / p = 0 \quad (31)$$

where $M = \Omega_H^2 + \omega_o k_\theta / p$. Solving Eq. (31) for Ω_o^2 gives

$$2 \Omega_o^2 = M \pm \sqrt{M^2 - 4 (\Omega_H^2 - \omega_o^2) \omega_o k_\theta / p} \quad (32)$$

For the motion to be stable $\Omega_o^2 > 0$ is required, that is $\Omega_H^2 > \omega_o^2$ which yields for the field index

$$1 - n > 1 + R^2 k_r / \beta pc \quad (33)$$

In order to satisfy Eq. (33) the field index n has to take very large negative values. It is not possible that the conditions of Eqs. (30) and (33) can be satisfied simultaneously. It derives that the Equilibrium Configuration of a Circular String is not a Stable Configuration that can be realized in a simple Betatron Magnet. This seems to be in agreement with the results of Wei, Li and Sessler [4].

7. STORAGE RING WITH ALTERNATING FOCUSSING GRADIENT

Let $r_o = 1.535 \times 10^{-18}$ m be the classical proton radius and A the mass number of a particle, and

$$n_o = R^2 k_z / \beta pc \tag{34}$$

Then the stability condition for the axial component of the motion is, from Eq. (30),

$$n > n_o \tag{35}$$

whereas the stability condition for the motion on the z = 0 plane is, from Eq. (33),

$$n < -n_o \tag{36}$$

This suggests that a solution can be found with an alternating gradient storage ring where the field index n takes very large values and changes sign periodically.

We shall apply these results to the case of a beam of ions of gold partially stripped (A = 197, Q = 51) is injected into a small storage ring from the Tandem-ALPI complex of the *Laboratori Nazionali di Legnaro* [3] with the magnetic rigidity of 1.2 T-m ($\beta = 0.1$). We derive $n_o = 4.9 \times 10^{-18} N^3$. It is seen that already for $N = 10^7$ particles, the field index gets a too large value. Not only this may be very difficult to achieve in practice, but also it causes concern about the stability of the storage ring lattice in the limit of a single particle.

We shall assume that the storage ring is made of n_p superperiods, each with a pair of combined function magnets of alternating gradient sign, that is having field index – n and + n respectively. Neglecting the presence of drift spaces, the motion of a single particle in the lattice is stable if the following condition is satisfied

$$|\cos \zeta \cosh \zeta| < 1 \tag{37}$$

where $\zeta = \alpha \sqrt{n}$ and $\alpha = \pi / n_p$ is the bending angle per magnet. The stability condition (37) can be satisfied by choosing $\zeta \sim (2h + 1)\pi / 2$ where h is an integer. This condition is equivalent of setting a betatron phase-advance per superperiod to about 90°.

The relations above combined together set a relation between the periodicity of the storage ring and the beam intensity since the critical field index depends with the number N of particles, and one requires $n > n_o$,

$$n_p \sim 4.4 \times 10^{-9} N^{3/2} / (2h + 1) \tag{38}$$

Small values of h are desirable, since for larger values the stability interval reduces considerably. It is then seen that a large periodicity is needed. For instance for $N = 10^7$ particles $n_p \sim 140 / (2h + 1)$, and a periodicity $n_p = 8$ can be obtained by choosing h = 8.

REFERENCES

[1] J. P. Schiffer and A. Rahman, *Feasibility of a Crystalline Condensed State in Cooled Ion Beams of a Storage Ring*, PHY-5121-ME-88, Argonne National Laboratory, Feb. 1988

[2] Proceedings of the Workshop on Crystalline Ion Beams, Werheim, Germany, Oct. 1988. GSI-89-10 Report.

[3] CRYSTAL. *A Storage Ring for Ion Beam Crystallization Studies*. LNL-INFN (REP) 59/92. Laboratori Nazionali di Legnaro, Via Romea 4, I-35020 Legnaro (Padova), Italy (1992)

[4] J. Wei, X. P. Li, A. Sessler, *Crystalline Beam Ground State*, BNL-52381, June 1993.

[5] A. G. Ruggiero, *Confinement and Stability of a Crystalline Beam*, BNL-49090 (May 1993)

[6] J. D. Jackson, *Classical Electrodynamics*, second edition. John Wiley & sons. 1975

[7] R. Becker, *Teoria della Elettricita'*, Vol. II, trans. by M. Ageno. Sansoni Edizioni Scientifiche, Firenze, 1950

[8] A. G. Ruggiero, *Demonstration of No Feasibility of a Crystalline Beam in a Betatron Magnet*, BNL - 49529 (Sept. 1993)

MOLECULAR DYNAMICS SIMULATIONS OF THE CRYSTALLIZATION OF ION BEAMS IN ALTERNATING FOCUSING FIELDS, AND FOR CURVED TRAJECTORIES

J. P. Schiffer
Argonne National Laboratory, Argonne, IL 60439, U.S.A.
and
J. S. Hangst
University of Århus, Århus, Denmark

The possibility that very cold ions in a beam would form a crystalline structure was noted some time ago [1]. The properties of ions cooled down to low internal temperatures were investigated through simulations using Molecular Dynamics [2]. Focusing was first approximated by a radially symmetric focusing force, constant in time, and a section of beam was studied with a repeating boundary condition (typically with a repeating distance that was about 100 interparticle spacings). In these simulations particles are given random initial spatial and velocity coordinates, and then their motion is followed, while gradually scaling down their relative velocities, i.e. reducing their temperature in the co-moving frame. As the temperature is lowered, the radius of the beam approaches the space-charge limit. As the cooling proceeds to even lower temperatures, a crystalline shell structure forms, becoming gradually better defined, as is shown in Fig. 1. No sharp phase transitions were seen in this process.

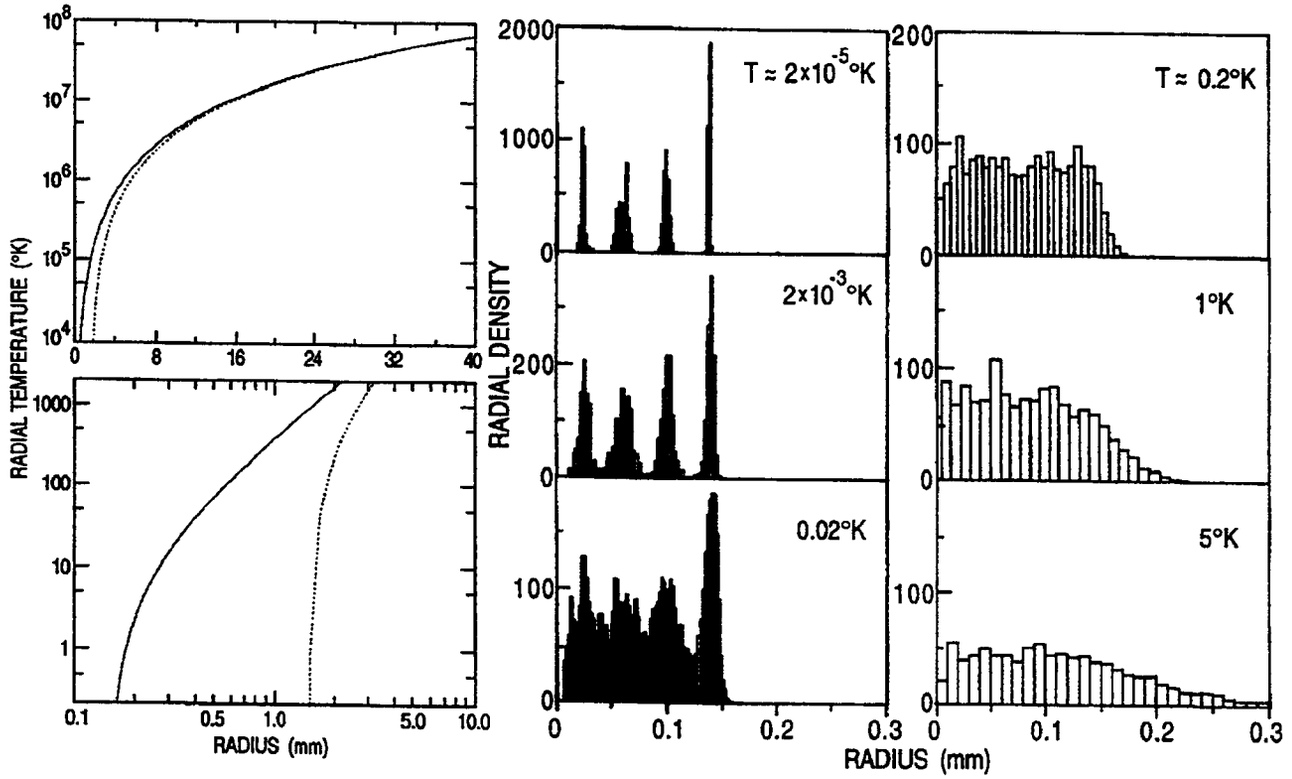

Fig. 1 Radial distribution of a beam as a function of its transverse temperature. The results shown are in degrees and millimeters, for singly charged particles in a ring approximating the Århus storage ring ASTRID. The two boxes on the left use an analytic expression for the rms radius for 10^7 (solid) and 10^9 (dotted) particles in ASTRID. The histograms on the right correspond to simulations for approximately 10^7 particles at lower temperatures.

The character of these structures is a function of density (the number of particles per unit length). While a dimensionless density λ has been defined [3], here, with several small storage rings of similar characteristics (radius between a few and 10 meters and betatron tunes around 2.5), we quote approximate total numbers of particles. The types of ordering are as follows:

$N < 10^6$	The ions form a one-dimensional string.
$N \sim 2\text{x}10^6$	The interparticle Coulomb interaction forces the particles into a two-dimensional zig-zag pattern.
$10^7 < N < 2\text{x}10^6$	The particles from various helical and other structures on a single cylindrical surface.
$N \gtrsim 10^7$	More cylindrical shells are formed.

For multi-shell structures the shells are uniformly spaced and each has the same surface density of ions, so that the number of ions on each shell is proportional to the shell radius. In each shell the ions are arranged, as far as possible, in equilateral triangles, the characteristic form of the two-dimensional Coulomb lattice. The number of shells is proportional to the square-root of the number of particles. Figure 2 shows a system corresponding to about $N = 10^8$. A detailed discussion of the properties of such static systems has been given in reference [3].

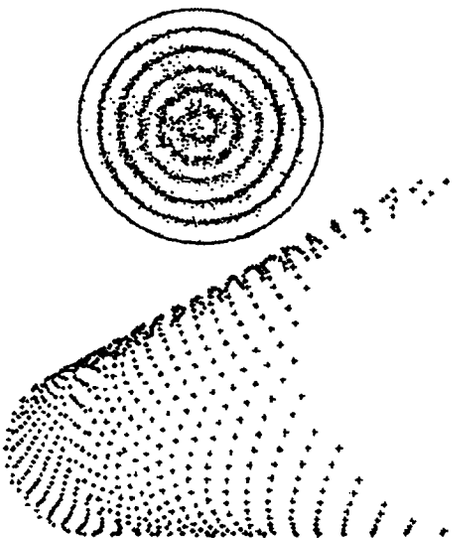

Fig. 2 Results of a MD simulation corresponding to $N \sim 10^8$ with focusing that is constant in time and no bending. The top shows the projection of particles onto a plane perpendicular to the beam, while the lower figure is a perspective view of half of the outermost shell in the crystallized beam. The structures in each shell are similar.

When, in the simulations, such static configurations are given a single transverse impulse, and then followed as a function of time two normal modes are seen, as shown in Fig. 3: a radial breathing mode and a quadrupole shape mode. The breathing mode (left) is excited in a crystalline system confined with constant focusing forces, when the focusing field is reduced for a short interval (much less than a betatron period) and then restored to its original value. This produces a radial *volume* oscillation with a frequency that is the plasma frequency: $\omega_{plasma} = \sqrt{2}\ \omega_\beta$.

The other mode is excited when a similar perturbation is introduced in the focusing field but increased in one dimension and reduced in the other. This induces a volume-conserving *shape* oscillation with a frequency that is equal to the betatron frequency.

The shape oscillation decays with a resonant $Q \approx 100$, which is somewhat dependent on the details of the simulation. The volume mode does not appear to be damped, $Q > 2000$, within the accuracy of the simulations. The longitudinal temperature is ~ 1° mK after 40 betatron periods.

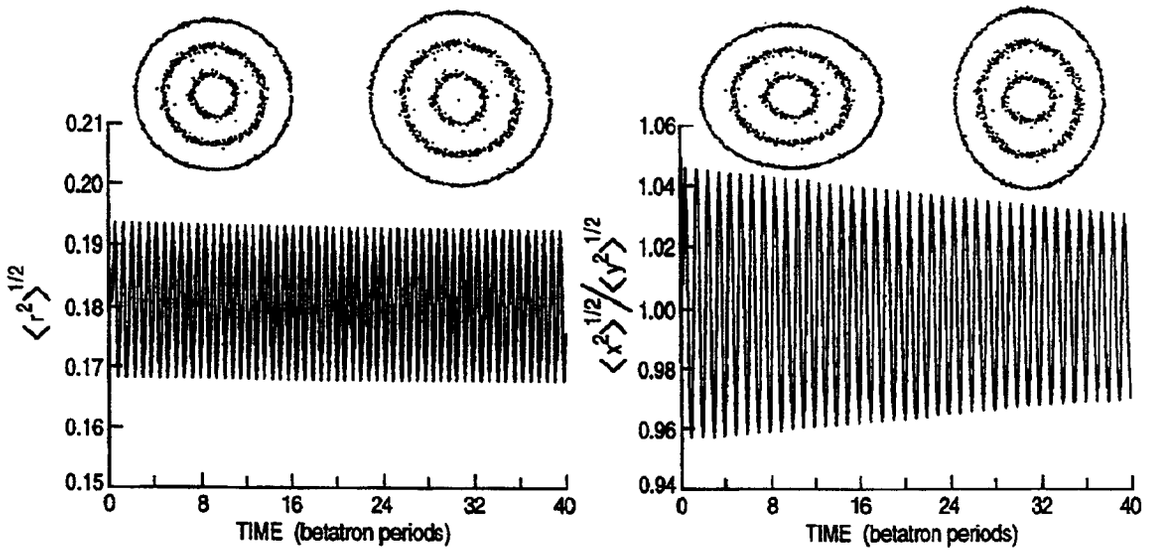

Fig. 3 Simulations of two normal modes.

What happens when the focusing field becomes time-dependent, as is the case in all existing storage rings? A simulation of such a system is shown in Fig. 4. Here the particles were again started with random coordinates, but

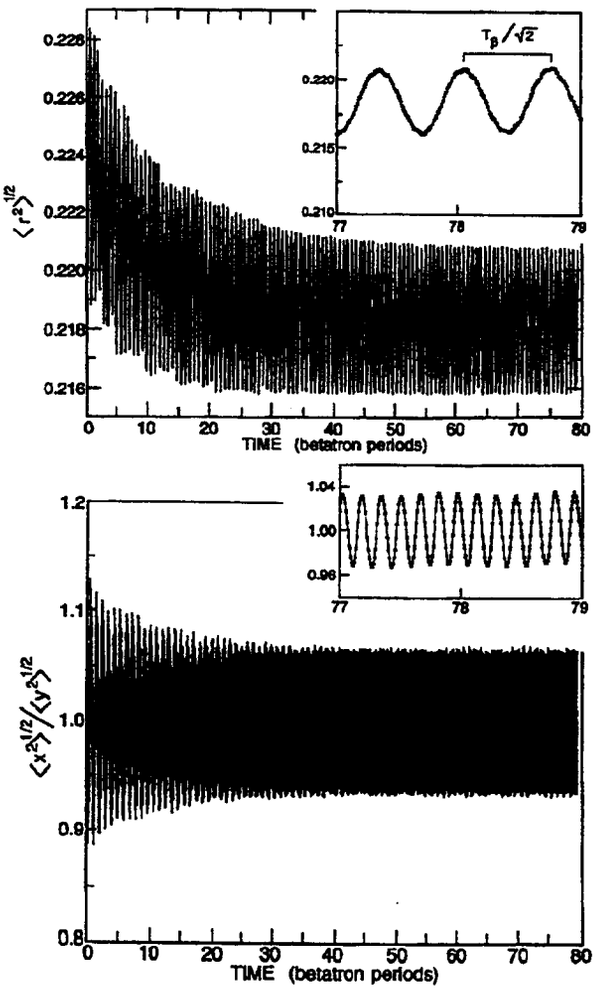

Fig. 4
Results of a Molecular Dynamics simulation of crystallization with the focusing force switched alternately on and off between the horizontal and vertical directions. Only the longitudinal temperature was cooled, once every 2.5 betatron oscillations, correspond-ing to once per turn in a storage ring. The system settles into a set of concentric shells almost identical to those seen in a static field, but with small residual oscillations: a (~7%) forced shape oscillation with the period of the imposed alternation in focusing, and a residual (~1%) radial oscillation with a period that is characteristic of the radial normal mode with its characteristic frequency.

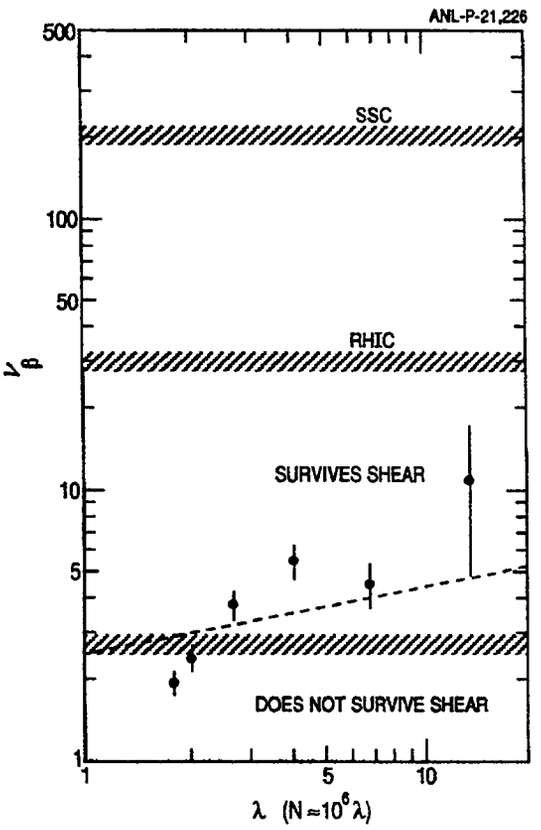

Fig. 5
Empirical limits imposed by the shear of bending on a beam crystallized with no prior bends. Note that a beam with $\lambda \sim 2$ corresponds to a single shell, $\lambda \sim 6$ to 2 shells, etc. The dotted line corresponds to $N_{lim.} \propto \nu_\beta^4$, a simple dimensional estimate. The betatron tunes for several storage rings are also indicated.

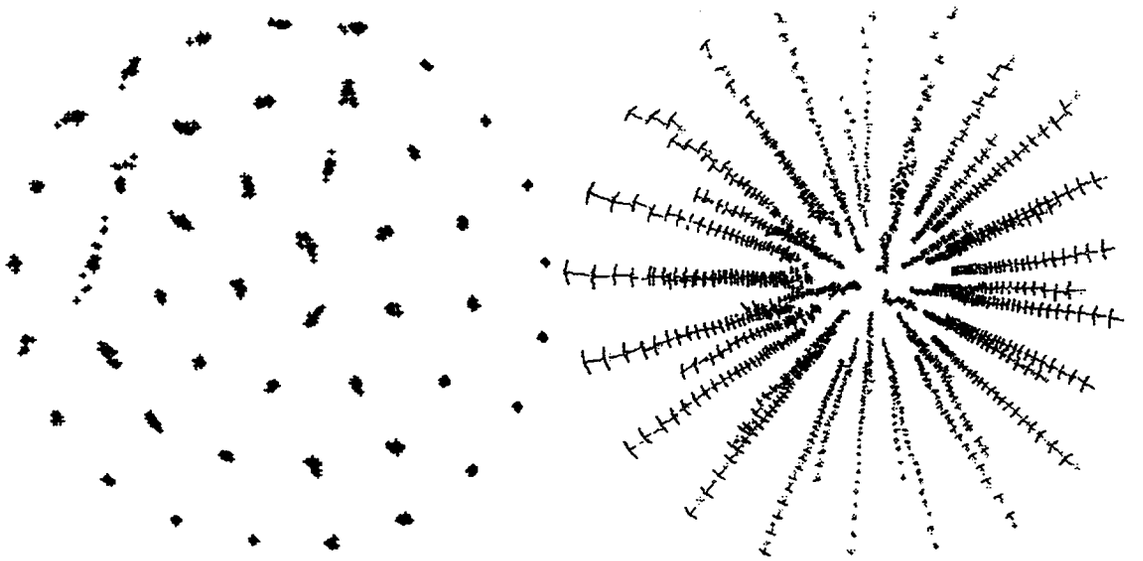

Fig. 6 MD simulations of a beam above the shear limit. The simulation assumes constant (as opposed to once-per-turn) cooling to the same linear velocity. The system eventually settles into a set of strings that slide with respect to each other, but the strings themselves form a pattern of equilateral triangles. The projection of the particle locations onto a plane perpendicular to the beam is shown on the left, and the motion of the particles for a horizontal bend to the right is indicated by arrows on the perspective view on the right side.

never reaches complete order, but the distribution of spacings in such a system has unique mathematical interest. In random matrix theory, the Gaussian orthogonal ensemble [13], which is basic to discussions of the distribution of level spacings in atoms and nuclei and is a major aspect of quantum chaos, corresponds to the properties of a one-dimensional Coulomb system at a particular temperature. Other temperatures correspond to other statistical ensembles.

On the level of "applications" there are many aspects which may pertain to very cold beams that still remain to be investigated and understood. For instance, it is amusing to note that if two beams could be cooled to the space-charge limit, and their crystalline structures could be aligned shell by shell to a micron or better, one might attain an improvement in luminosity by two orders of magnitude over the value for beams of the same diameter and no crystalline structure. Of course, even a slight misalignment would be catastrophic.

Finally on the human level, we always strive to try for the best, and it seems entirely appropriate that the limits of the "best" beam cooling be attempted, explored, and understood.

This research was supported by the U.S. Department of Energy, Nuclear Physics Division, under Contract W-31-109-Eng-38.

REFERENCES

[1] E. N. Dementiev, et al., *Sov. Phys. Tech. Phys.* 25, 1001 (1980).

[2] J. P. Schiffer and P. Kienle, Z. *Phys.* A 321, 181 (1985); A. Rahman and J. P. Schiffer, *Phys. Rev. Letts.* 57, 1133 (1986); J. P. Schiffer and A. Rahman, Z. *Phys.* A331, 71 (1988).

[3] J. P. Schiffer, *Proc. of Workshop on Crystalline Ion Beams*, Wertheim, FRG, Oct. 4-7, 1988, GSI-89-10 Report, April 1989, ISSN 0171-4546, p. 2.

[4] Alessandro Ruggiero, *Demonstration of No Feasibility of a Crystalline Beam in a Betatron Magnet*, Workshop on "Beam Cooling and Related Topics", October 3-8, 1993, Montreux, Switzerland.

[5] Jie Wei, Xiao-Ping Li, and Andrew M. Sessler, *Critical Densities and Temperatures for Crystalline Beam*, Workshop on "Beam Cooling and Related Topics", October 3-8, 1993, Montreux, Switzerland.

[6] J. P. Schiffer and J. S. Hangst, *Molecular Dynamics Simulations of the Crystallization of Ion Beams in Alternating Focusing Fields, and for Curved Trajectories*, Workshop on "Beam Cooling and Related Topics", October 3-8, 1993, Montreux, Switzerland.

[7] A. Labrador, S. Gustafsson, and A. Dainelli, *Computer Simulation of a Crystalline Ion Beam in a Storage Ring*, Workshop on "Beam Cooling and Related Topics", October 3-8, 1993, Montreux, Switzerland.

[8] H. J. Miesner, M. Grieser, R. Grimm, A. Gruber, D. Habs, W. Petrich, D. Schwalm, B. Wanner, H. Wernoe, *Intrabeam Scattering Losses in Laser Cooling*, Workshop on "Beam Cooling and Related Topics", October 3-8, 1993, Montreux, Switzerland.

[9] J. S. Hangst, J. S. Nielsen, O.Poulsen, J. P. Schiffer, P. Shi, and B. Wanner, *Laser Cooling of a Bunched Beam in ASTRID*, Workshop on "Beam Cooling and Related Topics", October 3-8, 1993, Montreux, Switzerland.

[10] J. P. Schiffer and J. S. Hangst, Z. *Phys.* A 341, 107 (1991).

[11] V. V. Avilov and I. Hofmann, *Theory of Longitudinal Schottky Spectra of Ordered Ion Beams in a Storage Ring*, Workshop on "Beam Cooling and Related Topics", October 3-8, 1993, Montreux, Switzerland.

[12] L. Tecchio, G. Lamanna, V. Stagno, V. Variale, R. Calabrese, V. Guidi,F. Petrucci, G. Bisoffi, G. Ciullo, A. Dainelli, S. Gustafsson, A. Labrador, M. F. Moisio, A. Pisent, A. Ruggiero, and B. Yang, *A Dedicated Storage Ring for Ion Beam Crystallization*, Workshop on "Beam Cooling and Related Topics", October 3-8, 1993, Montreux, Switzerland.

[13] Freeman J. Dyson, *J. Math. Phys.* 3, 140 (1961).

RESULTS FROM BEAM TRANSFER FUNCTION MEASUREMENTS AT THE LOW ENERGY ANTIPROTON RING (LEAR)

M. Chanel, U. Oeftiger
CERN, PS Division, CH-1211 Geneva 23

ABSTRACT

Beam transfer functions (BTF), giving the frequency domain response of the beam to an external excitation, are widely used to measure the impedance of the beam environment, to analyze stability conditions and to determine the true momentum distribution in spite of strong signal shielding in dense, cooled beams. In this report results obtained from longitudinal and transverse BTF measurements with protons and antiprotons will be discussed.

Electron cooling has been applied to reach a very low momentum spread of a 310 MeV/c proton or antiproton beam in LEAR. The transverse feedback system and the stochastic cooling system have been used to enhance the stability of the beam at high particle densities. By varying the gain of these two damping systems their influence on the stability diagrams and their contribution to the transverse coupling impedance has been studied.

1. INTRODUCTION

It is well known that the Beam Transfer Function (BTF) is a powerful technique to analyse the stability of dense beams, to measure the machine impedance characteristics and to adjust an active feedback system. The beams obtained by electron cooling are so dense that the longitudinal Schottky spectrum is completely deformed by space charge impedance. The BTF is a way to find the real distribution of the particles. In the transverse planes, tune shifts are large while Landau damping gets very small leading to beam instability. Stabilising systems have to be installed. Again the BTF is an essential technique to estimate the limit of the beam stability and to adjust these active feedback systems.

2. LONGITUDINAL PLANE

2.1. Theory

The longitudinal BTF $r_{\|}^{0}(\omega)$ neglecting the longitudinal coupling impedance $Z_{\|}$ is proportional to the following function of the excitation frequency ω and the revolution frequency ω_r

$$r_{\|}^{0}(\omega) \propto j \int \frac{\frac{d\psi}{d\omega_r}}{\omega - n\omega_r} d\omega_r \quad , \tag{1}$$

where $\psi(\omega_r)$ is the distribution of the particle revolution frequency and n the harmonic number [ref. 1, 2]. The integral is called the dispersion integral. It can be split into its principal value (PV) and the residue at the pole:

$$\int \frac{\frac{d\psi}{d\omega_r}}{\omega - n\omega_r} d\omega_r = PV \int \frac{\frac{d\psi}{d\omega_r}}{\omega - n\omega_r} d\omega_r + j \frac{\pi}{n} \left. \frac{\partial \psi}{\partial \omega_r} \right|_{\omega_r = \omega/n} \quad . \tag{2}$$

Taking into account collective effects $r_{\|}^{0}(\omega)$ is modified by the shielding function $\varepsilon_{\|} = 1 + Z_{\|}\, r_{\|}^{0}$ to [ref. 3]

$$r_{\|}^{c}(\omega) = \frac{r_{\|}^{0}(\omega)}{\varepsilon_{\|}(\omega)} \quad . \tag{3}$$

This influence of the coupling impedance can be seen in the longitudinal stability diagram $1/r_{\|}^{c}(\omega)$- a plot of the BTF in the complex plane - as a shift by the impedance vector. Instability threshold is reached, if the

inverted response curve touches the origin in the stability diagram. If the impedance vector $Z_{\|}$ is known, the true momentum distribution $\psi(\omega)$ can be evaluated from the measured $r_{\|}^{c}(\omega)$.

The longitudinal shielding function modifies the longitudinal Schottky power spectrum $P^{0}(\omega)$ to

$$P^{c}(\omega) = \frac{P^{0}(\omega)}{\left\|\varepsilon_{\|}(\omega)\right\|^{2}} \quad \text{with} \quad P^{0}(\omega) \propto \psi(\omega) \quad . \tag{4}$$

From the deformed Schottky power spectrum one can calculated the distribution $\psi(\omega)$ for an estimated vector $Z_{\|}$. A criterion for the exactness of the estimated $Z_{\|}$ is that the distributions obtained from the two computations do fit [ref. 4, 5].

2.2. Results from longitudinal measurements

At LEAR measurements have been performed in a frequency range up to 80 MHz and with a different number of protons and antiprotons. In figure 1 the coupling impedance calculated from the BTF measurements and the deformed Schottky power spectra is shown. The real and the imaginary part of the impedance per harmonic number have a maximum at around 7 MHz. This effect was due to a defect of the short circuit of the cavity gap during the coasting beam operation of the machine. The expected behaviour $\mathrm{Re}\{Z_{\|}/n\} \propto 1/\sqrt{n}$ of the real part could not be seen because of the strong spread of the results. Above 30 MHz the average real part of the coupling impedance is around (30 ± 90) Ohms. The imaginary part of the coupling impedance is constant above frequencies of 30 MHz as expected from theory.

Assuming that the momentum distribution of the beam is Gaussian and supposing that in the case of strongly cooled beams the coupling impedance is mainly due to space charge forces, the width of the revolution frequency distribution $\Delta\omega$ is related to the width $\delta\Omega$ and the distance $2\Delta\Omega$ of the two coherent peaks in the longitudinal deformed Schottky spectrum [ref. 6] by:

$$\delta\Omega = (\Delta\Omega)\left(\frac{\Delta\Omega}{n\,\Delta\omega}\right)^{3} \exp\left[-\frac{(\Delta\Omega)^{2}}{n^{2}(\Delta\omega)^{2}}\right] \quad . \tag{5}$$

This formula can be used to cross check the results for the momentum width derived from the BTF measurements. In figure 2 the width of the momentum distribution derived from the BTF measurement is compared with the one directly obtained from the corresponding deformed Schottky spectrum using equation (5). The correlation of the two is nearly linear, but the results from the Schottky spectra are about 25% larger than the results from the BTF analysis.

Taking into account the electron cooling and intra beam scattering [ref. 7] the equilibrium momentum width should vary with the number of protons or antiprotons N as:

$$\frac{dp}{p} \propto N^{1/3} \tag{6}$$

In figure 3 the width of the distribution is plotted against the number of protons. Fitting the data by a least square fit to the logarithmic values one observes an exponent of (0.31 ± 0.04) , which is in good agreement to the expected value of 1/3. In these measurements the calculated imaginary impedance reached twelve times the Keil-Schnell-circle.

The quality of the measurements has been improved by transforming the frequency data of the BTF measurements into time domain, gating out the incoherent signal contributions (mainly Schottky noise from the beam) and transforming the data back into frequency domain [refs. 8 and 9].

Using this time gating procedure to suppress the coherent signals one can extract the noise contribution of the BTF measurement. This noisy frequency spectrum has been fitted to the measured deformed Schottky spectrum that was taken directly after the BTF excitation has vanished, by minimizing the difference of both signals using the exponent x in the following equation as the fitting parameter:

$$\left(r_{noise}^{BTF}(\omega)\right)^{x} = P_{0}^{c}(\omega) \tag{7}$$

As in the example of figure 4 the two signals fit very precisely and the value for the exponent x is (1.00 ± 0.15), which shows that the noise of BTF measurements is mainly determined by the Schottky noise of the beam and not by electronic noise. Its suppression is therefore of great importance for the quality of the BTF measurements.

3. TRANSVERSE PLANE

3.1. Theory

Similar to the longitudinal plane the transverse BTF $r_\perp^0(\omega)$ neglecting the transverse coupling impedance $Z_\perp$ is proportional to

$$r_\perp^0(\omega) \propto j\, PV\int \frac{\psi(\omega_\beta)}{\omega_\beta-\omega} d\omega_\beta \pm \pi\ \psi(\omega_\beta)\Big|_{\omega_\beta=\omega} \quad . \tag{8}$$

where ω_β is the betatron frequency and $\psi(\omega_\beta)$ the betatron frequency distribution of the beam [ref. 1, 10]. The plus and minus sign stands for the response to the fast and slow wave. Collective effects modify this BTF by the shielding function $\varepsilon_\perp = 1 + Z_\perp\, r_\perp^0$ to

$$r_\perp^c(\omega) = \frac{r_\perp^0(\omega)}{\varepsilon_\perp(\omega)} \quad . \tag{9}$$

The influence of the coupling impedance leads again to a shift in the transverse stability diagram, whereas the transverse feedback system and the stochastic cooling system lead to an additional shift of each of the two traces away from the origin as shown in figure 5.

3.2. Results from transverse BTF measurements

Transverse BTF measurements have been used to estimate the impedance of the transverse feedback system and the impedance contribution of the transverse stochastic cooling system working as a broad band damper. From vertical and horizontal BTF measurements the transverse stability diagram has been calculated at different harmonic numbers and different values for the gain of the feedback system G_{fb} [dB] and the gain of the stochastic cooling system G_{st} [dB]. The total damper impedance $Z_\perp$ calculated from the stability diagram has a component $Z_{\perp,fb}$ due to the feedback system, and a component $Z_{\perp,st}$ due to the stochastic cooling system. Both are proportional to the linear gain of the corresponding system and to the sensitivity of their pick-up and kicker system. Calculation of the transfer function for the pick-up, the kicker and the amplifier electronics for both systems leads to a formula for the total damper impedance, which is given by a superposition of the transfer functions of the two damping systems [ref. 11].
Using the proportional constants A_{fb} and A_{st} the real part of the total damper impedance can be written as:

$$\mathrm{Re}(Z_\perp) = A_{fb}\frac{\sin(\pi\frac{f}{f_1})}{f/_{MHz}} 10^{G_{fb}/_{20dB}} + A_{st}(1+0.3\,f/_{MHz})\sqrt{f/_{MHz}}\ 10^{G_{st}/_{20dB}} \quad , \tag{10}$$

Fitting this function to a series of measurements with A_{fb} , A_{st} and f_1 as the fitting parameters one can calculate the impedance contributions due to the feedback system and the stochastic cooling system separately. In the example of figure 6 the real part of the total damper impedance derived from the BTF measurements is plotted together with the fitting curve $\mathrm{Re}\{Z_\perp(f)\}$. By averaging the results of three different measurement sets - each of them having different settings for the gains - we get as a mean value: $A_{fb} = 617\,M\Omega/m$ and $A_{st} = 0.158\,M\Omega/m$. The fitting parameter f_1 represents the zero in the kicker sensitivity function of the feedback system and was found to be 30 MHz (from a separate broad band BTF f_1 was obtained to be around 55 MHz - the reason for the discrepancy is not yet understood).

The impedance contributions $\mathrm{Re}\{Z_{\perp,fb}\}$ from the feedback system and the impedance contribution $\mathrm{Re}\{Z_{\perp,st}\}$ due to the stochastic cooling system are shown in figure 7. The accuracy of this result depends on the accuracy of the damper impedance derived from the stability diagram. In the horizontal plane the efficiency of the damper is very low (fig. 5), because of the small value of the Twiss parameters at the pick-up and at the kicker of the feedback system. The structure of the kicker of the feedback system will have to be changed to avoid the zero of the response at 30 MHz (fig. 7).

4. CONCLUSIONS

The Beam Transfer Function is now used extensively at LEAR in all the 3 planes. It permits us to find the longitudinal beam distribution (despite the strong coherent signals which modify the Schottky spectrum), to estimate the impedance of the machine in a large frequency range, to observe the effect of the two transverse active feedback on the beam stability, and to find the action that has to be taken to improve these systems.

5. ACKNOWLEDGMENTS

F. Caspers, D. Möhl and F. Pedersen have participated in many discussions about the measurement technique and the results. D. Williams and L. Söby have built a continuously improved active feedback system.

6. REFERENCES

[1] J. Borer, G. Guignard, A. Hofmann, E. Peschardt, F. Sacherer, B. Zotter: "Information from Beam Response to Longitudinal and Transverse Excitation", CERN-ISR-TH-BOM / 79-20

[2] K. Hübner, V.G. Vaccaro, "Dispersion Relations and Stability of Coasting Particle Beams", CERN-ISR-TH/70-44, 1970

[3] S. Cocher, I. Hofmann: "On the Stability and Diagnostics of Heavy Ions in Storage Rings with High Space Densities", Part. Accel. 34, 189 (1990)

[4] U. Oeftiger: "Measurements of Beam Properties and Beam Environment in LEAR and COSY using RF Excitation Methods", Thesis to be published

[5] J. Bosser, M. Chanel, R. Ley, D. Möhl, U. Oeftiger, G. Tranquille: "Electron Beam Cooling and Beam Instability Studies at LEAR", Proceedings of Workshop on Heavy Ion Storage and Cooler Rings, Smolenice, June 1st-5th, 1992, to be published, preprint CERN/PS 92-45 (AR)

[6] S. Chattopadhyay, "Some Fundamental Aspects of Fluctuations and Coherence in Charged-Particle Beams in Storage Rings", CERN 84-11, October 1984, p. 118

[7] I. Hoffmann, "Beam Dynamics in Cooled Heavy Ion Beams", IEEE Particle Accelerator Conference 1991, San Francisco, Vol. 4,p. 2492 .

[8] U. Oeftiger and F. Caspers: "Gating in Time Domain as a Tool for improving the Signal-to-Noise-Ratio of Beam Transfer Function Measurements", CERN Internal Note 1992, PS/AR/NOTE 92-19

[9] F. Caspers, M. Chanel, U. Oeftiger, "A Novel Method of Noise Suppression in Beam Transfer Function Measurements", IEEE Particle Accelerator Conference 1993, Washington, Proceedings to be published, preprint CERN/PS 93-19 (AR)

[10] D. Möhl, A.M. Sessler, "The Use of RF-knockout for the Determination of the Characteristics of the Transverse Instability of an Intense Beam", Proc. 8th Int. Conf. on High-Energy Accelerators, CERN, Geneva 1971, p. 33 .

[11] U. Oeftiger, M. Chanel, "Measurements of Transverse Active Feedback at LEAR", CERN Internal Note 1993, PS/AR/Note 93-20

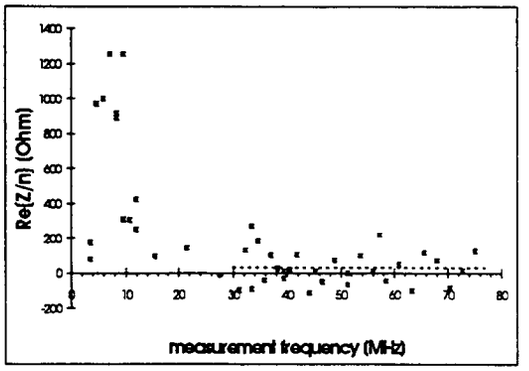

Figure [1a]

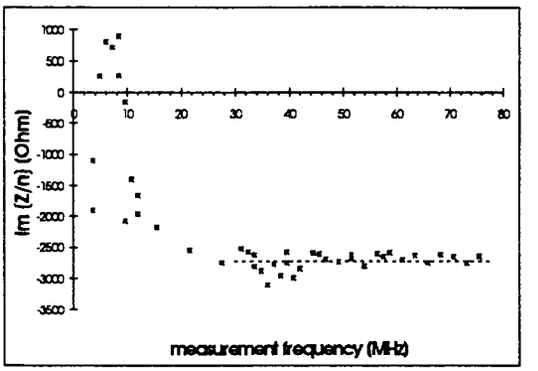

Figure [1b]

Measurement with $2 \cdot 10^9$ antiprotons with a momentum of 309 MeV/c, the average real part of the coupling impedance calculated from BTF's performed at frequencies above 30 MHz is about Re{Z/n} = (30 +- 90) Ohm, the average imaginary part is about Im{Z/n} = (-2730 +- 130) Ohm (see dotted lines)

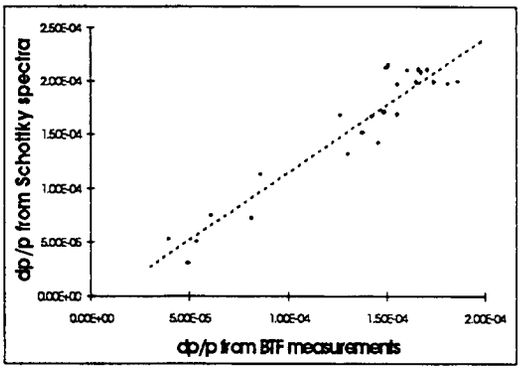

Figure [2]: Comparison of $(dp/p)_{FWHH}$ derived from a deformed Schottky power spectrum with the one calculated from BTF measurements with a proton beam of 310 MeV/c and proton numbers between 10^9 and $8 \cdot 10^{10}$

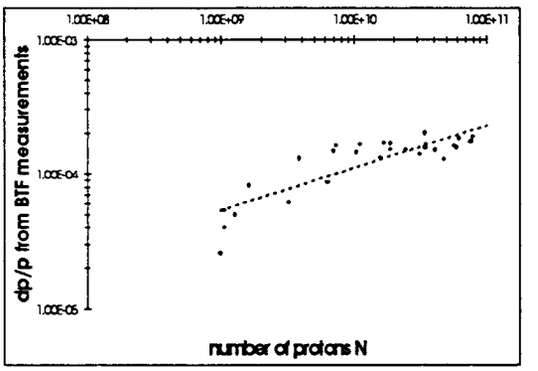

Figure [3]: Logarithmic plot of $(dp/p)_{FWHH}$ calculated from BTF measurements with a proton beam of 310 MeV/c versus the number of protons. A linear fit leads to the dotted line with a slope of (0.31 ± 0.04).

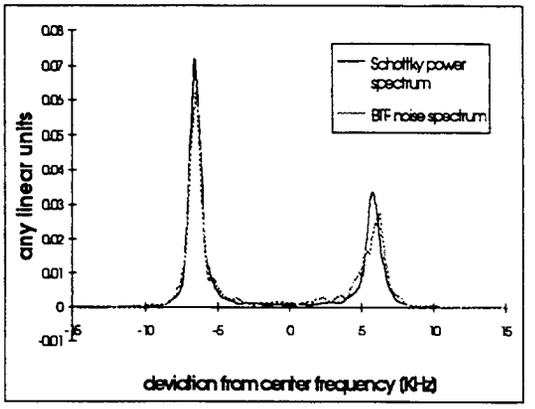

Figure [4]: Noise spectrum of a BTF measurement at the 25th harmonic with $5 \cdot 10^{10}$ protons at 310 MeV/c and with $(dp/p)_{FWHH} = 1.3 \cdot 10^{-4}$, compared with a deformed Schottky power spectrum measured directly after the excitation signal of the BTF source has vanished. A fitting to the formula of equation (7) leads to an exponent $x = 1.00$.

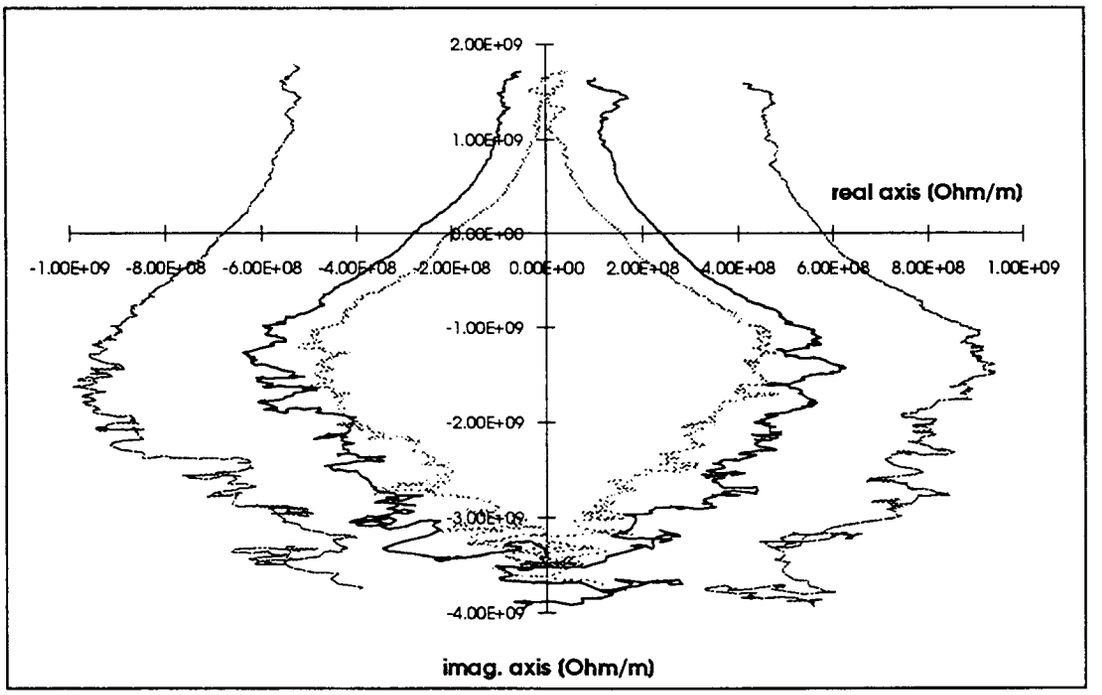

Figure [5]: Example of an horizontal stability diagram of a beam with $8 \cdot 10^9$ protons at 310 MeV/c at the 70th harmonic (= 84 MHz) with +50dB as the gain for the feedback system and different gains for the stochastic cooling system: +50dB, +70dB and +85dB (from inner to outer traces). Increasing the gain enhances the horizontal stability of the beam.

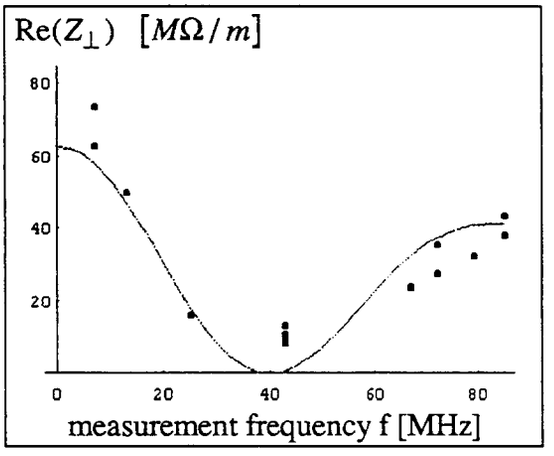

Figure [6]: The real part of the transverse damper impedance $\mathrm{Re}\{Z_\perp(f)\}$ for the gains G_{fb}= +50dB and G_{st}= +70dB has been calculated from transverse BTF measurements of a proton beam of 310MeV/c. The line represents the fitting function of equation (10) with the parameters f_1 = 30 MHz, $A_{fb} = 617 M\Omega/m$ and $A_{st} = 0.158 M\Omega/m$.

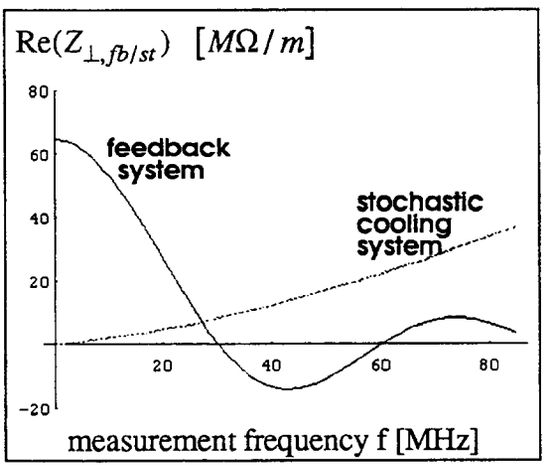

Figure [7]: Plot of the estimated real part of the transverse impedance $\mathrm{Re}\{Z_{\perp,fb}\}$ due to the feedback system and of the real part $\mathrm{Re}\{Z_{\perp,st}\}$ due to the stochastic cooling system used as a damper. The traces are related to G_{fb}=+50dB and G_{st}=+70dB.

CURRENT LOSSES IN SYSTEMS WITH THE ELECTRON BEAM ENERGY RECOVERY IN A LONGITUDINAL MAGNETIC FIELD.

A.N. Sharapa, A.V. Shemyakin
Budker Institute of Nuclear Physics, 630090 Novosibirsk, Russia

ABSTRACT

Efficiency of the secondary electron capture in the recuperator with a longitudinal magnetic field is discussed. To characterize this efficiency the value of the collector secondary emission coefficient is introduced, for calculation of which the simple formula is proposed. The effects determining the difference of current losses in rectilinear systems and devices with bending magnets are analyzed. It is experimentally shown that there is no unambiguous relation between the efficiency of the secondary electron capture by the collector and the current losses. The mechanism determined current losses in rectilinear systems is suggested.

In electron cooling devices using effective recovery of the electron beam energy, it is important to have low current losses. In such systems, a strong magnetic field keeps a primary beam far from electrodes, and the current losses are due to only ionization of residual gas and to secondary electrons from a collector. This paper is devoted to losses resulting just from the secondary electrons. A part of the device determining a flow of these electrons, i.e., the collector and electrodes forming a potential minimum will be named a recuperator.

Without a magnetic field, all the secondary electrons escaping from the recuperator go to electrodes having a high potential respecting a cathode. An efficiency of the recuperator can be characterized by the value

$$\sigma_{col} = \frac{\delta I}{I}, \tag{1}$$

where δI and I are currents of the secondary and primary electrons, respectively. A natural name for this value is a collector secondary emission coefficient.

In the devices with the magnetic field these secondary electrons are confined by the field. In rectilinear systems most of the electrons goes to the gun, reflects from the region near the cathode and is captured by the recuperator with the same efficiency as the primary beam. In this case, the current losses $\Delta I/I$ are much less than σ_{col}, if δI in 1 is a flow of the secondary electrons created by the primary beam on the collector surface and escaping from the recuperator. Hence, with the guiding magnetic field the current losses depend not only on the recuperator efficiency, but also on properties of the device as a whole. So, the losses can increase by orders when the recuperator is transferred from a rectilinear test device to one with turns. Such an effect was observed by authors at testing of the recuperator for the installation described in [1], the same is in [2]. In the electron cooling system [3] the losses decrease by two orders due to compensation of a centripetal drift. Therefore it is useful to separate the factors determining the value, i.e. the efficiency of the recuperator itself, and the mechanism of the current losses.

1. The collector secondary emission coefficient

To estimate the collector secondary emission coefficient, it is expedient to consider the secondary electron movement on the recuperator as an aggregate of its interaction with an electrostatic barrier, a magnetic mirror and walls of the collector ("a geometric factor" [4]).

1.1 "The geometric factor"

In the recuperators without the magnetic field, geometric dimensions of the collector are very important because the secondary electron flow diverges from the collector bottom surface and mainly goes to the collector walls. The use of such arguments for the systems with the magnetic field (for example, in 5) seems us inconsistent. A trajectory of the secondary electron can not deviate from a field line by more than Larmor radius

$$\rho_{col} = \frac{m \cdot c}{e \cdot H} \cdot v_{\perp} < \frac{m \cdot c}{e \cdot H} \cdot \sqrt{\frac{2 \cdot e \cdot U_{col}}{m}}, \tag{2}$$

where e and m are charge and mass of an electron, H is the magnetic field strength, $v_\perp$ is a component of the velocity transverse to the field line, U_{col} is a collector potential respecting the cathode. For the parameters of real recuperators ($H \approx 0.01T$, $U_{col} \approx 1kV$) $\rho_{col} = 1cm$. This is much less than transverse dimensions of the collectors. Therefore, "the geometric factor" is unessential for the systems under consideration. This conclusion is also confirmed by a computer simulation of the secondary particle movement 1.

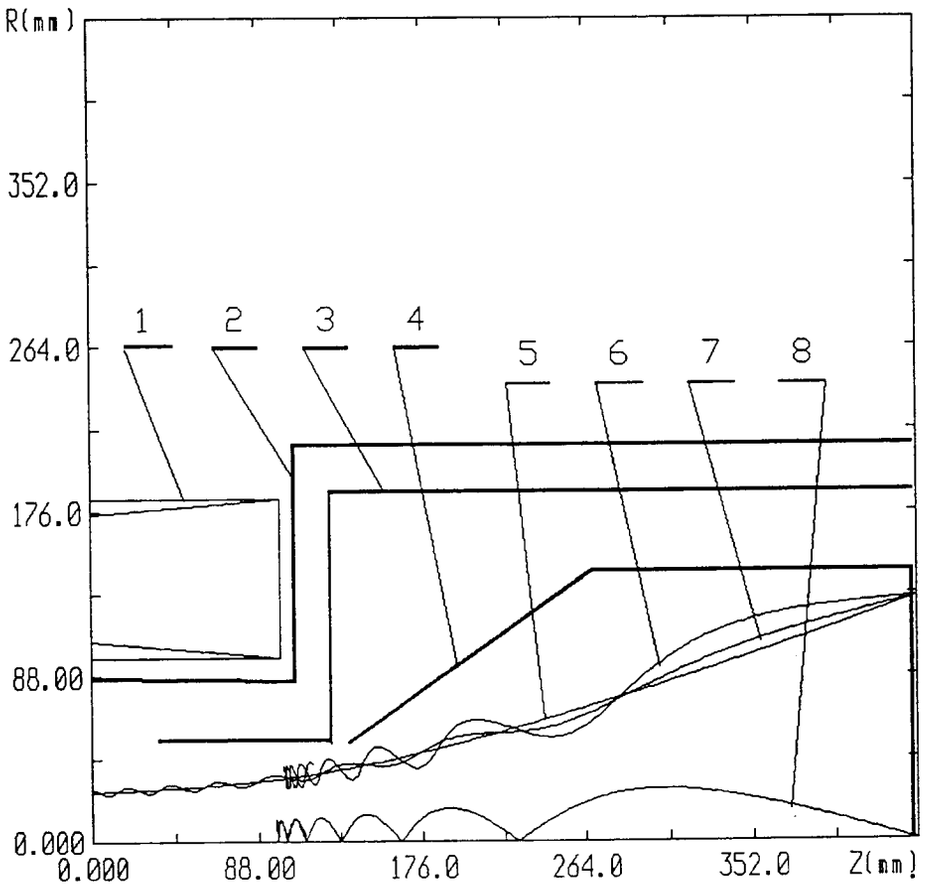

Figure 1: Drawing of the recuperator being test
1 — solenoid, 2 — vacuum chamber, 3 — suppressor, 4- collector. Trajectories 5-8 illustrate movement of particles inside the collector for a case of an equipotential space. Computer simulations for $H_0 = 0.06T$, $U_{col} = 3kV$. *5 — boundary trajectory of the primary beam, 6, 8 — trajectories of the secondary electron with* $\vartheta > \vartheta_c$, *7- the same for* $\vartheta < \vartheta_c$.

1.2 The magnetic mirror

The term "the magnetic mirror" means that the electrons created on the collector surface placed in a weak field H_c reflect from the region with a strong field H_0 near a recuperator exit if the angle ϑ between its velocity and the field line on the collector surface is more than the critical value ϑ_c 1. This critical angle is simply estimated if the magnetic field change slowly in comparison with the Larmor rotation:

$$\frac{1}{H} \cdot \frac{dH}{dZ} \cdot \rho_1 \ll 1, \tag{3}$$

where ρ_l is the Larmor radius calculated by the longitudinal velocity of the particle. In this case the movement is adiabatic, there is the invariant

$$\frac{v_\perp^2}{H} = const, \tag{4}$$

and the critical angle is

$$\sin \vartheta_c = \frac{H_c}{H_0}. \tag{5}$$

As a rule, the field strenght on the collector surface is much less than that in the homogeneous part, and condition 3 is not fulfilled. We made computer simulations of the particle movement in the field of a solenoid for the case of the equipotential space. Even for $H_c \ll H_0$, the calculated critical angle proves to agree with the estimation 5 with an accuracy of 10% if the Larmor radius is much less than the solenoid radius R_s:

$$\frac{m \cdot c}{e \cdot H_0} \cdot \sqrt{\frac{2 \cdot W}{m}} < 0.1 \cdot R_s, \tag{6}$$

This fact owes to a specific picture of the magnetic field lines of the solenoid which is closed to that of a point magnetic pole. In the field of the point pole, the adiabatic invariant 4 is an exact integral of movement [6]. As a rule, electric fields in the collector cavity weakly affect the transverse movement of the electrons, and, apparently, relation 4 asserts in the real collectors.

Using 4, the estimate for the magnetic mirror efficiency can be easily found if the magnetic field lines are perpendicular to the collector surface. The knocked secondary electrons are known to have a cosine angle distribution [7]

$$\frac{d\sigma}{d\Omega} = \frac{\sigma_0}{\pi} \cdot \cos \vartheta, \tag{7}$$

where σ_0 is a total secondary emission coefficient. From 4 the angle ϑ_1 between the trajectory and the field line at the exit of the mirror and the corresponding solid angle $d\Omega_1$ are obtained:

$$\sin \vartheta_1 = \sqrt{\frac{H_0}{H_c}} \cdot \sin \vartheta,$$

$$d\Omega_1 = d\Omega \cdot \frac{H_0 \cdot \cos \vartheta}{H_c \cdot \cos \vartheta_1}, \quad \vartheta < \vartheta_c, \tag{8}$$

From 7 and 8 we obtain that the angle distribution at the entrance of the mirror

$$\frac{d\sigma}{d\Omega_1} = \frac{\sigma_0}{\pi} \cdot \cos \vartheta_1 \cdot \frac{H_0}{H_c}, \tag{9}$$

is also cosine, and the total number of secondary electrons decreases by a factor of H_0/H_c.

So, if the collector is placed in the dropping solenoid field and the secondary electrons are confined only by the magnetic mirror, the collector secondary emission coefficient is equal to

$$(\sigma_{col})_H = \frac{H_c}{H_0} \cdot \sigma_0, \tag{10}$$

and doesn't depend on the absolute value of the magnetic field strength.

1.3 The electrostatic mirror

It is possible to estimate the electrostatic barrier influence using results of direct measurements of a share σ_1 of secondary electrons, overcoming the barrier U_m/U_{col} in a flat electric field from [8] 2.

In the magnetic field, the penetration of electrons through the potential barrier is determined by the longitudinal component of the velocity as in the case of the flat electric field. Therefore, in the recuperator with the homogeneous magnetic field and the potential minimum the flow of secondaries is the same as in 2.

The function $\sigma_1(U_m/U_{col})$ can be estimated also by energy spectra measured in [7]. These spectra can be approximated by a sum of δ- function for elastically scattered electrons and by homogeneous distribution for inelastic ones:

$$\frac{d\sigma}{dE} = \frac{a}{U_{col}} + b \cdot \delta(e \cdot U_{col}), \tag{11}$$

where a and b are material coefficients. The calculation results on distribution 7, 11 are shown in 2 by a solid line and are in reasonably good agreement with measurements [8].

For calculation, it is convenient to use the simple approximation of these data:

$$(\sigma_{col})_E = k \cdot \left(\frac{U_m}{U_{col}}\right)^2, \tag{12}$$

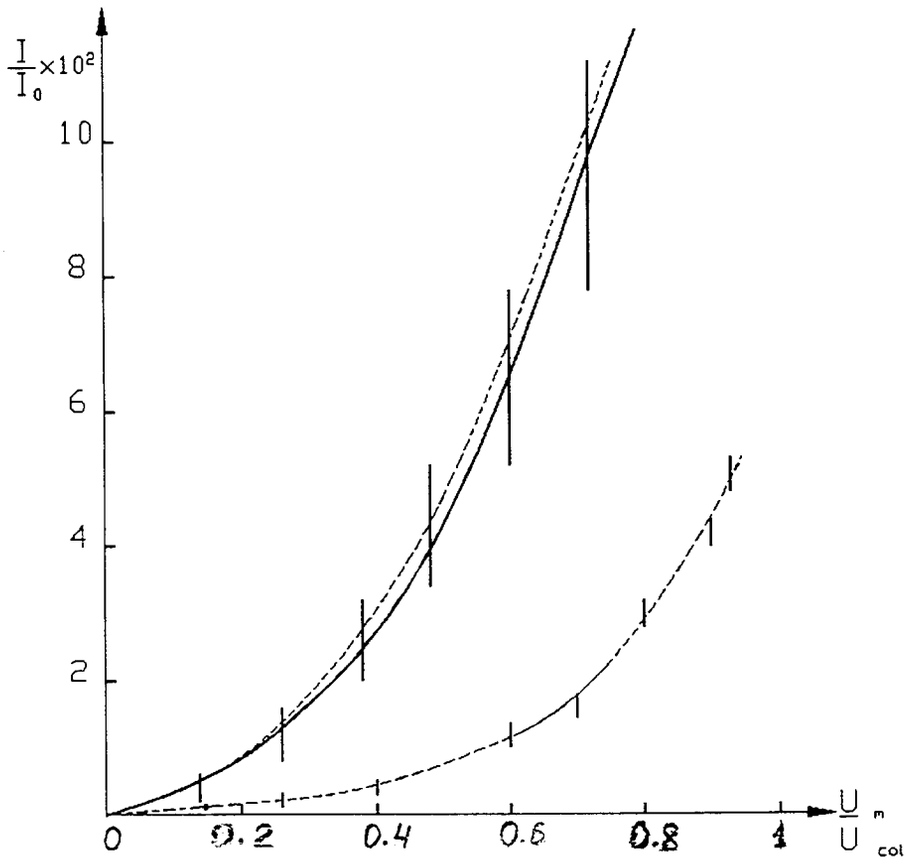

Figure 2: *The ratio σ_1 of the current of the secondary electrons overcoming the potential minimum in the flat electrostatic field as a function of depth of this minimum U_m/U_{col}. Vacuum is $5 \cdot 10^{-4} Pa$, a surface material is stainless steel (1), Be (2). A dashed curve is an approximation (12), solid one is a result of calculation by (11) for $a = 0.25$, $b = 0.01$.*

where k is the coefficient dependent on the collector surface material and vacuum conditions. For the surface of stainless steel and vacuum level of $5 \cdot 10^{-4} Pa$, $k = 0.2$.

Considering that the magnetic mirror keeps the cosine character of angle distribution 9, the estimation for the collector secondary emission coefficient with the potential barrier and the increasing magnetic field is reduced to multiplying 10 and 12:

$$\sigma_{col} = k \cdot \left(\frac{U_m}{U_{col}}\right)^2 \cdot \frac{H_c}{H_0}. \tag{13}$$

2. The current losses in the systems with the longitudinal magnetic field

The secondary electrons can strike the high potential electrodes only in the case, where its trajectories differ from those of the primary beam. In the electron cooling devices such a displacement is due to centripetal drift in toroidal bends:

$$\Delta_1 = 2 \cdot \alpha \cdot \rho_0, \tag{14}$$

where α is a full angle of turn, ρ_0 is the Larmor radius calculated by the total energy of electrons. If

$$\Delta_1 > R_0 + R_b, \tag{15}$$

where R_0, R_b are radii of a high voltage (resp. cathode) electrode and of a beam, all secondary electrons hit to the electrode and

$$\frac{\Delta I}{I} = \sigma_{col}. \tag{16}$$

For the low magnitude of Δ_1

$$\Delta_1 < R_0 - R_b \tag{17}$$

most of the electrons escaping from the recuperator returns again to it and is captured by the collector with the same efficiency as the primary beam. It is evident, that in this case

$$\frac{\Delta I}{I} \ll \sigma_{col}. \tag{18}$$

Condition 17 corresponds to a low magnitude of ρ_0 (a strong magnetic field, a low energy) or to $\alpha = 0$ (a compensated centripetal drift, S- configuration of the device, the rectilinear system). Mechanism of the losses for these possibilities seems to be similar. For definiteness, we consider the rectilinear system, in which the experiments were made.

Apparently, for such a system a main effect determining the current losses is increasing of the secondary electron beam due to large transverse velocities. The recuperator can be considered as an emitter of the secondary electrons with a temperature of $e \cdot U_m$. In this case the radius of the secondary beam is that:

$$R_2 = R_b + 2 \cdot \rho_m, \quad \rho_m = \frac{m \cdot c}{e \cdot H_0} \cdot \sqrt{\frac{e \cdot U_m}{m}}. \tag{19}$$

Hence, a variation of the minimum potential changes not only σ_{col}, but the radius of the secondary beam also.

If $R_2 < R_0$, the secondary beam doesn't hit the high voltage electrode and returns to the collector, where it creates a tertiery beam and so on. Each collision with the collector surface occurs in a random phase, and the maximum radius of the secondary emitted electrons after each successive generation increases $2 \cdot \rho_m$.

A quality pattern of an electron density distribution outside the primary beam boundary can be calculated at an assumption that after each collision the knocked electrons distribute homogeneously along the radius $\pm\rho_m$ from the collision point. Such a distribution is shown on 3 for the case, when after

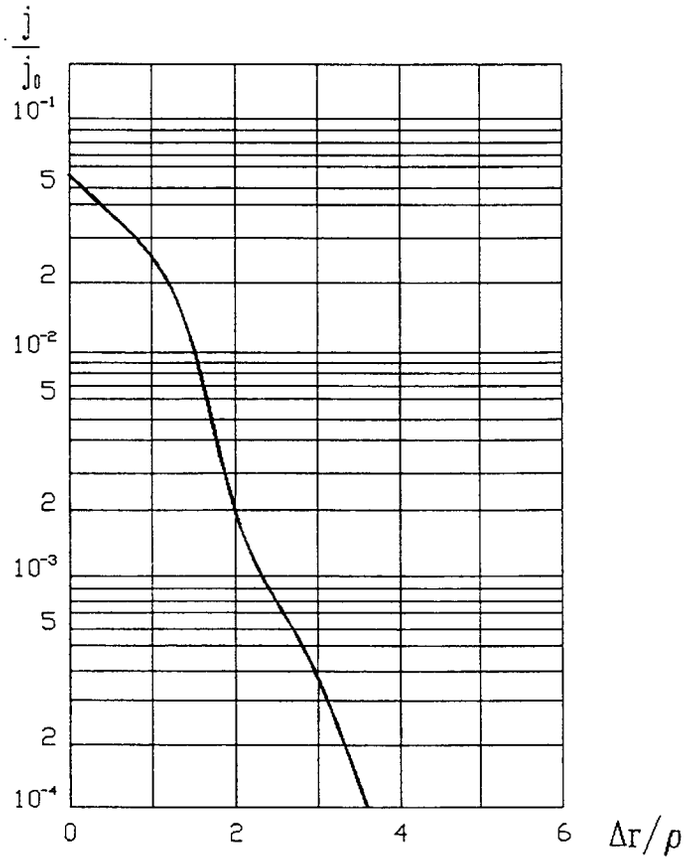

Figure 3: *Distribution of the secondary electron current density outside the boundary of the primary beam as a function of a distance from a beam boundary.* $\sigma_{col} = 0.1$.

third collision any electrons go to the high voltage electrode, and $\sigma_{col} = 0.1$. The density falls rapidly with

a coordinate r/ρ_m. It means also a strong dependence of the losses on the ratio of gaps to the Larmor radius. Therefore, the losses decrease with the magnetic field strength, whereas the value of σ_{col} remains constant.

3. Experimental results

A quality test of the model proposed was made at the recuperator, a scheme of which is shown in 1. The potential minimum is created by a tube-like suppressor having a potential U_s, the ratio of H_c to the field strength in the region of the potential minimum is 15.

The experimental functions $\Delta I/I\ (U_s/U_{col}), H_0)$ is presented in 4. The strong dependence of the

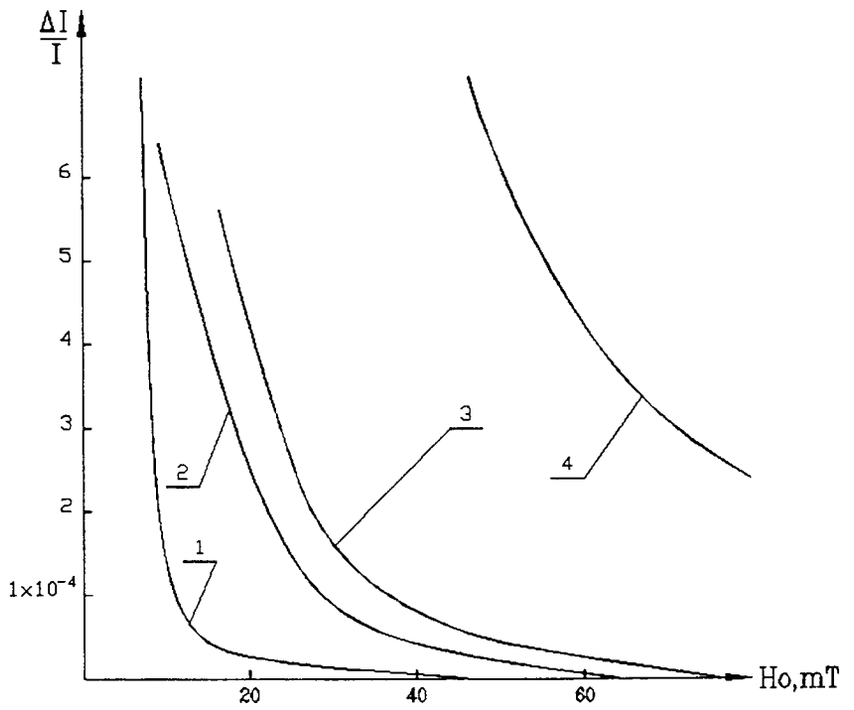

Figure 4: *Relative current losses as function of the magnetic field strength and the value of the potential minimum. For the curve 1* $U_s/U_{col} = 0.25$, $2 - 0.5$, $3 - 0.75$, $4 - 1.0$.

losses on the magnitude of the magnetic field agrees with the model proposed.

Using the curves of 4, it is possible to build up functions $\Delta I/I(\rho_m)$ for different suppressing potentials 5. For a given value of ρ_m a dependence of the losses on the suppressing voltage is close to quadratic one 13. The losses become zero (i.e. much less than 10^{-5}) for different values of ρ_m. This fact has a natural reason. For the low enough σ_{col} and $\Delta > 2 \cdot \rho_m$ the losses are extremely low because ones are merely due to the tertiery beam with the current of $\sigma_{col}^2 \cdot I$. Therefore for $\sigma_{col} = 10^{-3}$ $\Delta I/I < 10^{-6}$. In the regime $U_{col} = U_s$ (the curve 3 in the 5) $\sigma_{col} \sim 10^{-1}$. In this case the density even the tertiery beam is significant, and at $\Delta \cong 2 \cdot \rho_m$ the losses are $3 \cdot 10^{-4}$.

Notice, that to find the precise quantitative value of σ_{col} by the functions of $\Delta I/I\ (U_s/U_{col},\ H_0)$ it is necessary to know the beam diameter not only in the drift region, but in the suppressor also. In the experiments the last one wasn't knew with a good enough precision.

The model proposed assumes a gap between the beam and the high voltage electrode to be less than in the suppressor. It was just this relation, which was in the described above experiments. Otherwise a consideration is more complicated, but experiments show all qualitative relationships to be kept.

Conclusion

1. To characterize the efficiency of the secondary electron capture by the recuperator, the value of the collector secondary emission coefficient is introduced. To calculate this value, the simple formula is proposed. Using this conception makes it possible to describe the recuperator efficiency irrespectively of other system properties. The direct measurement of this value is possible in the U- configuration

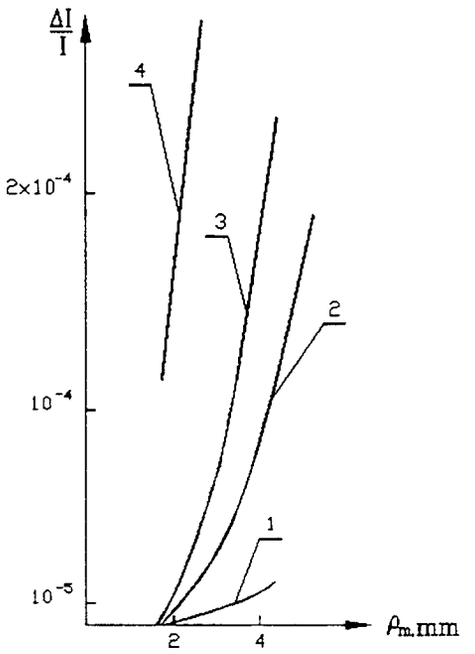

Figure 5: *Relative current losses as function of the Larmor radius calculated by the suppressor potential. For the curve 1* $U_s/U_{col} = 0.25$, $2 - 0.5$, $3 - 0.75$, $4 - 1.0$.

of the device under conditions of complete removal of the secondary beam by the centripetal drift during one turn.

2. In the systems with the longitudinal magnetic field the current losses due to the secondary electrons from the collector depend strongly on the system configuration and the magnetic field strength. In the rectilinear systems the value of the losses can be less than the collector secondary emission coefficient. This case is described qualitatively by the model on the aasumption that all secondary electrons having the maximum radius less than the aperture return into the collector and that the maximum diameter of each successive generation of the secondary electron beam increases.

3. The experiments performed on the rectilinear test bench agree qualitatively with the model proposed.

The authors acknowledge the assistance in calculations of T.N. Andreeva and in the assembly of the collector of V.M. Rybkin.

REFERENCES

[1] M.E.Veis et al., High voltage electron cooling device, in Proc. of $13 - th$ Int. Conf. on High Energy Accelerators, Novosibirsk, 7-11 August 1986, (Nauka, Novosibirsk, 1987), p.348.

[2] M.Steck et al., Electron cooling of heavy ions, Nucl. Instr. and Meth., A287(1990), 324.

[3] T.J.P. Ellison et al., The IUCF cooling system collector performance, Nucl. Instr. and Meth., *B*40/41(1989), 864.

[4] V.Kudelainen et al., Sov. Phys. Techn. Phys., 21(1976), 965.

[5] J.Bosser et al., The new collector for the electron cooling device at LEAR, Nucl. Inst. and Meth., A311(1992), 465.

[6] D.V.Sivuchin, in Problems of the plasma theory, N1, edited by M.A.Leontovich (Gosatomizdat, Moscow, 1969), p.69.

[7] I.M.Bronstein, B.S.Friman, Secondary electron emission (Nauka, Moscow, 1969).

[8] A.N.Sharapa, Candidate thesis, Novosibirsk, 1982.

STUDY ON PHOTOSOURCE FOR ELECTRON COOLING DEVICES

R.Calabrese[1], G.Ciullo[2], V.Guidi[1,2], G.Lamanna[2,5], P.Lenisa[3], B.Maciga[1,2], L.Tecchio[2,4] and B.Yang[2,5].

1) Dipartimento di Fisica dell'Università and INFN, I-44100 Ferrara, Italy.

2) Laboratori Nazionali di Legnaro, I-35020 Legnaro, Italy

3) Politecnico di Milano and INFN, I-20100 Milano, Italy

4) Dipartimento di Fisica Sperimentale dell'Università andINFN, I-10125 Torino, Italy.

5) PROEL Tecnologie, Firenze, Italy.

ABSTRACT

An intense cw electron beam is produced by GaAs photoemission. Some high performances have been achieved . In paricular, several weeks long lifetime has been achieved with an electron current as intense as 1 mA over a few mm^2 beam size.

1. INTRODUCTION

One of the most challenging applications would be the production of a very cold electron beam for electron cooling (subthermal cooling beams). This cooling precess[1] consists of the superposition of an electron beam with the lowest possible energy spread along a dedicated drift section of a circular machine, over an ion beam circulating at the same velocity. The thermal exchange induced by ion-electron collisions causes the compaction of the volume occupied by the ion beam in the 6-d phase-space. At low energy (1+30 keV), this application demands the production of relatively high current (about 1 mA over a few mm^2 beam size [2-4]), which quite contrasts with the request of low energy spread for the electron beam. In electron cooling devices operating at present, the electron source is a thermocathode [2-4]; in this case current density is related to cathode temperature T by the Richardson's law, $j=AT^2exp(-W/kT)$, W being the work function for the chosen material. In order to produce a current density j as high as needed for efficient cooling, the thermocathode is to operate at 1300 K [5]. The cathode temperature limits the energy spread of the electron beam δE, at the cathode, according to $\delta E \sim 5kT/2$ (FWHM) [6]. Thus, at T=1300 K it is roughly δE~270 meV. It is evident that a source with lower energy spread would allow significantly improved cooling efficiency lowering both the cooling time and the relative momentum dispersion $\delta p/p$ for the cooled ion beam.

The possibility to use subthermal electron beams in electron coolers opens up further opportunities in the field of ion beam cooling. Not only could a photosource replace standard sources, but they also be complementary to them. An ion beam, already pre-cooled by conventional electron cooling, could be cooled via subthermal electron beam. In this case, the requested diameter for the electron beam is 2 mm large [8].

Some of the authors have developed a specific acceleration optics considering the effects of relaxation mechanisms in the electron beam which minimizes the additional energy spread caused by the acceleration transient [9]. Combining this accelerating structure with the photocathode described in this paper an electron beam in which potential energy exceeds thermal energy (i.e. the plasma parameter is greater than one) was generated [10]. If applied to electron coolers, subthermic beam should improve the efficiency very much.

2. EXPERIMENTAL SET-UP AND RESULTS

The activation chamber is at a vacuum level of 10^{-11} and for a long time it has not been opened. The activations have been done in a way which is a mixed procedure between the two well known yo-yo and

saturation method. The experimental details have been described in Ref.[11] and the vacuum chamber is shown in Fig. 1.

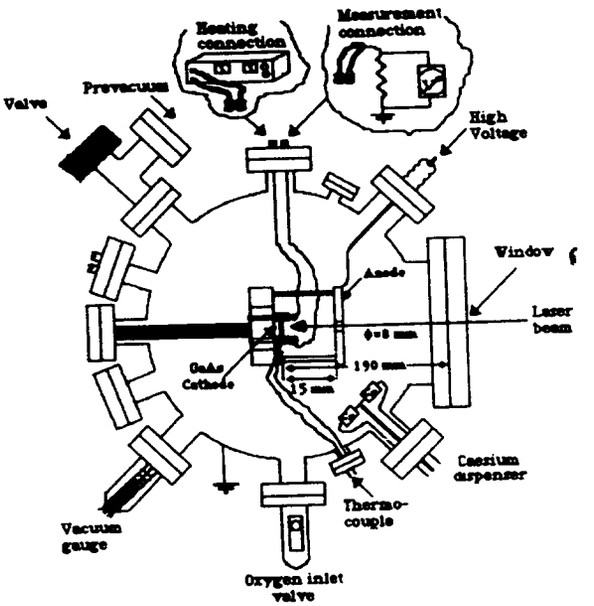

Fig. 1- Principal parts of the vacuum chamber in which the GaAs electron source is placed.

In order to achieve low energy spread of the emitted electrons we have used the laser wavelength in the 775-875 nm range. During working the photocurrnt's decay has been observed by many experiments and due to this large decrease the GaAs photocathode's application is very limited. Here we also studied this behaoir firstly. The results are exciting and are described as follows.

Fig. 2 shows the relation between 400 μA photocurrent and time at an accelerating voltage of 400 V with a laser wavelength of 800 nm (curve a) and 875 nm (curve b).

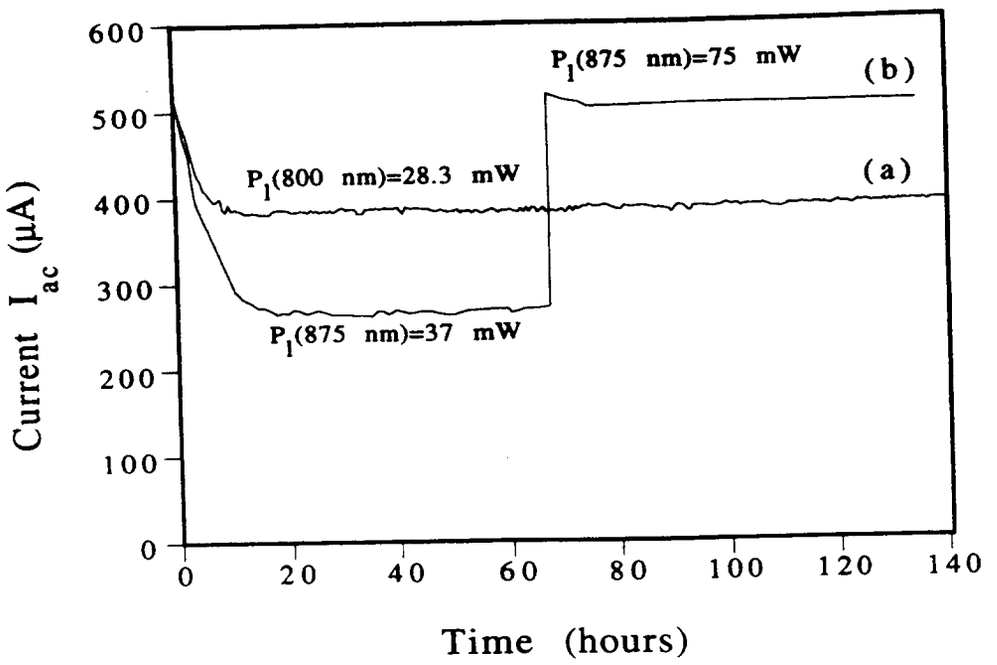

Fig. 2- Extracted current as a function of time (lifetime measurement) for two different wavelengthes l=800 nm *(a)* and l=875 nm *(b)*. Curve *(b)* shows how to restore the initial current by an increase of the laser power after that the initial decay has been accomplished.

As already mentioned before, a current value as high as 1 mA over a few mm^2 is requested by electron coolers for replacing usual thermoemissive sources. Therefore, we set the current to this level (V_{ac}=750 V) and similar results are obtained(Fig.3). However in this case the decay is shorter and stronger than those of Fig.2. We suppose that this is situable for the cooling process.

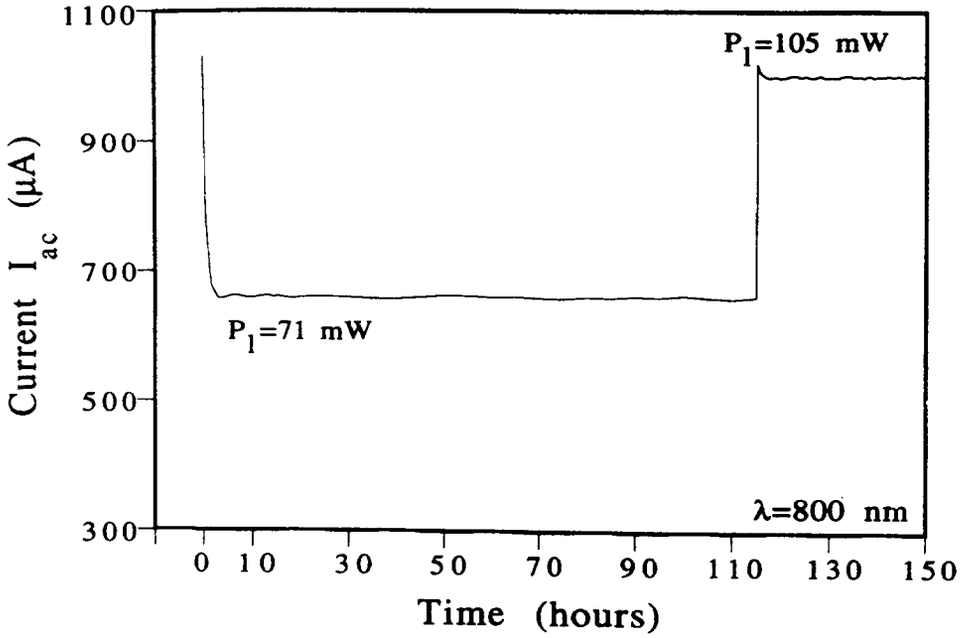

Fig. 3- Extracted current versus time starting at $I_{ac}(0)$=1 mA. After the first decay a further power increase restore the initial value permanently.

We try to obtain higher current in following experiments, but we fail to realize this due to very rapid current decay. The decay is supposed due to gas desorption from the collector as a high pressure ($8x10^{-8}$) is recorded. Fig. 4 shows quantum yield versus photon energy for a typical activation.

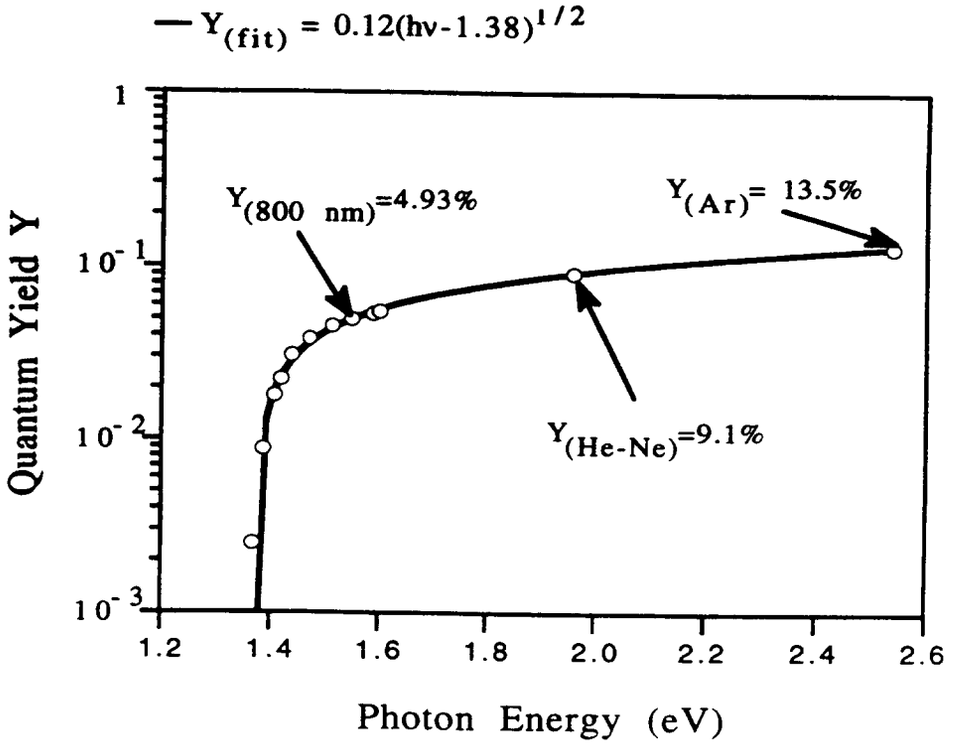

Fig. 4- Quantum yield *(Y)* versus photon energy. The curve is the fit of experimental data through the equation $Y=a(hn - E_g)^{1/2}$.

The dependence of lifetime on laser wavelength is shown in Fig. 5. We have not found significant difference between laser wavelength of 800 nm and 875 nm.

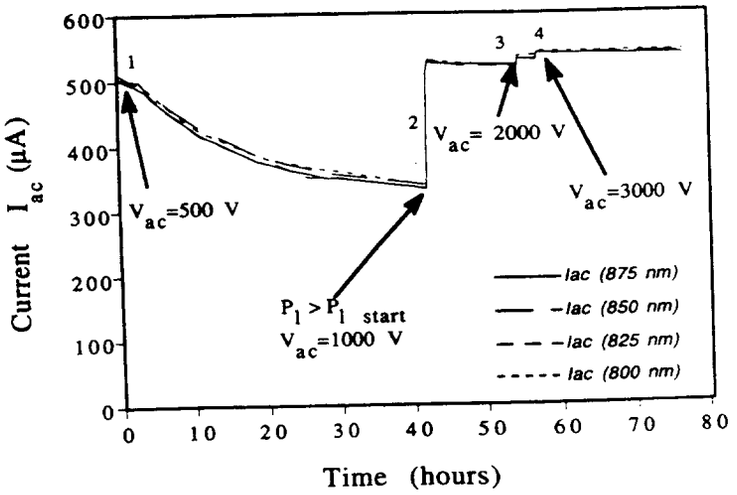

Fig. 5- Lifetime for different voltages and different wavelengthes (875, 850, 825, 800 nm). The laser is switched on only during the measurements.

1) P_{laser} at corresponding wavelenght: 46, 29, 24, 22.5 mW; V_{ac}=500 V.
2) P_{laser}: 71.5, 44.5, 37.5, 34.5 mW; V_{ac}=1000 V.
3) V_{ac}=2000 V. 4) V_{ac}=3000 V.

3. CONCLUSIONS

This paper has pointed out that the major drawback of NEA photoemission, namely the rapid current decay at relatively high current, has been overcome without feeding cesium and in a stable way. Unlike what was known we demonstrated that the lifetime can be very long independent of the exciting wavelength. The reason achieving above results are mainly due to very good vacuum (10^{-11} mbar), low-desorption materials used and long time of vacuum condition of the chamber.

The possibilities of this source are not limited to the field of electron cooling. As an example, when the photon energy is slightly greater than the semiconductor bandgap, GaAs allows the production of partially polarized electron beams (50% theoretically. A polarized electron beam as intense as 1 mA would be an excellent probe for solid state investigations where high current level are requested. A typical example is spin-resolved inverse photoemission.

ACKNOWLEDGMENTS

The Istituto Nazionale di Fisica Nucleare (Italy) is acknowledged for the financial support granted. Authors wish to extend their sincere gratitude to L. Milano for his technical aid and to G.Bisoffi for the critical reading of the manuscript.

REFERENCE

[1] G.I.Budker; Atom. Energ. 22 (1967) 346.
[2] M.Steck *et al.*; in Proc. of the Workshop on Electron Cooling and New Cooling Technique, pp. 64-79, Ed. by R.Calabrese and L.Tecchio, World Scientific, Legnaro, Italy, May 1990.
[3] M.Bell *et al.*; Phys. Lett. B 87 (1979) 275
[4] R.Foster *et al.*; IEEE Trans. Nucl. Phys. NS-28 (1981) 2386.
[5] H.Poth; Phys. Rep. 196 (1990) 135.
[6] W.Franzen, J.H.Porter; Adv. Elec. Phys. 39 (1975) 73.
[7] J.Javanainen *et al.*; J. Opt. Soc. Am. B2 (1985) 1768.
[8] D.Habs, J.Kramp, P.Krause, K.Matl, R.Neumann and D.Schwalm.; Phys. Scr. T 22 (1988) 269.
[9] A.V.Aleksandrov, R.Calabrese, G.Ciullo, V.Guidi, N.Ch.Kot, V.I.Kudelainen, G.Lamanna, V.A.Lebedev, P.V.Logachov and L.Tecchio; "Phys. Rev. A 46 (1992) 6628.
[10] A.V.Aleksandrov, R.Calabrese, N.S. Dikansky, V.Guidi, N.Ch.Kot, V.I.Kudelainen, V.A.Lebedev, P.V.Logachov and L.Tecchio; Europhys. Lett. 18 (1992) 151.
[11] R.Calabrese, V.Guidi, G.Lamanna and L.Tecchio; J.Phys. III France 2 (1992) 473.

APPLICATION OF ELECTRON COOLING IN ESR OPERATION AND EXPERIMENT

H. Eickhoff, K. Beckert, F. Bosch, B. Franzke, F.Nolden,
P. Raabe, H. Reich, M. Steck, P. Spädtke
Gesellschaft für Schwerionenforschung, Postfach 110552, D-64220 Darmstadt, Germany

ABSTRACT

The Experimental Storage Ring (ESR) [1], which is in operation at the GSI since 1990, is equipped with an Electron cooler [2], that is used for fundamental operation modes (injection, beam accumulation and extraction) and to deliver a brilliant heavy ion beam for experiments. The ions that have been stored cover the region from ^{12}C to ^{238}U; the particle intensities vary between a few thousand up to nearly 1×10^{10}. All experiments take advantage of the excellent quality of the cooled beam, some of them also use the cooler as a free electron target to investigate the interaction between the electrons and the ion beam.

1. INTRODUCTION

The heavy ion accelerator facility at GSI is capable to accelerate ions from protons up to Uranium to energies that range from the Coulomb-barrier up to relativistic values.

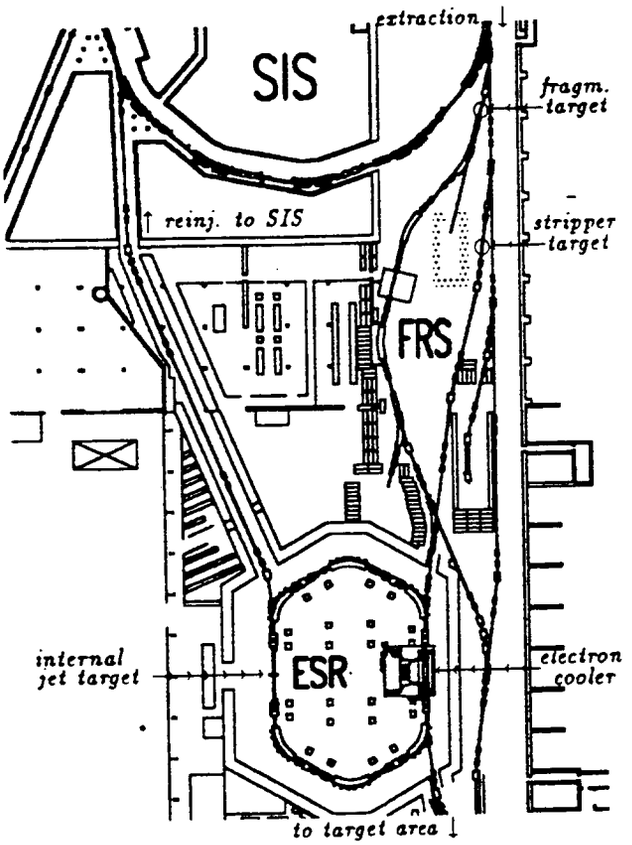

Figure 1: ESR with beam transfer lines from and to SIS

The beam, delivered by a Penning- or ECR ion source, is preaccelerated to 11 MeV/u by the UNILAC (in operation since 1975), multiturn-injected in the synchrotron SIS (in operation since 1989), accelerated up to a maximal magn. rigidity of 18 Tm (about 1 GeV/u U^{+72}), and fast or slowly extracted to the experimental high energy caves and/or the ESR. There are two beam lines to transport the SIS beam to the ESR: a direct line, equipped with a stripper target, for the injection of up to fully stripped heavy ions and the Fragment Separator (FRS) line, designed to inject unstable ions (Fig. 1). Ions up to maximal rigidity of 10 Tm (about 560 MeV/u U^{+92}) are fast injected into the ESR ('Bunch-to-Bucket-Transfer') and accumulated by means of RF-Stacking method.

2. COOLER APPLICATIONS IN ESR-OPERATION

Beam accumulation in the ESR is done by combining the conventional rf-stacking method with electron cooling; by switching the cooler voltage beam cooling is possible both on the injection- and the stack-orbit (Fig. 2).

Due to the compression of the injected bunches a reduction of losses during the deceleration to the stack takes place. As the accumulated ions are permanently cooled on the 'stack-orbit' the accumulation process is not limited by the ESR momentum acceptance, because a continous reduction of beam momentum spread takes place.

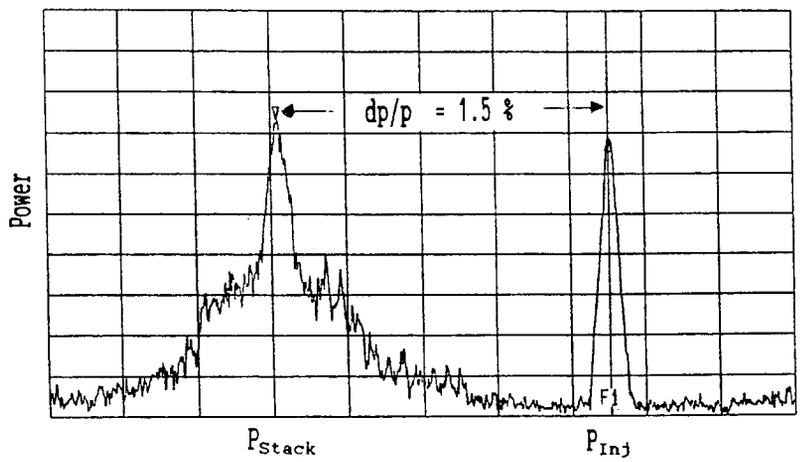

Figure 2: Longitudinal Schottky scan of combined RF-stacking and electron cooling

Especially for high-Z ions the maximum stored beam intensity is defined by the equilibrium between the Radiative Electron Capture (REC)-rate in the electron cooler and the accumulation rate. With Au^{79+} at 270 MeV/u, for instance, a saturation current of 1.4 mA, corresponding to 6×10^7 stored ions, was attained. The observed REC loss rate of about 5×10^{-4}/s is consistent with an injection of nearly 4×10^5 ions every 13 s. The REC-process also limits the life time of the stored ion beam; by minimizing the electron current this effect can be reduced (with an electron current of only 100 mA a life-time of 1 h was achieved for stored Bi^{81+}).

The optimal adjustment of the cooler parameters is done with the help of movable, position-sensitive particle detectors, that deliver the transverse distribution of ions after radiative electron capture in the cooler. For low beam intensities a beam diameter of less then 1 mm was measured, corresponding to an emittance of 0.05π mm mrad.

Due to the permanent action of the electron cooler on the circulating ion beam a continuous (multi-step) recombination process takes place. Thus different charge states are breeded and stored simultaneously, if they fit into the ESR momentum acceptance of about 3 %. As the dispersion function in the cooler region is close to zero these additional charges are cooled as well (Fig. 3). Because the energy of the different charge states is fixed by the electron cooler the relation between the frequency difference of the charge states is only determined by the orbit

length differences:

$$\frac{\Delta f}{f_q} = -\frac{\Delta C}{C_q} = \frac{1}{\gamma_t^2}\frac{\Delta q}{q} \tag{1}$$

As the charge states q are known exactly and the Schottky frequencies can be measured with high accuracy the transition point for the given lattice optics, γ_t, can be derived with a precision in the order of 1×10^{-4}.

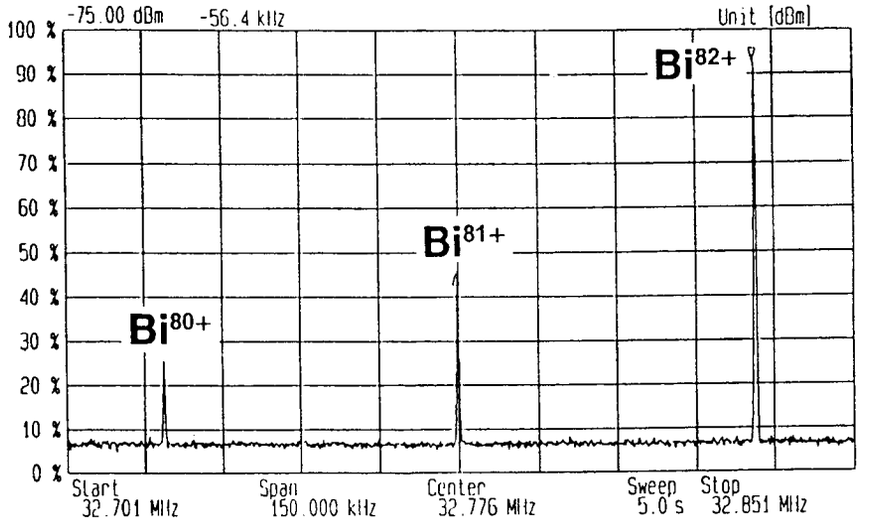

Figure 3: Simultaneous storage and cooling of three Bi charge-states

The ESR is also designed to work in the synchrotron mode, which allows beam acceleration, deceleration and both fast and slow extraction. Beam deceleration from 300 to 50 MeV/u was already successfully testet. Cooling on the low energy level, that allows to compensate the blow up of emittance and momentum spread during the deceleration process, will be possible after a ramped mode of the Cooler-high-voltage and the -magnets is established.

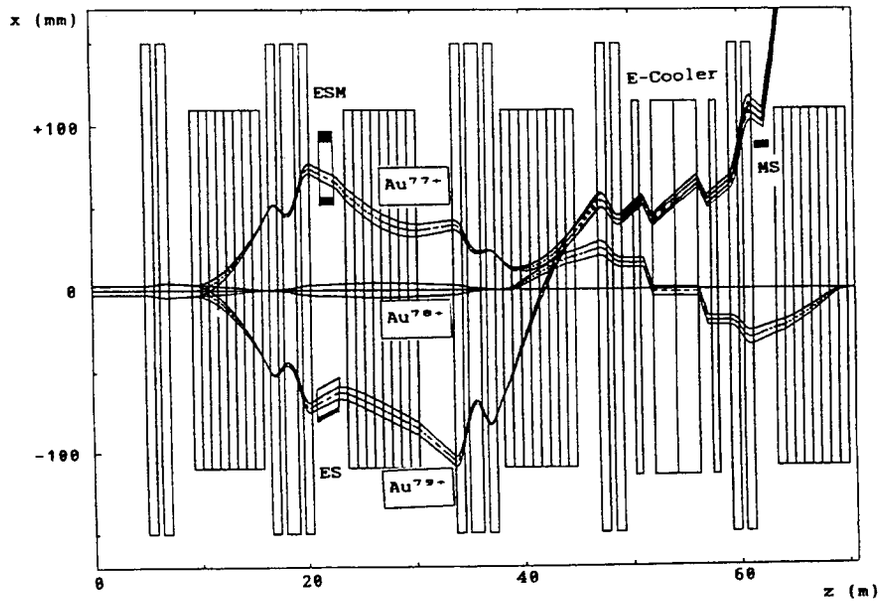

Figure 4: Slow beam extraction for recombined Au^{77+}- and stripped Au^{79+}-ions

A new type of slow extraction will be testet at the ESR in the near future. Beam simulations show (Fig. 4), that both recombined ions by the electron cooler and stripped ions by

the internal target may be deflected into the extraction channel without disturbing the primary beam. This kind of slow extraction process will preserve the excellent beam quality in the extracted beam.

A cooled, fast extracted beam is used for the external study of a high intense ion beam and for the reinjection back into the SIS. Due to the small beam emittance no beam losses could be detected in the extraction channel.

3. COOLER APPLICATIONS IN ESR-EXPERIMENTS

Whereas all internal experiments benefit from the high phase space density of the cooled beam, special experiments in addition use the electron cooler as a free electron target for the investigation of interactions between electrons, ions and even photons.

The Schottky diagnosis is a sensitive tool to detect fragments, that have been produced either within the FRS or by scattering of a stored intense heavy ion beam with the internal gas target. Due to the extremely small momentum spread of the cooled beam the signal to noise ratio of the Schottky spectra is very high, so that fragments with an intensity of less than 100 particles can be resolved. Mass determination with a rather high accuracy ($\frac{\Delta m}{m} \approx 1 \cdot 10^{-6}$) can be achieved by taking the particle energy, precisely defined by the cooler voltage, into account.

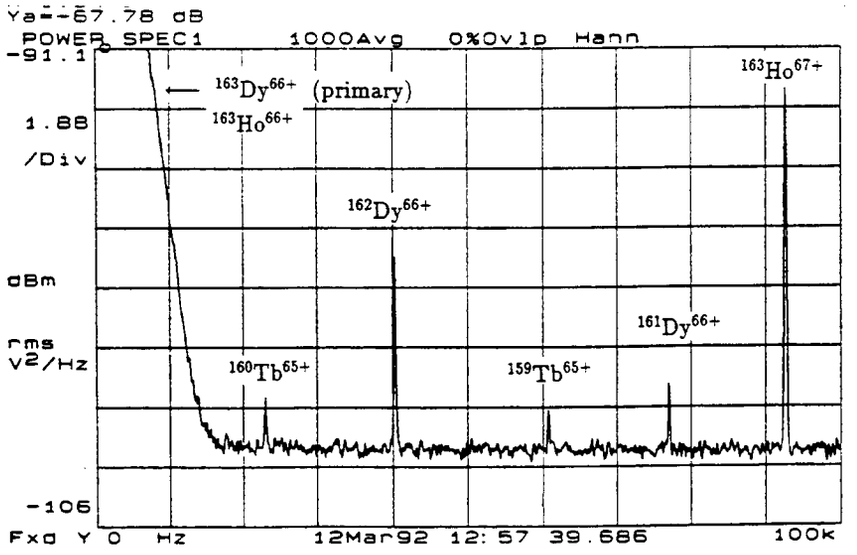

Figure 5: Longitudinal Schottky scan of stored and cooled nuclear fragments

Fig. 5 shows different fragments created by the collision between a primary Di-beam and an Ar gastarget-beam. The luminosity in this experiment was about $1 \times 10^{28}\ cm^{-2}\ s^{-1}$; the calculated cross-section of the visible fragments is in the region of 10 mbarn. It should be noted, that internal target experiments are only possible in combination with the electron cooler, which compensates for the emittance-, momentum-blow-up and the energy loss, that take place during the ion-/ target-interaction.

The GSI plasmaphysics-group has started to investigate effects of a cooled bunched beam with an experiment to achieve high phase space densities by fast bunch compression [3]. By quickly ramping the rf voltage from 100 V to 4 kV the bunch performed a synchrotron rotation, resulting in a bunch length reduction and an increase of the peak current by a factor of 6.

By using the electron cooler as a free electron target experimental studies of the interaction between the cooler electrons and the circulating ion beam are possible.

The cooler is equipped with x-ray detectors, that are used in coincidence with recombined particle detection for investigation of the REC-process; because of the small temperatures of the cooling electron beam and of the cooled ion beam REC in the electron cooler gives rise to narrow x-ray lines, which is important to precise spectroscopy.

The Dielectronic Recombination (DR) experiment [4] investigates the dependence of excitation energies (including Lamb-shift) by a two stage transition of electrons in heavy ions.

Fig. 6 shows a typical DR-spectrum, measured with Li-like gold, where the count rate of Be-like Au is plotted versus the electron energy in the c. m. frame between 0 and 50 eV. The energy variation of the electrons is possible by applying a variable pulsed voltage in a range of ± 5 kV to a drift tube in the cooler section.

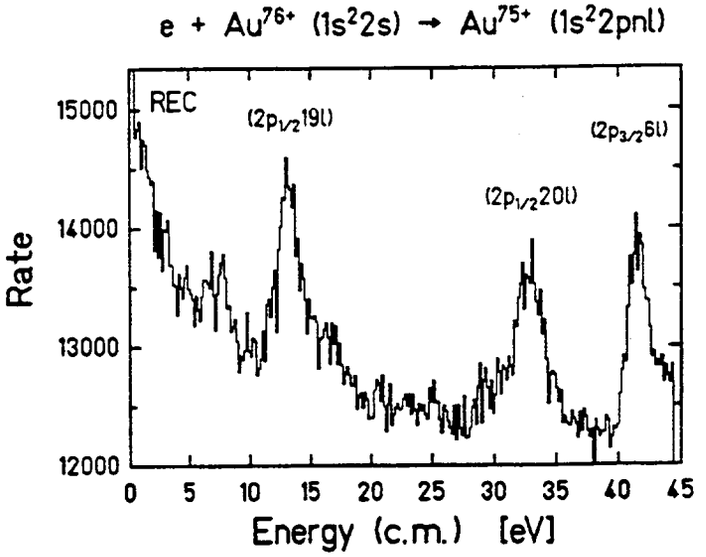

Figure 6: Dielectronic Recombination with Li-like Au-ions

In this experiment the cooler served three purposes at a time: it supplied electrons for the breeding of Li-like ions from the stored He-like ones, it cooled the beam, and it served as a target of electrons with tunable energy.

This year the first successful experiment of "Laser-Induced electron- ion Recombination" (LIREC) took place at the ESR [5]. A two-step laser induced recombination process was stimulated at an Ar ion-beam; The recombination of cooler electrons into n= 82 as a first step and sequentially to n=36/37 by a second laser frequency was detected.

References

[1] B. Franzke et al.; *Electron cooled Heavy Ion Beams in the ESR*; Int. J. Mod. Phys. A 2A (1993) 60

[2] M. Steck et al.; *Electron Cooling of Highly Charged Ions at the ESR*; this workshop

[3] I. Hoffman; *Physics of Cooled Beam*; this workshop

[4] W.Spies et al.; *Dielectronic and Radiative Recombination of Lithiumlike Gold*; Phys. Rev. Lett. 69 (1992) 2768

[5] S. Borneis; *Laser-Stimulated Two-Step Recombination of Ar^{18+} Ions*; GSI-Nachrichten 06-93

STATUS OF ELECTRON COOLING AT TARN II

T.Tanabe, I.Katayama, N.Inoue, K.Chida, T.Watanabe, Y.Arakaki, K.Noda†, T.Honma‡, T.Shoji¶, and Y.Sakawa¶ ,

Institute for Nuclear Study, University of Tokyo, Tanashi, Tokyo 188, Japan
† National Institute of Radiological Sciences, Chiba 260, Japan
‡Cyclotron and Radioisotope Center, Tohoku University, Sendai 980, Japan
¶ Plasma Science Center, Nagoya University, Nagoya 464, Japan

ABSTRACT

The electron cooler at TARNII has mainly been used for atomic and molecular physics experiments since 1991 when fundamental electron cooling tests finished. In this paper, some observed results during cooling and their analyses are reported.

1. INTRODUCTION

The TARNII is a storage ring [1] having a circumference of 78 m with electron cooler [2]. Light and heavy ions are injected from a sector focusing cyclotron with a K-number of 67. The first cooling experiments took place in September 1989. The electron cooler has recently been used mainly for the atomic and molecular physics experiments [3,4]. It is used to improve the momentum resolution and to reduce the transverse emittance of ion beams. It is also important for the stacking of low-intensity ion beams available from the cyclotron. The electrons of the cooler are a good electron target which can be adjusted to a finite velocity relative to the ion beams. Although time for studies of electron cooling has been quite limited, there has been some progress relating to the electron cooling technique.

For the parameters of the TARNII ring, the horizontal and vertical beta functions at the cooling section are 11 and 2.4 m, respectively. The dispersion function at the cooling section is as large as 4.9 m. Typical horizontal and vertical tune values during cooling are about 1.7 and 2.1, respectively. Average vacuum pressure is about 1×10^{-10} Torr. So far we stored molecular ion beams as well as atomic ion beams. They are p, d, $^3He^+$, He^{++}, N^{5+}, N^{7+}, H_2^+, H_3^+, HD_2^+, HeH^+, HeD^+ and CH^+.

The electron cooler has a layout with vertical U-shape. The electron energy and current can be changed over a wide range. The cooling experiments, however, have been performed only at the injection energies. So, electron energies are typically less than 12 keV and currents are at most 1 A. Electron beam diameter is 50 mm.

This paper describes typical results obtained in recent cooling experiments and their analyses.

2. BEAM PROFILE MEASUREMENTS

An accurate alignment of the electron and ion-beam axes is essential for efficient electron cooling. The beam width in transverse direction is very sensitive to such alignment accuracy. In order to observe the horizontal beam profile without destructing the circulating ion beam, a residual gas ionization beam profile monitor was designed. The ion-electron pairs produced by the impact of the ion beam on residual gas are accelerated in the uniform electric field, and the residual gas ions bombard the surface of a micro-channel plate (MCP). MCP event location is determined by a resistive anode using charge division or risetime encoding technique [5,6]. One-dimensional projection of the beam profile can thus be obtained.

Fig. 1 is a photograph of the profile monitor. A Chevron type MCP with a sensitive area of 100 mm (transverse)×15 mm (longitudinal) and one dimensional resistive anode are mounted together. The resistive anode comprises a sheet resistor with a total resistance of 250 kΩ. In order to identify the beam position, 4 parallel bars with a width of 1 mm are installed on the entrance of the MCP. A uniform electric field used to accelerate ionized residual gas was generated by applying a voltage of 10 kV between the upper and lower plates, which was divided by a resistor string and also applied to the intermediate electrodes. Since the electric field slightly steers circulating ion beams vertically, it is compensated by a reverse electric field formed by the same electrodes installed downstream of the profile monitor.

For position measurements, both charge-division and pulse-risetime methods have been tested. Although they gave almost the same position resolutions, the second method can work at higher count rates. Fig. 2 represents a measured beam profile of 85-MeV N^{5+} ions with and without electron cooling. The beam width changed from 60 mm (FWHM) to 1 mm with cooling. This means that the emittnance was compressed from 90 π mm mrad to 0.025 π mm mrad after cooling. The profiler is used for the diagnostics of cooling like Schottky signal.

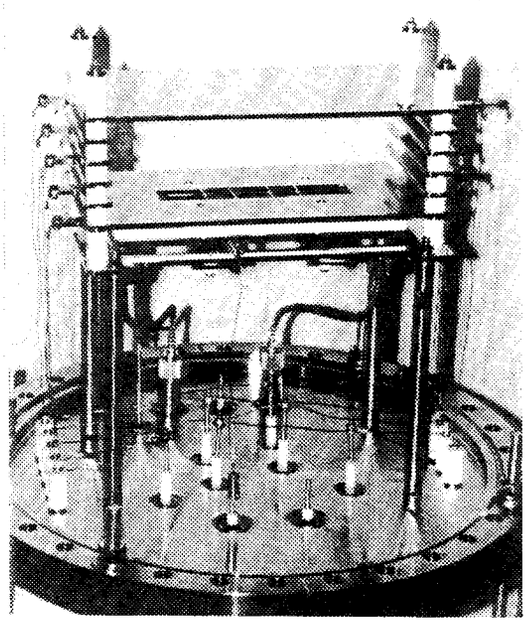

Fig. 1. Photograph of horizontal beam profile monitor.

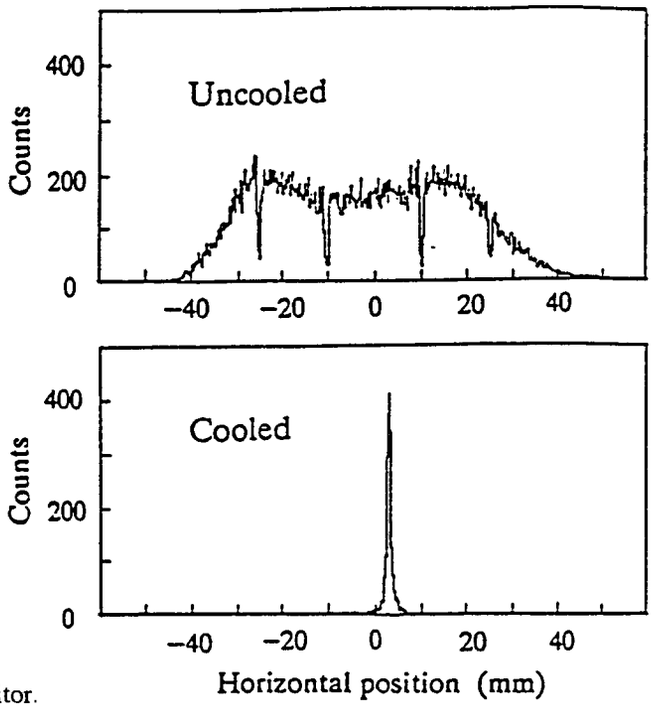

Fig. 2. Horizontal beam profiles for (a) uncooled and (b) cooled 85-MeV N^{5+} beams. The dips in the profile result from the shadows of 1-mm thick wires, which are inserted to calibrate the beam position.

3. BEAM STACKING

The beam intensity stored in the ring can be increased by the repeated multiturn injection with cooling, called "cool stacking". In this case, a part of the phase space volume prepared for the multiturn injection is occupied by the cooled and stacked beam. Fig. 3 shows an example of the cool stacking for 20-MeV proton beam, in which the beam was injected every 4 s and cooled. The intensity of the injected beam is about 10 μA at a multiturn batch. The injection and cooling were repeated many times. After 50 injections in a time of 3 min, an intensity multiplication factor of about 30 was reached, resulting in the total number of stored particles of 2.4×10^9. The intensity saturates gradually due to finite beam lifetime, increasing beam size and so on. Sometimes we observed sudden loss of the beam, probably due to some instabilities.

4. SCHOTTKY SIGNAL MEASUREMENTS

The frequency spectra of the cold beam Schottky signals show splitting. The splitting becomes remarkable with the increase in number of circulating particles. It is originated from two plasma waves propagating parallel and antiparallel to the beam direction with a characteristic frequency f_c that is half the peak distance [7]. Fig. 4 shows the splitting of frequency spectrum of 61st harmonics of Schottky signal for 16-MeV proton beam with electron current of 0.4 A. The spectrum shows splitting even at a low current as 3 μA. Estimated momentum resolution $\Delta p/p$ (FWHM) is 1.6×10^{-5} and 4.7×10^{-5} at the currents of 7 and 90 μA, respectively. The longitudinal coupling impedance (Z_n/n), which can be deduced from f_c and number of circulating particles, is about 1.5 kΩ. Sometimes a triple-peak structure was observed, where the central peak position corresponded to the position of the harmonics of the revolution frequency. Self bunching of the beam (60 μA) was observed even when we switched off the RF voltage. The Schottky spectrum becomes more stable and sharper when we detuned the frequency of RF cavity from the revolution frequency. The improvement of the momentum resolution from our previous measurements [2] seems partly due to the reduction of ripple voltages of the high -voltage power supply which accelerates electrons. This power supply has a fast response time of 1 ms and can reduce the slow component of ripple voltages to a level to 0.1 $V_{p\text{-}p}$ which is low in comparison with our previous ripple level of 3 $V_{p\text{-}p}$..

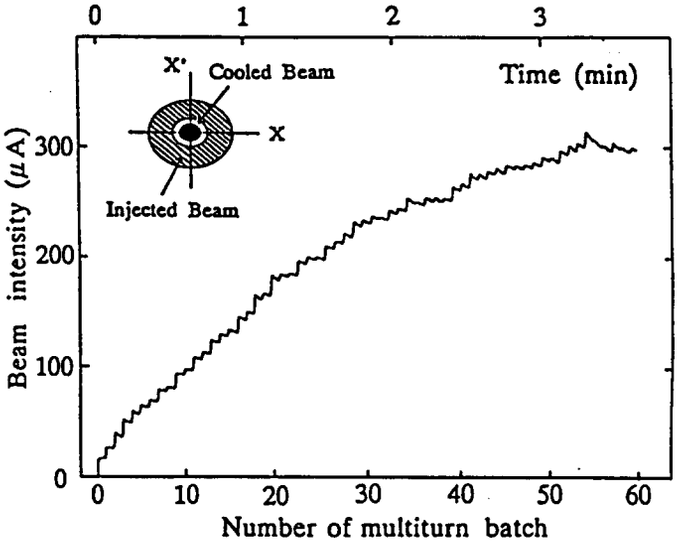

Fig. 3. Intensity increase during cool stacking as a function of the number of multiturn batches. The inset shows schematically represented phase spaces for the cooled and stacked beam and for the multiturn injected beam.

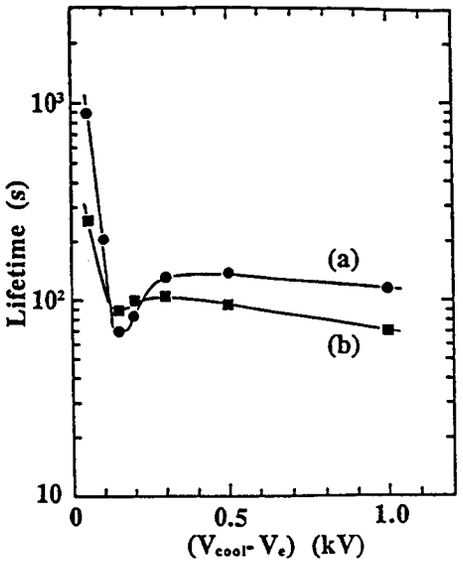

Fig. 5. Beam lifetime (1/e) as a function of electron acceleration voltage for (a) coasting beam and (b) bunched beam (voltage: 18 V_{p-p}) measured with a DC current transformer. Beam is 20-MeV proton and its current is about 40 μA. Tuned electron voltage (V_{cool}) and current are 11.218 kV and 0.3 A, respectively.

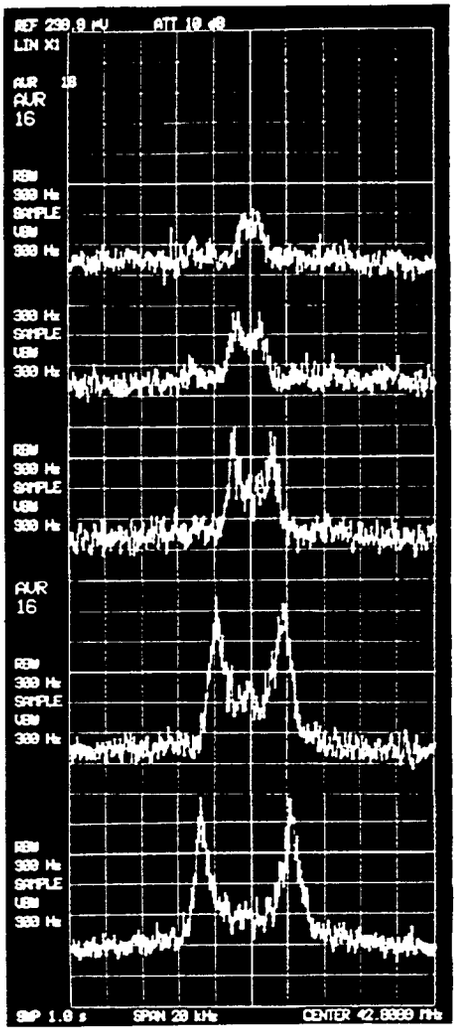

Fig. 4. Splitting of frequency spectrum of Schottky signal with increase in stored beam intensity (16-MeV p). From the top, intensities (number of particles) are 3 μA (2.6×10^7), 7 (6.2×10^7), 16 (1.4×10^8), 54 (4.8×10^8) and 90 (8×10^8).

5. EFFECTS OF DETUNED ELECTRON BEAM

An apparent beam loss in time of about 1 s after injection has been observed in a bunched beam cooling even with electron energy far detuned from the cooling energy. Such a decrease has been observed by using an electrostatic position monitor which is sensitive only to the bunched beam current. However, the current decrease, when measured with a DC-current transformer (DCCT) which was recently installed in the ring, was much slow. We try to understand the particle behavior when the electron velocity does not match the synchronous particle velocity. In order to find the electron cooling phenomenon easily, we used the small bucket with bucket height of 20 V_{p-p} (for 20-MeV proton) which corresponds to the proton momentum width of $\Delta p/p \sim 0.3\times10^{-3}$. On the other hand, the initial uncooled proton momentum width is equal to about 1×10^{-3}. If the electron energy is tuned to the bucket center, the injected beam is cooled into the bucket center. This can be observed by the fast increase of the AC beam current with time in contrast to almost constant DCCT current. If we now detune the electron energy from the bucket center by an amount less than bucket height, a "ring" of beam is formed inside of the bucket [8].

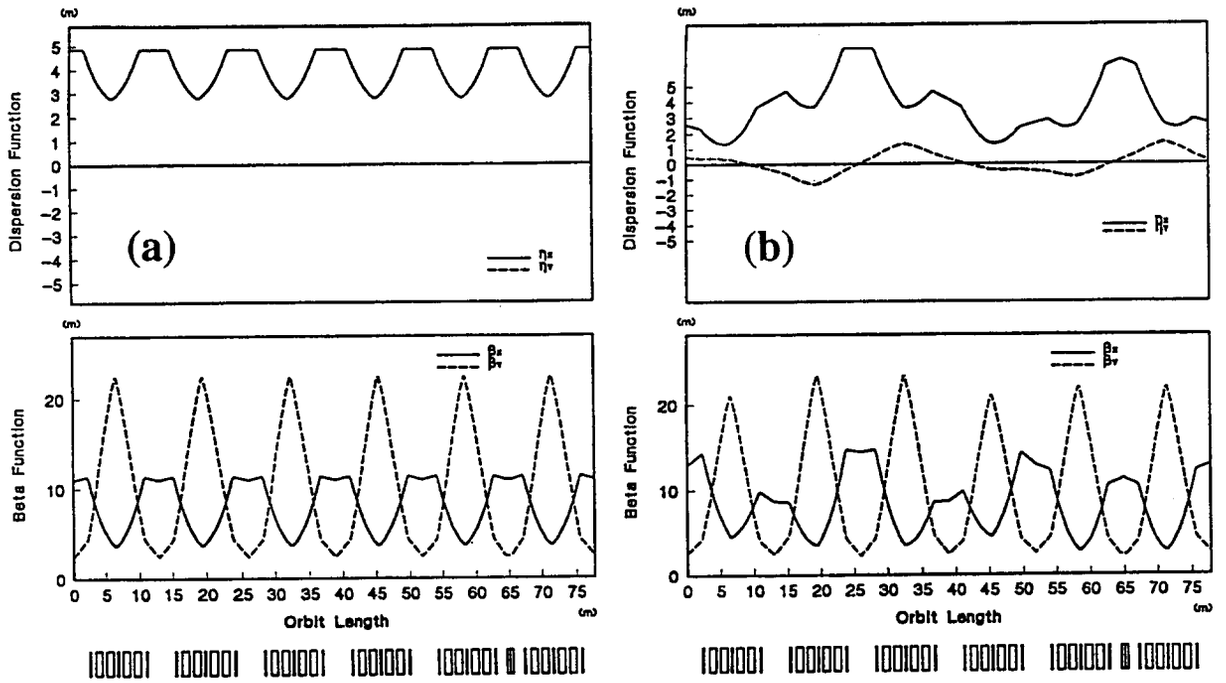

Fig. 6. Beta and dispersion functions (a) without electrons and solenoid field and (b) with an electron current of 4 A and a solenoid field of 0.6 kG. Electron cooler locates at the orbit length of about 65 m.

In this case, the AC and DCCT currents give almost the same results as the above ones. If we further detune the electron energy exceeding the bucket height, protons are siphoned out of the bucket, resulting in the fast decrease of the AC current after injection. The cooled DC component of the beam, however, still remains outside of the bucket, which gives slow decrease of the DCCT current. The experimental findings on the AC and DCCT currents behavior in case of the detuned electron energy can qualitatively be explained by such a consideration.

Fig. 5 shows the bunched and coasting beam lifetimes when the electron energy is shifted from the cooling energy. The lifetimes decrease rapidly and then get stabilized as the electron energies move apart from the tuning energy. There are minimums at around 0.15 kV. As the dispersion function at the cooling section is large, the beam moves horizontally by about the electron beam diameter of 50 mm if its energy is dragged to the one corresponding to the electron energy at the minimum. The dips seem to have a relation with such a beam movement. The coasting beam lifetime is generally longer than the bunched beam lifetime. The beam lifetimes at the far detuned electron energies are by about factor of 2-3 shorter in comparison with the ones without electron beam. The ion beam is affected by the electron beam despite negligibly small drag force at large detuning energies.

We try to understand such a phenomenon by taking account of the radial force due to the electron space charge. The radial electric field is linear inside the electron beam, while it changes as 1/r outside the electron beam. So particles feel different forces inside and outside of the electron beam. If the ion beam comes out of the electron beam due to the misalignment of the beams or the larger beam size than the electron beam, a deformation of phase space area occupied by the beam may happen. In order to study the behavior of the beam under the detuned electron beam, we did simulations using a program in ref. [9], neglecting the drag force under following conditions,

initial tunes: Q_x=1.75, Q_y=2.15, beta and dispersion functions at cooling section: β_x=11 m, β_y=2.4 m, η_x=4.9 m,
electron-diameter: 50 mm, -length: 1 m, solenoid field: 0.6 kG (uncompensated),
initial beam (20-MeV proton) at cooling section: $|x| \le 40$ mm, $|x'| \le 3.7$ mrad, $|y| \le 10$ mm, $|y'| \le 4.5$ mrad.

In the calculations, the magnetic field produced by the electron beam was neglected as its effect is small. Fig. 6 shows the differences of beta and dispersion functions with and without electrons and solenoid field which were calculated taking account of the linear part of the space-charge force. As can be seen in the figure, they change much and the vertical dispersion (η_y) newly appears due to the solenoid field. Tune shifts are ΔQ_x=+0.044 and ΔQ_y=+0.009 which are mainly due to the electron current of 4 A. Fig. 7 shows phase plots for particles with a momentum larger than the central particles by $\Delta p/p$=+0.2 % at I_e=0, 1 A and 4 A, including linear and non-linear space-charge forces. Particle phases are plotted every 10^3 turns up to 10^4 turns altogether on the horizontal and vertical phase spaces. As can be seen in the figure, the separatrix becomes unclear and the beam size expands with

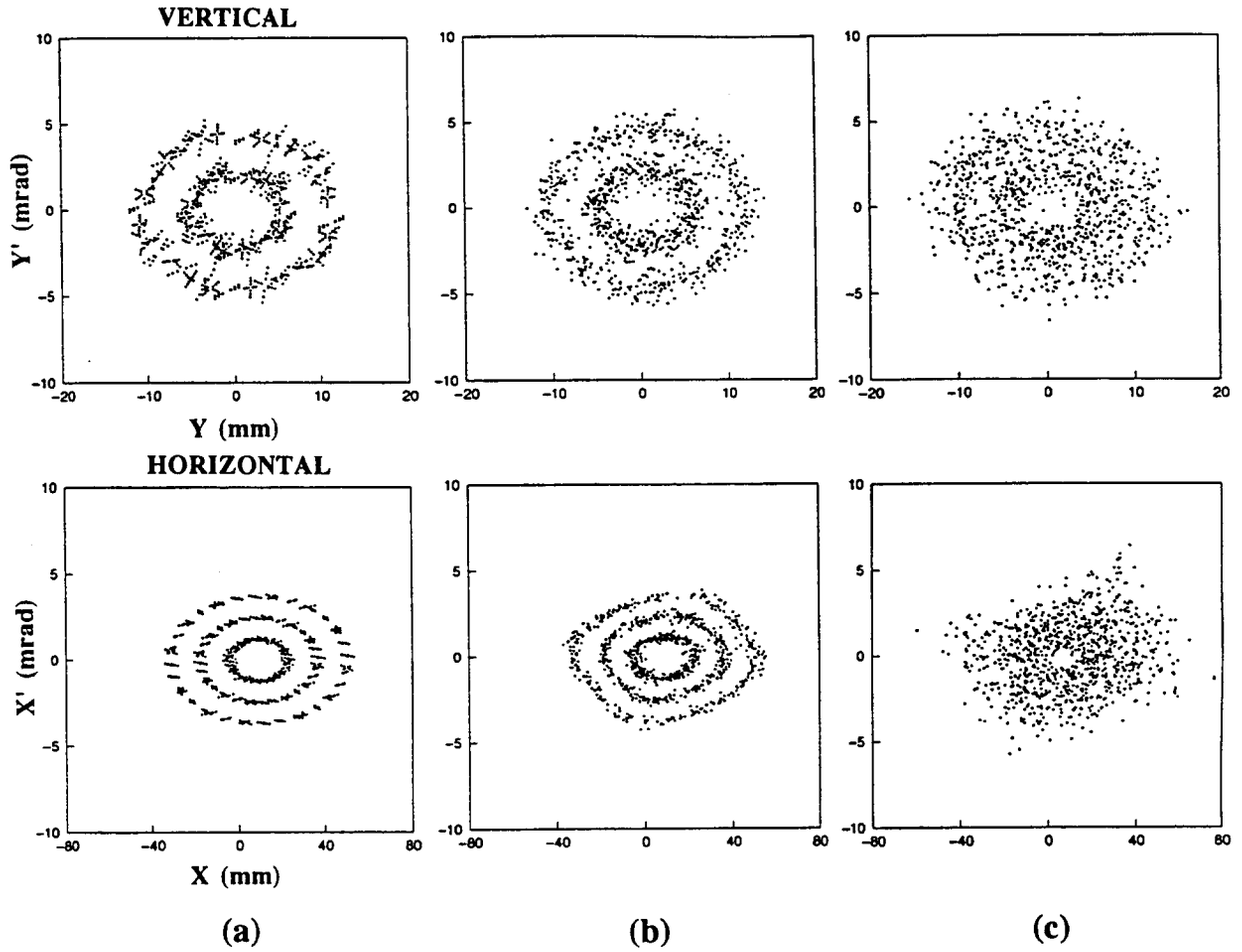

Fig. 7. Phase plots of 20-MeV protons with a momentum deviation of $\Delta p/p=+0.2$ % for the electron currents of (a) 0 A, (b) 1 A and (c) 4 A.

the increase of electron current. This tendency is especially remarkable for the particles outside of the electron beam and those having large momentum deviation. The plots are only 10^4 turns which correspond to 14 ms. So the beam quality becomes much worse in the time of the order of seconds. From these simulation studies, it can be concluded that followings are important in order to avoid the beam loss: 1) overlap of electron and ion beams, 2) compensation of solenoid field, 3) zero dispersion at the cooling section and 4) small beta functions. Although this phenomenon is not serious for our ring practically, the simulated results seem to suggest the origin of strong "electron heating" observed at CELSIUS [10].

REFERENCES

[1] T.Katayama et al., *Present status of cooler synchrotron TARNII*, Proc. of 7th Symposium on Accelerator Science and Technology, Osaka, pp. 35-37, (1989).

[2] T.Tanabe et al., *Electron cooling experiments at INS*, Nucl. Instrum. Methods, A307, pp. 7-25, (1991).

[3] T.Tanabe et al., *Dielectronic recombination of He^+ in a storage ring*, Phys. Rev. A45, pp. 276-280, (1992).

[4] T.Tanabe et al., *Dissociative recombination of HeH^+ at large center-of-mass energies*, Phys. Rev. Lett. 70, pp. 422-425, (1993).

[5] B.Hochadel, *Ein strahlprofilmonitor nach der methode der restgasionisation für den Heidelberger testspeicherring TSR*, MPI H-1990-V-19, (1990).

[6] J.L.Wiza, *Microchannelplate detectors*, Nucl. Instrum. Methods 162, pp. 587-601 (1979).

[7] H.Poth et al., *First results of electron cooling experiments at LEAR*, Z. Phys. A332, pp. 171-188, (1989).

[8] W.Kells and F.Mills, *Dynamics of R.F. captured electron cooled proton beams*, Fermilab TM-1153 (1983).

[9] K.Noda et al., *A use of a thin foil target in a cooler ring experiment*, Nucl. Instrum. Methods, A303, pp.215-225, (1991).

[10] D.Reistad el al., *Recent commissioning results at CELSIUS*, Proc. of 13th Int. Conf. Cyclotrons and Their Applications, Vancouver, pp. 266-273, (1992).

TECHNICAL FEATURES AND FINAL ELECTRON BEAM TESTS OF THE COSY ELECTRON COOLER AND FIRST PROTON BEAM COOLING

W. Derissen, R. Maier, U. Pfister, D. Prasuhn, W. Schwab, U. Schwarz, M. Sedlacek, K. Sobotta, H.J. Stein, J. Wimmer, J. Witt and A. Zumloh
IKP-Forschungszentrum Jülich GmbH, D-52425 Jülich, Germany

Abstract
The COSY electron cooler has been designed, constructed and tested during the years 1989 to 1992. After magnetic field measurements and corrections the electron cooler was mounted in a test position outside the COSY ring for first electron beam experiments. In February 1993 the electron cooler was moved into the COSY ring. First cooling experiments took place during spring and summer this year. Results of the comissioning and the first cooling experiments will be presented.

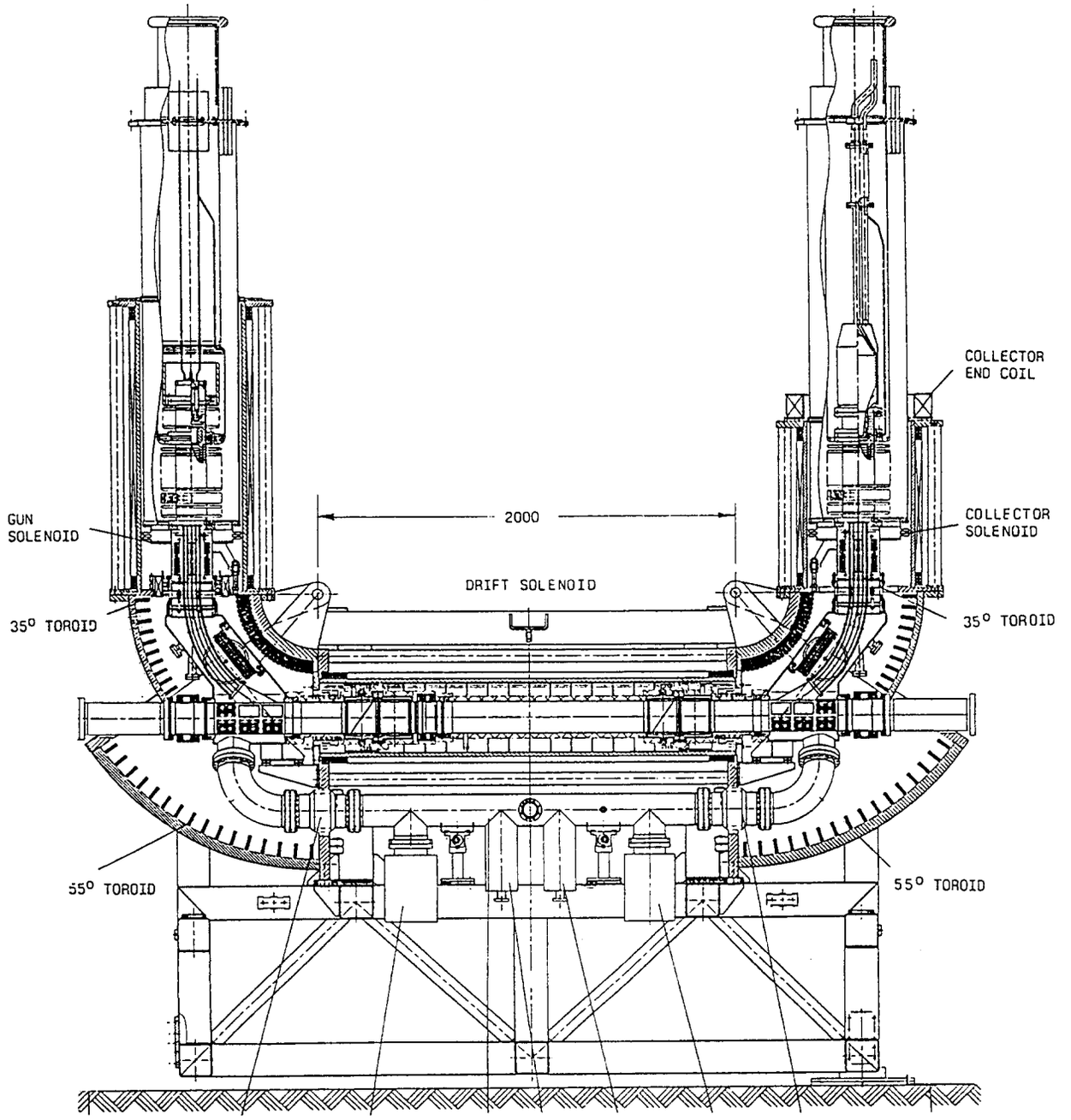

Figure 1: The COSY electron cooler

1. INTRODUCTION

The COSY electron cooler is designed to provide high brilliance proton beams at low energies between 40 MeV and 200 MeV. This energy regime defines the parameters of the electron cooler, 20 to 100 keV electron energy. A maximum electron current of 4 A within a diameter of 2.54 cm was chosen for fast cooling of high emittance beams. The maximum flux of the solenoidal field of the electron cooler amounts to 0.15 T. Results of the longitudinal and transverse magnetic field measurements and corrections are presented in Section 2.

Gun and collector conditioning took place in the test position outside the COSY ring. Results of the electron beam tests are described in Section 3.

The first cooling experiments in COSY were carried out at an energy of 40 MeV protons corresponding to 20 keV electron energy. Momentum cooling was obeserved with longitudinal Schottky-spectra, the transverse cooling with H^0-detectors. Cooling results are presented in Section 4.

2. THE MAGNETIC FIELD

2.1 The longitudinal field

The magnetic field configuration consists of three solenoids and two 90° toroids. Fig. 1 gives an overview over the magnet system. The solenoids are constructed similar to the IUCF design with iron rods as magnetic yoke. This design allows an easy access to the magnets to mount additional steeriing and correction coils. The two 90° toroids are splitted into a 55° and a 35° toroid each. Their mechanical layout is identical to the CELSIUS toroids. All main magnets are connected in series to one power supply, which also feeds the compensation solenoids in the COSY-ring. The final adjustment of the different current for each of the magnets is done by active shunts. In this way the ripple of the main power supply does not change the current ratio of the individual magnets, which decreases the requirements for the tolerances, especially for the compensation solenoids.

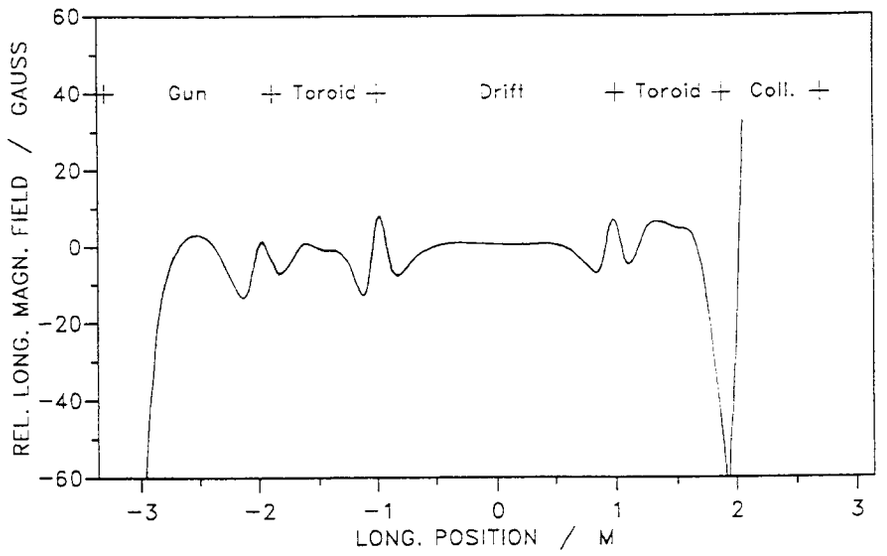

Figure 2: The longitudnal magnet field deviations at a level of 1200 T.

The expected field decrease in the transition regions between the solenoids and the toroids are compensated by separate gap coils. The longitudinal magnetic field was measured with a Hall probe drawn through the magnet system [1]. Fig. 2 shows the magnetic field deviations on the electron beam axis along the whole magnetic system from the gun to the collector solenoid. The active shunts and the gap coils are set to the optimum values for a magnetic field of 0.12 T. The field deviations are below 10^{-2}, which is in agreement with the specifications. The large deviation at the transition between collector toroid and collector solenoid is due the fact, that we did not care about the electron beam quality in front of the collector. Therefore we did not install a gap coil at

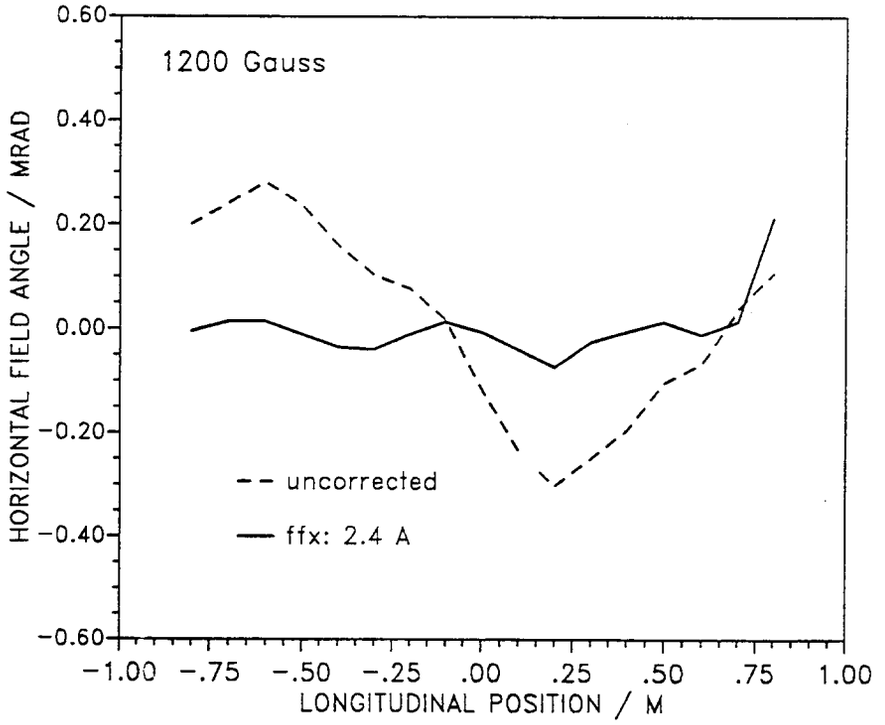

Figure 3: The transverse field component in the drift solenoid, uncorrected (dashed line) and corrected (solid line)

this transition. The remanent field of the cooler magnets amounts to 10^{-4} T, the reproducibility of the magnetic field after a rapid switch-off is better than 10^{-3}.

2.2 The tranverse magnetic field

High requirements have to be fulfilled by the tranverse field in the drift region, because any angular deviation from the pure longitudinal field simulates a higher temperature of the electron beam and increases the cooling time. For the transverse magnetic field measurements we used the same method as was used at the TSR cooler in Heidelberg [2]. A soft iron magnetic needle mounted perpendicular on a small mirror orientates itself freely in space due to a cardanic suspension. This mirror was drawn through the drift solenoid by a rod of balsa wood. The soft iron needle adjusts itself exactly along the magnetic field lines. An electronic autocollimator registers the angle deviations of the mirror. This gives directly the ratio between the tranverse and the longitudinal magnetic field at the measurement position. In Fig. 3 the result for the uncorrected horizontal field of the drift solenoid is displayed. Though the deviations are already in the order of $3 \cdot 10^{-4}$, we added saddle coils with varying angles according to the field measurements. The field error coils consist of 3 windings fixed on a plastic sheet, which could easily be mounted onto the coils of the drift solenoid due to the "open" construction. With these error coils we were able to suppress the transverse field component to less than $2 \cdot 10^{-5}$ in the effective cooling region of 1.5 m [3].

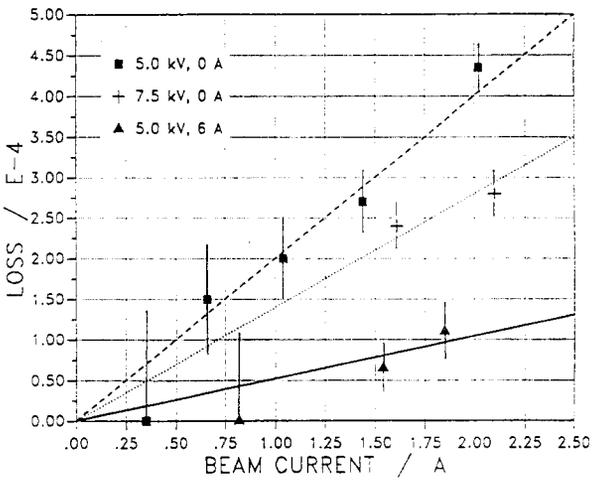

Figure 4: Electron loss current as function of the electron current, varied are the collector anode voltage and the collector end coil current.

3. ELECTRON BEAM TESTS

The first electron beam tests were made in an offline position outside of the COSY ring. This enabled us to check the different electron beam conditions without disturbing the comissioning of the storage ring itself. The vacuum system of the COSY electron cooler is not yet baked, so we achieved a vacuum of 10^{-9} hPa without electron beam, increasing to $5 \cdot 10^{-8}$ hPa with electron beam on. The conditioning of the electron cooler was done

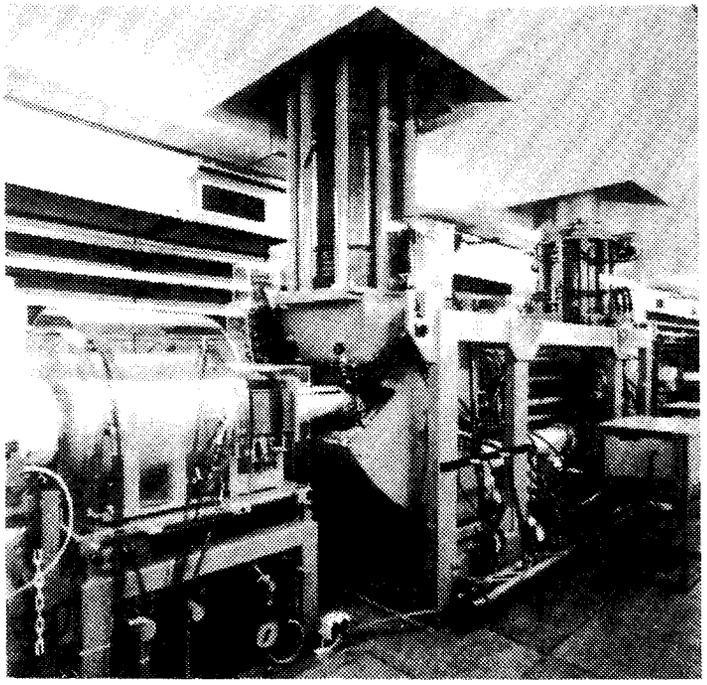

Figure 5: The electron cooler in its final position in the COSY tunnel

within 2 days, resulting in a stable operation at 100 keV and 1.5 A. At lower energies up to 25 keV electron currents up to 3 A were possible. These current limitations are due to the pressure increase of the unbaked vacuum system. The electron gun with the adiabatic acceleration allows an independant adjustment of the electron energy with the acceleration voltage and of the electron current with the gun anode voltage. The measured gun perveance of 0.88 μP is in good agreement with the EGUN-result [4] of 0.9 μP.

Fig. 4 displays the results of our collector efficiency measurements. We varied the collector voltage between 5 kV and 7.5 kV and the current of the collector end coil between 0 A and 6 A. The collector anode voltage was set to the minimum value to avoid beam reflection. The graph clearly shows a possible collector efficiency of better than $2 \cdot 10^{-4}$. The influence of the collector end coil is much more efficient than a higher collector voltage [5].

4. COOLING RESULTS

After the electron beam tests in the offline position the electron cooler was moved into the COSY ring during a 4 weeks shutdown in February 1993. Fig. 5 shows the electron cooler and the compensation solenoids in their final position in the COSY tunnel.

Our cooling experiments so far were carried out at injection energy, i.e. 40 MeV protons. A few tests were made to check the electron beam conditions after the movement of the electron cooler. Then we adjusted the correction steerers and the quadrupoles in the cooling telescope to compensate the magnetic disturbance of the cooler magnets to the storage ring. It turned out that the steering of the proton beam and the electron beam could be handled nearly independant to each other. By this it was a rather easy task to adjust the proton and the electron beam directions to better than 0.3 mrad. After a fine adjustment of the electron energy indications of cooling could be detected. Even with electron currents between 50 mA and 250 mA cooling times of 5 to 10 sec were observed. The first indication of cooling was detected with the bunch length reduction observed with the sum signal of a beam position monitor. The longitudinal Schottky-spectra indicated a momentum spread reduction from $2.5 \cdot 10^{-3}$ to less than 10^{-4} for 10^9 protons. Fig. 6 shows the longitudinal Schottky spectra for the uncooled beam (in logarithmic scale) and for the cooled beam (in linear

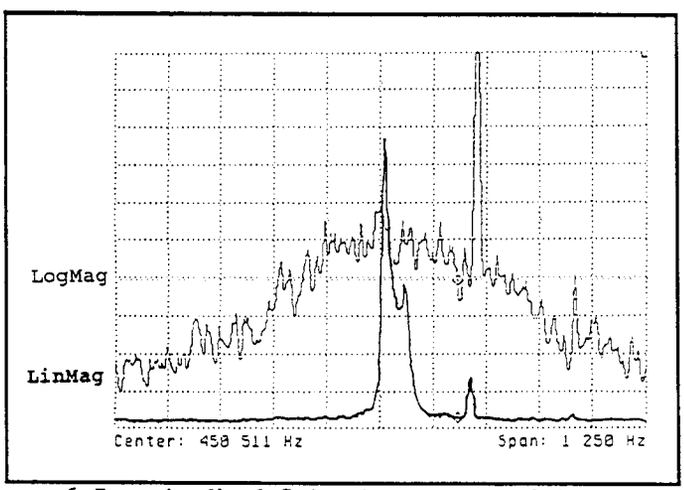

Figure 6: Longitudinal Schottky spectra of the uncooled (logarithmic scale) and the cooled (linea scale) proton beam in COSY

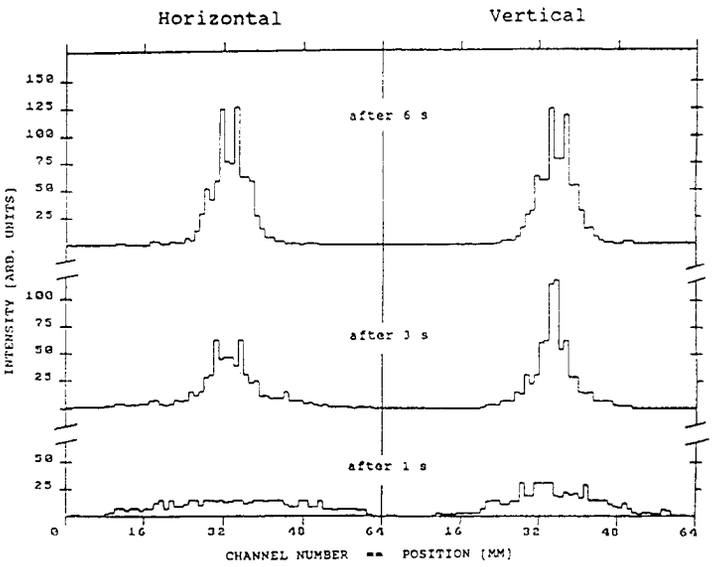

Figure 7: Horizontal and vertical H^0-spectra of the cooled proton beam in COSY

scale). An increase of the electron current to 400 mA lead to proton beam instabilities, whereas with 250 mA the proton lifetime was increased from 50 sec without cooling to 5 min.

After installation of our H^0-diagnostics, a two-dimensional multiwire proportional chamber behind the exit of the first bending magnet, we were able to measure the transverse beam profiles in the cooling region. Figure 7 shows the horizontal and vertical beam profiles 1s, 3s and 6 s after injection. The horizontal axes are calibrated in mm. The cooled beam emittance may be calculated according to formula 1:

$$\varepsilon = \frac{w^2}{\beta_c + d^2/\beta_c} \qquad (1)$$

Here, β_c is the betafunction in the cooling region, 6 m in the horizontal and 18 m in the vertical plane, d is the distance between cooling region and the H^0-diagnostics, for COSY 25 m, and w is the measured H^0 profile width. With these values we estimate a cooled beam emittance of better than 0.4 π mm mrad. The uncooled beam emitance is in the order of 25 π mm mrad.

Detailled measurments of our beam cooling, i.e. drag force measurements, high resolution Schottky-spectra etc. are foreseen for the beginning of next year. Acceleration of the cooled beam and cooling at higher energies also will take place in spring 1994.

REFERENCES

[1] Derissen et. al., Status of the COSY Electron Cooler, EPAC 92, Editions Frontiers (1992), p. 839
[2] M. Jung, Präzisionsmessung des Magnetsystems der Elektronenkühlung am TSR, MPI H-1989-V34
[3] W. Schwab et al., Magnetic Field Measurements of the COSY Electron Cooler, IKP Annual Report 1992, JÜL-2726 (1993), p. 215
[4] W.B. Herrmannsfeldt, SLAC-226, Stanford 1979
[5] R. Maier et al., Comissioning of the COSY Electron Cooler - Phase 1, IKP Annual Report 1992, JÜL-2726 (1993), p. 212

ELECTRON COOLING WITH AN ELECTRON BEAM OF 10 meV TRANSVERSE TEMPERATURE

H. Danared
Manne Siegbahn Laboratory, S–104 05 Stockholm, Sweden

ABSTRACT
The CRYRING electron cooler has recently been rebuilt to accomodate a magnetically expanded electron beam. Using a new electron gun with a cathode that has ten times smaller area than the old gun, and a magnetic field which decreases adiabatically after the gun solenoid by a factor of 10, the transverse electron temperature has been reduced from 100 meV to approximately 10 meV. The effect of a reduced electron temperature on cooling and resolution in recombination spectra is discussed. Measurements of the drag force and an example of the improved resolution in recombination experiments are shown.

1. INTRODUCTION

Most electron coolers are used both for cooling or stacking of heavy-particle beams and as electron targets in physics experiments. In both cases, the electron temperature is an important quantity. The cooling time or the drag force that the electrons exert on the ions depends strongly on the electron temperature, and the resolution in many atomic-physics experiments is determined directly by the spread in electron energy. A reduction of the electron temperature thus improves both machine performance and experimental resolution [1]. The CRYRING [2] electron cooler [3] was recently rebuilt to accomodate a magnetically expanded electron beam, lowering the transverse electron temperature by a factor of 10 from 100 to approximately 10 meV. This was accomplished by decreasing the longitudinal magnetic field by a factor of 10 between the gun solenoid and the small solenoid immediately below it (see fig. 1). At the same time, a new gun with 10 times smaller cathode area was installed.

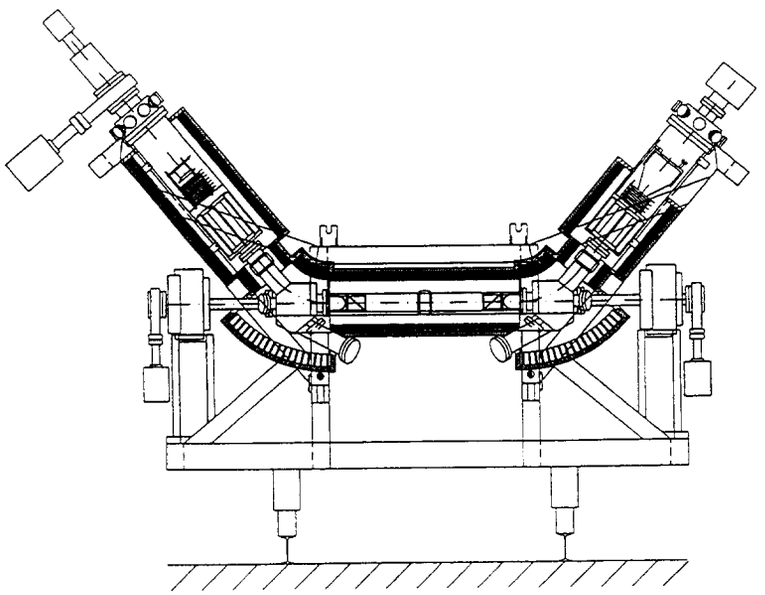

Fig. 1. Schematic diagram of the CRYRING electron cooler. The electron gun (before the cooler was rebuilt) is to the left and the collector to the right.

2. ELECTRON TEMPERATURES, COOLING FORCES, AND EXPERIMENTAL RESOLUTION

The longitudinal electron temperature in an electron cooler is in general quite low due to the acceleration of the electrons. At CRYRING, $kT_{e\|} = 6 \times 10^{-5}$ eV has been deduced from the line shapes of dielectronic-recombination spectra for an electron beam of 6 kV and 260 mA [4]. This value is in good agreement with the temperature resulting from the transverse–longitudinal relaxation in the electron beam [5]. The transverse temperature is unaffected by the acceleration of the electrons and has in all coolers been 100 meV (corresponding to the cathode temperature of around 1000°C) or higher. Measurements of the drag force created by the electrons have been performed at CRYRING for ions of three different charge-to-mass ratios [3]. The measurements agreed well with a transverse temperature $kT_{e\perp} = 100$ meV. The same dielectronic-recombination spectra as mentioned above gave $kT_{e\perp} = 150$ meV.

The simplest calculations of the cooling time use the binary-collision model and assume an isotropic electron temperature. If the velocity spread of the ions is smaller than the thermal velocities of the electrons, the cooling time is found to be proportional to $T_e^{3/2}$ and the drag force to $T_e^{-3/2}$. For a non-isotropic electron-velocity distribution, the drag force can be calculated analytically only in a few limiting cases. Thus, if the longitudinal temperature is negligible, the longitudinal drag force is proportional to $T_{e\perp}^{-1}$ and the transverse force to $T_{e\perp}^{-3/2}$, still provided that the velocity spread of the ions is smaller than that of the electrons. This implies that a reduction of the transverse electron temperature by a factor 10 (which is the factor that will be considered in the rest of this article) reduces cooling times with a factor between 10 and 30 if the electron current can be kept constant. We here neglect effects of "magnetised" cooling (adiabatic interactions between ions and electrons in collisions at impact parameters larger than the cyclotron radius of the electrons) since they have not been seen at CRYRING.

This improvement can be obtained only if there are no other contributions to the effective electron temperature than the cathode temperature. Transverse electron velocities can be induced by radial electric fields in the gun, the bending through the toroids, field errors in the solenoids (particularly the cooling solenoid), space charge, etc. Heating in the gun is not likely to be a problem since it is reduced by the expansion in the same way as the thermal spread from the cathode. In addition, the magnetic field is 10 times stronger, whereas the electric fields become larger (due to the reduced size of the gun) by only a factor of $10^{1/2}$. Dipole coils in the toroids are indispensable and have to be rather carefully adjusted. The same is true for the coils correcting the straightness of the field in the cooling solenoid—the field must be straight within $0.1 - 1$ mrad, depending on the ion energy. The transverse drift of the electrons, created by the space charge in combination with the longitudinal magnetic field, can become significant for high currents. The drift velocity is proportional to the distance from the centre of the beam, however, and once the ion beam has started to cool down and shrunk in diameter, this effect becomes less important. Also the longitudinal temperature is affected by the space charge. The velocity difference is here proportional to the radius squared, making the space-charge effects much smaller longitudinally than transversally for small ion-beam diameters. The longitudinal energy spread is generally set by the transverse–longitudinal relaxation mentioned above to something in the order of $e^2/(4\pi\epsilon_0)n_e^{1/3}$. This value is also larger than the extra longitudinal energy spread introduced by the expansion—the expansion transfers the transverse electron motion into a longitudinal energy spread.

The energy resolution in, e.g., atomic-physics experiments such as those studying radiative, dissociative, or dielectronic recombination between stored ions and cooler electrons, is sensitive both to the transverse and the longitudinal electron temperature. If the relative energy between ions and electrons is small, the transverse temperature limits the resolution, while the longitudinal temperature is important for high relative energies. More precisely, the transverse temperature gives a contribution to the peak width which is independent of the relative energy, whereas the contribution from the longitudinal temperature is proportional to $(E_{\rm rel}E_{\|})^{1/2}$ [6]. Decreasing the transverse temperature from 100 to 10 meV will thus have the biggest effect at relative energies $E_{\rm rel} < E_{\perp}^2/E_{\|}$, where the resolution will improve with a factor of 10.

3. ELECTRON-BEAM EXPANSION

The expansion of the electron beam will reduce its transverse temperature if the magnetic field decreases adiabatically with respect to the cyclotron motion of the electrons. More specifically, the transverse energy of a particle divided by the strength of the longitudinal magnetic field is an adiabatic

invariant under changes of the field strength:

$$\frac{W_\perp}{B_\parallel} \approx \text{const.}$$

(The author hereby and for all future apologises for using expressions such as "transverse energy", although he knows that energy is a scalar quantity.)

Adiabaticity requires that the region of decreasing field is much longer than the cyclotron wavelength λ_c, which is given by

$$\lambda_c = \left(\frac{8\pi^2 m_e}{e} \frac{U_{acc}}{B^2} \right)^{1/2}.$$

In the case of the CRYRING cooler, the field decrease occurs over approximately 30 cm, and setting $\lambda_c \ll 30$ cm gives $U_{acc} \ll 500$ kV if $B = 0.05$ T. To obtain more precise numbers, particles were traced through a field gradient that was calculated based upon the real cooler geometry. For particles with an initial transverse energy of 100 meV, a field in the gun solenoid of 0.3 T and with 0.03 T in the rest of the cooler, the transverse energy after the expansion is shown as a function of total energy in fig. 2. It is seen that the transverse energy becomes reduced to 10 meV up to an energy of approximately 30 keV, and that a significant effect remains up to 60 keV.

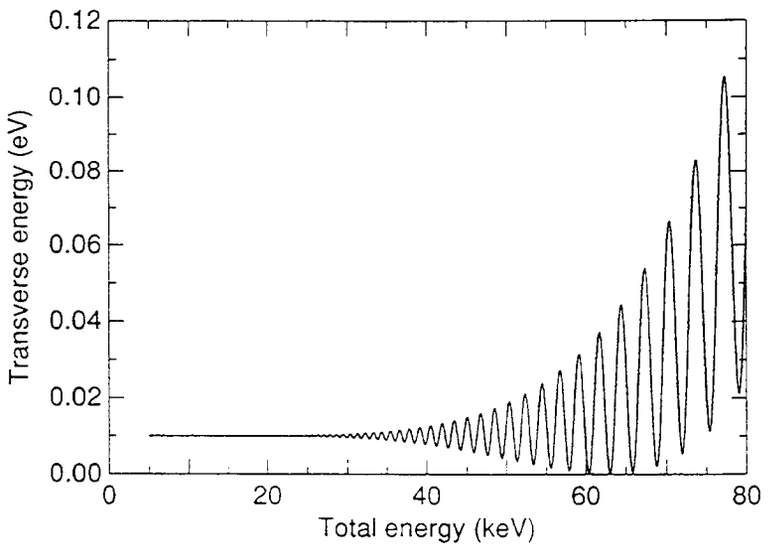

Fig. 2. Transverse energy (i.e., $m_e v_{e\perp}^2/2$) of an electron after the field gradient given in the text, as a function of the total electron energy. The initial transverse energy was 0.1 eV.

The area of the electron beam is inversely proportional to the magnetic field strength, so in order to keep the beam diameter unchanged in the cooling solenoid, the gun must be made correspondingly smaller in a cooler using an expanded electron beam. A gun's perveance, however, does not change when its size is changed, and the current (and thus the current density in the cooling solenoid) can remain the same as in a conventional cooler. The only limitation is set by the maximum current density that the cathode can deliver, which is several A/cm^2 for dispenser cathodes. For very high expansion factors, LaB_6 cathodes may be considered. They have a higher operating temperature, but this is more than compensated for by their higher emission.

4. RESULTS

During the winter and spring of 1993, a new electron gun was built for the CRYRING cooler, and it was installed during the summer. It has the same geometry as the old gun, but its linear dimensions are reduced by a factor 3.2, giving it a cathode diameter of 12.5 mm. All cooler magnets, including one pair of correction dipoles and a compensating solenoid, are connected in series to a single 600-A power

supply. The reduction of the magnetic field strength was accomplished by connecting a shunt resistor (a solenoid once used for a nuclear spectrometer) in parallel with all magnets except the gun solenoid. The resistance of the shunt is such that the field becomes 10 times weaker in the shunted magnets as compared to that of the gun solenoid. Since 600 A corresponds to 0.3 T in the solenoids, the field in the cooling solenoid is at present limited to 0.03 T.

A measurement of the drag force between ions and electrons with the new cooler configuration was made with a D^+ beam at 6 MeV per nucleon. The measurement was, as before [3], made by first cooling the ions and then changing the electron energy, observing from the Schottky signal how fast the ions accelerate toward the new electron velocity. The electron current was as low as 50 mA in order to reduce the drag rates, and the magnetic field in the cooling solenoid was 0.025 T. The result is shown in fig. 3 together with the old measurements. The theoretical curves are from the binary-collision model with a longitudinal electron temperature of 5×10^{-5} eV (the value expected from the transverse–longitudinal relaxation). Clearly, the new points are consistent with a transverse electron temperature of approximately 10 meV.

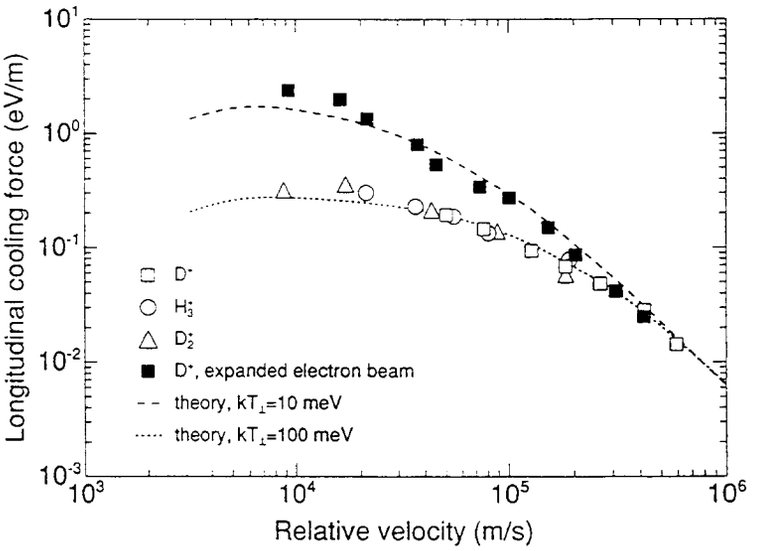

Fig. 3. The drag force created by the electrons on the ions as a function of the velocity between electrons and ions. The force is normalised to an electron density of 10^{14} cm^{-3}. The open symbols are from measurements with a conventional electron beam, the filled squares represent measurements with the expanded electron beam. The curves are from the binary-collision model with a longitudinal temperature of 5×10^{-5} eV.

One may argue that the strong drag force can be caused by the interaction with "magnetised" electrons. (In fact, taking this effect into account, one would expect an even larger drag force than the one observed even for electrons with 100 meV transverse temperature.) The only certain way of measuring the electron temperature is therefore to study the peak shapes in, e.g., some recombination process. Such a measurement was performed very recently, when dissociative recombination of HeH^+ ions was studied [7]. The spectrum of fig. 4 shows the measured yield of recombined molecules as a function of the relative energy between ions and electrons. The sharp rise between 20 and 30 meV shows that the transverse electron temperature indeed is close to 10 meV.

5. SUMMARY AND OUTLOOK

Although the idea to obtain a lower transverse electron temperature by expanding the electron beam has been discussed earlier [8], no attempts to realise such a scheme seem to have been made until now. We have shown, however, that this method works according to the theoretical expectations, and that a transverse electron temperature of approximately 10 meV can be reached. We have also seen how atomic-physics experiments can benefit from the low temperature. Obvious questions are if it can be

extended to higher expansion factors and higher energies.

We believe that expansion factors larger than 10 are feasible, at least at relatively low energies. Electron currents will then be limited to values below 1 A (unless LaB_6 cathodes are used), and a superconducting gun solenoid will probably be necessary. Preferably, the gun solenoid should be wound in such a way that the transition to the low magnetic field becomes smoother than in the present setup. This will also allow higher electron energies. The influence of the various heating mechanisms discussed in section 2 must be carefully considered, however.

At CRYRING we plan to improve the performance of the cooler further by replacing some of the parts used at present (magnets, power supplies) with new equipment made specifically for the use with an expanded electron beam.

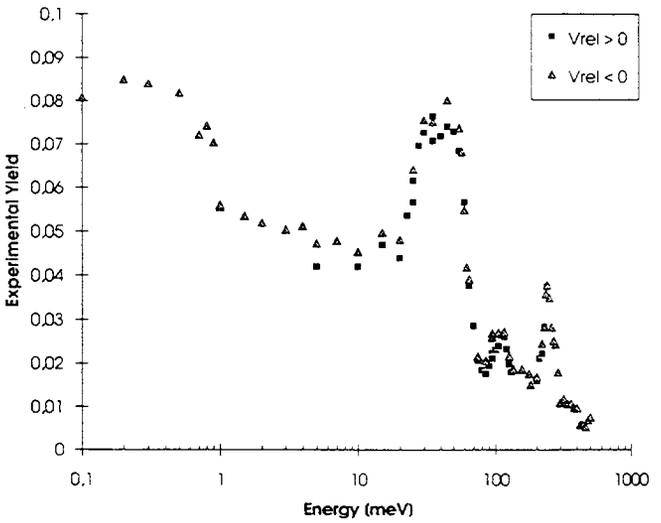

Fig. 4. Preliminary data from a recent experiment with dissociative recombination of HeH^+ ions. The figure shows the yield of recombined ions as a function of the relative energy between ions and electrons.

ACKNOWLEDGEMENT

I would like to thank L. Bagge, P. Dahl, J. Hilke, and A. Paál for their contributions to vacuum, electrical, and mechanical engineering, J. Jeansson, A. Källberg, and the other members of the CRYRING crew, as well as K.-G. Rensfelt.

REFERENCES

[1] H. Danared, Nucl. Instr. Meth., in press

[2] K. Abrahamsson, G. Andler, L. Bagge, E. Beebe, P. Carlé, H. Danared, S. Egnell, K. Ehrnstén, M. Engström, C.J. Herrlander, J. Hilke, J. Jeansson, A. Källberg, S. Leontein, L. Liljeby, A. Nilsson, A. Paál, K.-G. Rensfelt, U. Rosengård, A. Simonsson, A. Soltan, J. Starker, M. af Ugglas, and A. Filevich, Nucl. Instr. Meth. B79 (1993) 269.

[3] H. Danared, Phys. Scr. 48 (1993) 405.

[4] D.R. DeWitt, R. Schuch, T. Quinteros, H. Gao, W. Zong, S. Asp, H. Danared, M. Pajek, and N.R. Badnell, to be published.

[5] V.I. Kudelainen, V.A. Lebedev, I.N. Meshkov, V.V. Parkhomchuk, and B.N. Suchina, Sov. Phys. JETP 56 (1982) 1191.

[6] L.H. Andersen, J. Bolko, and P. Kvistgaard, Phys. Rev. A41 (1990) 1293.

[7] J.R. Mowat, H. Danared, G. Sundström, M. Carlson, L.H. Andersen, L. Vejby-Christensen, M. af Ugglas, and M. Larsson, to be published.

[8] M. Sedlaček, H. Poth, D. Krämer, L. Tecchio, and H.O. Meyer, Phys. Scr. T22 (1988) 204.

COHERENT INSTABILITIES AT ELECTRON COOLING

V. Parkhomchuk and D. Pestrikov
Budker Institute of Nuclear Physics, 630090 Novosibirsk, Russia

ABSTRACT
It is well known that very cooled beams tend to become unstable. Many causes of instabilities can be foreseen of which one is described in this paper.

1. INTRODUCTION

In the ion storage rings with electron cooling the beam emittance and momentum spread (ε, $\Delta p/p$) can reach very small values. Due to its dielectric reactance the electron beam gives additional contributions to the longitudinal and transverse impedances.

These facts generally increase the sensitivity of the cooled beam to various collective effects, including the instabilities of coherent oscillations, which can start from unusually small ion beam currents. As is well known, the strength of these instabilities is also determined by the so-called longitudinal or transverse coupling impedances.

Preliminary calculations [1, 2] have shown that the interaction with the cooling beam can result in the damping of transverse coherent oscillations of the ion bunch if its velocity coincides with the average velocity of electrons. If, however, the deviation in the longitudinal velocities exceeds the velocity spread of the electron beam, this interaction results in the rather fast instability of coherent oscillations of the ion bunch.

In this report we use a simplified model to calculate the increments of transverse coherent oscillations of the ion beam due to interaction with the cooling beam.

2. SINGLE-ION COOLING

An interaction of a single ion of mass M with cooling electrons produces the following friction force [3]:

$$\vec{F} = \frac{4\pi Z^2 e^4 n L_c}{m} \int \frac{\vec{V} - \vec{v}_e}{\left|\vec{V} - \vec{v}_e\right|} f(\vec{v}_e)\, d^3 v_e \tag{1}$$

where

n is the density of the electron beam in the phase space,
L_c is the Coulomb logarithm,
Z is the ion-charge number,
n is the electron density,
e, m are the electron charge and mass (the symbol < > will be used for averaging),
$\vec{V}, \vec{v}$ are the ion and electron beam velocities,
$f(\vec{v}_e)$ is the electron-beam velocity distribution

As a function of $<\vec{V}>$ the friction force attains its maximum value when the velocity deviation $\vec{u} = <\vec{V}> - <\vec{v}_e>$ occurs near the velocity spread in the electron beam $|\Delta|$. For higher $|\vec{u}|$ the friction decreases to u^{-2}. Then the decrements of betatron oscillations can be estimated using the expression:

$$\lambda_\alpha = \frac{1}{M}\frac{\partial F_a}{\partial V_\alpha}\cdot\frac{\ell}{\Pi}, \quad \alpha = \{x(\text{horizontal}), z(\text{vertical})\} \tag{2}$$

where ℓ is the length of the cooling region and Π is the perimeter of the closed orbit. If $u < \Delta$, the values λ_α are positive, which corresponds to the beam cooling:

$$\lambda = \frac{4\pi n Z^2 e^4 L_c}{mM\Delta^3}\frac{\ell}{\Pi} \tag{3}$$

Otherwise, $u > \Delta$ leads to beam heating [2] with increments:

$$\lambda(u) = \frac{4\pi n Z^2 e^4 L_c}{mM u^3} \frac{\ell}{\Pi} \tag{4}$$

3. COHERENT INCREMENTS

To simplify calculations, we estimate the increments of coherent oscillations of the ion bunch as the heating increments of macro-particles which contain N_a particles inside a sphere of radius a moving with a velocity υ_0 in the laboratory frame. This approach can be based, for instance, on the theorem about the sum of the decrements of collective modes [4]. Due to the collision with such a macro-particle electrons change their momenta by the amount:

$$\Delta p = \frac{Ze^2 N_a u}{a^3}\left(\frac{\ell}{\upsilon_0}\right) \tag{5}$$

and the average rate of the electron energy growth can be evaluated as follows:

$$\frac{dE}{dt} = \frac{(\Delta p)^2}{m} n a^3 \frac{\upsilon_0}{\Pi} \tag{6}$$

Then the decrement of coherent oscillations of the ion beam can be given by the following expression:

$$\lambda_c = \frac{1}{E}\frac{dE}{dt} = \frac{nZ^2 e^4 N_a}{mMa^3}\left(\frac{\ell}{\upsilon_0}\right)^4 \frac{1}{\Pi} \cong \lambda(u) u^3 N_a \left(\frac{\ell}{\upsilon_0 a}\right)^3 \tag{7}$$

where the kinetic energy of microparticles ΔE is expresssed by $\Delta E = (Mu^2/2)Na$.

If N is the number of ion beam particles, a_0 the beam radius, ℓ_p the length of the bunch, and $N/\pi a_0^2 \ell_b$ the ion beam density, then a sphere of radius a contains:

$$N_a = N \frac{a^3}{a_0^2 \ell_b} \tag{8}$$

Substituting this expression in Eq. (7) we obtain the increment of the transverse coherent oscillations:

$$\lambda_c = \lambda(u) u^3 N \left(\frac{\ell}{\upsilon_0}\right)^3 \frac{1}{a_0^2 \ell_b L_c} \tag{9}$$

In a more realistic case, when the electron beam is guided by the longitudinal magnetic field and the electron beam is magnetized, Eq. (9) still holds if we replace u by the deviation in the longitudinal velocities. The value λ_c is positive if $u < \Delta_{\|}$. In this case, the interaction with the cooling beam damps the coherent oscillations of the bunched ion beam provided that λ_c is smaller than the frequency of the synchrotron oscillations. In the inverse case, $u > \Delta_{\|}$, the value λ_c becomes negative and hence coherent oscillations become unstable. Since this instability is due to the space-charge type of wakes, we can expect that the increments of the higher-order betatron modes will slowly decay with the increase in the mode number.

4. CONCLUSIONS

For usual cooling device with the following parameters: $n = 10^8$ cm^{-3}, $u = 2 \times 10^5$ m/s, $\upsilon_0 = 10^8$ m/s, $\ell = 2$ m, $a_0 = 0.02$ m, $\ell_b = 10$ m, $L_c = 5$, Eq. (7) results in

$$\lambda_c = N\, 5 \times 10^{-7}\ \text{s}^{-1}$$

For the ring with $\Pi = 80$ m, $dQ/d(\ell np) \sim 1$ and for $\Delta p/p \sim 10^{-3}$, the frequency spread of betatron oscillations is:

$$\Delta w = w_0 \frac{dQ}{d(\ell n\, p)} \frac{\Delta p}{p} \cong 1.6 \times 10^{-4}\ \mathrm{s}^{-1}$$

If we take the value $w_S = 6 \times 10^3\ \mathrm{s}^{-1}$ as frequency of the synchrotron oscillations, then the comparison of Eqs. (10), (11) ans w_S gives $N_{th} = 10^{10}$ ions [5].

In principle, such an instability may cause the so-called "effect of electron heating" at CELSIUS [4].

The increment of the instability in Eq. (9) increases during the beam cooling. Provided that the dipole modes are damped by some feedback system, the next unstable will be the quadrupole modes. In the cold beam these modes can be stabilized by the frequency spread due to the Coulomb tune shift. In this case, both increment of instability and the Landau damping decrement are proportional to the ion beam current. Hence, the stability criterion will define the threshold current of the electron beam.

Note also than the heating of ions due to collisions inside the target will decrease the increments of this stability and will increase the threshold current of the beam.

REFERENCES

[1] N.S. Dikansky and D.V. Pestrikov, Preprint INP 76-40, Novosibirsk 1976.

[2] N.S. Dikansky and D.V. Pestrikov, *Physics of Intense Beams in Storage Rings*, Nauka (Novosibirsk), 1989.

[3] Ya. S. Derbenev and A.N. Skrinski, *Kinetics of Electron Cooling of Beams in Storage Ring of Heavy Particles*, Preprint INP 225, Novosibirsk, 1968; Part. Accel., Vol. 8, p. 1, 1977.

[4] Ya. S. Derbenev, N.S. Dikansky and D.V. Pestrikov, Proceedings of the 2nd All-Union Part. Conf., V. 2, p. 62, Moscow, Nauka 1970.

[5] T. Bergmark, C. Ekström et al., *The CELSIUS Ring*, TSL Progress Report 1987-1991, The Svedberg Laboratory, Uppsala 1992.

WHAT IS ELECTRON COOLING FOR HIGH-Z?

I. Hofmann
GSI Darmstadt, Postfach 110552, D-64220 Darmstadt, Germany

Abstract

We present a computer simulation of the cooling process for high-Z ions in the limit of no magnetic field and of an infinite magnetic field. Special emphasis is on the effect of initial conditions, a description of the origin of the cooling force in terms of the wake field of the ion, and of the nonlinear response of the electrons to the ion potential. We show that the usually assumed Z^2-dependence of the cooling force (and rate) in the linearized theory is modified due to the fact that the Coulomb potential of a highly charged ion can induce a strong perturbation of the electron distribution, which invalidates linear theory. Our numerical results suggest a scaling $\propto Z^{1.5}$ for $Z/N_D >> 1$, where $N_D$is the number of electrons per Debye sphere. Electrons are described here as a collisionless plasma by using a particle-in-cell code in r-z geometry, with the test ion moving in z-direction. This model is appropriate as long as N_D is larger than unity, hence Z should be much larger than unity to enter into the nonlinear regime.

1. INTRODUCTION

Recent measurements of the cooling force for medium [1] and highly [2] charged heavy ions have shown that the cooling force increases weaker than the Z^2-law suggested by the linearized dielectric theory [3] as well as the binary collision model [4]. It is obvious that a theoretical description of this phenomenon would be of great importance for interpreting the data as well as completing our understanding of electron cooling. Estimates on possible improvements of cooling with much colder electron beams than presently used have to take into account nonlinear effects, which may lead to a saturation. One aspect of such a saturation has been proposed in terms of collectively trapped electrons moving along with the ion and resulting in a considerably reduced effective charge of the ion projectile [5]. This effect was essentially due to the initial conditions of the ion starting to interact with the electron plasma in a non-adiabatic fashion (i.e. not arriving from infinity). An analytical description of the nonlinear plasma response in stopping of a negative ion has been performed in a 1-dimensional approximation using charge sheets rather than point particles [6]. These authors found that in the limit of small perturbation (i.e. linear response) their nonlinear result would lead to twice the stopping force than predicted by the linear dielectric theory, where there is no difference between positive and negative ion charge.

A different model has been suggested for the 3-dimensional problem extending the linearized theory in first order perturbation theory [7]. This semi-nonlinear treatment lead to the conclusion that there is an extra term $\propto Z^{5/2}$ for positive ions and a term $\propto Z^3$ for negative ions in the limit of very small ion velocities compared with the electron thermal velocity. These authors found that in both cases the (small) nonlinear terms result in an enhancement of the force.

A full description of nonlinear effects appears to be impossible analytically, hence the remaining tool is computer simulation. An alternative approch to the (nearly) collisionless plasma simulation presented in this paper is the "molecular dynamics" model [8]. This model is more appropriate to desribe strong coupling between the electrons for extremely cold electrons. It is confined to a relatively small number of electrons (typically 10^2), which are then periodically repeated in all spatial dimensions. The particle-in-cell model, on the other hand, ignores collisions between the electrons. Its advantage is that one can work with a large number of electrons (10^4 to 10^5) and thus describe relatively long-range collective interaction adequately (see Debye screening length below).

2. SIMULATION MODEL AND BASIC PARAMETERS

Our goal is to use a self-consistent computer simulation of the interaction process to describe the plasma response under the conditions of strong nonlinearity as well as with realistic initial conditions. We are using a particle-in-cell code in r-z geometry (SCOP-RZ) with the test ion moving in z-direction.

Procedure: The potential of the test ion is that of a point charge. The plasma response to the ion is calculated in a selfconsistent way by solving Poisson's equation on a mesh in r,z. To this end we push the electrons for one time step according to Newton's equations, deposit their charge on the nearest mesh points ("area weighting") and thus obtain a spatial density on the r-z mesh. The electron plasma is actually modelled as a beam, which is rotationally symmetric with respect to the z-axis. Electrons are radially confined by a harmonic potential, which is equivalent to a cylindrically symmetric smeared out ion background. In longitudinal direction the plasma is assumed to have periodic boundary conditions. In order to simulate magnetized cooling we have also foreseen the option to freeze the transverse motion, which corresponds to an infinite magnetic field. For zero magnetic field we assume that the plasma is isotropic, i.e. the transverse temperature is equal to the longitudinal.

Initial Condition: At time zero the ion starts interacting with the yet unperturbed electron plasma. This abrupt "non-adiabatic" entry of the ion into the electron plasma is justified by the small bending radius at which the electron beam merges with the ion beam [5]

Parameters: An important feature of our model is that the simulation plasma is extended, i.e. large compared with the Debye shielding length describing the effective range of interaction of a test particle (here an ion) with the electron plasma. For the ion at rest this static shielding length is given by

$$\lambda_D = v_{th,e}/\omega_p, \tag{1}$$

where the plasma frequency is defined by $\omega_p^2 = \frac{e^2 n_0}{\epsilon_0 m_e}$ and n_0 is the electron density. In practical units we can write

$$\lambda_D \approx 10 \times (\frac{kT(eV)/10^{-4}}{n_0(cm^{-3})/10^8})^{1/2} \quad (\mu m). \tag{2}$$

For an ion moving with relative velocity $\Delta v >> v_{th,e}$ ("fast ion") one introduces a dynamical shielding length, which is given by the same expression, but with $v_{th,e}$ replaced by Δv. It is thus necessary to choose the actual size of the simulation plasma large compared with the dynamical λ_D. We note that for infinite magnetic field the shielding radius is properly calculated by taking the parallel electron temperature [3].

Limit of Applicability: The model of an ideal or collisionless plasma is applicable as long as the number of particles per Debye sphere,

$$N_D = \frac{4\pi}{3} n_0 \lambda_D^3, \tag{3}$$

where n_0 is the electron density, is larger than unity. For $N_D < 1$ ("non-ideal plasma") reliable results can be obtained with the molecular dynamics method.

To give an example we find that $N_D \approx 1$ for $n_0 = 10^8$ (cm^{-3}) and $kT = 2 \times 10^{-4}$ (eV). It is easily verified that $N_D \propto n_0^{-1/2}(kT)^{3/2}$.

In the simulation we artificially increase the number of electrons per unit volume, keeping the charge to mass ratio invariant. This is desirable to obtain a consistent description of an ideal plasma; it also helps to reduce statistical fluctuations, which would cause a large error bar in each run. We note that our simulation plasma is not completely collisionless. The area-weighting method for density calculations introduces a small diffusion rate depending on the mesh size. This is well-known in particle-in-cell simulation; in our context it is even a desired deviation from the artificial ideality.

Nonlinearity Parameter: An important question is to define a dimensionless "nonlinearity parameter". We adopt the suggestion from analytical theory, where the scaled ion charge Z/N_D is used. The physical meaning of this is the following: an ion is attracting Z electrons to shield its own space charge; as long as $Z << N_D$ the ion shielding is a weak perturbation of the

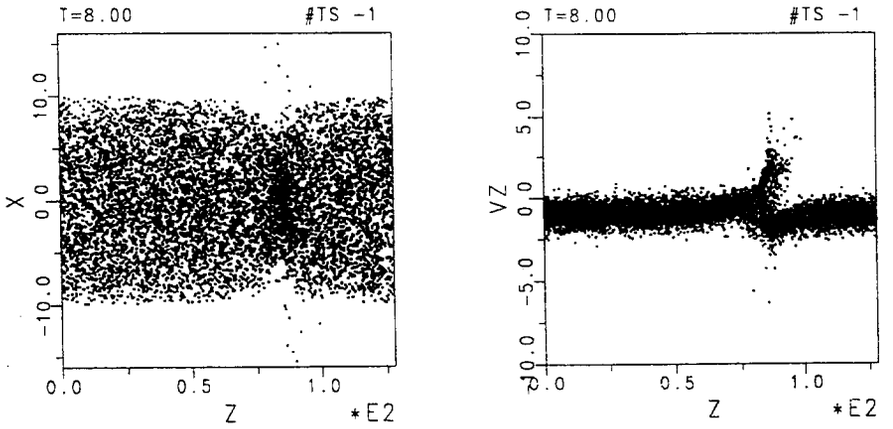

Figure 1: Scatter plots of simulation for strong nonlinearity(Z/N_D=135); left plot real space, right plot longitudinal phase space.

electron density. For $Z >> N_D$ the shielding implies a strong perturbation of the local electron distribution, hence linearized theory is violated.

We first present results for the isotropic plasma in the absence of a magnetic field. The result of a simulation with 1.3×10^5 electrons (only 8×10^3 plotted) describing an extended environment of the test ion is shown in Fig. 1. We are using a scaled time; in all examples the plasma oscillation period $2\pi/\omega_p$ is 20. The plot shown is at time T=16. The ion is at rest and the electron beam is moving to the left. The relative velocity Δv is measured in units of the electron thermal velocity spread, $v_{th,e}$, and is chosen 1 in this example. The scaled charge state Z/N_D is as large as 135 to demonstrate a strong nonlinearity. We note that for the largest physical charge (Z=92) this would mean N_D=0.68, which is actually beyond the range of validity of the ideal plasma approximation. The electron beam is strongly perturbed by the presence of the ion, both in density as well as in local "temperature".

3. DEBYE SHIELDING

The shielding of an ion with Z/N_D=45 is shown in Fig. 2, where we plot the axial electric field component in the neighbourhood of the test ion about a plasma period after start. The upper case refers to Δv=0, i.e. static shielding, the center case to Δv=1 and the bottom case to a fast ion with Δv=5. The ion is attracting a cloud of electrons, which shields the ionic electric field. The shielding is symmetric in the static case; for the moving case the shielding is seen to be more effective in the wake of the ion (left side). For the fast ion there is practically no shielding in front of the ion; the shielding cloud is found further away in the wake, where the sign of the bare ion electric field is reversed by it.

The theoretically expected shielding length (according to Eq. 1), is 3 scaled length units for the static case. This agrees well with the simulation result.

4. COOLING FORCE

The origin of the cooling force acting on the ion is the electric field produced by the electron "cloud" at the position of the ion (see Fig. 2. It is zero for an ion at rest; for a moving ion it is nonzero, since the "cloud" lags behind the ion. The shape of the electric field distribution indicates the well-known feature that there is a maximum force at an intermediate relative velocity, which drops to zero at large relative velocities. The cooling force for Δv=1 as a function of time is shown in Fig. 3 for the strongly nonlinear example of Fig. 1. Besides Z/N_D=135 we also show the result for a negative ion with Z/N_D=-135 (unphysical). It is recognized that for both cases the cooling force increases from zero during the phase where the shielding cloud is formed. The cooling force on the positive ion is considerably larger in the

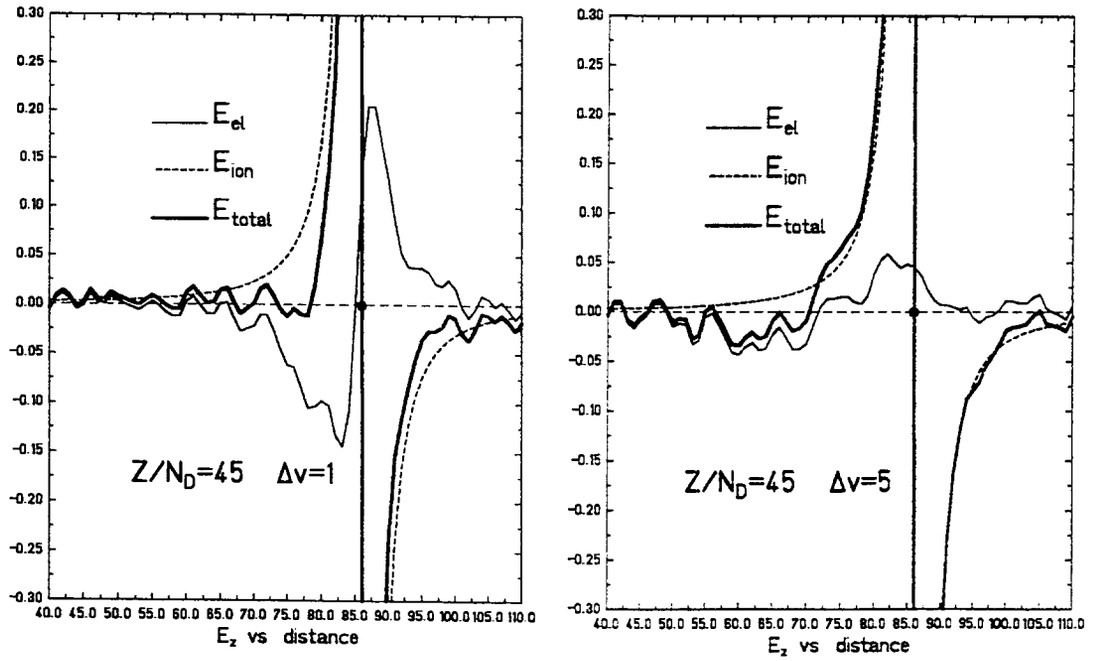

Figure 2: Debye shielding effect for different velocities

early phase, which we explain by trapping of electrons in the ionic potential. These electrons lead to a drag force only in the beginning. It should be noted here that according to Fig. 3 the effective cooling force comes to a stationary value only after a sufficient time, hence it may vary with the length of the cooler. After 3/4 of a plasma period the forces on positive and negative ion are identical.

It is also observed that the force for the negative ion is much smoother than for the positive. This might be connected with the phenomenon of trapping. It is of interest to plot the cooling force as a function of relative velocity. This is shown in Fig. 4 for Z/N_D=45. The maximum of the force occurs near Δv=2, with a linear dependence on velocity for slow ions. A comparison with the well-known linearized theory result [3] shows that the maximum force is approximately a factor of 4 smaller, which we ascribe to the nonlinear response. For large relative velocities the difference vanishes. This is consistent with the observation that Z/N_D should be calculated with the dynamical screening length entering into N_D according to Eq. 3.

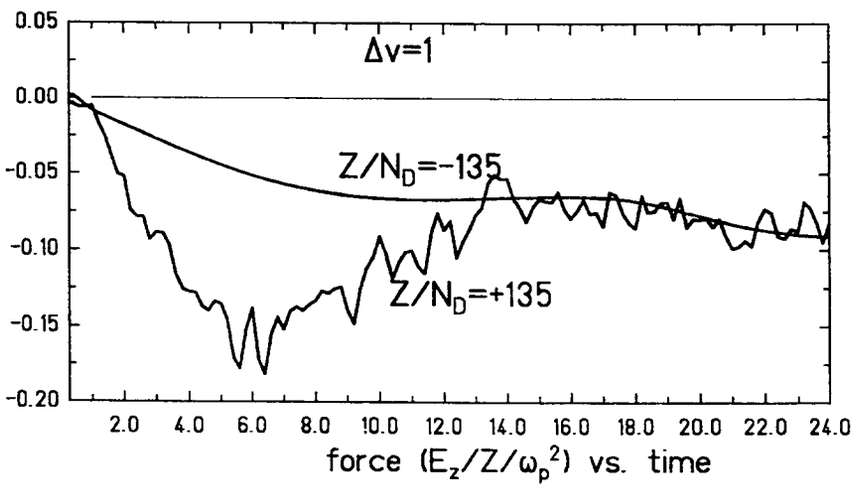

Figure 3: Cooling force for strongly nonlinear case as function of time

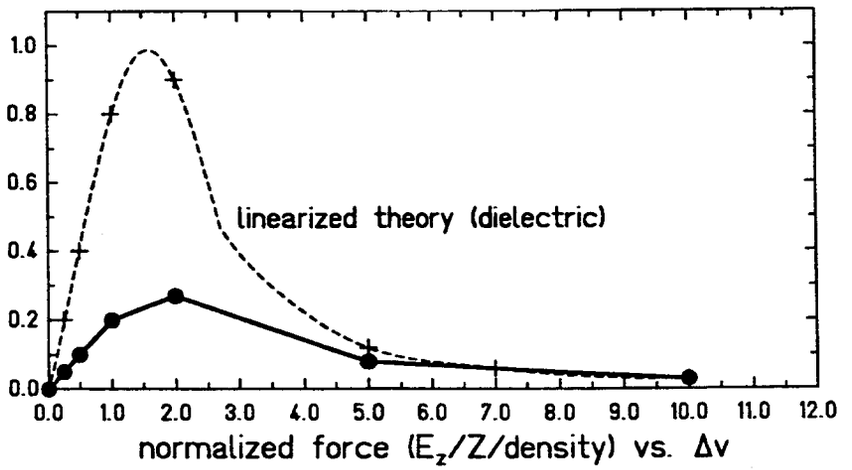

Figure 4: Cooling force as function of relative velocity

5. DEPENDENCE ON Z/N_D

Results of simulations for different values of the scaled charge state Z/N_D and Δv have been obtained. Here N_D is defined using the static Debye length. In Fig. 5 we have plotted E_z/Z, which should be a constant according to linear theory. Since the value Δv=1 is in the linear regime (Fig. 4) the cooling rate is directly proportional to this force (dashed line). It is noted that with increasing Z/N_D the force is decreasing for the slow ion, whereas it is almost constant for a fast ion with Δv=5. The latter case is thus close to the linearized theory behaviour (the gentle decrease is explained in linear theory by the decreasing Coulomb logarithm with increasing Z). This agreement can be explained by noting that N_D is proportional to $(\Delta v)^3$ for fast ions, hence the nonlinearity parameter is accordingly reduced. For $Z/N_D \approx 100$ we find that there is no difference between the forces on the Δv=1 and Δv=5 case. This indicates that the pronounced peak in the force for ion velocities near the electron thermal velocity vanishes for strong nonlinearity. It should be noted that for the slow ion it is not easy to simulate a case with Z/N_D equal to or smaller than unity, where the perturbation is small and linear theory should apply. This is due to the fact that small perturbations fall within the noise level of the simulation plasma, hence the error bar on the friction force is large.

The data of Fig. 5 suggest that for slow ions the cooling force follows an approximate scaling with $Z^{1.5}$ in the regime $1 < Z/N_D < 50$, which is about the regime of applicability of the ideal plasma simulation. A similar fitted scaling ($Z^{1.43}$) has been obtained recently by a molecular dynamics approach [8] in the regime, where strong correlations among electrons

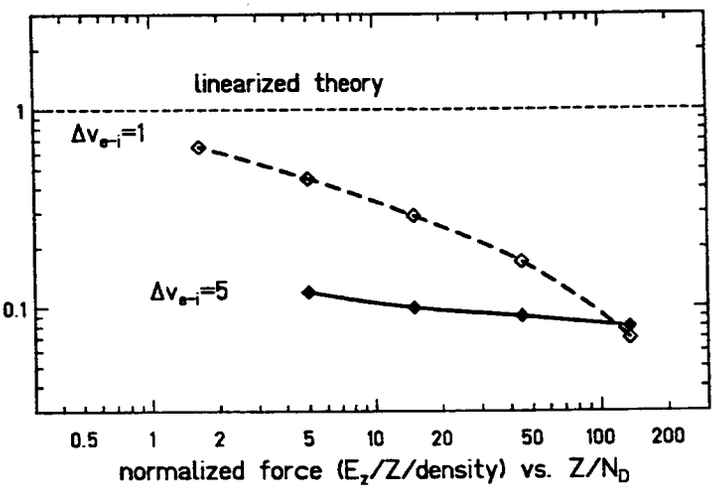

Figure 5: Scaling of normalized force E_z/Z

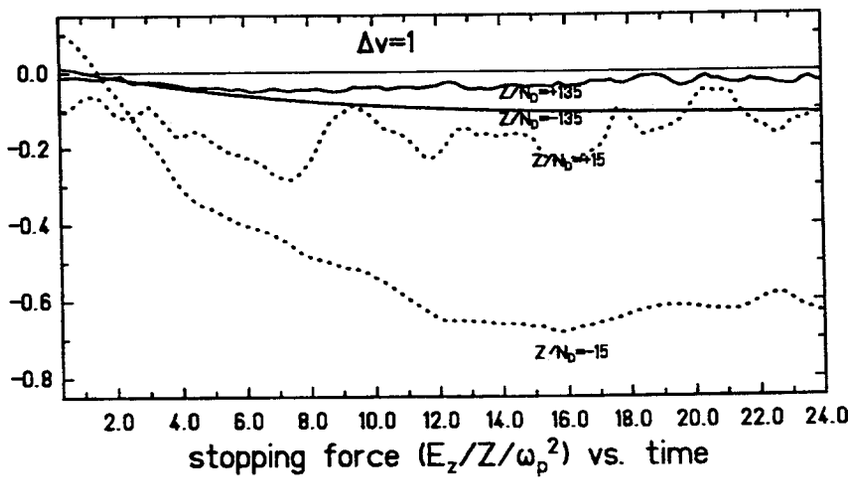

Figure 6: Cooling force for infinite magnetic field and Δv=1

play a role. This good agreement suggests that the nonlinear reduction of the cooling force is unsensitive to correlations between electrons, but a matter of the strong perturbation of the local electron temperature due to the ion potential.

6. MAGNETIZED COOLING

We have carried out preliminary studies on magnetized cooling. For this case we have assumed the limit of an infinite magnetic field by suppressing the transverse motion of electrons. Results are shown in Fig. 6 for Z/N_D equal to 15 and 135 and Δv=1. We have plotted E_z/Z as in Fig. 3 using the same scale. The plasma density and (parallel) temperature is identical to the isotropic plasma case without magnetic field. We find that for positive ions the force is almost a factor of two smaller than without the magnetic field (note that in the latter case we have not considered a "flattened" distribution with larger transverse than longitudinal temperature). For negative ions it is, however, about a factor of 3 larger, if one ignores the values at early times. This agrees well with experimental observations at MOSOL, where an enhanced force was found for H^- as compared with protons [9]. The enhancement factor was 3 for 4 kG magnetic field; no enhancement was found for 1 kG magnetic field.

A similar nonlinear force reduction as in the above case is again recognized from Fig. 6, where the linearized theory would predict identical values for E_z/Z. A comparison of different values of Z/N_D for Δv=1 confirms that approximately the same scaling $\propto Z^{1.5}$ applies as in the case of no magnetic field, both for positive and negative ions.

REFERENCES

[1] A. Wolf, "Nonlinear Effects on Ion Stopping in a Magnetized Electron Gas", these Proceedings

[2] M. Steck et al., " Electron Cooling of Highly Charged Heavy Ions", these Proceedings

[3] A.H. Soerensen, E. Bonderup, Nucl. Instr. Meth. 215, 27 (1983)

[4] Y.A. Derbenev, A.N. Skrinsky, Part. Acc. 8, 235 (1978)

[5] S.R. Goldman, I. Hofmann, Plasma Science 18, 789 (1990)

[6] V.V. Avilov et al., Phys. Rev. A 40, 7133 (1989)

[7] Th. Peter and J. Meyer-ter-Vehn, Phys. Rev. A 43, 1998 (1991)

[8] G. Zwicknagel, C. Toepffer, P.-G. Reinhard, " Molecular Dynamics Simulation of Electron Cooling", these Proceedings

[9] N.S. Dikansky et al., "Ultimate Possibilities of Electron Cooling", INP Novosibirsk preprint 88-61 (1988)

LASER COOLING OF $^{24}MG^{+}$ IN THE ASTRID STORAGE RING.

J.S. Nielsen, J.S. Hangst, O. Poulsen[#], J.P. Schiffer[†], P. Shi[#], and B. Wanner[‡]
Institute of Physics and Astronomy, Århus University
DK-8000 Århus C, Denmark

ABSTRACT
Laser cooling of $^{24}Mg^{+}$ has now begun at the ASTRID storage ring. In contrast to $^{7}Li^{+}$, which has been used up to now, it is now possible for the laser to interact with all of the beam. In this paper some of the results from the first beam time with $^{24}Mg^{+}$ are described. By frequency chirping a single laser, laser cooling has been performed on a coasting beam, and first evidence of sympathetic transverse cooling has been observed.

1. INTRODUCTION.

At the Institute of Physics and Astronomy at the University of Aarhus, the ion $^{7}Li^{+}$ has, during the last few years, been used to study laser cooling in a stored ion beam [1,2]. A longitudinal temperature of 1 mK ($\Delta p/p=1.5\cdot10^{-6}$) has been achieved[1]. However, this ultralow temperature was achieved in a very dilute beam, in which the momentum diffusion was dominated by the diffusion due to the laser and not by that due to intrabeam scattering. For a more dense beam the diffusion is dominated by intrabeam scattering, and the ultralow temperatures cannot be obtained.

$^{7}Li^{+}$ is an almost ideal ion for laser cooling. It has a nearly closed transition (branching ratio less than 10^{-5}) at a wavelength of 548.6 nm (green light), where CW lasers are very well developed. However, the lower state of the cooling transition is the metastable 1s2s $^{3}S_{0}$ state, 60 eV above the groundstate. It was hoped that the groundstate ions would be cooled sympathetically due to Coulomb interactions with the coolable metastable ions. Measurements have now shown that in the ionsource used at ASTRID, only $\sim10^{-4}$ of the ions are produced in the metastable state. There is therefore no hope of any significant sympathetic cooling, on the timescales of the storage lifetime. The energy which can be removed by the laser is too small to change the velocity distribution of the beam as a whole.

2. LASER COOLING OF $^{24}Mg^{+}$.

A new ion has therefore been chosen, which has a suitable cooling transition operating directly from the groundstate, so that all the ions can be addressed. This ion, $^{24}Mg^{+}$, has a closed transition, with a lifetime of the upper state of only 3.5 ns. The short lifetime implies that the maximum cooling force due to the spontaneous force can be potentially up to ~20 times larger than that in the case of $^{7}Li^{+}$. The range of the force in velocity is also larger because of a larger natural linewidth. Table 1 summarizes some of the different properties of $^{7}Li^{+}$ and $^{24}Mg^{+}$. Unfortunately, the transition wavelength is in the UV at 280 nm, where CW lasers are not very well developed, and it has up to now not been possible to produce enough CW UV laser power to use this ion to perform laser cooling in a storage ring.

By the technique of frequency doubling, a tunable CW UV laser system capable of routinely producing 50-60 mW has been developed at our institute. This power implies that the maximum force on a single $^{24}Mg^{+}$ ion is approximately the same as that on a $^{7}Li^{+}$ in the metastable state. But because all ions can interact with the laser in the case of $^{24}Mg^{+}$, the force on the beam as a whole is more than 10^{4} times larger than that in the case of $^{7}Li^{+}$. This increase in the force has allowed a manipulation of the velocity distribution of the ion beam as a whole.

In Fig. 1 are shown two longitidinal Schottky spectra of a 100 keV $^{24}Mg^{+}$ beam. One (dashed line) is taken without laser, and the second (solid line) is taken after a laser scan from -2 GHz ($\Delta p/p=-6.2\cdot10^{-4}$) to +12 GHz ($\Delta p/p=3.7\cdot10^{-3}$) relative to the linecenter. The laser is able to change the momentum by $\Delta p/p = 3.9\cdot10^{-3}$, corresponding to an energy shift of 780 eV. A slight decrease in the width of the distribution is also seen, but this effect has been reduced by the heat up after the laser scan, due to diffusion from intrabeam scattering. Some ions are left behind by the laser. This is partially due to intrabeam scattering events in which ions undergo so

large a velocity change that they end up on the "wrong" side of the scanning laser and are lost from the cooling process. Another reason is that as ions get accelerated their orbits in the ring shifts due to dispersion (D_x=2.7 m), and the physical overlap between the laser beam and the ion beam is thus reduced.

Table 1: Some of the different properties of $^{7}Li^{+}$ and $^{24}Mg^{+}$.

	$^{7}Li^{+}$	$^{24}Mg^{+}$
Coolable fraction	$\sim 10^{-4}$	1
Typical saturation parameter[a]	25	0.25
Max cooling force on a coolable ion, averaged over the ring circumference[b]	8 meV/m	42 meV/m
Max energy change per round trip, averaged over all of the beam	~33 μV	1.7 eV
Max cooling power, averaged over all of the beam[c]	1.4 eV/s	38 keV/s
Typical thermal energy in the beam (in the lab. frame)[c]	190 eV	190 eV
Range of force (FWHM Δp/p)[c]	$6 \cdot 10^{-6}$	$1.4 \cdot 10^{-5}$

[a] The saturation parameter is the ratio between the laser intensity and the saturation intensity for the transistion. A saturation parameter of 1 means that the spontaneous force on resonance is half of what it would be with infinite laser intensity.
[b] Assuming overlap for 4 m (1/10 of ring circumference)
[c] at E=100 keV

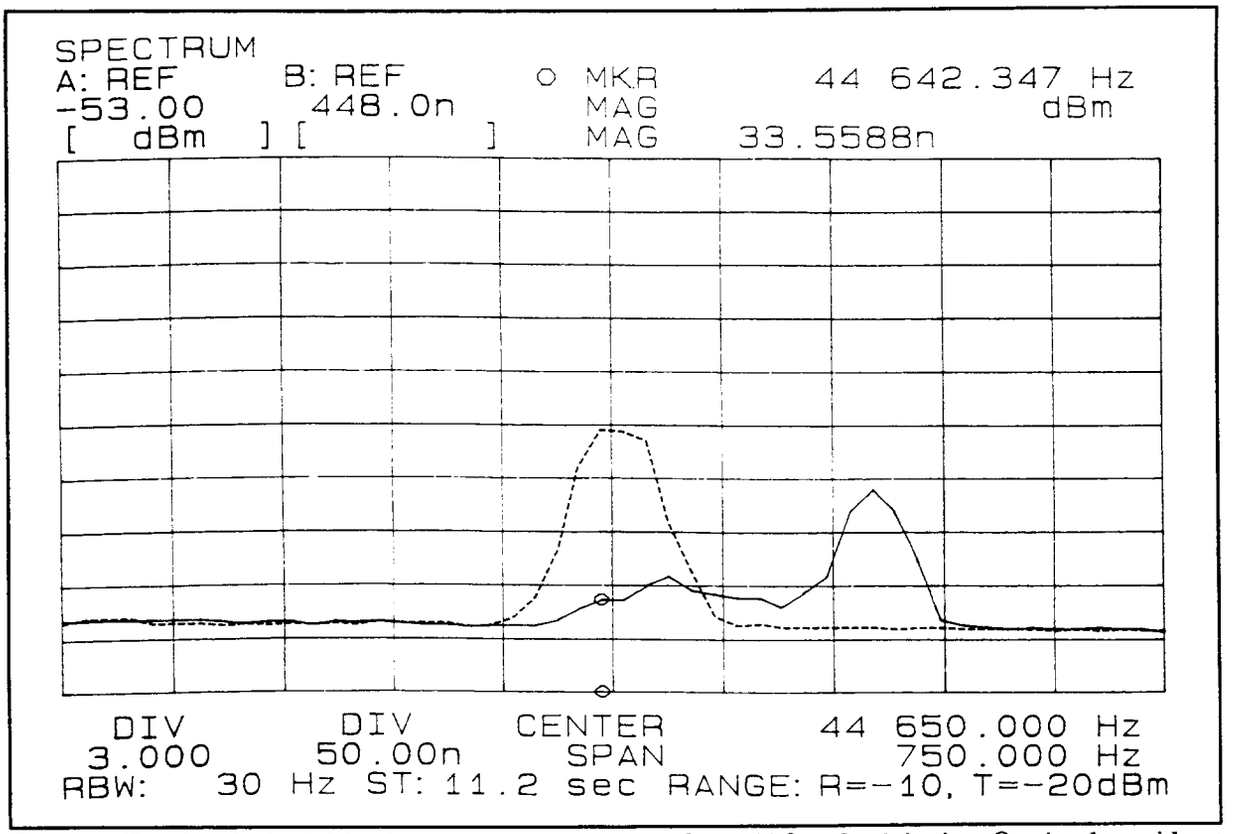

Figure 1. Two longitudinal Schottky spectra, measured from 0 s to 11.2 s after injection. One is taken without laser (dashed line) and one is taken after a laser scan from -2 GHz to +12 GHz.

3. LASER COOLING BY FREQUENCY CHIRPING.

With only one laser, fixed in frequency, no stable point is possible [3]. However, by scanning the frequency of the laser, laser cooling is possible by pushing the ions in front of the laser.

Figures 2 and 3 show the velocity distribution during the last part of two cooling scans. These are measured by scanning the voltage on a post acceleration tube, and thereby locally changing the velocity of the ions. Looking at laser induced fluorescence, the number of ions can be measured as function of velocity. Figure 2 shows the result for a low density beam ($n=2\cdot10^5$ cm^{-3}), and Fig. 3 shows the result for a higher density ($n=1\cdot10^6$ cm^{-3}). The scan ranges and the scan rates are the same for the two ((-2 GHz ($\Delta p/p=-6.2\cdot10^{-4}$) to +4 GHz ($\Delta p/p=1.2\cdot10^{-3}$)) and 24 GHz/s), but note the different scale on the X-axis. It is seen that for a low density the laser is able to collect all of the ions, whereas this is not possible in the case of a higher density. The reason for this is that intrabeam scattering or another diffusive mechanism is stronger for a higher density, and there are therefore many more scattering events which will change an ions velocity by more than the capture range of the force. For a lower scan rate the capture range is larger [3] and we find that the laser then is able to collect all of the ions, even for the higher density.

From the distance from zero relative velocity (which is at the maximum laser force) to the peak of Fig. 2 and the scan rate, one can get an estimate of the strength of the laser force. We find this to be ~26 meV/m averaged over the ring cirfumference, in reasonable agreement with the theoretic value calculated in Table 1.

4. TRANSVERSE SYMPATHETIC COOLING

Laser cooling has up to now only been accomplished on the longitudinal degree of freedom of a stored beam. The reason that direct transverse laser cooling has not been successful, is that the physical overlap between a laser beam propagating transversely to the ion beam will be much smaller than for a laser beam propagating parallel to the ion beam. It has long been believed that by cooling the beam longitudinally, the beam would also be cooled transversely, because energy would be transferred from the hot transverse degree of freedom to the cold longitudinal degree of freedom by intrabeam scattering. However, up to now no effect of this mechanism has been measured. We have now seen evidence for such a transverse cooling. Laser cooling was performed with a fixed frequency laser in an RF bunched beam as described in [4]. At a certain time after injection a vertical scraper was run into the beam, and the loss of ions was monitored by a neutral particle detector. Assuming a Gaussian distribution for the ion beam, the scraper spectra were fitted [5], and the resulting sizes are shown in Fig. 4. In Fig. 4 the open circles are the beam sizes measured with the laser blocked and the filled circles are with the laser on. Even though there is a large spread in the sizes for the laser on, the sizes with laser on are significantly smaller. The averaged difference is ~10%. The effect is not very big, and it will certainly be one of our goals in future beam times to improve this.

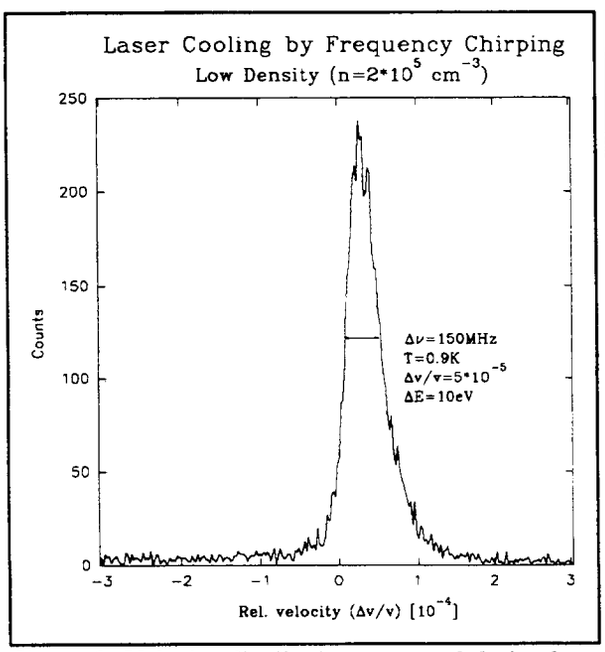

Figure 2. Velocity distribution measured during laser cooling by frequency chirping in a low density beam.

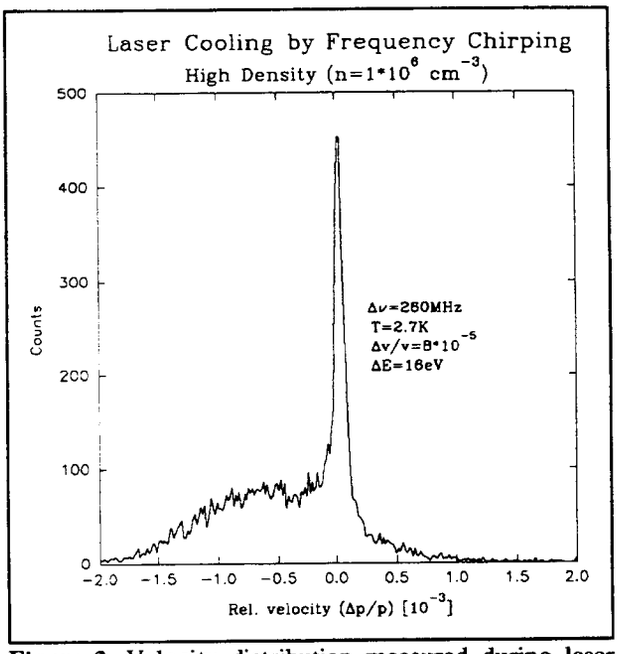

Figure 3. Velocity distribution measured during laser cooling by frequency chirping in a higher density beam.

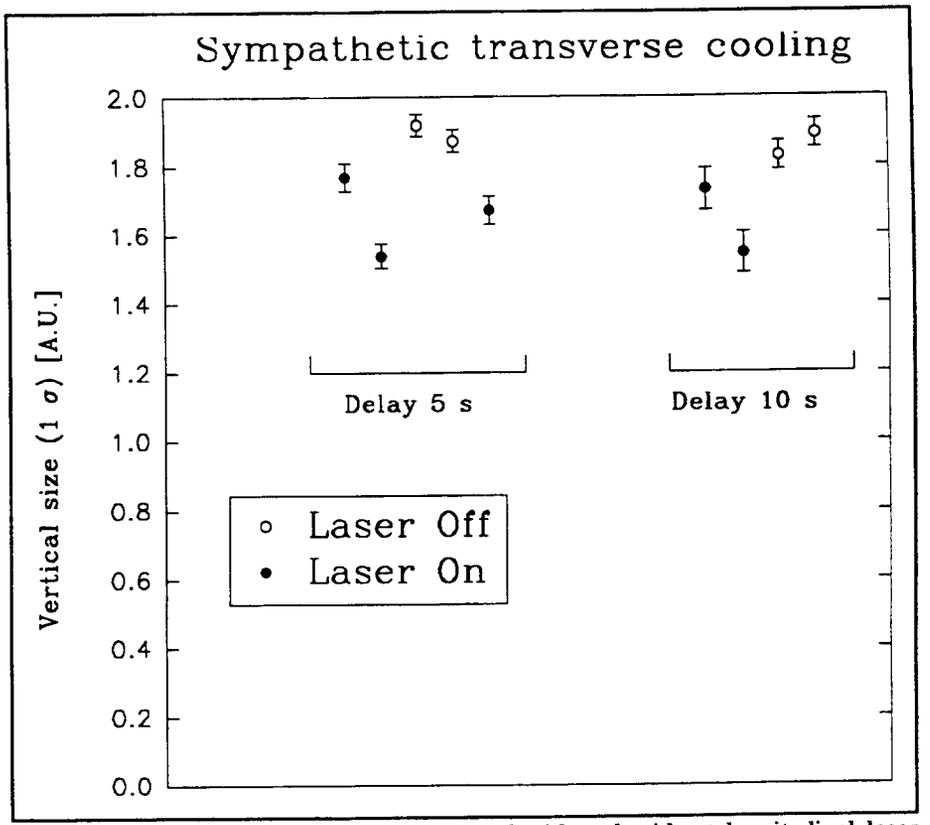

Figure 4. The vertical beam sizes measured with and without longitudinal laser cooling. The errors are the statistical errors from the fit to the data assuming a Gaussian distribution for the ion beam.

5. CONCLUSION

In this paper we have shown some of the results of our first beam time with $^{24}Mg^{+}$ in the ASTRID storage ring. We measured among other things the beam dynamic and equilibration processes with laser induced fluorescence, and we found that the laser was able to perturb and change the velocity distribution of the ion beam. In addition we have for the first time laser cooled a stored ion beam bunched by an RF cavity [4], and first evidence for indirect transverse cooling has been observed.

For our next beam time, planned to take place in winter 1993, we will have two UV lasers. We can then have one laser copropagating and one laser counterpropagating, which will allow us to have a stable point which is fixed in velocity. This will also allow us to get a much higher friction force, and therefore achieve a much lower beam temperature. The capture range of the force will also be increase, reducing the loss from the cold distribution due to large velocity changes from the intrabeam scattering. Another aspect which will be further pursued is the indirect transverse cooling.

REFERENCES

Also at Mikroelektronik Centret, DTH, Blgd. 345 E, DK-2800 Lyngby, Denmark

† Argonne National Laboratory, Argonne, IL 60439, and University of Chicago, Chicago, Il 60637

‡ Max-Planck-Institut für Kernphysik, D-6900 Heidelberg, FRG

[1] J.S. Hangst, M. Kristensen, J.S. Nielsen, O. Poulsen, J.P. Schiffer and P. Shi, Phys. Rev. Lett., **67**, 1238 (1991)

[2] J.S. Hangst, K. Berg-Sørensen, P.S. Jessen, M. Kristensen, K. Mølmer, J.S. Nielsen, O. Poulsen, J.S. Schiffer, P. Shi and S. Pape Møller, Nucl.Instrum.Meth. **B68**, 17 (1992)

[3] For an introduction to laser cooling in storage rings, see eg. W. Petrich et. al., Phys. Rev. A., **48**, 2127 (1993)

[4] J.S. Hangst, J.S. Nielsen, O. Poulsen, J.P. Schiffer, P. Shi, and B. Wanner, "Laser Cooling of a Bunched Beam in ASTRID", These proceedings

[5] K. Potter, in CERN 85-19, edited by P. Bryant and S. Turner, (CERN, Geneva, 1985), pp. 301-317

LASER COOLING OF A BUNCHED BEAM IN ASTRID

J.S. Hangst, J.S. Nielsen, O. Poulsen[*], *J.P. Schiffer*[†], *P. Shi* [*], *and B. Wanner*[‡]
Institute of Physics and Astronomy, Aarhus University
DK-8000 Aarhus C, Denmark

ABSTRACT
The ASTRID storage ring has been used to study laser cooling of low energy ion beams. We discuss the results of recent experiments involving the ion $^{24}Mg^{+}$. We have employed a single cooling laser and a radio frequency (RF) cavity to demonstrate the first laser cooling of a bunched beam.

1. INTRODUCTION

Laser cooling has, to date, been employed in two storage rings, the Test Storage Ring (TSR) in Heidelberg [1] and ASTRID [2] in Aarhus. Laser cooling is an attractive technique for beam cooling because of the potentially low momentum spreads and high cooling rates obtainable. The possibility of obtaining a crystalline ion beam [3] is often closely linked to the strength and speed of the laser cooling process. There are, unfortunately, few candidate ion/laser combinations for laser cooling of energetic beams. Following our early work using the ion $^{7}Li^{+}$ [2,4] and visible lasers, we have developed a tunable UV laser for use in cooling the ion $^{24}Mg^{+}$ [5]. The advantages of using this ion and tunable lasers are discussed elsewhere in these proceedings [5].

Several experimental configurations have been used for longitudinal cooling of ion beams using laser light. The first experiments in ASTRID employed two tunable lasers; a co-propagating laser to accelerate slow ions, and a counter-propagating laser to decelerate fast ions. This is analogous to the situation in ion or atom traps. Some experiments in the TSR employ a single, fixed-frequency laser and an induction accelerator. The induction accelerator sweeps ions into resonance with the laser, forming a cold distribution. A single scanned laser may also be used [5] in order to form a cold distribution. These last two methods have the disadvantage that the stable, cold distribution is only obtainable while the induction accelerator or the laser is scanning. There is no fixed stable point for the cooling force.

We have developed another method for producing a steady-state, cold distribution which combines laser cooling with standard RF bunching technique. This method offers the advantage of producing a stable, cold distribution with a single cooling laser. A further benefit is the ability to study bunched beam dynamics in a very cold beam.

2. DESCRIPTION OF THE COOLING METHOD

An RF cavity is used to bunch the injected ion beam. The frequency of the RF potential defines an ideal velocity (the synchronous velocity) for ions in the storage ring. For ions having velocity (or phase) errors relative to the synchronous particle, the RF potential represents a quasi-harmonic restoring force in longitudinal phase space. These particles undergo oscillations (synchrotron oscillations) in energy and phase relative to the synchronous particle.

Figure 1 illustrates, in the longitudinal phase plane, the principle of the cooling method for a single particle. A particle having non-zero longitudinal emittance undergoes synchrotron oscillations. Each dot in the diagram represents a single revolution. A laser beam, which is co-propagating with the ion beam, is tuned to be in resonance with the ion when it has its minimum energy in the oscillation cycle. The particle absorbs photons from the laser beam and is accelerated slightly. This alters the phase space trajectory, as shown in the diagram. The particle continues to scatter photons until its velocity is changed enough to take it out of resonance with the laser light. (The width in velocity of the radiation pressure force, which is determined by the line width of the optical transition, is taken to be much smaller than the particle's velocity error. It is, of course, this narrow width that defines the very small energy spreads obtainable in laser cooling.) By scanning the frequency of the laser, the amplitude of the synchrotron oscillations can be further damped, as illustrated in the figure.

For a distribution of particles, the method is essentially the same. The laser is initially tuned to be in resonance with particles having the largest synchrotron amplitudes. Scanning the laser frequency then damps the oscillations of all particles as the laser comes into resonance with particles having smaller longitudinal

emittance. The cooling process is stopped by halting the laser scan just short of being in resonance with the synchronous particle. The laser can then maintain the cold velocity distribution in the CW RF field. Note that the fixed-frequency laser can re-cool particles which may diffuse out of the cold distribution (because of intrabeam scattering, for example), since their synchrotron oscillations will periodically bring them into resonance with the laser. Note also that, in the projection of the phase space distribution onto the velocity axis, the signature of this cooling method is a distribution that narrows symmetrically around the synchronous velocity as the laser scans. The width of the distribution at any time should be approximately twice the velocity detuning of the laser from the synchronous velocity (if the distribution is broad enough that the transition line width can be ignored).

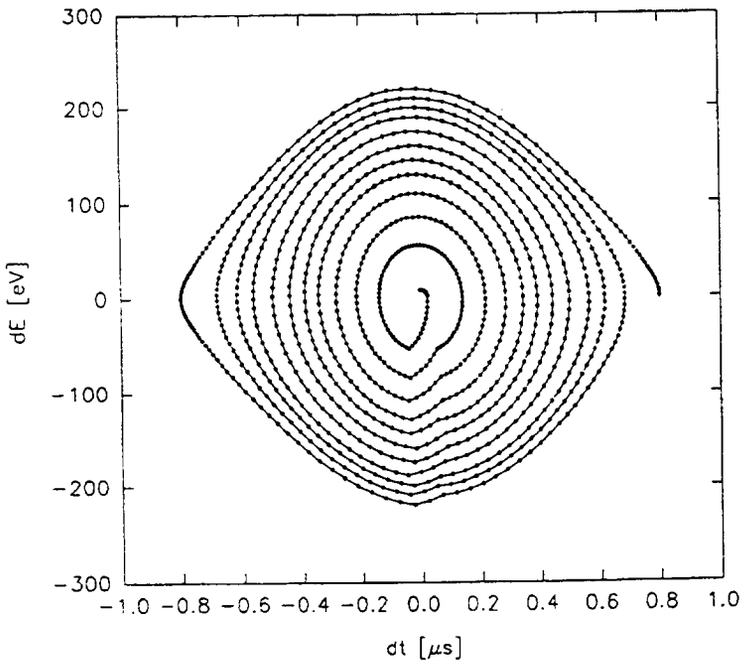

Figure 1. Longitudinal phase space plot illustrating the principle of bunched-beam laser cooling. Energy deviation and time deviation are plotted for a single particle in an RF bucket.

3. THE EXPERIMENTAL SETUP IN THE ASTRID STORAGE RING

Figure 2 shows the configuration used for bunched beam cooling in the ASTRID ring. The ring itself is described in reference [6]. The beam employed consisted of 100 keV $^{24}Mg^{+}$ ions produced in an ion source and electrostatically accelerated. Typical beam currents were of order 1 μA, corresponding to 10^8 particles stored. The initial momentum spread of the injected beam is very low ($\delta P/P \sim 10^{-5}$), but the beam blows up rapidly to $\delta P/P \sim 10^{-3}$ (for coasting beam). The RF cavity was operated at the 26th harmonic of the revolution frequency. Due to the very low longitudinal emittance of the beam, the RF cavity was operated at very low voltages, typically of order 10 V peak.

The laser employed was a frequency-doubled ring dye laser producing light at about 279 nm in the UV. The laser is co-propagating with the beam in one straight section of ASTRID, giving about 4 m of overlap. For more specifics of the laser cooling parameters see reference [5], these proceedings. Fluorescence light is detected by a photomultiplier tube (PMT) looking transversely at the beam. The beam observed by the phototube is passing through a post-acceleration tube (PAT) which is isolated from the vacuum chamber and upon which can be placed a voltage. This voltage locally alters the kinetic energy of the ions and therefore can be used to determine the velocity class of ions that is locally in resonance with the laser. Scanning the voltage on this tube while monitoring the fluorescence light from the beam allows rapid measurement of the ions' velocity distribution during the cooling process. The beam can also be observed using a longitudinal Schottky detector, but due to the difficulty in interpreting the coherent signals from a bunched beam, we have employed the laser fluorescence technique for characterizing the velocity distribution. The time structure of the bunched beam has been measured using the sum signal from standard beam position pickups.

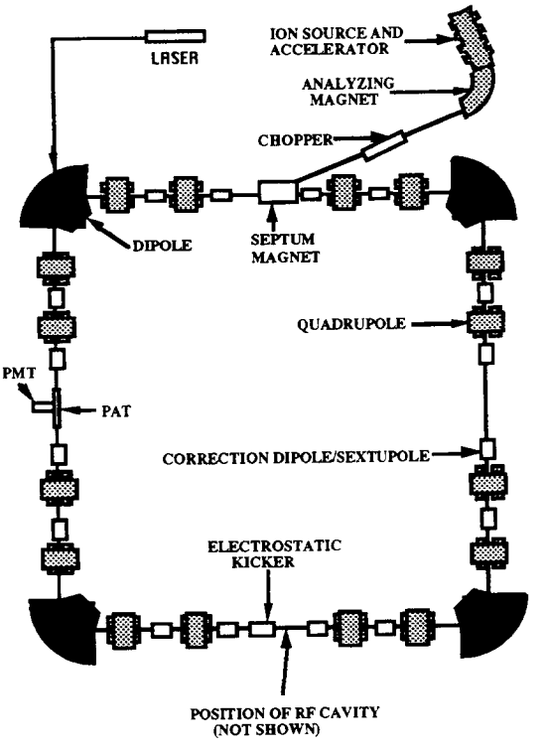

Figure 2. Layout of the ASTRID storage ring. The circumference is 40 m

4. DEMONSTRATION OF BUNCHED-BEAM COOLING

A typical cooling cycle starts with DC beam injected into the ring with the RF cavity operating CW. The laser is also operating CW at injection and is detuned -3 GHz, that is, initially in resonance with particles having $\delta P/P = -1x10^{-3}$. After a delay of two seconds, the laser is swept in frequency at rate of 3 GHz per second. As the laser is sweeping, the post-acceleration tube is scanned rapidly at intervals of 50 ms. The resulting fluorescence signal is thus a series of snapshots of the beam's developing velocity distribution as the cooling proceeds. Figure 3 shows the time development of the velocity distribution measured in this way. The plot shows 15 measurements of the beam's velocity distribution at intervals of 50 ms. The synchrotron period for the applied RF voltage is about 60 revolutions, or 2.7 ms (for small synchrotron oscillation amplitude). The decrease in peak signal for the scan just before 3.1 s delay reflects the fact that the laser has crossed the synchronous energy and has begun to accelerate the beam out of the RF bucket. The laser scan was not halted in this measurement.

Figure 4 shows the velocity widths extracted from the fluorescence signal in Figure 3. In the interval recorded, the velocity spread has been reduced by a factor of 10. The minimum corresponds to $\delta P/P \sim 5x10^{-5}$, or, in terms of longitudinal temperature, approximately 1 K. Note that this minimum could be optimized by stopping the laser scan at various points before the laser crosses the synchronous energy; this has not yet been attempted.

The other longitudinal phase space coordinate is monitored by measuring the bunch length as the laser scan proceeds. Figure 5 shows a typical oscilloscope trace of the signal from the beam pickup. For the low-velocity ($v \sim 9x10^5$ m/s) magnesium ions, the bunch lengths are much longer than the time constant of the detection electronics. The bunch widths were measured with and without laser cooling for various times. The bunch width with no laser cooling is found not to change in the time scale of interest. In Figure 6, the time development of the bunch width during the cooling scan is depicted. Each point represents an average over many bunches. The bunch length decreases by about a factor of four during the cooling. That this number is smaller than the associated decrease in energy spread may indicate that the minimum bunch length is limited by the longitudinal space charge force in the bunch [7]. This has not yet been studied systematically. Figure 6 also indicates a growth in bunch length (the point to the extreme right of the figure) as the laser crosses the resonant frequency corresponding to the synchronous velocity .

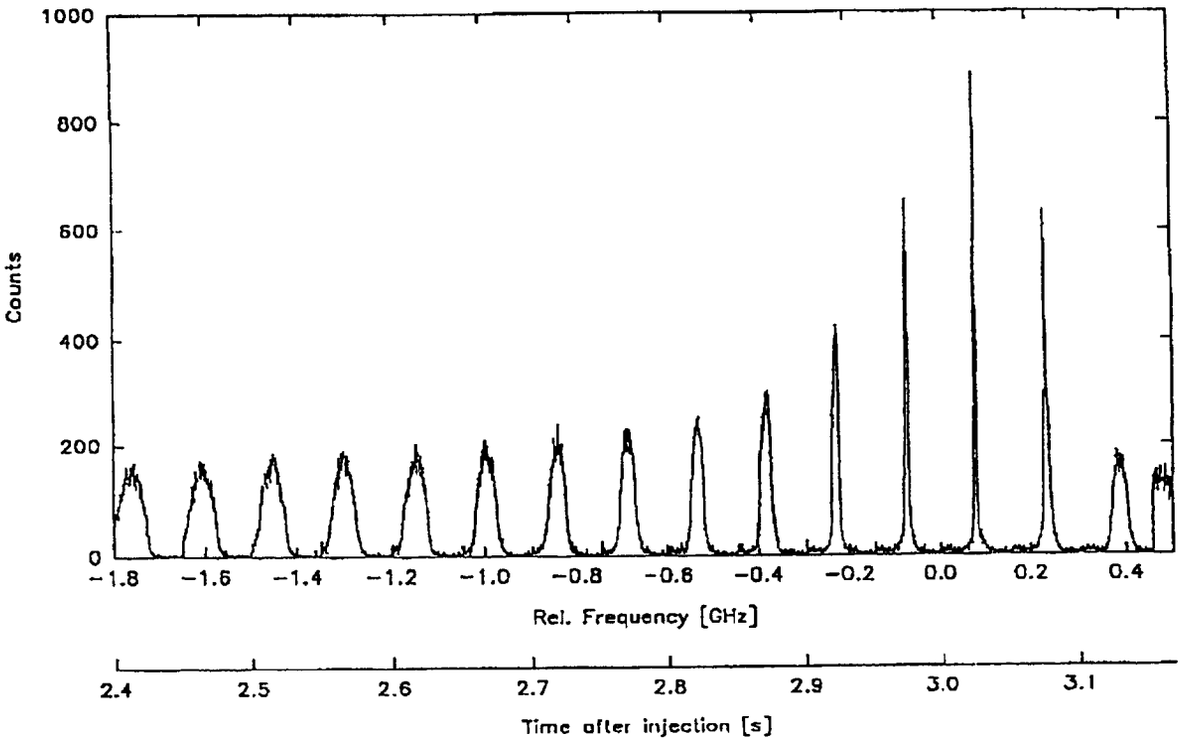

Figure 3. Time history of the ion velocity distribution during laser cooling. Each peak is an independent laser fluorescence intensity vs. velocity measurement. The numbers on the abscissa are the laser detuning at the time the measurement is made. The measurements are separated in time by 50 ms. The beam current is about 0.5 μA.

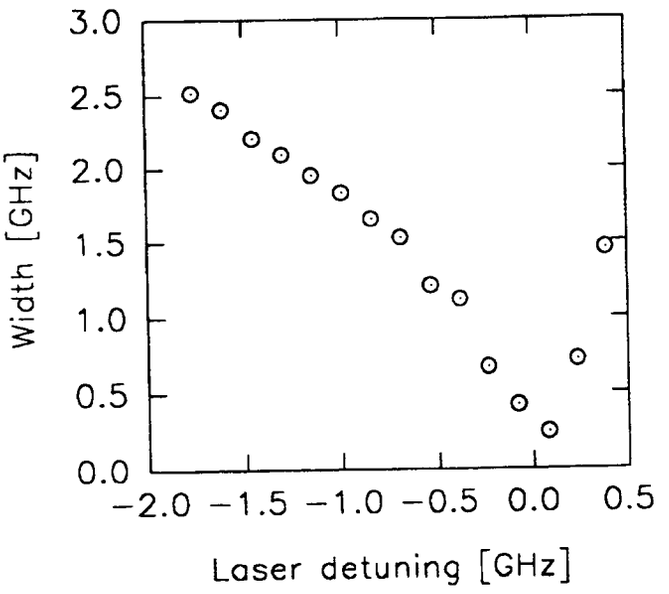

Figure 4. Width of the velocity distribution vs. laser detuning for the cooling scan depicted in Figure 3.

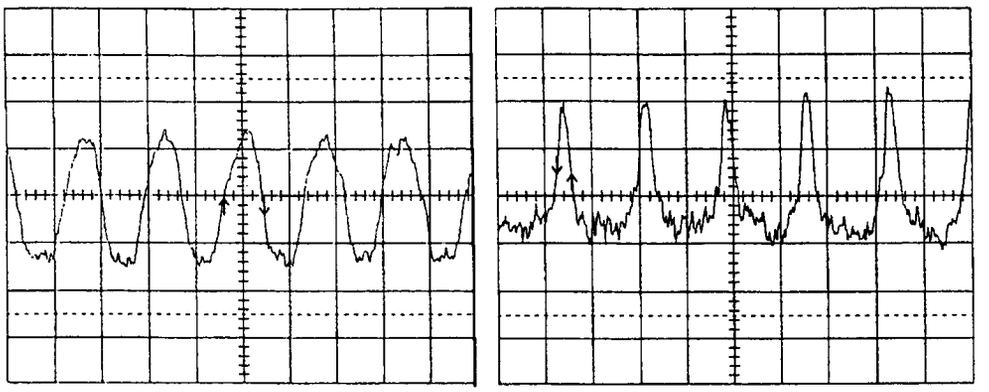

Figure 5. Bunch shapes measured early in the laser scan (detuning -2.0 GHz, left) and towards the end of the cooling process (detuning -0.3 GHz, right). Both traces are 1μs/div. and 10 mV/div.

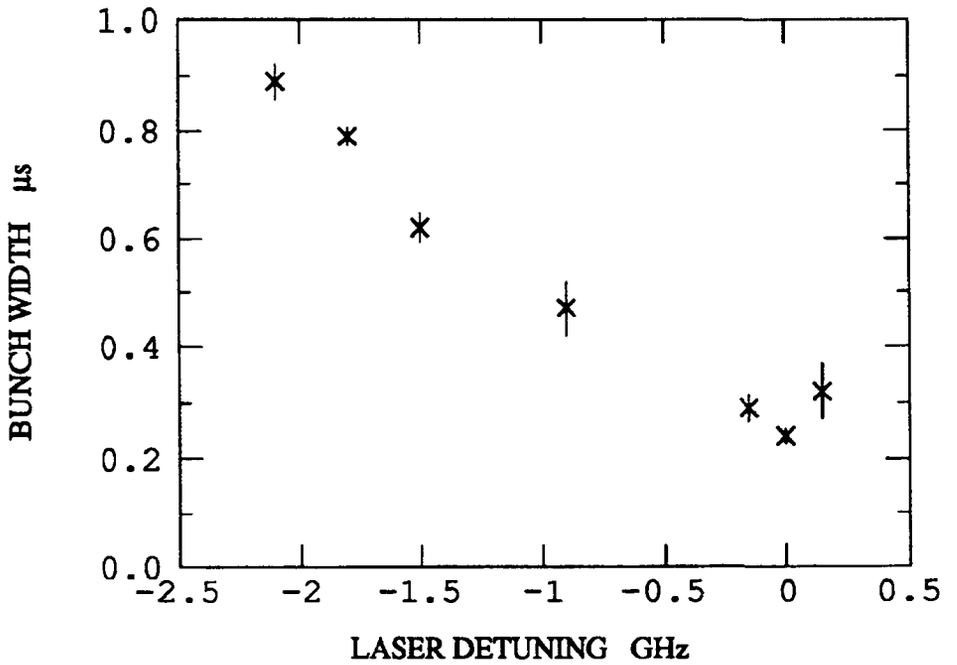

Figure 6. Bunch width (FWHM) vs. laser detuning measured during the cooling scan depicted in Figure 3.

5. CONCLUSIONS AND FURTHER STUDY

We have demonstrated the feasibility of laser cooling of bunched beams in a storage ring. Reduction of both beam energy spread and bunch width have been directly observed. Measurement of the beam velocity spread by a laser fluorescence technique is shown to be a unique, unambiguous method for diagnosing the effectiveness of the cooling. These techniques have great potential for contributing to the study of the dynamics of bunched beams in the space charge limited regime, such as observed in the experiment in the IUCF Cooler Ring [7]. The laser cooling method also offers considerable freedom in the preparation of a cold bunch, since the final momentum spread in the beam can be set by simply choosing the final detuning of the laser relative to the synchronous particle (assuming that no competing heating mechanisms are important).

In the near future, more systematic measurements of bunched beam laser cooling will be carried out in ASTRID. Of interest is the dependence of the bunch shape on the beam intensity. The minimum momentum spread obtainable must also be determined, and the effect of phase noise heating from the RF system must be addressed. The addition of a second UV laser in ASTRID (December 1993) should enhance the cooling and diagnostic capabilities in the ring.

REFERENCES

* Also at Mikroelektronik Centret, DTH, Bldg. 345 E, DK-2800 Lyngby, Denmark
† Argonne National Laboratory, Argonne, IL 60439, and University of Chicago, Chicago, IL 60637
‡ Max-Planck Institut für Kernphysik, D-6900 Heidelberg, Germany

[1] S. Schröder et al., Phys. Rev. Letts. **64**, 2901 (1990)

[2] J.S. Hangst, M. Kristensen, J.S. Nielsen, O. Poulsen, J.P. Schiffer, and P. Shi, Phys. Rev. Letts. **67**, 1238 (1991)

[3] A. Rahman and J.P. Schiffer, Phys. Rev. Letts. **57**, 1133 (1986)

[4] J.S. Hangst, Ph.D. Thesis, The University of Chicago, (1992), published as Argonne Report ANL/PHY-93/1

[5] J.S. Nielsen, J.S. Hangst, O Poulsen, J.P. Schiffer, P. Shi, and B. Wanner, "Laser Cooling of $^{24}Mg^{+}$ in the ASTRID Storage Ring", these proceedings.

[6] S.P. Møller, in proceedings of the 1991 IEEE Particle Accelerator Conference, IEEE 91CH3038-7, 2811 (1991)

[7] T.J.P. Ellison et al, Phys. Rev. Letts. **70**, 790 (1993)

EFFECTS OF INTRABEAM SCATTERING IN LASER COOLING EXPERIMENTS AT THE TSR

H.-J. Miesner, M. Grieser, R. Grimm, A. Gruber, D. Habs, W. Petrich, D. Schwalm, B. Wanner, H. Wernøe
Max-Planck-Institut für Kernphysik and Physikalisches Institut der Universität Heidelberg, D-69029 Heidelberg, Germany

ABSTRACT

Two substantial new effects of intrabeam scattering have been observed in a laser-cooled 7.3 MeV $^9Be^+$ beam. A loss of laser-cooled ions out of the velocity capture range of the cooling force occurs, which we can explain by single binary collisions transfering a large amount of kinetic energy out of the transverse motion into the longitudinal one. After a certain cooling time, however, this loss is surprisingly found to disappear. As a second important effect, we have observed an indirect transverse cooling of the longitudinally laser-cooled ion beam.

1. INTRODUCTION

Standard laser cooling techniques applied to stored ion beams allow a very fast reduction of the longitudinal beam temperature to extremely low values, but do not directly affect the transverse motion of the ions. Therefore laser cooling typically results in a longitudinally extremely cold beam which is transversely still hot. In this pronounced thermal non-equilibrium, the connection of the laser cooling process with the transverse ion motion by intrabeam scattering (IBS) processes leads to new interesting effects, occuring in addition to a simple heating of the longitudinal motion. In this paper, we focus on new surprising findings resulting from effects of IBS in a longitudinally laser-cooled beam of $^9Be^+$ ions stored in the Heidelberg Test Storage Ring (TSR) at 4.3% of the velocity of light.

2. LOSSES OF LASER-COOLED IONS

Suitable starting conditions [1] for the laser cooling process are reached by electron precooling the 7.3 MeV $^9Be^+$ beam for about 12 s. This reduces the ion beam diameter to ~ 1 mm (FWHM), corresponding to a transverse temperature of $T_\perp \approx 6000$ K. Laser cooling of typically 10^7 circulating ions is then performed in the following way (see also [1]): The ions are decelerated by an induction accelerator (INDAC) until they come into optical resonance with the cooling laser. Here the laser cooling sets in and the ions are kept in a force balance between the resonant accelerating laser force and the constant decelerating INDAC force. The total force acting on the ions as a function of the longitudinal velocity is shown in Fig. 1.

Of crucial importance for the following discussion is the *limited velocity capture range* in this cooling scheme: To be pushed towards the stable point at v^* the ion velocity must not be lower than $v^* - \Delta v_c$ (see Fig. 1). If an ion once enters the region $v < v^* - \Delta v_c$ it is more and more decelerated by the INDAC force and lost for the cooling process. In the following we refer to Δv_c as the *critical capture range* of the laser cooling scheme.

When performing a laser-cooling experiment, the laser frequency is chosen in such a way that the stable point v^* lies below the whole initial velocity distribution determined by the

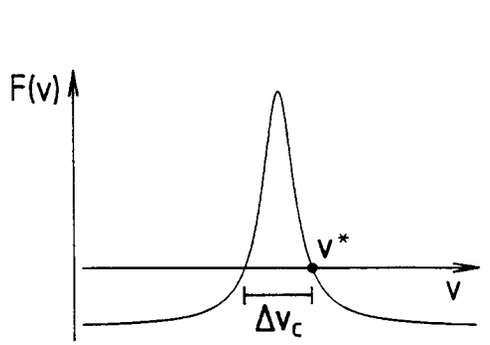

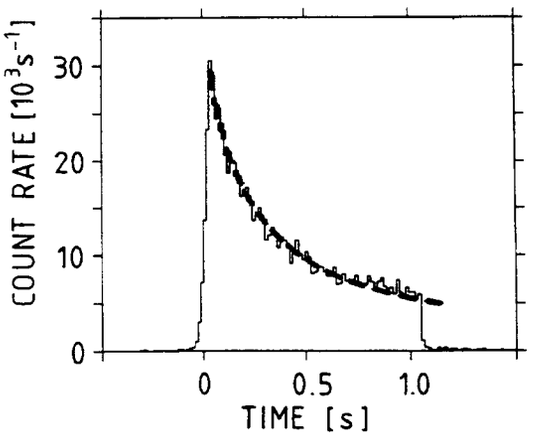

Figure 1: The longitudinal cooling force as a combination of the Lorentzian-shaped laser force and the constant counteracting auxiliary force provided by the INDAC. v^* is the *stable point* to which the ions are cooled, and Δv_c denotes the *critical capture range* for ion velocities below v^*.

Figure 2: Time dependence of the emitted fluorescence light, reflecting the number of ions taking part in the laser-cooling process. The dashed line is a fit corresponding to Eq.(2). The sudden drop of the fluorescence at $t \approx 1$ s is due to the finite ramping time of the INDAC.

electron precooling. Therefore one would naively expect that all ions, after having reached the stable point, can permanently be laser cooled. In this case, the fluorescence of the cooled ions, being proportional to the number of ions participating in the cooling, could be expected to decrease slowly with the beam lifetime (about 10 s). In practically all our experiments, however, we observe a different behavior: The fluorescence of the laser-cooled ions decreases much faster than one would expect from the beam lifetime. A typical example is shown in Fig. 2.

The observed decrease of the fluorescence light is due to a substantial loss of ions out of the velocity capture range, not obeying an exponential decay law. We attribute this behavior to IBS: A single scattering process between two ions diverts transverse momentum into the longitudinal degree of freedom. An electron-cooled $^9Be^+$-beam still has a transverse temperature of $T_\perp \approx 6000$ K, resulting in a mean velocity of $\langle v_\perp \rangle \approx 2300$ m/s. Therefore, after such a collision, a change of the longitudinal velocity that is large compared to the critical capture range Δv_c (typically being in the range 10-100 m/s) is no surprise. This loss due to single binary collisions of *two* ions can be described in a simple model by the the differential equation:

$$\frac{dN}{dt} = -rN^2 \,, \tag{1}$$

where r denotes the loss constant. If the laser cooling starts at $t = t_0$ with the initial particle number N_0, the solution is

$$N(t) = (r * (t - t_0) + 1/N_0)^{-1} \,. \tag{2}$$

This nicely fits to the experimental behavior (ses dashed line in Fig. 2), at least within the ramping time of the INDAC.

We have systematically investigated the loss process by measuring the loss constant r as a function of the critical capture range Δv_c for various laser intensities. The corresponding data are displayed in Fig. 3(a), assuming $N_0 = 1.0 \times 10^7$.

Following the IBS-theory of [2], one can calculate the cross section for a binary collision and the resulting loss constant r for the escape of one of the ions out of the given critical capture

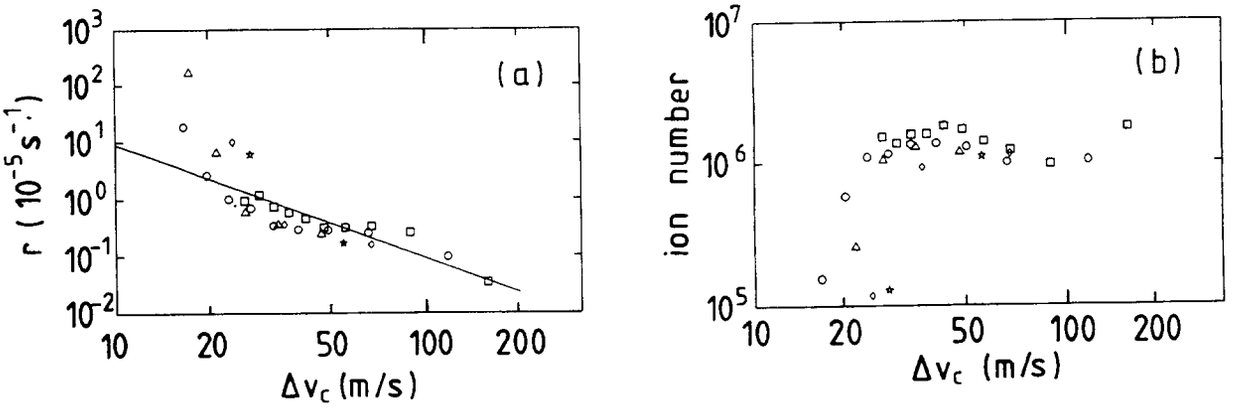

Figure 3: (a) The loss constant r and (b) the number of laser-cooled ions after the disappearance of the loss measured as a function of the critical capture range Δv_c for various values of the laser power (□ - 20mW, ○ - 10mW, △ - 5mW, ◇ - 3mW, large ⋆ - 2mW). The solid line in (a) is the result of an IBS calculation assuming single binary collisions.

range Δv_c of the cooling force. Under the assumption that both ions initially have the same longitudinal velocity v^* (stable point), one finds in the limit $\langle v_\perp \rangle \gg \Delta v_c$:

$$r = \frac{A}{\Delta v_c^2} \,. \tag{3}$$

The constant A is determined by the specific ion species, the ring lattice and the transverse beam temperature and, for our experimental parameters, is calculated to $A = 9 \times 10^{-3}\,\mathrm{m}^2/\mathrm{s}^3$. As shown by the solid line in Fig. 3(a), this agrees quantitatively with our experimental data for $\Delta v_c \geq 25$ m/s. At lower values of the critical capture range the loss is much stronger than we can understand by single binary collisions. We are presently investigating whether this can be explained by multiple scattering processes leading to a longitudinal diffusion or by the longitudinal heating caused by the laser itself.

Although the loss process described by Eq.(1) nicely fits to all our previous experiments, we have observed significant deviations in the most recent beam time, where the laser cooling process was greatly improved by much better optimizing the overlap of ion and laser beam. In these recent experiments longitudinal cooling rates (typically $\lambda_{||} \approx 10^4\,\mathrm{s}^{-1}$) about a factor of ten higher than in previous beam times were applied to the ion beam.

The typical behavior observed in these improved laser-cooling experiments is shown in Fig. 4. The inital loss stops after some time and the flourescence exhibits a plateau showing a constant number of laser-cooled ions. In practically all experiments of this last beam time, a significant loss occured only in the beginning of the cooling process; there, however, the loss was found to still follow the loss equation (1) in a wide parameter range. This suggests that we still understand the nature of the loss process by single binary collisions, but that something happens in the beam in addition to that. Another interesting experimental finding in this context is the number of laser-cooled ions after the disappearance of the loss: Fig.3(b) shows that for $\Delta v_c > 25\,\mathrm{m/s}$, where the binary collision model well explains the loss, the number of cooled ions was observed to be *independent* of both the critical capture range Δv_c and the laser intensity.

The explanation for this surprising behavior might be connected with an indirect transverse cooling of the ion beam by a heat transfer via IBS out of the hot transverse degrees of freedom into the cold longitudinal one. If this leads to a reduction of the transverse velocities to values

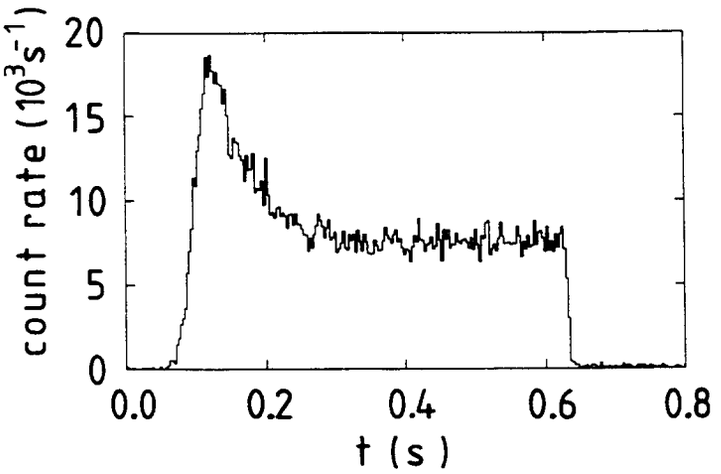

Figure 4: A typical result from the last beam time showing the time dependence of the emitted fluorescence during the laser-cooling process.

less than the (longitudinal) critical capture range Δv_c, then binary collisions can hardly lead to an escape from the capture range and the loss must stop. Simulations using an IBS computer code [3] confirm that an indirect transverse cooling should in fact occur; for our experimental parameters and a typical longitudinal cooling rate of $\lambda_{||} = 10^4\,s^{-1}$, however, a strong transverse cooling effect within ~ 200 ms, as necessary to explain the disappearance of the loss in Fig. 4, would require an initial transverse beam temperature below ~ 1000 K [3]. As another possible explanation, one could also imagine that a longitudinal ordering might set in which leads to an additional suppression of the IBS. Quite surprisingly, the constant number of laser-cooled ions observed after the disappearance of the loss in a wide parameter range corresponds to the maximum number of ions which can form a simple linear chain: For the relevant parameter, the dimensionless linear particle density λ defined in [4], we can derive $\lambda = (0.5 \pm 0.2)$ in comparison to $\lambda < 0.71$ for a string of ions. On the other hand, the maximum λ for which a strong suppression of intrabeam scattering was observed during electron cooling at the NAP-M ring [5] was about 4.0, which roughly corresponds to the region where a transition from a one-dimensional structure to a three-dimensional structure ($\lambda = 3.1$) occurs. Since the loss process in laser cooling and the onset of strong heating during electron cooling are quite different processes, the observed particle thresholds may be quite different, but both point to one-dimensional beam structures.

3. INDIRECT TRANSVERSE COOLING

In the last beam time, we have begun to investigate the indirect transverse cooling expected as a result of longitudinal laser cooling in connection with IBS. The standard laser cooling procedure with counteracting INDAC force was applied to the electron precooled beam for 10 s with a longitudinal cooling rate of $\lambda_{||} \approx 10^3\,s^{-1}$. In the last 5 s of the laser cooling process the vertical beam profile was measured by the TSR beam profile monitor [6]. In corresponding reference measurements, the same procedure was performed with both the laser and the INDAC switched off. Fig. 5 shows the summarized results of several pairs of cooling and reference measurements. The beam profile with laser cooling (bold line) is clearly narrower than the reference profile (thin line). Taking into account the resolution of the beam profile monitor of 0.6 mm (full width at half maximum), we derive a reduction of the transverse temperature from 6000 K to about 4000 K. This observation is close to the results of the IBS computer simulations presented in [3].

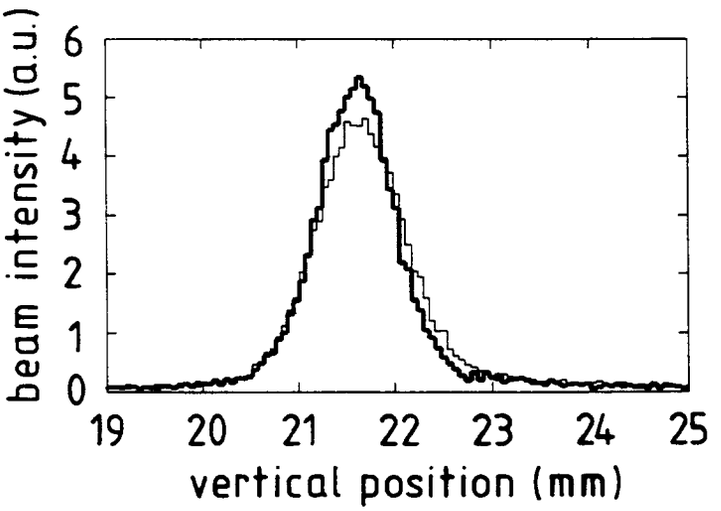

Figure 5: First observation of an indirect transverse laser-cooling effect. The vertical beam profiles recorded with and without laser cooling are displayed by the thick and thin line, respectively.

4. CONCLUSION

Our experimental results on 7.3 MeV $^9Be^+$ ions demonstrate the strong influence of IBS processes in laser cooling of stored ion beams. For the typical situation of the longitudinally extremely cold but transversely still hot beam, two important consequences of IBS have been identified: (i) Single binary collisions kick laser-cooled ions out of the capture range of the cooling force so that they are lost for the cooling process. (ii) The ion beam is also cooled transversely, as we have observed for the first time.

In the near future, our investigations will concentrate on the dynamics and the limits of the indirect transverse cooling. This should also clarify in how far this effect or a possible longitudinal ordering is responsible for the surprising disappearance of the IBS losses observed after a certain cooling time.

This work was supported by the Bundesministerium für Forschung und Technologie under contract No. 06HD525I.

References

[1] W. Petrich et al., Phys. Rev. A **48**, No.3 (1993);
R. Grimm, these proceedings.

[2] A. Piwinski in *Frontiers of Particle Beams*, edited by M. Month and S. Turner, Lecture Notes in Physics 296 (Springer, Berlin Heidelberg, 1988).

[3] B. Hochadel et al., these proceedings.

[4] R.W. Hasse and J.P. Schiffer, Ann. Phys. **203**, 419 (1990).

[5] Dementiev E.N. et al., Sov. Phys. Tech. Phys. **25**, 1001 (1980).

[6] B. Hochadel et al., submitted to Nucl. Instr. Meth.

NEW LASER COOLING SCHEMES BASED ON OPTICAL ADIABATIC EXCITATION

B. Wanner, M. Grieser, R. Grimm, A. Gruber, D. Habs, H.-J. Miesner, J.S. Nielsen [1], *W. Petrich, D. Schwalm, H. Wernøe*
Max-Planck-Institut für Kernphysik and Physikalisches Institut der Universität Heidelberg, D-69029 Heidelberg, Germany

ABSTRACT
By means of appropriately shaped and biased drift tubes and a collinear cw laser beam an adiabatic inversion of fast stored ions can be realized. Experimental results obtained at the TSR with 13.4 MeV $^7Li^+$ ions are in good agreement with theory. The force resulting from the adiabatic excitation offers new possibilities for laser cooling in storage rings. A stimulated force may be created allowing for cooling via weak optical transitions. Furthermore this force provides a very large capture range which is essential for effective indirect transverse cooling.

1. INTRODUCTION

The so-called adiabatic inversion [1] is a well-known process, which allows to obtain a nearly complete population inversion in an optical transition. This process is based on a frequency sweep through resonance and is not very sensitive to the exact laser frequency and intensity.

Adiabatic excitation of an ion beam can experimentally be achieved in a simple way: a cw laser counterpropagating to the ions and an appropriately shaped and biased drift tube are necessary. The local acceleration inside the electrostatic potential induces a velocity change and, via the Doppler effect, the required laser frequency sweep in the ion rest frame. The excitation process is inherently connected with a momentum transfer of $\hbar k$. For ions in a storage ring the force created in this way offers new and interesting possibilities for laser cooling.

2. OBSERVATION OF ADIABATIC INVERSION

In a recent experiment at the Test Storage Ring (TSR) in Heidelberg we have investigated this scheme with metastable $^7Li^+$ ions stored at an energy of 13.4 MeV. $^7Li^+$ provides a closed transition $2^3S_1(F=5/2) \rightarrow 2^3P_2(F=7/2)$ at a wavelength of 548.6 nm and a lifetime of τ=43 ns. The electrostatic potential was realized with a drift tube array consisting of six parts, which could invidually be connected to different voltages and which created a potential as shown in figure 1. The slow increase was designed to realize a smooth frequency sweep leading to an excitation by adiabatic inversion, whereas the steep drop is crucial to avoid a subsequent deexcitation of the ion which would cancel the net momentum transfer. The total length of the potential of 200 mm was chosen to be shorter than the distance of 840 mm an ion travels during one lifetime so as to minimize the effect of spontaneous emission.

The ions were first electron cooled to reduce the transverse temperature and afterwards laser cooled with the usual scattering force. This force was created by an argon-ion laser whose 514 nm line matches the Doppler-shifted resonance frequency and it was counterbalanced by an auxiliary force provided by the induction accelerator. In this standard laser cooling scheme

[1] permanent address: Institut of Physics, University of Århus, DK-8000 Århus C, Denmark

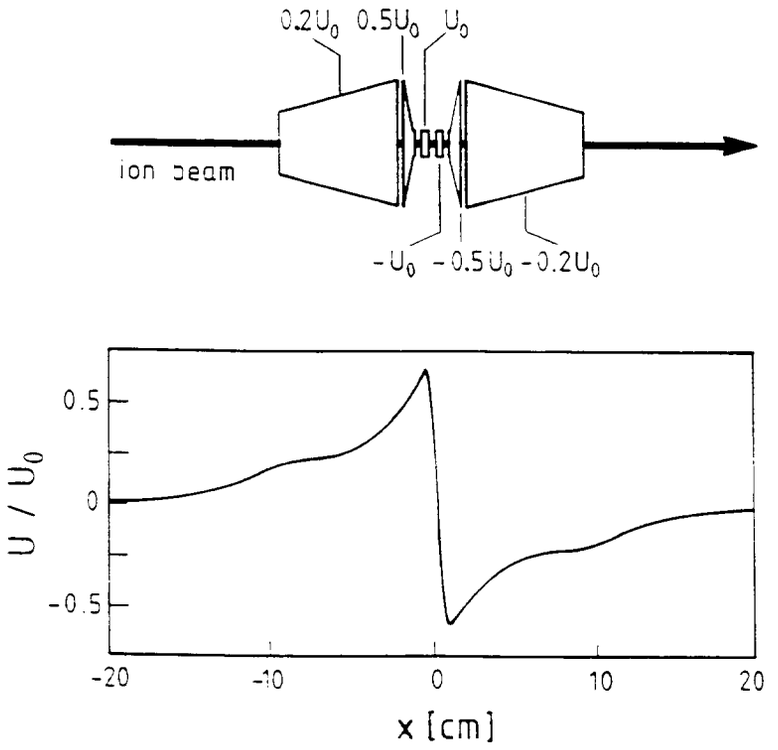

Figure 1: Electrostatic potential to achieve an excitation by optical adiabatic inversion. The potential is created by a drift tube array consisting of the six parts sketched on top of the potential curve.

the longitudinal width of the ion distribution was reduced to $T_{||} < 350$ mK. The practically monoenergetic ion beam prepared in this way was subjected to a transient interaction with a counterpropagating intensive tunable ring dye laser inside the electrostatic potential. With a photomultiplier situated right behind the drift tubes we detected the rate of spontaneously emitted photons, which is proportional to the excitation probability. To avoid modifications of the velocity distribution due to the interaction with this strong laser, it was chopped with a frequency close to 600 Hz and at a duty ratio of 1:25. The background due to scattered light was strongly reduced by synchronously gating the detection and by blocking the cooling laser during the short intervals of transient interaction. The experiment was performed for a variety of potentials and laser intensities. The latter determine the Rabi frequency which is the characteristic parameter for all optical interactions of ions with laser light and which is proportional to the square root of the laser intensity. An absolut calibration was provided by a measurement with grounded drift tubes. As the transition was strongly saturated the heigth of the saturation broaded line defined an excition probability of 50% whereas its width supplied the effective Rabi frequency.

For a saturation parameter of G=2000 (which corresponds to a Rabi frequency of $\omega_r = 31\,\tau^{-1}$) and a potential of U_0=800 V applied to the drift tube array the measured excitation probability is shown in figure 2(a). For comparison the saturation-broaded line obtained with grounded drift tubes is added with a thin line. One observes an excitation extending over an nearly three times larger detuning range with the potential applied. Furthermore the maximum excitation probability approaches 80%, i.e. a clear population inversion can be observed. The two peaks correspond to an adiabatic excitation in the negative and the positive part of the potential respectively. At zero potential the ions are in resonance with the laser field over several meters, all over the magnetic field free region of the experimental section, and the steady-state excitation of 0.5 is detected. The result of a numerical solution of the Optical Bloch Equations

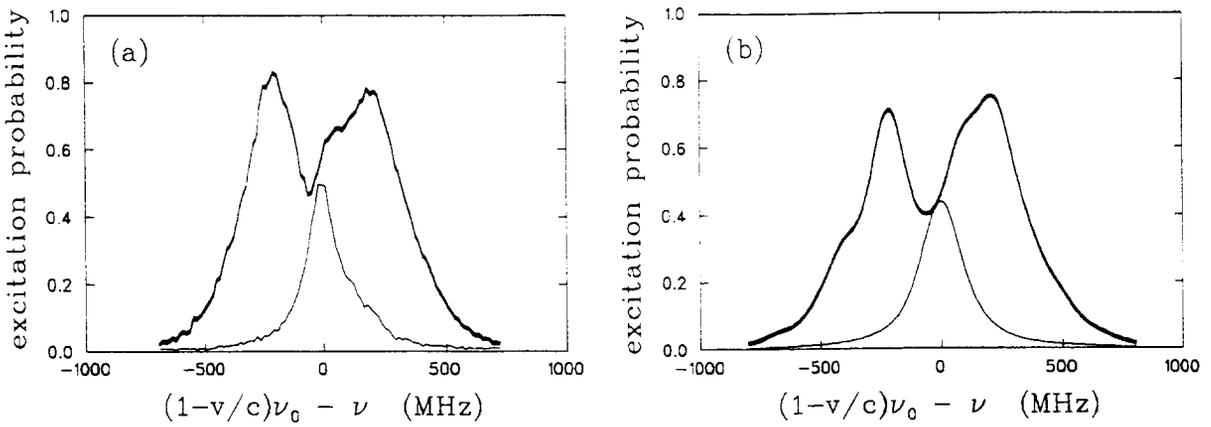

Figure 2: Excitation probability as a function of the detuning of the laser frequency ν with respect to the Doppler-shifted resonance ν_0. The saturation parameter is G=2000 and the applied voltage U_0=800 V. (a) experimental result and (b) numerical calculation based on the Optical Bloch Equations. For comparison the saturation-broaded line measured with grounded electrodes is drawn with a thinner line.

with the realistic potential, shown in figure 2(b), is in good agreement with the experimental data.

The process of adiabatic excitation may also be described in the "dressed states" picture [2]. The "dressed states" are energy eigenstates of the coupled atom-field system. They coincide with ground- and excited state for large detunings and form an avoided crossing at resonance. The probability for adiabatic transitions from the ground- to the excited state and vice versa is given by the Landau-Zener-formula:

$$p = 1 - \exp(-\pi \frac{\omega_r^2}{2|\dot{\Delta}|}) \tag{1}$$

As $\omega_r^2 \sim G$ and the sweep rate $|\dot{\Delta}| \sim U_0$ a scaling law of the form $p = f(\frac{G}{U_0}) = 1 - \exp(-const\frac{G}{U_0})$ is expected. This could indeed be verified for a large number of saturation parameters and potentials, see figure 3 . The dotted line describes the probability for an adiabatic excitation in the smooth part of the potential. For high saturation and low potentials however a finite probability for adiabatic transitions back to the ground state induced inside the steep drop of the potential occurs. This effect has been accounted for by the curve displayed with a solid line. The two constants, which depend on the gradient of the potential at the avoided crossing, have been determined by a least-square-fit to the experimental data.

3. NEW LASER COOLING SCHEMES

A stimulated force may be created using two counterpropagating lasers alternately exciting and deexciting the ion, see figure 4 (a). In each cycle 2 $\hbar k$ are transfered to the ion, the first one related to the absorption of a photon and the second one due to recoil in connection with the deexcitation stimulated by the counterpropagating laser beam. Such a stimulated force is of particular interest for laser cooling of heavy and highly charged ions, where only weak optical transitions are within the wavelength range accessible with lasers.

Adiabatic excitation is also important for improving ordinary cooling via strong E1 transitions. A simple cylinder can be used for this purpose. The idea is to adiabatically excite the ions in the increasing field and to let them decay spontaneously in the field free region. The next adiabatic excitation can then be performed when the ions leave the drift tube, see figure 4 (b).

In the next beamtime this scheme will be realized with $^9Be^+$ at the TSR. The high decay

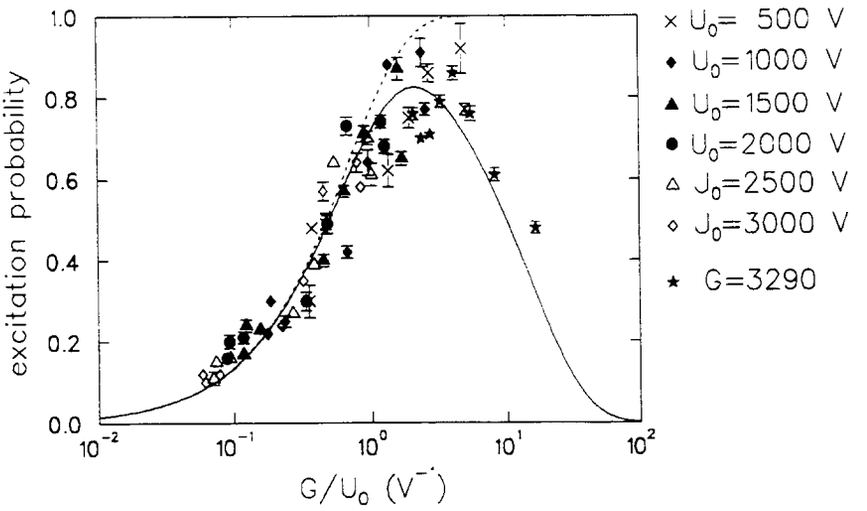

Figure 3: Maximum excitation probability as a function of G/U_0. The dotted curve describes the excitation probability for the case of a single adiabatic excitation inside the smooth part of the potential. At higher intensities and lower potentials adiabatic transitions in the steep part become relevant. This is taken into account by the curve drawn with a solid line.

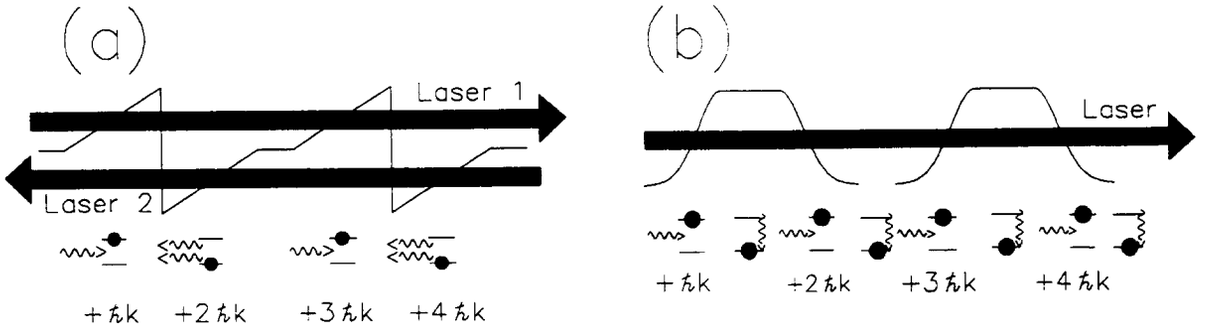

Figure 4: New laser cooling schemes based on adiabatic excitation. The velocity of ion on its way across the experimental section is displayed (thin line). By using two counterpropagating lasers (a) a stimulated force may be created which can further be increased by the use of several drift tube arrays. On the contrary, if the lifetime of the excited state is short enough, simple cylinders can be used, allowing for a spontaneous decay of the ion between subsequent excitations in the fringe field of the drift tube (b).

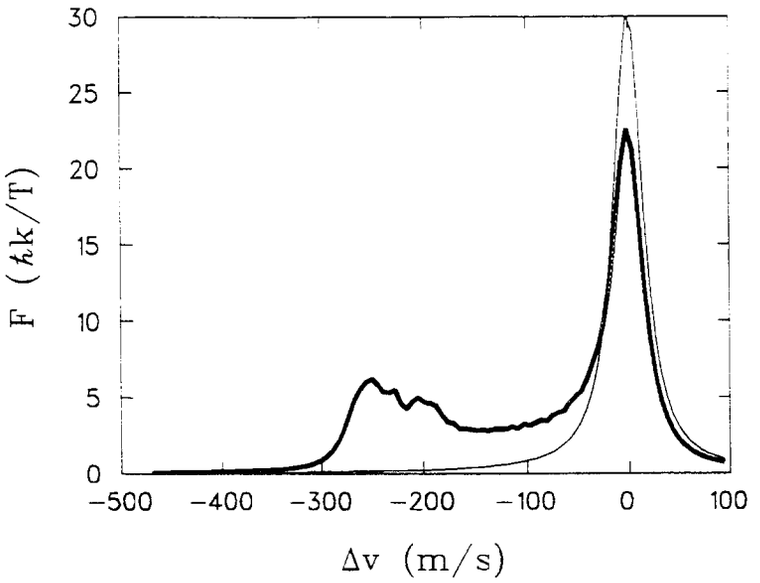

Figure 5: Calculated ring-averaged force on 7.5 MeV $^9Be^+$ under realistic conditions as it results from an adiabatic excitation in the electrostatic field of four cylinders and the scattering force in the field free area. The saturation parameter is G=30 ($\omega_\tau = 3.8\,\tau^{-1}$) and the applied potential U_0=0.3 kV. The force is given in units of photon momenta per round trip T. The capture range of this combined force is much larger than the one of the scattering force alone, thin line. Note that the force is ring-averaged so that the scattering force is stronger in the case of grounded drift tubes where the interaction length is larger.

rate of the closed transition in this ion of $\gamma = 2\pi \times 19.4$ MHz implies that all four drift tubes available in the experimental section of the TSR may be used. The ring-averaged force resulting from this scheme has been calculated for realistic parameters and is shown in figure 5 (thick line). With an auxiliary force of up to 2.5 $\hbar k$ per roundtrip the capture range is considerably larger than the one of the scattering force alone (thin line). For laser cooling of $^9Be^+$, where a strong loss of ions from the cooling process has been observed in recent experiments at the TSR [3], this feature is very much requested. One might even think of a two-step-process, where the potential is switched off and the auxiliary force encreased as soon as all ions have been cooled by the force due to adiabatic excitation. Indirect transverse laser cooling is expected to become much more efficient with this new force.

Supported by BMFT under contract No. 06HD525I

References

[1] L.Allen and J.H. Eberly, "Optical Resonances and Two-Level-Atoms" (Dover, New York 1987), and ref. therein.

[2] C. Cohen-Tannoudji, J. Dupont-Roc, G. Grynberg, "Atom-Photon Interactions: Basic Processes and Applications" (Wiley, New York, 1992), Chap. VI.

[3] H.J. Miesner et al., these proceedings.

THEORY OF LONGITUDINAL SCHOTTKY SPECTRA OF ORDERED ION BEAMS IN A STORAGE RING

V.V.Avilov and I.Hofmann*
GSI Darmstadt, D-6100 Darmstadt, Germany

Abstract

The longitudinal Schottky spectrum of an ultra-cold ion beam in a storage ring is calculated in the frame of harmonic oscillations of a 1d Coulomb lattice. It is assumed that the extremely high cooling rate required to bring the beam into a one-dimensional ordered chain can be provided by electron or laser cooling. The Schottky spectrum measured by the pick-up system consists of bands located near the harmonics of the revolution frequency of the beam. The total intensity of each band characterizes the temperature distribution of the phonons in an ionic chain. The amplitude and the width of the peaks in the spectrum are a function of the strength of relaxation processes (cooling and heating) as well as the Coulomb correlations, rsp. ordering. It is suggested that a careful analysis of these spectra could be a signature of the presence of 1d ordering in the beam.

1 Introduction

Electron cooling experiments at Novosibirsk [1] and more recently in the TSR storage ring at Heidelberg [2] and in the ESR storage ring at GSI [3] have shown that extremely small momentum spreads (below 10^{-6}) are possible for small intensities (typically $10^5 - 10^6$ ions). The temperatures of such beams is of the order of a $1K$ in beam direction, but several orders of magnitude higher transversely. Even lower temperatures (tens of mK) can be achieved with laser cooling, which works in the longitudinal direction [4, 5]. The dimensionless parameter that determines the conditions for ordering is the ratio of the Coulomb energy of the lattice to the longitudinal temperature T

$$\Gamma = \frac{(eZ)^2}{dT}, \tag{1}$$

where Z is the ion charge and d the interionic distance.

Computer simulation using molecular dynamics indicates that for $\Gamma > 170$ there exists a longitudinal ordering [6].

If the number of particles in the storage ring is below a certain threshold an ordered structure could be a simple linear chain of ions. For observation it is necessary to determine the temperature, energy distribution and structure of the ion beam. The most useful method of beam diagnostics is the analysis of the Schottky spectrum measured by a pick-up system.

The aim of the present paper is to calculate the Schottky spectrum of beams with external ordering. We must take into account some peculiarities of the phonon spectrum of the ordered ionic chain:

(a) the interaction of the ions is described by the Coulomb, which is a long-range force;

(b) the ion beam in a storage ring is not an infinite chain, but a circle of typically 10^5 or more ions;

(c) this system can have distinct temperatures longitudinally and transversely; the temperature of the transversal motion can be up to 10^3 times greater then the temperature of the longitudinal motion;

(d) from a thermodynamical point of view, the state of a typical ion beam is far from equilibrium and we must take into account that the cooling of the ion beam by an electron (or laser) cooler is accompanied by heating of the beam due to intrabeam scattering (transfer of temperature from the transverse to the longitudinal direction), which increases with the density of the beam and the charge state of the ion.

Our treatment is based on the harmonic approximation for an N-ionic periodic chain with interionic distance d in equilibrium and circumference $L = Nd$.

2 Longitudinal pick-up diagnostic of the ion beam

In the pick-up (PU) system a beam of N ions with the coordinates z_j produces a signal

$$j(t) = j_o L \sum_{j=1}^{N} \phi(z_j(t) + v_o t). \tag{2}$$

where $z_j(t)$ is the coordinate of j-th ion in a system that moves with the mean velocity of the beam v_o relative to the PU, $\phi(z)$ is the normalized sensitivity function of the PU, $\int \phi(z)dz = 1$. The mean value $j(t)$ is j_o. As we will see later if the frequency ω is small enough, the Fourier transform of the PU signal $J(\omega)$ is sum of nonoverlapping bands located near harmonics of the ion beam revolution frequency $\omega_o = 2\pi v_o/L$. The mean square of $J(\omega)$ (the Schottky power spectrum) is

$$<\mid J(\omega) \mid^2> = \sum_M <\mid J_M(\omega - M\omega_o) \mid^2> \tag{3}$$

where $< ... >$ denotes a thermal averaging. There is a direct relation between the M-th band of the Schottky power spectrum and the dynamical structure factor (see [7])

$$<\mid J_M(\Omega_M) \mid^2> = 2\pi N j_o^2 t_o (\phi_M L)^2 S(Q_M, \Omega_M). \tag{4}$$

where $\Omega_M = \omega - M\omega_o$ and $Q_M = 2\pi M/L$ is the wave number of the M-th harmonic, ϕ_M is the M-the Fourie transform of $\phi(z)$, t_o is the time of the measurement. The dynamical structure factor is determined as

$$S(Q,\Omega) = \frac{1}{N} \int_{-\infty}^{\infty} e^{i\Omega t} \sum_{l,j=1}^{N} < e^{-iQ[z_j(t+t') - z_l(t')]} > \frac{dt}{2\pi}. \tag{5}$$

In the rest of the paper we calculate the contribution of an isolated M-th band and can omit the index M in Q_M and Ω_M.

3 Phonons in a two-temperature 1d Coulomb lattice

The phonon amplitude $a(q,t)$ is determined as a Fourier transform of $u_j(t)$ $(j = 1, .., N)$, the ionic displacements from the equilibrium [8]. The longitudinale phonon frequency $\omega(q)$ is determineed as

$$\omega^2(q) = \frac{1}{m} \sum_{l=-\infty}^{\infty} [1 - \cos(\frac{qdl}{N})] U''(dl). \tag{6}$$

Here $U(z)$ is the modifide Coulomb potential of the interionic interaction, m is the ion mass. A firs modification is the effective screening by the charges induced on the metallic vacuum chamber of a storage ring, which limits the interaction to a maximum screening length D of the order of the diameter of the vacuum chamber. We take the effectic screening factor as $\exp(-z/D)$.

The finite amplitude of transversal thermal oscillations $a_\perp$ also modifies the potential of the interionic interaction at distances of the order of $a_\perp$. This rather anharmonic system may be described within the method of self-consistent phonon approximation. In the description of a slow system (longitudinal phonons) we can use the potential averaged over the motion of a fast subsystem (transversal motion). The transversal focusing potential of the ion beam $U_b(r) = m\omega_b^2 r^2/2$ is characterized by the betatron frequency ω_b. The distribution of radial charge density can be assumed to be a Boltzmann distribution with the transverse temperature $T_\perp$.

$$\rho(\mathbf{r}) = \frac{eZ \exp(-r^2/(2a_\perp^2))}{2\pi a_\perp^2} \delta(z), \tag{7}$$

where $a_\perp = (T_\perp/(m\omega_b^2))^{1/2}$ is the amplitude of transversal oscillations. The potential of interaction of two "charged disks" (as proposed to explain the observations of the Novosibirsk experiment [1]) can be evaluated by using the Fourier transform technique. It provides

$$\omega^2(q) = \frac{2(eZ)^2}{md^3} \int_o^{\infty} dw w^2 e^{-(W a_\perp/d)^2} [\frac{1}{\exp(d/D + w) - 1} - \frac{e^{d/D+w}\cos(qd) - 1}{e^{2(d/D+w)} - 2e^{d/D+w}\cos(qd) + 1}]. \tag{8}$$

Typical longitudinal phonon spectra are shown in Fig. 1.

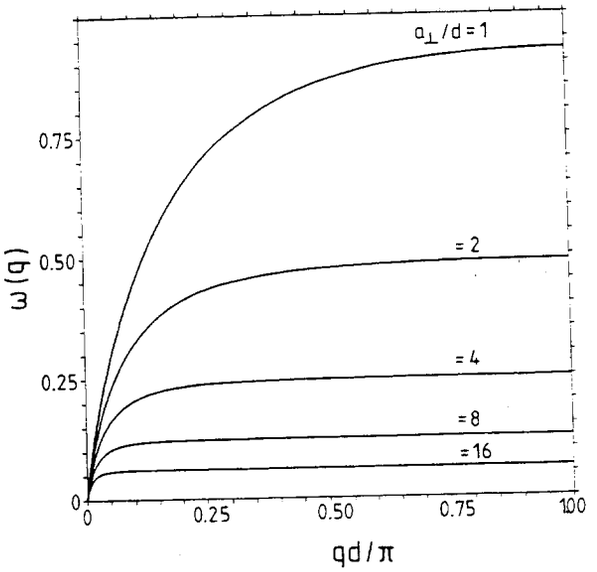

Fig.1 Typical longitudinal phonon spectra $\omega(q)$ (in units of $Z/(md^3)^{1/2}$) of the 1d Coulomb crystal for some values of the amplitude of transversal oscillations $a_\perp$. All curves are calculated for the ratio of the interionic spacing to the radius of effective screening of the Coulomb interaction $d/D = 10^{-3}$.

The phonon frequency tends to zero at small q as

$$\omega(q) \approx c_s \mid q \mid, \quad \text{where} \quad c_s^2 = 2(eZ)^2\Lambda/(md). \tag{9}$$

Here Λ the logarithm of the ratio of the screening length D to $\max\{d, a_\perp\}$. In any case typical values of Λ don't exceed 10.

We can use the phonon formalism to calculate all thermally averaged characteristics of the ion beam. The use of the basis of phonon amplitudes is preferable because on this basis the total potential energy is a simple sum of terms, each related to a single q and there are no terms containing the product of phonon amplitudes with distinct q. The mean square of the phonon amplitude is [8]

$$<\mid a(q,t) \mid^2>= \frac{T}{m\omega^2(q)}. \tag{10}$$

From Eq. (9) it follows that in thermal equilibrium the maximum of the phonon amplitude corresponds to the phonons with smallest q.

4 The dynamical structure factor of an ion beam

To obtain the mean value of $\exp(-iQdj - iQ[u_{j+l}(t+t') - u_l(t')])$ in Eq. (5) we can perform independent thermal averaging of each phonon mode q. The detales of calculation of the dynamical structure factor are published in [7]. In the case of an ion chain with no dissipation

$$S(Q,\Omega) = \sum_{k=-\infty}^{\infty} B_k \delta(\Omega - k\Omega_s), \tag{11}$$

where $\Omega_s = 2\pi c_s/L$ is the revolution frequency of a sound wave in the storage ring,

$$B_k = NH(\frac{M-k}{2})H(\frac{M+k}{2}) \quad \text{if } M \pm k \text{ are even numbers} \tag{12}$$

and $B_k = 0$ if $M \pm k$ are odd numbers,

$$H(k) = \frac{i}{2\sqrt{\pi\alpha}} e^{(-k/\alpha + i\pi\alpha/2)^2} \times [\mathrm{erf}(k/\alpha - i\alpha\pi/2) - \mathrm{erf}(k/\alpha + i\alpha\pi/2)], \tag{13}$$

and $\alpha^2 = M^2/(2\Gamma\Lambda N)$.

Typical profiles of the dynamical structure factor are presented in Fig. 2.

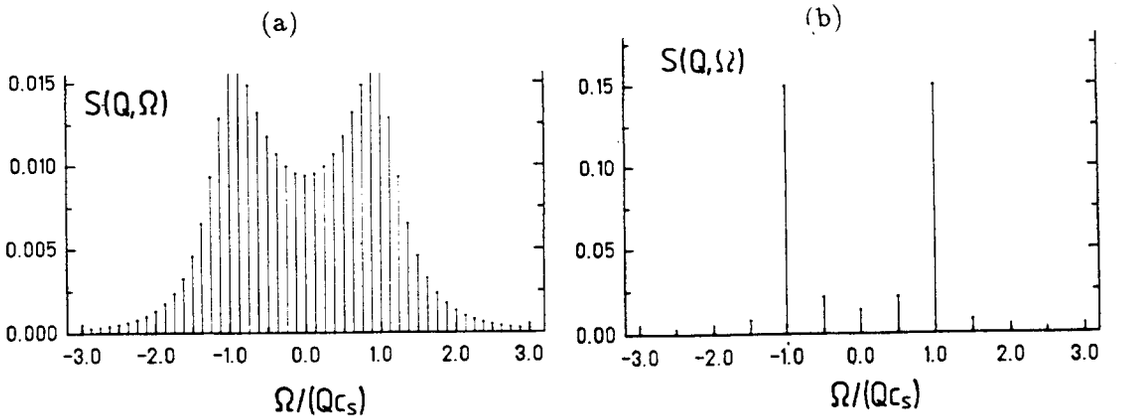

Fig.2 Typical plots of the dynamical structure factor of a 1d ordered beam in a storage ring without dissipation. Profiles have a δ-peak structure with spacing $2\Omega_s$ between peaks: (a) in the "high-temperature" ($\alpha \gg 1$) case with $M = 16$, $\alpha = 1.6$ the envelope curve of δ-peaks is a product of two Lorentzians;
(b) in the "low-temperature" ($\alpha \ll 1$) case: $M = 4$, $\alpha = 0.4$ there are two main peaks at $\Omega = \pm\omega(Q)$.

In the general case our ion beam is not an isolated system but rather interacts with cooling and heating baths through rates $\nu_c(q)$ and $\nu_h(q)$. The form of the function $\nu_c(q)$ depends on the details of the cooling force. The longitudinal heating is a result of collisions of the ions, which are supposed to have a transverse temperature (emittance).

For the PU diagnostic it is important to consider a case of small enough M ($M^2 \ll 3\Gamma\Lambda N/(2\pi^2)$) or $\alpha \ll 1$. We simply denote this case as the low-temperature case, where α also depends on both T and M.

$$S(Q,\Omega) = [\frac{(Qc_s)^2}{2\pi\Lambda\Gamma(Q)}]\frac{\nu(Q)}{(\Omega^2 - \omega^2(Q))^2 + \nu^2(Q)\Omega^2} \tag{14}$$

The plots of the dynamical structure factor for this case of small α are shown in Fig. 3(a,b) for some values of ν. In the case of $\nu \ll \omega(Q)$ the profile has two well distinguished peaks at $\Omega = \pm\omega(Q)$ with the width of the order of ν. If $\nu \gg \omega(Q)$ then the profile has a central diffuse peak. The total power of the M-th band of the Schottky spectrum is related to the static structure factor

$$S(Q) = \int S(Q,\Omega)d\Omega = Q^2 <\mid a(Q,t) \mid^2>= \frac{1}{2\Gamma(Q)\Lambda}, \tag{15}$$

where we have taken into account that Γ my be a function of Q. The static structure factor is independent of ν and may be used for a direct measurement of the temperature distribution function $T(Q)$. The information on the relaxation frequency is available from the width of the peaks of $S(Q,\Omega)$ in Fig. 3.

In the opposite "high-temperature" case, $\alpha \gg 1$,

$$S(Q,\Omega) = \frac{4c_s}{\pi d}\frac{\gamma_Q^2}{[\gamma_Q^2 + (c_sQ + \Omega)^2][\gamma_Q^2 + (c_sQ - \Omega)^2]}, \tag{16}$$

where $\gamma_Q = dc_sQ^2/(4\Lambda\Gamma)$. A typical plot of $S(Q,\Omega)$ for this case is presented in Fig. 3(c). The profile has two well-distinguished peaks at $\Omega = \pm c_sQ$ with width γ_Q (the ratio of γ to Qc_s is equal to $(Qd)/(4\Lambda\Gamma) \ll 1$). In the case of large relaxation rate $\nu > \gamma_Q$ the width of these peaks is of the

order of ν.

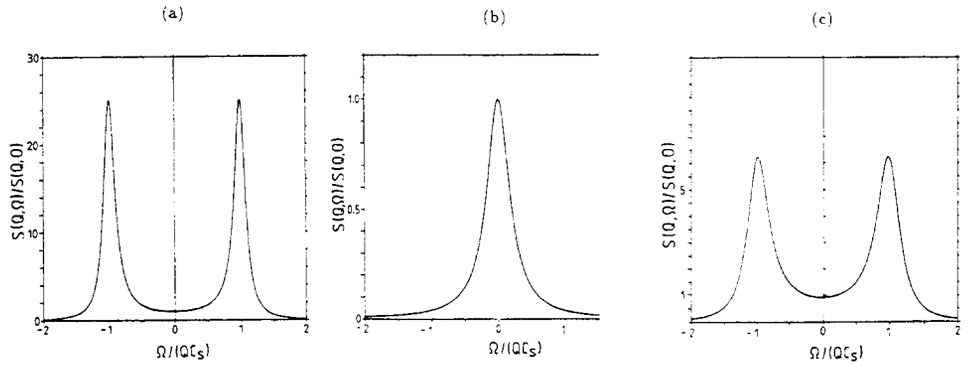

Fig.3 Plots of the dynamical structure factor $S(Q,\Omega)$, for some values of T, M and ν:
(a) at $\alpha \ll 1$ and $\nu \ll Qc_s$ there are two well distinguished peaks located at $\Omega = \pm Qc_s$ with the widths of the order of ν;
(b) at $\alpha \ll 1$ but $\nu \gg Qc_s$ there is only a central peak with the width $\delta\omega \approx Q^2c_s^2/\nu$;
(c) in the "high temperature case" ($\alpha \gg 1$) the width γ_Q of two peaks located at $\Omega = \pm Qc_s$ does not depend on ν.

It is interesting to compare the Schottky spectrum of a strongly correlated phonon system with the case of the ideal gas. Each band of the spectrum of the harmonic system has a width of the order of $2Qc_s$ whereas the width of peaks in the case of an ideal gas is of the order of $2Qv_{th}$. From Eq. (9) it follows that $v_{th}^2/c_s^2 = 1/(\Gamma\Lambda)$ and in our case $\Gamma > 1$ we have $v_{th} \ll c_s$. For a system with $\Gamma > 1$ and not too large M (i.e. $\alpha \ll 1$) the form of the Schottky spectrum depends on M, if the cooling rate is large enough. A single-peaked spectrum at low M is changing into a double-peaked at a sufficiently large M. This is opposed to the ideal gas case, where one expects that the two peaks merge into one peak due to a reduction of c_s for short wavelength. It is proposed that this dependence on M can be used in the experiment as a signature of correlations or ordering.

References

[*] Present address: Institute for Theoretical Physics, TU Braunschweig, Germany

[1] E.N. Dementev, N.S. Dikanskii, A.S. Medvedko, V.V. Parkhomchuk and D.V. Pestrikov, Sov. Phys. Tech. Phys. **25**, 81 (1980) ;

[2] E. Jaeschke et al., Part. Acc. **32**, 97 (1990);

[3] B. Franzke, Proc. 1991 Part. Accel. Conf., San Francisco, May 6-9, 1991, p. 2880;

[4] S. Schröder et al., Phys. Rev. Lett. **64**, 2901 (1990);

[5] I. Waki, S. Kassner, G. Birkl, H. Walther, Phys. Rev. Lett. **68**, 2007 (1992);

[6] R.W Hasse, Phys. Rev. A **46**, 5189 (1992);

[7] V.V. Avilov, I. Hofmann, Phys. Rev. E **47**, 2019 (1993).

[8] A.A. Maradudin, E.W. Montroll, G.H. Weiss, I.P. Ipatova, *Theory of Lattice Dynamics in the Harmonic Approximation*, Second Edition, Academic Press, N.Y. 1971;

CRITICAL TEMPERATURES FOR CRYSTALLINE BEAM*

Jie Wei, Brookhaven National Laboratory, Upton, New York 11973, USA
Xiao-Ping Li, Rutgers University, and *Andrew M. Sessler*, Lawrence Berkeley Laboratory

ABSTRACT

Based on the previously derived equations of motion in the beam rest frame, we study the melting conditions of the crystalline beam confined in an actual alternating-gradient (AG) focusing storage ring. The temperatures defined in the rest frame are directly related to the transverse emittances and momentum deviation conventionally used in the accelerator community. Using molecular dynamics (MD) method, we obtain the critical emittances and momentum deviation as functions of beam density and machine parameters.

1. INTRODUCTION

The ground states of crystalline beams were studied, first in seminal work by Schiffer and his colleagues,[1] and then by others[2]. Recently, we derived equations of motion in the rotating beam rest frame taking into account the time-dependent AG focusing force and the effect of the bending curvature.[3] We include in the formalism that the particles are confined by the guiding and focusing magnetic fields, and that they are confined in a conducting vacuum pipe while interacting with each other via a Coulomb force. Numerical simulations using MD methods has been performed to obtain the equilibrium crystalline beam structure. The effect of the shearing force, centrifugal force, and azimuthal variation of the focusing strength are investigated. It is found that a constant-gradient (weak focusing) storage ring can not give a crystalline beam, but that an AG structure can. In such a machine the ground state is, except for one-dimensional (1-D) crystals, time dependent. The ground state is a zero entropy state, despite the time-dependent, periodic variation of the focusing force. The nature of the ground state, similar to that found by Schiffer *et al.*[1-2] depends upon the density and the relative focusing strengths in the transverse directions. At low density, the crystal is 1-D. As the density increases, it transforms into various kinds of 2-D and 3-D crystals. In both 2-D and 3-D cases, the time-dependent crystalline structure has the same periodicity as that of the focusing forces. The crystal "breathes" transversely with no shearing and almost no oscillation in azimuthal direction. However, if the energy of the beam is higher than the transition energy of the machine, the crystalline structure can not be formed for lack of radial focusing.

In this paper, we study the melting condition of the crystalline beam. In section 2 we summarizes the previously derived equations of motion and the ground-state results. Section 3 describes the method used for determining the critical temperature. The critical temperatures, also expressed in terms of beam emittances and momentum deviation, are obtained in section 4 as functions of density and storage ring parameters. With this information, suitable cooling system can be designed in order to achieve crystalline beams. Discussions and conclusions are given in section 5.

2. EQUATIONS OF MOTION AND THE GROUND STATE

The motion of the particles under Coulomb interaction and external electromagnetic forces can be most conveniently described in the rotating rest frame (x, y, z, τ) of the reference particle of which the orientation of the axes are constantly aligned to the radial (x), tangential (z) and vertical (y) directions of the motion, with τ the proper time. Within this frame, particle motion becomes non-relativistic, and a periodic state simply corresponds to the desired crystalline state.

For simplicity but without losing generality, we assumed in the following discussion a circular storage ring with no straight sections. The beam is guided by a bending field B_0, and focused by a quadrupole field of gradient B_1

$$B_x = B_1 y, \quad B_y = B_0 + B_1 x, \quad B_z = 0, \tag{1}$$

* Work performed under the auspice of the U.S. Department of Energy, supported by NSF Grant DMR-91-15342, and by the DOE, Office of Energy Research, Office of High Energy and Nuclear Physics, under Contract No.DE-AC03-76SF00098.

where B_1 may vary for different piece of magnets, and the field variation at the magnet end is neglected. Assume that there exists no electric field so that the particle beam is not focused azimuthally. The magnitude of the B_0 is determined by the velocity βc and the bending radius R of the reference particle as $eB_0R = m_0c^2\beta\gamma$. For the convenience of later analysis, we express the equations of motion in terms of dimensionless variables. Let $n \equiv -B_1R/B_0$ represent the strength of the focusing magnetic field, and ξ (with $\xi^3 \equiv r_0R^2/\beta^2\gamma^2$) be a characterization of the inter-particle distance in the presence of Coulomb interaction in the storage ring, where $r_0 = Z^2e^2/m_0c^2$ is the classical radius of the particle. Express the time t in unit of $R/\beta\gamma c$, the spacial coordinates x, y, and z in unit of ξ, and the energy in unit of $\beta^2\gamma^2Z^2e^2/\xi$. The Hamiltonian $H(x, P_x, y, P_y, z, P_z; t)$ becomes in these reduced units

$$H = \frac{1}{2}\left(P_x^2 + P_y^2 + P_z^2\right) - \gamma x P_z + \frac{1}{2}\left[(1-n)x^2 + ny^2\right] + \frac{1}{\beta^2\gamma^2}\sum_j \frac{1}{\sqrt{(x_j-x)^2 + (y_j-y)^2 + (z_j-z)^2}} \quad (2)$$

where the cross term $-\gamma x P_z$ describes the coupling between the tangential and normal motion that leads to shearing. The equations of motion are given by the Hamilton's equations

$$\begin{cases} \dot{x} = P_x, & \dot{P}_x = \gamma P_z - (1-n)x - \dfrac{\partial V_C}{\partial x}, \\ \dot{y} = P_y, & \dot{P}_y = -ny - \dfrac{\partial V_C}{\partial y}, \\ \dot{z} = P_z - \gamma x, & \dot{P}_z = -\dfrac{\partial V_C}{\partial z} \end{cases} \quad (3)$$

where the Coulomb potential V_C is the last term in Eq. 2. With Eq. 3, we have studied the ground state of a crystalline particle beam under time-dependent, realistic storage ring environment. It has been shown that in a weak-focusing storage ring, the crystalline beams can not be formed for lack of transverse focusing. In an AG focusing ring, on the other hand, the crystalline beams can exist in spite of the variation in the focusing strengths, as long as the energy of the beam is less than the transition energy of the machine. If γ is higher than γ_T, the crystalline structure again can not be formed for lack of radial focusing.

We tested the effectiveness of the conventional cooling method by simply reducing, in our simulation, the momentum deviation $\Delta p/p$ of the particles by a certain fraction. It has been found that 1-D, 2-D, and 3-D crystals can all be formed depending on the beam density. The particles self adjust under the Coulomb interaction and the cooling effect (reduction of P_z in the rest frame) to form a certain structure. The actually required cooling rate, however, depends upon the noise level in the system.

3. METHODS FOR DETERMINING CRITICAL TEMPERATURES

We seek numerical solutions using molecular dynamics to the Hamiltonian in Eq. (2). Since Coulomb interaction is long ranged, an Ewald-type summation has to be performed to calculate the energy and the forces. To simulate a real storage ring, we consider a bunch of charged particles confined in a perfectly conducting, infinitely long pipe. The periodic boundary condition is used only in the z direction, where the "supercell" of length L (in unit of ξ) repeats itself to infinity. The integration used for evaluating the image-charge potential is performed by a 15th order Gauss-Laguerre method. The equations of motion in Eq. (3) is integrated by the 4th order Runge-Kutta algorithm. The storage ring is assumed to consist of 10 identical focusing-drift-defocusing-drift (FODO) lattice cells. Within each cell, the lengths of the F, O, D, and O elements are assume to be 15%, 35%, 15%, and 35% of the cell length, respectively. The focusing and defocusing gradients n are set to be 50 and -50, respectively. This arrangement results in transverse tunes $\nu_x = 2.7$ and $\nu_y = 2.3$ in the absence of the Coulomb interaction. The transition energy γ_T is about 2.5. The energy γ of the reference particle is set to 1.4. The time step for the integration is 1/20 of the period T_c of the focusing field.

Notice that the Hamiltonian we are solving is time-dependent, therefore the total energy is not a constant of motion, and the "temperature" as conventionally defined is no longer meaningful. On the other hand, since the ground state structure has the same periodicity as that of the focusing forces, we can define the relative "temperature" T_x, T_y, and T_Z as

$$T_x = \langle(\Delta P_x)^2\rangle, \quad T_y = \langle(\Delta P_y)^2\rangle, \quad \text{and} \quad T_z = \langle(\Delta P_z)^2\rangle, \quad (4)$$

where Δ denotes the deviation from the ground-state value, and $\langle\ \rangle$ denotes the average both over different particles and over a time period that is long compared with the focusing period but short compared with the total time of observation.

Initially, the ground-state crystalline structure is obtained for each density after 20,000 time steps (or 1,000 FODO cells) of simulated cooling and stability testing starting from randomly chosen positions and momenta of the particles. Then, particles are perturbed in certain direction x_i (x_i=x, y, z) by randomly adding a δP_{x_i} to its momentum P_{x_i}. The average of δP_{x_i} over all the particles is zero, and the r.m.s. of

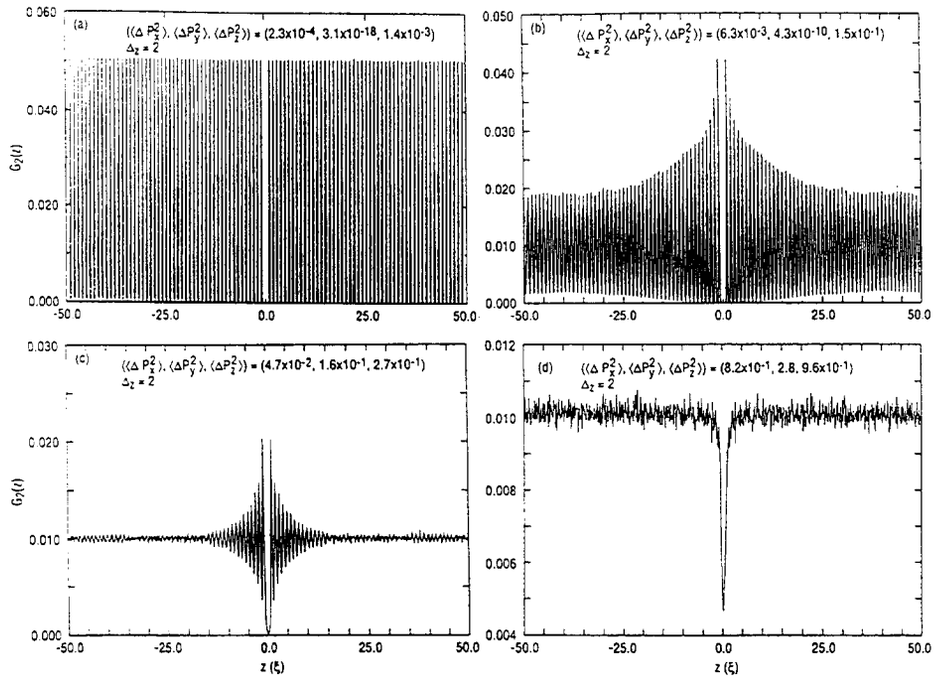

Figure 1: Two-body correlation function $G_2(z)$ for a) ground state; b) non-zero temperature solid state; c) liquid state; d) gas state for the case $N = 100$ and $L = 100$.

δP_{x_i} is chosen according to the desired initial temperature. Thereafter, particles are tracked for another 10,000 time steps when the temperatures are controlled within the desired range by simulated cooling or heating. The simulated cooling is achieved by, at the end of each focusing period, imposing the periodic condition on all the positions and momenta of the particles, while the simulated heating is achieved by randomly perturbing the momentum in a certain direction. The ordering of the system is determined after an equilibrium state is reached by evaluating the correlation functions. The critical temperatures are obtained when the beam structure transforms in z from long-range (solid) to short-range ordered (liquid) state, and also from short-range to random (gas) state.

The ordering in azimuthal direction can be characterized by the two-body correlation function $G_2(z)$

$$G_2(z) = \langle \frac{1}{N^2} \sum_{i,j=1, i\neq j}^{N} \delta\left(z - |z_i - z_j|\right) \rangle \Big|_t \tag{5}$$

where $\langle\ \rangle|_t$ denotes the average over time after the thermal equilibrium is reached. Figs. 1a–d show $G_2(z)$ of various states for the case $N = 100$ and $\Delta_z \equiv L/N = 1$. The beam is long-range ordered in z in solid state, short-range ordered in liquid state, and randomly distributed (except for the effect of the repulsive Coulomb force) in the gas state.

The ordering in transverse directions may be described by the deviation from that of the ground state the time-averaged density distribution functions $G(\rho)$ and $G(\phi)$,

$$G(\rho) = \langle \frac{1}{N} \sum_{i=1}^{N} \delta\left(\rho - \sqrt{x_i^2 + y_i^2}\right) \rangle \Big|_t, \quad G(\phi) = \langle \frac{1}{N} \sum_{i=1}^{N} \delta\left(\phi - \phi_i\right) \rangle \Big|_t \tag{6}$$

where ϕ_i is the polar angle of the ith particle. These functions have been used for determining the melting in the transverse directions.

The relative temperatures T_x, defined in the beam rest frame by Eq. 4 can be expressed in terms of the quantities in the laboratory frame. In the conventional case where the transverse velocity is much less than the longitudinal velocity in the laboratory frame, the momentum P_x, P_y, and P_z in the rest frame are related to the transverse velocities $x' \equiv dx/ds$, $y' \equiv dy/ds$, and the momentum deviation $\Delta p/p$ in the laboratory frame by the equation[4]

$$\left(x', y', \frac{\Delta p}{p}\right) = \frac{\xi}{R}\left(P_x, P_y, \gamma P_z\right) \tag{7}$$

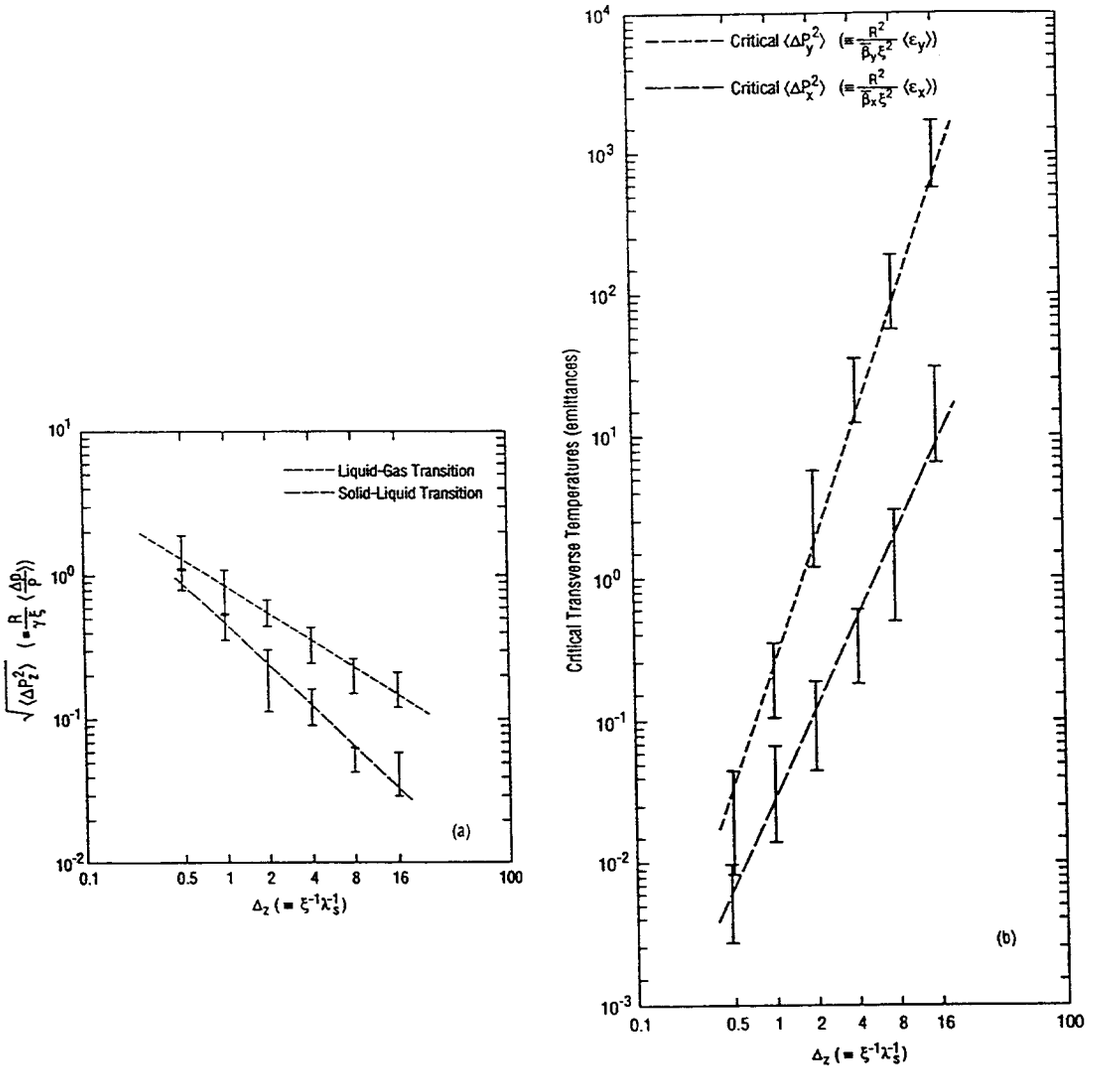

Figure 2: a) Azimuthal critical temperatures for solid-liquid and liquid-gas transition in z as functions of the inverse of the beam density. b) Transverse critical temperatures for solid-liquid transition in z as functions of the inverse of the beam density. λ_s is the line density in the laboratory frame.

where s is the azimuthal distance. Define the transverse emittances $\epsilon_x = \bar{\beta}_x \langle x'^2 \rangle$ and $\epsilon_y = \bar{\beta}_y \langle y'^2 \rangle$, with $\bar{\beta}_{x,y}$ the effective Courant-Snyner parameter. The temperatures can be expressed in terms of the deviation in emittances $\epsilon_{x,y}$ and momentum using Eq. 7

$$\left(\Delta\epsilon_x, \Delta\epsilon_y, \frac{\Delta p}{p} \right) = \left(\frac{\xi^2}{R^2} \bar{\beta}_x T_x, \frac{\xi^2}{R^2} \bar{\beta}_y T_y, \frac{\xi}{R} \gamma \sqrt{T_z} \right) \tag{8}$$

where $T_{x,y,z}$ have been defined by Eq. 4.

4. NUMERICAL RESULTS

Because of the time-dependent focusing force, we obtain the equilibrium state by numerically iterating the equations of motion Eq. 3. At each iteration step, the Coulomb potential including image charges has to be numerically integrated and summed.[3] This time-consuming process limits the number of particle used for MD calculation. In the following, we report results calculated with $N = 100$ with the size L of the supercell ranging from 50 to 1600. The ground state is 1-D at low density ($\Delta_z \geq 1.2$), 2-D at intermediate density, and 3-D at high density ($\Delta_z \leq 0.5$).

The short-dash line in Fig. 2a indicates the critical temperature in azimuthal (z) direction when the

beam transforms in z direction from liquid to gas state. The approximate relation

$$\langle P_z^2 \rangle \approx 0.6/\Delta_z \tag{9}$$

implies that the melting in azimuthal direction occurs when the average kinetic energy is comparable to the potential energy difference needed for some of the particles to traverse a significant fraction of the distance Δ_z. The long-dash line in Fig. 2a indicates the critical temperature when the beam transforms in z direction from solid to liquid state. When T_z is lower than the critical temperature, particles vibrate azimuthally around their ground-state positions. Almost no thermal energy is transferred into y direction, and very little is transferred into x direction (due to $x-z$ coupling). In the 1-D case, the vibrational frequency $\omega_z(k)$ in z direction can be derived from Eq. 3 as

$$\omega_z^2 = \frac{4}{\Delta_z^3}\sum_m \frac{1}{m^3} - \frac{4}{\Delta_z^3}\sum_m \frac{\cos(mk\Delta_z)}{m^3}, \quad -\frac{\pi}{\Delta_z} < k_z \leq \frac{\pi}{\Delta_z} \tag{10}$$

where k is the crystal momentum. On the other hand, when T_z is above the liquid-gas critical temperature, thermal equilibrium is reached in all the directions after the thermal energy in z is transferred into transverse directions.

Fig. 2b indicates the critical temperatures T_x and T_y in radial (x) and vertical (y) directions when the beam transforms in z direction from solid to liquid state. The fact that T_x and T_y increase with decreasing beam density can be understood in the low-density regime as the following. The melting in z occurs when the thermal energy (Eq. 9) in azimuthal direction reaches the critical value. When the particles are mainly perturbed in transverse directions, the amount of Coulomb energy that can be transferred into azimuthal direction to cause melting corresponds to a transverse displacement $d_{x,y} \approx \Delta_z$. On the other hand, the vibrational frequencies $\omega_{x,y}(k)$ in transverse directions

$$\omega_x^2 = (\nu_x^2 - \gamma^2) - \frac{2}{\Delta_z^3}\sum_m \frac{1}{m^3} + \frac{2}{\Delta_z^3}\sum_m \frac{\cos(mk\Delta_z)}{m^3}, \quad \omega_y^2 = \nu_y^2 - \frac{2}{\Delta_z^3}\sum_m \frac{1}{m^3} + \frac{2}{\Delta_z^3}\sum_m \frac{\cos(mk\Delta_z)}{m^3}. \tag{11}$$

are mainly determined by the external transverse focusing in the low-density case. Therefore, the critical temperatures $T_{x,y}$ are approximately proportional to Δ_z^2. The fact that T_x is lower than T_y is partly due to the coupling between x and z motion. The results of the calculation has been verified by comparing cases with different L and N (N =10, 20, 50, 100, and 200) while keeping the density $\Delta_z^{-1} = N/L$ constant ($\Delta_z = 2$).

5. CONCLUSIONS AND DISCUSSION

In this paper, we have studied the melting conditions of crystalline particle beams of different density under time-dependent, realistic storage ring environment. The temperatures defined in the rest frame are directly related to the transverse emittances and momentum deviation conventionally used in the accelerator community. Using molecular dynamics method, we obtain the critical emittances and momentum deviation as functions of beam density and machine parameters.

Consider the storage ring example discussed at the beginning of section 3 with $2\pi R$ =24 m and $\bar{\beta}_{x,y} \approx 10$ m. Therefore, ξ is equal to 1.8×10^{-6} m for proton, and is equal to 2.2×10^{-5} m for electron. Hence, the condition to form the crystalline beam is

$$\left(\Delta\epsilon_x, \Delta\epsilon_y, \frac{\Delta p}{p}\right) < \begin{cases} (0.8\times10^{-11}T_x, 0.9\times10^{-11}T_y, 1.3\times10^{-6}\sqrt{T_z}) & \text{(proton)} \\ (1.2\times10^{-9}T_x, 1.3\times10^{-9}T_y, 2.1\times10^{-5}\sqrt{T_z}) & \text{(electron)} \end{cases} \tag{12}$$

where T_x, T_y, and $\sqrt{T_z}$ are given by Fig. 2. In order to achieve this condition of crystallization, cooling techniques have to be applied to the beam.

REFERENCES

[1] For example, J. P. Schiffer and P. Kienle, Z. Phys. A **321**, 181 (1985); J. P. Schiffer and O. Poulsen, Europhys. Lett. **1**, 55 (1986); A. Rahman and J.P. Schiffer, Phys. Rev. Lett. **57**, 1133 (1986).
[2] For example, D. Habs, MPI Heidelberg preprint MPIH-1987-V10 (1987); J. P. Schiffer and A. Rahman, Z. Phys.A – Atomic Nuclei 331, 71–74 (1988); R. W. Hasse, Phys. Rev. Lett. **67**, 600 (1991); R. W. Hasse and J. P. Schiffer, Ann. Phys. **203**, 419 (1990); R. W. Hasse, GSI preprint GSI-90-23 (1990); R. W. Hasse and V. V. Avilov, Phys. Rev. A **44**, 4506 (1991); J. P. Schiffer, Phys. Rev. Lett. **70**, 818 (1993).
[3] J. Wei, X-P. Li, and A.M. Sessler, BNL Report BNL-52381, Upton, New York (1993).
[4] J. Wei and A.G. Ruggiero, BNL Informal Report BNL-45269, AD/RHIC-81 (1990).

A DEDICATED STORAGE RING FOR ION BEAM CRYSTALLIZATION

L. Tecchio
University of Torino and INFN, Torino, Italy

G. Lamanna, V. Stagno and V. Variale
University of Bari and INFN, Bari, Italy

R. Calabrese, V. Guidi and F. Petrucci
University of Ferrara and INFN, Ferrara, Italy

G. Bisoffi, G. Ciullo, A. Dainelli, S. Gustafsson, A. Labrador, M.F. Moisio, A. Pisent, A. Ruggiero and B. Yang
Laboratori Nazionali di Legnaro-INFN, Legnaro, Italy

ABSTRACT
A feasibility study of a storage ring dedicated to crystallize ion beams is actually in progress at the LNL Legnaro Laboratory. As result of computer simulations, a 38 m circumference storage ring with six super-periods was selected among other possible configurations. Simulation programs suggest the possibility to use such a storage ring in order to study ordered beam structures (string, zig-zag, helix, shell). The problems connected to the shear forces induced in the dipoles have been taken into account and are still under study.

1. INTRODUCTION

After the advent of efficient electron coolers the possibility of generating crystallised ion beams has gained the interest of particle accelerator physicists [1,2].

In addition, new cooling methods like laser cooling gives a further opportunity to reach ultracold system of particles in which ions can have a state transition to the crystalline phase.

The reason for the interest in crystalline beams has many aspects: for example the fascination of a new research field or some of the applicative potentials which are connected with this subject would justify a careful investigation of this kind of beams.

Apart from the pioneering work performed by E.N. Dementiev *et al.* in 1980 [3], no further indication about crystalline beams have been found in a storage ring.

During the last decade computer simulations have been carried out whose results describe the structure of crystalline beams.

Very recently two relevant experiments have been done: H. Walther *et al.* [4] achieved the crystallisation of ions in a small ring-like ion trap by employing laser cooling; while [5] A.V.Aleksandrov *et al.* have produced, for the first time, an electron beam where the potential energy exceeds the thermal energy, thus obtaining a liquid-like phase in the electron beam. These efforts are very promising for further experimental investigations in this direction.

At present, a feasibility study of a dedicated storage ring (CRYSTAL) for ion beam crystallization is in progress at the Laboratori Nazionali di Legnaro (LNL). The existing facilities, the XTU Tandem [6] and the ALPI superconducting post-accelerator [7], can be used as Heavy Ion Injector systems for the CRYSTAL Storage Ring.

Heavy ion beams of different charge states and kinetic energies can be injected in an indipendent way, either directly from the XTU Tandem or from the ALPI post-accelerator, following the requirements of the experiments.

The first step is to store in the ring all stable ion species with kinetic energies and intensities produced by the accelerator facilities. The stored beams will be cooled by electron and laser cooling methods in order to induce the phase transition from the gas state to the crystalline one. Several ordered structures (string, zig-zag, helix, multishell) will be studied accumulating many pulses in order to increase the beam density.

The CRYSTAL Storage Ring is planned to be housed in an experimental area located close to the ALPI building as shown in Fig. 1

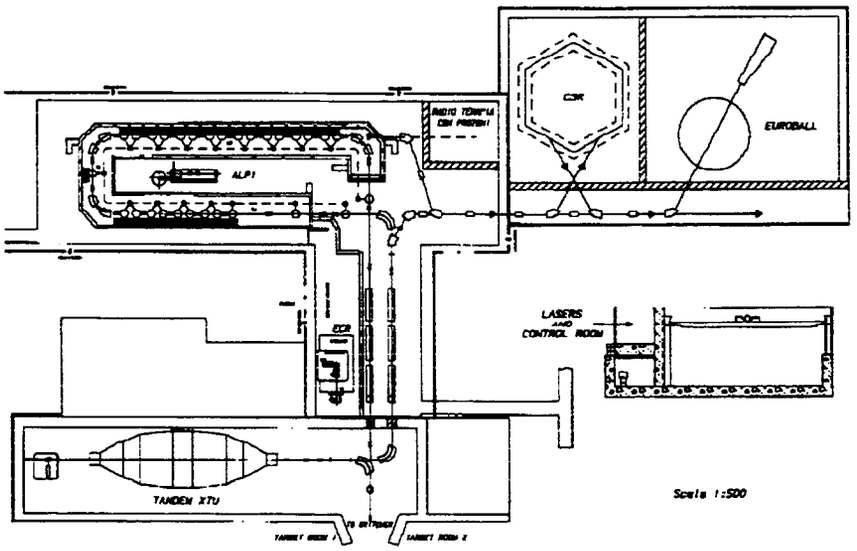

Fig. 1 - The LNL accelerator complex.

2. THE CRYSTAL STORAGE RING

2.1 Lattice and general layout

The overall size of the storage ring has been determined by some general considerations such as the largest specific kinetic energy of the ions which have to be stored, the matching with the heavy ion injector systems and the avaible space in the Laboratory. The kinetic energy depends on the ion species extracted from the XTU Tandem/ALPI complex; the maximum specific kinetic energy for fully stripped C is about 24 MeV/u and 3.90 MeV/u for U^{54+}. The shape and symmetry of the ring is determined by a compromise between an ideal circular machine where the beam is preserved from external perturbations and the need of several straight sections where to accomodate injection, extraction, cooling and diagnostic devices.

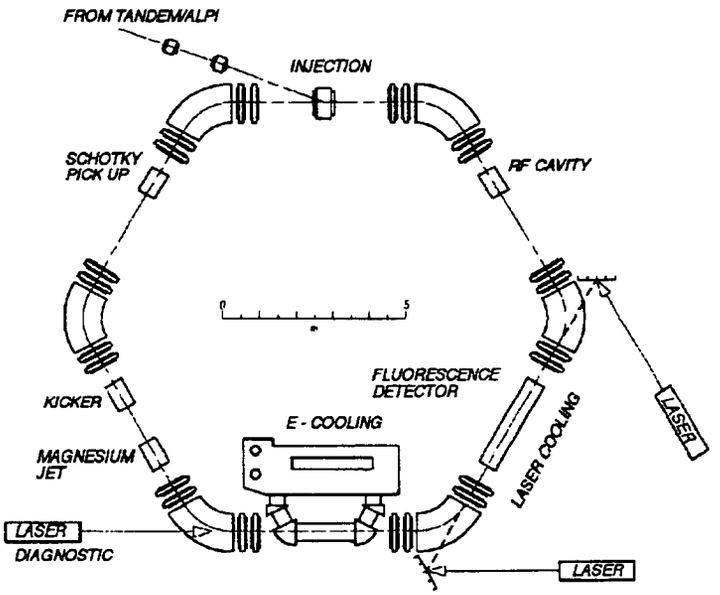

Fig. 2 - A scheme of the CRYSTAL Storage Ring.

The storage ring is conceived as a fully symmetric six super-periods alternating gradient focusing machine with an hexagonal geometry. The lattice has a sixfolded symmetry and general considerations on technical feasibility and machine operation make the choise of the betatron tunes $Q_{h,v} = 1.8$ the preferable ones.

The storage ring has a total length of about 38 metres and is schematically shown in Fig. 2. The magnetic lattice consists of six 60 degrees bending magnets and six drift sections 4.0 metres long in which electron and laser cooling devices can be installed. Moreover, correction coils, conventional diagnostic devices and special systems for crystalline beams will be located in the drift sections as well. Twelve couples of focusing and defocusing quadrupoles are placed near each end of the bending magnets. Lattice and dispersion functions are displayed in Fig. 3 for one sixth of the machine.

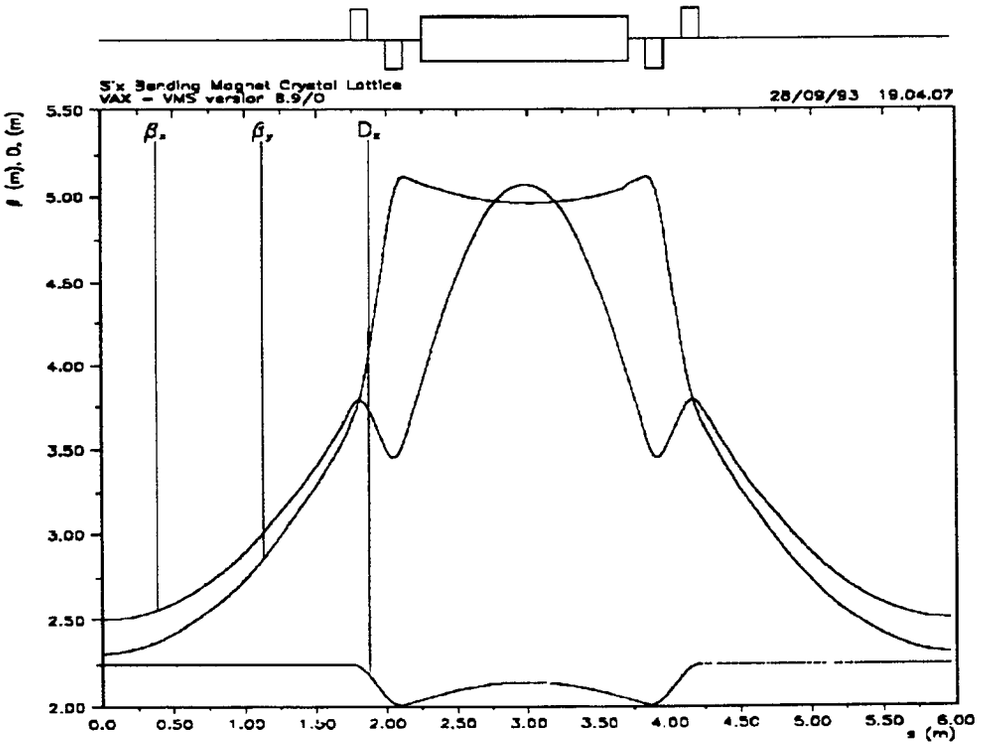

Fig. 3 - The lattice and dispersion functions of the CRYSTAL Storage Ring.

The transition energy γ_t = 1.6 has a large value which keeps the machine operating well below it. The main characteristics of the storage ring are given in Table 1.

Table 1 - Main characteristics of the CRYSTAL Storage Ring.

Perimeter [m]	38	Max. hor. beta function [m]	5.2
Magnetic rigidity [Tm]	3.0	Max. vert. beta function [m]	5.2
N. of dipoles	6	Dispersion [m]	2.4
N. of quadrupoles	24	Gamma transition	1.6
Hor. and vert. apertures [cm]	10	Straight section length [m]	4.0
Hor. and vert. tune	1.8	N. of super-periods	6

2.2 XTU Tandem and ALPI post-accelerator injection complex

Beam injection of heavy ions takes place in one of the drift sections as shown in Fig. 2 . Injection can be done in a single turn in case of low intensity operation or in several beam turns in order to reach higher beam intensities. After injection the beam is self-debunched in a few turns and the storage ring operates with a

coasting beam. An estimation of the injection parameters for different ion species and injector type are summarized in Table 2.

Table 2 - Beam parameters at the exit of the XTU Tandem and ALPI post-accelerator.

Ion species		C	S	Cu	I	Au	U
XTU Tandem	Charge state	-	9	11	12	13	13
	β (v/c)	-	0.103	0.0808	0.059	0.0494	0.045
ALPI Post-accel.	Charge state	6	16	27	40	51	54
	β (v/c)	0.22	0.185	0.148	0.114	0.099	0.091
Energy spread		10^{-4}					
Emittance		1 π mm mrad					

2.3 The cooling systems

Very efficient phase-space cooling is required to attain crystalline ion beams, i.e. a beams with very small temperature (in the rest frame system), compared to the average Coulomb interaction energy. Electron cooling and laser cooling techniques are foreseen to be applied in the CRYSTAL Storage Ring to attain beam crystallisation since they have complementary features.

Electron cooling provides a phase-space contraction for an ion beam, through the overlappping of a ultracold electron beam, continuously renewed. Coulombian scattering between ions and electrons, in force of their different masses, allows a transfer of a net amount of thermal energy from the ion beam to the electrons. Afterwards the electron beam is removed and a relatively low momentum spread, $\Delta p/p = 10^{-5} \div 10^{-6}$, is attained.

Laser cooling acts by virtue of momentum exchange between an ion beam and laser light whose frequency is chosed in correspondence of high values of the electric dipole for the stored ions. Photon excitation and subsequent re-emission causes, in princicle, longitudinal momentum $\Delta p/p$ even three orders of magnitudine lower than in the electron cooling case. This latter method has a working regime that recommends a precooled ion beam; the former can therefore be considered as complementary to the laser cooling. Furthermore laser cooling acts only along the longitudinal axis, so that transverse cooling is determined by the electron cooling efficiency. It is also clear that the laser cooling imposes a selection on the kind of ion to be employed. Thus, electron cooling reduces emittance and momentum spread without decreasing the ion current, allowing the application of laser cooling on a dense ion beam with still enhanced efficiency.

The devices for cooling are housed in two different drift sections, as schematically shown in Fig. 2. The possibility to operate the laser cooling in some straight section of the CRYSTAL Storage Ring is outlined.

3. SIMULATION OF CRYSTALLINE BEAMS

The lattice design and the possibility to obtain crystalline structures in the CRYSTAL Storage Ring has been investigated by computer simulation codes.

An intense low emittance beam in presence of space charge, to simulate a space charge dominated crystalline beam, has been used in order to study the lattice parameters matching the beam. The used code (TRACE-2D) is an interactive, first order, envelope-tracing, beam-dynamics program in which space charge forces are linearized [8]. TRACE-2D calculates the beam envelope and shows (Fig. 4) that the beam is stable for different emittances.

A dedicated computer code (LICCRY: LIquid Coulomb CRYstal) to study the detailed behaviour of a crystallized beam in a storage ring is under development. At present, a two dimensional version is ready and an initial study concerning the interaction of a crystalline beam with a storage rings magnetic structure has been performed. The trajectories of the particles in a beam cell are determined using a straightforward ray tracing method (Runge-Kutta). The space charge effect is computed before each step of trajectory calculation. A coulombian particle-particle interaction is considered in a static approach (non-relativistic approximation). A coasting beam is simulated by calculating the electric field contribution from all particles in the beam within a cell length distance.

The computer simulation of a zig-zag cell configuration passing through a super-period of the storage ring has shown the possibility to match the beam not only to achieve symmetry in dimensions and divergencies but also to reconstruct the same internal beam structure. In addition, the simulation shows that the initial structure is

preserved between the dipoles and has a behaviour similar to a laminar "Liquid Coulomb Crystal" flow. This phenomenon is very sensible to the interplay between space-charge and focusing forces.

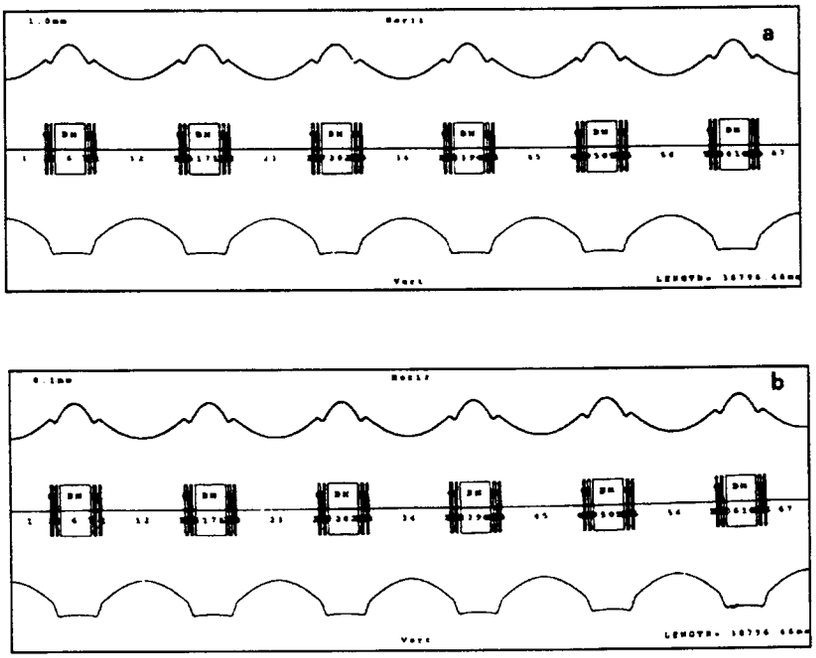

Fig. 4 - Beam envelop for different emittances; a) 0.1 mm mrad, b) 0.001 mm mrad.

The possibility to obtain ordered structures in the CRYSTAL Storage Ring has been investigated by the computer simulation code PARMTRA [9]. This is a Monte-Carlo program to simulate the transport of an ion beam through a system of optic elements under space charge condition. Coordinates and momenta are transformed around the ring by matrices incorporating the effect of quadrupoles and dipoles.

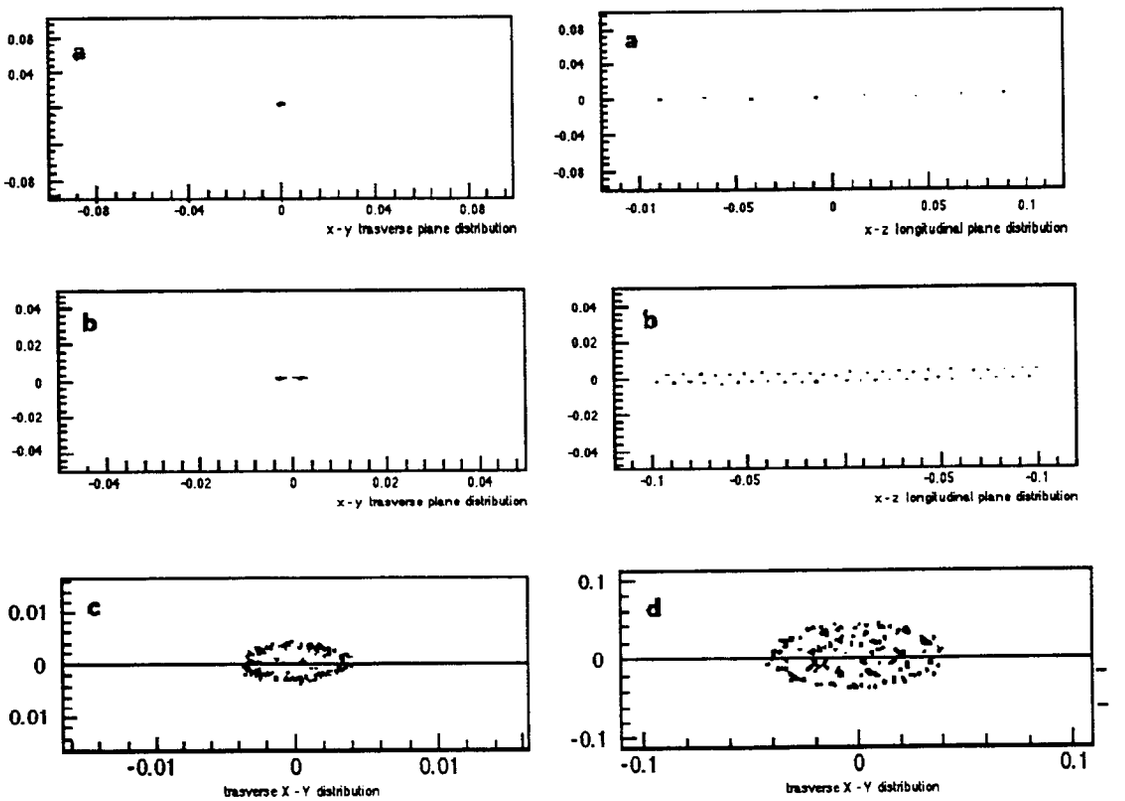

Fig. 5 - Computer simulations of several crystalline beam configurations: a) string, b) zig-zag, c) shell, d) multishell. Horizontal and vertical dimensions are in centimetres.

Coulomb forces between all particles of a beam sample can be calculated at arbitrary step and added to the magnetic element matrix. The simulation code is configurated in order to model the appropriate Coulomb force of a continuous coasting beam.

Several kinds of ordered structures (string, zig-zag, one shell, multishells) have been studied suggesting that the CRYSTAL lattice could be consistent with the formation and maintaining of such kind of structures. Results of computer simulations are shown in Fig. 5; in all examples the ion is Au^{51+} with $\beta = 0.1$ and the number of particles varies according to the structure configurations.

Being the cooling system the main tool to obtain ordered ion beam, the corresponding parameters have to be chosen in an appropriate way. The cooling forces, applied in one straight section of the storage ring, reduces the beam temperature by a certain factor that, for the most simple structure configurations, it is consistent with the realistic case. Actually, while for string and zig-zag configurations realistic cooling forces have been used, for more complex structures the cooling forces were chosen on the base of theoretical estimations [10] because of the very long computer time required for simulations.

Since the single elements composing the storage ring influences the crystalline beam its behavior has been investigated when the beam is passing through each element. The bending magnets are the most important elements to be investigated, in fact the ordered structures can be prevented from the viscous heating due to the shear induced in the bending dipoles of the ring. Shear will transfer some of the energy of coherent motion to thermal energy and may prevent reaching the very low temperatures required for formation of the ordered state. Computer simulations [9] for the CRYSTAL Storage Ring shown that the shear effect can be rather small and that the ordered structure seems to be quite elastic to compensate such an effect conserving the initial order in the beam.

ACKNOWLEDGEMENTS

We are very grateful to R. Hasse, I. Hofmann and J. Struckmeier of GSI - Darmstadt for their strong active collaboration, helpful suggestions and encouragements to continue the design of a dedicated ring for beam crystallization studies.

REFERENCES

[1] J.P. Schiffer and P. Kienle; Z. Phys. A 321 (1985) 181.
[2] J.P. Schiffer and O. Poulsen; Europhys. Lett. 1 (1986) 55.
[3] E.N. Dementiev, N.S. Dikansky, A.S. Medvedko,V.V. Parkhomchuk and D.V. Pestrikov; Sov. Phys.Tech.Phys. 25 (1980) 1001.
[4] I.Waki, S. Kassner, G. Birkl and H. Walther;*"Observation of Ordered Structure of Laser-cooled Ions in a Quadrupole Storage Ring"*, to be published.
[5] A.V. Aleksandrov, R. Calabrese, N.S. Dikansky, V. Guidi, N.Cl. Kot, V.I. Kudelainen, V.A. Lebedev, P.V. Logachov and L. Tecchio; Europhys. Lett.,18 (1992) 151.
[6] R.A. Ricci and C. Signorini; NIM 184 (1981) 35.
[7] G. Fortuna et al.; NIM A287 (1990) 253.
[8] K.R. Crandall and D.P. Rusthoi; *Documentation for TRACE-2D: An Interactive Beam-Transport Code*; LA-10235-MS UC-32.
[9] J. Struckmeier and I. Hofmann; GSI Annual Report 1987, GSI-87-1, p. 389.
J. Struckmeier; *PARMTRA Simulation Code*; GSI-ESR-87-03
[10] I. Hofmann and J. Struckmeier; *Interaction of Crystalline Beams with a Storage Ring Lattice*; Proceedings of the Workshop on Crystalline Ion Beam; GSI-89-10, p. 140.

COOLED BEAM INTENSITY LIMITS IN THE IUCF COOLER

Daniel Anderson, Mark S. Ball, Vladimir Derenchuk, Gary East, Michael Ellison, Tim Ellison, Dennis Friesel, Brett J Hamilton, Sergei S. Nagaitsev, Terry Sloan, Peter Schwandt

IUCF - 2401 Milo Sampson Ln., Bloomington IN 47405

ABSTRACT

In the case of stripping injection, electron cooling enables the IUCF Cooler to accumulate beam currents about 10 times higher than what can be obtained without cooling; in the case of kicked injection of fully-stripped beams, this ratio is greater than 1,000. Paradoxically, the electron cooling system also appears to be responsible for limiting the peak current in the ring at 45 MeV to about 6 mA; this limit is more than an order of magnitude below what we might expect without cooling. Thus the tool which allows us to accumulate beam also prevents us from accumulating more beam.

1. INTRODUCTION

The maximum cooled proton beam peak current stored in the IUCF Cooler at 45 MeV is about 6 mA (i.e., coasting beams of 6 mA, and 1 mA of rf−bunched beams with bunching factors [$BF = I_{peak}/I_{average}$] of about 6). These currents have been obtained using a combination of stripping injection with electron cooling accumulation and transverse beam damping. This performance limitation appears to be similar to that reported at other laboratories operating with similar beams:

--The LEAR ring has stored coasting cooled beam currents of up to 3 mA using both electron cooling and dampers[1].

--CELSIUS has been able to accumulate 2 mA using the electron cooling accumulation mode of injection and dampers[2].

The *un-cooled* beam limit in the Cooler, however, may be 1 to 2 orders of magnitude higher. CELSIUS, for example, has accumulated and accelerated 40 mA (corresponding to 200 μA assuming a bunching factor of 5) using stripping injection *without* cooling[3]. This is about 40 times greater than what has been achieved at IUCF; the principal reason being the higher CELSIUS injector current, ≈ 75 μA as compared to ≈ 0.75 μA at IUCF.

At this point we do not know what causes this intensity limit, nor do we have any techniques to raise this limit. We hope that discussion of these limitations at the workshop will provide us will ideas which can bring back to IUCF. Below we summarize what we know about this intensity limit.

2. INTENSITY LIMITATIONS

2.1 Peak Current Limitation

As might be expected, the intensity limit in the IUCF Cooler is a peak current (I_{peak}) limit, rather than an average current (I_{ave}) limit. Since to first order we expect the bunch length to vary as $I_{ave}^{1/3}$ in the space charge dominated regime[4][5], where V_{rf} is the rf voltage, it can easily be shown that I_{ave} should vary as $V_{rf}^{-1/2}$ for a constant peak current. Such is the case in the Cooler, as illustrated in Figure 1, where we plot the measured average current as a function of the $h = 1$ rf voltage (h is the harmonic number). This does, however, suggest an operating mode to maximize I_{ave} without actually addressing the I_{peak} limit: I_{ave} should vary as $h^{1/2}$ for constant V_{rf}. Since the required bucket area for cooled beams is so small, the rf voltage requirement is almost entirely determined by the required energy gain per turn; we thus operate in a regime where V_{rf} is not a function of h, and should be able to increase I_{ave} by a factor of 2 to 3 by operating with a larger value for h (we presently operate at $h = 1$ for historical reasons). Instituting a "parabola" at the beginning of ramping would also lead to increased I_{ave} without increasing I_{limit}.

2.2 Injection Efficiency

As also might be expected, the I_{peak} limit is independent of the amount of injected beam current, as well as, within limits, the repetition rate at which we inject beam. We can thus conclude that the limit is not related to beam lifetime. This is illustrated in Figure 2 which shows the stored average current as a function of time during the process of cooling accumulation using stripping injection. The beam current does not increase to its maximum value as $I_{limit}(1 - e^{-t/\tau})$, where τ is the beam lifetime; rather the current increases with no apparent change in rate until just below the limiting current. More detailed information on how cooling is used as an injection aid can be found in another contribution to this workshop[6].

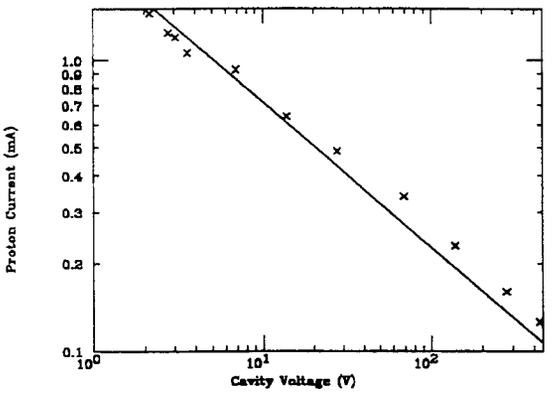

Figure 1. I_{ave} vs. V_{rf} (h = 1) in the IUCF Cooler. Solid line is $V_{rf}^{1/2}$.

2.3 Increased Transverse Beam Size

One could conjecture that the intensity limit is due to an increase in the beam size. Such a conjecture is supported by the large decrease in the geometrical constant g[4], which is proportional to the natural logarithm of the beam radius to the vacuum chamber radius for a centered beam inside a round pipe, as shown in Figure 3. This conjecture was tested by measuring the effective ring aperture as a function of beam current. The aperture was "measured" by exciting a coherent betatron oscillation with the injection pulse kicker magnet and observing the percentage loss of beam. The results, shown in Figure 4, however, would seem to indicate the opposite: that the available aperture in the machine *increases* with beam current! This is a mystery, and the explanation could be quite complicated. We do know that at high beam currents the decoherence of both longitudinal and transverse coherent oscillations is suppressed, so very different things happen to the beam in the low and high current regimes when a coherent oscillation is excited.

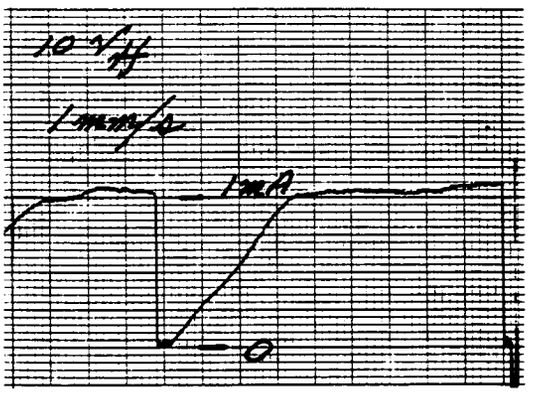

Figure 2. Beam current as a function of time during stripping injection with cooling accumulation.

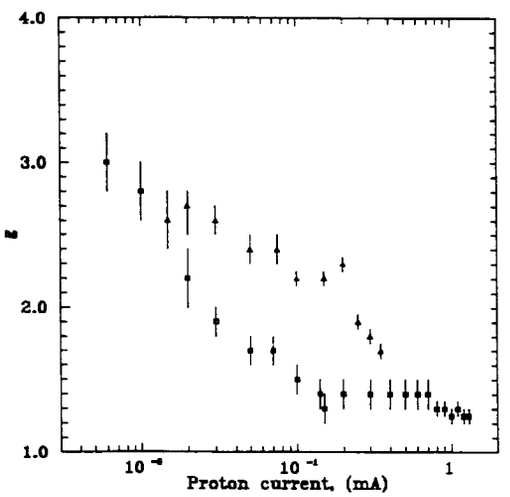

Figure 3. Geometrical constant g as a function of current.

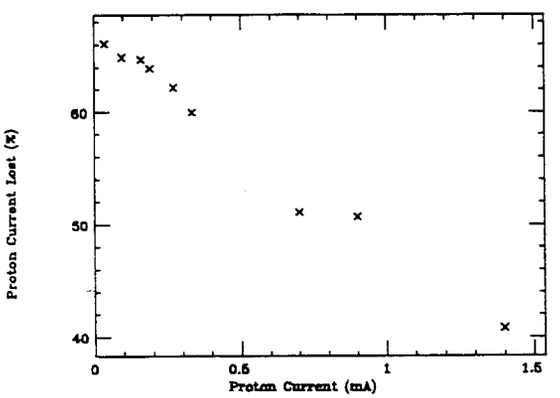

Figure 4. Percentage beam loss as a function of beam current for a fixed kicker strength corresponding to 10 $\pi\mu$m (non-normalized).

We could also conjecture that if the beam size increased substantially as the current increased, a limit might be reached due to a sudden beam loss at injection due to the stacked beam striking an aperture when the injection magnets are pulsed. This also does not appear to be the case; Figure 5 shows the stored beam current as a function of time between injection cycles. A sudden beam loss at injection is not observed; instead the beam current smoothly decreases between injection cycles.

2.4 Beam Lifetime as a Function of Intensity

The manner in which the beam intensity approaches its limiting current can be explained by the beam lifetime being a highly nonlinear function of the beam intensity. This is illustrated in Figure 6 which shows the beam current as a function of time after the injection system is turn off. However, the mechanism responsible this behavior in unknown.

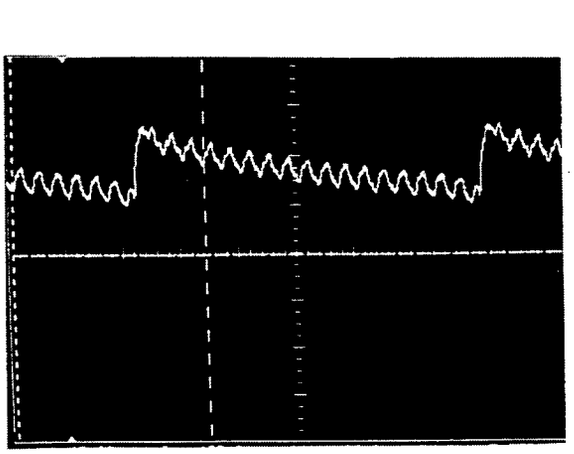

Figure 5. $I_{ave}(t)$ between injection cycles; 50 μA, 50 ms per div ($I_{ave,max}$ = 1.5 mA).

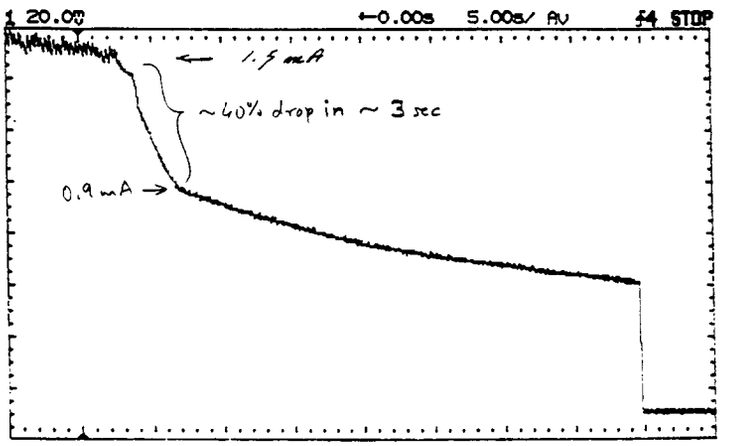

Figure 6. Beam current as a function of time after the injection system is turned off.

2.5 Coherent Transverse Instabilities

Although coherent transverse instabilities have been observed, they do not appear to be a limit[7]:

-- Coherent transverse instabilities are usually observed only when the Cooler is operated in a non standard mode (i.e., cooling the beam after injection for many seconds before beginning acceleration).

-- A transverse feedback (damping) system can damp these instabilities at rates up to two orders of magnitude faster than the measured growth rates.

2.6 Space Charge Effects

The limit appears to be due to space charge effects. Space charge effects in synchrotrons are usually quantified by the space charge tune shift, ΔQ_{SC} which can be expressed as:

$$\Delta Q_{SC} = \frac{BF \cdot I_{DC} C r_p}{4\pi e c \beta^2 \gamma^2 \epsilon_N}$$

where I_{DC} is the average beam current, C the ring circumference, r_p the classical proton radius, e the proton charge, c the speed of light, β and γ the usual relativistic parameters, and ϵ_N the normalized rms beam emittance. ΔQ_{SC} is the amount the incoherent betatron tune is reduced due to defocussing effects from the beam space charge. We note that ΔQ_{SC} is not directly measured; the tune shift is a mathematical quantity which can be exactly calculated but does not necessarily accurately represent what is happening physically.

In order to estimate the value of ΔQ_{SC} it is necessary to measure ϵ_N; this quantity is usually determined by measuring the beam size in a region with known beta functions. An emittance dominated model is then used to determine the beam emittance. We note, however, that as the longitudinal beam size is not a measurement

is not a measurement of the longitudinal emittance, but rather the beam current, so too the transverse beam size may not be a measurement of the transverse beam emittance if the beam properties in the transverse plane are also space charge dominated. Previous measurements[8] using the emittance dominated optics model indicated that the space charge shift may be as high as 0.3, corresponding to what is typically considered to be the practical space charge limit.

It is easy to understand how a large ΔQ_{SC} can lead to emittance growth: the small amplitude particles have the largest tune shift and could be shifted onto a major resonance line. It is less easy to understand why instead the high tune shifts should lead to a beam loss. It may be that the particles with high amplitudes are lost; these particles experience a smaller tune shift, but also experience more nonlinear fields which may drive higher order resonances.

We have observed that very small (< 0.01) changes in the coherent betatron tunes can make greater than order of magnitude changes in the equilibrium beam intensity; this is somewhat unexpected for situations in which the incoherent tune shift is presumed to be more than an order of magnitude larger.

2.7 Beam Heating?

At present we have not found a technique which will preserve the beneficial aspects of electron cooling, thus allowing us to accumulate beams, while alleviating the detrimental effects (presumably very small beam emittances). In the future we will try various "heating" mechanisms, which have been tried without success in the past, though not under controlled conditions.

In the past we have tried heating the beam using white noise applied to a transverse kicker. To first order there was no change in the beam emittance (as measured by a "flying beam" scanner) but a large change in the beam lifetime. At high intensities we found this noise, to first order, merely excited coherent transverse instabilities and decreased the beam current. It turns out to not be such an easy problem to increase the beam emittance -- at high intensities, coherent oscillations tend not to decohere as rapidly as would be expected with an emittance dominated beam. In the future we will try using high frequency white noise (such that the beam wavelength is much longer than the noise wavelength) in conjunction with a coherent transverse damping system. The equilibrium proton beam emittance can be increased by mis-aligning the electron and proton beams in the cooling region[9] (Figure 7). We have demonstrated that the highest stored beam currents are obtained when the electron and proton beam are *not* exactly aligned so as to maximize the measured cooling forces. We do not, however, think that there is a lot to be gained here -- the operators routinely use the stored beam current as feedback in adjusting the beam alignment.

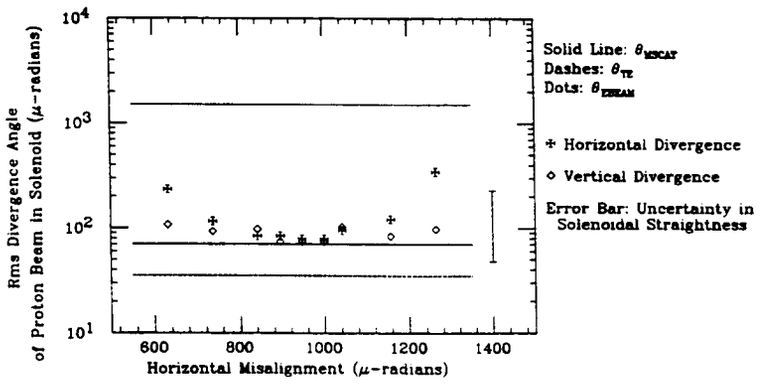

Figure 7. Proton beam H and V angular divergences in the cooling region vs. the H angular alignment between the beams.

We will also try heating the beam using multiple scattering from an internal target, though we do not expect this technique to have great potential. One can show that, for a zero-emittance beam, the small angle multiple scattering beam lifetime is $\approx 0.2Z/(Z + 1)$ times the single scattering lifetime. We would consequently expect that the single scattering lifetime will be $\approx 0.1\,\mathrm{s} \times A/\epsilon_{eq}$ where A is the ring acceptance and ϵ_{eq} is the equilibria emittance.

3. CONCLUSIONS

We have just begun to explore means for increasing the stored beam limitations. Thus far, we have identified no techniques which can substantially increase the limiting beam current without compromising our ability to quickly accumulate beam. There are many unanswered questions and mysteries. In early November we will systematically explore the beam transverse equilibrium using a flying wire profilometer; the information from this monitor should answer many of our question. In the meantime, we are beginning to take more seriously the possibility of drilling a small hole in the center of the cathode!

ACKNOWLEDGEMENT

This work was supported by the National Science Foundation under grant NSF PHY 90-15957.

REFERENCES

[1] Jacques Bosser, CERN (private communication: FAX's 14 and 15 January 1993).

[2] Dag Reistad, CELSIUS (private telephone communication 11 March 1993).

[3] Dag Reistad, CELSIUS (private communication, E-Mail 26 November 1992).

[4] Sergei S. Nagaitsev, Timothy J.P. Ellison, Michael J. Ellison, Daniel Anderson, "The investigation of space charge dominated cooled bunched beams in a synchrotron", these proceedings.

[5] Timothy J.P. Ellison, Sergei S. Nagaitsev, Mark S. Ball, David D. Caussyn, Michael J. Ellison, and Brett J Hamilton, Phys. Rev. Lttr. **70** No. 6 (1993) 790.

[6] R. E. Pollock "Experience at IUCF With Electron Cooling as an Injection Aid", these proceedings.

[7] M. Ball, D.D. Caussyn, T. Ellison, B. Hamilton, and S.Y. Lee, "Coherent transverse instabilities" in IUCF Scientific and Technical Report -- May 1990 - April 1991 (edited by E.J. Stephenson and R.D. Bent) p. 139.

[8] M. Ball, D.D. Caussyn, J. Collins, D. Duplantis, V. Derenchuck, G. East, T. Ellison, D. Friesel, B. Hamilton, B. Jones, S.Y. Lee, M. G. Minty, and T. Sloan, "Beam property measurement in the IUCF Cooler" (1991 IEEE Particle Accelerator Conference, 6 - 9 May 1991, San Francisco) p. 1770.

[9] Mark Ball, Dave Caussyn, Scott Curtis, Pete Dittner, Mike Ellison, Tim Ellison, Jeff Frey, Brett Hamilton, Jeff Hudson, Bill Lozowski, Chris Merton, Tom Rinckel, and Bill Jones, "Measurement of the equilibrium emittance of an electron-cooled 45 MeV proton beam", in IUCF Scientific and Technical Report -- May 1991 - April 1992 (edited by E.J. Stephenson and C. Olmer) p. 163.

EXPERIENCE AT IUCF WITH ELECTRON COOLING AS AN INJECTION AID*

R. E. Pollock
Indiana University Department of Physics and IUCF, Bloomington, IN, USA 47405

ABSTRACT
Methods have been developed to use electron cooling to assist in beam accumulation, both for stripping injection of unpolarized beams and for rf stacking of polarized beams, in the cooling ring-synchrotron at the Indiana University Cyclotron Facility (IUCF). In both modes, stored currents in excess of 0.5 mA are obtained, about one thousand times the cyclotron output current. Cooling-assisted injection is sensitive to the strength of the cooling force. New measurements of the longitudinal cooling drag rate are presented and some details of the stacking process are compared to numerical simulations. Limits to the performance in these injection modes are discussed.

1. INTRODUCTION

The IUCF Cooler [1, 2], a cooling ring-synchrotron of 3.6 T-m maximum rigidity has been operating, primarily for internal target experiments in nuclear and particle physics, since 1988. The low peak beam current, from the CW accelerator complex (the IUCF cyclotrons) used for injection, requires a current gain by beam accumulation of order one thousand to obtain useful event rates in experiments. Methods have been developed to use electron cooling to assist in the accumulation process, both for stripping injection of unpolarized beams and for rf stacking of polarized beams. In the stripping mode, an H_2^+ beam of 90 MeV from the cyclotron is employed. A stored proton beam current up to 1 mA at 45 MeV can be obtained after a few seconds of injection. Following acceleration, this beam can give a cycle-averaged luminosity approaching 10^{31} $cm^{-2}s^{-1}$ with a hydrogen jet target in threshold meson production experiments [3, 4]. Cooling during the experiment counteracts emittance growth from target scattering, with the transverse cooling rate setting the upper limit to target thickness [5]. Stored beams of deuterons and $^3He^{++}$ are prepared also by this method.

Because polarized ions with attached electrons are not presently available from the IUCF accelerators, the stripping mode cannot be employed to accumulate polarized beams. A more intricate method which employs fast kickers, rf manipulations and cooling has been developed [6]. The current state of this method is summarized in Section 4. Injecting polarized protons at 198 MeV, a current of 0.56 mA has been reached, and accumulation rates in excess of 2 μA/s have been observed. The slow build-up of stored current by stacking makes this mode useful primarily for experiments with very much thinner targets than are used with stripped injection. Filling and measurement portions of a run cycle are then measured in minutes rather than seconds. Polarized beam-polarized target experiments, for example, have been carried out with cycle-averaged luminosity of 10^{29} $cm^{-2}s^{-1}$. Polarized deuteron beams are also being delivered by the cooling-assisted stacking method.

The prospects for further improvements to IUCF Cooler injection methods are of considerable interest to our user community. Studies of limiting phenomena continue to be pursued. Some comments on the present state of our understanding are presented in Section 7.

2. RELEVENT MACHINE PARAMETERS

Typical cyclotron beam current is about 0.5 μA. The time microstructure is a stream of ±0.2 ns pulses normally spaced at 1/6 of the Cooler ring circumference. The beam normalized emittance is about 1 π μm and the momentum spread about ±0.03%. Beam is often directed to other users between Cooler injection pulses.

* Work supported in part by the U. S. National Science Foundation under grant NSF PHY 90-15957.

The IUCF Cooler, for economy of design, has a small phase space volume for beam storage. The acceptance in each transverse plane is about 16π μm, while the momentum acceptance is ± 0.2%. The uniform length of the confinement solenoid of the electron cooling system occupies about 2.5% of the 87 m ring circumference. The electron beam is 25 mm diameter and operates at currents up to 2.5 A at 100 keV, a limit set by a collector power dissipation of 20 kW. The electron system can cycle between two energies so cooling is available at injection and again after synchrotron acceleration. Protons up to 415 MeV have been cooled.

3. STRIPPING MODE

A carbon foil, of nominal thickness 10^{18} atoms/cm^2 is mounted above the closed orbit, with its lower edge unsupported. A macropulse of a few ms duration is split from the cylotron output beam, directed down the injection path, into the ring and onto the foil edge. A set of bumper magnets with about 20 ms rise and 0.5 ms fall times raise the ring closed orbit locally at the foil, so that the stripped beam lies within the ring acceptance in transverse phase space, but cooled beam from prior injection cycles is below the foil edge. As soon as the beam pulse ends, the closed orbit is lowered and transverse cooling begins to reduce the emittance of the halo of freshly-injected particles. After about 0.4 s, the process is repeated. The measured beam lifetime while intercepting the foil is 3 ms, about 3000 turns. Both emittance growth and energy spread contribute to the loss rate. The stored current increase per bump is about 0.1 mA or 200 times the cyclotron ion current. This indicates a rather low proton injection efficiency of about 3%. However, the stored current limit set by beam stability is reached after a few repetitions, so the filling time is comparable to times for acceleration and high energy cooling, and performance is not very sensitive to this efficiency factor.

The cooling-assisted stripping process is found to be very sensitive to the exact position of the closed orbit with respect to the foil edge, because of the limited acceptance of the storage ring. Macropulse width and repetition period are other tuning variables. Higher electron beam currents permit higher repetition rates.

Filling rate in the stripping mode improved in 1992 after a chance observation with a new diagnostic [7] that the cooled beam was being decelerated when brought close to the foil edge. The flat top of the bump pulse was then reduced from about 50 to about 5 ms. This smaller time for interaction of the beam distribution tail with the foil led to an increase in the added stored current from about 0.04 to about 0.1 mA per bump, probably by permitting a more efficient sharing of the available transverse phase space during the macropulse.

4. STACKING MODE

The rf stacking mode employs a single turn of beam, placed onto the closed orbit by a pair of fast kickers. The aperture function β_x is 1.8 m at the injection point and 11 m at the matched kicker pair at $\pm 90^\circ$ of phase advance from that point. The "fast" kicker pulses have 0.1 μs rise and fall times, adjustable duration and amplitude, and may be synchronized to ring or cyclotron rf systems. The kickers produce an 8 mm local orbit excursion at the injection septum in a region with 4 m dispersion. By lowering the momentum after injection by 0.2%, the new beam can survive subsequent kicks. To prepare the beam for rf deceleration, a debunching 90° rotation in the longitudinal phase space is performed, turning the subnanosecond time spread of the cyclotron microburst into a momentum spread of less than 0.005%, so that a small bucket can contain the decelerating beam. Rf synchronization and careful matching of the cyclotron orbit radius at extraction to the Cooler radius is essential in avoiding dilution in the debunching step. The sixth harmonic rf system of the Cooler ring performs the debunching phase space rotation on the kick-injected pulses. This requires an amplitude of about 1 kV and a duration of about 0.1 ms. The amplitude is then reduced to about 50 V to match the bucket volume to the cyclotron pulse. A pause of 5 ms is inserted to allow the operator to view the intensity at this stage as a tuning aid. The deceleration begins with a phase jump, and takes about 15 ms. The rf amplitude is turned off to release the beam near the stack momentum. Electron cooling then slowly contracts the phase space. After a 0.1 s delay, the kick/debunch/decelerate/cool cycle can be repeated.

A limit to this process is set by the action of the kickers on a coasting stack. Despite careful matching to produce a purely local orbit excursion, there is some transverse beam heating from the residual mismatch. Slow time drifts due to kicker thyratron temperature changes are particularly troublesome in maintaining an optimum match over long runs. If the cycle repetition rate is too high, emittance growth overwhelms the transverse

cooling rate, signalled by a reduction in beam lifetime with kickers firing. Since the tail of the beam is being removed, the loss rate increases if target material in the path of the beam regenerates tails.

Beginning in 1991, the stacking method has been improved by employing two rf cavities, one for debunching and deceleration and a second for bunching of the cooled stack. The kicker fire is synchronized to this second cavity to ensure that the cooled bunch is centered on the kicker pulse flattop. The main part of the stored beam does not then see the edges of the kicker pulses and time matching becomes much less critical. With this change, the optimized performance has increased from a kicker loss rate of about 10^{-4} /kick at a 2 Hz rate to about 10^{-5} /kick at a 10 Hz rate. The rate limit is no longer set by transverse cooling and kicker mismatch but by the time needed for longitudinal cooling into the stack bucket. Beam which has not cooled enough before the next kick is vulnerable and a loss of injection efficiency is observed if the repetition rate is too high. Phase displacement would set a separate limit if the decelerating buckets were larger. The optimum repetition rate increases with electron current so that we now operate at 2.5 A (0.5 A/cm^2) to reach 10 Hz. Stored current increasing at 2 μA/s may be obtained under these conditions, corresponding to about 40% efficiency in transfer of one turn's worth of 200 MeV polarized cyclotron output into the cooled stack pulse.

5. NUMERICAL SIMULATIONS

The suite of programs developed to study and optimize the debunching procedure [6] has been extended to observe details of the capture by cooling in a small first harmonic bucket. It was found that the simplified step cooling force used in this earlier work underestimated the time delay in the formation of narrow time structure. When a more realistic velocity-dependent drag rate was incorporated, the simulation began to show good qualitative agreement with observations. A sample of the simulation output is given in Fig 1.

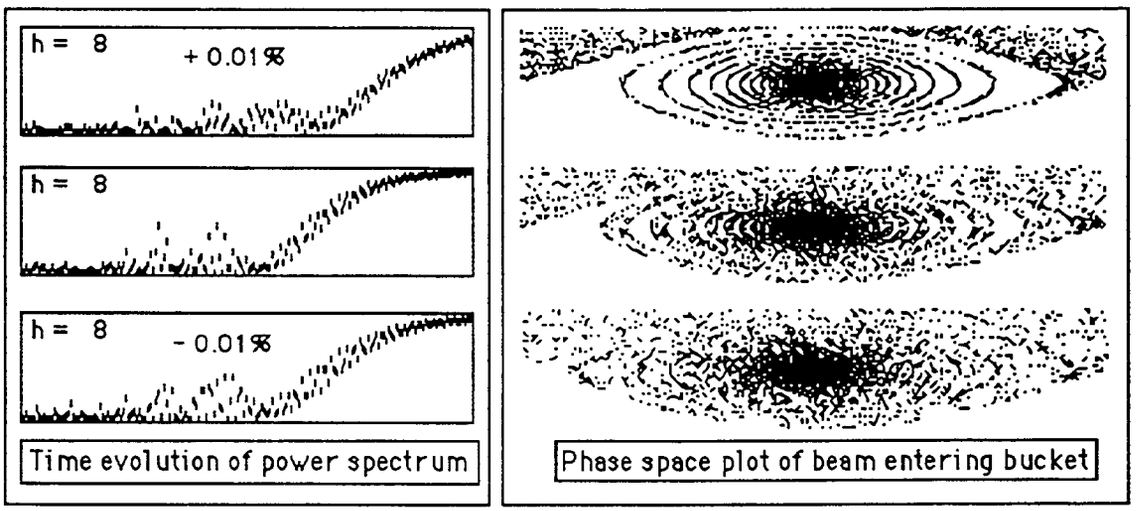

Figure 1. An ensemble of particles with a random distribution of initial phases and identical initial momenta is drawn down into a first harmonic stacking bucket by electron cooling. The simulation cooling rate is higher by a factor of 8 than in our ring. The three cases represent slightly different electron momentum relative to the momentum defined by the bucket rf frequency. On the left is shown the time evolution of the peak in the power spectrum at the eighth harmonic of the orbit frequency. Note the precursor peaks which are visible before the narrow time structure of complete cooling has developed. A peak occurs when the shrinking ellipse width passes a sub-multiple of the bucket width. On the right is a cumulative phase space plot of particle positions recorded at equal intervals of time. Note that the phase space spiral for all particles passes near the unstable fixed point on entering the bucket. This region is vulnerable to kicker transverse heating.

Precursor peaks which appear in a spectrum analyzer display at higher harmonics are quite similar to those observed in the simulated power spectrum. Understood as a consequence of the cusped projected density distribution of the shrinking hollow ellipse, which produces a peak at harmonic h when the two cusps are

separated in phase by $2\pi/h$, the time delay before observation of peaks at different h can be used to extract a cooling rate. See next section. Figure 1 shows that the process is not strongly sensitive to changes in electron momentum of $\pm$ 0.01%. It is interesting that the phase space trajectory for any initial phase passes close to the unstable fixed point as each particle enters the bucket. If the kickers are fired for the next injection cycle while particles from the previous cycle are slowly passing this point, transverse heating through kicker time mismatch may reduce the injection efficiency.

6. DRAG RATE MEASUREMENTS

A method of measuring the longitudinal drag rate as a function of relative velocity while stacking has been developed. The rf deceleration is interrupted after a selected fraction of the frequency change is completed, leaving much slower cooling to finish the velocity change. The time delay between injection and cooled bunch formation is measured. The change in delay per unit energy change is the inverse of the longitudinal drag rate, shown as a function of relative velocity in Fig. 2. This data is supplemented in Fig. 2 by the drag rate at very low relative velocity extracted from the delay in precursor peak formation for h = 2 . . 24, as shown in Fig. 3.

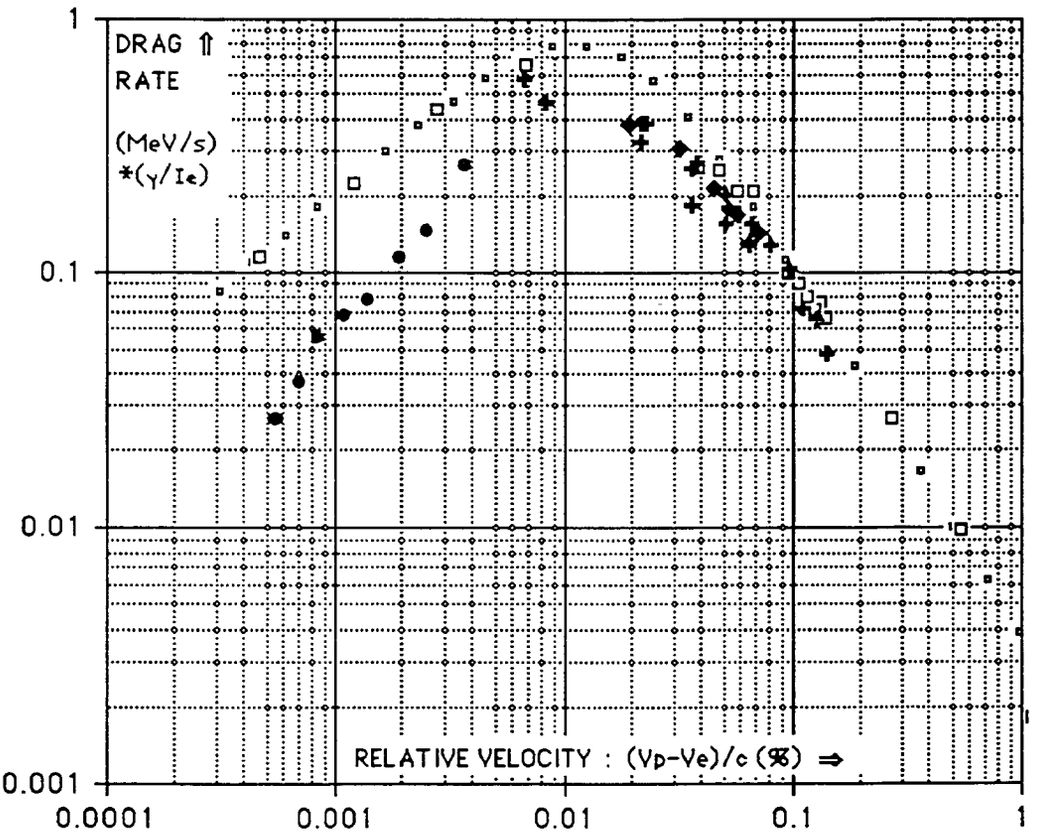

Figure 2. The large squares are 45 MeV proton data [8]. The small squares are a four parameter analytic expression fit to this data which is useful for longitudinal simulations. The filled diamond and + symbols show measurements from the time delay in the power spectrum for injected beam of 200 MeV. Data are normalized to 1 Ampere of electron current (25 mm cathode diameter) and to $E/mc^2 = 1$. The solid circles are normalized drag rates extracted from the precursor peak delay. See Fig. 3.

Agreement between data sets is reasonable at large relative velocity but the stacking method data near the peak drag rate are seen to fall below the cooled equlibrium data. This is attributed to the short time delay which has not allowed the freshly injected beam to cool transversely to equilibrium emittance. Minimizing this delay

is a useful tuning aid in matching the injection trajectory to the closed orbit. There is a significant disagreement in slope at low relative velocity. The cooled equilibrium data show a drag rate proportional to v^n where the best fit has n = 0.7, while the stacking data are consistent with n = 1.05 ± 0.15. The low relative velocity region is known to be sensitive to power supply ripple [8], which has not been cancelled in stacking operation, as well as to magnetized cooling. These data may well indicate the strong influence of incomplete transverse cooling for low relative velocity.

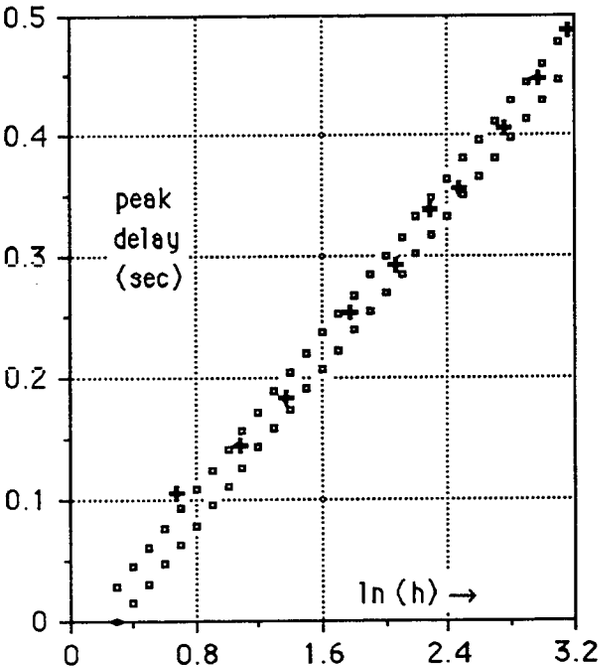

Figure 3. The delay before the cooling precursor peak forms is linear vs. the natural logarithm of the harmonic number h. The best fit slope (small squares) gives an emittance cooling time of 80±2 ms (1.82 A, 198 MeV).

7. FUTURE PROSPECTS

The proton current in stripping mode would benefit most from raising the cooled beam stability limits. Active damping of transverse instabilities and flat-bottomed buckets for reduced tune shifts are under investigation. For other stripped ion species, more development effort may be expected to yield an improved transfer efficiency between cyclotron and Cooler. A thinner stripper foil would be helpful for these beams.

The stacking mode, with its higher injection energy, would seem now capable of reaching several mA of polarized beam. Multiplication of an observed filling rate of 0.12 mA/min with a best observed lifetime while kicking of 1 hour would give 7 mA. However the best stored current to date with this mode is lower by an order of magnitude. There is evidence for a stored-current-dependent loss of transfer efficiency with a threshold near 0.4 mA. Longitudinal space charge effects [9] may play a role by limiting the time contraction. Other physics cannot be excluded at this stage. A more intense polarized beam source coming into operation in the next few months will allow more rapid exploration of the phenomena setting the present limit.

The present performance of the stacking mode is critically dependent on good cooling. Drag rates above 1 MeV/s and longitudinal cooling time of 60 ms are being exploited with electron beam power densities of 55 kW/cm^2. It is not clear that much better cooling is to be expected. Further injection improvements must be obtained instead by improvements to or radical changes in the procedures preceding the cooling step.

REFERENCES

[1] R. E. Pollock, Proc. IEEE Part. Accel. Conf. (1989), IEEE Publ. 89CH2669-0, p. 17.

[2] R. E. Pollock, Proc. 19th INS Symposium, Tokyo, 1990, "Cooler Rings and their Applications", ed. T. Katayama, A. Noda, World Scientific, 1991, p. 4.

[3] H.-O. Meyer et al, Nucl. Phys. **A539** 633 (1992).

[4] H. Rohdjess et al, Phys. Rev. Letters **70** 2864 (1993).

[5] R. E. Pollock et al, Nucl. Instrum. Methods **A330** 380 (1993).

[6] A. Pei, PhD dissertation, Indiana University (1991).

[7] R. E. Pollock et al, Nucl. Instrum. Methods **A330** 27 (1993).

[8] T. Ellison, PhD dissertation, Indiana University (1991).

[9] T. J. P. Ellison et al, Phys. Rev. Letters **70** 790 (1993).

THE DEVELOPMENT OF THE TECHNOLOGY FOR ELECTRON COOLING IN THE 2-20 GeV/nucleon ENERGY RANGE*

S. Nagaitsev, D. Anderson, M. Ball, D. Caussyn, T. Ellison, B. Hamilton, P. Schwandt
The Indiana University Cyclotron Facility
2401 Milo B. Sampson Lane, Bloomington, IN 47405, USA

J. Adney, J. Ferry, M. Sundquist
The National Electrostatics Corporation, Graber Rd., Middleton, WI 53562, USA

D. Reistad
The Svedberg Laboratory, Box 533, S-751 21 Uppsala, Sweden

M. Sedlaček
The Alfvén Laboratory, S-100 44 Stockholm, Sweden

ABSTRACT

The use of low energy electrons, in the energy range of $\leq$ 300 keV, for cooling $\leq$ 550 MeV/nucleon ion beams, is a well-developed technology. In the past 5 years, 8 systems have been commissioned[1],[2] in the U.S. (1), Europe (6), and Japan (1). In all cases, these systems are functioning splendidly, allowing accumulation of polarized and rare isotope beams, and providing beams of unsurpassed quality for high resolution atomic, nuclear, and particle physics research. We believe that intermediate energy electron cooling, in the electron energy range of 1 − 10 MeV for cooling 2 − 20 GeV/nucleon ion beams, would be exploited on a similar scale today if the technology were available. Such systems could enhance the performance of light and heavy ion colliders, provide the same opportunities for performing high precision nuclear and particle physics in a storage ring environment as are available now at lower energies. These applications are discussed in the following section. Above electron energies of about 500 keV, however, the traditional approach of using a Cockcroft-Walton power supply and a magnetically-confined electron beam becomes impractical. A non-magnetically confined electron beam generated and collected in the terminal of a Pelletron accelerator, however, seems ideally suited for these higher energy systems[3]. Although this technology has been partially developed, order of magnitude improvements in the performance demonstrated to date are necessary to exploit this technology. This paper will outline the design considerations behind the system and the current status of the project.

1. MOTIVATION AND APPLICATIONS

1.1 Increasing the luminosity of light ion colliders

The luminosity, L, of a bunched-beam collider depends upon the ion beam current, I, and normalized rms emittance, ϵ, as I^2/ϵ; the space charge tune shift, (ΔQ_{SC}) limit, however, varies as I/ϵ. Consequently, when pushing colliders to higher luminosities after the tune shift limit has been reached at low energies, I and ϵ are usually increased together, keeping the quantity I/ϵ constant, resulting in $L \propto I$.

Another possible approach is to reduce ϵ after acceleration in lower-energy injector. Since ΔQ_{SC} is usually only significant in the lowest energy synchrotron, smaller values of ϵ may be allowed later in the chain

*This work was supported by the TNRLC under grants RGFY9158 & RGFY9258. Additional support by Indiana Univ. and NEC.

of accelerators providing the beam−beam tune shift is not a limitation ($\Delta Q_{SC} \propto C/\gamma^2$ where $C \propto \gamma$ is the ring circumference; thus $\Delta Q_{SC} \propto 1/\gamma$). Stochastic cooling is not able to quickly increase the already high phase space density of beams in synchrotrons fed by modern sources, but such beams are just "cold" enough for rapid intensity-independent electron cooling. Such an approach could provide increased luminosity via operation with the same beam current and reduced emittance, or provide the same luminosity via operation with a reduction in the beam current and a greater reduction in emittance[4]. There are advantages resulting from either reduction: the lower beam current reduces radiation damage and synchrotron radiation at very high energies; the lower beam emittance reduces the aperture requirements in all the following machines -- a *very* considerable economic benefit. Since luminosity is a direct measurement of the physics research potential of a machine, the $1 - 10$ M$ electron system cost makes intermediate energy electron cooling a very economical option in light of the capital and daily operating costs of large colliders such as the SSC and DESY.

Although $\Delta Q_{SC} > 0.3$ for the 0.6 GeV beam injected into the SSC LEB, $\Delta Q_{SC} \approx 0.06$ at injection into the MEB[5] at 12 GeV; consequently the beam emittance could be reduced by up to a factor of $3 - 4$ at this point. An electron cooling system installed in an available straight section of the SSC MEB *without* lattice modifications could reduce larger-than-design beam emittances by an order of magnitude in about 26 s, and thus not significantly increase the SSC filling time. The cooling rates could be over an order of magnitude higher in the MEB if lattice modifications were made to incorporate electron cooling as an integral component.

The emittance of proton beams in HERA is limited by space charge effects in the first synchrotron[6], DESY III. In the following ring, PETRA II, $\Delta Q_{SC} \approx 0.03$; consequently the emittance could be reduced by approximately a factor of 10. An electron cooling system installed in an available straight section could attain this reduction in about 1/10th of the ring cycle time of 240 s.

The benefits of electron cooling in high energy colliders would be even more dramatic if the machines were operated with less bright polarized beams, or with heavy ion beams.

1.2 Increasing the luminosity of heavy ion colliders

The beam emittance in heavy ion storage rings and colliders is often limited by intrabeam scattering, IBS, the rate for which scales as Z^4/A^2. In very high energy colliders electron cooling can reduce the beam emittance before acceleration in the final machine, compensating for IBS at low energies. For colliders operating with beam energies less than 30 GeV/nucleon, the colliding beams can be continuously electron cooled.

The electron cooling time would be as low as 0.1 s for the $4 - 7$ GeV fully-stripped gold beams in the proposed KEK-PS[7] heavy ion collider due to the A/Z^2 scaling of the cooling time and relatively low beam energy. Since the space charge and beam-beam tune shifts are estimated to be $< 10^{-3}$ and 10^{-5}, respectively, the beam emittance could potentially be reduced by over a factor of 100, resulting in a 10 to 100 fold luminosity increase.

1.3 Improving the performance of light ion storage rings

Using a storage ring with internal targets and cooled beams has proven to be a far superior environment for many classes of experiments[8]. At IUCF the possibility of extending this technology from the 500 MeV energy limit of the IUCF Cooler ring to 15 GeV energies (in a conceptual ring called "LISS" -- the Light Ion Spin Synchrotron) is currently being explored[9].

An electron cooling system installed in one of the 4 straight sections reserved for stochastic cooling in the 2.5 GeV CoSy ring in Jülich could provide order of magnitude higher cooling rates than can be achieved with stochastic cooling at a fraction of the cost.

2. TECHICAL PROJECT OVERVIEW

This project, which began in April 1991, has two principal goals: (1) to determine the feasibility of electron cooling the 12 GeV/c beams in the SSC MEB; and (2) to develop and demonstrate the necessary technology, leading to its commercial availability. The first goal has been completed. In the attached recently-completed design report[10] we have shown that all the necessary subsystems are technically feasible; potential problems have either been determined to be unimportant, or straightforward solutions have been identified.

2.1 Demonstration of electron recirculation

The work thus far, however, still leaves unresolved the primary problem, which is to convincingly demonstrate that such a system as a whole can indeed be built and made to operate reliably. The principal technical problem is to demonstrate successful recirculation of a dc, multi-MeV, multi-ampere electron beam. The recirculation principle is shown schematically in Figure 1. The primary current path is from the cathode (at the high voltage terminal potential) to ground (where the electron beam interacts with the ion beam and cooling takes place), then to the collector located in the terminal, and finally through the collector power supply back to the cathode.

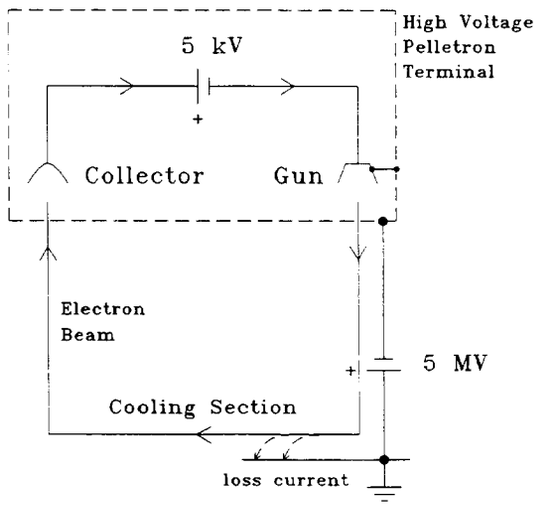

Figure 1. Simplified electrical schematic of the electron recirculation system.

Recirculation allows recovery of $\approx$ 99.9% of the beam energy. By illustration, if the terminal potential, W, (beam energy/e) were 5 MV, the beam current, I_e = 2 A, and the collector power supply voltage, V_{col} = 5 kV, although the *imaginary* beam power would be 10 MW ($W \cdot I_e$), only 10 kW of real power ($V_{col} \cdot I_e$) would be needed to recirculate the beam providing no current were lost to ground, $I_{loss} = 0$.

Collection inefficiencies, $\delta \equiv I_{loss}/I_e$, in the present low energy ($\leq$ 0.3 MeV) electron cooling systems are typically $\approx 10^{-4}$, though values as low as 1×10^{-6} have been demonstrated[11] at IUCF. We estimate that collection inefficiencies must be in the range from 10^{-5} to 10^{-4} for the higher energy systems for manageable power dissipation. To date the necessary electron collection efficiencies have been obtained in beam tests at the National Electrostatics Corporation (NEC), though with insufficient (0.12 A) current[12]; the required currents have been obtained (> 6 A) in a system used as a free electron laser driver at the University of California - Santa Barbara, though only in a pulsed mode with insufficient collection efficiencies[13]. Our goal is to demonstrate reliable *high efficiency dc* recirculation of a 2 A electron beam using the 2 MV Pelletron accelerator at NEC.

2.2 Plans to achieve stable high efficiency recirculation

The electron recirculation system design incorporates many improvements based upon the experience of previous work. Some of these improvements include:

--*Improved beam diagnostic systems*. The previous system tested at NEC had no working beam diagnostic systems for beam currents exceeding 10^{-4} A. The present system design includes specially-designed diagnostics to allow measurement of the beam position and beam profile for currents in the range from 10^{-6} to 10^{1} A.

--*Improved electron collector*. Our collaborators from Novosibirsk have already demonstrated an electron collector suitable for this application. IUCF is also building a collector which includes a dipole suppressor which may allow δ as small as 10^{-6}.

--*Improved electron gun*. The present gun design will produce a much smaller beam emittance and has true Pierce geometry in the gun region.

--*Ion clearing electrodes*. These high-intensity, low-emittance electron beams have space charge, rather than emittance, dominated optics. The system pressure will be improved using nonevaporable getter pumps, and ion clearing electrodes will be employed to prevent space charge neutralization.

The beam optics have been calculated from the gun through to the collector as a function of electron beam current, and all the ion optical elements have been field mapped. This preparation, together with a computer control system, ion clearing and improved vacuum systems, and beam diagnostic systems, (all of which were lacking in the previous system), will allow systematic comparison of the calculated and measured beam optics as a function of current; such a systematic approach was not possible in the past. It will thus be possible to understand problems as they inevitably arise during the commissioning of this system.
Technical details on the design of the electron gun, acceleration system, recirculation beamline, electron collector, beam diagnostic systems, etc. may be found in the MEB E-Cool Design Report (Ref. [10]) and in Ref. [14].

2.3 Project Status and Schedule

Nearly all components for the electron recirculation beamline have been procured. The magnets have been machined, assembled, mapped and shimmed. Figure 2 shows the schematic status of the procurement process. The Pelletron accelerator has been raised to allow more room for the beamline and alignment systems, and concrete radiation shielding has been poured around it. The Pelletron has been refurbished and operated at the design voltage and the radiation monitoring system and power supplies have been installed.

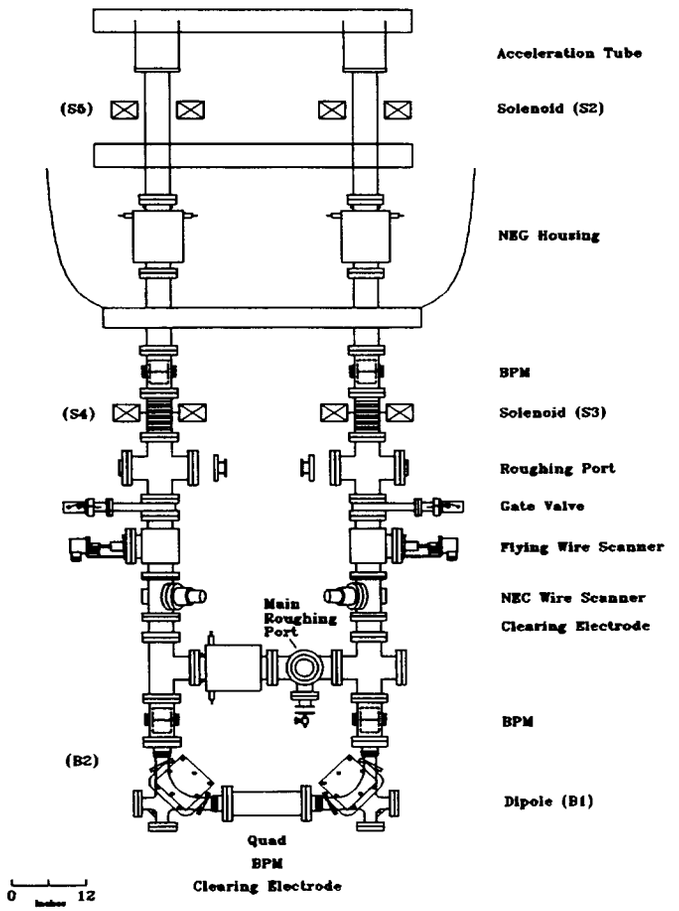

Figure 2. Schematic of recirculation system beamline procurement.

The schedule for the completion of this project is divided into two principal parts. During the first 10 months the procurement, assembly, and system checkout will be completed. The following 14 month period will be devoted to operation and modifications of the recirculation system. We expect stable low current (< 0.1 A) operation within the first three months; at that time the low-current beam diagnostic (rotating wire)

systems will be replaced with higher current (residual-gas ionization detection) systems, and the remaining 11 months will be devoted to operation at high currents (up to 2 A).

REFERENCES

[1]. Robert E. Pollock, "Ion synchrotrons and storage rings for nuclear and atomic physics", Proc. of the 1987 IEEE Particle Accelerator Conference", edited by Eric R. Lindstrom and Louise S. Taylor (IEEE, Piscataway-NJ, 1987) pp. 245-248.

[2]. D. Möhl, "Perspective of ion cooling rings", *Proc. 11th Int. Conf. on Cyclotrons and their Applications*, edited by M. Sekiguchi, Y.Yano, and K. Hatanaka (Ionics, Tokyo 1987) pp. 116 - 122.

[3]. D.B. Cline, D.J. Larson, W. Kells, F.E. Mills, J. Adney, F. Ferry, and M. Sundquist, "Intermediate energy electron cooling for antiproton sources using a Pelletron accelerator", IEEE Trans. Nucl. Sci. Vol. **NS-30** No. 4 (August 1983) pp. 2370−2372.

[4]. Tim Ellison, Jim Adney, Dan Anderson, Mark Ball, Dave Caussyn, Mike Ellison, Jim Ferry, Brett Hamilton, Sergei Nagaitsev, Dag Reistad, Mark Sundquist, Peter Schwandt, Miro Sedlacek, "Multi-MeV electron cooling -- a tool for increasing the performance of high energy hadron colliders?", Fifth Annual International Industrial Symposium on the Super Collider (IISSC) (6-8 May San Francisco CA).

[5]. *Superconducting Super Collider Laboratory Site-Specific Conceptual Design Report* (SSCDR, July 1990).

[6]. Ferdinand Willeke, DESY (private e-mail communication, 25 March 1993).

[7]. J. Chiba et al., "The PS Collider design report 2 (in English)", KEK Report 90-13 (September 1990).

[8]. R.E. Pollock, "Storage rings for nuclear physics", Ann Rev. of Nucl. and Particle Science **41** (1991) 357.

[9]. S.E. Vigdor, "Advantages of cooled, stored, polarized beams for precision symmetry tests at Multi-GeV Energies", *Proc. of Workshop of Future Directions in Part. and Nucl. Physics at Multi-GeV Hadron Beam Facilities*, (Brookhaven Nat. Lab. March 1993).

[10]. The MEBEC Group, *Design report on the feasibility of decreasing the emittance of beam in the SSC by electron cooling in the Medium Energy Booster* (I.U.C.F. publication, October 1992).

[11]. Timothy JP Ellison, Robert J. Brown, and Brian D. DeVries, "The IUCF electron cooling system collector performance", Nucl. Instr. and Meth., **B40/41** (1989) 864-869.

[12]. D.J. Larson, D.R. Anderson, J.R. Adney, M.L. Sundquist, F.E. Mills, "Operation of a prototype intermediate-energy electron cooler", N.I.M. **A311**(1992) 30−33.

[13]. Luis R. Elias and Gerald Ramian, "Recirculating electrostatic accelerators", IEEE Trans. Nucl. Sci. **NS−32** No. 5 (October 1985) 1732.

[14]. Dan Anderson, Jim Adney, Mark Ball, Dave Caussyn, Tim Ellison, Jim Ferry, Brett Hamilton, Sergei Nagaitsev, Dag Reistad, Mark Sundquist, Peter Schwandt, Miro Sedlacek, "The development of a prototype multi-MeV electron cooling system", 1993 Particle Accelerator Conference, 17-20 May 1993, Washington, DC.

ELECTRON COOLING OF HIGHLY CHARGED HEAVY IONS AT THE ESR

M. Steck, K. Beckert, F. Bosch, H. Eickhoff, B. Franzke, O. Klepper, R. Moshammer, F. Nolden, H. Reich, P. Spädtke

Gesellschaft für Schwerionenforschung, Postfach 110552, D-64220 Darmstadt, Germany

Abstract

The temperature of heavy ion beams in equilibrium between electron cooling and heating by intrabeam scattering has been measured over a large range of ion and electron beam intensity. Momentum spread and emittances increase with the ion beam intensity and decrease for stronger cooling with higher electron currents. The dependence of the ion beam temperature in equilibrium on the ion charge is not very pronounced. A comparison of cooling forces at small relative velocity for C^{6+}, Ti^{22+} and Au^{79+} shows a strong increase with the ion charge which however favours a proportionality to $Z^{1.5}$ rather than a Z^2- dependence which is expected from a straightforward theoretical estimate. Longitudinal cooling rates determined from the cooling force are in reasonable agreement with measured heating rates by intrabeam scattering.

1. INTRODUCTION

The electron cooling system of the heavy ion storage ring ESR [1] is designed for cooling of heavy ions from the variable injection energy of the heavy ion synchrotron SIS [2] down to the minimum energy that can be achieved after deceleration. Moreover it opens a large field of atomic physics investigations concerning the interaction between bare or few electron ions and free electrons. Studies of radiative electron capture and associated X-ray emission, dielectronic recombination and laser induced recombination have already been performed successfully [3]. Cooling of stored beams which are heated by the internal gas target particularly in connection with radioactive beams is another application of electron cooling with growing importance.

2. STATUS OF THE ESR ELECTRON COOLING SYSTEM

Several problems with respect to the ambitious objectives of electron beam operation at high energy, strong magnetic guiding field and intense electron beam have been faced. Design parameters for the electron cooler can be found elesewhere [4], therefore only a short status report is given here. The operation voltage was limited by an unsuitable connection tube between high voltage platform and power transformer. First tests after replacement of the troublesome connection and separate tests of most of the components raise expectations to be soon able to achieve stable conditions for voltages up to 250 kV. Operation at very low energies after ion beam deceleration seems to be restricted by a fast regulation ripple (in the range of a few kHz) at voltages below 50 kV. Beam experiments have to show whether this ripple on the order of ± 5 V (compared to ± 1 V for voltages above 50 kV) is adequate for beam cooling or whether a scheme with an additional power supply for better energy stabilization has to be considered.

Although the cooler has been tested off line with electron currents up to 3 A the cooling current is usually less than 0.5 A as the high recombination rate in the cooler determines the lifetime of cooled heavy ion beams. Moreover fluctuations of the electron beam energy due to varying space charge compensation have been observed for higher electron currents. A proper electrode system for clearing or trapping such ions is desirable to achieve for currents in excess of 0.5 A the same level of energy stability ($\delta E/E \approx 10^{-6}$) that was observed in cooling experiments with electron currents below 0.5 A. An improvement of the current collection efficiency of the collector system has already been achieved by reduction of the length of the collector entrance electrode resulting in a current collection efficiency better than 0.9998 for electron currents up to 1 A and better than 0.9995 up to 2 A.

The magnetic field is at present limited to 1.1 kG because of an underdesigned power supply for the ion beam correction. Electron beam tests have shown that operation with higher magnetic field ($B \geq 1.0\ kG$) may be limited by discharge phenomena most likely occurring in the gun region. Installation

of a screening electrode to avoid a field configuration in which slow electrons can be trapped is expected to be a cure for such discharges.

First tests to decelerate ions in the ESR were successful, but cooling of decelerated beams will not be available before installation of the control hardware for ramped cooler operation. Modification of the existing control hardware for ramped operation is foreseen for early next year.

3. COOLING TO EQUILIBRIUM

Beams of bare ions from C^{6+} to U^{92+} have been stored and cooled in the ESR, but also some partially stripped ions have been prepared for atomic physics experiments. The energy was determined by the injection energy from the synchrotron SIS between 150 and 300 MeV/u with the maximum energy corresponding to the high voltage limit for reliable operation of the cooling system. The major concern of the cooling experiments was the attainable phase space density of heavy ion beams with electron cooling. The momentum spread of the ion beam in equilibrium was determined either by FFT analysis of the Schottky noise or BTF measurements with the standard ESR diagnostic system [5], emittances were determined with charged particle detectors measuring the transverse distribution of down charged ions produced by radiative electron capture in the cooling section [6]. All measurements were routinely preceded by a procedure to minimize angular misadjustments of electron and ion beam [7]. Fig. 1 exemplifies the dependence of the ion beam emittance (2σ) and momentum spread (FWHM) for a medium and a very heavy ion beam (Ti^{22+} and Au^{79+}) as a function of the number of stored particles under constant cooling conditions. The increase of the ion beam temperature with the particle number can be well explained with stronger intrabeam scattering in an ion beam of higher intensity. In all experiments by now a $N^{1/3}$-dependence of the momentum spread on the number of stored particles N has been observed. For the transverse emittance results varied in the range $N^{1/3}$ to $N^{2/3}$ [7] indicating a high sensitivity to the actual cooling conditions.

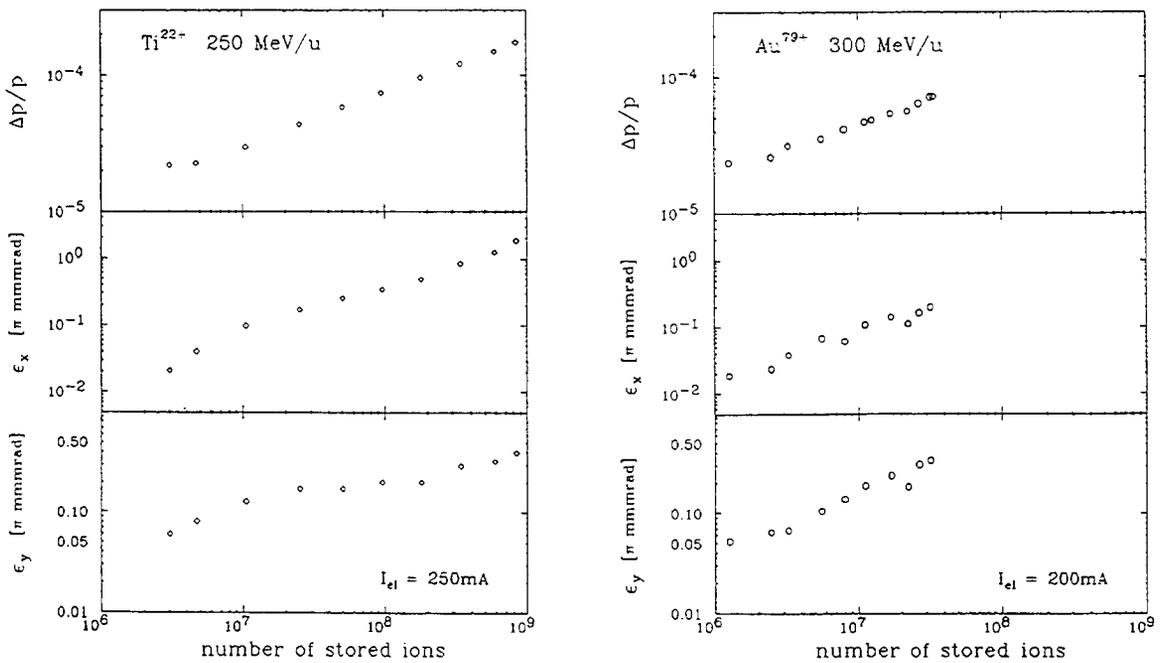

Figure 1: Ion beam momentum spread and emittances as a fuction of the number of stored particles for a lighter (Ti^{22+}) and a heavier (Au^{79+}) ion species.

Assuming a balance between cooling and heating rate by intrabeam scattering the equilibrium state must depend on the electron beam intensity which determines the cooling rate. Higher electron currents result in an increased cooling rate which corresponds to a lower equilibrium temperature of the ion beam. Calculations for the gun design indicate no considerable dependence of the quality of the electron beam on the electron current up to 1 A. The equilibrium beam temperatures as a function of the electron current are shown in Fig. 2. The systematic decrease for higher electron currents is attributed to a cooling rate that increases proportional to the electron current. The momentum spread dependence in

all experiments was close to $I_{el}^{-0.3}$, the decrease of the horizontal and vertical emittance can be described by a $I_{el}^{-\alpha}$-dependence with $\alpha \simeq 0.1 - 0.5$. The vertical emittance usually shows a weaker dependence on I_{el} and is also less sensitive to the vertical alignment, since the profiles of down charged ions which are utilized for the optimization procedure are within a range of ± 1 mrad not affected significantly by angle misadjustments.

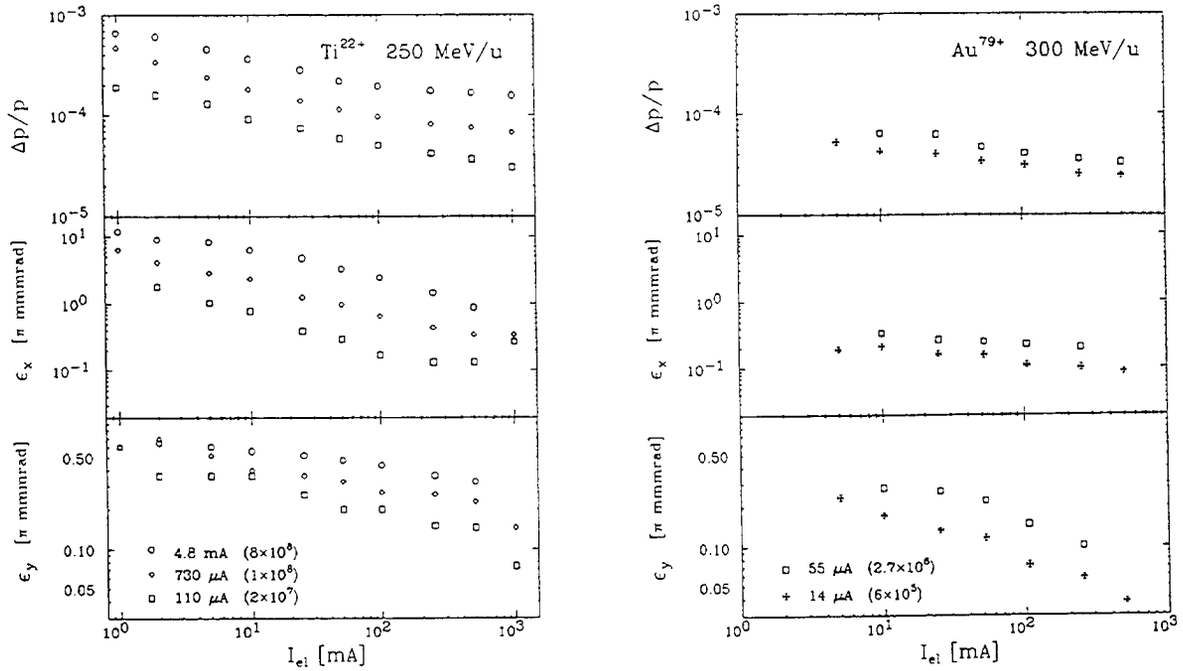

Figure 2: Equilibrium temperature of two ion species (Ti^{22+} and Au^{79+}) descends as a function of the electron current due to stronger cooling. (Ion currents as indicated.)

The dependence of the equilibrium temperature of the ion beam on the ion charge and mass for constant cooling current is not very expressed as can be derived from Figs. 1 and 2. This is clearly indicated by the dependence of the momentum spread as a function of the particle number shown in Fig. 3 which includes additional results from experimental runs. Only Schottky spectra without strong indications of collective beam behaviour were analysed for this comparison because the analysis of such spectra has caused discrepancies which are not in agreement with the systematic temperature dependence on the ion number and the electron current. Small variations over the large range of charge states in Fig. 3 indicate that the higher intrabeam scattering rate for higher charged ions is nearly balanced by the larger cooling rate. The $N^{1/3}$-dependence seems to change for low particle numbers to a $N^{1/2}$-dependence explicable by reduced intrabeam scattering from the transverse to the longitudinal degree of freedom. The observed lower limit for detectable beam momentum spread $\Delta p/p = 7 \cdot 10^{-7}$ at small particle numbers is likely to be caused either by power supply ripple of the main ring magnets or by the energy stability of the electron beam.

The amount of data for the transverse degree of freedom is not so abundant, but the dependence on the ion charge can be deduced from a comparison of the two ion species in Fig. 1 or when properly scaled also from Fig. 2. The results for the equilibrium emittance agree quantitatively for both ions indicating an almost neglible variation of the equilibrium ion beam emittance for constant ion and electron beam intensity with the ion charge or mass.

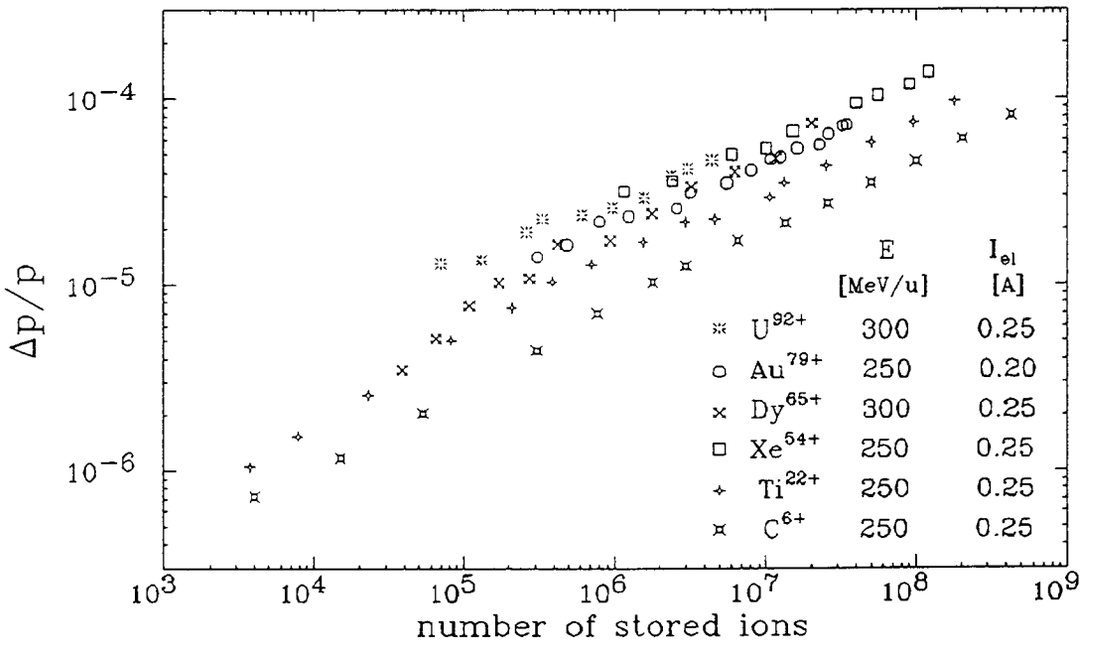

Figure 3: The momentum spread of cooled ion beams increases with the number of stored particles approximately $\propto N^{1/3}$. Ion species, ion energy and cooling current according to inscription.

4. COOLING FORCE AND INTRABEAM SCATTERING

The two determinant quantities for the quality of electron cooled ion beams the cooling force of the electron beam and the intrabeam scattering rate of the dense ion beam were investigated in separate experiments. For lack of adequate diagnostics for the transverse degree of freedom the experiments were concentrated on longitudinal cooling force, cooling rate and longitudinal heating rate. For measurements of the longitudinal cooling force at small relative velocities between electron and ion beam the cooled beam was heated by white noise and the cooling force of the electron beam was determined according to $F \cdot v_o = D \cdot \partial\psi(E)/\partial E \cdot \psi^{-1}$ with the diffusion coefficient D and with the energy dependent distribution function $\psi(E)$. The measurements shown in Fig. 4 were performed with an electron current of 50 mA, an ion current of approximately 100 μA and an identical set up for longitudinal beam excitation. Although an absolute calibration of the diffusion coefficient is not yet finished this comparison allows a statement on the ion charge dependence for the investigated ions C^{6+}, Ti^{22+}, Au^{79+}.

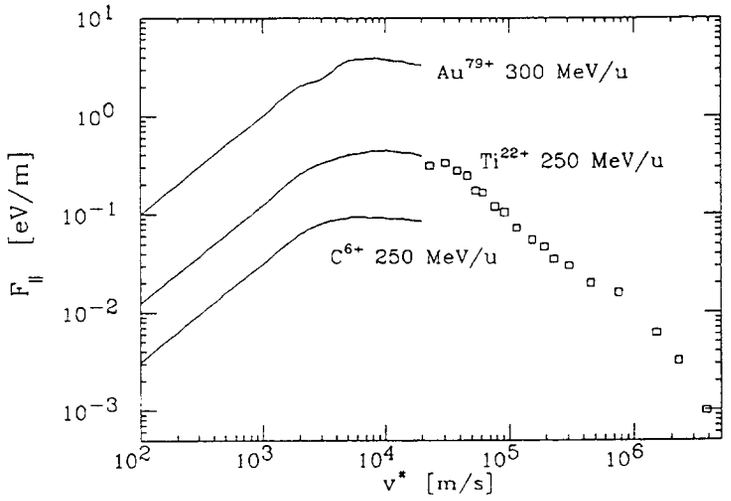

Figure 4: Longitudinal cooling force of a 50 mA electron beam determined for 100 μA ion beams of C^{6+}, Ti^{22+} and Au^{79+}, respectively. Straight curves are mesurements with simultaneous rf noise heating. Fitting of the Ti curve to data points from HV stepping allows an estimate of the absolute value of the cooling force at small relative velocity.

The increase for the three ion charges can be described by a proportionality to $Z^{1.5}$ which can be determined without knowledge of the absolute value of the diffusion coefficient. This is in agreement with a previous result [8] comparing Ne^{10+} and Bi^{82+} but contradicts a simplified model predicting a Z^2-dependence. More elaborated theories are obviously required for highly charged ions. For relative velocities $v^* \geq 2 \cdot 10^4\ m/s$ the cooling force for Ti^{22+} was measured by high voltage stepping. The measurement for Ti^{22+} in the low relative velocity regime was fitted to the absolutely known cooling force for larger relative velocities originating from measurements with an electron current of 250 mA which are scaled down to 50 mA.

Longitudinal heating rates by intrabeam scattering can be determined by FFT analysis of Schottky noise. The Schottky noise signal is analysed within a time interval of 16 ms typically which is delayed with respect to a fast cooler switch off. The cooling action is interrupted by fast detuning of the electron energy (5 kV step in less than 5 ms) which causes instantaneous growth of the momentum distribution. Fig. 5 shows the increase of momentum spread for a 0.4 mA Ti^{22+} beam cooled with a 100 mA electron beam. The initial growth rate compares after scaling to 50 mA and regarding the ratio of cooler length to ring circumference $\eta = 0.0185$ reasonably with the previous cooling force measurement. The cooling force gives a cooling time of 5 ms for the central part of the particle distribution whereas the initial intrabeam scattering rate corresponds to a cooling time of 4 ms which has to be considered as a satisfactory result regarding the accuracy of the applied methods.

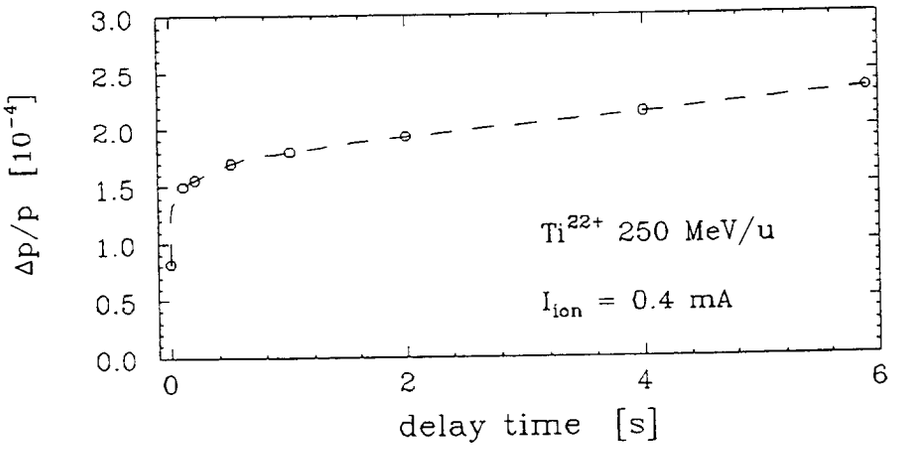

Figure 5: Increase of the momentum spread after cooler switch off for a 0.4 mA Ti^{22+} beam. Electron beam (100 mA) was switched off the cooling energy by a fast 5 kV step of the accelerating voltage.

REFERENCES

[1] B. Franzke et al., Proc. of the 1993 Part. Acc. Conf., Washington D.C., May 1993
[2] K. Blasche et al., Proc. of the 1993 Part. Acc. Conf., Washington D.C., May 1993
[3] H. Eickhoff et al., contribution to this workshop
[4] N. Angert et al., Proc. of the 2^{nd} Europ. Part. Acc. Conf., Nice 1990, pp. 1374-1376
[5] K. Beckert et al., Proc. of the 2^{nd} Europ. Part. Acc. Conf., Nice 1990, pp. 777-779
[6] O. Klepper et al., Nucl. Instr. Meth. Phys. Res., Sect. B70 (1992) 427
[7] M. Steck et al., Proc. of the 3^{rd} Europ. Part. Acc. Conf., Berlin 1992, pp. 827-829
[8] M. Steck et al., Proc. of the 1993 Part. Acc. Conf., Washington D.C., May 1993

EMITTANCE GROWTH OF INTENSE HEAVY ION BEAMS*

M. Seurer, C. Toepffer and P.-G. Reinhard
Institut für Theoretische Physik II, Universität Erlangen,
D - 91058 Erlangen, Germany

ABSTRACT
We investigate growth of the emittance in intense, strongly coupled heavy ion beams. A set of coupled differential equations is developed which describe the dynamics of the beam's envelopes and the emittances. The emerging estimates of emittance growth are compared with numerical results from molecular dynamics computer simulations.

1. INTRODUCTION

In most applications of high-current beam transport, a good quality of the beam and thus low emittances are desired. So, in these cases one has to deal with both the strong coupling between the ions and space charge effects. The usual treatment describes the dynamics of the beam's spatial extension through envelope equations which require the emittances as input (usually treated as constant). We aim to develop an extension of the envelope equations which allows to describe the coupled dynamics of the envelope and of the emittance. To this end, it is necessary to include collisional effects which play an important role in beam transport at high phase-space densities. The derivation of the extended envelope equations is presented in the following steps:
We first recall the well-known envelope equations in their special form when the beam's cross section is elliptic. We then give a schematic outline of our model and derive a set of temperature-relaxation equations which extend the envelope equations. Finally, we derive formulas for the averaged emittance growth rates and compare the predictions of our model with results derived from molecular dynamics (MD) simulations.

2. COLLISIONLESS BEAM TRANSPORT

We investigate a beam in a periodic quadrupole channel. Here, the external transversal forces F_x and F_y are proportional to the displacements x and y from an ideal trajectory. We will derive all our results in the rest-frame of the beam. We parametrize all quantities by means of the elapsed time $t = \frac{s}{v_z}$, where s is the distance along the accelerator and v_z is the mean beam velocity. Usually, the beam's transversal dimensions vary rather slowly in z-direction of beam propagation. Thus we can assume that the external forces act uniformly on the beam over its whole length and are switched on and off periodically. In space-charge-dominated beams one describes the beam dimensions in terms of the second moments $\langle x^2 \rangle$ and $\langle y^2 \rangle$ where the brackets denote avaraging over the whole phase-space:

$$\langle x^2 \rangle = \frac{\int d^3r \int d^3v \, n(\mathbf{r}, \mathbf{v}) x^2}{\int d^3r \int d^3v \, n(\mathbf{r}, \mathbf{v})} \quad . \tag{1}$$

We further assume, that the beam's cross section is elliptical and that the density is homogeneous. We derive the equations of motion for $x_{\mathrm{rms}} = \sqrt{\langle x^2 \rangle}$ and $y_{\mathrm{rms}} = \sqrt{\langle y^2 \rangle}$ by the second time-derivative of Eq. (1) and inserting the equations of motion for the phase-space density $n(\mathbf{r}, \mathbf{v})$. This yields the envelope equation [1]

$$\ddot{x}_{\mathrm{rms}} = k_{\mathrm{ext},x} x_{\mathrm{rms}} + \frac{n_0 Z^2 e^2 x_{\mathrm{rms},0} y_{\mathrm{rms},0}}{\varepsilon_0 m} \frac{1}{x_{\mathrm{rms}} + y_{\mathrm{rms}}} + \frac{\varepsilon^2_{\mathrm{rms},x}}{x^3_{\mathrm{rms}}} \tag{2}$$

where $k_{\mathrm{ext},x}$ describes the external forces, Ze and m are the ions charge and mass, n_0 is the beam density, and $x_{\mathrm{rms},0}$ and $y_{\mathrm{rms},0}$ are the x- and y-envelopes at $t = 0$. The quantity

$$\varepsilon_{\mathrm{rms},x} = \sqrt{\langle x^2 \rangle \langle \dot{x}^2 \rangle - \langle x \dot{x} \rangle^2} \tag{3}$$

is the root-mean-square emittance of the beam in x-direction. An analogous definition exists for the y-direction. The emittances $\varepsilon_{\mathrm{rms},x}$ and $\varepsilon_{\mathrm{rms},y}$ of the beam remain constant if the total forces F_x and F_y acting on an ion are proportional to its displacements x and y. In that case the equations for the envelopes are complete and one can solve them numerically where one looks in particular for solutions which are 'matched', which means that they have the same periodicity as the focussing structure.

3. TEMPERATURE OSCILLATIONS

We consider a FODO-section, where the beam is focussed and defocussed alternatingly.

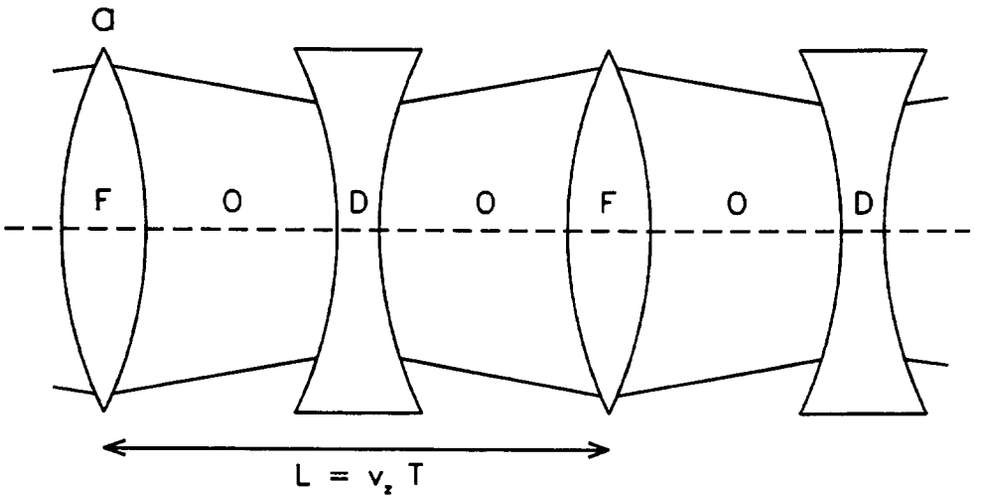

Figure 1: *Lens arrangement of a FODO-section in the x-z-plane. L is the length of one focussing period.*

Fig. 1 shows the arrangement of the lenses in the x-z-plane. A corresponding arrangement exists for the y-z-plane such that the beam is defocussed in y-direction when it is focussed in x-direction and vice versa. Now consider point a) in Fig. 1. There, the x-envelope is large and thus the y-envelope must be small. The phase-space volume in x-$\dot{x}$- and y-$\dot{y}$-space is approximately conserved, and consequently, the width of the phase-space density must be small in $\dot{x}$-direction and large in $\dot{y}$-direction, delivering a small kinetic energy in x-direction and a large one in y-direction. Relating a temperature to the kinetic energy, one can interpret this as a temperature anisotropy in x- and y-direction driven by beam guiding fields. Collisions between the ions drive towards thermal equilibrium, diminishing the anisotropy, increasing the entropy, and also increasing the emittance. The repeated deformation of the beam will then lead to a steady growth of the emittance.

4. TEMPERATURE-RELAXATION EQUATIONS

We define the local beam temperature in x-direction from the kinetic energy as

$$T_x(\mathbf{r}) = \frac{m}{k_B}\overline{(\dot{x} - \bar{\dot{x}}(\mathbf{r}))^2} \tag{4}$$

where the bar denotes averaging over the velocity space

$$\bar{\dot{x}}(\mathbf{r}) = \frac{\int d^3v\, n(\mathbf{r},\mathbf{v})\dot{x}}{\int d^3v\, n(\mathbf{r},\mathbf{v})} \quad . \tag{5}$$

In the case of linear external forces the correlation between $\bar{\dot{x}}(\mathbf{r})$ and x is linear and we can write

$$\bar{\dot{x}}(\mathbf{r}) = \frac{\langle x\dot{x}\rangle}{\langle x^2\rangle}x \quad . \tag{6}$$

In addition, we assume that the beam temperature varies little over $\mathbf{r}$ such that we can approximate the local temperature by its global value

$$T_x = \frac{\int d^3r\, n(\mathbf{r})T_x(\mathbf{r})}{\int d^3r\, n(\mathbf{r})} = \frac{m}{k_B}\frac{\langle x^2\rangle\langle\dot{x}^2\rangle - \langle x\dot{x}\rangle^2}{\langle x^2\rangle} = \frac{m}{k_B}\frac{\varepsilon^2_{\mathrm{rms},x}}{\langle x^2\rangle} \tag{7}$$

This establishes a relationship between beam temperature, emittance and envelope. As discussed above, there are two mechanisms which change the temperature:

1. envelope oscillations cause the temperature to oscillate with the squared inverse envelope as

$$\dot{T}_{x,\mathrm{osc}} = \frac{m}{k_B}\varepsilon_{\mathrm{rms},x}^2 \frac{d}{dt}\frac{1}{\langle x^2\rangle} = -\frac{m}{k_B}\varepsilon_{\mathrm{rms},x}^2 \frac{\langle x\dot{x}\rangle}{\langle x^2\rangle^2} \tag{8}$$

2. collisions diminish the temperature anisotropy. We describe this with a relaxation ansatz:

$$\dot{T}_{x,\mathrm{rel}} = -D\left[(T_x - T_y) + (T_x - T_z)\right] \tag{9}$$

where D is an inverse relaxation time.

The total time derivative of the temperature is thus $\dot{T}_x = \dot{T}_{x,\mathrm{osc}} + \dot{T}_{x,\mathrm{rel}}$. This is inserted into Eq. (7) and yields the time evolution for the emittance

$$\frac{d}{dt}\varepsilon_{\mathrm{rms},x}^2 = -D\left[2\frac{\varepsilon_{\mathrm{rms},x}^2}{\langle x^2\rangle} - \frac{\varepsilon_{\mathrm{rms},y}^2}{\langle y^2\rangle} - \langle \dot{z}^2\rangle\right]\langle x^2\rangle \quad . \tag{10}$$

Analogous results are obtained for $\varepsilon_{\mathrm{rms},y}^2$ and $\langle \dot{z}\rangle^2$. The envelope equation (2) together with the emittance equation (10) and with the analgous equations in y- and z-directions form a set of coupled differential equations taking care of space-charge as well as collisional effects. The inverse relaxation time D is a parameter of the model. The dielectric theory predicts for weak coupling [2]

$$D \propto \omega_p \Gamma^{3/2} \ln\Lambda \tag{11}$$

where $\omega_p = \sqrt{\frac{n_0 Z^2 e^2}{\epsilon_0 m}}$ is the plasma frequency and $\ln\Lambda \propto \ln 3 - \ln\Gamma$ is the Coulomb-logarithm. In practice, we adjust D to data from MD simulations.

5. AVERAGE EMITTANCE GROWTH

The total emittance $\varepsilon_{\mathrm{rms}}^6 = \varepsilon_{\mathrm{rms},x}^2\varepsilon_{\mathrm{rms},y}^2\langle \dot{z}^2\rangle$, serves as a measure of total phase-space volume. Its time derivative is $\frac{d}{dt}\varepsilon_{\mathrm{rms}}^6$ as:

$$\begin{aligned}\frac{d}{dt}\varepsilon_{\mathrm{rms}}^6 &= -D\varepsilon_{\mathrm{rms}}^6\left[\left(2 - \frac{\varepsilon_{\mathrm{rms},y}^2\langle x^2\rangle}{\varepsilon_{\mathrm{rms},x}^2\langle y^2\rangle} - \frac{\varepsilon_{\mathrm{rms},x}^2\langle y^2\rangle}{\varepsilon_{\mathrm{rms},y}^2\langle x^2\rangle}\right) + \left(2 - \frac{\langle \dot{z}^2\rangle\langle x^2\rangle}{\varepsilon_{\mathrm{rms},x}^2} - \frac{\varepsilon_{\mathrm{rms},x}^2}{\langle \dot{z}^2\rangle\langle x^2\rangle}\right)\right. \\ &\quad \left. + \left(2 - \frac{\langle \dot{z}^2\rangle\langle y^2\rangle}{\varepsilon_{\mathrm{rms},y}^2} - \frac{\varepsilon_{\mathrm{rms},y}^2}{\langle \dot{z}^2\rangle\langle y^2\rangle}\right)\right]\end{aligned} \tag{12}$$

The terms in the round brackets are each of the form $2 - \frac{1}{c} - c \leq 0$ and thus the total emittance is monotonously increasing,

$$\frac{d}{dt}\varepsilon_{\mathrm{rms}}^6 \geq 0 \quad , \tag{13}$$

similar as the entropy. In order to estimate the average growth of the emittance, we approximate the beam's envelopes as

$$\langle x^2\rangle(t) = r^2\left(1 + \Delta\sin\frac{2\pi t}{T}\right) \tag{14}$$

$$\langle y^2\rangle(t) = r^2\left(1 - \Delta\sin\frac{2\pi t}{T}\right) \quad . \tag{15}$$

It turns out, that the emittance growth is dominantly driven by the oscillations of the envelopes. Integration of Eq. (12) over one period yields

$$\varepsilon_{\mathrm{rms}}^6(t_0 + T) = \varepsilon_{\mathrm{rms}}^6(t_0)\left(1 + 6DT\frac{1 - \sqrt{1-\Delta^2}}{\sqrt{1-\Delta^2}}\right) \quad . \tag{16}$$

And thus the average growth of the emittance can be written approximately as

$$\Delta\varepsilon_{\mathrm{rms}} = \varepsilon_{\mathrm{rms}}(t_0 + T) - \varepsilon_{\mathrm{rms}}(t_0) \approx DT\frac{1 - \sqrt{1-\Delta^2}}{\sqrt{1-\Delta^2}}\varepsilon_{\mathrm{rms}}(t_0) \quad . \tag{17}$$

6. NUMERICAL RESULTS

The results from MD-simulations for the envelopes and emittances in x- and y-direction are shown in Figs. 2 and 3. The emittances oscillate as discussed in section 3. For example, if the x-envelope is larger

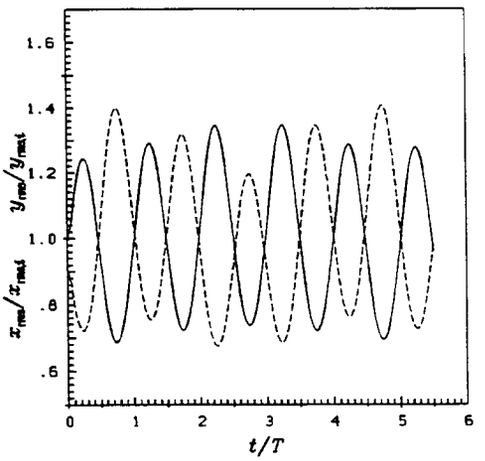

Figure 2: *Envelopes in x-direction (solid curve) and in y-direction (dashed curve).*

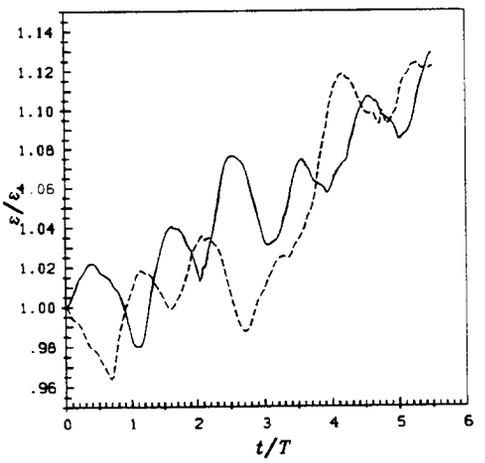

Figure 3: *Emittances in x-direction (solid curve) and in y-direction (dashed curve).*

than the y-envelope, then the emittance in x-direction increases because the temperature T_x is lower than the temperature T_y. Similar patterns are obtained by solving the extended envelope equations. Note that the emittance increases on the average because the relaxation process is irreversible. This is in accordance with the result of Eq. (17) from the extended envelope equations. The development of the emittance over a long distance of about 350 focussing structures is shown in Fig. 4, for the MD-simulation (solid curve) as well as for a solution of the extended envelope equations (dashed curve).

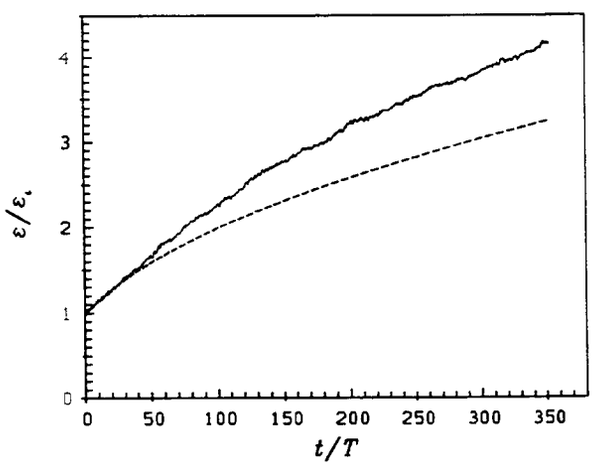

Figure 4: *Emittances drawn from MD-simulations (solid line) and from a solution of the extended envelope equations*

The beam parameters were identical in both calculations. The relaxation coefficient D in the extended envelope equations was fitted to reproduce the initial emittance growth of the MD simulation. The Fig. 4 shows that the temperature model provides an appropriate description of the general trend and order of magnitude, but it underestimates the emittance growth somewhat in comparison to the MD-simulation.

Finally, we want to discuss the dependence of the emittance growth rates on the plasma frequency ω_p and the plasma parameter Γ of the beam. According to Eqs. (17) and (11) one expects $\frac{d}{dt}\varepsilon_{\rm rms}/\varepsilon_{\rm rms}$ to be proportional to $\omega_p \Gamma^{3/2} \ln \Lambda$. We test this hypothesis against the results of full MD simulations.

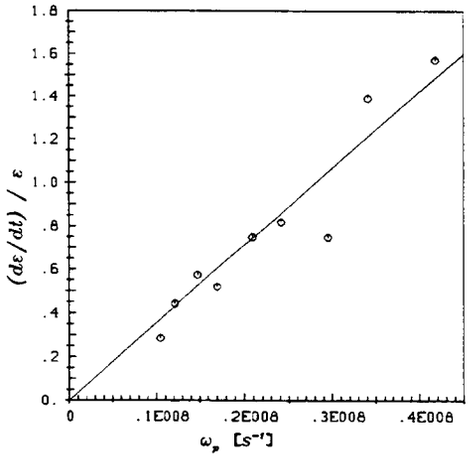

Figure 5: *Emittance growth rates versus plasma frequency (arbitrary units).*

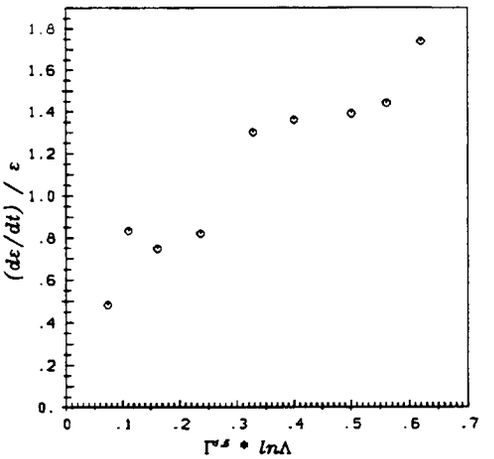

Figure 6: *Emittance growth rates versus plasma parameter (arbitrary units).*

The dependence of $\frac{d}{dt}\varepsilon_{\rm rms}/\varepsilon_{\rm rms}$ versus ω_p for fixed Γ is shown in Fig. 5. The linear dependence on ω_p as predicted by the dielectric theory is nicely visible. The dependence of $\frac{d}{dt}\varepsilon_{\rm rms}/\varepsilon_{\rm rms}$ on $\Gamma^{3/2} \ln \Lambda$ for fixed ω_p is shown in Fig. 6. The growth rate increases with increasing $\Gamma^{3/2} \ln \Lambda$, but there remains a non-zero intercept at $\Gamma^{3/2} \ln \Lambda = 0$ deviating from the dielectric prediction. The most probable reason is that the dielectric theory overestimates the relaxation coefficient D at high Γ. Moreover, our starting configuration for the MD-simulation (elliptical cylinder with sharp edge in ordinary space and Maxwellian in velocity space) may lead to a transient softening of the beam edge at high temperatures (i.e. low Γ) which causes an additional emittance growth.

7. CONCLUSION

We have shown that the envelope oscillations produce emittance growth in space-charge-dominated, strongly coupled heavy ion beams. The MD-simulation results confirm the prediction of our simple model based on a temperature anisotropy and equilibration.
The emittance growth rates increase with increasing Γ. Therefore, we think that this effect must be taken into account in attempts to produce crystalline ion beams with a more complicated structure than a linear chain.

REFERENCES

[*] Supported by the "Gesellschaft für Schwerionenforschung" (GSI), Darmstadt.

[1] F.J. Sacherer, IEEE Trans. Nucl. Sci. **NS-18**, 1105, (1971).

[2] S. Ichimaru, *Basic Principles of Plasma Physics* (Benjamin, Reading, Massachusetts, 1973).

THE INVESTIGATION OF SPACE CHARGE DOMINATED COOLED BUNCHED BEAMS IN A SYNCHROTRON

Sergei S. Nagaitsev, Timothy J.P. Ellison, Michael J. Ellison, Daniel Anderson
The Indiana University Cyclotron Facility
2401 Milo B. Sampson Lane, Bloomington, IN 47405, USA

ABSTRACT

The longitudinal equilibrium distribution of electron-cooled protons stored in a synchrotron ring is well described by theory based on the Fokker-Plank equation. Having made the assumption that the longitudinal coupling impedance is almost completely space charge dominated one can find the relative momentum spread of the beam and longitudinal space charge impedance by two independent methods. The first method relies upon fitting the measured longitudinal bunch shape to the theoretical one. The second method finds the momentum spread and impedance by analyzing the frequencies of the dipole and quadrupole longitudinal bunch modes. In this paper we present the results of bunch shape and bunch oscillation measurements as a function of proton beam current in the IUCF Cooler ring. A comparison of these two methods is also presented in this paper.

1. INTRODUCTION

Knowledge of the longitudinal momentum spread of an electron-cooled proton beam is important for experiments which rely on the unique properties of this beam. Since the rf cavity produces a conservative force, it cannot change the beam longitudinal phase density. Consequently, for a known rf voltage, the beam time spread normally provides a direct measurement of the beam momentum spread. An electron-cooling system[1], however, can reduce the ion beam emittance to extremely small values. In this regime the ion beam, interacting with its surroundings, generates the longitudinal self-fields which significantly modify the bunch shape[2]. It can be shown that for ion beams below transition, the most significant part of this interaction comes from the electrostatic repulsion between the ions within the bunch. Since in all cases of interest the bunch lengths are much greater than the radius of the surrounding vacuum chamber one can treat the beam as a thin thread and, consequently, reduce the electrostatic problem to one dimension. Further, the Vlasov technique must be used to find the self-consistent longitudinal particle distribution function[3]. The simplest solution for a linear rf force in the presence of space-charge is given in Ref. [3] and has a parabolic line density function with bunch length determined by the rf amplitude, space charge impedance and longitudinal momentum spread. The measurement of the bunch length, however, does not allow the determination of both momentum spread and longitudinal impedance. One needs another independent measurement to complete the system and eliminate this ambiguity. Section 3 discusses a possible solution to this problem. For electron-cooled ion beams, one needs to modify Vlasov equation to include both damping and diffusion[4]. The implication of cooling on the distribution function will be described in section 2.

To avoid confusion in the following sections, we would like to explain some notations we use. We define three rf voltages V_o, V_{rf} and V_{eff} as follows: V_o is the rf voltage amplitude measured across the rf cavity gap, V_{rf} is the rf voltage amplitude determined from the synchrotron frequency (see section 4) and V_{eff} is the effective rf voltage amplitude inside the bunch in the presence of space charge. V_{rf} data were not available for the measurements, described in the section 2, therefore we assume $V_{rf} = V_o$ there.

2. FOKKER-PLANK EQUATION

Although a cooling force is generally a complex function of proton momentum[5], one can consider the cooling force to be a linear function of the relative proton momentum δ, if it is smaller than the relative longitudinal momentum spread of the electron beam. The latter is typically determined by the high-voltage power supply ripple, which for the IUCF Cooler is $\approx 5\ V_{rms}$ at $22\ kV$. This implies that the linear approximation is valid for $\sigma < 1.1 \times 10^{-4}$, where σ is the relative rms proton momentum spread. The modified Vlasov equation

then can be written in a Fokker-Plank form:

$$\frac{\partial \Psi}{\partial t} + \dot{s}\frac{\partial \Psi}{\partial s} + \dot{\delta}\frac{\partial \Psi}{\partial \delta} = \frac{\partial}{\partial \delta}\left(\lambda \delta \Psi + \frac{d}{2}\frac{\partial \Psi}{\partial \delta}\right) \tag{1}$$

Here $\Psi = \Psi(t,s,\delta)$ is the longitudinal distribution function, t is time, s the longitudinal coordinate, λ the cooling rate, d the diffusion rate and the dot indicates the derivative with respect to time. The equations of motion for a particle experiencing synchrotron oscillations within the stationary bucket can be written as:

$$\dot{\delta} = f_o \frac{eV_{rf}}{\beta^2 E}\sin\left(\frac{hs}{R}\right) + \frac{1}{p}\frac{dU(s)}{ds} \tag{2}$$

$$\dot{s} = 2\pi R \eta f_o \delta \tag{3}$$

where $E = \gamma Mc^2$ is the energy of synchronous particle, $p = \beta\gamma Mc$ is its momentum, f_o its revolution frequency, γ and β are the usual relativistic parameters, c is the speed of light, e is the ion charge, V_{rf} is the amplitude of rf voltage, h is the harmonic number, R is the radius of synchrotron storage ring ($\approx$ 13.8 m for the IUCF Cooler ring) and $\eta = -\Delta f/f_o\delta$ is the phase slip factor ($\approx$ -0.86 for the IUCF Cooler ring). The potential energy due to space-charge interaction is:

$$U(s) = \frac{Z_o g}{\gamma^2 \beta} e f_o R \rho(s) \tag{4}$$

where $Z_o = 377\ \Omega$, g is a geometrical factor (= *ln(pipe radius/beam radius) + 1/2* for a perfectly conductive cylindrical vacuum chamber) and $\rho(s)$ is the longitudinal linear charge density. The bunch is assumed to be moving in a perfectly conducting smooth vacuum chamber therefore no other longitudinal self-fields are taken into account. For a stationary distribution, the time dependence of Ψ vanishes and the solution of (1) in the case of linear rf voltage can be written as[6]:

$$\Psi(s,\delta) = \frac{1}{(2\pi)^{1/2}\sigma} e^{-\delta^2/2\sigma^2}\ \rho(s) \tag{5}$$

where $\sigma^2 = d/2\lambda$ and $\rho(s)$ is given by the expression:

$$\rho(s) e^{-\alpha\rho(s)} = \rho(0) e^{-\alpha\rho(0)} e^{-s^2/2\sigma_s^2} \tag{6}$$

The value of $\rho(0)$ must be chosen so that $\rho(s)$ is normalized to eN, where N is the total number of particles per bunch. The constants α and σ_s are given by the expressions:

$$\alpha = \frac{Z_o g}{\gamma^2 \beta}\frac{e f_o}{E \beta^2}\frac{R}{\sigma^2 \eta} \tag{7}$$

$$\sigma_s = \left(\frac{2\pi\beta^2|\eta|}{h}\frac{E}{eV_{rf}}\right)^{1/2} R\sigma \tag{8}$$

Equation (6) has two unknowns: σ and g. The first is a measure of the longitudinal beam temperature, the second is a measure of potential energy. For small α (resulting from large σ or small g), the linear density $\rho(s)$ is Gaussian with the rms bunch length given by Eq. (8). On the other hand, if the beam is cooled, the linear density becomes a more complex function of s with a well defined parabolic central part and Gaussian-like tails (Fig. 1). One can now fit the measured longitudinal density to the theoretical prediction, given by Eq. (6) to obtain the values of σ and g. A comparison between the predicted, Eq. (6), and measured bunch shape is presented in Fig. 1. The fit and measured data are difficult to resolve in Fig. 1 except near the tail of the bunch. With two unknowns, the fit is unambiguous, because the value of g influences the

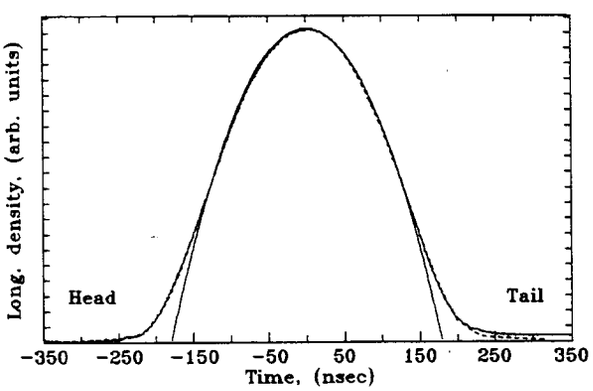

Figure 1. Measured(solid) and theoretical(dashed) linear density. $I_p=800\ \mu A$, $V_{rf}=10\ V$, $g=1.3$, $\sigma=5.7\times10^{-5}$. Parabolic fit with $g_o=1.8$, $\sigma=0$ is also presented.

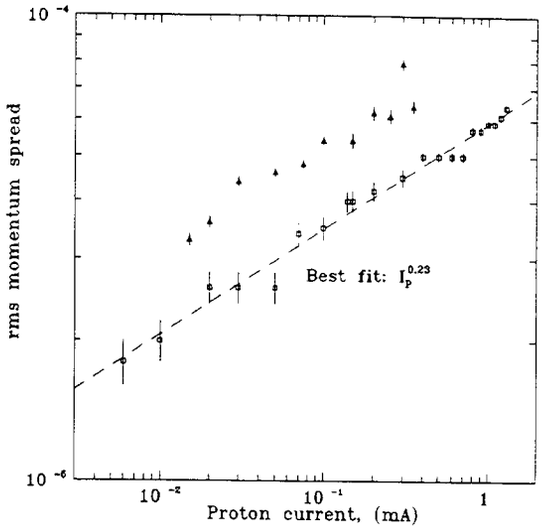

Figure 2. Proton beam rms momentum spread vs. total beam current at 45 MeV. V_{rf} = 10 V (□), V_{rf} = 126.4 V (△).

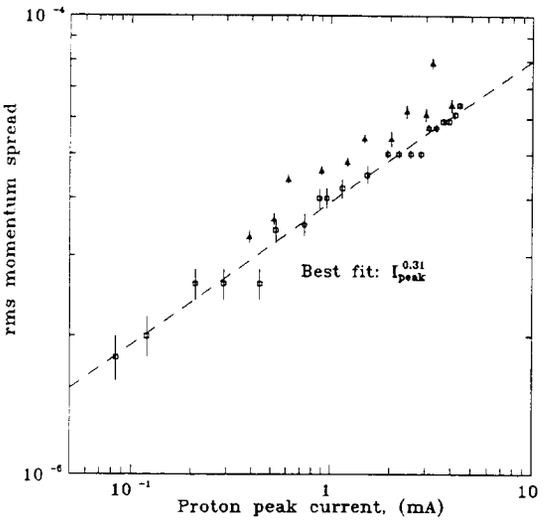

Figure 3. Proton beam rms momentum spread vs. proton peak current. V_{rf} = 10 V (□), V_{rf} = 126.4 V (△).

width of the central part, whereas σ defines the tails. In Figs. 2-4, the geometrical factor g and the rms momentum spread σ are shown for two different rf voltages. One can also fit the measured longitudinal density to a parabolic function by setting σ equal to zero. It requires larger values of g (Fig. 1) because the space-charge force in this case completely compensates the rf force. In fact, by fitting both with finite momentum spread and without momentum spread ($\sigma = 0$) one can obtain the ratio of the rf voltage, reduced by presence of space charge, to the rf voltage in the cavity:

$$\frac{V_{eff}}{V_{rf}} = 1 - \frac{g}{g_o} \tag{9}$$

where g_o is the value of g, obtained by fitting the bunch shape with $\sigma = 0$. In Fig. 5 this ratio is shown as a function of proton beam intensity.

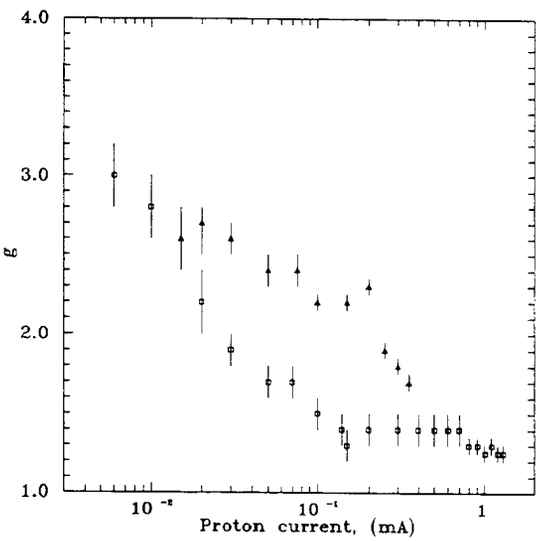

Figure 4. Geometric factor g vs. proton beam current. V_{rf} = 10 V (□), V_{rf} = 126.4 V (△).

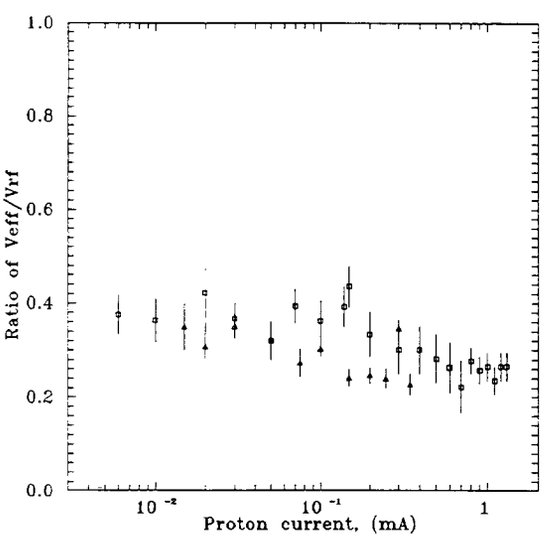

Figure 5. Ratio of the effective rf voltage to the applied rf voltage derived from the bunch shape fitting. V_{rf} = 10 V (□), V_{rf} = 126.4 V (△).

3. BUNCH MODES

Once the stationary solution of Eq. 1 is found, one can look for a time dependent solution. Eq. 1, however, does not have a simple analytic time dependent solution, and a perturbation approach, developed in Ref. [7] must be used. Nevertheless, if the synchrotron frequency, ω_s, is much greater than $\lambda/2$ (typically, $\lambda \approx 40 \div 60$ Hz for the IUCF cooler), the damping and diffusion in Eq. 1 can be neglected and the Fokker-Plank equation becomes the Vlasov equation, the time dependent solution of which for a parabolic bunch density was derived in Ref. [3]. Following Ref. [3] we shall write the solution of Eq. 1 in the form of an envelope equation:

$$\ddot{L} = \left(\frac{2\pi f_o|\eta|}{\beta}\right)^2 \left(\frac{\epsilon^2}{L^3} + \frac{I}{I_o}\frac{1}{L^2} - AL\right) \tag{10}$$

where $L = cT_{FWHM}/R$ is the unitless full width at half max bunch time spread, $\epsilon = L\delta_{FWHM}$ is the unitless longitudinal emittance, I is the proton current per bunch and the constants A and I_o are given by:

$$I_o = \frac{\beta^4\gamma^3 h|\eta|M}{12\sqrt{2}\pi g m}\frac{ec}{r_e}\ ;\quad A = \frac{heV_{rf}}{2\pi|\eta|E} \tag{11}$$

where r_e is the classical electron radius and m is its mass. In a stationary case, the bunch length can be found by setting the right-hand side of Eq. 10 equal to zero, but unlike the situation in section 2, one cannot obtain both the momentum spread, δ_{FWHM}, and the geometrical factor, g, simultaneously, because we have only one equation for the stationary bunch length, L_o, and two variables to satisfy it. A second constraint equation can be obtained by measuring the frequency of small bunch length oscillations. Assuming, that $L(t) = L_o + x(t)$, where $x(t) \ll L_o$ one can rewrite Eq. 10 after linearization:

$$\ddot{x} = -\omega_q^2 x\ ;\quad \omega_q = \frac{2\pi f_o|\eta|}{\beta}\sqrt{\frac{3\epsilon^2}{L_o^4} + \frac{2}{L_o^3}\frac{I}{I_o} + A} \tag{12}$$

The expression for ω_q in Eq. 12 can be now used to eliminate one of the variables. Using Eq. 10 with RHS set to zero L_o satisfies the equation:

$$AL_o^3 - \delta^2_{FWHM}L_o - \frac{I}{I_o} = 0 \tag{13}$$

one can obtain a simple relation for the bunch length (quadrupole) oscillation frequency:

$$\left(\frac{\omega_q}{\omega_s}\right)^2 = \frac{V_{eff}}{V_{rf}} + 3 \tag{14}$$

where ω_s is the synchrotron (dipole) frequency given by:

$$\omega_s = 2\pi f_o\sqrt{\frac{heV_{rf}|\eta|}{2\pi\beta^2 E}} \tag{15}$$

In the absence of space-charge interaction ($V_{eff} = V_{rf}$) $\omega_q = 2\omega_s$, which simply corresponds to the rotation of the bunch in the longitudinal phase space, whereas in the case of the zero momentum spread ($V_{eff} = 0$) $\omega_q = \sqrt{3}\omega_s$.

4. EXPERIMENTAL RESULTS

Experimental measurements of bunch profiles and bunch oscillation modes were performed in the IUCF cooler ring at the energy 45 MeV for various rf voltages and beam currents. To measure the bunch shape, a broad band-width longitudinal pick-up electrode was used together with a digitizing scope (10-bit full scale resolution, 1 GSample/sec). Data were then transferred to a PC computer for offline analysis. A parametric current transformer was used to measure proton current with 1 μA precision. The rf cavity voltage was measured both with an rf probe, coupled to the cavity, and by measuring the frequency of 20° p-p synchrotron phase oscillations (Eq. 15). These oscillations were excited by nonadiabaticaly shifting the phase of the cavity voltage by 10° in less than 40 μsec. Together with this phase jump, the amplitude of the rf voltage was incremented by a fixed value ($\approx$ 6 V) to excite the bunch length oscillations. The frequency of the bunch length oscillations was measured by monitoring the power in one of the higher revolution frequency harmonics as a function of time. The harmonic number (typically $20 \div 40$) was chosen to be sensitive to the bunch length changes. The intervals between measurements were long enough to ensure sufficient cooling time. The electron current in all measurements was kept at 480 mA. Improved electronics overcame the difficulties, encountered

in the previous experiments, connected with the filtering, AC coupling and cable losses.

After analyzing the experimental data, it was found that the amplitude of the rf voltage, measured in the cavity, was different from the voltage derived from synchrotron frequency (Eq. 15). While the value of the former was independent on beam intensity, the latter showed a noticeable current dependence. The synchrotron frequency, $\omega_s/2\pi$, and the corresponding rf voltage as a function of proton current are shown in Figs. 6 and 7. For all cavity voltages, V_o, used in the experiment the value of the rf voltage derived from Eq. 15 satisfies the empirical relation:

$$V_{rf} \approx V_o - 3\,\mathrm{k\Omega} \cdot I_p \tag{16}$$

It is not clear to the authors how the dipole oscillation frequency can depend on the proton current when the measured voltage across the rf cavity gap remained constant.

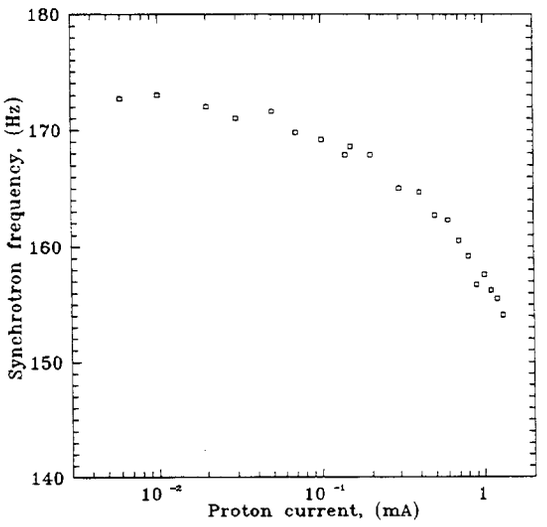

Figure 6. Synchrotron frequency ($\omega_s/2\pi$) as a function of proton beam current.

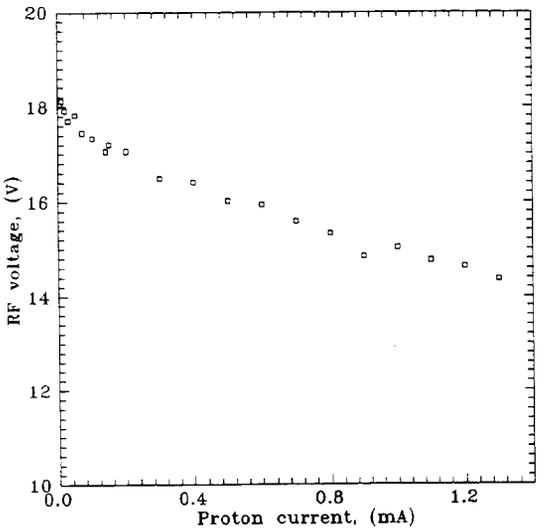

Figure 7. Amplitude of the rf voltage as a function of proton beam current.

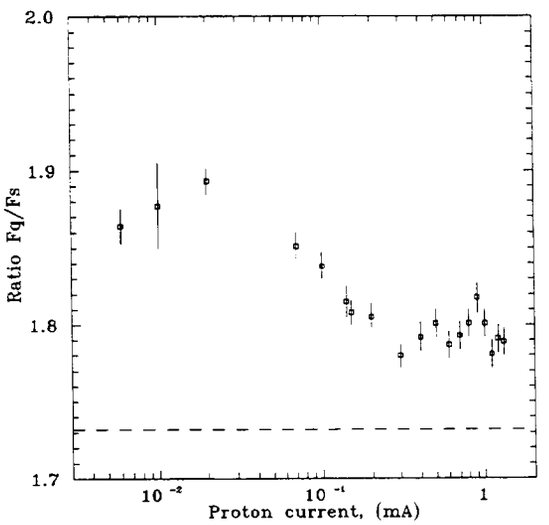

Figure 8. Ratio of quadrupole frequency to synchrotron frequency vs. beam current. Dashed line shows $\sqrt{3}$ value.

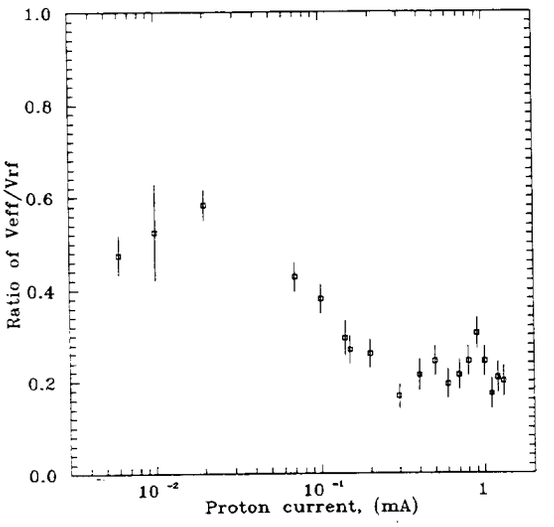

Figure 9. Ratio of effective rf voltage to applied rf voltage derived from the ratio of the frequencies.

The ratio of the bunch length oscillation frequency to the synchrotron frequency (Fig. 6) is shown in Fig. 8. Using Eq. 14 the amplitude of the effective rf voltage within the bunch was derived. Fig. 9 shows the

ratio of this voltage to the rf voltage (Fig. 7). While this ratio is in reasonable agreement with the ratio derived from bunch shape fitting (Fig. 5), the direct comparison of these two figures is difficult for two reasons. The first reason is that once the cavity voltage was increased to excite quadrupole oscillations, it remained at this increased level. These oscillations were, therefore, around a slightly different equilibrium determined by the new rf voltage. Secondly, the rf voltage depends on beam intensity, whereas we used a constant value of V_o for the bunch shape fitting.

5. DISCUSSION

We presented in this paper two methods of determining the momentum spread of bunched beams. Both methods indicate that the voltage inside the bunch is significantly reduced by the presence of the space charge. The monitoring of the bunch modes has the potential to be used online in future experiments which require knowledge of the momentum spread. Figure 4 indirectly indicates a strong dependence of the beam size on the beam intensity. In upcoming experiments we shall measure the transverse profile together with the longitudinal properties of the beam to verify this dependence. If a correlation between the geometrical factor g and the transverse beam size were to be found, one could imagine having a powerful tool to measure 6-d beam properties by merely the fitting bunch shape or by exciting bunch oscillations. We shall also continue the measurements of the longitudinal properties of the beam as a function of beam energy and internal target thickness.

ACKNOWLEDGEMENTS

The authors are grateful to M. Ball, V. Derenchuk, G. East, D. Friesel, B. Hamilton, T. Sloan and P. Schwandt for their help in performing this experiment, special thanks to Mark Ball who designed the electronics for the bunch shape measurements. This work was supported by the National Science Foundation (Grant No. NSF PHY 90-15957).

REFERENCES

[1]. G.I. Budker, Atomnaya Energia **22** (5), 246-248 (1967).

[2]. Timothy J.P. Ellison, Sergei S. Nagaitsev, Mark S. Ball, David D. Caussyn, Michael J. Ellison and Brett J Hamilton, Phys. Rev. Lttr. **70** No. 6, p. 790-793 (1993).

[3]. David Neuffer, IEEE Trans. Nucl. Sci. **26**, No. 3, 3031-3033(1979).

[4]. J. Haïssinski, Nuovo Cimento **18B**, No. 1, 72 (1973).

[5]. Tim Ellison, Ph.D. thesis, Indiana University, p.83 (1990).

[6]. Alexander Wu Chao, *Physics of Collective Beam Instabilities in High Energy Accelerators*, John Wiley & Sons, Inc., p.287, 1993.

[7]. F. Sacherer, *Methods for computing bunched-beam instabilities*, CERN/SI-BR/72-5(1972).

LEAD ION ACCUMULATION SCHEME FOR LHC

P. Lefèvre, D. Möhl

CERN, PS Division, CH - 1211 Geneva 23, Switzerland

ABSTRACT

After a summary of the beam qualities required for LHC as lead ion collider, the reasons for accumulation and cooling of ions at low energy are given. A description of the scheme and the expected beam qualities are indicated. The performance limitations are listed.

1. INTRODUCTION

The accumulation of heavy ions at low energy is part of the scheme adopted in the LHC project proposal [1]. The basic idea is to use a ring like LEAR with strong electron cooling to cool and accumulate the pulses from the heavy ion Linac 3 [2] during the time of a PS cycle thus increasing the intensity to be accelerated via the PS by an order of magnitude. In fact the operation of the LHC with Pb ions is limited by the requirement to have a sufficient beam lifetime in the presence of nuclear effects in the beam-beam interaction [3]. This leads to an upper limit for the luminosity per bunch ($3.6\ 10^{24}\ cm^{-2}\ sec^{-1}$). However the corresponding phase space density cannot be reached with conventional beams like those foreseen for the standard CERN Heavy Ion Facility, under construction for fixed target experiments at the SPS. The missing factors in intensity and luminosity are in the order of 30 and 10^3 respectively. The stacking scheme aims at gaining back these factors by means of cooling and accumulation.

The scheme is based on the accumulation of Pb^{53+} at 4.2 MeV/u in the cooling ring with a stack of up to $1.2\ 10^9$ ions per batch. Then with about 500 bunches per LHC ring the total luminosity is close to the desired $2\ 10^{27} cm^{-2}\ s^{-1}$.

To fix ideas we consider the conversion of LEAR "in situ" into a Low Energy Accumulator Ring. This is a possibility only, should the antiproton programme be wound up in a few years from now. In the opposite case a new dedicated ion accumulator can be built. Most of the following considerations pertain to both alternatives.

We limit the presentation to Pb ions, but the case of lighter ions (Nb, Ca, O) has been also investigated in the more detailed feasability study [4].

2. THE BASIC SCHEME FOR LEAD IONS

The Linac 3 parameters are given in table 1. Using LEAR in situ the transfer to the accumulation ring proceeds via the existing loop (E0) and injection line (E2), Fig. 1. The injection is a classical horizontal multiturn scheme with an orbit bump decreasing in about 50 μs (i.e. over 20 turns) from typically 50 mm to 0 amplitude at the septum. Up to 20 turns are injected around the dense cooled stack, Fig. 2. They are transferred into the stack by the electron cooling system before the new pulse arrives. Cooling times fast enough to accomplish this during 100 ms must be obtained.

After 2 sec of stacking the required intensity of $1.2\ 10^9$ ions ($6.4\ 10^{10}$ charges) is reached and the beam is bunched at harmonic number 4 ($f_{rf} \approx 1.4$ MHz), accelerated and transferred to the PS at 654 MeV/c per charge (14.8 MeV/u), close enough to the present 609 MeV/c used for antiproton transfer. The time available for acceleration is about 1 s. The full LEAR-cycle is matched to a standard PS-cycle with a length of 3.6 s.

The train of the 4 bunches is transferred into matched PS buckets (h = 32). After acceleration to 258 MeV/u, the 4 bunches are gradually stepped down from h = 32 to 28, 24, 20 and finally 16. Thereafter the acceleration continues at h = 16.

Ejection and full stripping to Pb^{82+} are done at 3078 MeV/u (≈ 10 Gev/c per charge after stripping). At this energy the bunch separation (135 ns at the $\beta = 0.97$) matches both the 200 MHz rf structure in the SPS and the bunch harmonic number of 660 in the LHC [3].

Table 1 : Source and Linac 3 parameters

1. General Parameters	
Pulse length	≤ 100 μs
Repetition rate	10/s
2. Ion source	
Ion species	$^{208}Pb^{28+}$
Output energy	2.5 keV/u
Transverse emittances (1σ), normalised	0.07 μm
Pulse current	80 μA
Corresponding flux dN/dt	1.8 10^7 ions/μs
3. RFQ	
Output energy	250 keV/u
Transmission efficiency	0.9
4. LINAC	
Output energy	4.2 MeV/u
Transmission efficiency	0.9
5. Stripping foil (Carbon)	
Charge state selected after stripping	$^{208}Pb^{53+}$
Stripping efficiency 28+ to 53+	18 %
6. Beam at injection to LEAR	
Pulse current (after stripping)	22 μA
Corresponding flux	2.6 10^6 ions/μs
Transverse emittances (1σ)	
physical $\varepsilon_h = \varepsilon_v$	2.1 μm
normalised $\varepsilon^*_h = \varepsilon^*_v$	0.2 μm
Momentum spread σ_p after debunching	<0.2 10^{-3}

Prior to acceleration in the SPS 32 PS trains of 4 bunches are stored at injection energy (3078 MeV/u). The holding time of about two minutes is sufficiently short compared to the time constant for blow-up by intra-beam scattering.

The distribution of the 660 bunch places in LHC for the 4 bunch basic scheme is summarised by the formula : 660 = [(4 + 1) 32 + (5)] 3 + [(4 + 1) 28 + (25)] where the filled bunch places are underlined, the empty ones are needed to avoid losses during kicker rise and fall times and rf acceleration in the SPS.

This leads to a total of 496 bunches per LHC ring from 4 SPS pulses. With a 3.6 s LEAR and PS cycle and 10 s for acceleration in the SPS the filling time per LHC ring is then about 8.1 min. The LHC parameters for this operation are given in table 2.

Table 2 : LHC parameters for operation with $^{208}Pb^{82+}$

Number of ion/bunch		0.94 10^8
Luminosity/bunch ($cm^{-2}s^{-1}$)		3.6 10^{24}
Normalised emittances at collision		
$\varepsilon^*_h = (\beta\gamma)\sigma_h^2/\beta_h$	(μm)	1.5
$\varepsilon^*_v = (\beta\gamma)\sigma_h^2/\beta_v$	(μm)	1.5
$\varepsilon^*_l = 4\pi\sigma_{T/A} \cdot \sigma_t$	(eV·s/u)	0.8
Collision energy (TeV/u)		3.1
Injection energy (GeV/u)		118
Bunch harmonic number		660
Bunch spacing (ns)		134.7

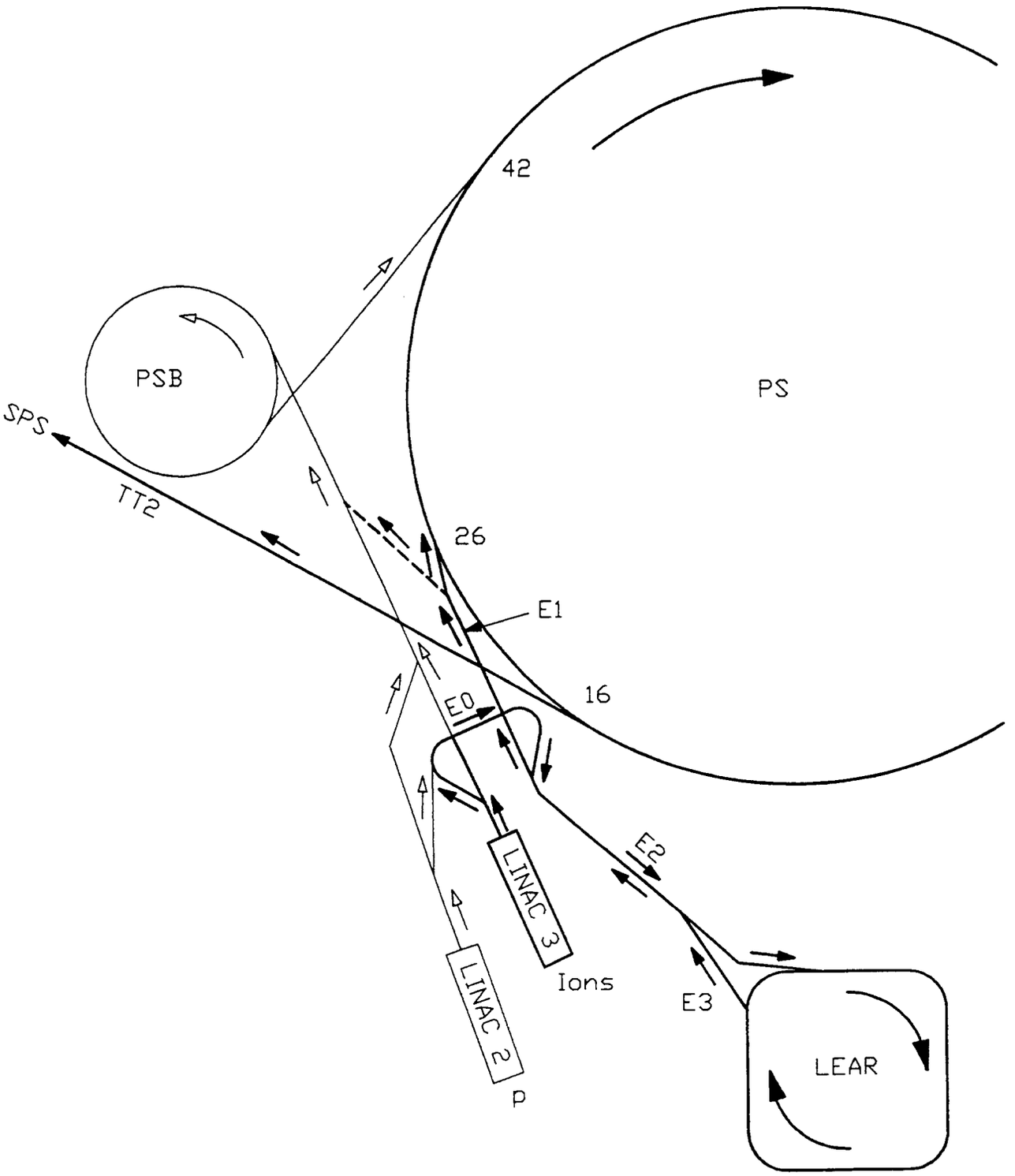

Fig. 1 : Ion scheme for LHC with accumulation in LEAR

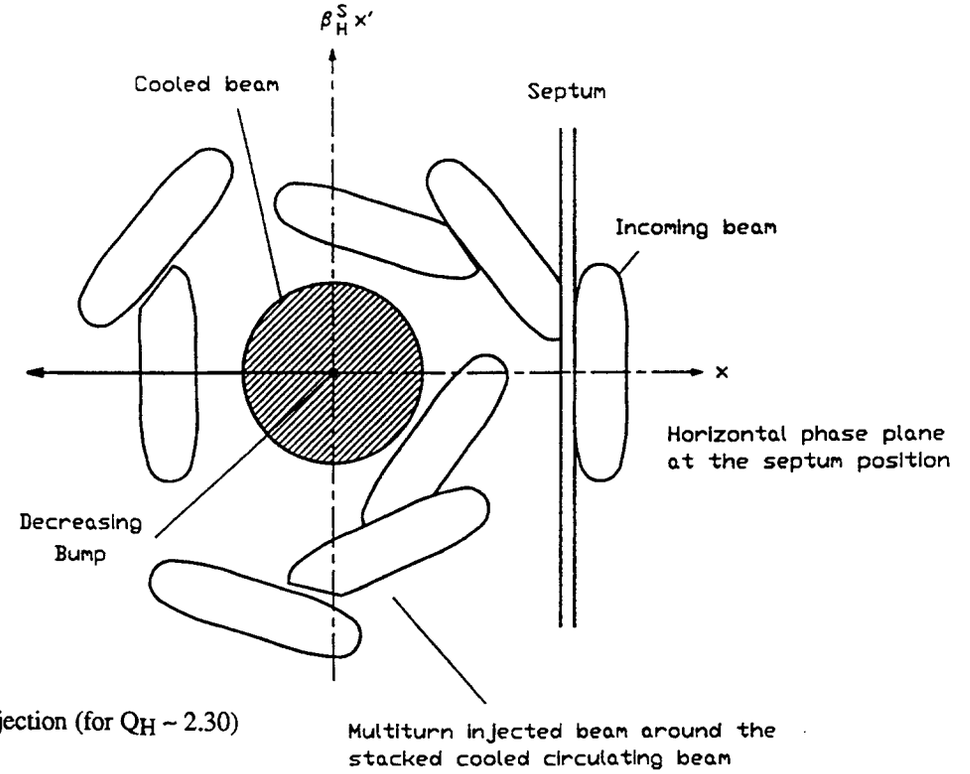

Fig. 2 : Multiturn injection (for $Q_H \sim 2.30$)

3. INJECTION AND COOLING

3.1 Aperture and stacking considerations

The acceptances of LEAR are given in table 3. We assume that for multiturn injection and stacking with cooling an effective space of ± 3 standard deviations (i.e. an emittance in phase space of 9 times the rms emittance of the beam) is required to accommodate each incoming turn. Then from tables 1 and 3 one concludes that ideally about 10 turns fit into the horizontal acceptance. In reality, with an overall efficiency of 50%, about 20 turns are needed to reach the intensity gain of 10. Thus to some extent the vertical acceptance, too, has to be used for multiturn stacking.

Table 3: LEAR acceptances

Acceptances	Theoretical	Practical	
horizontal, A_h	200	150	μm
vertical, A_v	60	40	μm
momentum, $\Delta p/p$	±5	±3	10^{-3}

The 20 turns are injected around the stack in much the same way as in a classical multiturn injection. Then, to improve the efficiency, some controlled amount of coupling is used to transfer particles from the horizontal into the vertical phase plane, where "spare" acceptance is available. The coupling can be provided by the solenoidal fields of the electron cooling device and possibly by skew quadrupoles [5]. The electron cooling system is working continuously to merge the injected beam into the stack. After 100 ms, when the next pulse is available the particles must be contained in an r.m.s. phase space emittance of a few μm.

In principle the injection scheme can be achieved with the existing elements, namely the fast bumpers to be relocated in section SS11 and SS12 with the addition of a third one in SS42 or in SL1 and the DC magnetic septum in SL1.

Nevertheless the multiturn injection efficiency will suffer due to the magnetic septum thickness (9 mm), a higher efficiency could be produced by using a thin electrostatic septum (≤0·1mm).

Additional longitudinal stacking which could improve the transverse scheme will be investigated.

3.2 Electron cooling times

The cooling times are discussed in ref. [6]. The problem is different from the cooling of a normal beam as pulses have to be transported from injection orbit into the stack. To estimate the time for this we write the cooling rate for the amplitude of betatron oscillation as:

$$1/\tau = \frac{1}{k}\frac{Q^2}{A}\eta_c L_c r_e r_p \frac{j}{e}\frac{1}{\beta^4\gamma^5\theta^3} \qquad (1)$$

with : k (=0.16) : a constant, depending on the distribution of ions and electrons; η_C (= 0.018) : the fraction of the circumference occupied by the cooling device; $L_c \cong 10$: the Coulomb logarithm; $r_e = 2.8\ 10^{-13}$cm and $r_p = 1.5\ 10^{-16}$cm : the classical electron and proton radii; j (= 0.02 Amp/cm^2) : the current density of the electron beam; e = 1.6 10^{-19} C and Θ (= 4 mrad) : the angular spread between the electron and the ion beam.

We then obtain a time constant of 65 ms, for the charge state Q = 53 and the mass number A = 208.

In summary we expect that horizontal and vertical cooling in 0.1 s, to clear space for the new pulse, can be achieved. In a first phase one might use a slower filling rate with a linac pulse every 0.2 s. This would increase the LHC filling time to about 14 instead of 8 minutes.

Beam properties expected at the end of stacking are summarised in table 4.

Table 4: LEAR batch (coasting beam) at the end of stacking.

number of ions		1.2 10^9
normalised emittances		
ε_h*	(μm)	1.
ε_v*	(μm)	0.5
ε_l	(eV·s/u)	0.05
momentum spread, coasting beam σ_p		5 10^{-4}

3.3 Beam lifetime limitations in LEAR.

To estimate charge exchange with the residual gas, we use Franzke's formula for the electron caputre and loss cross sections [7]. For the LEAR vacuum of 10^{-12} Torr N_2 equivalent, the resulting losses are less than 2%.

To estimate the recombination with cooling electrons we scale the observed proton recombination with Q^2. The resulting beam lifetime (about 200 s for the conditions of the upgraded LEAR cooler) is sufficiently long even if mechanisms other than radiative capture increase the cross section by an order of magnitude.

The intra beam scattering times, worked out using the computer code INTRAB, are long compared to the electron cooling times and thus can be neglected.

The maximum space charge tune shift of the bunched beam is close to 0.1 which may well be the limit for the proposed scheme.

As to longitudinal stability, for the wall impedance $|Zn/n| \approx 100\ \Omega$ of LEAR the "Keil-Schnell" criterion requires a $\sigma_p > 2\ 10^{-4}$ which is safely below the expected 5 10^{-4}. The direct space-charge impedance of about 5 kΩ is not important as for capacitive impedance the stability zone is much larger than predicted by the simple "Keil-Schnell circle".

4. CONCLUSIONS

The use of LEAR or a LEAR-like machine with strong electron cooling opens up the possibility of obtaining the desired luminosity with lead. More work is necessary to reach the level of a design study.

REFERENCES

[1] The Large Hadron Collider, LHC Project Proposal to be submitted to CERN Council in December 93.

[2] D. Warner editor, CERN Heavy Ion Facility Design Report, CERN 93-01.

[3] D. Brandt, E. Brouzet, H. Gareyte, Heavy Ions in the SPS-LHC Complex, CERN/SL/Note 92-47 (AP).

[4] P. Lefèvre, D. Möhl, A Low Energy Accumulator Ring of Ions for LHC, CERN-PS Report to be published.

[5] K. Schindl, P. van der Stok, A Method for Increasing the Multiturn Injection Efficiency in AG Synchrotrons by Means of Skew Quadrupoles, IEEE Trans. Nucl. Sci., Vol. NS-24, No.3, June 1977, p. 1390.

[6] J. Bosser, G. Tranquille (CERN/PS), I. Meshkov (Capt Lipetsk, Russia), Expected Cooling Times, CERN/PS/Note to be published.

[7] B. Franzke, Vacuum Requirements for Heavy Ion Synchrotrons, IEEE Trans. Nucl. Sci., Vol. NS-28, No. 3, June 1981, p. 2116

CHARGE DEPENDENCE OF THE ELECTRON COOLING FORCE FOR HEAVY IONS

A. Wolf, C. Ellert, M. Grieser, D. Habs, B. Hochadel, R. Repnow, and D. Schwalm
Physikalisches Institut der Universität Heidelberg and
Max-Planck-Institut für Kernphysik, Heidelberg, Germany

ABSTRACT

The longitudinal friction force on heavy ions in charge states between 1 and 16 was measured using the electron cooler and the induction accelerator of the Heidelberg Test Storage Ring at a beam energy of 6.1 MeV/u. At higher relative velocities, typical for the cooling of a newly injected ion beam, very good agreement with the usual linear theory was observed for all charge states. At low relative velocities close to the equilibrium, the agreement with the linear dielectric theory of 'magnetized' electron cooling was reasonable for $q = 1$, but at higher charge states the measured force came short of the predicted value by up to 60%. The observed cooling force close to equilibrium scales with $q^{3/2}$ rather than q^2 predicted by the linear theory.

1. INTRODUCTION

Electron cooling of ion beams is based on the energy loss of an ion in the electron gas formed by a collinear, velocity-matched electron beam superimposed on the ion beam. Usually the dominant part of this energy loss is caused by "distant" electron-ion collisions. For these, the Coulomb interaction represents only a small perturbation of the relative motion so that the momentum transfer increases linearly with the strength of the interaction, that is, proportional to the ion charge number q and inversely proportional to the impact parameter b. Considering the integrated effect of such collisions, the friction force should increase proportional to the ion charge squared. This is expected also in the presence of the magnetic guiding field of the electron beam applied in beam direction in most electron cooling devices.

In this paper, however, we present experimental investigations of a regime where the dominant part of the energy loss is caused by "close" collisions for which the condition of a small perturbation of the electrons by the ions no longer holds and thus deviations from the q^2 scaling of the friction force are observed. In particular, we consider the "magnetized electron cooling" effect [1] where the magnetic field causes a strong enhancement of the friction force as compared to the case without a magnetic field. In the equilibrium of an electron-cooled ion beam, this leads to very low effective temperatures of both the electrons and the ions, and predictions of the friction force using the assumption of a linear scaling of the momentum transfer with the strength of the interaction are expected to fail, especially for higher ion charges $q \gg 1$.

2. NON-LINEAR EFFECTS IN 'MAGNETIZED' ELECTRON COOLING

For a situation in which the distant collisions are dominant, the deviations from the scaling of the friction force $\propto q^2$ can be estimated by considering the relative importance of close collisions, for which the condition of a small perturbation of the electron-ion relative motion no longer holds. The electron-ion distance d which marks the onset of close collisions is that for which the Coulomb interaction potential qe^2/d reaches the order of magnitude of the initial kinetic energy of the relative motion, $mv^2/2$, where m is the electron mass and v the relative velocity. Conventionally, twice the kinetic energy is set equal to the potential energy and the resulting length $d = qe^2/mv^2$ is called the collision diameter. (By this definition d is the impact parameter at which the electron deflection angle becomes 90° in a Coulomb collision with a heavy ion.)

Let us first consider the case without magnetic field. For the typical parameters of an electron cooler, i.e., a relative energy corresponding to the electron temperature of 0.1 eV and an electron density of $n_e = 3 \times 10^7$ cm^{-3}, the collision distance $d = q \cdot 7 \times 10^{-7}$ cm is 4-5 orders of magnitude smaller than the Debye screening length $\lambda = 6 \times 10^{-2}$ cm. The usual integration of the momentum transfer over

the impact parameters between d and λ then leads to a large Coulomb logarithm $L_C \approx 10 - \ln q$ and correspondingly [2], a reliable prediction of the friction force can be made even for high ion charges q.

In a magnetic field, the dynamics of the electron-ion collisions is essentially modified for those electrons that always stay further away from the ion than the adiabatic distance $r_1 = u/\omega_c$. Here, u is the relative velocity between the ion and the *guiding center* of the electron motion, and $\omega_c = eB/mc$ is the electron cyclotron frequency for the magnetic field strength B. The distance $2\pi r_1$ is the displacement of the ion with respect to the electron after a full cyclotron revolution. For collisions at $b \gg r_1$ ("slow collisions") the velocity u, obtained by neglecting the electron motion in the transverse direction, represents the effective relative velocity. On the other hand, for $b \ll r_1$ ("fast collisions") the collision dynamic is essentially not modified by the magnetic field and the effective relative velocity continues to be given by v.

The magnetic field strength applied in typical electron coolers is of the order of 0.1 T. The related cyclotron frequency ω_c is higher than the plasma frequency $\omega_p = (4\pi e^2 n_e/m)^{1/2}$ by about one to two orders of magnitude. Hence, r_1 is considerably smaller than the Debye screening length $\lambda = u/\omega_p$ [2] and the range of impact parameters for "slow" collisions extends over one to two decades. On the other hand, the size of the associated Coulomb logarithm is typically only between 2 and 4, which requires a more careful treatment of screening than for the unmagnetized case [2].

The typical longitudinal velocity spread in the electron beam of average velocity v_0 is given by $\Delta v_\parallel = \langle (v_\parallel - v_0)^2 \rangle^{1/2} \approx 10^6$ cm/s, whereas the average transverse electron velocity (corresponding to the temperature of 0.1 eV at the cathode) is $\Delta v_\perp = \langle v_\perp^2 \rangle^{1/2} = 1.9 \times 10^7$ cm/s. For decreasing ion velocity V in the comoving frame, the friction force is first dominated by the fast collisions as long as $V > \Delta v_\perp$ and increases $\propto V^{-2}$. In the range $\Delta v_\parallel < V < \Delta v_\perp$ the contribution due to fast collisions decreases, being strongly influenced by the transverse velocity spread of the electrons [it is in fact suppressed by a factor of $(V/\Delta v_\perp)^3$], whereas the contribution from slow collisions continues to rise as V decreases; the increase is $\propto V^{-n}$ with $1 < n < 2$, as numerical calculations [2] show. For $V \approx \Delta v_\parallel$ the friction force reaches its maximum; it is now mainly due to slow collisions occuring at a distance $b \gtrsim r_1$. For $V < \Delta v_\parallel$ the longitudinal electron velocity spread finally counteracts any further increase and the force becomes $\propto V$, leading to an exponential damping of the ion velocity towards $V = 0$.

Let us now make a rough estimate of the 'collision diameter' $d^{\rm slow} = qe^2/mu^2$ for the slow collisions, which represents the distance at which the potential energy is of the order of the kinetic energy of the guiding-center motion. As u decreases, $d^{\rm slow}$ can become larger than r_1 so that we have to consider also for 'magnetized' collisions the situation where the assumption of a small perturbation of the electron-ion relative motion no longer holds. Obviously, a close Coulomb collision in a magnetic field is much more difficult to handle than one without external fields. The velocity u_1 at which $d^{\rm slow} = r_1$ can be expressed in terms of the classical electron radius r_e as $u_1/c = [q r_e(\omega_c/c)]^{1/3}$. Its numerical value of $u_1 = [q \cdot (B/\mathrm{T})]^{1/3} \cdot 3.545 \times 10^6$ cm/s is of the order of 10^6 cm/s for the typical magnetic field strength in electron coolers and $q = 1$. The ion velocity in the comoving frame is likely to become lower than $\Delta v_\parallel$ in the equilibrium of electron cooling (at least for not too dense ion beams), so that average relative velocities $u \approx \Delta v_\parallel < u_1$ should be reached especially at higher ion charge q. Finally, the collision diameter can exceed even the screening distance λ; the velocity u_2 where this occurs is lower than u_1 by only a factor of $(\omega_p/\omega_c)^{1/3}$ which lies in the range of 0.25–0.5.

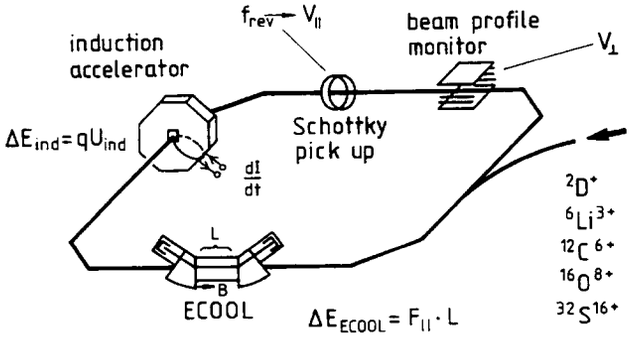

Fig. 1: Experimental setup for cooling force measurements at the TSR observing the equilibrium between the energy change at the induction accelerator and that in the electron cooler ($\Delta E_{\rm ind} + \Delta E_{\rm ECOOL} = 0$).

3. EXPERIMENTAL METHOD

We have performed measurements of the longitudinal friction force on ions with charge numbers between 1 and 16 in the Test Storage Ring (TSR) at the Max-Planck-Institut für Kernphysik in Heidelberg. Fully stripped ions with a charge-to-mass (q/A) ratio of 0.5 (d, $^6Li^{3+}$, $^{12}C^{6+}$, $^{16}O^{8+}$, $^{32}S^{16+}$) were stored at a specific energy close to 6.1 MeV/u, keeping the magnetic field of the storage ring elements and the parameters of the electron cooling device practically fixed for all ions. The longitudinal friction force was measured with an induction accelerator [3] in which a constant and well-defined acceleration can be applied to the circulating ions during time intervals of some seconds, ramping the excitation current around a large iron core as sketched in Fig. 1. The voltage induced in a monitoring loop around the iron core yields a direct absolute measurement of the acceleration applied. The average relative longitudinal velocity of the ions with respect to the electrons is derived from the Schottky noise spectrum of the ions, representing the ion revolution frequency and hence their velocity. After cooling to the equilibrium, a specific constant acceleration is applied and the shift of the average revolution frequency of the ions is extracted from the noise spectrum. This yields the longitudinal ion velocity $V_\parallel$ (in the comoving frame) for which the friction force is equal in size and opposite to the ring-averaged accelerating force. Probing the frequency shift for different values of the inductive acceleration yields the longitudinal friction force as a function of the longitudinal ion velocity $V_\parallel$.

Since only minimal changes of the electron-beam energy (3.4 keV) are required and the magnetic settings of the storage ring are not touched at all, a direct comparison of the friction force as a function of the ion charge can be performed. However, in order to compare the different measurements, also the average transverse velocity $V_\perp$ of the ions in the electron cooler must be monitored. This is accomplished by the residual-gas ionization beam-profile monitor [4] of the TSR (see Fig. 1), which yields the horizontal emittance of the ion beam. In fact, the transverse emittance increases with the stored ion current. Using the information on the transverse emittance, the longitudinal cooling force $F_\parallel$ is thus obtained as a function of $V_\parallel$ and $V_\perp$ and can then be compared to corresponding theoretical calculations of $F_\parallel(V_\parallel, V_\perp)$.

Results for the longitudinal friction force as a function of $V_\parallel$ for different ions but for average transverse velocities $V_\perp$ equal within ±10% are shown in Fig. 2. For normalization the measured force is divided by q^2; thus, the results for the different ions should coincide in the graph if the scaling $\propto q^2$ is observed. The data measured with the method described above are all in the velocity range $< 10^6$ cm/s, i.e., below the expected longitudinal electron velocity spread $\Delta v_\parallel$. Measurements at higher relative velocities were performed by a different method, changing the average electron velocity by applying a step of the electron-beam acceleration voltage and then finding the inductive acceleration which exactly compensates the drag force seen by the ions in the electron beam; for details see Refs. [4,5]. All measurements were

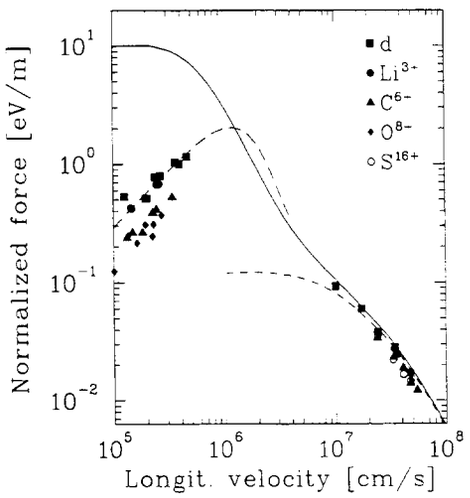

Fig. 2: Measured normalized longitudinal cooling force $F_\parallel/[q^2(n_e/10^8\,\mathrm{cm}^{-3})]$ as a function of the longitudinal ion velocity $V_\parallel$ for average transverse ion velocities in the range $V_\perp = (0.59 \pm 0.05) \times 10^6$ cm/s (ion current 11 ± 2 μA), $n_e = 0.72 \times 10^7$ cm^{-3}. The calculated curves are discussed in the text.

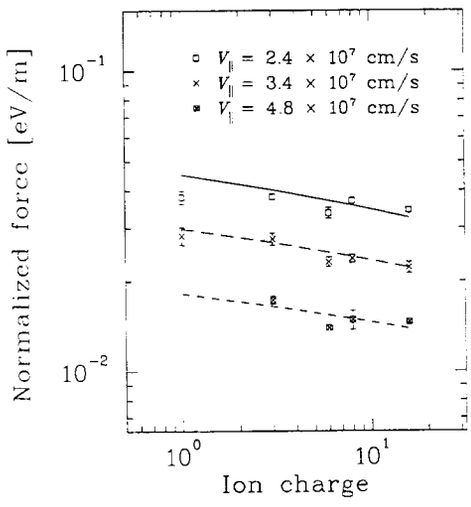

Fig. 3: Normalized longitudinal friction force as a function of the ion charge number q at high relative velocity for three values of $V_\parallel$. The curves represent the charge dependence expected because of the variation of the Coulomb logarithm.

performed a magnetic field strength of $B = 0.042$ T. The time of passage of an ion through the electron beam was 50 ns, whereas the plasma period ω_p^{-1} was shorter by a factor of 8 or 16 at the two electron densities of 0.72 and 3.4×10^7 cm^{-3}, respectively.

4. RESULTS

4.1 High relative velocities

As seen in Fig. 2, results for ions of different charge numbers are available for various values of the average longitudinal velocity $V_\parallel$ close to $\Delta v_\perp$. These relative velocities are typical for the cooling of a newly injected ion beam at moderate beam velocity ($v_0 \lesssim 0.4 \cdot c$). The longitudinal force in this relative-velocity region is mainly given by the effect of fast collisions ($b < r_1$), which can be calculated in a straightforward manner by averaging the $1/v^2$ behaviour of the friction force over the flattened electron velocity distribution [2, 6]. The absolute size of this force contribution is obtained from the Coulomb logarithm $L_C = \ln(r_1/d)$, which was directly calculated from the known parameters of the electron beam and the relative velocity v (lower dashed line in Fig. 2, for $q = 1$). At $V_\parallel \lesssim 10^7$ cm/s, an additional contribution due to the slow collisions shows up, which was calculated [6] using the dielectric approach and the impact-parameter subdivision proposed by Sørensen and Bonderup [2]. This yields the full curve in Fig. 2 which was also directly calculated from known parameters without any fitting. In particular, the transverse velocity spread $\Delta v_\perp$ was taken from earlier measurements [7] of dielectronic recombination in the TSR at similar electron beam parameters.

Very good agreement between the measured and the calculated cooling forces is observed. The Coulomb logarithm introduces a slight dependence of the normalized force $F_\parallel/q^2$ on the ion charge, since $d \propto q$. This is illustrated by Fig. 3, which shows the q dependence of the normalized force at three relative velocities. The calculated curves represent the decrease of the Coulomb logarithm [$L_C(q) = L_C(q=1) - \ln q$] and are in good agreement with the data. Thus, the present measurement enables us for the first time to perform a precise and detailed verification of the theoretical model used to describe the friction force in this range of relative velocities.

4.2 Low relative velocities

Whereas the longitudinal electron velocity spread $\Delta v_\parallel$ and the transverse ion velocity $V_\perp$ can be neglected at high velocity $V_\parallel$, they are essential at low velocity for a comparison of the data with theory

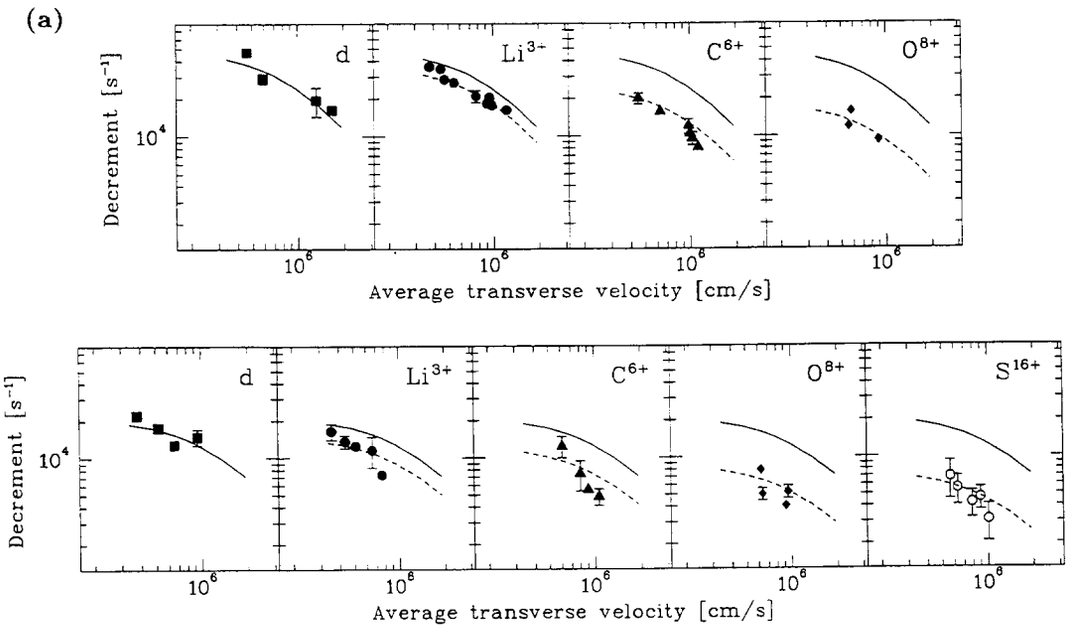

Fig. 4: Normalized cooling decrement $\alpha/[(q^2/A)(n_e/10^8\,\mathrm{cm}^{-3})]$ as a function of the average transverse ion velocity $V_\perp$ measured for ions of different charge. (a) Electron density $n_e = 0.72 \times 10^7$ cm^{-3}, theoretical curve (full line) for $\Delta v_\parallel = 0.86 \times 10^6$ cm/s; (b) electron density $n_e = 3.4 \times 10^7$ cm^{-3}, theoretical curve (full line) for $\Delta v_\parallel = 1.03 \times 10^6$ cm/s. The dashed curves are explained in the text.

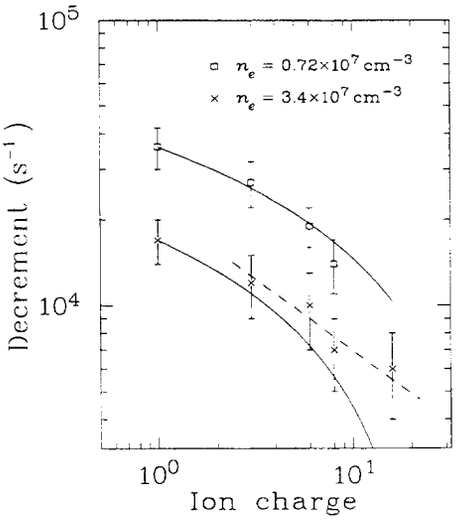

Fig. 5: Normalized cooling decrement $\alpha/[(q^2/A)(n_e/10^8\,\mathrm{cm}^{-3})]$ at an average transverse ion velocity $V_\perp = 0.5 \times 10^6$ cm/s as a function of the ion charge number q for the two electron densities of Fig. 4. (For the lines see text.)

and for extracting the variation of the friction force with the ion charge. The upper dashed curve in Fig. 2 shows the influence of $\Delta v_\parallel$ on the longitudinal friction force at low relative velocity; it has been obtained from folding the full line, representing $F_\parallel(V_\parallel, V_\perp)$ from the dielectric theory [2, 6] for the given fixed transverse velocity $V_\perp$, with a Gaussian distribution of standard deviation $\Delta v_\parallel = 1 \times 10^6$ cm/s for the longitudinal electron velocity. A more detailed comparison with theory at low velocity is presented in Fig. 4. Here, the decrement α has been determined by fitting a straight line defined by $F_\parallel = -(M\alpha)V_\parallel$ to the measured cooling force at low velocity, where M is the ion mass; the result has then been normalized to unit charge, to ion mass number $A = 1$, and to an electron density of 10^8 cm^{-3}.

As seen in Fig. 4, the normalized cooling decrement decreases not only for increasing transverse ion velocity but also for increasing ion charge. Comparing the results for $q = 1$ with the theoretical curves from the folded dielectric theory, we obtain a good fit of the data when values close to 1×10^6 cm/s, as given in the caption of Fig. 4, are chosen for $\Delta v_\parallel$. These values of $\Delta v_\parallel$ are close to those determined independently for the TSR electron cooler [7], and as expected a slightly higher value is obtained at the higher electron density. The functional depence of the cooling decrement on $V_\perp$ is thus well represented by the linear dielectric theory. On the other hand, this theory does not predict any dependence of the normalized decrement on q.

In order to extract from these data the q dependence of the normalized cooling decrement, we have first multiplied the curve obtained from the linear theory by a factor independent of $V_\perp$, chosen to fit the data for each q as shown by the dashed curves in Fig. 4. This allows us to find interpolated values of the normalized cooling decrement at a fixed average transverse ion velocity $V_\perp$ for all q, presented in Fig. 5. For high ion charge, the decrement and hence the friction force is up to 60% lower than predicted by the linear theory. Looking for a simple power law describing the decrease of the normalized cooling decrement as a function of q, one finds that a dependence $\propto q^{-1/2}$ (indicated by the dashed line in Fig. 5) fits the data well. Theoretical calculations on the friction force in the non-linear regime presented at this conference [8,9] in fact predict quite the same power law, and also the first electron cooling experiments at very high ion charge [10] indicate that the friction force increases $\propto q^{3/2}$ rather than $\propto q^2$.

In Ref. [8] a nonlinearity parameter was defined as the ratio of the ion charge number q to the number N_D of electrons in the Debye sphere, given in terms of the Debye screening length λ as $N_D = (4\pi/3)\lambda^3 n_e$. This parameter is related to the ratio of the 'collision diameter' d^{slow} to the screening length λ discussed in Section 2 ($q/N_D = 3d^{\mathrm{slow}}/\lambda$). We obtain $N_D = 4.3$ and 5.5 for the higher and the lower electron density, respectively; hence, the data represent the range of q where nonlinearities are expected to become significant ($q/N_D = 1$ for $q \approx 5$). A similar nonlinearity limit is considered in Ref. [9].

Based on the discussion of Section 2, we could also directly consider the variation of d^{slow} with q and describe its influence on the cooling force by a reduction of the effective Coulomb logarithm for the slow collisions. In the linear dielectric theory used in Figs. 3 and 4, no Coulomb logarithm occurs explicitly; however, from the spatial region around an ion considered in this approach [2], the approximate value

of the effective Coulomb logarithm can be estimated to be $\ln(\lambda/r_1) = \ln(\omega_c/\omega_p)$. Taking into account the lower cutoff due to the 'collision diameter', this transforms into $L_C^{\rm slow} = \ln(\lambda/d^{\rm slow})$. Now for the present experimental conditions, $d^{\rm slow} \approx r_1$ for $q = 1$; thus we can write the effective Coulomb logarithm as $L_C^{\rm slow}(q) \approx \ln(\omega_c/\omega_p) - \ln q$. The decrease of the normalized cooling decrement for increasing ion charge with respect to the result at $q = 1$ is then given by the factor $L_C^{\rm slow}(q)/\ln(\omega_c/\omega_p)$ (full lines in Fig. 5). This description, suggested in similar form also by Ref. [1], is in reasonable agreement with the data except for $q = 16$, where $\ln q = 2.77$ is already very close to $\ln(\omega_c/\omega_p) = 3.11$ (or, equivalently, $d^{\rm slow} \approx \lambda$). Thus, the logarithmic dependence at lower q possibly merges into the $q^{-1/2}$ power law for the normalized friction force as q increases further and the collision diameter $d^{\rm slow}$ approaches the screening length λ, or as $q/N_D \gtrsim 1$.

5. CONCLUSION

We have explored the charge dependence of the friction force in electron cooling of heavy ions, performing high-precision measurements of the longitudinal drag force in different ranges of the relative velocity. The results at high relative velocity confirm the cooling-force calculations based on the linear theory and thus demonstrate the accuracy of the experimental method. At low relative velocity, where the interaction between ions and 'magnetized' electrons yields the dominant contribution to the cooling force, a few basic estimates show that for $q > 1$ the linear description will no longer be appropriate. In fact, the available linear dielectric theory of the friction force turns out to be in reasonable agreement with the data for $q = 1$, but it cannot explain the observed variation of the friction force with q, which approximately follows the power law $\propto q^{3/2}$. Remarkably, already simplified theoretical models, developed recently to describe the friction force in the nonlinear regime, predict a similar scaling behaviour.

To arrive at a proper description of the electron cooling force at high ion charge and low relative velocity, it appears necessary to consider the Coulomb interaction of an ion with several surrounding electrons in a magnetic field for a strong perturbation of the electron orbits by the ion. This situation may also lead to the formation of bound electron orbits around the ion. The possible influence of such processes on the recombination of electrons and ions in the electron cooler is being investigated at the TSR by measuring spontaneous and laser-stimulated electron-ion recombination rates [11].

This work has been supported by the German Federal Minister for Research and Technology (Bundesministerium für Forschung und Technologie) under Contract No. 06 HD 525 I.

REFERENCES

[1] I.N. Meshkov, Electron cooling: Status and perspectives, these Proceedings.
[2] A.H. Sørensen and E. Bonderup, Nucl. Instrum. Methods **215**, 27 (1983).
[3] Ch. Ellert, D. Habs, E. Jaeschke, T. Kambara, M. Music, D. Schwalm, P. Sigray, and A. Wolf, Nucl. Instrum. Methods Phys. Res. **A314**, 399.
[4] B. Hochadel, A residual-gas ionization beam-profile monitor for the Heidelberg Test Storage Ring TSR, subm. to Nucl. Instrum. Methods Phys. Res. A.
[5] A. Wolf, "Wechselwirkung zwischen hochgeladenen Ionen und freien Elektronen in einem Ionenspeicherring: Dynamische Reibung und Rekombination", MPI H–V 15–1992 (MPI für Kernphysik, Heidelberg, 1992).
[6] A. Wolf, "Elektronenkühlung für niederenergetische Antiprotonen", KfK 4023 (Kernforschungszentrum, Karlsruhe, 1986).
[7] G. Kilgus, D. Habs, D. Schwalm, A. Wolf, N.R. Badnell, and A. Müller, Phys. Rev. A **46**, 5730 (1992).
[8] I. Hofmann, What is electron cooling for high Z?, these Proceedings.
[9] G. Zwicknagel, C. Toepffer, and P.-G. Reinhard, Molecular dynamics simulation of electron cooling, these Proceedings.
[10] M. Steck, K. Beckert, F. Bosch, H. Eickhoff, B. Franzke, O. Klepper, R. Mooshammer, F. Nolden, H. Reich, and P. Spädtke, Electron cooling of highly charged heavy ions at the ESR, these Proceedings.
[11] A. Wolf, D. Habs, A.Lampert, R. Neumann, U. Schramm, Th. Schüßler, and D. Schwalm, in: "Atomic Physics 13", edited by H. Walther, T.W. Hänsch, and B. Neizert, AIP Conference Proceedings, vol. 275 (American Inst. of Physics, New York, 1993), p. 228.

K4-K10 PROJECT. TREBLe: TWO RING EXOTIC BEAM LABORATORY

V.A.Gorshkov, O.N.Malyshev, Yu.Ts.Oganessian, G.S.Popeko, A.M.Rodin, R.N.Sagaidak, V.P.Sarantsev, S.I.Sidorchuk, Ye.A.Sokol, S.V.Stepantsov, G.M.Ter-Akopian and V.A.Timakov
Joint Institute for Nuclear Research, Dubna 141980, Russia
I.I.Averbukh, V.P.Cherepanov, Ye.N.Dementiev, A.M.Kalinin, V.I.Kudelainen, V.V.Parkhomchuk, A.N.Skrynski and A.M.Zelenin
Budker Institute of Nuclear Physics, Novosibirsk 630090, Russia
V.F.Byckovski, R.M.Lapik, I.N.Meshkov, Ye.M.Syresin
Center of Applied Physics and Technology, Lipetsk 398055, Russia
V.P.Belov, A.A.Makarov, I.A.Shuckeylo, Yu.P.Severgin and M.N.Tarovik
Efremov Research Institute, St.Petersburg 189631, Russia

ABSTRACT
The concept of the Dubna project of two coupled storage rings intended to provide cooled beams of short lived exotic nuclei is briefly described and the evaluated luminosity values are presented. As the first stage of the project the construction of one of the rings is proposed. Due to the high peak beam intensity of the injector cyclotron U400M this ring will give high luminosity exotic beams.

1. DESCRIPTION OF THE PROJECT

TREBLe is a modification of the Dubna project of the heavy ion storage ring complex K4-K10 [1, 2, 3]. The specific feature of this modification is to provide high precision beams of exotic nuclei with mass numbers of A<50 in the energy range from few MeV to about 200 MeV/amu. We preserve the principal concept of the K4-K10 project (see Fig.1). The first ring is intended to accumulate the primary heavy ion beam from the JINR sector focusing cyclotron U400M, to cool this beam and to increase the energy up to about 120-170 MeV/amu. The primary beam obtained as a result of fast extraction from the first ring is used to produce the exotic beam which, after separation by an energy loss achromat, is injected into the second ring. The nuclei with the lifetime of $\geq$1 s can be cooled and accumulated on the ring orbit and their beam energy can be controlled. For the short lived nuclei ($T_{1/2}$<1 s), a target irradiation will be preferable immediately after cooling. The cooling time in the second ring will be of the order of 50 ms. This very short cooling time can be obtained due to a low initial phase space of the secondary beam. The small transverse emittance is resulted from the fact that the secondary beam is produced after focusing the high quality primary beam onto a very small target spot of less than 1 mm in diameter. The longitudinal emittance of the secondary beam is also considerably reduced due to the possibility to extract from the first ring the high quality primary beam in the form of very short (20 ns) bunches.

2. INJECTOR CYCLOTRON U400M

The sector focusing cyclotron U400M is a new machine which being tested during the 1993 commissioning cycle proved its ability to produce, with a PIG ion source, high intensity beams of ions ranging

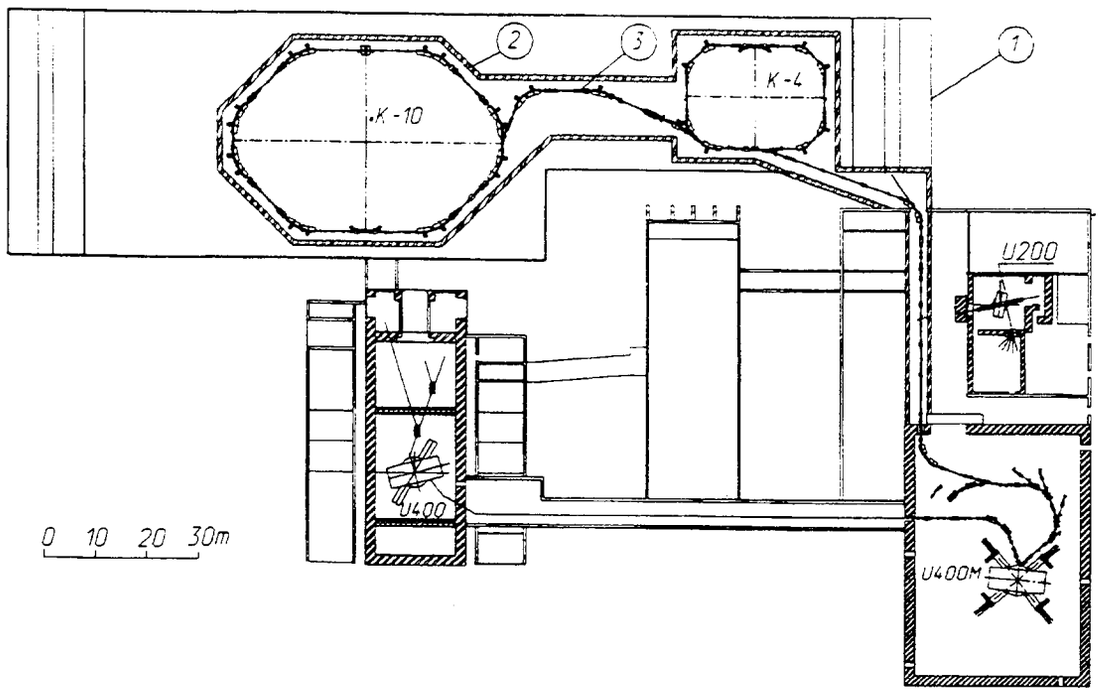

Fig.1 - Diagram of the complex K4-K10.
1-injection beam line, 2- production target, 3-separation channel.

Table 1 - Peak Beam Intensities of U400M

ION	NUMBER OF IONS PER 1μS			ENERGY
	ECR	Laser source	PIG	MeV/amu
$^{14}C^{+4}$		10^9	$5*10^8$	43
$^{15}N^{+5}$	$4*10^9$		10^7	56
$^{18}O^{+6}$	$3*10^8$	10^8		56
$^{20}Ne^{+7}$	$2*10^8$			59
$^{30}Si^{+7}$		$8*10^8$		31
$^{36}S^{+8}$		10^9		29
$^{40}Ar^{+10}$	10^8			35
$^{46}Ti^{+12}$		$3*10^8$		38
$^{48}Ca^{+10}$	$4*10^7$	$3*10^8$		27

from carbon to neon. Table 1 gives the intensities of some of the beams in terms of the number of ions which will be produced by the cyclotron within one microsecond, i.e. the time interval of the order of one period of beam revolution on a ring orbit. The data for the ECR ion source are from literature [4]. The numbers for the laser plasma ion source are obtained in experiments carried out at the sector focusing cyclotron U200 [5]. The program of installation of an ECR ion source is running in 1993 as an essential part of the funded U400M project. The routine operation of the cyclotron with this ion source will begin in 1994. Specially for the project TREBLe the work on a new version of the laser ion source for U400M is carried out in 1993. The tests are planned for 1994.

3. COOLER RINGS

The ring K4 described in [1] meets the conditions imposed on the first ring in TREBLe. Its basic parameters are listed in Table 2. Two beam injection schemes foreseen for this ring are considered in detail in our previous papers [1, 2, 3]. Both schemes, the injection by ion stripping and multiple single turn injection, provide for the fast primary beam accumulation and cooling. This can be accomplished

Table 2 - Basic Parameters of the Ring K4

Ring	K4
$B\rho_{max}$, T*m	4
Circumference , m	83.11
Acceptance $\mathcal{E}_x$, π*mm*mrad	35
$(\Delta p/p)_{max}$, %	1.0
Cooling electron maximum energy , keV	100
Length of the cooling section , m	3
Electron maximum current , A	5
Cathode diameter , cm	3
RF amplitude, kV	14
Range of the RF frequency , MHz	0.5–3.4
Vacuum, Pa	10^{-8}

Table 3 - Some exotic beams attinable at TREBLe

BEAMS	$T_{1/2}$ (sec)	$\lvert N-N_{drip}\rvert$	$E_{inj.}$ (MeV/amu)	$E_{max.}$ (MeV/amu)	NUMBER OF IONS ON ORBIT	LUMINOSITY ($s^{-1}cm^{-2}$)
^{6}He	0.808	2	105	175	10^{7}	10^{27}
^{8}He	0.122	0	110	120	10^{5}	10^{25}
^{9}Li	0.178	2	110	175	10^{7}	10^{27}
^{11}Li	0.009	0	110	120	10^{4}	10^{24}
^{11}Be	13.8	3	125	210	10^{7}	10^{27}
^{14}Be	0.05	0	120	130	10^{2}	10^{22}
^{12}B	0.02	5	85	265	10^{8}	10^{28}
^{17}B	0.006	0	120	140	10^{2}	10^{22}
^{16}C	0.75	6	115	220	10^{6}	10^{26}
^{18}C	0.1	4	120	175	10^{3}	10^{23}
^{14}O	70.6	2	110	455	10^{8}	10^{28}
^{22}O	0.76	2	120	210	10^{4}	10^{24}
^{24}Ne	225	8	125	265	10^{8}	10^{28}
^{28}Ne	0.014	2	120	200	10^{3}	10^{23}
^{44m}Sc (J^{p}=6^{+})	$2*10^{5}$	9	110	335	10^{10}	10^{30}

within 100 ms for 10^{11} and 10^{10} ions of carbon and calcium, respectively, accumulated and cooled on the orbit of the ring. Formation of 20 ns bunches on the K4 orbit will cause some increase of the beam momentum spread while it does not affect the small transverse emittance of the cooled beam. A beam having the transverse emittance of 1 π mm*mrad and momentum spread of $\pm$0.2% will be easily focused onto a production (beryllium) target of a diameter of 0.8 mm. The beam of exotic nuclei produced on this target will be separated and focused by the ion optical system of the fragment separator shown in Fig.1. The separator is designed to manage, for the injection into the second ring, with the exotic beam having the momentum spread of $\pm$0.5% and emerging from the target within a solid angle of about 3 msr. The maximum magnetic rigidity of the second ring is not specified at this stage. Other essential parameters can be borrowed from the K10 ring described in [1]. In Table 3 we show, for some exotic nuclei, the evaluated numbers of ions on the orbit of the second ring and the luminosity values which will be attainable in experiments carried out with internal ring targets. We assumed that a long term irradiation will be possible in the case when the thickness of the target does not exceed 10^{14} atoms per cm^2 and that the beam accumulation time of up to 1000 s will be possible for the long lived nuclei.

4. FIRST STAGE OF THE PROJECT

We determine the first stage of the project realization which implies the building of the first ring K4. The peak primary beam intensities presented in Table 1 give us favorable conditions to produce the beams of exotic nuclei suitable for accumulating and cooling in the ring K4. Immediately after splitting (see Fig.2), the beam is focused on a target (diameter of 1 mm), and secondary beams are produced.

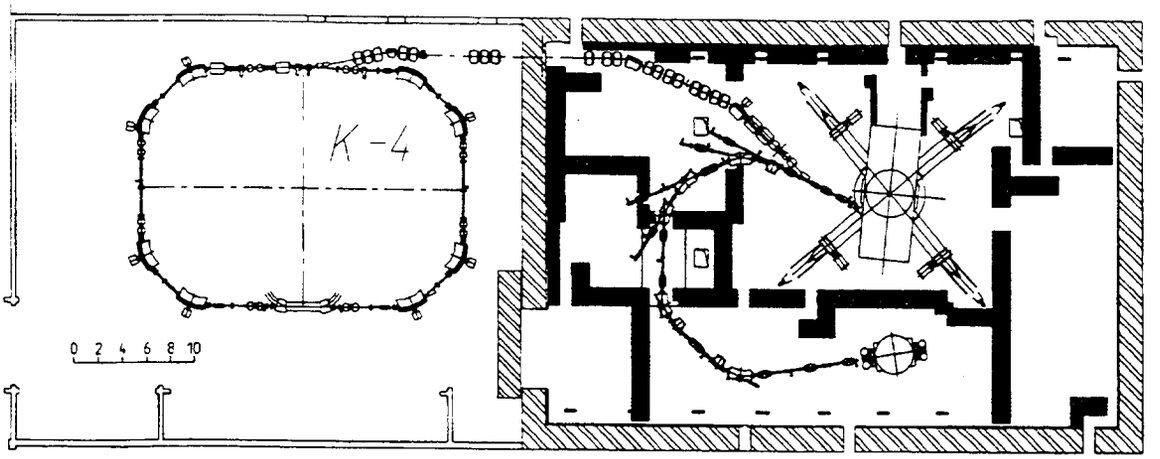

Fig.2 - First stage of TREBLe.

The secondary beam emerging from the target within the solid angle of 3.5 msr will be captured by this separation channel and injected into the K4 ring. To widen the accessible momentum range of the beam accumulated in the ring a beam debunching (see Fig.3) will be provided before the injection. This reduces, by a factor of about ten, the initial momentum spread (±1.0%) of the secondary beam. In Table 4 we give the parameters of some exotic beams which will be obtained after the completion of the project first stage.

Table 4 - Exotic Beams in K4.

BEAMS	$T_{1/2}$ (sec)	$\lvert N-N_{drip}\rvert$	E inj. (MeV/amu)	E max. (MeV/amu)	NUMBER OF IONS ON ORBIT	L (s^{-1} cm^{-2})
^{6}He	0.808	2	42	80	10^{4}	10^{24}
^{8}He	0.122	0	43	50	10^{2}	10^{22}
^{8}Li	0.84	3	41	105	10^{4}	10^{24}
^{9}Li	0.178	2	44	80	10^{3}	10^{23}
^{11}Be	13.8	3	44	100	10^{5}	10^{25}
^{12}B	0.02	5	40	125	10^{5}	10^{25}
^{16}C	0.75	6	42	105	10^{3}	10^{23}
^{14}O	70.6	2	36	225	10^{5}	10^{25}
^{24}Ne	225	8	20	125	10^{6}	10^{26}
^{28}Mg	$7*10^{4}$	12	20	130	10^{7}	10^{27}
^{38}S	$1*10^{4}$	14	17	130	10^{7}	10^{27}
^{44m}Sc ($J^{P}=6^{+}$)	$2*10^{5}$	9	22	160	10^{8}	10^{28}

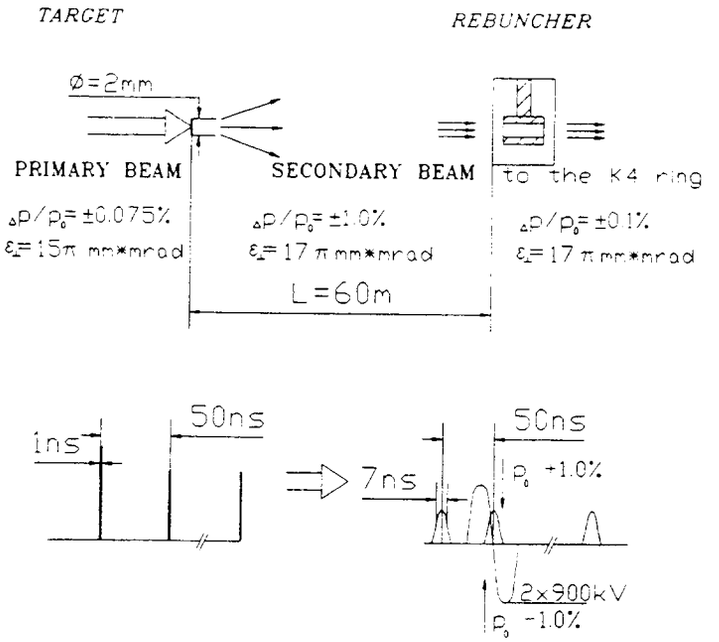

Fig.3 - Schematic diagram illustrating the production and debunching of a secondary beam.

One of the authors (G.M.T.-A.) acknowledges the fact that Dr. B. Franzke (GSI Darmstadt) attracted his attention to the advantage of the radioactive beam debunching in the ring injection line.

REFERENCES

[1] G.M.Ter-Akopian (Ed.) Heavy Ion Storage Ring Complex K4-K10. A Technical Proposal, JINR E9-92-15, Dubna 1992.

[2] Yu.Ts.Oganessian et al. Z.Phys. A, v.341, p.217, 1992.

[3] O.N.Malyshev et al. 1991 IEEE Particle Accelerator Conference, San Francisco, California, May 6-9, 1991, 91CH3038-7 Conference Record, v.5, p.2888-2890.

[4] C.M.Lyneis and T.A.Antaya, Rev. Sci. Instr., V.61, p.221, 1990.

[5] V.B.Kutner et al. Rev. Sci. Instr., v.63, n.4, p.2835, 1992.

REPORT OF THE WORKING SESSION ON CYCLOTRON MASER COOLING

D. Möhl and A. M. Sessler[*)]
CERN, PS Division, CH - 1211 Geneva 23

ABSTRACT
A report is presented of the Working Sessions on Cyclotron Maser Cooling in which the concept is presented, various comments upon it are reported, and it is concluded that there is no cooling.

1. INTRODUCTION

The Working Sessions on Cyclotron Maser Cooling (CMC) met on Monday evening, October 4, and on Tuesday afternoon, October 5. The total time was about $3^1/_2$ hours. Presentations were made by Hidetsugu Ikegami, David Whaley, Erkki Brändas, Takeshi Katayama, Simon van der Meer, Gerald Jackson, and Igor Meshkov. There was ample discussion and the audience reached a number of general conclusions.

In this report we shall, very briefly, describe the contributions of each of the people listed above and then present the general conclusions.

2. HIDETSUGU IKEGAMI

The concept of Cyclotron Maser Cooling (CMC) recently also referred to as Coherent Microwave Cooling, is due to H. Ikegami [1] and is described in the Proceedings of this Workshop [2]. Particles circulate in a storage ring which contains a cooling section consisting of solenoids, deflecting magnets, and rf cavities as shown in Fig. 1. The beam is deflected transversely and its transverse energy changes in time according to

$$\frac{d\gamma_\perp}{dt} = \frac{1}{2}\left(\frac{eE_{rf}}{m_0 c\gamma_\perp}\right)\tau F(x), \tag{1}$$

where
E_{rf} = electric field amplitude,
τ = a quantity which H. Ikegami calls the damping time of the oscillator,
$F(x)$ = $[1/(1+x^2)] + [2ax/(1+x^2)^2]$,
x = $2\tau[\omega_c/\gamma_\perp - \omega_{rf}]$,
ω_{rf} = angular frequency of the rf,
ω_c = cyclotron frequency ($\gamma = 1$) of the particles,
a = $2\omega_c\tau[1 - 1/\gamma_\perp]$.

Considering the case when $a \gg 1$, H. Ikegami concludes that not only does a particle's transverse energy, characterized by $\gamma_\perp$, get reduced in time, but a collection of particles will have its spread in $\gamma_\perp$ reduced. The cooling time for this process is given as

$$\tau_\perp = \frac{ecB_0}{\pi r_0 I(\omega_{rf})}\left(\frac{\gamma_\perp}{2\omega_c t}\right)^3 \frac{\gamma_\perp^2}{\left(1-\beta_{//}\beta_{rf}\right)\left(\gamma_\perp - 1\right)} \tag{2}$$

where
B_0 = solenoidal magnetic field,

---

*) Visitor from Lawrence Berkeley Laboratory, Berkeley, California 94720, USA.

r_0 = classical particle radius,
$I(\omega_{rf})$ = intensity of the rf,
t = "time in the cooler section",
β_{rf} = propagation velocity of the rf field.

The phenomenon is purely classical, although stimulated radiation is a key element.

H. Ikegami has performed an experiment on CMC using the apparatus shown in Fig. 2. He has obtained a number of results; a typical set is shown in Fig. 3.

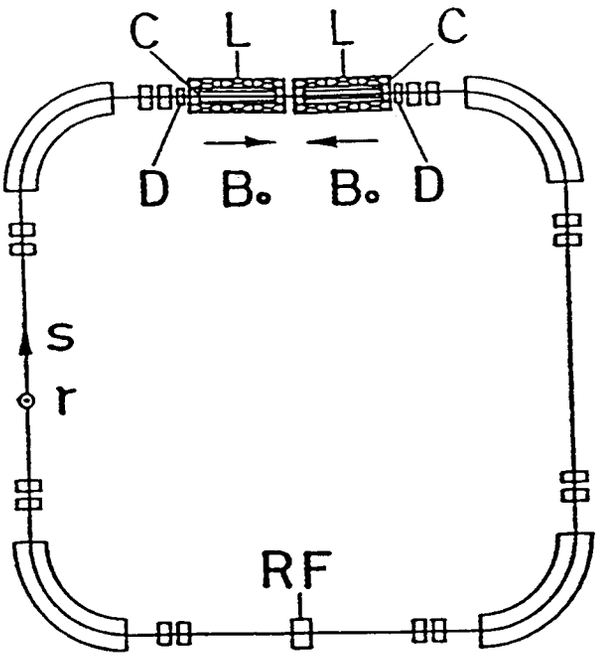

Fig. 1 - A basic configuration of a facility for coherent microwave cooling. C: rf cavity for stimulating emission or absorption of photons; D: small deflection magnet; L: solenoidal magnet; RF: accelerating rf system. Elements without abbreviation are lattice magnets and r and s are the transverse and longitudinal coordinates, respectively. (Figure and caption from Ref. [2].)

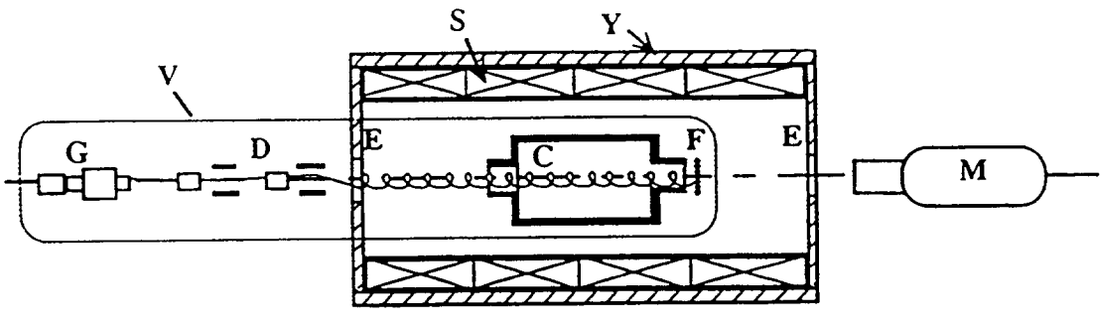

Fig. 2 - Experimental arrangement. G: electron gun; D: dual deflector system; E: end plate of magnet; C: rf cavity; F: conducting ZnS screen; Y: magnet yoke; S: solenoidal coil; V: vacuum enclosure; M: monitoring system. (Figure and caption taken from Ref. 2.)

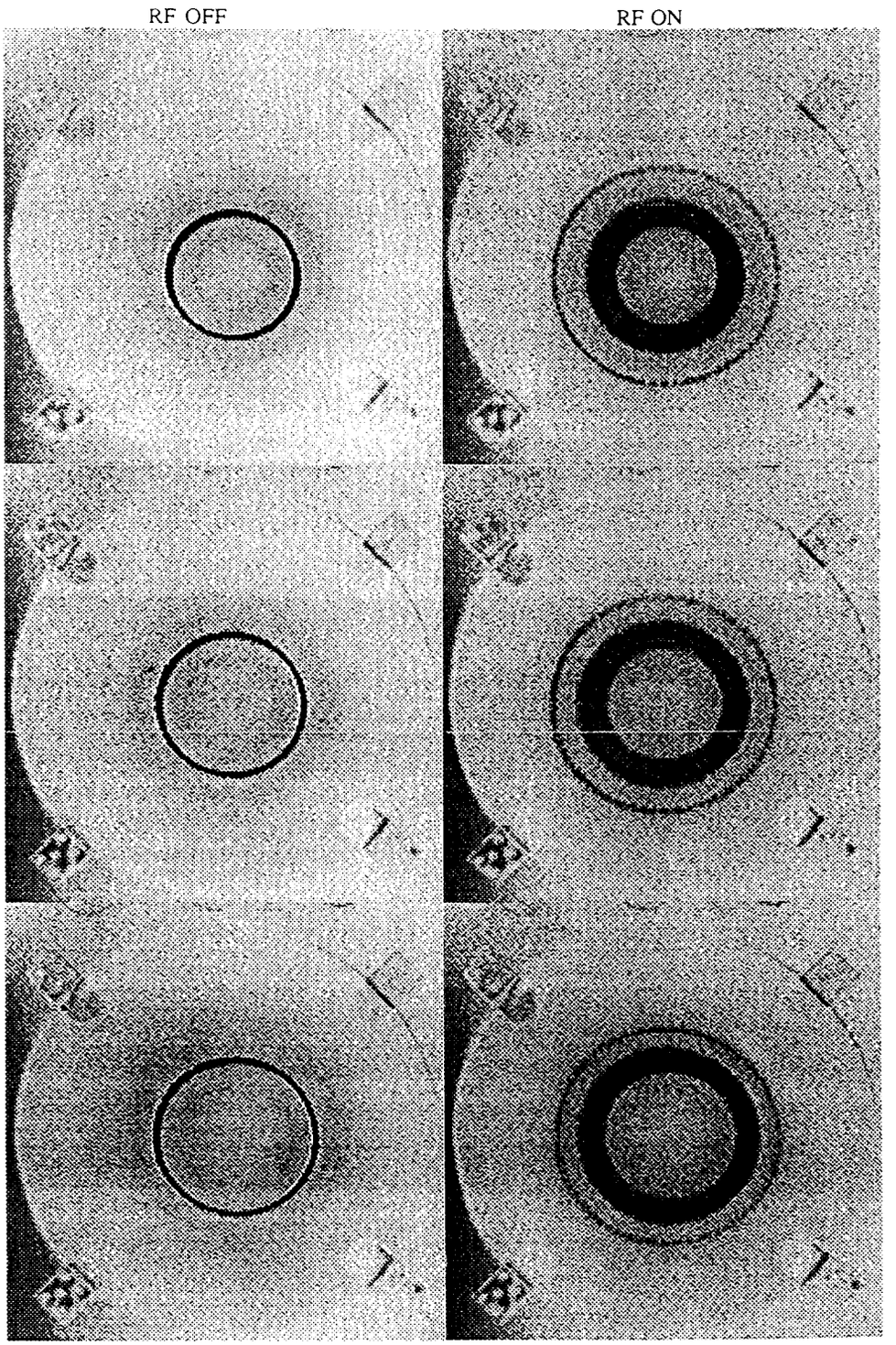

Fig. 3 - Comparison of the Larmor radii arising from *heating* and *absorptive cooling* of electrons. The patterns depicted on the ZnS screen for *rf on* and *rf off* at $\omega_c/2\pi$ = 2.16 GHz and $\omega_c/2\pi$ = 2.09 GHz for the initial transverse kinetic energies: (a) 8 keV, (b) 10 keV, (c) 12 keV. The sharp outer circles correspond to the electron energy of 23 keV, which were observed without accompanied by the broad band of inner circles when the longitudinal drift energy spread was reduced. (Figure and caption taken from Ref. 2.)

3. DAVID WHALEY

A presentation was given of the numerical simulation work of the Ecole Polytechnique Fédérale de Lausanne [3]. Their work is described in the Proceedings of this Workshop. They consider a rectangular cavity excited in the TE_{102} mode. Particles are sent through the cavity with typical results as shown in Fig. 4. A careful study reveals that there is no CMC cooling. Similar results have been obtained by B. Karlsson in Uppsala and are described in the Proceedings of this Workshop [3].

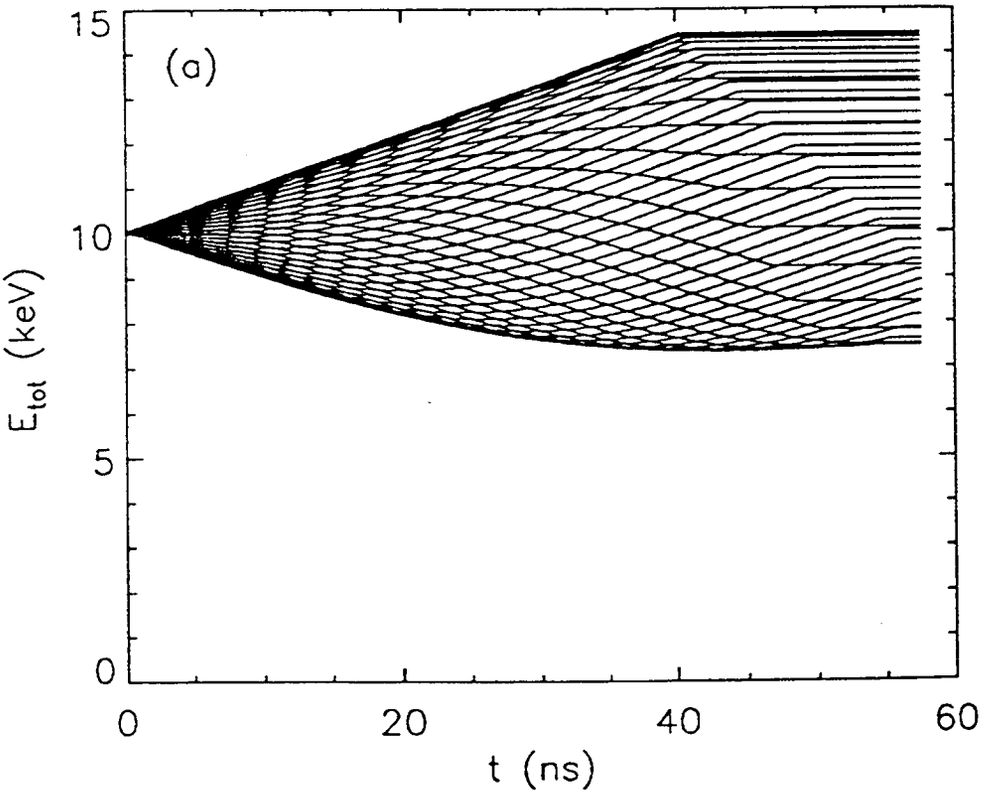

Fig. 4 - Energy vs. time trajectories of beam during passage through resonant cavity. Simulation begins with 50 injection particles distributed randomly in phase with respect to the RF waveform. Beam parameters: $E_{11} = 50eV$ and $E_{\perp} \sim$ ~10 keV (from Whaley et al., [3].

4. ERKKI BRÄNDAS

A general quantum mechanical formalism was presented and it was shown that in the classical limit there is no CMC cooling [4]. E. Brändas has determined the form of a term in the density matrix which would give cooling, but no physical relation has yet been developed between CMC and the required term.

5. TAKESHI KATAYAMA

A presentation was given of an analytic analysis of the cyclotron motion. Proceeding by considering cyclic motion in the beam reference frame he has:

- Cyclotron frequency

$$\Omega = \frac{eB_0}{m} = \frac{\Omega_0}{\gamma_\perp}$$

$$\Omega_0 = \frac{eB_0}{m_0}$$

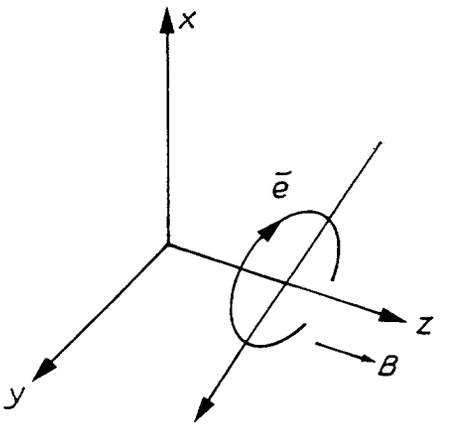

$$E_y = E_0 \cos(\omega t + \delta)$$

- Larmor Radius:

$$r = \frac{mv_\perp}{eB_0} = \frac{v_\perp}{\Omega}$$

- Equation of Motion

$$\frac{d\vec{P}}{dt} = e\left(\vec{E} + \vec{v} \times \vec{B}\right)$$

$$\downarrow$$

$$\begin{cases} \dfrac{dP_\perp}{dt} = \dfrac{|e|E_0}{2}\sin(\psi) \\ \dfrac{d\psi}{dt} = \omega - \dfrac{\Omega_0}{\gamma_\perp} + \dfrac{|e|E_0}{2P_\perp}\cos(\psi) \end{cases}$$

$$\psi \equiv \omega t - \phi(t) + \delta$$

"Modified Phase Equation"

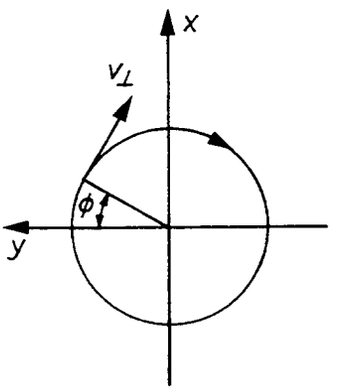

He concluded that since he is dealing with a conservative system there is no cooling or heating. The "coarse grained density", however, always decreases so that, in practice, whether there is deceleration or acceleration there is heating, as shown in Fig. 5.

6. SIMON VAN DER MEER

Simon van der Meer presented general arguments [6] showing that in μ-space Liouville's Theorem will be valid under the conditions where coherent cyclotron maser radiation is created, i.e. that there is **no** CM cooling. The basic reason for the absence of cooling is that there are no short range forces which vary over a length of the order of the inter-particle spacing.

7. GERALD JACKSON

G. Jackson focused on the experiment discussed in H. Ikegami's paper [2]. Following the remarks of others in the audience he emphasized that it is necessary to measure **phase-space** before and after the CMC section. A reduction of only the transverse velocity is, clearly, no proof of phase-space cooling.

He then developed an analogue where the bunching in the CM section is compared to rf motion in a storage ring. The wide and the narrow rings observed in the experiment can then be well-explained as due to some particles trapped inside the rf bucket and some particles moving outside the bucket. Clearly, there is no phase-space cooling in these circumstances.

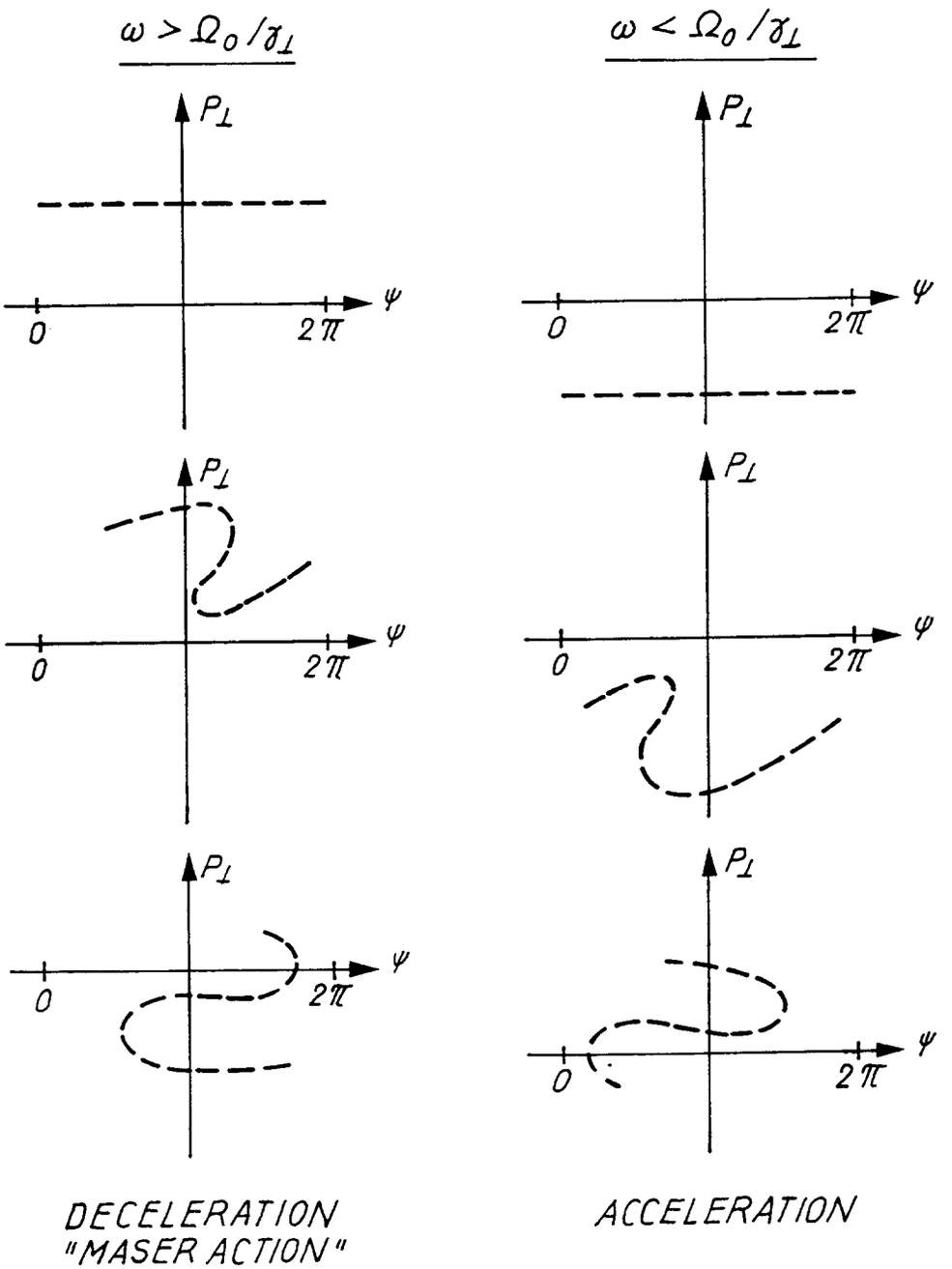

Fig. 5 - Phase space for cyclotron resonance

8. IGOR MESHKOV

Igor Meshkov realised independently the same analogue as presented by G. Jackson. In addition he proposed an improvement of the experiment consisting of a beam deflection and emittance measuring device to determine phase space prior to and after the CM section.

9. CONCLUSIONS

At first, in the discussion, questions were raised, and comments were made, on the various presentations. Some of the more salient points were:

1. It was not clear to the audience how there is phase-space cooling in CMC. Everyone agreed that a deflected beam, characterized by $\gamma_\perp$, would change its energy as suggested by Eq. (1). It was, however, most unclear how this process would lead to a damping of energy spread. In particular, people felt that there was "a jump in logic" between Eqs. (1) and (2) in the sense that loss of energy does not automatically imply loss of energy spread.

2. None of the analytic work of H. Katayama, or the numerical work of D. Whaley and M. and D. Tran as well as that of B. Karlsson, includes **stimulated** cyclotron radiation. This stimulated radiation into a state characterized, say, by wave vector $\boldsymbol{k}$ and polarization ε, would only occur if that state is already occupied by photons. If there are n photons in that state then the transition probability to the state is $(1+n)$, which for $n \gg 1$ can be very large.
   The presented work has the interaction of particles with a single rf mode (for which n is very large indeed), but no stimulated emission in any other mode. It was generally felt that stimulated emission needs not be included.

3. Only for short wavelengths can one "beat Liouville's Theorem", as discussed in the first paper [9] presented to this Workshop and re-empasized by S. van der Meer. Thus, in order to have fast ($n \gg 1$) cyclotron cooling one would need many photons in states of very short wavelengths (wavelength « inter-particle spacing). That, however, is not the case in cyclotron masers, which is why stimulated emission has not been --quite properly-- included in the work cited above.

4. The experiments reported by H. Ikegami were not considered to be definitive, as they could be explained in alternative (non-cooling) ways. For example, when the injection is changed, corresponding to non-central orbits in the rf cavity, only the narrow circle (made by increased energy electrons) shifts back to the cavity center while the broad circles of heated electrons (of low energy) remain displaced. This can be explained in terms of trapping and non-trapping, rather than being compelling evidence for cooling.

Following these detailed comments, there were general discussions and the group agreed (although, of course, no note was taken and there was no call for position) upon the following:

1. The derivation of cyclotron maser cooling is not compelling.
2. The experimental evidence for cyclotron maser cooling is not convincing.
3. There are analytic calculations, numerical simulations, and general arguments all of which say that there is no cyclotron maser cooling.

REFERENCES

[1] H. Ikegami, Pys. Rev. Lett. 64 (1990) 1737; 64 (1990) 2593.

[2] H. Ikegami, *Coherent Microwave Cooling (CMC) of Electron and Ion Beams*, this Workshop Proceedings.

[3] D. Whaley, M. Tran and T. Tran, *Particle Simulation of Cyclotron Maser Cooling Experiment*, this Workshop Proceedings, 1993.
B.R. Karlsson, *The CMC Concept and Test Experiment*, this Workshop Proceedings.

[4] E. Brändas, *Organization of Particle Beams - A possible New Cooling Concept*, this Workshop Proceedings.

[5] T. Katayama, private communication.

[6] S. van der Meer, *Discussion on Ikegami's Paper*, this Workshop Proceedings.

[7] G. Jackson, private communication.

[8] I. Meshkov, private communication.

[9] A.M. Sessler, *Liouville's Theorem and Phase-Space Cooling*, this Workshop Proceedings.

REPORT OF THE WORKING SESSION ON STOCHASTIC COOLING

T. Katayama
Institute for Nuclear Studies (INS), Tokyo, Japan

M. Chanel
CERN, Geneva, Switzerland

ABSTRACT

A report is presented of the overview talk by John Marriner on Monday, October 4 and of the Working Session on Stochastic Cooling which met on Wednesday morning, October 6. Presentations were made by Gerald P. Jackson, Jie Wei and Fritz Nolden. Summaries of discussions on the Fokker-Planck equation and cooling systems above 10 GHz are also presented.

1. HISTORY AND PRESENT STATUS OF STOCHASTIC COOLING

The idea of stochastic cooling, which was given first by S. van der Meer in 1968, was soon followed by the observation of proton-beam Schottky noise at the CERN ISR. In 1975 the first experimental demonstration was performed at the Intersecting Storage Rings (ISR) at CERN, and a proposal for a $\bar{p}p$ collider with stochastic cooling was immediately presented. Thereafter, stochastic cooling experiments were extensively performed at CERN, FNAL and INS-Tokyo during the years 1977-1983. In 1982, the CERN $\bar{p}$ accelerator complex projects, AA, SPS collider and LEAR started and, in 1986, the $\bar{p}$-source project was started at FNAL for the Tevatron collider. As the culmination of the stochastic cooling, in 1984, the Nobel Prize was awarded to C. Rubbia and S. van der Meer. After this work for the $\bar{p}$ ring, the application of the stochastic cooling is at present prepared or planned for the low-energy light-ion cooler ring at Jülich, and for the pre-cooling of hot fragments of heavy ions at GSI-ESR and at several heavy ion laboratories. The suppression of emittance growth due to the intra-beam scattering at the Relativistic Heavy Ion Collider (RHIC, BNL) is planned with the stochastic cooling device.

Twenty five years have passed since the beginning of stochastic cooling and much experience has been accumulated along with the development of physics of cooling itself and the industrial engineering, especially on digital and analogue electronic devices. In this sense, stochastic cooling is mature, steadily progressing on the theoretical and technological aspects.

2. KEY ISSUES OF STOCHASTIC COOLING

2.1 Bandwidth, Pick-ups and Kickers, and Low-Noise Amplifiers

The crucial parameters of stochastic cooling are:

1) The system bandwidth W, characterising principally the cooling time. At the early experimental rings such as ICE and TARN, it was around 0.1-0.2 GHz, while recently it has become an order of magnitude larger from 1-8 GHz according to the development of microwave technology and accelerator designs. Cooling people are now discussing the possibility of 30-100 GHz, mm wavelength range frequencies.
2) The structure of pick-ups and kickers with high pick-up sensitivity and shunt impedance is the main concern for the cooling technology. At present, most of high-energy stochastic cooling systems employ the $\lambda/4$ strip lines while loop couplers or slow-wave structures such as helical-type couplers are used for low-energy cooling.
3) In order to get a good signal-to-noise ratio, the cryogenic pick-ups and pre-amplifiers with low-noise figure should be used, especially at the cooler ring of small number of stored particles.

2.2 Review

In the present Workshop, an excellent review of the theory and technological implementation of the stochastic cooling was excellently given by J. Marriner (FNAL), who explained the simple theoretical model of betatron and momentum cooling, stressing the importance of the design of the cooler ring with proper lattice

structure to ensure the "good mixing" from kicker to pick-up, and the "bad mixing" from pick-up to kicker. Concerning the technological aspects, he described the design of pick-ups and kickers which have a similar structure due to Lorentz reciprocity theorem, especially on $\lambda/4$ strip-line structures currently used in most of the cooler rings. To get a good signal-to-noise ratio, arrays of 100 or more pick-ups are used. The output power of two pick-ups is combined in a transmission line of the same characteristic impedance of the pick-ups. The cascading transmission line of proper impedance transformation can effectively transfer the beam signal to a pre-amplifier. These are implemented for a bandwidth of an octave, i.e. the upper frequency is twice the lower frequency, such as 4-8 GHz, using micro-strip circuit board techniques.

One of the key issues, which determine the cooling rate and the equilibrium emittance or momentum spread, is the ratio of the thermal noise to Schottky noise. The thermal noise comes from two sources, one is due to the terminating resistor R of the pick-ups where the thermal noise voltage is $V_n = \sqrt{kTR}$ at the temperature T. In order to reduce the thermal noise, the pick-ups including resistors are cooled to cryogenic temperature. The second factor is due to the noise figure of the pre-amplifier. At present, low-noise amplifiers are made of GaAs devices used for stochastic cooling such as amplifiers, filters, delay lines for low-loss skin effect and an amplitude modulator of a laser coupled to an optical fibre followed by a demodulator using a photo diode. J. Marriner mentioned the measurement techniques such as open-loop gain measurement, Schottky signal suppression, beam profiles and beam instabilities which are commonly used in most of the storage rings as a standard beam diagnostic method.

3. REPORTS FROM LABORATORIES

3.1 Gerald Jackson (FNAL) reported on the plan and some preparatory works on the bunched beam cooling at the Tevatron collider. The purpose of this plan is to suppress the emittance growth and resultant luminosity decrease induced mainly by the noise and ripple of power supplies. The emittance growth rate is measured at 0.3π mm·mrad/h and then the cooling time is specified as 50 h for protons and 18 h for antiprotons. These long cooling times are a compromise between the beam-beam tune shift (already ~0.01) and the integrated luminosity lifetime. The major difficulties in the bunched beam transverse cooling are the unwanted/unexpected large signals at just the harmonics of the revolution frequency related to the coherent synchrotron beam motion. A number of techniques have been tried for the solution of this problem. The adjustment of positions of pick-up arrays, transversely and longitudinally, was tried with an inchworm motor with a step size of 1 μm. Another innovative technique reported is a new hybrid system to detect closed-orbit information except for betatron oscillations, where they use the photon storage ring which exponentially averages away the betatron modulation.

3.2 J. Wei (BNL) discussed the plans for the 4-8 GHz bunched-beam stochastic-cooling system for RHIC which will compensate the deterioration of luminosity due to the intra-beam scattering (IBS). The growth rate of the rms betatron amplitude $\sigma_{x,y}$ and the fractional deviation σ_p are inversely proportional to the 6-D phase volume and proportional to Z^4N/A^2 where Z is the charge state of ion, A the mass number and N the number of ions. At the typical operation of RHIC, Au beam of 100 GeV/u $N = 10^9$ is expected. The transverse cooling rate $(1/\sigma)(d\sigma/dt) = 0.1$/hr could give the equilibrium emittance of 30π mm·mrad balanced with IBS growth rate. Using the 4-8 GHz stochastic cooling for both the transverse and longitudinal directions could improve the integrated luminosity by a factor of 2 over the entire 10-hours storage period. To accommodate for the future upgrade of the beam intensity, the bandwidth of 8-16 GHz is desirable and detailed technical aspects are to be examined.

3.3 F. Nolden (GSI) explained the concept of cooling system for the 500 MeV/u secondary fragment beam which is injected on the injection orbit of ESR with a momentum spread $\Delta p/p = \pm 0.35\%$ and a transverse emittance of 20π mm·mrad. The bandwidth is from 0.9 to 1.7 GHz and the Palmer method is conceived for longitudinal cooling because the Schottky bands will overlap due to a large momentum spread and to the ring dispersion parameter $\eta = 0.25$. The number of particles of fully stripped, highly charged heavy ions is around 10^8, and the thermal noise is negligible. The cooling time is estimated to be of the order of seconds.

3.4 F. Caspers et al. (LEAR) reported the present status of the stochastic cooling scheme at LEAR which provides antiproton beams from 61 MeV/c to 2 GeV/c. To accommodate the beam cooling for a wide range of energy, a number of techniques are implemented. Now the pick-ups and kickers are of the loop-coupler type with precisely variable delays between each coupler for the adjustment of the signal propagation velocity to be matched with the beam velocity. The bandwidth extends from 5 MHz to 1.1 GHz. The upper limit of the frequency range is limited by the Schottky band overlapping at high frequency due to a large momentum spread $\Delta p/p = 0.6\%$. Digital system delays using 16-bit data word can be varied in steps of 41 ps. Non-cryogenic low-noise pre-amplifiers of 1.4 dB noise figure are used for the high-momentum lines, and the head amplifiers at 80 K physical temperature are used for the low-momentum system along with the 20 K cooled termination

resistor (50 Ω). They use 12 pick-ups of plate pairs connected to form a travelling wave structure with precisely adjusted delay lines. The other slow-wave structures, helical and meander types, were tested but with moderate success. At high-momentum (1 to 2 GeV/c) operation, the stochastic cooling is used for the retrieval of the diffused particles at the ultra-slow extraction, and for getting a very good beam quality at the jet gas target experiments, namely beam emittances less than 3π mm·mmrad for both vertical and horizontal directions and the momentum spread less than 0.2%. At low-momentum (105-609 MeV/c) operation, the stochastic cooling is used to reduce the beam dimensions before deceleration and to compensate the adiabatic emittance increase. The cooling system is also used for counteracting the diffusion mechanism such as intra-beam scattering during the slow-extraction process. Better wide-band power amplifiers, BAW (bulk acoustic wave) filters and printed structures of pick-ups and kickers are envisaged for future improvement.

Specifications of the stochastic cooling

		Tevatron	RHIC	LEAR	ESR	ADRIA
T	(GeV)	1 000	100	0.006 to 1.4	0.5	1
Beam		p-$\bar{p}$	Au^{79+}	$\bar{p}$	Fragments	Fragments
W	(GHz)	4-8	4-8	0.01-1	0.9-1.8	1-2
N	(10^9)	120/40	1	0.1-50	~0.1	~0.1
τ	(sec)	18/50 h	16 h	100-500	~1	~1
$\Delta p/p$	(‰)	0.14	1	3	3.5	4
ε	(mm·mrad)	20π	30π	20π	20π	20π
$d\varepsilon/dt$		0.3/h	0.1/h	5π-20π/nn		
Purpose		Constant luminosity		Low emittances	Pre-cooling	

4. DISCUSSION MEETINGS

Two discussion meetings took place during the Workshop, one about the Fokker-Plank (FP) equation and the other on the pick-ups and kickers for 30-100 GHz and beyond.

- The subject of the former meeting (proposed by A. Gerasimov and moderated by D. Möhl) was the FP equation which can well describe the cooling process evolution not only of the longitudinal cooling process but also of the transverse cooling process. From the beginning of the stochastic cooling history, the longitudinal cooling has been well explained by the FP equation with the measured cooling coefficient F and that of diffusion D. Could we reliably extend that approach to a 4-D or 6-D cooling process, especially in the case of dominant diffusion term of intra-beam scattering in a heavy ion collider or in the case of cooling of horizontal and momentum cooling of large momentum spread. During the discussion, A. Ruggiero explained his idea of the FP equation for the bunched beam cooling, numerically applied to the RHIC gold beam. The participants agreed that, up to now, there is no reliable formulation of the FP equation describing the 4-D or 6-D beamssatisfactorily; however, efforts are in progress at GSI and BNL, and their results should be compared to the experimental and tracking simulation results.
- The second brain storming meeting on pick-ups and kickers at high frequency was proposed by F. Caspers (CERN). The following subjects were discussed: at present, slot structures, printed loops and slot lines are in preparation or in use up to a frequency of 16 GHz. Printed loops or slot lines seem to be possible up to 30 GHz. What kind of structure could be envisaged for the bandwidth 30-100 GHz and beyond? The detailed technological problems discussed are: What are the frequency limits for printed metal structures due to metallic losses? Can we use high T_c superconductors for pick-ups and kickers on dielectric substrata instead of copper? Does the beam pipe become an over-moded wave guide for such a high frequency? The beam may be several wavelengths away from the pick-up surface, so there is no longer a near field. In this case, would a kicker be a "far field accelerator" or is the Lorentz reciprocity theorem valid outside the near field? When do we get into the regime of "quantum noise"? Are materials available for mm-wave integrated structure in an accelerator environment (e.g. vacuum, radiation)?

All the problems are related with high-level microwave engineering which is rapidly developing in connection with industrial requirements. During the meeting, several solutions and suggestions were presented. However, it seems too early to draw conclusions here. The more concrete plans for the 30-100 GHz bandwidth are expected to be deliberated at the next beam cooling workshop.

CRITICAL ISSUES IN MUON COLLIDERS - A SUMMARY

S. Chattopadhyay, W. Barletta, S. Maury,** D. Neuffer,*** A. Ruggiero,**** A. Sessler*

Lawrence Berkeley Laboratory, University of California,
Berkeley, CA 94720, USA

ABSTRACT

We present a brief summary of the current state of conception and understanding of high-energy muon colliders, associated technological challenges and future research directions on this topic.

1. MOTIVATION AND CHALLENGES

It is well known that multi-TeV e^+-e^- colliders are constrained in energy, luminosity and resolution, being limited by "radiative effects" which scale inversely as the fourth power of the lepton mass $[(E/m_e)^4]$. Thus collisions using heavier leptons such as muons offer a potentially easier extension to higher energies [1]. It is also believed that the muons have a much greater direct coupling into the mass-generating "Higgs-sector", which is the acknowledged next frontier to be explored in particle physics. This leads us to the consideration of TeV-scale μ^+-μ^- colliders. However, with the experimental determination of the top quark being heavier than the Z boson, there is increasing possibility of the existence of a "light" Higgs particle with a mass value bracketed by the Z-boson mass and twice that value. This makes a 100 GeV $\mu^+ \otimes$ 100 GeV μ^- collider as "Higgs Factory" an attractive option. The required luminosity is determined to be 10^{30} $cm^{-2}s^{-1}$. We note that the required luminosity for the same "physics reach" scales inversely as the square of the lepton mass and implies a significantly higher luminosity required of a similar energy e^+-e^- collider, in order to reach the same physics goals.

The challenges associated with developing a muon collider were discussed at the Port Jefferson workshop [1, 2], subsequent mini-workshops at Napa [3], Los Alamos [4] and at the present workshop [5, 6]. Basically, the two inter-related fundamental aspects about muons that critically determine and limit the design and development of a muon collider are that muons are secondary particles and that they have a rather short lifetime in the rest frame. The muon lifetime is about 2.2 μsec at rest and is dilated to about 2.2 msec at 100 GeV in the laboratory frame by the relativistic effect. The dilated lifetime is short enough to pose significant challenges to fast beam manipulation and control. Being secondary particles with short lifetime, muons are not to be found in abundance in nature, but rather have to be created in collisions with heavy nuclear targets. Muon beams produced from such heavy targets have spot size and divergence-limited intrinsic phase-space density which is rather low. To achieve the required luminosity, one needs to cool the beams in phase space by several orders of magnitude. And all these processes - production, cooling, other bunch manipulations, acceleration and eventual transport to collision point - will have to be completed fast in 1-2 ms and there lies the challenge. Bunch manipulation and cooling of phase space are some of the primary concerns. In the following section, we describe the two scenarios, and associated parameters being considered at present for muon colliders.

2. SCENARIOS, PARAMETERS AND COMMENTS

Basically, there are two scenarios that have been considered to date for muon colliders. These two scenarios start with very different approaches to the production of the secondary muon beam from a primary beam hitting a heavy target. The subsequent acceleration, cooling, stacking, bunching and colliding gymnastics are all dictated and differentiated by these production schemes, which are very different. We consider them in sequence in the following.

---

* Reporting author.
** CERN, CH-1211 Geneva 23, Switzerland.
*** CEBAF, 12000 Jefferson Ave., Newport News, VA 23606, USA.
**** BNL, Upton New York 11973, USA.

The first approach considers production of the muons starting from a primary "proton" beam hitting a heavy target according to the following reaction:

$$p + N \rightarrow \pi + X$$

$$\rightarrow \mu\nu$$

Since proton bunches are typically long (few ns), one basically obtains long bunches of low phase-space density, unless further phase-space manipulations are done to bunch and cool the beams. The situation is similar to the use of the Proton Ring as a pion source in the Los Alamos Meson Physics Facility (LAMPF-II) or conventionally considered kaon factory sources, for example. In order to reduce the length of the produced muon beam bunches, considerable gymnastics is required of the proton ring rf system. Ultimately, of course, a bunch rotation in the longitudinal phase space to reduce bunch length comes at the expense of the relative momentum spread, $(\Delta p/p)$, which could be as high as 5%. The produced muon bunches will need to be cooled longitudinally from $(\Delta p/p)$ of 5% to about 0.1% in order to have acceptable spectral purity at the collision point. In addition, the muon bunches will have to be cooled in the transverse phase space by a significant amount in order to meet the luminosity demand at the collision point. The cooled muons are subsequently accelerated and injected into a 100 GeV μ^+-μ^- collider where the bunches collide in at most a few hundred to a thousand turns (the number of turns, $n \simeq 300\overline{B}$ [Tesla]). Clearly the constraint of short muon lifetime puts a premium at every stage on minimizing the time for production, cooling, acceleration and bunch processing, so as to still leave a few hundred turns in the collider to produce luminosity. Thus, it is clear that high field magnets play crucial role in the collider. Details of this scenario have been considered by D. Neuffer [5]. In Fig. 1, we depict schematically the scenario of a muon collider based on production via protons [5].

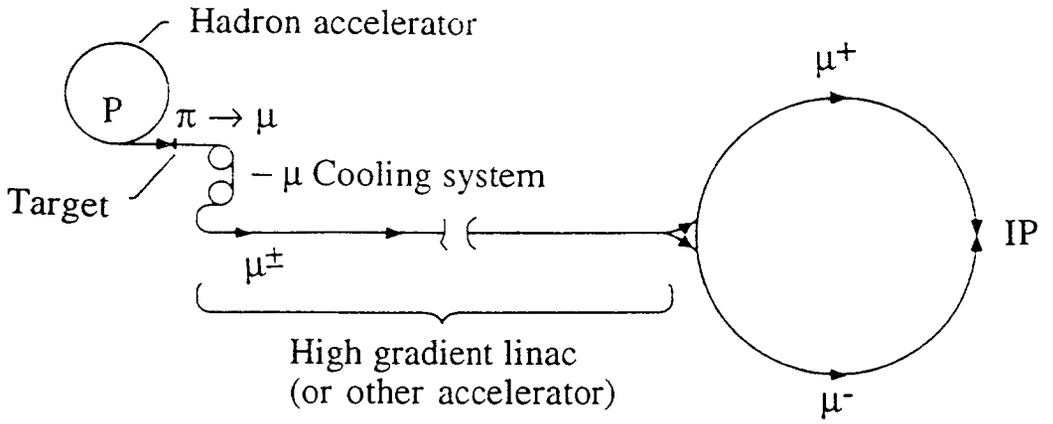

Fig. 1 - Overview of a μ^+-μ^- collider, showing a hadronic accelerator, which produces π's on a target, followed by a μ-decay channel ($\pi \rightarrow \mu\nu$) and μ-cooling system, followed by a μ-accelerating linac (or recirculating linac or rapid-cycling synchrotron), feeding into a high-energy storage ring for μ^+-μ^- collisions. (from Ref. [5])

A second approach considers production of the muons starting from a primary "electron" beam hitting a heavy target according to the following reaction:

$$e + N \rightarrow e + N + \gamma$$

$$\rightarrow \mu^+\mu^-$$

In this electro-production scenario, one obtains short bunches most naturally, since it is compatible with the normal mode of operation of high energy linacs. Although one obtains the "optimum bunch format" naturally, one has to consider unprecedently high power and high repetition rate electron linacs, not explored before in order to meet the required collision luminosity. This is so because of the rather low yield of muons per electron, even at the optimum energy of incident electrons of 60 GeV, and the difficulty of packing more electrons per bunch in the linac. The low transverse phase-space density of the muons will require significant improvement via cooling, similar to the proton production scenario, and, in addition, calls for a non-trivial beam stacking scheme before collision described in Ref. [6]. Details of this scenario have been considered by Barletta and Sessler [6]. In Fig. 2, we depict schematically the scenario of a muon collider based on electro-production [6].

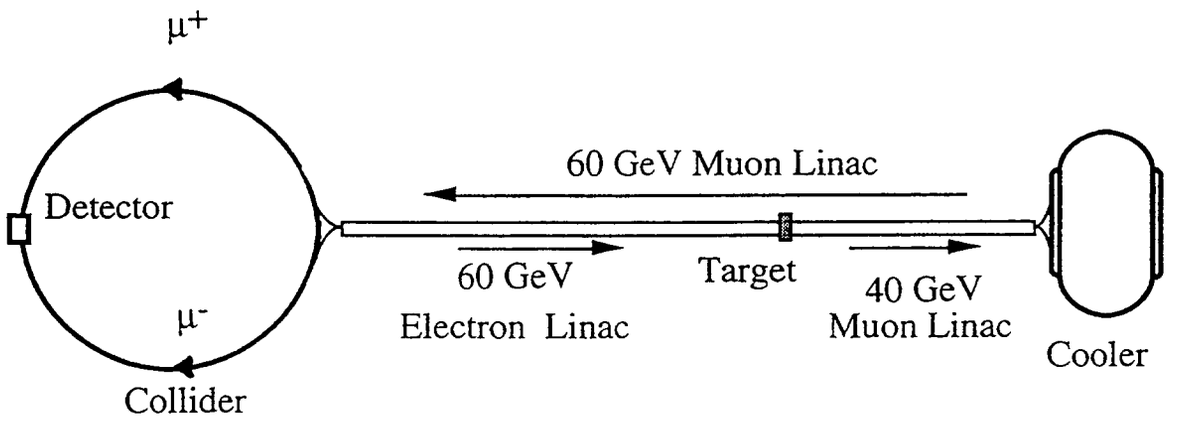

Fig. 2 - A muon collider scenario with electro-production of muons. (from Ref. [6])

Table 1 presents a comparison of parameters for the above two scenarios for a 100 GeV $\mu^+ \otimes$ 100 GeV μ^- collider, with an average luminosity of 10^{30} cm^{-2}s^{-1}. We assumed a collider scenario with a low beta at the collision point of 1 cm, about 1 000 bunches colliding in the ring and muon production limited by a 5 MW power at the target. It is clear that while powerful pion sources, bunch compression and cooling are essential for the proton-production scenario, high current electron linacs, cooling and stacking are essential for the electro-production scenario. It is fair to say from an inspection of Table 1 that, fundamentally, both scenarios are equally amenable to a muon collider configuration with comparable luminosities, given the fact that in both cases equally difficult and challenging technological problems will have to be addressed and solved.

Table 1 - Parameters for a muon collider

100 GeV $\otimes$ 100 GeV

$$L = M\frac{N_+ N_- f}{4\pi\,\varepsilon_N \beta^*}\gamma \sim 10^{30}\ \text{cm}^{-2}\text{s}^{-1}$$

M = 1 000; γ = 1 000; β^* = 1 cm; P = 5 MW @ target

	Production via Electrons	Production via Protons
$E_{e\,\text{or}\,p}$ (GeV)	60	30
Intensity	5×10^{11}/pulse	10^{14}/pulse
# pulses	100 (stacked later)	1
Repetition rate (Hz)	10	10
E_μ (GeV)	40	1.5
ε_N (π m·rad)	2×10^{-3}	2×10^{-2}
$\Delta p/p$	±3%	±3%
(μ/e) or (μ/p)	4×10^{-3}	10^{-3}
Ionisation cooling	$\varepsilon_n^f = 2 \times 10^{-5}\pi$ m·rad	$\varepsilon_n^f = 2 \times 10^{-5}\pi$ m·rad
Bunch Rotation Factor	None	100

The most difficult and challenging of these technological problems is probably that of "ultra-rapid" phase-space cooling of "intense" bunches. One can consider radiation cooling via synchrotron radiation which is independent of the bunch intensity. However, it is too slow for our purposes. Stochastic cooling rate, on the other hand, depends on the number of particles per bunch and, although too slow usually, can be made significantly faster by going to an extreme scenario of a few particles per bunch with ultra-fast phase mixing or

an ultra-high bandwidth (~10^{14} Hz) cooling feedback loop. Both the latter cases will require significant technological inventions. A promising scheme that is both "fast" and "intensity-independent" is that of "Ionization Cooling", which looks feasible in principle. We have assumed ionization cooling in arriving at the parameters of Table 1. We discuss cooling considerations briefly in the next section.

3. COOLING OF MUONS

The cooling of the transverse phase-space assumed in Table 1 is of the kind known as "Ionization Cooling". In this scheme the beam transverse and longitudinal energy losses in passing through a material medium are followed by coherent reacceleration, resulting in beam phase-space cooling [5-7]. The cooling rate achievable is much faster than, although similar conceptually to, radiation damping in a storage ring in which energy losses in synchrotron radiation followed by rf acceleration result in beam phase-space cooling in all dimensions. Ionization cooling is described in great detail in Ref. [5] in these proceedings. It seems that the time is ripe to make a serious design of an ionization cooling channel, including the associated magnetic optics and rf aspects, and put it to real test at some laboratory.

Exploration of the alternate cooling scheme of stochastic cooling takes us to a totally different regime of operation of the collider, determined by the very different nature and mechanism of cooling by an electronic feedback system. Here, the muon lifetime and the required low emittance demanded by the luminosity requirements determine the necessary stochastic cooling rate of the phase space. This rate scales directly as the bandwidth (W) of the feedback system and inversely as the number of particles (N) in the beam (stochastic cooling rate $\propto W/N$). If we limit our consideration to practically achievable conventional feedback electronics, amplifiers, etc. with bandwidth not exceeding 10 GHz, the number of particles per bunch must be less than a thousand (1 000) in order to meet the desired rate. This then would imply a very different pulse format. This alone drives all the parameters back to the source and issues of "targetry" and "muon source", etc. are not critical. The critical issues for stochastic cooling are: (1) large bandwidth, (2) ultra-low noise, as the cooled emittance reaches the thermal limit of the electronics, (3) rapid mixing and (4) bunch recombination techniques.

Critical issues in the stochastic cooling scenario are discussed by Ruggiero [8], where he also explores a conventional cooling scheme with modest bandwidth but with a special non-linear (magnetic) device that stirs up the phase space rapidly and provides "ultra-fast mixing". It is clear that we need new technical inventions in stochastic cooling for application in a muon collider. Another novel scheme [9] being explored currently is that of "optical cooling" where one detects the granularity of phase space down to a micron scale by carefully monitoring the incoherent radiation from the beam, which is a measure of its Schottky noise, then amplifying this radiation via a laser amplifier of high gain and bandwidth (10^7, 100 THz) and applying it back to the beam. Various issues regarding quantum noise and effective pickup and kicker mechanisms will have to be understood before it can be considered for a serious design.

4. SUMMARY AND OUTLOOK

As we have seen, both scenarios - production of muons from protons and electro-production of muons - are competitive but very ambitious and challenging. Production of muons from protons will clearly require non-trivial and sophisticated target design and configuration. In addition, in order to match the bunch length of the colliding (but secondarily produced) muon beams to the low-beta function at the collision point, the primary proton beams must be bunched by a large factor (~100). The complicated bunch rotation and rf manipulations are cumbersome and must be done at the low-energy proton end before the target, which implies an associated increase in the relative momentum spread, ($\Delta p/p$). On a positive note, however, targetry with protons and rf gymnastics with proton beams are relatively familiar affairs at hadron and kaon facilities, albeit at a lower level of power and rf manipulation of the bunches. Electro-production of muons, on the other hand, requires high-peak current, high-repetition rate linacs, so far unexplored, in order to meet the luminosity demand. Besides, "stacking" of many electron bunches from a linac into a single bunch poses a non-trivial problem. The significant and most attractive feature of the electro-production scenario, however, is that the "optimal pulse format" is produced directly at the target by electrons from a linac, without complex bunch compression schemes in a ring.

No matter what the optimal scenario would turn out to be, should the muon collider concept turn into reality, further consideration of such a collider at 200 GeV center-of-mass energy with an average luminosity of ~10^{30} $cm^{-2}s^{-1}$ would have to assume major advances in an eventual operation of: (1) megawatt muon targets, (2) multi-kiloampere peak current electron linacs, (3) efficient transfer, compression and stacking schemes for charged particle beams, (4) high-field magnets and (5) most importantly, feasible phase-space cooling technologies with low noise and large bandwidth. While "Ionization Cooling" looks promising, it needs experimental demonstration. A possible feasibility test of muon production and ionization cooling at existing facilities, e.g., CERN, FNAL, etc. would be highly desirable. The "stochastic Cooling" approach, however, would need fundamental invention of a new technique, as elaborated earlier. The emerging new ideas of "Optical Stochastic Cooling", "Ultra-rapid Phase-Mixer", etc. are ambitious, but may hold the key to the success of such

high-frequency stochastic cooling. Finally, the synchrotron radiation and muon decay in the collider ring vacuum chamber and detector area pose issues that cannot be overlooked.

In conclusion, surely a muon collider is exotic! But even as we contemplente the value, utility and eventual realizability of such a collider in future, there is no doubt that the necessary conceptual and technological explorations forced upon us by these considerations are much too valuable to many fields to be simply passed up.

ACKNOWLEDGEMENTS

This work was supported by the Director, Office of Energy Research, Office of High Energy and Nuclear Physics, High Energy Physics Division, of the US Department of Energy under contract No. DE-AC03-76SF00098.

REFERENCES

[1] M. Tigner, *in Advanced Accelerator Concepts*, Port Jefferson, NY 1992, AIP Conf. Proc. 279, 1 (1993).

[2] P. Chen and K.T. Mac Donald, in AIP Conf. Proc. 279, 853 (1993).

[3] Proceedings of the Mini-workshop on μ^+-μ^- Colliders: Particle Physics and Design, Napa, CA, to be published in Nucl. Inst. and Meth. A (1993).

[4] Proceedings of the Muon Collider Workshop, February 1993, Los Alamos National Laboratory Report LA-UR-93-866 (1993).

[5] D. Neuffer, *Muon Cooling and Applications*, these Workshop Proceedings.

[6] W.A. Barletta and A.M. Sessler, *Prospects for High Energy Muon Collider Based On Electro-production*, these Workshop Proceedings.

[7] D. Neuffer, Particle Accelerators, 14, 75 (1983).

[8] A.G. Ruggiero, Stochastic Cooling Requirements for a Muon Collider, these Workshop Proceedings.

[9] A.A. Mikhailichenko and M.S. Zolotorev, *Optical Stochastic Cooling*, SLAC-PUB-6272, July 1993.

REPORT OF THE WORKING SESSION ON TECHNIQUES AND TECHNOLOGY

V. Parkhomchuk
Budker Institute of Nuclear Physics, 630090 Novosibirsk, Russia

F. Caspers
CERN, PS Division, CH - 1211 Geneva 23

ABSTRACT
In the following summary each of the 11 papers (7 oral presentations, 4 posters) is discussed individually. This is because the subjects treated in the presentations are rather different, and a global evaluation is nearly impossible.

1. INTRODUCTION

The Working Session on Techniques and Technology met on Tuesday morning, October 5, and the Poster Session on Tuesday afternoon. Oral presentations were made by Evgeny Syresin, Gérard Tranquille, Jacques Bosser, Dag Reistad, Dietrich Habs, Sebastian Zwickler, and Bernd Hochadel. Poster presentations were made by Alexander Shemyakin, Alexander Sharapa, Vincenzo Guidi (represented by Bin Yang), and Michel Chanel.

2. ORAL PRESENTATIONS

2.1 Evgeny Syresin

The optical analyzer [1] consists of a cutting diaphragm followed by a luminescent screen and an observation microscope (Fig. 1). The device is operated in a pulsed mode by switching the steering electrode potential with a pulse of 20-50 μs. The screen shows an "electro-optical" image of a small hole (diaphragm). Transverse temperatures evaluated with this technique are in the range of 0.1-0.3 eV. This method is a direct way to measure transverse energies. An analysis was carried out for energy spreads in a parameter range corresponding to the operational condition of the new LEAR gun.

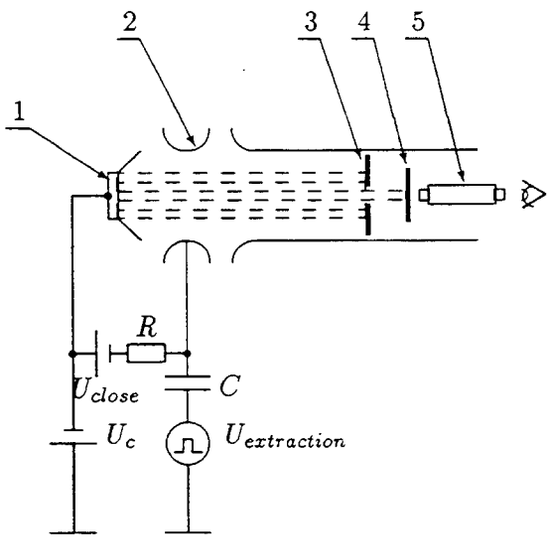

Fig. 1 - The schematics of the optical analyzer (Figure 1 of Ref. [1]). 1) the gun cathode, 2) the steering electrode, 3) the cutting diaphragm, 4) the luminescent screen, 5) the microscope.

2.2 Gérard Tranquille

The initial transverse emittances of 45π mm·mrad were cooled to about 4-6π mm·mrad within 30-60 s [2]. The possibility of controlling the beam current opens new options for electron cooling at ultra-low energies and is useful for optimisation of the cooling system. The measured H° profiles from the recombination of protons and electrons have been recorded by a CCD camera, viewing a screen at the end of the straight beam-line section containing the electron cooler.

2.3 Jacques Bosser

A relative flight-time measurement for the electron beam through the cooling section was carried out [3] by means of a vector network analyzer (Fig. 2) with a short-term stability and time resolution of about 1 ps.

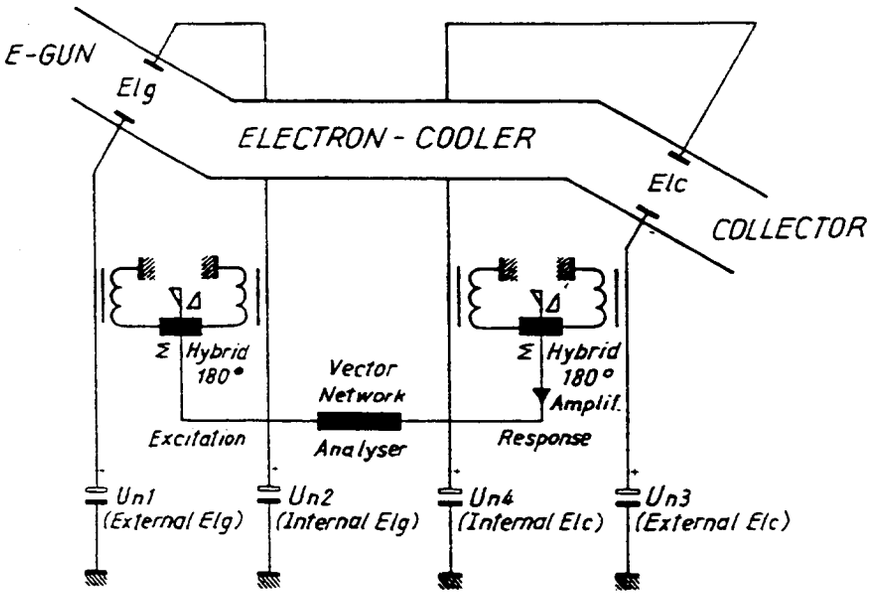

Fig. 2 - Principle of the flight-method time (Figure 2 of Ref. [3])

Space-charge variations as a function of time due to neutralization of positive, ions are clearly visible. Neutralization levels of 60% have been obtained. As an independent tool to measure the neutralization, momentum changes in the proton beam were observed. A servo-system (Fig. 3) to stabilise the proton-beam momentum during electron-beam current changes and neutralization fluctuations, has been tested successfully. The system shows a response time of about 2 s.

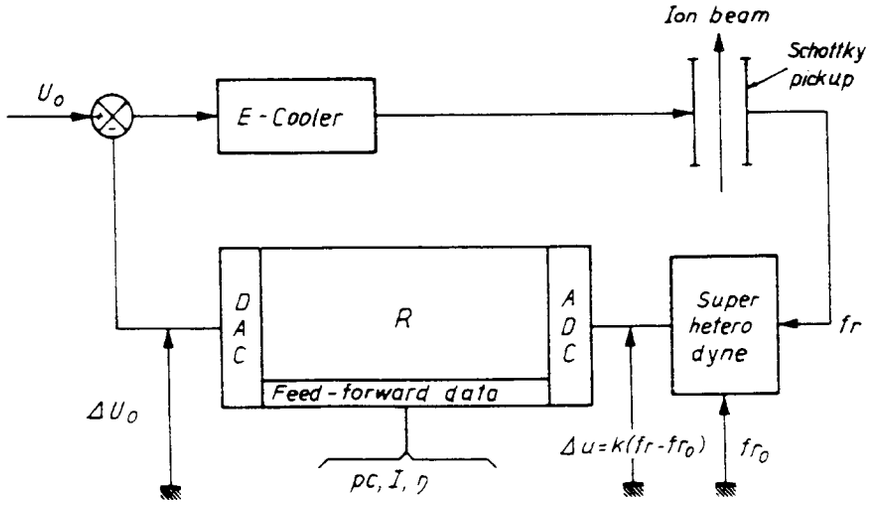

Fig. 3 - Principle of the servo-system (Figure 4 of Ref. [3])

2.4 Dag Reistad

The CELSIUS electron cooler [4] is used to reduce the momentum spread and transverse emittances of protons and deuterium ions. A comparison of measured data from CELSIUS, with electron coolers in several other laboratories, shows similar results. However, very short lifetimes have been observed for injected 25 mA proton beams with high-emittance values. With an initial lifetime of 0.5 s most of the beam has been lost very quickly. A thorough study of this phenomenon did not lead to a complete understanding of all mechanisms involved. One hypothesis is electron heating due to higher order resonances driven by non-linear electric fields from the electron beam; as an alternative theory electron heating linked with coherent effects is under discussion. Over a current range from 4 to 25 mA no large differences in lifetime have been observed. For the future, new solenoids on the electrons gun and collector are foreseen, allowing the adjustment of a variable diameter electron beam.

2.5 Dietrich Habs

One important design feature of this contribution [5] is the electron gun (Fig. 4) to be immersed in a high-magnetic field of a superconducting solenoid. An adiabatic transition to the lower magnetic field in the drift region and adiabatic expansion of the electron beam permits the maintenance of low-transverse temperatures in the order of 1 to 10 meV. Transverse momentum can be converted into longitudinal momentum in a diverging magnetic field. For the optimum design of this configuration four adiabatic invariants have to be taken into account. Adiabatic expansion has been practised in order to measure transverse electron-beam temperatures.

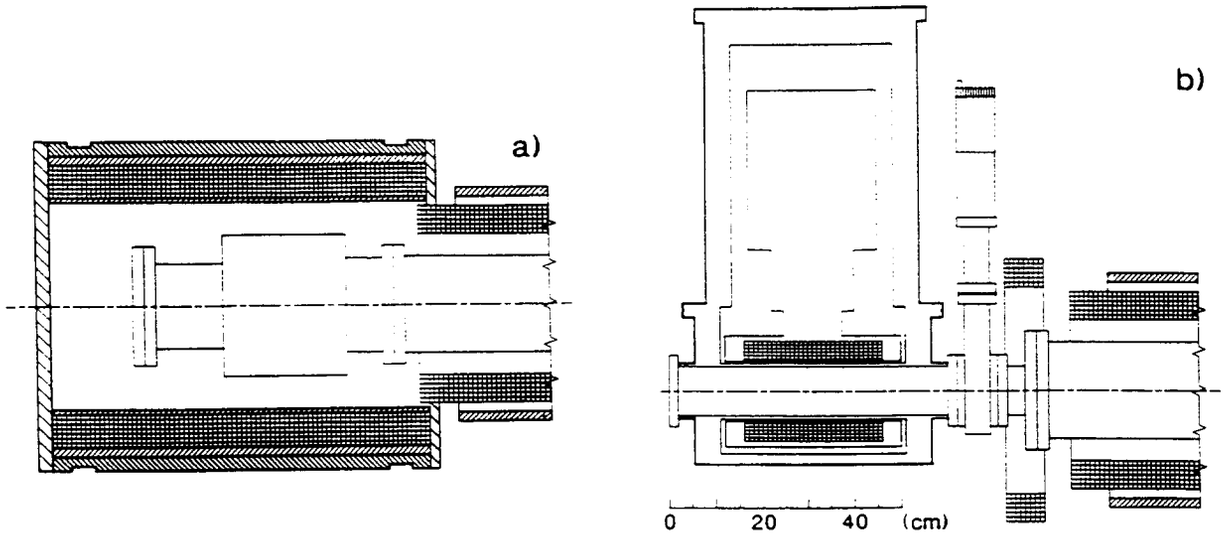

Fig. 4 - a) Present gun solenoid of the TSF cooler. b) New technical design with superconducting magnet and old solenoid. The electron gun is separated by a valve from the rest of the cooler (Figure 1 of Ref. [5]).

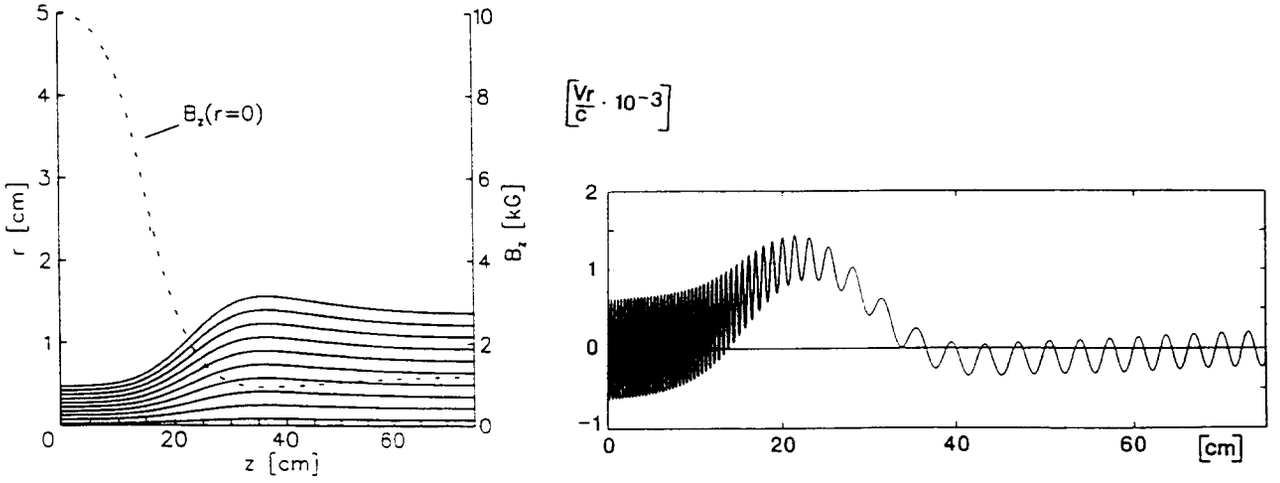

Fig. 5 - a) Longitudinal B-field distribution on the axis and typical electron trajectories. b) Radial velocity for an electron ray starting 1 mm of axis with an energy of 30 keV (Fig. 3 of Ref. [5].

2.6 Sebastian Zwickler

GaAs photocathode [6] activated by cesium and NF_3 layers exhibits negative electron affinity. However, the lifetime of this cathode for high (~0.1 mA/cm^2) current density levels may still be improved. Measurements are presented on the longitudinal and transverse momentum spread for different current densities and various longitudinal magnetic fields, respectively. The accuracy of the transverse energy amounts to 3 meV independently of space charge and relaxation effects.

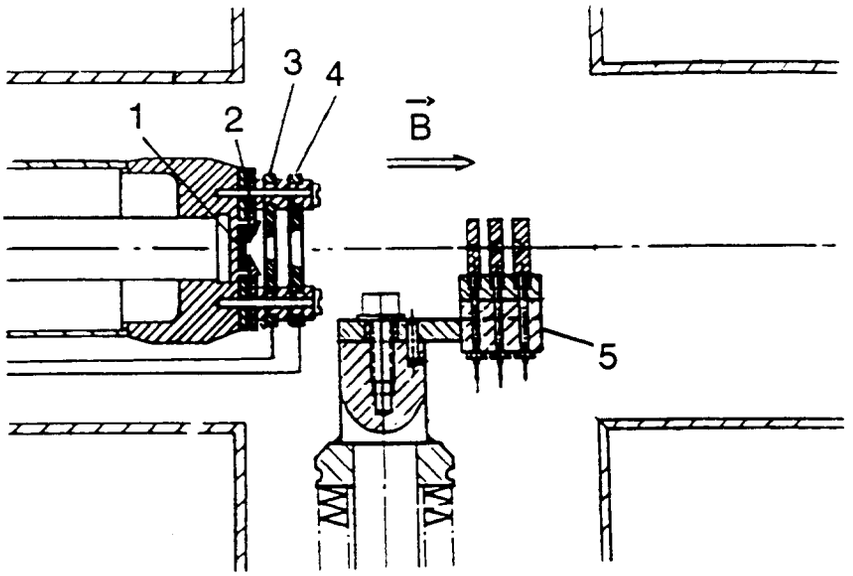

Fig. 6 - Experimental setup with electron gun and retarding field energy analyzer (Figure 1 of Ref. [6])

2.7 Bernd Hochadel

The studies of intrabeam scattering at TSR [7] showed results in good agreement with data obtained from IBS computer code simulations, assuming strong coupling between transverse degrees of freedom. Evidence of linear ordered structures has been observed on laser-cooled Be-ion beams (7.29 MeV $^9Be^+$). After initial electron-beam cooling subsequent laser cooling leads to further and very fast decrease of emittance. According to predictions for $N < 2 \times 10^6$ particles, a strong suppression of IBS, linked with the appearance of linear ordered structures should occur.

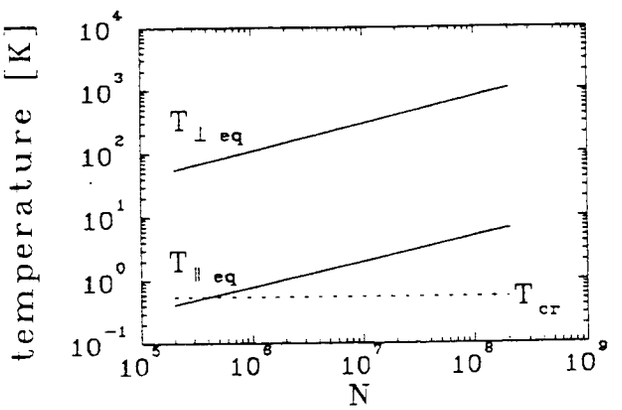

Fig. 7 - Dependence of the equilibrium temperatures $T_{\|eq}$ and $T_{\perp eq}$ on the particle number N for a laser cooled $^9Be^+$ beam assuming a cooling constant of $\lambda_{\|} = 3 \times 10^4$. Also shown is the critical temperature T_{cr} discussed in the text (Figure 6 of Ref. [7]).

3. POSTER SESSION

3.1 Alexander Shemyakin

This paper [8] describes an interesting system to reduce current losses on the electron-beam collector, linked to secondary electron emision (SEE) and capture. The influence of electrostatic and magnetic "mirrors" on the collector SEE coefficient has been investigated both experimentally and theoretically. The experiments indicate good agreement with the theoretical model proposed.

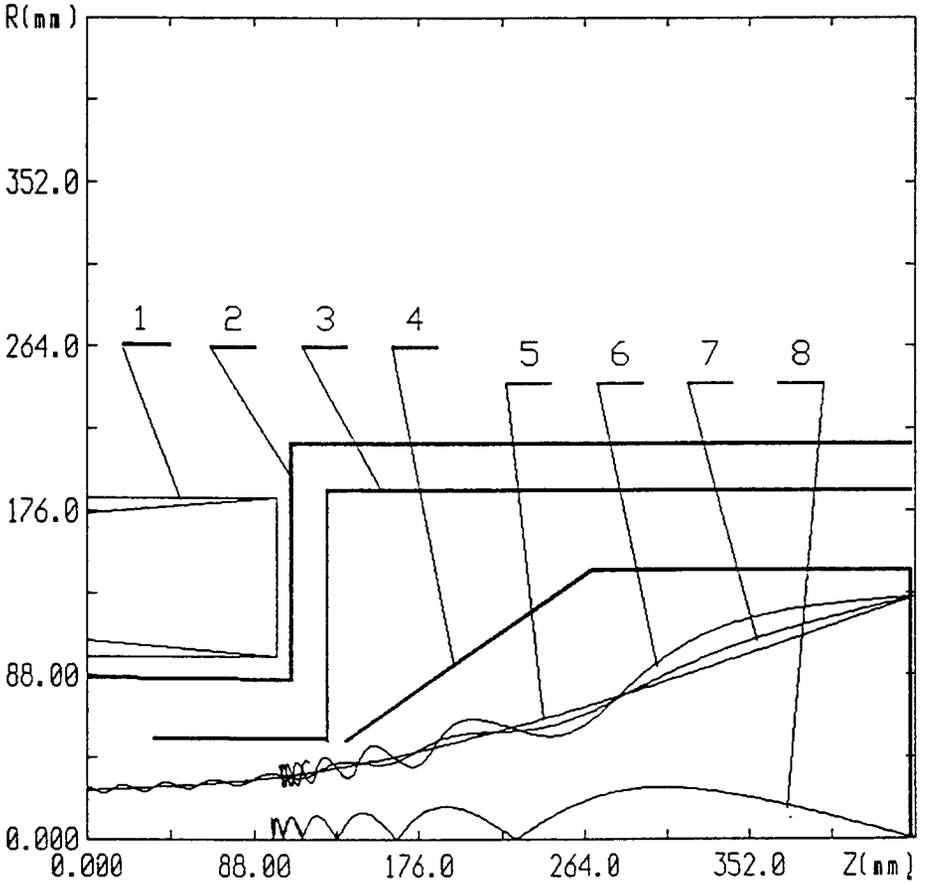

Figure 8 - Drawing of the recuperator being tested. 1) Solenoid; 2) Vacuum chamber; 3) Suppressor; 4) Collector: Trajectories 5-8 illustrate the movement of the particles inside the collector for a case of an equipotential space, computer simulations for H_0 = 0.06 T, U_{col} = 3kV; 5) Boundary trajectory of the primary beam, 6) and 8) Trajectories of the secondary electron with $\vartheta > \vartheta_c$; 7) The same for $\vartheta > \vartheta_c$ (Figure 1 from Ref. [8]).

3.2 Anatoly Sharapa

It is shown [9] that the most effective solution for configuration of the collector electrodes is similar to a Pierce electron gun. Then along the beam the minimum potential exists but the conditions for trapping ions will not be met.

3.3 Vincenzo Guidi (represented by Bin Yang)

Lifetimes of GaAs cathodes of about a hundred hours with currents close to 1 mA have been demonstrated [10].

3.4 Michel Chanel

Longitudinal and transverse BTF measurements on dense cooled proton and $\bar{p}$ beams have been carried out [11]. The results are discussed and permit an analysis of stability conditions, momentum distribution and impedance of the transverse feedback systems. To improve the effectiveness of this system (damper), the transverse stochastic cooling has also been operated with reduced gain like a damper. The influence of both systems on the beam was studied.

4. CONCLUSIONS

The fast development of beam cooling techniques over the last 20 years was clearly demonstrated at this Workshop on "Beam Cooling and Related Topics". The first electron-beam cooler NAP-M became operational in October 1973. It is interesting to display the improvements obtained on different cooling parameters.

	NAP-M (1974)	Ratio	Now (1993)
Electron energy	30 keV	0.07 - 10	2 keV (LEAR) 300 keV (CELSIUS)
Cooling time	3 s	1/30 1/300 2/30000	$\tau_{\perp}$ = 0.1 s (TSR) $\tau_{\parallel}$ = 0.01 s (TSR) τ_{Laser} = 20 ms (TSR)
Ion current	0.02 mA	1200	25 mA (CELSIUS)
Electron beam perveance	1 $\mu A/V^{3/2}$		5 $\mu A/V^{3/2}$ (LEAR)
Initial ion beam emittance	10π mm·mrad		100π mm·mrad (LEAR)
Cooling temperature	2000 K		1/20 = 100 K = $T_{\perp}$ $1/(2\times10^4)$ = 0.1 K = $T_{\parallel}$ $1/(2\times10^5)$ = 0.01 K = $T_{\parallel Laser}$

It is clearly seen that most parameters have improved by a few orders of magnitude.
Problems for future developments not solved up to now:

1. The secondary ions and electrons linked to high-intensity beams, for example at LEAR. The system of electron cooler can trap secondary electrons which oscillate from gun to collector or inside a specific electrode with maximum potential. These electrons can produce uncontrolled fluctuation of space charge.
2. The problem of "electron heating" and beam intensity losses due to non-linear resonances and coherent instabilities as seen at the CELSIUS experiment.
3. The cooling near gamma transition.
4. The combination of electron cooling and subsequent laser cooling methods. Ordering effects for extremely cooled ion beams. For example, crystallisation may be soon an experiment.

REFERENCES

[1] V. Gobulev, I. Meshkov, V. Polyakov, I. Seleznev, A. Smirnov, E. Syresin, *The Optical Analysis of the Electron-Beam Temperature. The Measurement of Transversal and Longitudinal Velocities of an Electron Beam*, this Workshop Proceedings, 1993.

[2] J. Bosser, R. Lapik, R. Ley, I. Meshkov, V. Polyakov, I. Seleznev, A. Smirnov, E. Syresin, G. Tranquille, and A. Zapunjako, *The First Results of Electron Cooling at LEAR with the Variable Current Electron Gun*, this Workshop Proceedings, 1993.

[3] J. Bosser, F. Caspers, M. Chanel, R. Ley, S. Maury, R. Maccaferri, I. Meshkov, G. Molinari, U. Ramos Sanchez, E. Syresin, G. Tranquille, and F. Varenne, *Neutralisation and Beam-Transfer Function of a Dense Electron Beam. A Servo-System on the LEAR Electron Cooler*, this Workshop Proceedings, 1993.

[4] L. Hermansson, T. Bergmark, O. Johansson, D. Reistad, A. Simonsson, *Measurements of Electron Cooling and "Electron Heating" at CELSIUS*, this Workshop Proceedings, 1993.

[5] D. Habs, S. Pastuszka, D. Schwalm, A. Wolf, and S. Zwickler, A *Cold Electron Beam for Cooling and Collision Experiments by Adiabatic Transverse Expansion in a Magnetic Field*, this Workshop Proceedings, 1993.

[6] D. Habs, P. Krause, S. Pastuszka, D. Schwalm, A.S. Terekhov, A. Wolf, and S. Zwickler, *Energy Analysis of Electrons Emitted by a Semiconductor Photocathode*, this Workshop Proceedings, 1993.

[7] F. Albrecht, G. Bisoffi, M. Grieser, D. Habs, B. Hochadel, D. Schwalm, and A. Wolf, *Studies of Intrabeam Scattering (IBS) at the TSR*, this Workshop Proceedings, 1993.

[8] A.N. Sharapa and A.V. Shemyakin, *Current Losses in Systems with the Electron Beam Energy Recovery in a Longitudinal Magnetic Field*, this Workshop Proceedings, 1993.

[9] A.N. Sharapa, *Formation of the Potential Minimum in the Intense Electron Beam Recuperator*, this Workshop Proceedings, 1993.

[10] R. Calabrese, G. Ciullo, V. Guidi, G. Lamanna, P. Lenisa, B. Maciga, L. Tecchio, and B. Yang, *Study on Photosource for Electron Cooling Devices*, this Workshop Proceedings, 1993.

[11] M. Chanel and U. Oeftiger, *Results from Beam Transfer Function Measurements at the Low-Energy Antiproton Ring (LEAR)*, this Workshop Proceedings, 1993.

SUMMARY TALK ON LASER COOLING

Ove Poulsen[1]
Mikroelektronik Centret, DTH, Blgd. 345e, 2800 Lyngby, Denmark

ABSTRACT
Beam cooling methods like stochastic- and electron cooling play an increasingly important role in the utilization of stored beams for molecular, atomic and nuclear physics. Whether it be excited nuclei or rotationally cold molecules, a succesful control of the phase space of the particles often directly influences the outcome of a given experiment. A third cooling scheme, laser cooling, has been developed extensively in the atomic physics community. Compared with the two beam cooling methods, laser cooling is **not** universal. Laser cooling requires an electronic transition for optical excitation, thus limiting the method to cooling of only a few selected elements. This restriction is amply compensated for by the strong cooling force, its excellent velocity control, and the ultra low cooling limits. Laser cooling must therefore be viewed as a test methods for studying the dynamics of stored beams in its extreme limits, the ultimate limit of beam cooling, an ordered "crystalline" array of particles, being the final goal.

1. INTRODUCTION

Today lasers are routinely used for manipulation and cooling of free atoms and ions. In high precision spectroscopy the detrimental Doppler effect can be eliminated to first order only by applying non-linear spectroscopic methods. The ultimative resolution limits will eventually be given by the second-order Doppler broadening. This observation led to the development of laser cooling of both atoms [1] and trapped ions [2]. This field has experienced an explosive development. New cooling principles have been introduced, and temperatures have dropped steadily. Doppler cooling is still the workhorse as a precooler, allowing temperatures in the mK-range. Temperatures in the μK-range are obtained by newer cooling methods like polarization gradient cooling and velocity-selective coherent population trapping [3].

New phenomena occur at these low temperatures. Optically induced potentials become larger than the kinetic energy of the particles, resulting in trapping of "free" atoms in optical potentials. One and two-dimensional atom lattices have been created [4] and solid state properties of these cold "solids" have been studied by non-linear spectroscopy [5]. By optical potential engineering, slow atoms can be deflected, focused and velocity dispersed. The traditional role between matter and light is thus reversed in this new field known as atom optics[6].

A similar rapid development has been realized in the field of laser cooling of trapped ions. The plasma physics properties of ultra-cold ions have been studied [7] and the ultimate state of the field-matter interaction, that of a single ion cooled to the vibrational ground state of the external electrostatic trapping potential, has been observed [8]. Of special interest to the storage ring community is the observation of shell structures in magnetically confined strongly coupled plasmas [9].

It is in the perspective of this rapid development that laser cooling of stored ions must be summarized.

LASER COOLING OF FAST AND STORED BEAMS

The possibilities of laser cooling stored fast beams was recognized early and discussed briefly from a spectroscopy point of view [10]. The fast beam laser cooling scenario was subsequently analysed theoretically [11], followed by an experimental demonstration of laser induced acceleration of a fast beam in a single-pass experiment, using a traditional low energy accelerator [12].

---

[1]associated with **ACAP**, Aarhus University, 8000 Aarhus C, Denmark

The advent of storage rings drastically changed the perspectives of laser cooling fast ion beams. In addition, the field was dramatically accelerated by the discussions on the ultimate cooling limits or ordered "crystalline" beams [13,14].

Laser cooling of stored ions are pursued at only two laboratories, the Max planck Institute für Kernphysik at Heidelberg (the TSR storage ring) and at the ASTRID storage ring at Aarhus University. Shortly after the completion of these facilities, laser cooling was succesfully demonstrated, first by the TSR-group [15], who laser cooled a 13 MeV Li^+-beam and shortly thereafter by the ASTRID-team, who laser cooled a 100 keV Li^+ beam [16]. Temperatures in the range 1 mK - 1 K were experimentally observed, the temperature strongly depending on the density of the stored beams.

This summary will focus on the progress achieved since these initial experiments were performed. At this Workshop four areas of importance to further progress in the field were presented. Development of new cooling methods for obtaining a stronger cooling forces, development of new lasers for efficient cooling of new ions, laser cooling in a rf-bucket and new tantalizing evidence for a laser cooled low dimensional structure.

LASER COOLING BASED ON ADIABATIC OPTICAL EXCITATION

"Conventional" laser cooling is limited in several ways. The laser force is limited by the spontaneous emission rate γ as $F < \hbar k\gamma$, where k is the wavenumber of the photon. Another limiting factor in laser cooling is the small capture range $\Delta v_c \approx (\sqrt{I/I_{sat}})\,\gamma$, leading to intra-beam scattering (IBS) scattering losses. During the Workshop these points were made by Rudi Grimm, who then described a new method for laser cooling of stored beams. The aggressive environment found in storage rings necessitates a continuing development of novel laser cooling schemes and, in particular, to avoid the problem of a small spontaneous emission rate. Rudi Grimm discussed laser cooling based on adiabatic optical excitation in the dressed atom picture using the Landau-Zener picture to calculate the transition probability in frequency chirped fields. The fast beam environment is particularly suited for such excitation schemes due to the precise time and spatial control of the stored ions.

In a normal cw excitation of an atomic system, the rate of stimulated processes equals the rate of absorptive processes when 50% of the upper level is populated. By applying frequency chirped fields the Landau-Zener picture in an avoided crossing scenario allows a full inversion of the population of a quantum system. This well known effect has been applied to the TSR-ring at Heidelberg. Experimentally, more than 80% of the initial state of a 13 MeV Li^+ beam was transferred to the excited state utilizing a custom tailored electrostatic potential for optimizing the adiabatic excitation probability.

This cooling scheme has several attractive features. The cooling force has a range substantially larger than "normal" Doppler cooling and the process can be repeated several times in a straight section. Rudi Grimm discussed a multi-electrode geometry, with longitudinal dimensions tailored to the spontaneous decay of the stored ion. The problems of IBS losses will be greatly reduced with this new cooling scheme and the transverse sympathetic cooling will be more efficient due to the size and the range of the force.

NEW LASERS AND COOLING OF MAGNESIUM IONS

A different way of obtaining stronger cooling is by a careful selection of ions with a fast spontaneous scattering rate. One of the best ions for laser cooling is magnesium. This ion was, so far, avoided due to the difficult excitation wavelenght of 280 nm. Jørgen Nielsen presented a solution to this problem: a highly effective external cavity second-harmonic generation unit, capable of generating up to 100 mW of radiation at 280 nm. This has been possible by two recent developments, a new super effective dye at 560 nm and the construction of external ring cavities, fully coma and astigmatic compensated and electronically servo-locked.

With this laser system Jørgen Nielsen laser cooled Mg^+ with only one frequency chirped laser. Injecting 10^8 ion in ASTRID, he reported temperatures around 1 K, while higher temperatures were observed at higher densities. He demonstrated a good cooling efficiency, with only a modest loss of ions during the laser cooling process. In addition to cooling experiments, Jørgen Nielsen described heating studies, using laser induced fluorescence as a tool for measuring the longitudinal temperature as function of storage time and of density of the ions. Such data are of importance in understanding the dynamics of cold stored ionbeams. A result of these studies, revealing a strong, probably coherently driven, initial heating, points towards the low intensity regime as the best starting point for obtaining a condensed beam.

One of the most difficult aspects of laser cooling of stored ion beams is the transverse degree of freedom. Laser cooling is only effective at cooling the longitudinal degree of freedom in a fast beam. IBS is one mechanism coupling the transverse (hot) and longitudinal (cold) movement of the ions. The picture is by no

means simple due to betatron oscillations and loss mechanisms. Jørgen Nielsen presented data, indicating a transverse sympathetic cooling. Transverse temperatures were measured as a function of injection (cooling) time using a scraper to determine the transverse size of the beam. A 15% effect was reported, but conclusive evidence for sympathetic transverse cooling is still pending in the ASTRID experiment.

LASER COOLING IN A RF-BUCKET

Laser cooling experiments in storage rings are traditionally performed on coasting beams. This corresponds to a two dimensional confinement of the ions. They are bound by the quadrupole fields in the x-y plane, while they are freely propagating in the z-direction. Laser cooling of fast stored ions therefore requires two opposing forces in order to achieve stable cooling around a fixed velocity. The first experiments, at the TSR-ring [15] and at ASTRID [16], were performed using two counterpropagating lasers. Adding two counterpropagating laser fields, a resulting dispersion-like cooling force results due to the directionality of the photon recoil and the different Doppler shifts.

In later experiments the TRS-group introduced a new element, an induction accelerator (INDAC). The circulating ions constitute the secondary loop in a transformer. Applying a time varying flux at the primary loop, the beam energy is conviniently tuned. The INDAC provides a convinient holding force, which together with an opposing laser cooling force, provides a stable cooling point. The electron cooling force has been employed in a similar scheme, again by the TSR-group.

At the Workshop Jeffrey Hangst of the ASTRID team reported experiments on laser cooling in a rf-bucket. This experiment is conceptually different from the previously reported laser cooling experiments at storage rings, because of the 3-dimensional confinement of the ions in the bucket. The experiment effectively turns a storage ring into a trapping facility. ASTRID is equipped with a tunable rf-gap for accelerating the ions. This rf-device was excited by only a few volts of rf-pover, tuned for the 26^{th} harmonic of the revolution frequency. A single laser was applied in another arm of the ring. Jeffrey Hangst showed a simulation of the particles "trapped" in the rf-potential, subjected to a laser cooling force. Both cooling and localization was simulated. This simulation was confirmed by experiments, showing effective laser cooling of a 100 keV Mg^+ beam in rf-potentials as low as 5 V. Jeffrey Hangst showed cooling results with a scanned laser and 10^9 particles injected. The velocity distribution of the ions was measured as function of storage time, showing warm ions trapped in the rf-bucket effectively being cooled as function of cooling time. The experiment, however, was limited by the bandwidth of the Schottky reciever. Beam pick-up signals showed distinct narrowing of the bunches due to laser cooling.

TRANSVERSE COOLING AND (NEW) LOW DIMENSIONAL STRUCTURES

Dieter Habs of the TSR-team gave an inspiring contribution on some of the outstanding challenges of laser cooling of fast stored ions, that of transverse cooling of the final low temperature state of a cold beam.

By careful measurements of the diffusion coefficients, obtained by heating curves and by measurements of the longitudinal laser cooling force, temperatures in the low mK-range are derived for a Be^+ beam of 8×10^8 particles. This temperature was found to be in agreement with a direct temperature measurement by laser induced fluorescence. Based on this good understanding of the longitudinal degree of freedom, Dieter Habs proceeded by showing evidence for transverse (sympathetic) cooling. Without laser cooling a transverse temperature of 6000 K was found, whereas longitudinal laser cooling resulted in a transverse temperature of only 3800 K. This reduction of temperature corresponds to a reduction of the radius of the stored beam of 15%.

The most fascinating aspect of the laser cooling section of the Workshop was the discussion on the final low temperature state of a stored beam. Dieter Habs presented results, which clearly point towards new and puzzling horisons. Using the full power of the INDAC and the laser cooling force, the Heidelberg-group measured longitudinal temperatures as a function of the density of the beam. By changing the laser cooling force and thus the capture range of the force, a naive consideration would predict more ions cooled. Quite the opposite, the TSR-team reported a constant number of particles cooled above a certain laser cooling force. Dieter Habs discussed the possible scenarios implied by this observation, the most intriging being the creation of a string of ions embedded in a halo of warm ions. To verify this scenario, careful transverse temperature measurements must be carried out and better beam diagnostics employed.

Another way of studying such phenomena is by numerical simulations of cold beams. Dieter Habs showed IBS studies of laser cooled beryllium beams. Assuming temperature equilibrium, sympathetic transverse cooling was investigated, as was longitudinal cooling. Careful loss measurements supported aspects of these simulations.

OUTLOOK AND CONCLUSIONS

During the workshop "laser coolers" and "beam crystallizers" met to discuss the present state-of-affairs. One question concerned the optimum strategy for obtaining a 3-dimensional cold beam. The ASTRID-team has started with a dense and very cold beam. Strong coherent and IBS heating is observed resulting in a low density, longitudinal very cold beam, as a result of laser cooling. The TSR-team traditionally has worked with less dense beams, resulting in a week initial coupling between the longitudinal and transverse degrees of freedom. They have overcome this problem by electron pre-cooling.

During the discussions at the Workshop it was agreed, that an optimum strategy must avoid too dense beams, as the dynamics of these strongly coupled and coherently excited beams was not understood. To succesfully use a low density beam as the starting point for obtaining a low dimensional coupled state requires development of "seeding" schemes. The use of rf or laser stacking to slowly add particles to a cold system is an intriguing possibility.

Finally, the "laser coolers" need better diagnostics. Longitudinal and transverse Schottky pick-ups are urgently needed in order to study the plasmas allready produced. With lower temperatures and higher densities of the beams, the need for new advanced (low noise, high bandwidth) pick-ups is high. An alternative scheme, based on the correlation between neutralized particles escaping the ring, is another interesting possibility for detecting a possible ordering of the beam.

Based on the presentations at the Workshop, new and dramatic progress is expected. New cooling schemes, new lasers, cooling in rf-buckets and new tantalizing evidence from the beryllium experiments at the TSR-ring all clearly point towards a rapid development towards crystalline beams.

REFERENCES

[1] T.W.Hänsch and A.L.Schawlow, Opt. Commun., **13**, 68 (1976)

[2] D.J.Wineland and H.Dehmelt, Bull. Am. Phys. Soc., **20**, 637 (1975)

[3] See special feature *Laser Cooling and Trapping of Atoms*, eds. S.Chu and C. Weiman, in J. Opt. Soc. Am., **B6**, 2109-2278 (1990)

[4] P. Jessen, C. Gerz, P. Lett, W. Phillips, S. Rolston, R. Spreeuw and C. Westbrook, Phys. Rev. Lett.,**69**, 49 (1992) and A. Hemmerich and T.W. Hänsch, ibid, **70**, 410 (1993)

[5] P. Verkerk, B. Lounis, C. Salomon, C. Cohen-Tannoudji, J. Courtois and G. Grynberg, Phys. Rev. Lett.,**68**, 3864 (1992)

[6] See special feature *Atom Optics and Interferometry*, eds. J. Mlynek, V. Balykin and P. Meystre, in Appl. Phys., **B54**, 321-477 (1992)

[7] L.R.Brewer, J.D.Prestage, J.J.Bollinger, W.M.Itano, D.J.Larson and D.J.Wineland, Phys.Rev.A,**38**,859-873 (1988)

[8] J.C. Bergquist, W.M.Itano and D.J. Wineland, Phys. Rev. A, **36**, 428-430 (1987)

[9] S.L. Gilbert, J.J. Bollinger and D.J. Wineland, Phys.Rev.Lett., **60**, 2022-25 (1988)

[10] Laser Cooling of Fast Accelerated Ion Beams, M. Kaivola, U. Nielsen and O. Poulsen, Proc. of CELCIUS Workshop, Uppsala (1983)

[11] Juha Javanainen, Matti Kaivola, Ulrik Nielsen and Erling Riis, J.Opt.Soc.Am.B2,1768(1985)

[12] Erling Riis, Lars-Ulrik Aaen Andersen, Ove Poulsen, Harald Simonsen and Torben Worm, Phys.Rev.A37,2958(1988)

[13] A. Rahman and J.P. Schiffer, Phys.Rev.Lett., **57**, 1133 (1986)

[14] J.P. Schiffer and O. Poulsen, Europhys. Lett., **1**, 55 (1986)

[15] S. Schröder *et al.*, Phys.Rev.Lett., **64**, 2901 (1990)

[16] J.S.Hangst, M.Kristensen, J.S.Nielsen, O.Poulsen, J.P.Schiffer and P.Shi, Phys.Rev.Lett., **67**, 1238 (1991)

SUMMARY TALK ON BEAM CRYSTALLIZATION

J. P. Schiffer
Argonne National Laboratory, Argonne, IL 60439 U.S.A.

The logical ultimate limit of beam cooling leads to an ordered "crystalline" array of particles. It should occur when the thermal energy (not counting collective oscillations) becomes much less than the Coulomb energy stored between two neighboring particles in the beam:

$$kT_{incoh.} << q^2/a$$

where "a" is a parameter reflecting the interparticle spacing. As cooling techniques improve this limit is gradually coming within grasp. In fact, some think that it perhaps had already been reached in Novosibirsk [1] over a decade ago, but the evidence on this is not clear.

In this summary I would like to give a brief primer on what has been done in this area, indications from simulations of what one might expect in such a crystalline beam, and where some of the problems may be. I would like to fold in the contributions we heard and saw at this Workshop, give an assessment of where we now are, and of what the future may hold.

The idea and first simulations of a crystalline beam occurred around 1986 [2], and were then developed further and presented at the Wertheim Workshop in 1988 [3]. It was clear that the lowest energy configuration of particles, traveling in a focusing field that was cylindrically symmetric and constant in time, would be as is shown schematically in Fig. 1. The configuration depends on the linear density of particles. But since several small storage rings are similar in their size and focusing properties, we may here refer to these densities in terms of the approximate total number of particles N for a typical small storage ring. For $N < 10^6$ stored ions, the particles, when absolutely cold, would settle in a string. Then, as the density of particles increases so that the interparticle Coulomb forces became stronger than the focusing force, the particles would undergo dimensional phase transitions, first breaking out of a line into a two-dimensional zig-zag pattern around $N = 10^6$, then into various three-dimensional helical configurations on cylindrical surfaces above about $N \approx 2x10^6$, and for $N > 10^7$ into several concentric shells. For the larger N values these shells are equally spaced, with the surface density of particles on each shell the same, and thus the number of shells proportional to $\sqrt{N}$.

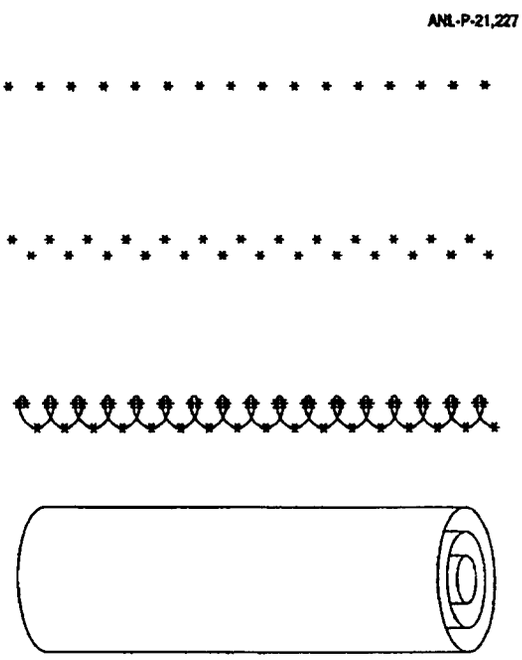

Fig. 1 Schematic representation of particles in a cold beam at various particle densities. The top view corresponds to one-dimensional order expected for $N < 10^6$, the next to a two-dimensional zig-zag, then to a helix, and at the bottom to multiple shells.

But one has to deal with reality, both in the focusing method, and in considering the curvature inherent in a storage ring. What can one say about the best focusing scheme for a crystalline beam? One can obtain constant focusing in a weak-focusing betatron -- could this be the right method? At Wertheim some thought that this was a solution, most others thought otherwise, but at the present Workshop Ruggiero [4] has shown rigorously that weak focusing cannot work, strong focusing is absolutely needed for this ordered regime.

Can this ordering survive an alternating focusing field? At Wertheim, some simulations were discussed [3] that indicated that with the alternating field and with only longitudinal cooling, the early simulations assumed ideal cooling in both transverse and longitudinal directions. These simulations indicated that the beam did seem to remain in a multiple shell structure, very similar to the static case, but undergoing small shape oscillations. At the present Workshop Wei, Sessler and Li [5] presented

simulations that included explicitly repeating FODO cells and bending, as well as vacuum chamber image charges that had not been considered in the earlier work. They also assumed cooling to constant angular velocity. Their systems for $N \lesssim 10^7$ undergo simple oscillations and settle into a mode that requires no further cooling. Results were also shown [6] for larger ($N \approx 10^8$) systems that indicate no problems with alternating focusing, even if the longitudinal cooling is applied only once per orbit.

Next is the question of curvature. Since present beam cooling techniques force particles to travel with the same *linear* velocity, this introduces a problem when the particles are forced into a curved orbit with dipole elements. An ideal case was presented in the poster by Labrador, et al. [7] for a two-dimensional zig-zag pattern that was bent just the right amount for particles on the two strips of the zig-zag to move over by one spacing. This is a very special case. One would like to see a scheme in which the particles are "cooled" into a mode where they all travel with the same *angular* velocity, as was assumed in the contribution by Wei, et al. [5]. Note that this would imply a large coherent momentum spread across the beam, which could be as much as $\Delta p/p = 10^{-4}$. Also, if the bending is not continuous, (continuous bending was assumed in Ref. 5) even a constant angular velocity beam would be subject to a longitudinal shear oscillation that may disrupt the order, particularly if individual elements bend by angles $\gtrsim 60°$.

For normal cooling to constant linear velocity, one may still wonder whether the interparticle forces within an ordered beam might be sufficient to resist shear. Simulations shown at Wertheim indicated that, not surprisingly, the amount of shear a given density of particles could resist depended on the ratio of the focusing force to the curvature of the storage ring, which is just the betatron tune. For the small storage rings, with betatron tunes around 2.5, only the lowest density ordered beams would survive the shear: the one-dimensional string, which of course is not subject to shear, the zig-zag pattern and perhaps some of the simplest helical systems. The larger multi-shell systems would be too fragile and be disrupted by shear. Storage rings with large radii and large betatron tunes could sustain the more complex patterns of larger particle density because the shear would be smaller. The number of particles that can sustain bending should increase roughly as the 4th power of the betatron tune [6].

We need more realistic simulations however, that combine the periodic focusing with periodic bending, in order to better understand the limits at which cooling to fixed linear velocity might produce structures that can survive bending with conventional cooling schemes.

Where do we stand with results? At the time of Wertheim the only data in existence was the original Novosibirsk measurement. Since that time considerable progress has been made at a number of facilities, and at this Workshop very low temperatures have been reported both at the TSR and the ASTRID rings. We heard of the measurements at the TSR in Heidelberg from Habs [8], and they suggest that some sort of a limit may be approached at around 2×10^6 particles -- which is tantalizingly close to the limit to shear estimated earlier [3,6]: a one- or two-dimensional beam. It will be interesting to hear whether slight modifications in the tune of the ring modify this limiting number. Hangst [9] reported on measurements at Aarhus in ASTRID where low longitudinal temperatures, in much more dense beams of ~ 10^9 particles, show instabilities -- which conceivably could also be related to such problems.

Perhaps in these rings it would be best to focus on the low densities, $N < 10^7$ particles, as an initial goal. But at these low densities it is important to understand how long it takes to equilibrate longitudinal cooling with the perpendicular temperatures $T_\perp$. This may be a difficult issue to treat correctly in simulations [10] and the test against reality is going to happen soon.

Diagnostics are a major issue in this regime. We heard a paper by Avilov and Hofmann [11] on the Schottky spectra to be expected for one-dimensional beams -- but the relatively easy transition between one- and two-dimensional configurations may complicate matters.

We heard about a possible new dedicated facility for crystalline beams from Tecchio: the CRYSTAL storage ring project at Legnaro [12]. This project has the potential of learning from and building on the detailed experiences at the existing small storage rings: the TSR and ASTRID, and thus optimizing their design for a new generation of specialized rings.

What does the future hold for this area? My guess is that within the next two years the evidence for ordering in one- and two-dimensional beams will become firmer at the storage rings with laser cooling. Beyond $N = 10^7$, I would guess that there will have to be some conceptual technical developments that would allow beams to attain constant <u>angular</u> velocity rather than constant <u>linear</u> velocity, before these forms of order may be realized in storage rings. But in the meantime many diagnostic questions need to be assessed. For instance, some thought and ideas are needed on how to separate the transverse beam temperature from coherent oscillations that are inherent to the beam and that do not disrupt order. And the consequences of the issue that was already mentioned, that the momentum spread in a crystalline beam <u>must</u> be quite appreciable -- though coherent, need to be considered.

Finally, one is confronted with the question: "What are crystalline beams good for?" I would like to answer this on three levels.

On the level of "basic science" these systems represent a unique form of condensed matter, that is some 15 orders of magnitude less dense than "normal" forms of matter in the solid state. Some of the features of such matter can also be studied in ion traps. But others are unique to beams. For instance, the one-dimensional Coulomb system

the focusing field was continuously alternating between the horizontal and vertical directions, to approximate the alternating focusing in a real storage ring. For this simulation the system was cooled only in the longitudinal direction, and the longitudinal velocities were scaled down only once every 2.5 betatron period, to simulate the once-per-turn cooling in a storage ring with a betatron tune of 2.5. As is seen, the system does settle into a multi-shell structure very similar to the one obtained in a static field, though it undergoes collective oscillations, both of the radial type (with the frequency of that normal mode) and a shape oscillation (with the driving frequency of the repeating cell of the alternating focusing field). Clearly the "crystallization" is not appreciably inhibited by the alternating focusing [4] though the "crystal" is oscillating in time. The residual oscillations depend on details of the simulation, such as the size of the system and the period of the repeating focusing cell compared to the betatron period.

The next problem has to do with the inevitable curvature of orbits in a storage ring. Since all present cooling techniques force beams to travel with the same *linear* velocity in the longitudinal direction, and since in the condensed state the Coulomb interactions between particles will prevent orbits of adjacent particles from crossing, it follows that horizontally adjacent particles may not complete an orbit in the same time. The appropriate motion for the lowest state would be constant *angular* velocity, instead of constant *linear* velocity. What does this imply for the ordering phenomena discussed above?

In the co-moving frame of particles with constant angular velocity, a cooler that imposes constant linear velocity represents a shearing force, that pushes particles ahead on the inside of the curved orbit, and pushes them backward on the outside. The first question is whether the interlocking lattice has enough rigidity to withstand this shearing effect. Simulations were carried out for various systems in order to determine the force constant resisting a shear displacement in these lattices [4,5]. The test system was subjected to a small shear displacement and then the motion of the particles was followed in time to determine the period of a shear oscillation ω_{shear}. The condition for a given system to withstand the shear is that this frequency be higher than the frequency driving the shear: the cyclotron frequency.

$$\omega_{shear} > \omega_{cyclotron}$$

At the same time we note that, because of the nature of the Coulomb force, all the elastic forces in the condensed structure scale with the focusing force, or the betatron frequency. Thus the relevant parameter must be the ratio of the cyclotron to the betatron frequency, which is the betatron tune ν_β for the ring.

The results of these tests are shown in Fig. 5. Simulations do show a shear oscillation frequency, though it is not a very simple mode, especially for the larger systems. The results indicate that the system is more and more likely to break up from shear as the number of particles is increased. In fact, in the small storage rings with betatron tunes around 2.5, the simplest three dimensional structures can barely survive, and the order may be constrained to one- and two-dimensional systems. Clearly, to attain a three-dimensional structure, one needs to think hard to find schemes that may allow this problem to be circumvented, for instance by cooling particles to a constant angular velocity [4,6]. The problem is much less severe when the radius of the storage ring (and the betatron tune) are large.

Alternatively, one may look at what happens if the system is allowed to shear. Here, if cooling to a linear velocity is imposed continuously (rather than once per turn as was done in the simulations discussed above), the particles eventually settle into a new form of order: a set of strings that are continuously sliding with respect to each other, and the strings themselves arranged in a pattern of equilateral triangles as is shown in Fig. 6. It is not clear whether realistic cooling forces will permit this intriguing form of order to be realized in real storage rings.

This research was supported by the U.S. Department of Energy, Nuclear Physics Division, under Contract W-31-109-Eng-38.

REFERENCES

[1] J. P. Schiffer and P. Kienle, *Z. Phys.* *A 321*, 181 (1985).
[2] A. Rahman and J. P. Schiffer, *Phys. Rev. Letts.* *57*, 1133 (1986).
[3] R. W. Hasse and J. P. Schiffer, *Ann. of Phys.* *203*, 419 (1990).
[4] J. P. Schiffer, *Proc. of Workshop on Crystalline Ion Beams*, Wertheim, FRG, Oct. 4-7, 1988, GSI-89-10 Report, April 1989, ISSN 0171-4546, p. 2.
[5] J. P. Schiffer and A. Rahman, *Z. Phys.* *A331*, 71 (1988).
[6] R. E. Pollock, *Z. Phy.* *A341*, 95 (1991).

REPORT OF THE WORKING SESSION ON HEAVY IONS AND HIGH-ENERGY COOLING

D. Koshkarev
Institute for Theoretical and Experimental Physics (ITEP), Moscow, Russia

J. Bosser
CERN, Geneva, Siwtzerland

ABSTRACT
A report is presented of the Working Session on Heavy Ions and High Energy Cooling.

1. INTRODUCTION

The Working Session on Heavy Ions and High-Energy Cooling met on Wednesday morning, October 6. Presentations were made by Robert Pollock, Tim Ellison, Markus Steck, Michael Seurer, Pierre Lefèvre, Andreas Wolf, and Gurgen Ter-Akopian.

The contributions of this session can be divided into three groups:

a. new projects with electron cooling,
b. new applications of the electron cooling,
c. experimental and theoretical investigations of the electron cooling physics.

2. NEW PROJECTS WITH ELECTRON COOLING

2.1 LHC Project

In this group the possibility is examined of using electron cooling for the storage of more intense heavy ion beams in order to enhance a luminosity.

The one proposed for the LHC scheme is based on the accumulation of Pb^{53+} at 4.2 MeV/n in the cooling ring with a stack of up to 1.2×10^9 ions per bunch. When, with about 500 bunches per LHC ring, the total luminosity is close to the desired 2×10^{27} $cm^{-2}s^{-1}$, asolution based on the performances achieved with an ECR source is the conversion of LEAR into a Low-Energy Accumulator Ring. The beam lifetime limitation in LEAR is carefully estimated taking into account the intra-beam scattering ion recombination with cooling electrons, charge exchange on the residual gas, microwave instability, and space-charge tune shift

2.2 K4-K10 Project TREBLé

The aim of the Dubna project of heavy ion storage rings complex is to provide high precision beams of exotic nuclei with a mass number ≤50 in the energy range from a few MeV to about 200 MeV/μ. The first ring, K4, is intended to accumulate the primary ion beam from the JINR sector focusing cyclotron U400M, to cool this beam and to increase the energy up to 170 MeV/u. After cooling the beam is ejected and used to produce the exotic nuclei which are injected into the second ring. The nuclei with a lifetime ≥1 s can be cooled and accumulated in the ring and their energy can be optimized. For the short-lived nuclei (lifetime <1 s), a target illumination will be preferable immediately after cooling.

At the first stage of the project only one ring (K4) will use the exotic nuclei for injection and cooling. Then the luminosity will be of 2 or 3 orders of magnitude less.

3. NEW APPLICATIONS OF THE ELECTRON COOLING

3.1 New Applications at the IUCF

Some new applications of the electron cooling have been developed in the cooling-ring synchrotron, at the Indiana University Cyclotron Facility (IUCF).

Methods have been developed to use electron cooling to help in beam accumulation, both for stripping injection of unpolarized beams and rf stacking of polarized beams.

Typical cyclotron beam current is about 0.5 μA. The beam normalized emittance is about 1 μm and the momentum spread of about 0.03%. After a few seconds of injection a stored proton current up to 1 μA at 45 MeV can be obtained. Multiplication of an observed rate of 12 mA/min with a best observed lifetime while kicking of 1 hour would give 7 mA. However, the best stored current to-date with this mode is lower by an order of magnitude. There is evidence for a stored current-dependent loss of transfer efficiency with a threshold near 0.4 mA. Longitudinal space-charge effects may play a role by limiting the time contraction. Other physics also cannot be excluded. The present performance of the stacking mode is critically dependent on a good cooling.

IUCF is also studying a new project: the development of the technology for electron cooling in the 2-20 GeV/n energy range.

3.2 The Development of the Technology for Electron Cooling in the 2-20 GeV/n Range

Two principal goals are defined:

1. to determine the feasibility of the electron cooling the 12 GeV/c beams in the SSC Meadl Energy Booster and
2. to develop and demonstrate the necessary technology, based on High-Voltage Pelletron Accelerator, leading to its commercial availability.

Above electron energies of about 500 keV the traditional approach of using a Cockroft-Walton power supply and a magnetically-confined electron beam becomes unpractical. A non-magnetically confined electron beam generated and collected in the terminal of a Pelletron accelerator seems ideally suited for these higher energy systems.

The first goal has been completed. Remains the last main problem-collection δ (δ is the inefficiency) which must be in the range 10^{-5}-10^{-4}. [$\delta = J_{loss}/J_e$)

The following improvements may be useful:

a) Improved diagnostics systems

The previous system did not work for beam currents exceeding 10^{-4}. The present system design might allow measurements of the beam position and profile for currents in the range 10^{-6}+10^{0} A.

b) Improved electron gun

The present gun design will produce a much smaller beam emittance and has true Pierce geometry in the gun region.

c) Improved electron collector

IUCF is building a collector which includes a dipole suppressor which may allow $\delta \cong 10^{-6}$.

d) Ion clearing electrodes

The system pressure will be improved using non-evaporable getter pumps, and ion clearing electrodes will be employed to prevent space-charge neutralization.

The author expects that collection inefficiencies will be in the range 10^{-5}-10^{-4} for the higher energy systems for manageable power dissipation.

4. THE EXPERIMENTAL AND THEORETICAL INVESTIGATIONS OF THE ELECTRON COOLING PHYSICS

Experimental and theoretical investigations on the beam cooling parameters have been made at IUCF. Assuming that the longitudinal coupling impedance is almost completely space-charge dominated, one can find the relative momentum spread of the electron-cooled proton beam and the longitudinal space-charge impedance.

Two independent methods have been used:

- fitting the measured longitudinal bunch shape to the theoretical one found from equilibrium the solution of the Fokker-Planck equation for the electron-cooled case.
- analyzing the frequencies of the dipole and quadrupole longitudinal bunch modes.

The results of both methods coincide with a satisfactory accuracy and show the presence of the significant space-charge forces.

Both methods may be useful, but the first one seems to be not very reliable because of difficulties to measure exactly the tails of the bunch longitudinal density.

The last two papers are devoted to a detailed examination of the physics of electron cooling for heavy ions (up to Au^{79+}).

At GSI, in Darmstadt (Germany), the temperature of heavy ion beams in equilibrium between electron cooling and heating by intra-beam scattering has been measured over a large range of ion and electron beam intensities. A comparison of cooling forces at small relative velocity for ions C^{6+}, Ti^{22+} and Au^{79+} shows a strong increase with the ion charge which, however, favours a proportionality to $Z^{1,5}$ than Z^2. In all experiments by now a $N^{1/3}$-dependence of the momentum spread versus the number (N) of stored particles has been observed.. For the transverse emittance results varied in the range $N^{1/3}$ to $N^{2/3}$ note that the observed lower limit for the detectable beam momentum spread 7×10^{-7} is likely to be caused either by the power supply ripple of the main ring magnets or by the energy instability of the electron gun.

Moreover, the cooling force of the electron beam and the intra-beam scattering rate of the dense ion beam were investigated in separate experiments. Because of lack of adequate diagnostics for the transverse degree of freedom the experiments were concentrated on longitudinal cooling force, cooling rate and longitudinal heating rate. For measurements of the longitudinal cooling force at small relative velocities between electrons and ions the cooled beam was heated by white noise and the cooling force of the electron beam was determined according to

$$F = D \cdot \psi^{-1} \frac{\partial \psi(E)}{\partial E}$$

where D is the diffusion coefficient and ψ the energy-dependent distribution function.

For three ion charges, 6+, 22+ and 79+ increasing of the longitudinal cooling forces can be described by a proportionality $\cong Z^{1,5}$. Note that this law can be determined without knowing the absolute value of the diffusion coefficient D, and that the same charge dependence of the electron cooling force was measured at the TSR ring in Heidelberg for D^+, Li^{3+}, C^{6+}, O^{8+} and S^{16+} ions.

5. CONCLUSIONS

1. The new heavy ion projects (CERN, Dubna) show that it is practically impossible to obtain the designed high luminosity without electron cooling.
2. The technology of electron cooling of high energy ions has been developed. It will open new feasibility in very high-energy project.
3. As a result of new experimental investigations (GSI, Heidelberg, IUCF) the electron cooling physics for heavy ions has been understood in more details.

LIST OF PARTICIPANTS

ANDERSEN, Lars Henrik, ISA, Aarhus University, DK-8000 AARHUS C, Denmark
AVILOV, Viatcheslav V., Inst. für Theoret. Phys., TU-Braunschweig, D-38116 BRAUNSCHWEIG, Germany
BAIRD, Simon, PS Division, CERN, CH-1211 GENEVA 23, Switzerland
BARLETTA, William A., Fusion Research Div., Lawrence Berkeley Lab. (LBL), BERKELEY, CA 94720, USA
BOSSER, Jacques, PS Division, CERN, CH-1211 GENEVA 23, Switzerland
BRÅNDAS, Erkki, Dept. of Quantum Chemistry, Uppsala University, S-751 20 UPPSALA, Sweden
CAPPI, Roberto, PS Division, CERN, CH-1211 GENEVA 23, Switzerland
CARRON, Georges, SL Division, CERN, CH-1211 GENEVA 23, Switzerland
CASPERS, Friedhelm, PS Division, CERN, CH-1211 GENEVA 23, Switzerland
CHANEL, Michel, PS Division, CERN, CH-1211 GENEVA 23, Switzerland
CHATTOPADHYAY, Swapan, Beam Physics, Lawrence Berkeley Laboratory (LBL), BERKELEY, CA 94720, USA
CHURCH, Michael, Fermi National Accelerator Laboratory (FNAL), BATAVIA, IL 60510, USA
DAINELLI, Antonio, Ist. Naz. di Fisica Nucleare (INFN), Lab. Naz. di Legnaro, I-35020 LEGNARO, Italy
DANARED, Håkan, Manne Siegbahn Institute of Physics, S-10405 STOCKHOLM, Sweden
EICKHOFF Bernhard, Ges. für Schwerionen-Forschung mbH (GSI), D-64220 DARMSTADT 11, Germany
ELLISON, Tim, Indiana University Cyclotron Facility (IUCF), BLOOMINGTON, IN 47405, USA
GAILLARD, Nicole, PS Division, CERN, CH-1211 GENEVA 23, Switzerland
GERASIMOV, Andrei, Fermi National Accelerator Laboratory (LBL), BATAVIA, IL 60510, USA
GOLDBERG, David, Lawrence Berkeley Laboratory (LBL), BERKELEY, CA 94 720, USA
GRIESER, Manfred, Max-Planck Inst. für Kernphysik (MPI), D-69029 HEIDELBERG 1, Germany
GRIMM, Rudolf, Max-Planck Inst. für Kernphysik (MPI), D-69029 HEIDELBERG 1, Germany
GUSTAFSSON, Stellan, Ist. Naz. di Fisica Nucleare (INFN), Lab. Naz. di Legnaro, I-35020 - LEGNARO, Italy
HABS, Dietrich, Max-Planck Inst. für Kernphysik (MPI), D-69029 HEIDELBERG 1, Germany
HANGST, Jeffrey S., ISA, Aarhus University, DK-8000 AARHUS C, Denmark
HERMANSSON, Lars, The Svedberg Laboratory, S-751 21 UPPSALA, Sweden
HOCHADEL, Bernd, Max-Planck Inst. für Kernphysik (MPI), D-69120 HEIDELBERG 1, Germany
HOFMANN, Ingo, Ges. für Schwerionen-Forschung mbH (GSI), D-64220 DARMSTADT 11, Germany
HUBER, Gerhard, CERN & Institut für Physik, Univ. Mainz, D-55099 MAINZ, Germany
HÜBNER, Kurt, PS Division, CERN, CH-1211 GENEVA 23, Switzerland
IKEGAMI, Hidetsugu, Dept. of Radiation Sciences, Univ. of Uppsala, S-751 21 UPPSALA, Sweden
JACKSON, Gerald P., Fermi National Accelerator Laboratory (FNAL), BATAVIA, IL 60510, USA
KATAYAMA, Takeshi, Institute for Nuclear Study (INS), Univ. of Tokyo, Tanashi, TOKYO 188, Japan
KOSHKAREV, Dimitri, Inst. of Theoretical and Experimental Physics (ITEP), MOSKOW 117259, Russia
LABRADOR, Ana, Ist. Naz. di Fisica Nucleare (INFN), Lab. Naz. di Legnaro, I-35020 - LEGNARO, Italy
LEFEVRE, Pierre, PS Division, CERN, CH-1211 GENEVA 23, Switzerland
LEY, Rudolf, PS Division, CERN, CH-1211 GENEVA 23, Switzerland
MAIER, Rudolf, Forschungszentrum Jülich, Institut für Kernphysik, D-52425 JÜLICH, Germany
MARRINER, John, Fermi National Accelerator Lab., P.O. Box 500, MS-341, BATAVIA, IL 60510, USA
MAURY, Stéphan, PS Division, CERN, CH-1211 GENEVA 23, Switzerland
MEINCKE, Olaf, DESY, Notkestrasse 85, D-22603 HAMBURG, Germany
MESHKOV, Igor, CAPT, Budker Institute of Nuclear Physics, 398055 LIPETSK, Russia
MÖHL, Dieter, PS Division, CERN, CH-1211 GENEVA 23, Switzerland
MOLAT-BERBIERS, Anne-F., PS Division, CERN, CH-1211 GENEVA 23, Switzerland
NEUFFER, David, CEBAF, Newport News, VA 23606, USA
NIELSEN, Jørgen S., ISA, Aarhus University, DK-8000 AARHUS C, Denmark
NOLDEN, Fritz, Ges. für Schwerionen-Forschung mbH (GSI), D-64220 DARMSTADT 11, Germany
OEFTIGER, Uwe, PS Division, CERN, CH-1211 GENEVA 23, Switzerland
PAPE MOLLER, Søren, ISA, University of Aarhus, DK-8000 AARHUS C, Denmark
PARKHOMCHUK, Vasily, Budker Inst. of Nuclear Physics (INP), 630 090 NOVOSIBIRSK, Russia
POLLOCK, Robert E., Indiana University Cyclotron Facility (IUCF), BLOOMINGTON, IN 47405, USA,
POULSEN, Ove, Mikroelektronik Centret, DTH, DK-2800 LYNGBY, Denmark
PRASUHN, Dieter, Forschungszentrum Jülich, Institut für Kernphysik, D-52425 JÜLICH, Germany
REISTAD, Dag, The Svedberg Laboratory, S-751 21 UPPSALA, Sweden
RENSFELT, Karl-Gunnar, Manne Siegbahn Laboratory, Stockholm University, S-10405 STOCKHOLM, Sweden
RUGGIERO, Alessandro G., Brookhaven National Laboratory (BNL), UPTON, NY 11973, USA
SARANTSEV, Vladislav, Joint Institute for Nuclear Research (JINR), 141 980 DUBNA, Russia

SCHIFFER, John P., Argonne National Laboratory (ANL), Physics Division, ARGONNE, IL. 60439-4843, USA
SEDLACEK, Miroslav, The Alfvén Laboratory, Royal Institute of Technology, S-100 44 STOCKHOLM, Sweden
SESSLER, Andrew M., Lawrence Berkeley Laboratory (LBL), BERKELEY, CA 94720, USA
SEURER, Michael, Institut für Theoretische Physik II, D-91058 ERLANGEN, Germany
SHARAPA, Anatoli N. , Budker Institute of Nuclear Physics (INP), 630 090 NOVOSIBIRSK, Russia
SHEMYAKIN, Alexander, Budker Institute of Nuclear Physics (INP), 630090 NOVOSIBIRSK, Russia
SIMON, Daniel-Jean, PS Division, CERN, CH-1211 GENEVA 23, Switzerland
SKRINSKI, Alexander, Budker Institute of Nuclear Physics (INP), 630090 NOVOSIBIRSK, Russia
STECK, Markus, Ges. für Schwerionen-Forschung mbH (GSI), D-64220 DARMSTADT 11, Germany
SYRESIN, Evgeny, CAPT, Budker Institute of Nuclear Physics, 398 055 LIPETSK, Russia
TANABE, Tetsumi, Institute for Nuclear Study (INS), Univ. of Tokyo, Tanashi, TOKYO 188, Japan
TECCHIO, Luigi, Univ. of Torino & Ist. Naz. di Fisica Nucleare (INFN), Sez. di Torino, I-10125 TORINO, Italy
TER-AKOPIAN, Gurgen M., J.I.N.R., Dubna, 141980 DUBNA, Russia
THORNDAHL, Lars, SL Division, CERN, CH-1211 GENEVA 23, Switzerland
TOEPFFER, Christian, Inst. für Theoretische Physik II, Univ. Erlangen, D-91058 ERLANGEN, Germany
TRAN, Minh-Quang, Centre de Recherches en Physique des Plasmas, EPFL, CH-1007 LAUSANNE, Switzerland
TRANQUILLE, Gérard, PS Division, CERN, CH-1211 GENEVA 23, Switzerland
VAN DER MEER, Simon, 4, chemin des Corbillettes, 1298 GRAND-SACONNEX, Switzerland
VEJBY-CHRISTENSEN, Lise, ISA, Aarhus University, DK-8000 AARHUS C, Denmark
WEI, Jie, Brookhaven National Laboratory (BNL), UPTON, NY 11973, USA
WHALEY, David, Centre de Recherches en Physique des Plasmas, EPFL, CH-1007 LAUSANNE, Switzerland
WOLF, Andreas, Max-Planck Inst. für Kernphysik (MPI), D-69029 HEIDELBERG 1,Germany
YANG, Bin, Ist. Nazionale di Fisica Nucleare, Lab. Nazionali di Legnaro, I-35020 LEGNARO, Italy
ZENKEVITCH, Pavel, Inst. of Theoretical & Experimental Physics (ITEP), 117 256 MOSKOW, Russia
ZWICKLER, Sebastian, Max-Planck Inst. für Kernphysik (MPI), D-69117 HEIDELBERG 1, Germany

AUTHOR INDEX

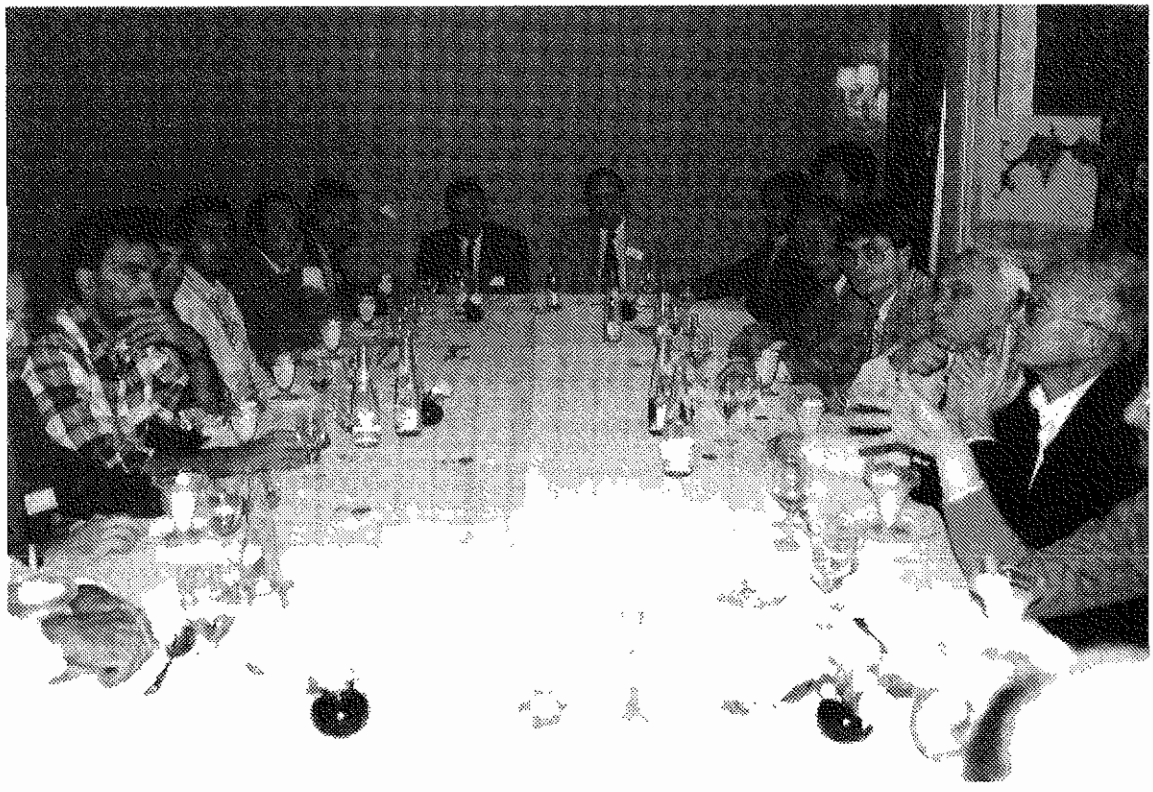

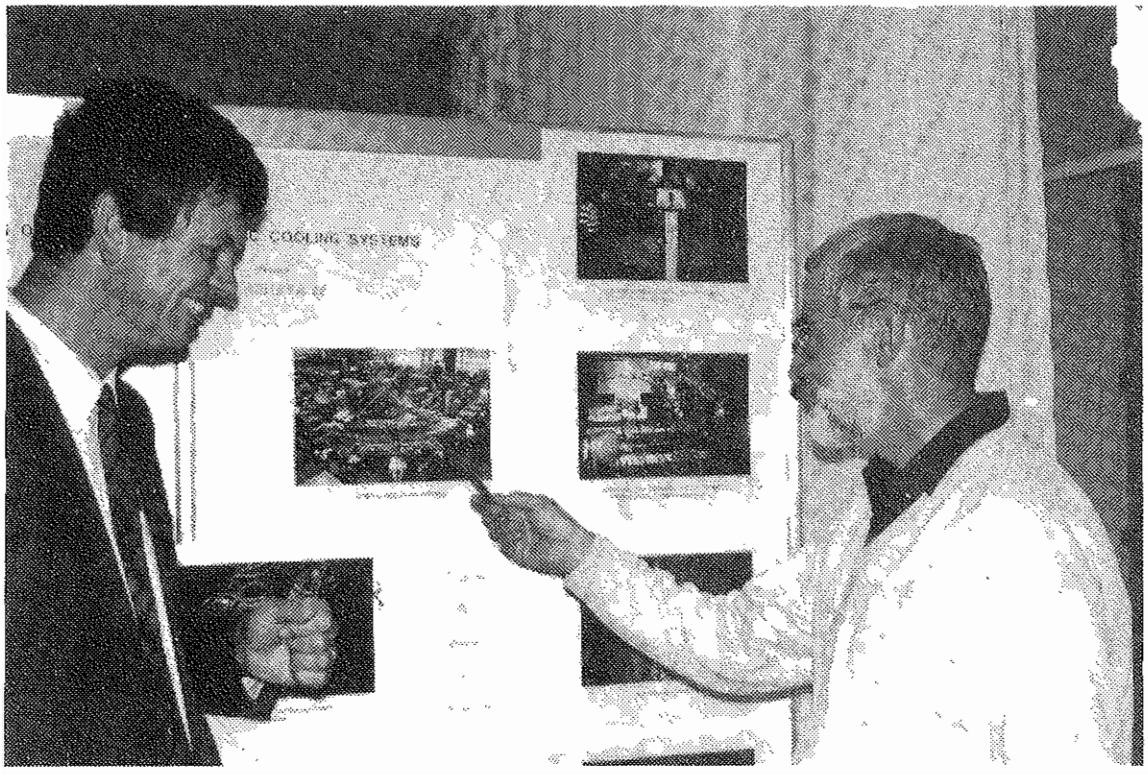
COOLING SYSTEMS

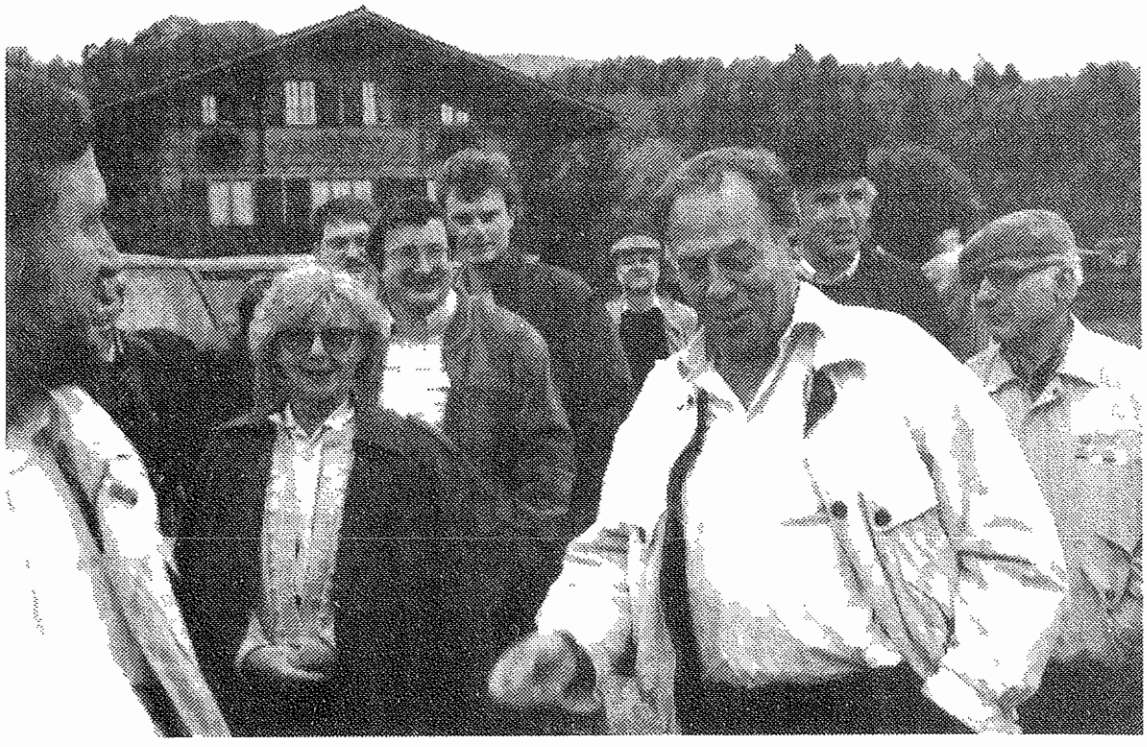

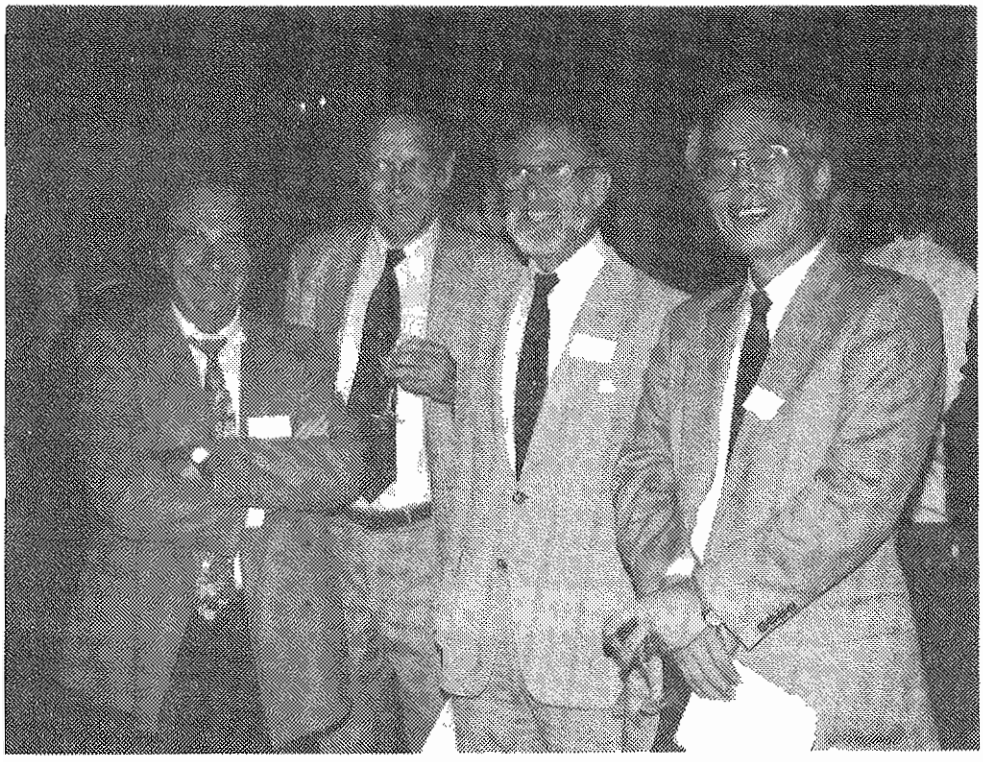

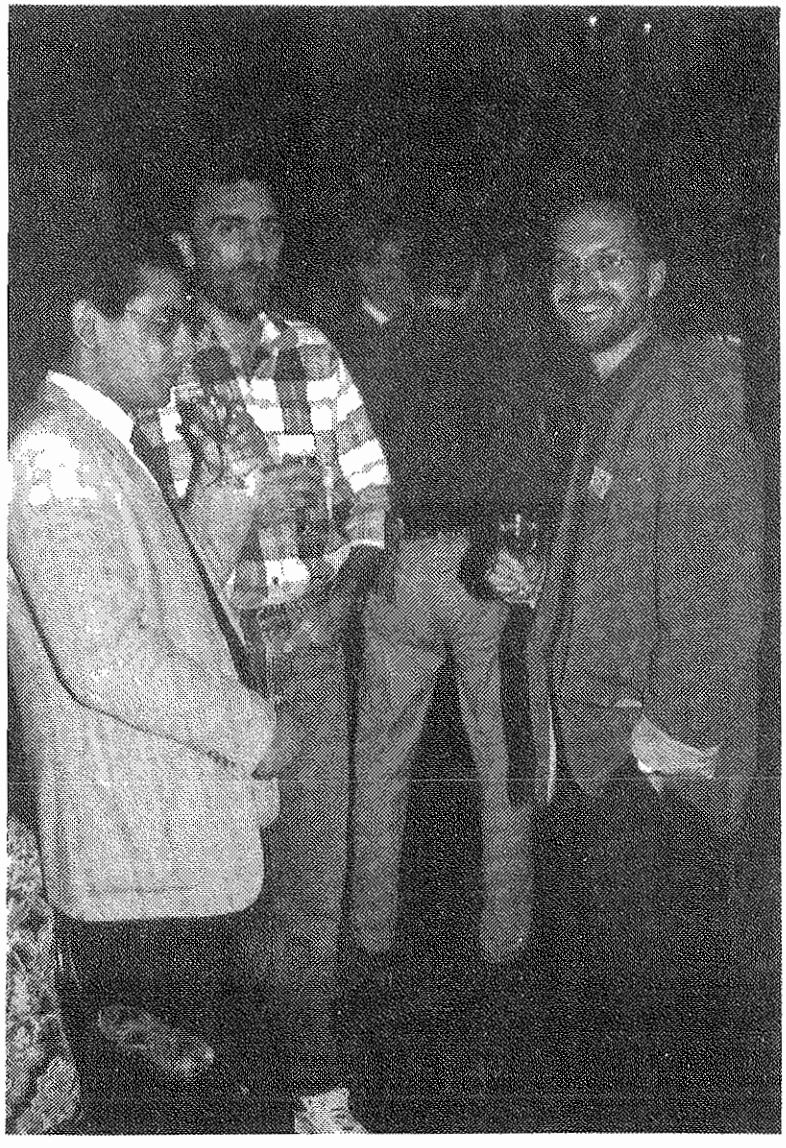

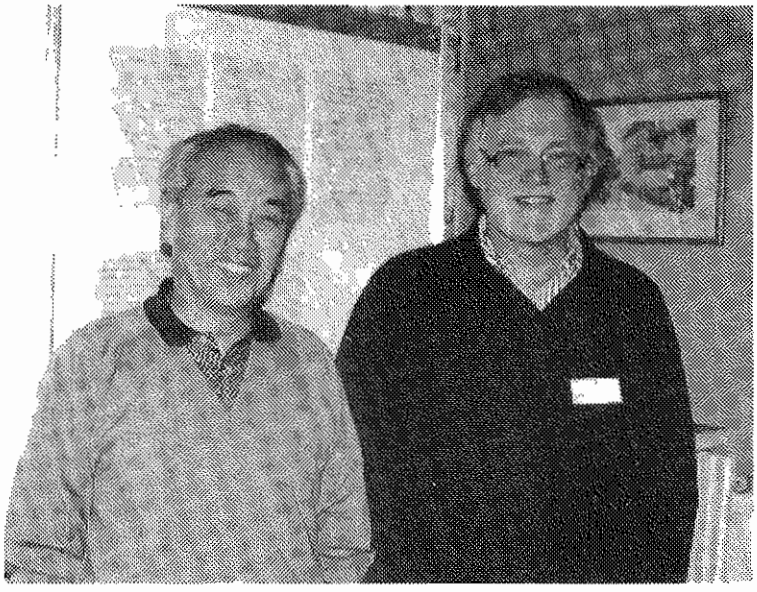

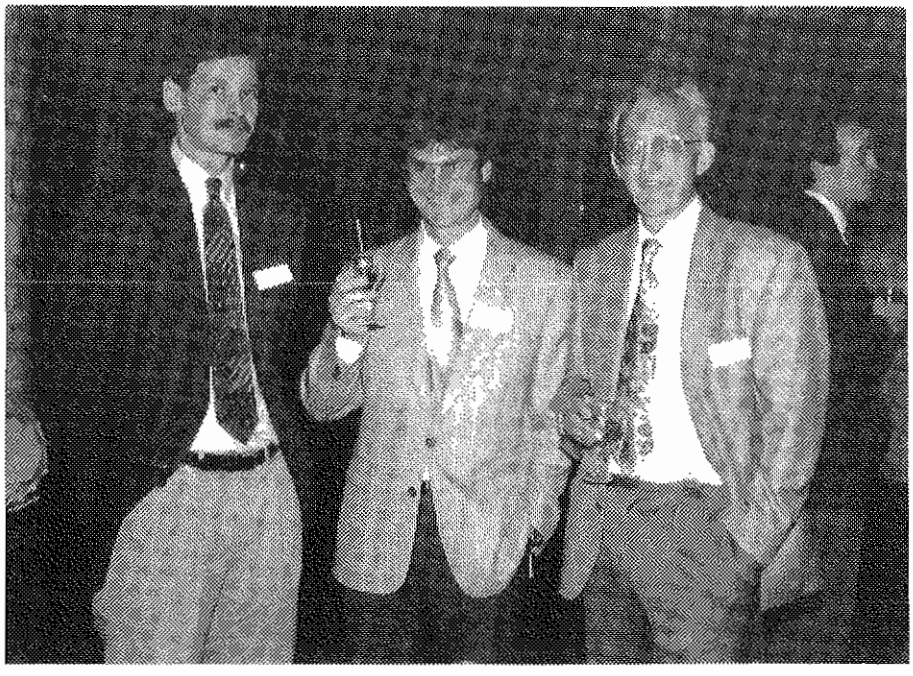

LIST OF PARTICIPANTS

ANDERSEN, Lars Henrik, ISA, Aarhus University, DK-8000 AARHUS C, Denmark
AVILOV, Viatcheslav V., Inst. für Theoret. Phys., TU-Braunschweig, D-38116 BRAUNSCHWEIG, Germany
BAIRD, Simon, PS Division, CERN, CH-1211 GENEVA 23, Switzerland
BARLETTA, William A., Fusion Research Div., Lawrence Berkeley Lab. (LBL), BERKELEY, CA 94720, USA
BOSSER, Jacques, PS Division, CERN, CH-1211 GENEVA 23, Switzerland
BRÅNDAS, Erkki, Dept. of Quantum Chemistry, Uppsala University, S-751 20 UPPSALA, Sweden
CAPPI, Roberto, PS Division, CERN, CH-1211 GENEVA 23, Switzerland
CARRON, Georges, SL Division, CERN, CH-1211 GENEVA 23, Switzerland
CASPERS, Friedhelm, PS Division, CERN, CH-1211 GENEVA 23, Switzerland
CHANEL, Michel, PS Division, CERN, CH-1211 GENEVA 23, Switzerland
CHATTOPADHYAY, Swapan, Beam Physics, Lawrence Berkeley Laboratory (LBL), BERKELEY, CA 94720, USA
CHURCH, Michael, Fermi National Accelerator Laboratory (FNAL), BATAVIA, IL 60510, USA
DAINELLI, Antonio, Ist. Naz. di Fisica Nucleare (INFN), Lab. Naz. di Legnaro, I-35020 LEGNARO, Italy
DANARED, Håkan, Manne Siegbahn Institute of Physics, S-10405 STOCKHOLM, Sweden
EICKHOFF Bernhard, Ges. für Schwerionen-Forschung mbH (GSI), D-64220 DARMSTADT 11, Germany
ELLISON, Tim, Indiana University Cyclotron Facility (IUCF), BLOOMINGTON, IN 47405, USA
GAILLARD, Nicole, PS Division, CERN, CH-1211 GENEVA 23, Switzerland
GERASIMOV, Andrei, Fermi National Accelerator Laboratory (LBL), BATAVIA, IL 60510, USA
GOLDBERG, David, Lawrence Berkeley Laboratory (LBL), BERKELEY, CA 94 720, USA
GRIESER, Manfred, Max-Planck Inst. für Kernphysik (MPI), D-69029 HEIDELBERG 1, Germany
GRIMM, Rudolf, Max-Planck Inst. für Kernphysik (MPI), D-69029 HEIDELBERG 1, Germany
GUSTAFSSON, Stellan, Ist. Naz. di Fisica Nucleare (INFN), Lab. Naz. di Legnaro, I-35020 - LEGNARO, Italy
HABS, Dietrich, Max-Planck Inst. für Kernphysik (MPI), D-69029 HEIDELBERG 1, Germany
HANGST, Jeffrey S., ISA, Aarhus University, DK-8000 AARHUS C, Denmark
HERMANSSON, Lars, The Svedberg Laboratory, S-751 21 UPPSALA, Sweden
HOCHADEL, Bernd, Max-Planck Inst. für Kernphysik (MPI), D-69120 HEIDELBERG 1, Germany
HOFMANN, Ingo, Ges. für Schwerionen-Forschung mbH (GSI), D-64220 DARMSTADT 11, Germany
HUBER, Gerhard, CERN & Institut für Physik, Univ. Mainz, D-55099 MAINZ, Germany
HÜBNER, Kurt, PS Division, CERN, CH-1211 GENEVA 23, Switzerland
IKEGAMI, Hidetsugu, Dept. of Radiation Sciences, Univ. of Uppsala, S-751 21 UPPSALA, Sweden
JACKSON, Gerald P., Fermi National Accelerator Laboratory (FNAL), BATAVIA, IL 60510, USA
KATAYAMA, Takeshi, Institute for Nuclear Study (INS), Univ. of Tokyo, Tanashi, TOKYO 188, Japan
KOSHKAREV, Dimitri, Inst. of Theoretical and Experimental Physics (ITEP), MOSKOW 117259, Russia
LABRADOR, Ana, Ist. Naz. di Fisica Nucleare (INFN), Lab. Naz. di Legnaro, I-35020 - LEGNARO, Italy
LEFEVRE, Pierre, PS Division, CERN, CH-1211 GENEVA 23, Switzerland
LEY, Rudolf, PS Division, CERN, CH-1211 GENEVA 23, Switzerland
MAIER, Rudolf, Forschungszentrum Jülich, Institut für Kernphysik, D-52425 JÜLICH, Germany
MARRINER, John, Fermi National Accelerator Lab., P.O. Box 500, MS-341, BATAVIA, IL 60510, USA
MAURY, Stéphan, PS Division, CERN, CH-1211 GENEVA 23, Switzerland
MEINCKE, Olaf, DESY, Notkestrasse 85, D-22603 HAMBURG, Germany
MESHKOV, Igor, CAPT, Budker Institute of Nuclear Physics, 398055 LIPETSK, Russia
MÖHL, Dieter, PS Division, CERN, CH-1211 GENEVA 23, Switzerland
MOLAT-BERBIERS, Anne-F., PS Division, CERN, CH-1211 GENEVA 23, Switzerland
NEUFFER, David, CEBAF, Newport News, VA 23606, USA
NIELSEN, Jørgen S., ISA, Aarhus University, DK-8000 AARHUS C, Denmark
NOLDEN, Fritz, Ges. für Schwerionen-Forschung mbH (GSI), D-64220 DARMSTADT 11, Germany
OEFTIGER, Uwe, PS Division, CERN, CH-1211 GENEVA 23, Switzerland
PAPE MOLLER, Søren, ISA, University of Aarhus, DK-8000 AARHUS C, Denmark
PARKHOMCHUK, Vasily, Budker Inst. of Nuclear Physics (INP), 630 090 NOVOSIBIRSK, Russia
POLLOCK, Robert E., Indiana University Cyclotron Facility (IUCF), BLOOMINGTON, IN 47405, USA,
POULSEN, Ove, Mikroelektronik Centret, DTH, DK-2800 LYNGBY, Denmark
PRASUHN, Dieter, Forschungszentrum Jülich, Institut für Kernphysik, D-52425 JÜLICH, Germany
REISTAD, Dag, The Svedberg Laboratory, S-751 21 UPPSALA, Sweden
RENSFELT, Karl-Gunnar, Manne Siegbahn Laboratory, Stockholm University, S-10405 STOCKHOLM, Sweden
RUGGIERO, Alessandro G., Brookhaven National Laboratory (BNL), UPTON, NY 11973, USA
SARANTSEV, Vladislav, Joint Institute for Nuclear Research (JINR), 141 980 DUBNA, Russia

SCHIFFER, John P., Argonne National Laboratory (ANL), Physics Division, ARGONNE, IL. 60439-4843, USA
SEDLACEK, Miroslav, The Alfvén Laboratory, Royal Institute of Technology, S-100 44 STOCKHOLM, Sweden
SESSLER, Andrew M., Lawrence Berkeley Laboratory (LBL), BERKELEY, CA 94720, USA
SEURER, Michael, Institut für Theoretische Physik II, D-91058 ERLANGEN, Germany
SHARAPA, Anatoli N. , Budker Institute of Nuclear Physics (INP), 630 090 NOVOSIBIRSK, Russia
SHEMYAKIN, Alexander, Budker Institute of Nuclear Physics (INP), 630090 NOVOSIBIRSK, Russia
SIMON, Daniel-Jean, PS Division, CERN, CH-1211 GENEVA 23, Switzerland
SKRINSKI, Alexander, Budker Institute of Nuclear Physics (INP), 630090 NOVOSIBIRSK, Russia
STECK, Markus, Ges. für Schwerionen-Forschung mbH (GSI), D-64220 DARMSTADT 11, Germany
SYRESIN, Evgeny, CAPT, Budker Institute of Nuclear Physics, 398 055 LIPETSK, Russia
TANABE, Tetsumi, Institute for Nuclear Study (INS), Univ. of Tokyo, Tanashi, TOKYO 188, Japan
TECCHIO, Luigi, Univ. of Torino & Ist. Naz. di Fisica Nucleare (INFN), Sez. di Torino, I-10125 TORINO, Italy
TER-AKOPIAN, Gurgen M., J.I.N.R., Dubna, 141980 DUBNA, Russia
THORNDAHL, Lars, SL Division, CERN, CH-1211 GENEVA 23, Switzerland
TOEPFFER, Christian, Inst. für Theoretische Physik II, Univ. Erlangen, D-91058 ERLANGEN, Germany
TRAN, Minh-Quang, Centre de Recherches en Physique des Plasmas, EPFL, CH-1007 LAUSANNE, Switzerland
TRANQUILLE, Gérard, PS Division, CERN, CH-1211 GENEVA 23, Switzerland
VAN DER MEER, Simon, 4, chemin des Corbillettes, 1298 GRAND-SACONNEX, Switzerland
VEJBY-CHRISTENSEN, Lise, ISA, Aarhus University, DK-8000 AARHUS C, Denmark
WEI, Jie, Brookhaven National Laboratory (BNL), UPTON, NY 11973, USA
WHALEY, David, Centre de Recherches en Physique des Plasmas, EPFL, CH-1007 LAUSANNE, Switzerland
WOLF, Andreas, Max-Planck Inst. für Kernphysik (MPI), D-69029 HEIDELBERG 1,Germany
YANG, Bin, Ist. Nazionale di Fisica Nucleare, Lab. Nazionali di Legnaro, I-35020 LEGNARO, Italy
ZENKEVITCH, Pavel, Inst. of Theoretical & Experimental Physics (ITEP), 117 256 MOSKOW, Russia
ZWICKLER, Sebastian, Max-Planck Inst. für Kernphysik (MPI), D-69117 HEIDELBERG 1, Germany